NASA Conference Publication 10113

Second International Microgravity Combustion Workshop

Proceedings of a workshop
held at the Cleveland Airport Marriott Hotel
Cleveland, Ohio
September 15–17, 1992

NASA

NASA Conference Publication 10113

Second International Microgravity Combustion Workshop

Proceedings of a workshop cosponsored by
NASA Headquarters,
Microgravity Science and Applications Division,
and Lewis Research Center,
Space Experiments Division,
and held at the Cleveland Airport Marriott Hotel
September 15–17, 1992

National Aeronautics and
Space Administration

Office of Management

**Scientific and Technical
Information Program**

1993

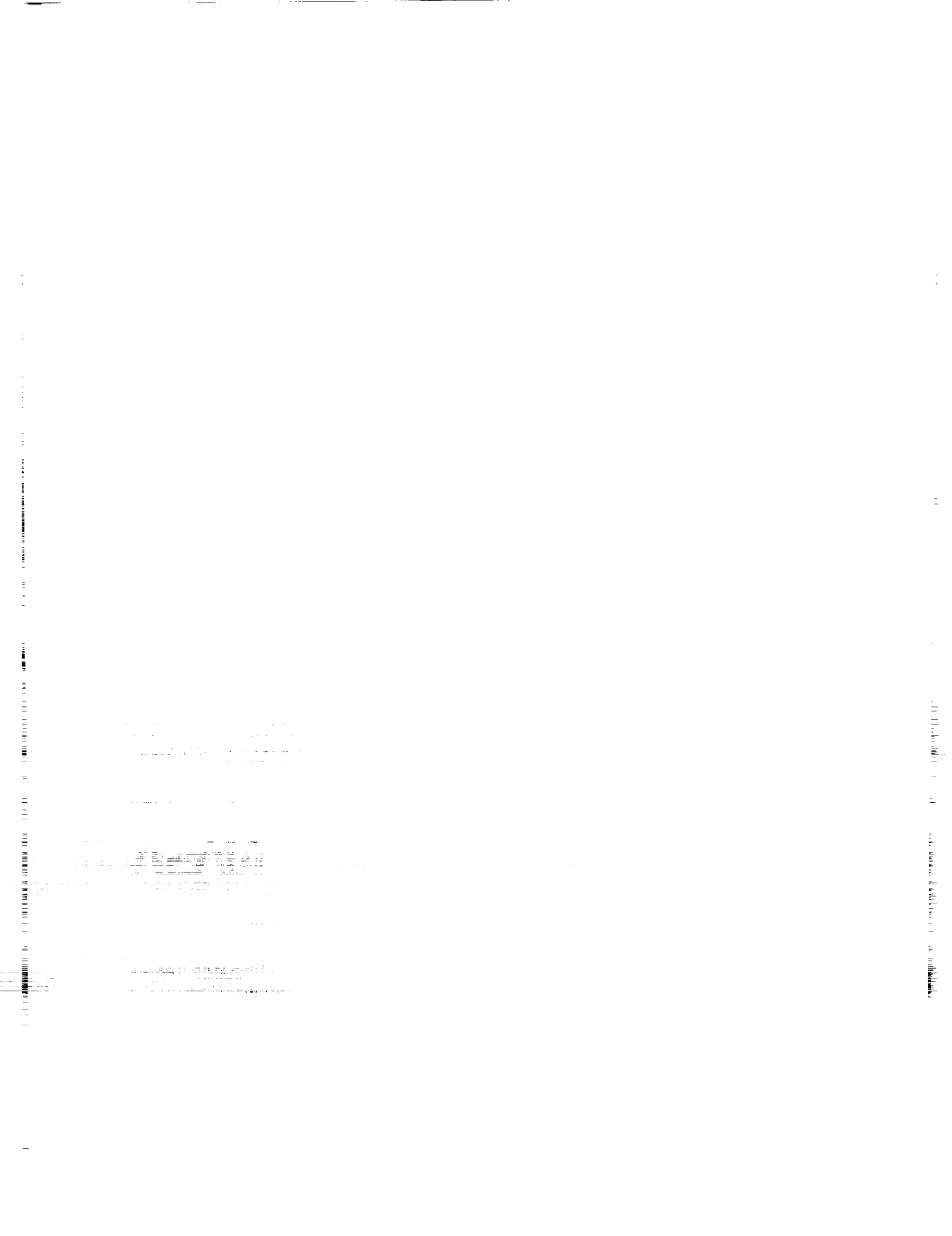

PREFACE AND ACKNOWLEDGEMENTS

The Second International Microgravity Combustion Workshop, held in Cleveland, Ohio on September 15-17, 1992, was attended by about 160 people, mostly university professors and graduate students, from fourteen countries. The purpose of the workshop was twofold: first, to exchange information with fire safety and combustion researchers and managers about the progress and promise of combustion research in microgravity, specifically in ground-based facilities like the NASA Lewis drop towers and the NASA JSC/KC-135 as well as space-based facilities like the Shuttle and the planned Space Station *Freedom*. Second, the workshop was a forum for an open discussion of areas into which microgravity combustion science investigations could expand profitably, and which should be included in any upcoming NASA Research Announcement (NRA).

Independent assessments by leading combustion researchers stated that combustion science in a microgravity environment now has a proven record of accomplishment and surprising discoveries; in the coming decades it will continue to offer a unique opportunity and challenge for generating new fundamental understanding of widespread interest to people concerned with novel combustion processes here on Earth and in space. Recommendations for new or expanded emphasis in an NRA included combustion synthesis of high-value materials in space, metals combustion studies in microgravity, and soot-generation mechanisms.

Forty papers were presented, including the first-look by the peer community at the results of the USML-1 (STS-50) mission, which flew four successful combustion experiments. All papers are included in these proceedings (along with one paper which was not presented at the authors' request). Also in these proceedings are all of the audience's written questions or comments and the authors' replies, included at the end of the relevant paper. When no questions or comments appear, it is not because none was offered at the workshop; instead either the question/comment forms were mistakenly not passed out to the questioner, or the questioner chose not to submit it for response, author reply, and publication. A closing plenary meeting was held, at which oral summaries of the contents of parallel technical sessions were provided by the session chairmen; a brief synopsis of their summaries is also included in these proceedings.

A number of the papers included color plates, and because the color in microgravity combustion is often critical to visualization of the process, these are included. Production requirements make it necessary to group these color plates at the end of the proceedings; all figures in the main body are black and white.

Sincere appreciation is offered to all who participated in this highly successful workshop, especially to the microgravity combustion "discipline working group" who served as the steering committee for the workshop (see attached list), Col. Carl Meade of the STS-50 astronaut crew for sharing in a keynote dinner speech his experiences on two shuttle missions, the members of the Microgravity Combustion Branch at NASA Lewis and of NASA Headquarters' Microgravity Science and Applications Division for serving as session chairman and facilitators, and finally to the conference organizer's support team (see attached list).

Dr. Howard D. Ross, Workshop Organizer
Mail Stop 500-217
NASA Lewis Research Center
21000 Brookpark Road
Cleveland, OH 44135
Phone (216) 433-2562 -- FAX (216) 433-8660

LISTS

DISCIPLINE WORKING GROUP MEMBERS

Professor Gerard Faeth, University of Michigan (Chair)
Professor Robert Altenkirch, Mississippi State University
Dr. Bradley Carpenter, NASA Headquarters
Dr. Raymond Friedman, Factory Mutual (retired)
Professor Jack Howard, Massachusetts Institute of Technology
Professor Chung K. (Ed) Law, Princeton University
Mr. Kurt Sacksteder, NASA Lewis
Professor Robert Santoro, Pennsylvania State University
Professor Mitchell Smooke, Yale University
Professor Forman Williams, University of California--San Diego

CONFERENCE SUPPORT CORE TEAM

Sverdrup Technology, Inc. team: Richard Ziegfeld, John Toma, Karen Fandrich, and Jack Harper.

TABLE OF CONTENTS

*Presenter

*Presenter

*Presenter

SESSION A - PLENARY SESSION

(Chair, Jack Salzman)

THE WORLD OF NASA MICROGRAVITY SCIENCE

Robert C. Rhome, P.E.*
National Aeronautics and Space Administration
Washington, D.C. 20546

Introduction

It has been said the the decade of the 1990's represents a second golden age of science. We are in the midst of one of the most exciting and interesting periods in the history of exploration - - a period which holds the potential for expanding our understanding of scientific phenomena ranging from intricacies of the universe to the subtleties of our own planet. The opportunities to study the effects of microgravity in space seem limitless during the next decade. Using the European Space Agency (ESA) built Spacelab, we will maximize opportunities for development of new microgravity facilities in order to obtain new information and increase our understanding of the effects of gravitational forces on phenomena in biological, chemical and physical systems. NASA intends to move aggressively, but sensibly, to develop additional space research facilities as we build toward the unique Space Station Freedom resources becoming available towards the end of this decade.

In the Space Studies Board's 1992 report, *Toward a Microgravity Research Strategy*, the Committee on Microgravity Research recommended that a long term research strategy be developed for microgravity sciences. The report defined the the overall goals of the field and summarized the current knowledge of its subdisciplines. In addition, the Committee concluded that this strategy should identify the fundamental questions that need to be addressed and the scientific community's ability to address them. For those of us involved in developing and supporting a growing microgravity science research program, this was yet another indicator that the field of low gravity research is beginning to prove its merit.

---

* Director, Microgravity Science and Applications Division
Office of Space Science and Applications

NASA's Microgravity Science Research Program

NASA funds a robust microgravity research program in a wide variety of microgravity related disciplines. Each research task is designed to yield a better understanding of phenomena within the areas of biotechnology, combustion, fluid dynamics and transport phenomena, and materials sciences. The knowledge gained from research in one field often has impacts in another. Investigations sponsored as part of the microgravity science program share one characteristic; they required reduced or very low gravity conditions in order to achieve their objectives.

The overall Microgravity Research Program is conducted through integrated ground-based and flight programs. The primary functions of the ground-based research program is to develop concepts that lead to flight experiments - - to determine limitations of various terrestrial processing techniques - - and to provide analysis and modeling support to the flight program. Although we support research than can be completed in the ground-based program, a successful ground-based research program is generally the first step in the process towards flight experimentation. At the start of 1992, the Microgravity Science and Applications Division was supporting a total of 115 microgravity research Principal Investigators; 73 in the ground-based program and 42 in the flight program.

Ground-based Research

The ground-base research program has continued to perform the essential functions of providing theoretical and experimental background to support current flight experiments, and to nurture ideas and efforts that may later form the basis of future flight experiments. The program has used several types of unique facilities providing varying durations of reduced gravity environments such as drop tubes, drop towers, and aircraft. The most active of these ground facilities include two drop towers here at Lewis Research Center, wherein the sample and equipment can be protected from the drop environment and provide a low gravity environment for 2-5 seconds, and a drop tube at Marshall Space Flight Center. Aircraft in parabolic flight trajectories can provide reduced gravity durations of up to nearly 30 seconds; a KC-135 aircraft at the Johnson Space Center and a Learjet Model 25 here at the Lewis Research Center are available. In addition to the test facilities, the Microgravity Materials Science Laboratory here at Lewis Research Center provides an extensive computational and modeling capability.

In a continuing effort to expand the microgravity research community, we have supported several ground-based efforts in the academic community. The Graduate Student Researchers Program is one means where students, under the guidance of a faculty sponsor, can perform microgravity research using ground-based low gravity facilities. Secondly, government, industry, and university cooperation is encouraged through an active post-doctoral and Visiting Senior Scientist program. Recent Ph.D 's, tenured professors, and nationally known experts can spend one to two years conducting research at a NASA center or can participate in science planning and management at NASA Headquarters.

In addition, we disseminate results from both the ground-based and flight-based research programs to the scientific community-at-large through participation in conferences, forums, and workshops. These include such meetings as Gordon Research conferences, American Institute of Aeronautics and Astronautics science meetings, Committee on Space Research (COSPAR) conferences, International Astronautical Federation conferences, European Symposia on Materials and Fluid Sciences in Microgravity, and at workshops such as this Second International Workshop on Combustion Science in Microgravity. In this way we are expanding our base throughout the low-gravity research community.

The Flight Program: Research-in-Space

As our experience becomes more fine-tuned and as we more effectively use gravity as an experimental parameter, we will be able to realize the potential offered by this new age of low-gravity research. The sheer number of space science missions related to microgravity sciences in the years between 1991 and 1993 is dramatic. More microgravity research will have been conducted within these years than has been conducted over the preceding decade.

Significant effort is spent in preparation for a number of upcoming Space Shuttle missions. Multi-user and experiment-unique apparatus will be flown abroad the Shuttle periodically over the next six years in various payload configurations. The European developed Spacelab module is an important tool in supporting low gravity research. This year the International Microgravity Laboratory (IML), the United States Microgravity Laboratory (USML), and the Japanese/U.S. collaborative Spacelab-J mission utilized the pressurized Spacelab module. The U.S. Microgravity Payload (USMP), an unpressurized system in the Shuttle payload bay is to be first flown in October 1992. These Spacelab missions form a foundation for future microgravity research on space Station Freedom. This research will continue as Shuttle and

Spacelab flights are projected into 1998 as our basic research vehicle prior to access to Space Station. Another payload configuration is the commercial middeck accommodations module, Spacehab, scheduled to begin a series of flights in 1993.

Most of the recently launched and upcoming microgravity missions have an international component, fostering cooperation and an exchange of knowledge benefiting the entire science community. When combined with other international cooperative flight programs, such as the European Retrievable Carrier (EURECA) series, the German Spacelab-D2, the Japanese/ U.S. collaborative Spacelab-J mission, and the European Space Agency (ESA) proposed Spacelab-E1 and Spacelab-E2 missions, there should be frequent and routine access to space and its research opportunities during the remainder of the decade.

Supporting Research & Technology

Flight experience has demonstrated that an early investment in technology specific to the microgravity program is essential. In order to achieve this, NASA funds research activities that seek to create or refine equipment that would enhance the scientific quality of future microgravity flight experiments. Technology development not specifically on the critical path of any particular flight project is funded through the Advanced Technology Development (ATD) program. The supporting technology development includes fundamental research that supports the goals and objectives of the overall microgravity science program. An example of this activity is the development of systems to characterize the reduced-gravity environment of space experiments.

Space Station Freedom Utilization

Beginning as early as 1997, the Space Station will offer the environment, power, and duration necessary to pursue a wide range of scientific research. Extending on-orbit research time from the seconds and minutes of sounding rockets to the hours and days of the Shuttle and Spacelab program was a key element in the growth in research in which gravity is the experimental parameter. The Space Station extends the opportunity several orders of magnitude. Definition of several multi-user microgravity facilities for potential use on the Space Station began during the 1990-1991 time period. Hardware requirements necessary to support these facilities continue to be identified in order to influence Space Station design. The precursor payloads

flown on Shuttle missions and the research conducted provide experience for the operations and development of instrumentation and subsystems for use on the Space Station .

Space Station Freedom will provide a stable platform on which highly productive and flexible microgravity science experiment modules can be based. A key long term program goal is the development of several multi-user facilities specifically designed for long duration scientific research missions. We are studying several facility concepts to support the microgravity science research we expect will be conducted aboard the Space Station during the period 1997 and 2004. Some of this early hardware could be of Spacelab heritage - - consistent with our "go as you learn" strategy.

The Modular Combustion Facility, probably of most interest to this Workshop, could support a wide range of science experiments dealing with the study of combustion and its by-products. The facility is currently planned for flight aboard the Space Station as early as 1998. Advanced combustion experiment hardware is presently being defined for Spacelab missions in the mid 1990's as precursors to the Modular Combustion Facility experiments. It is likely that recommendations from this workshop will influence the research announcement leading to the selection of many of the early Space Station Freedom combustion Principal Investigators.

The Future for Microgravity Science Research

Microgravity Research within the United States has an optimistic future. The President proposed a budget for Fiscal Year 1993 that represented a doubling of the funding for microgravity research over three years.

We have established four science Discipline Working Groups in the areas of Biotechnology, Combustion, Fluids and Transport Phenomena, and Materials Science. These groups are responsible for maintaining an overview of the efforts in the discipline areas and for providing an annual assessment of the program. They are to recommend refinements and science priorities within the discipline, and to identify the programs, strengths and weaknesses, as well as the most promising areas for investigation and the most advantageous approaches for experimentation.

We are using a series of NASA Research Announcements (NRA's), all open to the international science community, to select principal investigators for ground-based research, for flight experiment definition, and for space-based research. The NRA for combustion science issued in 1989 to solicit

ground-based and flight experiments produced 65 proposals, the NRA for Fluids and Materials Science Containerless Processing released in 1990 produced 69 proposals. Four NRA's were released in 1991 -- the fluid dynamics and transport phenomena NRA produced 205 proposals; the biotechnology NRA produced 94 proposals; the materials science NRA produced 141 proposals; and the NRA for fundamental science produced 51 proposals -- or a total of 491 proposals from NRA's released in 1991. In August 1992 we selected 122 Principal Investigators from these four NRA's - - a selection rate approximating 25%. This raises the number of Principal Investigators in the microgravity science program from 115 in 1992 to over 190 in 1993.

We are looking toward a 3-fold increase in funded Principal Investigators prior to Space Station Freedom Permanently Manned Capability in 1999. We plan to release research announcements in the coming years in order to continue to obtain high quality scientific investigations. Workshops such as this one will contribute to the content definition of future research announcements.

Conclusions

The research in space we applaud in 1992 and 1993 is based upon plans laid in the mid to late 1980's. It has taken several years to develop and define a successful research plan. The present series of microgravity research missions is based upon work that was started almost a decade ago, and has evolved through successful international cooperation, planning and establishment of clearly defined research goals.

These are exciting times for those of us involved in microgravity research -- and we have only begun to define the work that needs to be done. So at the onset of this Second International Workshop on Combustion Science in Microgravity -- let us agree to start the cycle again, to plan for the research opportunities in the years ahead, using the Spacelab, free-flyers and, of course Space Station Freedom. Clearly, securing the promise of successful microgravity research for the late 1990's, both in the laboratory and in space, demands a science dialogue such as that supported by workshops like this one. I wish you well in your endeavors this week.

OVERVIEW OF NASA'S MICROGRAVITY COMBUSTION SCIENCE AND FIRE SAFETY PROGRAM

N93-20180

Howard D. Ross
NASA Lewis Research Center
Cleveland, Ohio 44135

The study of fundamental combustion processes in a microgravity environment is a relatively new scientific endeavor. A few simple, precursor experiments were conducted in the early 1970's. Today the advent of the U.S. space shuttle and the anticipation of the Space Station *Freedom* provide for scientists and engineers a special opportunity -- in the form of long duration microgravity laboratories -- and need -- in the form of spacecraft fire safety and a variety of terrestrial applications -- to pursue fresh insight into the basic physics of combustion. Through microgravity, a new range of experiments can be performed since:

* ***Buoyancy-induced flows are nearly eliminated.*** Due to the hot, less dense reaction products of combustion, buoyancy-induced flows tend to develop in normal gravity experiments, promoting self-turbulization and instabilities. Microgravity reduces these flows and their attendant complications, thus, furthering understanding of low-gravity behavior and, by direct comparison, related normal-gravity combustion processes.
* ***Normally obscured forces and flows may be isolated.*** Buoyancy frequently obscures weaker forces, such as electrostatic, thermocapillary, radiative and diffusional forces, which may be important near flammability limits. Further, the effect of low velocity forced flows can not normally be studied due to the onset of mixed convection. By removing buoyancy, the roles of these forces and flows may be observed, and compared to theory.
* ***Gravitational settling or sedimentation is nearly elimlnated.*** Unconstrained suspensions of fuel droplets or particles may be created and sustained in a quiescent environment, eliminating the need for mechanical supports, levitators, or stirring devices and enabling a high degree of symmetry and/or quiescence to be achieved.
* ***Larger time or length scales in experiments become permissible.*** To limit buoyancy effects in normal gravity experiments, the size or duration of tests is often constrained. Microgravity permits larger scale experiments which in turn allow more detailed diagnostic probing and observation. Microgravity also enables new tests of similitude through experiment.

Combustion experiments have now been completed in drop towers and aircraft and have flown successfully on the Shuttle. As will be discussed in various papers at this workshop, unexpected and unexplained phenomena have been observed -- with surprising frequency -- in microgravity combustion experiments, raising questions about the degree of accuracy and completeness of our textbook understanding and our ability to estimate spacecraft fire hazards.

The interest in microgravity combustion science is not strictly academic. There have been four internal "fire" incidents in the U.S. Shuttle program, involving overheating or smoldering of wire insulation and electrical components from localized loss of cooling air or electrical short circuits. In each case, the crew observed the evolution of particles and odors; the potential fire was immediately suppressed by switchin g off the appropriate circuits, without resorting to the discharge of fire extinguishers. A severe incident was reported for the Soviet Salyut 7, requiring both the discharge of an extinguisher and venting of the uninhabited cabin atmosphere to the vacuum of space. The atmosphere of the space station was later replenished by stores from a supply flight. This experience has demonstrated that present spacecraft fire protection can respond to a variety of in-flight incidents. Nevertheless, there is growing appreciation for

---

This paper is excerpted in part from NASA TM105410 entitled "Microgravity Combustion Science: Progress, Plans, and Opportunities" which was authored by members of the Microgravity Combustion Branch, Space Experiments Division, NASA Lewis Research Center. I have expanded it with several personal opinions and assessments.

the need for fundamental research and technology development with the longer-term objective of investigating and improving spacecraft fire-safety practices. A more complete understanding of combustion phenomena and flame characteristics contributes to the improvement of material acceptance standards, fire detection, extinguishment, and postfire rehabilitation in space. Moreover, low-gravity combustion research is necessary in assessing the effects of certain hazards that may be unique to or aggravated in space — smoldering or aerosol fires, for example.

Low-gravity combustion experiments may also yield methods to produce exotic materials such as fullerenes or highly ordered ceramic - metal composites. In this author's opinion, the costs of producing such materials in a space environment will probably prohibit their widespread manufacture in space; however, the results from space-based experiments could lead to needed understanding to produce these or related materials more readily or cheaply on Earth. Similarly fundamental experiments in heterogeneous combustion systems such as particle or aerosol clouds support improved understanding of Earth-based fire environments (e.g. grain bins, mine safety, spray combustion processes). One recent idea this author has heard involves using the long soot residence times available in microgravity to study agglomeration phenomena to be used to understand atmospheric contamination by particles from large-scale fires such as those which occurred recently in the oil fields in the Persian Gulf.

MICROGRAVITY LABORATORIES AND FACILITIES

There are several test facilities which provide a free fall or semi-free fall condition where the force of gravity is offset by linear acceleration, thus enabling a reduced gravity environment available for scientific studies. Each of the facilities has different capabilities and characteristics that must be considered by an investigator when selecting the one best suited to a particular series of experiments. Perhaps the most unique and challenging feature for researchers working in these facilities is the facility constraints. The researcher must place new emphasis on experimental requirements for power, volume, operating time, and weight. Operation is remote, being automated in the drop towers or through astronauts on the shuttle. Delicate hardware must be considered for shock isolation in the drop towers although items such as mirrors and incandescent lights regularly survive landing. Compatibility with vacuum environments may be needed as well. Balanced against these difficulties or constraints is the unique opportunity for scientific discovery, already verified in combustion experiments in microgravity: thought-provoking and surprising observations are the norm for nearly every experiment we have conducted.

To date, the majority of combustion studies have taken place in the NASA Lewis Research Center's (LeRC) two drop towers and Model 25 Learjet. The 2.2 Second Drop Tower, as the name implies, provides 2.2 seconds of low gravity test time for experiment packages with up to 150 kilograms of hardware mass. To lower residual acceleration, the experiment freely falls inside in an air drag shield. The facility offers both low cost and rapid turnaround time between experiments. It is often used for proof-of-concept or precursor experimentation; most microgravity combustion experimental investigations start here. The 5.18 second Zero-Gravity Facility with its 132 meter free fall distance in an evacuated drop chamber (again to lower residual accelerations) allows experiments of up to 450 kilograms in mass mounted in a one meter diameter drop bus. This facility probably provides the lowest available accelerations available today.

Specially modified jet aircraft flying parabolic trajectories can provide significant increases in low-gravity experiment time when compared to drop towers but not without the penalty of higher gravity levels. For an experiment fixed to the body of an aircraft, accelerations in the range of 10^{-2} g can be obtained for up to 20 seconds. During one flight several trajectories are possible. While aircraft may not offer true microgravity, they offer the significant advantages of permitting researchers to monitor their experiments in real-time, reconfigure them between trajectories and utilize delicate instrumentation precluded in drop tower tests because of severe shock loadings at the end of the drop. NASA's larger KC-135 aircraft at the Johnson Space Center also permits free-floated experiments achieving acceleration levels in the range of 10^{-4} g for 5 to 8 seconds. Up to 40 trajectories can be performed in a single flight.

Although they have not yet been used by the U.S. microgravity combustion program, sounding rockets can provide a reduced gravity environment of 10^{-4} g for about 300 seconds. Their use is presently being considered for experiments in flame spread over liquid pools and thick solids; the hardware is being built with plans for future users to fly the same or similar hardware for other combustion experiments.

Truly long duration microgravity combustion experiments require space-based laboratories such as the U.S. space shuttle or Space Station *Freedom*. Qualification of materials and assurance of safety for combustion experiments imposes an all-new set of concerns to the new researcher, although here NASA engineers who are experienced with the voluminous handbooks and requirements provide a great deal of help. The shuttle flight duration for science missions is 7 to 13 days; our experience with combustion experiments is they required as little as 0.5 crew-hours or, for the set of experiments on USML-1 (STS-50), up to 20 crew-hours (this is not a hard limit). Power, volume, and weight allowances depend on where an experiment is mounted in the shuttle (e.g. mid-deck locker, glovebox, cargo bay) and the type of mission (e.g. Spacelab). Substantial astronaut involvement is not only possible but encouraged for mid-deck or Spacelab experiments. While the crew is not necessarily expert in combustion, they are quite knowledgable on the unique features of microgravity and have improved, in real-time, the scientific yield from several experiments due to this knowledge.

The most common complaint of microgravity researchers is the long hardware development time and the difficulty in gaining frequent access to a space environment. In the future, Space Station *Freedom* will provide more opportunity as well as the highest quality, longest duration reduced gravity laboratory. Within its instrument racks will be dedicated space, electrical power, and advanced diagnostic instrumentation for microgravity combustion experiments. Multi-user experiments will be conducted in experiment "modules" by scientific specialists. Principal investigators on Earth will have the capability of monitoring and modifying in real-time the performance of their experiments. This future facility, along with the means by which investigators' experiments will be selected for flight, are discussed elsewhere in this workshop.

MICROGRAVITY COMBUSTION EXPERIMENTS AND SPACECRAFT FIRE SAFETY

In this workshop, the currently supported microgravity combustion studies are reviewed; they are listed in Table 1, noting that this list does not include completed or nearly completed microgravity combustion studies such as those experiments which have flown on the Shuttle (Solid Surface Combustion Experiment; Smoldering Combustion in Microgravity; Wire Insulation Flammability; and Candle Flames in Microgravity). Also shown in the table are the current facilities for the currently supported experiments; the NASA HQ-selected candidates for space-based testing are listed with their likely carrier. The flight candidates were selected through a NASA Research Announcement (see Program Participation section below) and began their efforts in the ground-based facilities several years ago.

Substantial differences between normal and microgravity flames have been observed in combustion systems such as burning droplets, Burke-Schumann flames, laminar, transitional and turbulent gas-jet diffusion flames, flame spread over solids and liquid pools, cellular and freely propagating premixed gaseous flames, smoldering combustion, and candle flames. Normally considered weak, diffusional and radiative processes have been shown to have significant influence on low gravity flames. In addition to new examinations of classical problems, current areas of interest include soot formation and agglomeration and weak turbulence, as influenced by gravity. The next generation of experiments will likely include and may expand beyond these areas, into such endeavors as combustion synthesis of materials.

Currently NASA and international human-crew space missions incorporate various means of fire protection, emphasizing fire prevention but including provisions for fire detection and extinguishment. There are several reasons for ongoing scientific and engineering interest. Safety strategies are evolutionary processes and must be subject to periodic review and updating as the knowledge of microgravity combustion grows and new consensus standards in aircraft and related fields are developed. The complex

missions and environment of future spacecraft, particularly the permanently orbiting Space Station *Freedom*, create a demand for unique and innovative approaches to fire safety. Improved knowledge can optimize safety factors and provide tradeoffs of minimal risk against greater utilization of spacecraft facilities. A series of experiments is underway examining fire detection methods, extinguishment methods, and combustion product evolution and dispersion.

MICROGRAVITY COMBUSTION DIAGNOSTICS DEVELOPMENT

Compared to normal gravity experiments, low-gravity instrumentation has been simple, consisting of movie films and intrusive temperature and velocity probes such as thermocouples and hot wire anemometers (calibration of the latter for low-gravity applications is a concern, especially for the low-velocities usually of interest). This was due to the forementioned constraints on reduced gravity experimentation. However, to better understand the unique results obtained in low-gravity combustion experiments, more sophisticated diagnostic systems are strongly needed. This has motivated an emphasis on developing small, low-power and lightweight optical techniques because they are non-perturbative, and suited to the acquisition of multi-dimensional data fields (e.g. two and three dimensional imaging) while being usable in flight hardware. As with all microgravity experiments, development proceeds from development and testing in a normal gravity laboratory to demonstration in the ground-based facilities to repackaging / design and use in space flight hardware.

Table 2 lists methods in active design, development, testing, or demonstration in the low gravity facilities. Intensified CCD array cameras with sensitivity below conventional detectors or photographic films have revealed heretofore unseen flame structures and behaviors, especially in dilute hydrogen mixtures aboard the KC-135. Platinum silicide arrays for imaging in the near and mid-infrared are now available with sensitivity permitting bandpass filtering to isolate weak spectral emissions. This allows two dimensional temperature field measurements of known emissivity radiators, such as soot or grids of thin (15 micron) ceramic fibers. Such fibers are already being used in the drop towers for the qualitative assessment of temperature distributions in droplet and gas jet diffusion flames. A more complete characterization of the IR spectrum may enable the determination of major species concentrations and temperatures.

Relative to phase-sensitive, interferometric methods, the rainbow schlieren method tends to be simpler, more tolerant to mechanical and thermal fluctuations, and readily adaptable to large fields of view. The present system with continuously graded color filters has achieved comparable sensitivity to conventional interferometry. A quantitative determination of the refractive index distribution has been completed and is in being prepared for publication. This system has been employed in normal gravity to measure refractive index distributions in and above liquid pools and in axially symmetric jet diffusion flames. A system of this type is being assembled in a rig for reduced gravity tests in the 2.2 second drop tower facility, and has flown successfully aboard the KC-135.

Soot measurements are being conducted using transmission, scattering, and sampling techniques to determine soot size and concentration. These techniques have been incorporated into a 2.2 sec drop tower rig with the initial configuration accommodating full-field absorption measurements using a low power laser source, and soot sampling using a thermophoretic probe. For the latter, small wire electron microscopy grids are rapidly inserted into the flame and withdrawn (total residence time of approximately 30 milliseconds) with the size distribution of the soot particles then determined from the analysis of scanning electron micrographs.

In the longer range, particle image and laser doppler velocimetry systems are in development for use in low-gravity facilities. Prototype hardware is available for these measurements. Instrumentation for the determination of temperature and species concentration via near-IR laser light absorption is also under development.

MULTI-USER SPACE FLIGHT HARDWARE

Multi-user hardware is planned, intended to reduce cost and development time for space-based experiments. Elements of the flight hardware must be compatible with experiments several years from conception, but predictions of need are difficult; it is recognized that most experiments will need some unique subsystems to be developed especially and individually. NASA has adopted an evolutionary approach to multi-user space flight hardware. Experiment payloads, such as the Solid Surface Combustion Experiment, dedicated to the requirements of a single investigator are to be followed by more advanced Shuttle payloads each of which can accommodate a class of experiments.

The next set of combustion flight hardware will attempt to utilize a common set of components and subsystems in required configurations for a first series of flight experiments. Carriers such as Getaway Special Canisters (GASCANs), sounding rockets and cargo-bay mounted systems will be analyzed by NASA engineers for potential use in the next generation of experiments. Table 1 includes the currently planned carrier for flight project candidates. The first complete multi-user facility where many of these components and subsystems will be permanently mounted will be the Combustion Module (CM-1) to fly on Space Station *Freedom* or possibly on Spacelab. Finally, a Modular Combustion Facility (MCF), evolving from CM-1, is planned for Space Station *Freedom*.

OPPORTUNITIES FOR PROGRAM PARTICIPATION

NASA provides financial and facility support, typically for a three year "definition study" period, to academic and industrial principal investigators. Their initial proposals and subsequent progress are evaluated via the peer review process which addresses the following types of questions:

**Is there a clear need for microgravity experimentation, particularly space-based experimentation?*
**Is the effort likely to result in a significant advance to the state of understanding?*
**Is the scientific problem being examined of sufficient intrinsic interest or practical application?*
**Is the conceptual design and technology required to conduct the experiment sufficiently developed to ensure a high probability of success?*

Principal investigators (P.I.'s) collaborate with a NASA technical monitor to conduct the necessary research. Work in the drop towers and aircraft is strongly encouraged in this period. If it is believed that, following the definition study, space flight experiments are justified, the P.I.'s propose through a competitive solicitation (described below) a shuttle flight experiment. If they win award through this solicitation, they become flight candidates. Soon thereafter, the P.I.'s present their detailed objectives, test requirements, and the conceptual hardware design to another independent review panel comprised of scientific and engineering peers who assess the ability of the proposed flight experiment to meet its objectives. If this "Conceptual Design Review" is successful, NASA assigns a team of engineers and scientists to the multi-year development of space flight hardware which meets the P.I.'s specifications. NASA continues to support the P.I.'s throughout this development to conduct further research, provide consultation, and support the design and safety reviews prior to space flight. The nominal timeframe from flight experiment candidacy to manifest on the shuttle is five years. The P.I.'s then monitor the conduct of the experiment in flight, and subsequently analyze and are obliged to publish the data in an archival journal.

The above scenario is "typical" for shuttle-based experiments, however NASA also supports theoretical and diagnostics research as well as microgravity experiments which can be completed in the drop towers or aircraft.

Proposals for either definition study or flight experiment candidacy are solicited via a NASA Research Announcement (NRA); the first NRA focussed on microgravity combustion science was issued in December, 1989. It resulted in 13 definition study awards and 6 flight experiment candidacy awards out

of 65 proposals. *The only path to selection for flight project candidacy is through an NRA, i.e. through a competitive, peer-reviewed selection process.* It is planned that an NRA for microgravity combustion science will be issued every three years. It is planned that a multi-disciplinary NRA, which will permit proposals for ground-based studies in microgravity combustion science, will be issued in the three-year period between combustion-specific NRAs. Finally, NASA offers graduate students financial support through its Graduate Student Research Program, and post-doctorate fellowships through the National Research Council. More information about the details of these programs and the process of proposal submission, progress reviews and space flight project selection is available by writing to the Microgravity Combustion Branch, MS 500-217, NASA Lewis Research Center, 21000 Brookpark Road, Cleveland, Ohio 44135.

Table 1: Today's Microgravity Combustion Science and Spacecraft Fire Safety Projects

Nomenclature: DT -- 2.2 sec Drop Tower; HDT -- Hokkeldo (Japan) Drop Tower; ZGF -- 5.18 sec Zero Gravity Facility; SR -- Sounding Rocket; GAS -- GASCan in cargo bay of Shuttle; SSF -- Space Station *Freedom*; Middeck -- Middeck of Shuttle

TITLE	INVESTIGATORS	FACILITIES
"Low-Velocity, Opposed-flow Flame Spread in a Transport-Controlled, Microgravity Experiment"	Robert A. Altenkirch Subrata Bhattacharjee Sandra L. Olson	DT; ZGF; Learjet; SR or Middeck
"Risk-Based Fire Safety Experiment"	George E. Apostolakis Ivan Catton	DT; Learjet
"An Experimental and Theoretical Study of Radiative Extinction of Diffusion Flames"	Arvind Atreya Indrek S. Wichman	DT
"Gravitational Effects on Turbulent Gas-Jet Diffusion Flames"	Yousef Bahadori Dennis Stocker Raymond Edelman	DT; ZGF; KC-135
"Ignition and Combustion of Bulk Metals in a Microgravity Environment"	Melvin C. Branch John Daily	KC-135
"Modeling of Microgravity Combustion Experiments"	John Buckmaster	
"Gravitational Effects on Premixed Turbulent Flames: Studies of Dynamics of Wrinkled Laminar Flames in Microgravity"	Robert K. Cheng	DT
"Combustion of Interacting Droplet Arrays in a Microgravity Environment"	Daniel L. Dietrich	DT
"Investigation of Laminar Jet Diffusion Flames in Microgravity: A Paradigm for Soot Processes in Turbulent Flames"	Gerard M. Faeth	KC-135; SSF
"A Fundamental Study of Smoldering Combustion in Microgravity"	A. Carlos Fernandez-Pello	Learjet; KC-135; GAS
"Combustion of Electrostatic Sprays of Liquid Fuels in Laminar and Turbulent Regimes"	Alessandro Gomez Mitchell Smooke Marshall Long	TBD
"Ignition and Subsequent Flame Spread in Microgravity"	Takashi Kashiwagi Howard Baum	DT
"Modelling of Premixed Gas Flames in Microgravity"	K. Kailasanath Gopal Patnaik	
"Measurements and Modeling of Sooting Turbulent Jet Diffusion Flames Under Normal and Reduced Gravity Conditions"	Jerry C. Ku Paul Greenberg	DT
"Studies of Flame Structure in Microgravity"	C. K. Law	DT

"Spacecraft Material Flammability Testing with Radiative Self-Heating"	Thomas J. Ohlemiller	
"Laminar Premixed Gas Combustion Experiments in Space"	Paul D. Ronney	DT; KC-135; SSF
"Ignition and Flame Spread Across Liquid Pools"	Howard D. Ross William A. Sirignano	ZGF; SR
"The Structure of Particle Cloud Premixed Flames"	K. Seshadri Abraham L. Berlad	
"Combustion Experiments in Reduced Gravity with Two-Component Miscible Droplets"	Ben Shaw	DT
"Combustion of Solid Fuel in Very Low Speed Oxygen Streams"	James S. T'ien Kurt R. Sacksteder	DT; KC-135
"High-Pressure Combustion of Binary-Fuel Droplets"	Forman A. Williams Jun'ichi Sato T. Niioka	DT; HDT
"Droplet Combustion Experiment"	Forman A. Williams Frederick L. Dryer	DT; ZGF; Middeck
"Laser Diagnostics for Microgravity Droplet Combustion"	Michael Winter Gregory Dobbs	DT; Learjet

Table 2: Today's Microgravity Combustion Diagnostics

Nomenclature: x -- completed, i.e. developed and demonstrated; i -- testing is imminent; d -- active design or development

MEASUREMENT OR INSTRUMENT	1G	DT	ZGF	LEARJET	KC-135	SOUNDING ROCKET	SHUTTLE OR SSF
Cine Cameras	x	x	x	x	x		x
Thermocouples, Radiometers and Pressure Transducers	x	x	x	x	x	d	x
Soot Sampling via Thermophoretic Probing	x	x					d
Soot Volume Fraction via Light Attenuation and Scattering	x	i			i		d
Soot Temperature via Pyrometry	i						d
Rainbow Schlieren	x (liquid and gas phases)	i			x (gas phase)	d (liquid phase)	
Standard CCD Video	x	x	x	x	x	d	x
Intensified Array Video w/ Bandpass Filtering	x			x	x	d	d
UV Intensified Array Video w/ Bandpass Filtering	x			i		d	
IR Video w/ Bandpass Filtering	x					d	
Planar (2D) Temperature and CH and OH Concentrations via Rayleigh Scattering and LIF	d						
Light Sheet Flow Visualization or Velocimetry	x (liquid phase)	x (smoke)				d (liquid phase)	
Laser Doppler Velocimetry	d						
Reactive Mie Scattering	x						
Liquid Surface Temperature and Vapor Phase Concentration via Exciplex Fluorescence	d						
Thin Fiber Pyrometry	d	d					
CH_4, CO_2, H_2O Concentration via Line Absorption	x	d					
Stable Species Concentration via Miniature Gas Chromotography	i						d

COMMENTS

Question: (Clayton Meyers, NASA Lewis Research Center): (1) How does the fire safety program "interact" with the evaluation of materials listed in MSFC-HDBK-527? Could a materials test program evolve to evaluate new material proposed for space use critical for future mission(s) success?

(2) Could optical diagnostics initialized by other directorates (2000, 5000) be shared via some commonality program/conference or other structured mechanism? Combustion byproducts analysis. laser ignition, laser diagnostics, and seeding technologies are available.

Answer: (1) We have joint efforts with both MSFC and JSC on the exchange of information of fire safety and combustion science research findings. We all are interested in, and we at LeRC are developing hardware for evaluating the flammability of common materials in low-gravity to assess the degree of conservatism of the 1-g test methods in the handbook you cite.

(2) Again, collaboration between directorates at LeRC exists. We presently share laboratories and expensive instruments with the groups you cite, and attend each other's seminars. I assure you we do not suffer from the "Not Invented Here" syndrome-- we are all too busy to reinvent existing measurement methods.

AN OVERVIEW OF EUROPEAN ACTIVITIES ON

MICROGRAVITY COMBUSTION

N93-20181

Iskender Gökalp
Centre National de la Recherche Scientifique
Laboratoire de Combustion et Systémes Réactifs
45071 Orléans cédex 2, France

Introduction

The global objective of the European efforts in microgravity combustion is to combine theoretical and experimental work, both under normal and reduced gravity, to progress in the basic understanding of gravity dependent phenomena in various combustion situations.

The first phase of the European activities on microgravity combustion has been summarized in refs. 1, 2 and 3. This overview will summarize the more recent developments. The focus will be on new experimental facilities, new research topics, and new collaborative efforts.

European experimental facilities for microgravity combustion research

Parabolic flights of aircrafts have been and still are the most common reduced gravity means used in Europe for combustion experiments. After the 1986-88 period during which the NASA KC-135 aircraft was used by the European combustion community (ref.2), combustion experiments have been conducted since 1989 in the Centre d'Essais en Vol, at Brétigny-sur-Orge, France during the parabolic flights of the CNES Caravelle, under the auspices of CNES or ESA/ESTEC. The Caravelle aircraft, with modified engines and hydraulics and reinforced structure, provides, during approximately 20 seconds per parabolae, mean reduced gravity levels of 10^{-2} g_0 when the measuring equipment is attached to the aircraft structure, and between 10^{-3} and 10^{-2} g_0 if free floated in the cabin. Some combustion experiments are also taking advantage of the succession of normal-high-low-high gravity levels (ref. 4).

With the construction of the ZARM-Bremen Drop Tower, European combustion community has a new facility providing much lower gravity levels than those obtained during parabolic flights. The ZARM Drop Tower is a 145.5 m high concrete tower which contains the drop tube of diameter 3.5 m and 110 m height. The tower is designed as a vacuum chamber with a residual air presure of 1 Pa. The free fall duration is 4.74 s. In a later development phase, the experiment capsule could be launched from the bottom up to the tower top, almost doubling the flight time up to 9.4 s. The microgravity level is of the order of 10^{-6} g_0. During the free fall period the drop capsule is in constant contact with the command centre via telemetry, remote control and television (ref. 5). A smaller drop tower (height 25 m, free fall time approximately 2 s) is also operated for combustion experiments in Forrejon, Madrid, Spain, by INTA (Instituto Nacional de Tecnica Aerospacial) (ref. 6).

The use of sounding rockets for microgravity combustion research is under preparation by ESA/ESTEC since few years. The combustion experiments module under design aims the use of TEXUS sounding rocket program, which is a proven system, having been flown

successfully many times from ESRANGE in Kiruna, Sweden, since 1977. With an experimental payload weight of about 250 kg subdivided into four to six experiment modules, the apogee is typically between 250 and 300 km. This corresponds to a free fall time of 6 to 7 minutes with residual accelerations of less than 10^{-4} g_o. The use of sounding rockets for combustion experiments offers many additional advantages such as direct experiment operation by the scientist using telescience, reduced safety and hazard requirements, short recovery time and the possibility of late access (ref. 7).

Examples of European microgravity combustion research programs

This chapter summarizes briefly some of the European microgravity research programs using the above listed facilities. The emphasis is mainly put on new research topics.

Microgravity combustion experiments with gas phase flames is conducted during the parabolic flights of the Caravelle aircraft by the group at the Laboratoire d'Aerothermique of the CNRS at Meudon. Part of the investigation is devoted to the effects of gravity on polyhedral flames. Propane-air premixed flames are burner stabilized and tests are conducted under normal gravity, reduced gravity and at 1.8 g_o during the pull-up period of the aircraft. Several theoretical results are verified on cellular flames in the polyhedral configuration and it is shown that gravity does have a stabilizing effect for a downward propagating flame. On average, it is observed that one facet of the polyhedron is lost at reduced gravity in those configurations where the number of facets are between 5 and 8 under normal gravity (ref. 8). Another part of the research program focuses on the influence of gravity on laminar premixed and diffusion gas flames (refs. 9 and 10).

Another example of microgravity combustion experiment using the parabolic flights of the Caravelle is the research program on high pressure droplet burning conducted at the CNRS-LCSR at Orléans. A High Pressure Droplet Burning Facility has been developed for this purpose. It allows the investigation of burning and vaporizing single droplets up to an ambient pressure of 12 MPa. A powerful image analysis system is added to the facility. N-heptane and methanol droplets undergoing pure vaporization or burning are investigated. Preliminary results show that the pressure effect on the gasification process differs strongly depending on the gasification regime and that the instantaneous gasification rate can be obtained by the techniques developed (refs. 11, 12).

With the availability of the Bremen drop tower, new combustion experiments have started to take advantage of the very low gravity levels provided by this facility. One recent research program is developed by the team of the CNRS-LCPC in Poitiers, in collaboration with the University of California, Berkeley (ref. 13). The global aim of the research is to study the diffusion flame combustion of gaseous, liquid and solid fuels in a non-buoyant, low velocity, flat plate boundary layer established in an oxidizing flow. The research program is planned in progressive stages. The forced flow boundary layer flame combustion produced by a gaseous flame injected through a porous plate is first studied in the Bremen Drop Tower. An experimental apparatus has been developed and the first drops were realized in 1992. Methane flames were ignited under both normal gravity and microgravity and the flame behaviour is recorded by CCD cameras and thermocouples. Several parameters have been varied. Preliminary observations indicate that microgravity flames are wider and more diffuse, and less flickering. The flame temperature is lower in microgravity (ref. 13). In parallel, modelling activities devoted to similar problems are conducted at the Universidad Politecnica de Madrid (ref. 14).

The Bremen Drop Tower allowed also the development of another international collaboration on the topic of high pressure droplet evaporation between German and Japanese teams (ref. 15).

Another example of new microgravity combustion research in Europe is provided by the future use of the Texus sounding rocket program by the team of the Polytechnic University of

Madrid. They developed the conceptual design and expected operational characteristics of a multipurpose Microgravity Combustion Module for sounding rocket experiments. The same team proposed also to carry out one particular experiment on flame spreading with forced convection along the surface of a solid fuel at reduced gravity. It is proposed to use hollow cylinders of PMMA samples of 8 mm external diameter and 4 mm internal diameter. Three series of experiments are proposed including the influence of small flow velocities at constant ambient composition with parallel and cross flow conditions, and the influence of oxygen concentration. In parallel, a theoretical program will be developed and will include the search of an analytical solution for flame spreading under forced convection in all upwind or opposed flow cases and an approximate theory of the downwind flame spreading processes. This program is also conducted in collaboration with CISE, (Milano, Italy) and CNR/CNPM (Milano, Italy) concerning the development of laser diagnostics for microgravity combustion applications.

A new European collaboration program on Gravity Dependent Phenomena in Combustion

In 1990, ESA started to organize Expert Working Groups (EWG) in various domains of fluids and materials sciences in order to structure at the European level the corresponding microgravity relevant research programs, by seeking strong complementarities between (1) ground and space based experimental activities (2) theoretical, numerical and experimental approaches, and (3) basic and technologically relevant research objectives. Another objective of the EWGs is to seek collaboration possibilities between ESA programs and those of the Commission of the European Community (CEC). An EWG in combustion has also been constituted. It is composed of the following individuals: Profs. K.N.C. Bray, N. Peters, A. Linan, A. d'Alessio, Drs. M. Champion and I. Gökalp (chairman). After several preliminary meetings and workshops a research program on "Gravity Dependent Phenomena in Combustion" has been put together and submitted to the Human Capital and Mobility program of the CEC. The global structure of the program constructed along four tasks, and which is currently under evaluation, is as follows:

Task I. Flame spread over liquid or solid surfaces

University of Madrid (A. Linan, S. Tarifa)
University of Naples (C. di Blasi)
CNRS, Poitiers (P. Joulain, J.M. Most)

Task II. Flammability limits in gaseous premixtures

RTWH, Aachen (N. Peters)
University of Cambridge (B. Rogg, K.N.C. Bray)

Task III. Droplet Combustion

CNRS, Orléans (I. Gökalp, C. Chauveau)
University of Naples (P. Massoli, A. D'Alessio)
University of Madrid (A. Linan)

Task IV. Laser Diagnostics

University of Naples (P. Massoli, A. D'Alessio)
CNPM, Milan (G. Zizak, F. Cignoli)
CNRS, Orléans (I. Gökalp, C. Chauveau)
CISE, Milan (I. Gianinoni)

The construction of this collaborative program is based on the understanding that analysis of gravity dependent phenomena in combustion necessitates both ground based studies and space (or reduced gravity) experiments. Theoretical studies are also an important part in this

conducted with the aid of ESA and National Space Agencies. The reduced gravity experiments will use parabolic flights of the Caravelle aircraft of CNES, the Bremen drop tower, and the Texus sounding rockets. Theoretical and numerical work will be performed in order to analyze and predict gravity effects on combustion.

In building this programme, the basic research relevance and the technological relevance of the proposed studies are taken into account. The elucidation of gravity effects on combustion phenomena has important general basic consequences as combustion induced buoyancy is always present on ground. The technological relevance of the programme appears through its interest i) on flammability limits of essentially hydrogen/air mixtures **(Task II)** which is the fuel selected for the future high speed civil transport (the so called scramjet technology based on supersonic combustion); ii) on droplet combustion **(Task III)** as liquid fuels such as liquid oxygen will power the next generation rocket motors (such as the Vulcain engine of the launcher Ariane V) and iii) on flame spread over solid and liquid surfaces **(Task I)** which constitutes the basic mechanisms of flame propagation during fires. Finally, **Task IV** is of importance for all combustion work as the development of laser diagnostics is today an essential companion of combustion studies. The adaptation of laser diagnostics to space conditions will benefit other applications (for example in medical sciences) through their miniaturization and enhanced stability or user friendliness.

References

1. Dordain, J.J. and Lockwood, F.C. Combustion. in **Fluid Sciences and Materials Science in Space. A European Pespective**. H.U. Walter (ed.), Berlin: Springler-Verlag, 1987, pp. 291-309.
2. **Combustion experiments during KC-135 parabolic flights**. ESA SP-1113, 1989, 69p.
3. Gökalp, I., **Microgravity News from ESA**, vol. 3, no. 1, 1990, pp. 18-22.
4. Pletser, V. and Couffy, J.F. (eds), **Microgravity experiments during parabolic flights with Caravelle**, ESA WPP-021, 1991, pp. 53-96.
5. Rath, H.J. and Dreyer, M., **Proceedings of the First European Symposium on Fluids in Space**. ESA SP-353, 1992, pp. 27-46.
6. The INTA Microgravity Combustion Laboratory, **Appl. microgravity tech I**, vol. 4, 1988, pp216-217.
7. **Summary Review of Sounding Rocket Experiments in Fluid Science and Material Sciences** (prepared by O. Minster), ESA SP-1132, 1991, 371p.
8. Durox, D., To appear in **Twenty-Fourth International Symposium on Combustion**. The Combustion Institute, 1992.
9. Durox, D., Baillot, F., Scouflaire, P. and Prud'homme, R., **Combustion and Flame**, vol. 82, 1990, pp. 66-74.
10. Villermaux, E. and Durox, D., **Combustion Science and Technology**, vol. 84, 1992, p. 279.
11. Chesneau, X., Chauveau, C. and Gökalp, I., Proceedings of the First European Symposium on Fluids in Space, ESA SP-353, 1992, pp. 407-418.
12. Chauveau, C., Chesneau, X. and Gökalp, I., **AIAA Paper no. 93-0824, to be presented at the 31st Aerospace Sciences Meeting & Exhibit**, January 11-14, 1993, Reno NV.
13. Bonneau, L., Most, J.M., Joulain, P. and Fernandez-Pello, A.C., **AIAA Paper no. 93-0826, to be presented at the 31st Aerospace Sciences Meeting & Exhibit**, January 11-14, 1993, Reno NV.
14. Crespo, A. and Hernandez, J., **Microgravity sci. technol.** vol. 4, 1991, p. 126
15. Nomura, H., Kono, M., Sato, J., Marks, G., Igleseder, H. and Rath, H.J., **Microgravity sci. technol.** vol. 4, 1991, p. 12

COMMENTS

Question (Howard D. Ross, NASA Lewis Research Center): (1) What types of laser diagnostics are being provided in ESA's microgravity combustion program?

(2) You showed a photograph of flame spread over a liquid pool. Could you please describe the ESA research in this area in a little more detail?

Answer:

(1) Several groups in Europe are developing laser diagnostics relevant for microgravity combustion. Previous studies at the Istitute Motori - CNR in Naples, Italy, have shown that the velocity, diameter and temperature of homogeneous droplets can be obtained by measuring the light scattered at two timely angles. These techniques are presently extended to non-homogeneous droplets by developing a theoretical model for the light-scattering by droplets with a radial gradient of the refractive index to determine the temperature and species profiles inside multicomponent droplets.

In parallel, a differential interferometer to determine the temperature distribution around a burning droplet is being developed at ZARM, University of Bremen, Germany.

The Research Institute on Propulsion and Energetics of CNR in collaboration with CISE, both in Milan, Italy, are developing a planar laser induced fluorescence system for combustion diagnostics in microgravity. A multi-purpose PLIF system based on a 2-D solid state array sensor is under development. The objective is to investigate the structure of diffusion flames by measuring molecular distributions. The simultaneous detection of the resonant scattering will give indication of the presence of particulate matter such as soot and/or liquid droplets. Also, temperature measurements will be obtained by exploiting the anomalous fluorescence of pyrene. A PLIF system is also under development at ZARM, University of Bremen, with the support of the German space agency. The system is based on a tunable narrow band excimer laser, a sheet-forming optical device and an intensified digital high-speed CCD camera.

(2) An experimental program on the simulation of pool fires with a gas flame stabilized above a porous burner of 7-cm in diameter is in progress at the LCPC-CNRS in Poiters in collaboration with Laboratoire d'Aerothermique in Meudon. The ZARM drop tower and the parabolic flights of the Caravelle are used for this purpose. The influence of macrogravity on the structure of simulated pool fires is also investigated in a centrifuge; LDA measurements have already been performed in this last case. In parallel, a numerical modeling study of flame spread over liquid fuels is being conducted at the University of Naples. The objectives of this study are: (a) the simulation and analysis, by means of a constant property model, of the effects of gravity level on flame spread over sub-flash liquid fuels; (b) the development of variable property gas-phase models (full Navier-Stokes equations) and simulation of the effects of hot-gas expansions; and (c) the simulation and analysis of the effects of slow forced-flow conditions on the pulsating flame spread and extinction mechanisms.

JAPAN'S MICROGRAVITY COMBUSTION SCIENCE PROGRAM

Jun'ichi Sato
Research Institute
Ishikawajima-Harima Heavy Industries Co., Ltd.
Tokyo, Japan

N93-20182

Introduction

Most of energy used by us is generated by combustion of fuels. On the other hand, combustion is responsible for contamination of our living earth. Combustion, also, gives us damage to our life as fire or explosion accidents. Therefore, clean and safe combustion is now eagerly required. Knowledge of the combustion process in combustors is needed to achieve proper designs that have stable operation, high efficiency, and low emission levels. However, current understanding on combustion is far from complete. Especially, there is few useful information on practical liquid and solid particle cloud combustion. Studies on combustion process under microgravity condition will provide many informations for basic questions related to combustors.

In Japan, origin of the microgravity combustion was Kumagai's droplet combustion conducted about 35 years ago (ref. 1), and until now, most of studies on the microgravity combustion has been conducted for the droplet combustion. Recently, many types of studies on the microgravity combustion have been planed, started, and carried out by using the droptowers. They are droplet arrays, sprays, solid, coal particle cloud, and premixed gas combustion studies.

At last year, the biggest dropshaft facility in the world for the microgravity science was opened at Hokkaido. It produces 10 second of good quality microgravity field. Also, 4.5 second dropshaft facility is now under constructed and will be opened in 1994. The new sounding rocket operation was started from this year. Preparation of a space station combustion experiments has been started also from this year. Increasing opportunity for getting good microgravity field has stimulated recent microgravity combustion studies in Japan. The combustion scientists who do and hope to do the microgravity combustion have made the consortium, and it discusses with the government agencies on the governmental support microgravity combustion programs.

This presentation describes the Japanese microgravity facilities, recent research activities, and planed future activities.

Microgravity Facilities

Droptowers: About six small droptowers of 5 - 20 m have been used for combustion research at universities and companies. Up to now, most of

microgravity combustion studies have been done by using these droptowers.

From October 1991, Japan Microgravity Center (JAMIC) opened its commercial operations at Kamisunagawa, Hokkaido (see Fig. 1). Capabilities of JAMIC facility are 10 second of free fall duration, 10^{-5} g of microgravity level, 8 g of maximum deceleration level, 1000 kg of maximum payload weight, and 870 x 870 x 918 mm of experimental equipment mounting capacity.

The other big dropshaft facility is now under constructed at Toki, Gifu prefecture and will be opened in 1994. Its capabilities are 4.5 second of free fall duration, 10^{-5} g of microgravity level, 10 g of maximum deceleration level, 650 kg of maximum payload weight, and 0.7 m diameter x 0.8m length of experimental equipment mounting capacity.

Parabolic flights: A small jet airplane named MU-300 is employed for the parabolic flight. Its capabilities are about 20 second of microgravity field, 10^{-2} g of microgravity level, and two 700 x 450 x 900 mm experimental rack. Up to now, there has been no combustion experiments by using the parabolic flight.

Sounding rockets: A new sounding rocket named TR-1A has been operated from 1991. The microgravity level and duration are 10^{-4} g and about 6 minute. The maximum payload is 750 kg and experimental equipment mounting capacity is 770 mm diameter x 2380 mm length. For the combustion experiments, it can be used after 1995. Preparation of TR-1A combustion experiments will be started from next year.

Space station Japan module: Preparation of microgravity Experiments in the space station "Freedom" has been started at this year. Combustion is planed as one of the space station microgravity experiments.

Recent research activities

Droplet and spray combustion: Effects of fuel nature on the burning process have been studied by using a free droplet method at atmospheric pressure by Hara and Kumagai (ref. 2). From this research, it has been found that the quasi-steady theory of droplet combustion cannot be applied for four kinds alkane fuel from n-heptane to n-decane.

The other droplet combustion studies are for the high pressure evaporation and combustion. For the evaporation, experiments have been done up to the ambient pressure of 5 MPa by Nomura et al (ref. 3). and the data were compared with results obtained at normal gravity condition. This experiments have been carried out by using 5 second droptower of University of Bremen, Germany, as a collaborative research. Quite different evaporation behavior compared with that of under normal gravity was observed at subcritical and supercritical condition.

Evaporation constant and evaporation life time were obtained for the various conditions.

Effects of oxygen concentration have been studied experimentally on the burning life time and on the carbon zone formation behavior around the droplet by Niwa et al. (ref. 4). The burning life time takes minimum at the critical pressure of fuel also in the low oxygen concentration.

Extinction diameter of a burning droplet was predicted theoretically by Niioka et al. (refs. 5 and 6). For the prediction, they used the extinction data of diffusion flame established in a stagnation flow on a liquid fuel and the analogy between its diffusion flame and the flame surrounding a liquid droplet. The droplet diameter at extinction was found to decrease rapidly with pressure, take minimum, and then increase.

Multi-components fuel problems have been studied experimentally by using a two-components fuel of n-heptane and n-hexadecane by Mikami et al. (ref. 7). This research used the NASA LeRC 2.2 second droptower as a collaborative research. Three-stage burning of the binary fuel droplets is observed, and the onset time of the second stage is compared with the previous theoretical predictions.

For the ignition, experimental studies are being carried out. Numerical studies have been done by Tsukamoto et al. (ref. 8), and the results will be compared with the experiments.

Experimental studies on ignition and combustion of droplets array have been started from this year. Also, studies on generation of homogeneous droplet cloud under microgravity have been started for preparation of the spray combustion research in the space station.

Others: Ignition of premixed gas by a hot surface has been studied experimentally and theoretically by Nagata et al. (ref. 9). Ignition delay under microgravity is shorter than that under normal gravity.

Fire spreading behavior over a paper honeycomb has been studied by Itoh et al. (ref. 10), and the effects of fire spreading direction, oxygen concentration, and honeycomb cell size were obtained and compared with that of under normal gravity. The fire spreading velocity does not depend on the honeycomb cell size under microgravity.

Flame propagation behavior through the coal particle ---- have been studied by using 10 second dropshaft to study the coal gasification process by Sato and Itoh. Nearly homogeneous particle cloud was obtained and spherical flame propagation was observed.

Demonstration experiments of 10 second dropshaft were conducted by some combustion experiments, such as candle burning, paper burning, string burning, and large solid fuel burning by Itoh et al. The candle did not extinguish during 10 second of microgravity. These studies will be continued as microgravity combustion science.

Future research activities

Preparation of space station combustion experiments has been started from this fiscal year. Based on the discussion in the Japanese microgravity combustion consortium, spray combustion experiments are planed to do in the space. Details of experiments are being discussed and some experimental preparations will be started in this year.

Two large governmental research programs on microgravity combustion science by using 10 second dropshaft are planed for five years from next year to keep clean the earth by the fundamental combustion science point of view. This year is preparation for the next year. One program will be conducted as international research collaboration. Details how to conduct these have been started to be discussed and will also be discussed with the governmental agencies concerning microgravity combustion science in the world. In the Japanese side, many combustion scientists will participate these research programs

Concluding Remarks

Up to now, most of the research budget for microgravity science in Japan has been used for material science. But recently, the research budget for combustion is increased and then Japan's microgravity combustion science programs are being increased remarkably. Furthermore, 10 second dropshaft facility was opened in Japan at last year. Many Japanese combustion scientists will join the microgravity programs in the near future.

For the combustion scientist, it is required to explore the combustion phenomena in order to solve the emission problems from the combustors. Microgravity field is suitable for the fundamental combustion research. However, opportunity to use a good quality microgravity field of over 3 second is not so much for many combustion scientists because of the limited number of big facilities. Therefore, more effective use of the limited number of big facilities is important and should be discussed.

References

1. Kumagai, S. and Isoda, H.: Combustion of Fuel Droplets in a Falling Chamber, Sixth Symposium (International) on Combustion, 1957, pp. 726-731.

2. Hara, H. and Kumagai, S.: Studies on free droplet combustion under microgravity, 28th Symposium (Japanese Section) on Combustion, 1990, pp. 170-172.

3. Nomura, H., Marks, G., Iglseder, H., Rath, H. J., Sato, J., and Kono, M.: Effects of the natural convection on fuel droplet evaporation, Microgravity Science and Technology, Vol. 4, 1991, pp. 124-126.

4. Niwa, M., Mikami, M., Kono, M., Tsue, M., and Sato, J.: Effects of pressure and oxygen concentration on burning of fuel droplets under microgravity condition, 28th Symposium (Japanese Section) on Combustion, 1990, pp. 167-168.

5. Niioka, T., Hasegawa, S., tsukamoto, T., and Sato, J.: Diffusion flame extinction of liquid fuel at elevated pressures, Combustion and Flame, Vol. 86, 1991, pp. 171-178.

6. Hiraiwa, T., Ono, N., and Niioka, T: High-pressure combustion characteristics of liquid fuel in the stagnation point flow, Abstract book of 24th Symposium (International) on Combustion, 1992, p. 15.

7. Mikami, M., Kono, M., Sato, J., Dietrich, D. L., and Williams, F. A.: Combustion of miscible binary-fuel droplets at high pressure under microgravity, Abstract book of 24th Symposium (International) on Combustion, 1992, p. 229. (to appear in Combustion Science and Technology)

8. Tsukamoto, T., Okada, H., and Niioka, T.: Numerical analysis on fuel droplet ignition under high pressures, 29th Symposium (Japanese Section) on Combustion, 1991, pp. 385-387.

9. Nagata, H., Ishii, K., Tomioka, S., Sato, J., and Kono, M.: Ignition delay of premixed gases under microgravity conditions, Microgravity Science and Technology, Vol. 4, 1991, pp. 117-118.

10. Itoh, K., Fujita, O., and Itoh, H.: Observation of fire spreading over porous materials under microgravity, 29th Symposium (Japanese Section) on Combustion, 1991, pp. 16-18.

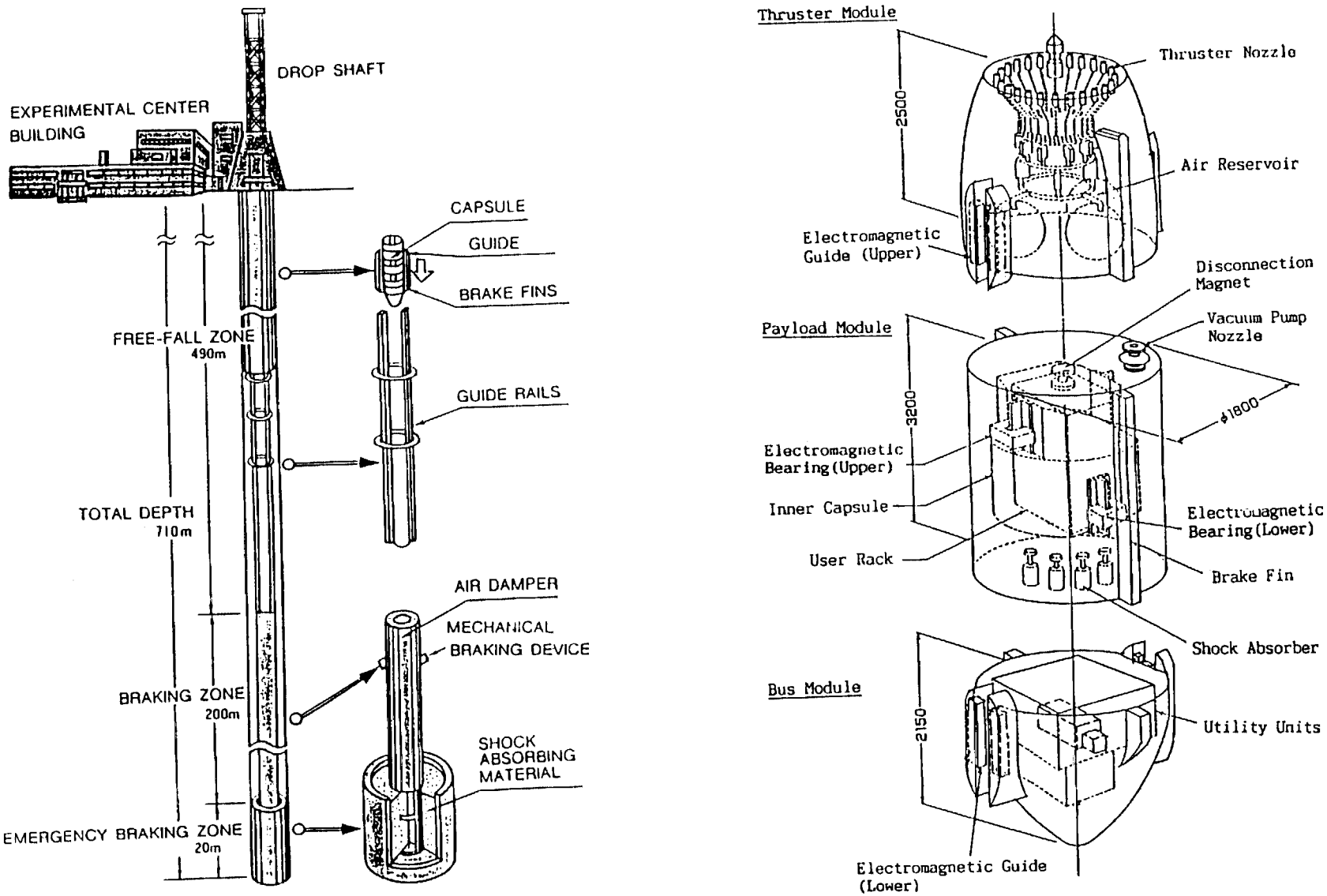

Figure 1.-Schematic of JAMIC 10 second dropshaft.

SESSION B - PLENARY SESSION

(Chair, Kurt Sacksteder)

CAPABILITIES AND CONSTRAINTS OF TYPICAL SPACE FLIGHT HARDWARE

N93-20183

John M. Koudelka
NASA Lewis Research Center
Cleveland, Ohio 44135

Introduction

The Space Experiments Division is in the business of performing ground based low gravity testing and designing experiment hardware for space flight on the Space Shuttle and in the future, Space Station Freedom. As witnessed in combustion work, the reduction of gravity brings forward previously negligible processes and parameters. In a similar manner, the design of experiments for microgravity operation aboard the Space Shuttle must consider parameters that are often not factors for laboratory hardware.

Accommodations

One of the first requirements that needs to be defined is the size selection for Shuttle accommodations. This selection is mostly driven by experiment requirements and manifest availability. The accommodations aboard Shuttle fall into two categories, that is habitable areas and the cargo bay. Obviously, the habitable areas permit crew interaction (hands on options) with the experiment. Cargo bay experiments are required to be more automated. Also, the safety requirements associated with crew presence are not a concern in the cargo bay.

The Space Shuttle provides several accommodations within the habitable area. Options consist of the Middeck area and the Spacelab (Spacehab is future option). Each area has its limitations and advantages. A summary of the resources available in each area is provided in Table 1.

Middeck

The Middeck area is the crews' living space. The prime experiment accommodation is in the place of middeck stowage lockers. The lockers are used mainly for Shuttle and crew stowage items but based upon the mission, several of the locker spaces are available for experiment hardware. The hardware can be designed to fit into a stowage container which provides 0.56 m^3 of volume and 24 kg weight carrying capacity.

Additional volume and weight is accommodated by interfacing in place of the stowage container(s). Experiment hardware can occupy the space of two middeck stowage lockers structurally and several lockers if not structurally connected. The more space that is allocated for a single experiment, however reduces the opportunities for flight. The services provided to an experiment in the middeck locker area are basic (namely; space, low power and crew interaction). The middeck locker area does provide ample flight opportunities since it is an integral section of the Shuttle. Experiments slated for Middeck opportunities are considered as secondary payloads which are evaluated for each Shuttle flight.

The Middeck area can also provide accommodations in a Middeck Accommodations Rack (MAR). This rack is mounted along port side in the Middeck. It provides additional services such as cooling, increased volume (0.42 m^3) and increased weight. The MAR has not been yet integrated into a Shuttle for flight.

Spacelab

The Spacelab module provides a complete laboratory setting for conducting experiments. The module consists of twelve equipment racks and additional mounting locations along the floor for experiment hardware. A summary of the rack features are listed in Table 1.

The Spacelab racks provide a variety of resources to the experimenter. The Spacelab rack services closely resemble the services associated with normal laboratories. Along with the larger volume and weight capacity available compared to the Middeck accommodations, the rack has provisions for thermal control (avionics air loop or liquid cooling loop), and command and data management.

Another provision for experiment operation within the Spacelab is a glovebox facility. The glovebox is a sealed work area for the performance of small experiments. The glovebox experiments are manifested as stowage items and operated in the confines of the glovebox. The facility provides a level of containment that permits operations using small quantities of toxic, irritant or potentially harmful materials.

A small version of the Spacelab is the Spacehab. The Spacehab is being developed to provide either 61 lockers (Middeck type) or 41 lockers with 2 racks. A Spacehab rack provides 1.2 m^3 of volume (two areas of 2.03m x .48m x .56 m) and is able to support 567 kg of payload. Other services provided by the Spacehab rack is similar to those provided by the Spacelab rack. The Spacehab is a new Shuttle accommodation that is yet to be flown.

Crew operation and observations of experiments is available to all accommodations within the habitable areas of the Shuttle. The rack accommodations generally offer the most resources/services to the experimenter but the lockers have the greatest flight opportunities.

The other accommodation area for microgravity experiments (secondary payloads) is in the Shuttle cargo bay. Two of the accommodations are the Getaway Special (GAS) Canister and as a payload on the Mission Peculiar Experiment Support Structure (MPESS).

GAS CAN

The GAS can is a cylindrical pressure vessel that can house up to a 90 kg experiment payload. The GAS can provides the simple services of 0.14 m^3 sealed volume and activation control. The GAS can being basic simplifies the integration and design work for the experimenter. The GAS cans are generally manifested as ballast on the Shuttle so flight opportunities are determined relatively late in the processing flow, but are often.

MPESS

Two MPESS's have been connected to form the United States Microgravity Payload (USMP). A description of the payload accommodations on USMP are described in Table 1. The USMP accommodation has resources similar to the Spacelab. It only lacks the crew interaction.

The cargo bay accommodations lack the crew interaction provided within the habitable areas of the Shuttle. The loss of this feature requires the experiments to be more automated. For USMP payloads, interactive control is available through the command and data management system (CDMS).

The accommodations described are the common ones aboard the Shuttle. For all these accommodations, the experimenter time-line is limited to the length of the Shuttle mission which is generally about five to ten days (extended duration of 13 days has been achieved) and sharing of resources among experimenters. The time-line will be expanded with the future use of Space Station Freedom (SSF). Rack accommodations are being developed for SSF.

HARDWARE DESIGN

The experiment hardware design gets its origins from the laboratory rigs developed in performing 1-g tests. The process to get to a flight experiment would seem to be one of packaging. Requirements based on Shuttle safety and environment, however does not allow us to just package components. Parameters are

added or more importance is placed on parameters as the hardware is transitioned to the Shuttle.

MATERIAL SELECTION

Today, health concerns from materials are addressed in their uses in the laboratories. Material Safety Data Sheets (MSDS) provide guidelines for safe use of materials and protective equipment necessary when handling certain materials. The measures taken on the ground, however, are not always available on the Shuttle, therefore extra precautions must be taken. All materials used on the space flight hardware must be evaluated for its acceptability.

Metallic materials are evaluated for their resistance to corrosion and contamination, resistance to stress corrosion cracking, compatibility with oxygen and fluid systems, strength, and fatigue endurance. Along with the metallic material selected, attention must be paid to the coatings applied to the metals.

Non-metallic materials generally come under the majority of the scrutiny. The major concerns for non-metallics are flammability and toxicity. Both of these are of less concern for experiments located in the cargo bay (depending on experiment provided environment). Common plastics, tapes and adhesives used in the lab are usually not acceptable for space flight use.

ENVIRONMENTAL CONSTRAINTS

The hardware components must be evaluated for their ability to operate and survive the environment imposed by a Shuttle flight (launch, orbit and landing). An area of concern for components is the ability to survive the launch random vibration loads. The vibration loads are dependent upon the accommodation but generally range up to 12 g's [rms] (at the interface with the experiment; might be larger at component due to amplification). In order to deal with the vibration environment, some components require vibration isolation, modifications for vibration resistance, or substitution.

The thermal environment of the Shuttle is also a concern for the experiments in the cargo bay. The cargo bay temperatures exceed the operating limitations of most commercial electronics and the temperatures affect experiment gases and liquids (phase change, pressure changes). Due to the elimination of buoyancy driven convection flows in the microgravity environment, even the shirt sleeve environment of the manned areas causes thermal problems. With the lack of convection, some experiments design in forced convective flows to keep hardware within operating limits and below Shuttle temperature limits (touch temperature limit of 45 °C). The thermal concerns also direct component

selection to be based upon power consumption.

An obvious aspect of space flight that is sometimes overlooked in evaluating component acceptability is gravity dependency. Some mechanisms rely on gravity for proper or safe operation. An example of this is the ejection of a storage disk. The mechanism consisted of a spring load to overcome frictional drag due to the weight of the storage disk. Without the gravity force, the spring load propelled the storage disk into the Shuttle cabin area.

These factors and others make the transition to space flight hardware more than a packaging task. They also work to add constraints to the hardware.

OPERATIONS

Even though some of the Shuttle accommodations resemble laboratories in terms of services provided, they do not in terms of operations. All experiment operations and crew interactions with hardware are controlled by the Shuttle safety requirements. Safety has to be at the center of hardware design and hardware operations. Experiment hardware or operation shall not damage or impair the Shuttle nor harm the crew.

This requirement has far reaching implications in the hardware design and operation. Simple operations performed on the ground such as sample change out are complicated in space. The procedures for the sample change out must consider items such as sharp edges, surface temperatures, release of hazardous materials (combustion gases) or electrical shock. The experiment procedure during a space flight must have controls to prevent any of the possible unsafe conditions before it would be approved for performance. Operation of the experiment requires extra steps and extra hardware features to aid the crew in the weightless environment.

The automated operation of experiments are still subjected to the requirement of safe operations. For those type of experiments, electrical and software protection are required.

CONCLUSION

The accommodations for experiments provide space up to 1.75 m^3 and structural capacity of 300 kg. The services usually available in ground based laboratories such as power, cooling, data management can be found within the Shuttle accommodations. The experimenter receives the services necessary to conduct their experiment. Space flight safety and environmental requirements constrain the design of the experiments. Factors such as material acceptability, vibration survival and non hazardous operations at times eliminate experiment components or operational flexibility.

TABLE 1 SUMMARY OF SPACE SHUTTLE / SPACE STATION ACCOMODATION RESOURCES

RESOURCE	MIDDECK LOCKER SINGLE	MIDDECK LOCKER DOUBLE	SPACELAB RACK SINGLE	SPACELAB RACK DOUBLE	GLOVEBOX
VOLUME	0.066 m^3 .46x.27x.52m	0.13 m^3 .46x.55x.52m	0.42 m^3 .44x1.0x.61m .44x.71x.40m	0.83 m^3 .88x1.0x.61m .88x.71x.40m	0.025 m^3 .48x.24x.21m
WEIGHT (maximum)	29 kg	45 kg	290 kg	580 kg	Stowage Dependent
POWER	28 VDC 5 amp max 110 W cont.	28 VDC 5 amp max 110 W cont.	28 VDC 35 amp limited	28 VDC 35 amp limited	5, 12 & 24 VDC 20W, 18W & 60W
ENVIRONMENTAL CONDITIONS					
PRESSURE	101.3 kPa	101.3 kPa	101.3 kPa	101.3 kPa	100.5 kPa
OXYGEN	25.9%	25.9%	21.7%	21.7%	21.7%
TEMPERATURE	18-35 °C	18-35 °C	10-35 °C	10-35 °C	18-35 °C
THERMAL CONTROL	Cabin Air	Cabin Air	Avionics Air Liquid cooling	Avionics Air Liquid cooling	Cabin Air
COMMAND & DATA MANAGEMENT	NONE	NONE	AVAILABLE*	AVAILABLE*	NONE
PHOTOGRAPHIC	AVAILABLE video, still	AVAILABLE video, still	AVAILABLE video, still	AVAILABLE video, still	AVAILABLE video, still
EXAMPLE	Space Acceleration Measurement System	Solid Surface Combustion Experiment (one module)		Surface Tension Driven Convection Experiment	Smoldering Combustion in Microgravity

* Commanding, monitoring, recording, processing & transmitting

TABLE 1 SUMMARY OF SPACE SHUTTLE / SPACE STATION ACCOMODATION RESOURCES

RESOURCE	GETAWAY SPECIAL (GAS) CANISTER	UNITED STATES MICROGRAVITY PAYLOAD	SPACE STATION FREEDOM
VOLUME	0.14 m^3 .50 dia x .72 m	1.75 m^3 .85x2.0x1.0m	1.1 m^3
WEIGHT (maximum)	90 kg	308 kg	700 kg
POWER	Experiment supplied	28 VDC 470 W (865 W peak)	120 VDC
ENVIRONMENTAL CONDITIONS			
PRESSURE	Experiment specific normally 101.3 kPa	Zero unless experiment provided	70 - 101.3 kPa
OXYGEN	Experiment specific	None	21%
TEMPERATURE	-100 to 40 °C	-157 to 144 °C	20 - 30 °C
THERMAL CONTROL	Passive (Insulation)	Coldplate Available	Avionics Air Water Cooling
COMMAND & DATA MANAGEMENT	NONE	AVAILABLE*	AVAILABLE*
PHOTOGRAPHIC	NONE	NONE	
EXAMPLE	POOL BOILING EXPERIMENT	ISOTHERMAL DENDRITIC GROWTH EXPERIMENT	

* Commanding, monitoring, recording, processing & transmitting

References:

1. NSTS 21000-IDD-MDK Shuttle/Payload Interface Definition Document for Middeck Accommodations

2. SLP / 2104 Spacelab Accommodations Handbook

3. GET AWAY SPECIAL (GAS) Small Self-Contained Payloads Experimenter Handbook

4. MSFC-HDBK-527 / JSC 09604 Materials Selection List for Space Hardware Systems

5. SPACEHAB User's Handbook January 1991 prepared by McDonnell Douglas

CAPABILITIES AND CONSTRAINTS OF NASA'S GROUND-BASED REDUCED GRAVITY FACILITIES

N93-20184

Jack Lekan, Eric S. Neumann, and Raymond G. Sotos
NASA Lewis Research Center
Cleveland, Ohio 44135

Introduction

The ground-based reduced gravity facilities of NASA have been utilized to support numerous investigations addressing various processes and phenomena in several disciplines for the past 30 years. These facilities, which include drop towers, drop tubes, aircraft, and sounding rockets are able to provide a low gravity environment (gravitational levels that range from $10^{-2}g$ to $10^{-6}g$) by creating a free fall or semi-free fall condition where the force of gravity on an experiment is offset by its linear acceleration during the "fall" (drop or parabola). The low gravity condition obtained on the ground is the same as that of an orbiting spacecraft which is in a state of perpetual free fall. Figure 1 summarizes the gravitational levels and associated duration times associated with the full spectrum of reduced gravity facilities including spaced-based facilities. Even though ground-based facilities offer a relatively short experiment time, this available test time has been found to be sufficient to advance the scientific understanding of many phenomena and to provide meaningful hardware tests during the flight experiment development process. Also, since experiments can be quickly repeated in these facilities, multistep phenomena that have longer characteristic times associated with them can sometimes be examined in a step-by-step process. There is a large body of literature which has reported the study results achieved through using reduced-gravity data obtained from the facilities.

Over the past several years these ground-based facilities have grown in their importance, particularly in the vital role they play in the support of research programs sponsored by the Microgravity Science and Applications Division (MSAD) of the NASA Office of Space Science and Applications. These facilities support the development of long duration space flight experiments aboard the Space Shuttles and eventually Space Station Freedom. The resources required to execute space-based experiments require thorough scientific justification and proven technological feasibility. Many of these requirements can be met in ground-based facilities. Drop towers and aircraft are employed to perform precursor tests to define space experiment science requirements and conceptual designs, perform tests for space experiment technology development and verification and to also provide baseline normal and reduced gravity data. The NASA facilities have enhanced the success and value of space experiments to such an extent, that when appropriate, their utilization is a prerequisite prior to flight. The facilities are also utilized for the execution of ground-based science programs. The requirements of these investigations can be fully met in the facilities and thus avoid the need for longer duration flight experiments.

While the value of the NASA ground-based reduced gravity facilities is clear, that value is enhanced by considering the capabilities and characteristics of each facility and selecting the one best suited for a particular series of experiments. This document will focus on the capabilities of the facilities located at the Lewis Research Center (LeRC) in Cleveland, Ohio which include a 2.2 Second Drop Tower, the Zero-Gravity Research Facility, and a model 25 Learjet. The capabilities of the KC-135 aircraft of the Lyndon B. Johnson Space Center (JSC) in Houston, Texas will also be presented.

Background

The initial low gravity test activities at LeRC focused on testing to enable the development of technologies and systems for space power and propulsion. Fundamental studies were performed to gain an understanding of fluids under reduced gravity conditions. These studies allowed NASA to develop on-orbit fluid management and handling functions including storage, conditioning , and transfer with a variety of liquids, gases, and supercritical fluids. Along with addressing the needs of propellant systems, smaller studies were initiated in other areas such as combustion, including fire safety. Through a large number of tests performed in the LeRC facilities in the 1960's and 1970's, including a progression from the Aerobee sounding rocket to an AJ-2 airplane to the 2.2 Second Drop Tower and finally the Zero-Gravity Research Facility, our understanding of many low gravity processes was greatly enhanced. During the late 1970's and early 1980's ground-based reduced gravity research declined. This reduction was due to the fact that the many critical enabling low gravity technologies had been successfully developed and implemented and some experimentation had moved to space as components of the Apollo and Skylab programs.

Reduced gravity or microgravity research (a term synonomosly used with research activities conducted at less than normal earth gravity) was reborn with the new era of the Space Shuttle and plans for the Space Station. NASA's MSAD program developed and grew since a restructuring in 1978. The MSAD program now sponsors over 115 researchers in several disciplines. The large growth in the MSAD program has been paralleled by an explosive growth in the number of programs, testing, and experiment complexity in ground-based facilities.

Facility Descriptions

The 2.2 Second Drop Tower, due to its relatively simple mode of operation and associated low cost, is the most heavily utilized facility as it now routinely supports over 1000 test drops per year. The Drop Tower, while only providing a test time of 2.2 seconds, does represent an easy and timely method of acquiring low gravity data. A schematic of this facility is shown in Figure 2. The components of the Drop Tower include a shop for experiment build-up, integration and testing, several small laboratories for experiment preparation and normal gravity testing, an electronics support area, and an eight story tower in which is contained the drop area.

Since experiment packages are dropped under normal atmospheric conditions, air drag on the package is minimized by enclosing it in a drag shield which has a high rate of weight to frontal area and a low drag coefficient. The drag shield/experiment assembly is hoisted to the top of the drop area where the necessary electrical connections are made. The entire package is then suspended by a highly stressed music wire which is attached to the release system. A drop is initiated by the pressurization of an air cylinder which drives a hard steel knife against the wire which is backed by an anvil. The resulting notch causes the wire to fail and the drag shield and experiment package are smoothly released into free fall. Accelerations of approximately 10^{-5} g are obtained as the experiment falls freely a distance of 20 centimeters within the drag shield while the whole assembly falls from a height of 27 m. The only external force acting on the freely falling experiment is the air drag associated with the relative motion of the experiment within the enclosure of the drag shield. A drop is terminated when the drag shield assembly impacts a 2.1 m deep rectangular container that is filled with sand. The sand is aerated prior to a drop to help reduce deceleration levels. The deceleration rate is controlled by selectively varying the tips of three 1.9 m long aluminum spikes that are mounted on the bottom of the drag shield. At the time of impact of the spikes with the sand, the experiment package has traversed the available vertical distance within the drag shield and is resting on the floor of the drag shield. The deceleration levels at impact vary from approximately 40 to 100 g's for several milliseconds. Precautions taken during design, coupled with various cushioning foams permit the utilization of many off-the-shelf electronic items including video cameras, low-power lasers, light bulbs, and data acquisition and control systems. For sensitive hardware such as optical diagnostics which require

decelerations of no more than 40 g's, a shock absorption system has been successfully employed to meet these requirements.

A large variety of experiment packages or "drop rigs" with differing capabilities have been tested in the Drop Tower. Hardware provided by investigators is integrated into a rectangular aluminum frame to form the experiment package. Experiment hardware weight is limited to 140 kg. The frame or drop bus has varied over the years according to the experiment needs. The current "standard" frame is 81cm high, 91cm long , and 40 cm deep. Standard frames need not be utilized however. Examples of two experiment packages are shown in Figures 3 and 4. The Laser Diagnostics rig (Figure 3) represents the most recent and sophisticated experiment package. For the purpose of clearly showing the experimental hardware, the supporting framework was removed. Figure 4 shows a rig utilized for premixed gas combustion. The rig is in the partially assembled drag shield undergoing final preparations prior to a drop test.

Experiment power is provided by onboard battery packs which are generally 28 VDC. A 110 VAC power cord has been dropped along with the package for two experiments. Data is acquired by high-speed motion picture cameras supplied by NASA with framing rates up to 1000 frames per second and also by a variety of video cameras. The video signal can be recorded onboard or transmitted to a remote recorder via a fiber optic cable that can be dropped with the experiment. Onboard data acquisition and control systems are also employed to record data supplied by instrumentation such as thermocouples, pressure transducers, and flow meters. The data acquisition and control system is supplied by NASA in many instances. Table 1 summarizes the characteristics of the Drop Tower operations.

The Zero Gravity Research Facility when compared to the Drop Tower represents an expansion in research capabilities and and in some instances experiment sophistication. Microgravity test time is increased to 5.18 seconds while experiment size and weight can be increased considerably and new experiment features are added. A schematic diagram of the facility is shown in Figure 5. The above-grade portion of this unique facility, which is a registered U.S. national landmark, consists of mechanical and electronics shop areas for experimental build-up, integration, and testing , a class 10000 clean room, shop offices, a control room for drop operations, and the attendant mechanical and electrical systems. A test chamber shaft, deceleration system, and support systems comprise the below-grade portion of the facility.

The shaft component of the facility, which extends 155 m below-grade elevation, consists of a .45 m thick unreinforced concrete casing with an inside diameter of 8.7 m in which is housed a 6.1 m diameter steel walled vacuum chamber which is 145 m deep. Unlike the Drop Tower, aerodynamic drag on the free-falling experiment vehicle is reduced to less than 10^{-5} g's by evacuating the vacuum chamber to a pressure of 10^{-2} torr. A multiple staged vacuum pumping system is capable of evacuating the chamber to the desired drop pressure in one hour. After an experiment has been prepared, the experiment vehicle is enclosed in a protective cover. The experiment vehicle is then suspended by its support shaft from a hinged-plate release mechanism at the top of the vacuum chamber. An umbilical cable is attached to the support shaft to maintain monitoring and control of the experiment during the pump down process. The umbilical is remotely pulled one-half second prior to release. The experiment vehicle is released by hydraulically shearing a bolt that is holding the hinged plate in a closed position. No measurable disturbances are imparted to the experiment by the release procedure. 5.18 seconds of reduced gravity are obtained by allowing the experiment vehicle to free fall in a vacuum through a distance of 132 m. After the experiment vehicle traverses the 132 m distance, it is decelerated in a 3.6 m diameter, 6.1 m deep container which is filled with small pellets of expanded polystyrene. An average deceleration rate of 35 g's is controlled by the flow of the pellets through the annular area between the experiment vehicle and the container wall. Peak deceleration loads reach 65 g's for several milliseconds.

The experiment vehicle, or drop bus, serves as the load bearing carrier structure for the experiment and protects the research equipment mounted within from the deceleration shock loads. The experiment vehicle also provides services such as power and programmable controllers. The primary vehicle

configuration currently used is cylindrical (with a conical tip). The vehicle, which is shown in Figure 6 outfitted with the Solid Surface Combustion Experiment engineering model, has an overall height of 3.4 m and gross weight of 1135 kg. The test section of another vehicle equipped with a general purpose combustion chamber is shown in Figure 7. This test section, which facilitates the mounting of experiment hardware, is 1 m in diameter and 1 m in height. Experiments with hardware weight up to 455 kg can be accommodated in the vehicle. As in the Drop Tower, data from experiments is acquired using high speed motion picture cameras with framing rates of up to 1,000 frames/second, video cameras (with onboard video recorders) and data acquisition systems which are utilized to record data such as temperature, pressure, and flow rates. Onboard battery packs supply the necessary power after the experiment is dropped. The key features of the Zero-Gravity Research Facility are summarized in Table 2.

The Lewis Research Center operates a specially modified Learjet model 25 in support of microgravity programs. The aircraft can obtain 18 to 22 seconds of low gravity by flying a parabolic (Keplerian) trajectory. The aircraft accomplishes this with a rapid climb to a 50 to 55 degree angle (pull up), then slows as it traces a parabola (pushover), and then descends at a 30 degree angle (pull out). It is during the pushover that gravity levels on the order of 10^{-2} are obtained. During the pull up and pull out the aircraft experiences brief periods of increased g, ranging from 2.5 - 3 g. The Learjet can also provide intermediate levels of 1/20 to 3/4 of earth gravity. Although the reduced gravity levels obtained aboard the aircraft are not as low as those obtained in drop towers, the aircraft offers the advantages of increased low gravity duration, real time monitoring and reconfiguration of the experiment in low gravity by an onboard operator, and a very minimal high gravity recovery.

The Learjet has 185 cm of cabin length available for experiment mounting and researcher seating. As many as three researchers can be accommodated. Due to the limited cabin volume, experiments must be attached to the aircraft, and generally only one experiment is installed at a time (Figure 8). Experiments are typically mounted in standard racks which were developed specifically for Learjet experiments. These racks have a usable volume 72 cm high, by 60 cm wide, by 52 cm deep. Each rack is limited to a total weight of 85.2 kg. Two racks can easily be accommodated in the aircraft. Experiment specific racks can be designed when the standard racks are not adequate. For example, a special rack was developed to mount a Get Away Special Canister in the Learjet. All hardware mounted in the aircraft must be designed to withstand the following loads, when applied one at a time: 9.0 g forward, 7.0 g downward, 2.0 g up, 1.5 g aft, 1.5 g side.

Accelerations aboard the Learjet are measured by three servo-accelerometers which are oriented along the pitch, lateral, and longitudinal axes of the aircraft. The inherent accuracy of the accelerometer system is +/- 0.005 g's, but the lowest accelerations achievable during a trajectory are somewhat higher due to air turbulence and other flight control factors. Output from the accelerometers is sent to the cockpit displays for use by the pilots for control of the trajectory. The analog outputs are also stored on a strip chart recorder aboard the aircraft, and can be supplied to experimenters for storage on their data systems.

The Learjet can complete a maximum of six trajectories before landing if minimum accelerations are obtained. Typical flight time for a six trajectory flight is approximately 1.5 hours. One to two flights are generally conducted per day. Because experiments aboard the aircraft do not experience the high g recovery periods associated with drop towers, virtually any ground-based laboratory equipment can be supported aboard the Learjet. Three sources of electrical power are available to researchers: 28 VDC, 80 amps maximum; 115 VAC 60 Hz, 7.5 amps maximum; and 115 VAC 400 Hz, 18.3 amps maximum. Table 3 summarizes the pertinent characteristics of the Learjet.

The Johnson Space Center operates a Boeing KC-135A aircraft in support of low gravity research. The aircraft is a four engine jet transport similar to the Boeing 707. The aircraft achieves low gravity by flying a parabolic (Keplerian) trajectory similar to the one described for the Learjet. Up to 23 seconds of reduced gravity conditions can be obtained during each trajectory. The gravity level experienced by an

experiment fixed to the aircraft floor is approximately 10^{-2} g's. Due to the larger cabin space available, experiments flown aboard the KC-135 can also be free-floated during a trajectory. Free-floating enables an experiment to experience a gravity level on the order of 10^{-3} g's to 10^{-4} g's . However, depending on the experiment size, free-float packages usually impact the aircraft walls or ceiling before the end of the trajectory, shortening the low gravity time to 5 to 8 seconds. The KC-135 is also capable of flying partial gravity trajectories. Typically, about 40 trajectories are completed per flight. Flights generally are 2 to 3 hours in duration and one flight is conducted per day. The KC-135 has a much larger volume than the Learjet. The aircraft has a usable cabin length of 18.28 m and a width of 3.25 m. Experiment size is limited by the cargo door of the aircraft which measures 1.90 m high by 2.99 m wide. Experiment weight is limited by the aircraft's maximum floor loading of 976.5 kg/m^2.

Experiment hardware must be designed to withstand the following emergency loading condition: 9 g's forward load, 3 g's aft, 2 g's lateral, 2 g's up, and 6 g's down. Because of the aircraft's large volume it is common to have numerous experiments, both fixed and free floating integrated for the same flight (see Figures 9 and 10). The KC-135 has 3 types of electrical power available to experimenters: 28 VDC, 80 amps; 110 VAC, 60 HZ, 20 amps; and 110 VAC, 400 HZ, 3 phase, 50 amps per phase. The aircraft is also equipped with bottle racks to carry standard K-bottles of inert gases, as well as an overboard vent system to allow for manual or automatic venting of liquids or gases in flight.

Like the Learjet the KC-135 can support a wide range of instrumentation and data systems. Gravity level data in the z-axis (vertical) only is measured during the trajectories and is available for input into research data systems. JSC can also provide photographic equipment and personnel, to support the needs of flight researchers. Further information and documentation regarding KC-135 operation can be found in the "JSC Reduced Gravity Program User's Guide" (JSC-22803).

From the above summary of the description of the NASA low-gravity facilities, it is evident that each facility has its own unique capabilities and limitations regarding the amount of test time, purity of reduced gravity levels, experiment size, operations and researcher interaction. Even though there are limitations, particularly in the amount of available low gravity time, the facilities have enjoyed a high level of effectiveness in meeting the needs of many investigations. The effectiveness of the facilities is evident in a large body of literature which has reported the results achieved using low gravity data obtained from the facilities particularly in the disciplines of combustion and fluids. Also, there have been a number of successful technology developments and successful space flight experiments based on activities executed in the facilities. Specific information regarding facility operations and some experiment hardware will follow.

Facility Operations/Guidelines

Effective utilization of the reduced gravity facilities begins with the selection of the appropriate facility in which to conduct an investigation. Facility selection generally is based on the following guidelines: experiments which are exploratory or require a large number of tests and do not require more than 2.2 seconds of test time should be conducted in the Drop Tower; well-defined experiments that require additional test time and high purity low gravity levels are candidates for the Zero-Gravity Research Facility; experiments which require longer test times and/or can tolerate higher reduced gravity levels and/or require operator interaction or are simply too large for the drop facilities should be considered for testing on the Learjet or KC-135 aircraft. The above represent initial guidelines. Discussions with the respective facility managers and experienced NASA investigators are also required in making a final determination. Note that for all facilities, investigators have the option of providing their own hardware up to a completely assembled experiment, utilizing existing NASA hardware (sometimes in a sharing arrangement) when feasible, or working with their technical monitor and facility operations personnel who will oversee experiment build-up.

The Drop Tower offers the greatest opportunity for "hands-on" investigations as well as the opportunity for the execution of a large test matrix (some hardware has been utilized for hundreds of

drops) and easy utilization of investigator-provided hardware. In most instances drop frames are sent to the investigator's institution for experiment assembly. Drop Tower personnel are available for consultation regarding all phases of an experiment, and also for limited hardware integration and assembly. Investigators are ultimately responsible for the testing and maintenance of their hardware. NASA-provided hardware besides the drop frame, can include cameras, certain electronics components, and data acquisition and control systems. A review of Table 1 will serve as guidance for design criteria for the Drop Tower. As mentioned previously, in some cases existing hardware or general purpose drop packages can be used with minor modifications and sharing of that equipment can be arranged.

The Zero Gravity Research Facility operations philosophy is unique particularly when compared to that of the Drop Tower. Except for a few experiments, the design, fabrication, assembly, integration, checkout and test operations are the responsibility of the facility operations personnel. For programs where hardware is furnished, facility personnel are available to consult on the design and buildup of the experiments. Operations personnel also have the responsibility to integrate the experiments into the drop vehicles and conduct the drop tests. Another major characteristic of the Zero Gravity Facility is that there are four experiment vehicles available to support experiments. Due to costs and complexity of the hardware involved, experiment vehicles become multi-user/multipurpose in nature. This situation is very different from the Drop Tower, where, in most cases due to lower costs and complexities, experiment-specific drop frames and experiments can be built-up if needed.

Table 2 summarizes the criteria that should be considered for Zero-Gravity Facility experiments. However, a few of them, due to their importance, are stated here. These design criteria include the following: experiments must be designed to operate in a vacuum environment; experiments should be capable of unattended control for a minimum of one hour after final checkout to allow for experiment vehicle integration into the facility in preparation for the drop test; because of the uniqueness of the facility and potential hazardous conditions to personnel working around the experiment vehicle during facility operations, the experiment must pass a stringent safety review (safety reviews are required for testing in all of the facilities); and because of environmental concerns, limits may be imparted on the types and quantities of fluids or gases available for testing.

Aircraft experiments require a close interface between the investigator and the operations engineering staff to ensure safety, and thus personnel at LeRC are an integral component of this type of testing. For the Learjet, an operations engineer and support staff similar to that of the Zero-Gravity Facility are available to integrate investigator-provided hardware into an experiment package or to have the responsibility for the design, fabrication, assembly, integration and checkout of new hardware. A summary of some of the design constraints can be found in Table 3. In either case, the operations engineer is responsible for the preparation of detailed safety documentation that must meet the approval of the LeRC Airworthiness Review Panel. The investigator will be required to provide certain elements of this documentation. Investigators who plan to fly on the Learjet are required to provide the LeRC Aircraft Operations Office with certification of both a current flight physical (minimum FAA Class III or Air Force Class III) and record of attendance at either a military or FAA passenger/crew physiological training class.

KC-135 experiments can also be supported by LeRC personnel in the same capacity as for Learjet experiments. Even though the KC-135 is operated out of JSC, the Marshall Space Flight Center (MSFC) has the responsibility for coordinating and scheduling flights for experiments sponsored by the MSAD of NASA Headquarters. LeRC personnel are available to assist investigators with the various documentation and contacts (MSFC and JSC) necessary for meeting the requirements for KC-135 flights. Also, LeRC-sponsored KC-135 experiments per JSC guidelines must be reviewed and approved by the LeRC Airworthiness Review Panel. The hardware will also be reviewed by a JSC safety committee for approval prior to flight. The "JSC Reduced Gravity Program User's Guide" provides complete details of experiment design guidelines and requirements for personnel who will be flying on the KC-135.

Another aspect of facility utilization involves coordination with NASA personnel. A NASA researcher or scientist is assigned to be a contract technical representative to any LeRC-sponsored investigation in the ground-based facilities. This individual will have the responsibility to provide the sponsored researcher with the necessary guidance regarding facility utilization and also assist in establishing an interface with operations personnel in the various facilities. The activities that will be coordinated with this individual include the following: arrangement of a pre-design meeting with the appropriate operations and design engineers to discuss the investigation, objectives, measurements required, hardware needs, design and procurement responsibilities and the like; maintenance of communications with operations personnel during the design and build-up phase; assistance in the preparation of a Test Request Document (directed to the appropriate operations engineer) which formally defines experiment details and experiment milestones, etc. ; assistance in scheduling tests; and consultation during the testing phase. LeRC mechanical and electronics technicians are available during the testing phase for repairs or modifications that cannot be performed by the investigator. This support may not always be available in a timely manner due to the many investigations that are ongoing.

Experiment Hardware/Investigations

As stated earlier, the NASA ground-based facilities have supported a wide range of investigations over the past thirty years particularly in the fields of combustion and fluids. Table 4 represents a sampling of a few of the recent experiment programs that have been carried out in the facilities. Many of the investigations have utilized more than one facility. A description of some of the hardware will be presented to show what is feasible. Of course these descriptions represent examples of capabilities. Simpler or more complex systems have been or can be engineered depending on the needs of the investigation.

The inventory of operational drop rigs at the Drop Tower has reached twenty-five with several more in the build-up phase. One of those that will soon become available is an updated multipurpose, multi-user combustion rig that will address investigations including solid material flammability, gas-jet diffusion flames, candle flames, and spacecraft fire safety. The test chamber for this rig will have an internal volume of .027 m^3 (.25 m I.D., .53 m length), a working pressure of 4.8 atmospheres, five viewing windows, and several feedthroughs and penetrations for mechanical and electrical hardware connections. The data acquisition capabilities will include accommodations for four thermocouples, one pressure transducer, and movie and video systems. The rig will also have provisions for a laser light sheet and a shock absorption plate system for the mounting of sensitive components.

Since there are fewer experiment vehicles available at the Zero-Gravity Facility, more multipurpose hardware exists, particularly for combustion research. There are three combustion experiment vehicles available. They contain combustion chambers with the following specifications:

1. The general combustion vehicle shown in Figure 7 contains a 113 m^3, 0.4 m internal diameter hemispherical domed cylindrical pressure vessel. The vessel has a centerline length of 0.98 m and a maximum working pressure of 13.6 atmosphere. This chamber has been utilized to support investigations in pool fires, solid materials flammability, spacecraft fire safety, candle flames, etc. This vehicle is adaptable to many investigations.

2. The Gas Jet Diffusion Flame Experiment contains a hemispherical domed cylindrical pressure vessel with an internal volume of 0.087 m^3. The pressure vessel has a 0.41 m internal diameter and a centerline length of .71 m. The maximum working pressure of the vessel is 4 atmospheres. An internal movable thermocouple and gas sampling probe rake is a part of the vessel configuration. This vehicle is currently employed solely for gas-jet diffusion flame research.

3. The convection/combustion vehicle contains a horizontal cylindrical pressure vessel with a centerline length of .91 m and a 0.31 m internal diameter. The maximum working pressure of the

vessel is six atmospheres. Internal to the vessel is a .19 m square fan duct, .61 m long. The fan duct is capable of providing flow velocities of 5 to 50 cm/sec at two atmospheres. A mechanical translation device expands testing into the 0-5 cm/sec velocity range. The convection/combustion vehicle should be adaptable to many investigations also.

All the above experiment vehicles provide high speed movie camera or video photography, programmable controllers, batteries (nominal 28 VDC), a data acquisition system and essential mechanical support systems such as valves and gas charging systems.

A number of combustion and fluids investigations have been conducted aboard the Learjet. Unlike the drop tower facilities, there are currently no dedicated combustion experimental facilities available. This is due to the fact that many of the programs on the Learjet have been development tests for specific shuttle flight hardware. However, a multipurpose combustion experiment known as the Spacecraft Fire Safety Experiment is currently being developed for use on the Learjet and the KC-135. This hardware is being designed for the following investigations:

1. Extinguishment of established fires by addition of extinguishing agents.
2. Extinguishment of established fires by pressure reduction.
3. Measurement of flame spread rate on engineering materials in various oxidizing atmospheres.
4. Measurement of flame spread rate on engineering materials in flowing oxidizer streams.
5. Development and testing of space-based smoke/fire detection systems.
6. Development and testing of combustion diagnostics instrumentation.

The experimental hardware will consist of a domed cylindrical pressure vessel with a centerline length of 74.3 cm and a diameter of 25.4 cm. The maximum working pressure of the chamber will be 3 atmospheres. The maximum oxidizing flow velocities will be 40 cm/s at 1 atmosphere and 20 cm/s at 3 atmospheres. Instrumentation for the chamber will include thermocouples, pressure transducers, video and motion picture cameras, and mass flow controllers. Data acquisition and experiment control will be handled by a personal computer. The combustion chamber will also be equipped with extra ports for additional instrumentation or diagnostics equipment. This apparatus is scheduled for completion in late October, 1992.

LeRC-developed KC-135 hardware to date has been quite experiment specific. The Gravitational Influences on Flammability and Flamespread Test System (GIFFTS) is one of those experiments. The sophisticated hardware supports a fundamental investigation into the combustion of thin solid fuels in the presence of very low-speed concurrent airflows that are induced by buoyancy in various levels of inertial acceleration, thereby simulating upward burning combustion behavior over a range of gravity levels. This is the first project to utilize a schlieren system in a reduced-gravity environment. Data obtained from this investigation includes motion picture imaging of the thermal field constituting the flame in order to deduce its size, shape and propagation speed, local temperatures of the fuel in the surrounding gases and three-axis measurements of the local accelerations. The hardware is mounted in two racks and utilizes a gas bottle support rack necessary for the various atmospheric test conditions. One rack can be fixed to the aircraft or free-floated. This rack is equipped with a test chamber with an interior volume of 25 liters, a sample holder, the test specimen, up to 6 type K thermocouples, a Kanthol alloy ignitor wire and an incandescent light bulb. The schlieren optical system which consists of 30 optical elements, a light source, a miniature video camera, and video cassette recorder is also a component of this main rack along with the system control and management computer, three-axis accelerometer, pressure transducer, power supply box and batteries. The support rack, which supports sample changeout and data storage functions, consists of a gas handling subsystem, sample storage, video display and power supply and laptop computer. This experiment has been flown at "normal" parabolic maneuvers in both a fixed and free-float mode, and at 1/6 g (lunar gravity) and 1/3 g (Martian gravity) in only the fixed mode.

Concluding Comments

Over the past 30 years the LeRC reduced gravity facilities have provided data which have significantly advanced the understanding of low gravity processes and phenomena and enabled the development of space-based technology. Research executed under low gravity conditions will continue to grow through the era of space-based research in order to provide critical, economical pre-flight scientific data and technology verification. Experiments are destined to grow in complexity, particularly in the area of diagnostics.

References

1. The Microgravity Combustion Group, Microgravity Combustion Science: Progress, Plans, and Opportunities. NASA TM-105410. 1992.

2. Low-Gravity Fluid Physics: A Program Overview. NASA TM-103215. 1990.

3. JSC Reduced Gravity Program User's Guide. JSC-22803. 1991.

Table 1.
2.2 Second Drop Tower: Characteristics and Capabilities

Operational Parameters
- Low gravity duration : 2.2 seconds (free fall: normal atmosphere with drag shield system)
- Gravitational acceleration : ~ 10^{-5}g
- Deceleration levels : 40 to 100 g's for several milliseconds (< 40 g's with shock absorption system)

Experiment Envelope Summary
- Drop Frame "standard" (aluminum bus for mounting hardware)
  - width (depth): 40cm
  - length: 91cm
  - height: 81 to 102 cm
  - dimensions identified are maximum
  - variations of standard frame are feasible

- Experiment hardware weight: 140 kg (maximum)

Experiment Instrumentation/Data Acquisition Capabilities
- High speed movie cameras
- Video cameras (fiber optic link to recorder)
- Battery packs (110VAC feasible)
- Data acquisition and control system
- Thermocouples
- Pressure transducers
- Flow meters
- Lasers

Mode of Operation
- Engineering support for consultation
- Technical staff to support electronics and mechanical integration and maintenance
- Technician and investigator perform drops
- Twelve drops per day (minimum of two drops per day per investigator)
- Safety review required

Additional Features
- Compressed gas (fuels, oxidant, and diluents) storage, handling, and delivery support available
- Limited community tool supply
- Film motion analyzer

NASA contacts:
Jack Lekan: (216) 433-3459
Mike Johnston: (216) 433-5002

Table 2.
Zero-Gravity Research Facility: Characteristics and Capabilities

Operational Parameters
- Low gravity duration: 5.18 seconds (free fall: evacuated chamber @ 10^{-2} Torr)
- Gravitational Acceleration: $<10^{-5}$ g
- Deceleration levels: up to 65 g's for several milliseconds (mean: 35 g)

Experiment Envelope Summary
- Cylindrical experiment vehicle
  - diameter: 1 m
  - total height: 3.4 m
  - paylod height: 1 m
  - payload weight: up to 455 kg
  - cold gas thrust system available for: 0.003 g to 0.015 g*
- Rectangular Experiment Vehicle*
  - L x W x H: 1.5 m x 0.5 m x 1.5 m
  - payload envelope L x W xH: 0.61 m x 0.40 m x 0.45 m
  - payload weight: up to 69 kg
  - cold gas thrust system available for: 0.003g to 0.037g (positive); 0.013 g to 0.070 g (negative)

Experiment Instrumentation/Data Acquisition Capabilities
- Telemetry: 18 channels of continuous data telemetered from experiment (standard IRIG FM/FM, frequency range: 6 to 10000 cps, and overall system accuracy of 2% to 3%)
- High speed movie cameras
- Video cameras
- Battery packs
- Data acquisition and control system
- Closed-circuit television system
- Thermocouples
- Pressure transducers
- Flow meters
- Lasers

Mode of Operation
- Engineering staff to support design, build-up and testing
- Facility engineering staff perform drops
- One to two drops per day
- Safety review required

Additional Features
- Compressed gas (fuels, oxidant, and diluents) storage, handling, and delivery support available
- Film motion analyzer
- Class 10000 clean room

NASA contact:
Ray Sotos: (216) 433-5485

* These options are not currently in use, but could be made available to satisfy specific requirements.

Table 3.
Learjet: Characteristics and Capabilities

Operational Parameters

- Low gravity duration: 18 to 22 seconds (parabolic trajectory)
- Gravitational acceleration: 10^{-2} g (1/20 to 3/4 normal gravity levels possible)
- Number of trajectories per flight: 6 (maximum at 10^{-2} g)
- Maximum power: 28 VDC, 80 amps
  110 VAC, 60Hz, 7.5 amps
  110 VAC, 400Hz, 18.3 amps

Experiment Envelope Summary

- NASA-provided racks
  - length: 60.9 cm
  - width: 52.7 cm
  - height: 90.8 cm
  - stress limits: weight: 85.27 kg , total moment: 369.23 Nm
- Cabin length: 1.85m

Experiment Instrumentation/Data Acquisition Capabilities

- Three-axis accelerometer system
- LeRC-approved instrumentation provided by the investigator
- High speed movie cameras
- Data acquisition and control system

Mode of Operation

- Engineering staff to support design and integration of hardware
- Flight-qualified investigators conduct in-flight experiments (flight physical and physiological training required)
- Two flights per day are possible
- Safety review required

Additional Features

- LeRC personnel available to fly with payload
- Accommodations for Get Away Special Cannister experiments

NASA contact

Eric Neumann: (216) 433-2608

Table 4.
Examples of Investigations Performed in Ground-Based Facilities

Investigation	Drop Tower	Zero-G Facility	Learjet	KC-135
Laminar Gas Jet Diffusion Flames	•	•		•
Droplet Combustion - Pure Fuels at Low and Ambient Pressures	•	•		
Laminar and Turbulent Flames at Microgravity	•			•
Flame Spread over Solids in Quiescent Environments	•	•		
Fundamental Study of Smoldering Combustion in Microgravity	•		•	•
Ignition and Flame Spread over Liquid Fuels	•	•		
Candle Flames in Microgravity	•	•	•	
Interface Dynamics	•			
Vibration Isolation Technology Development			•	
High Pressure Combustion of Binary-Fuel Droplets	•			
Studies of Flame Structure in Microgravity	•			
Combustion of Solid Fuel in Very Low Speed Oxygen Streams	•			•
Flame Spread over Thin Solid Fuels in Quiescent and Slow, Opposed Flow Environments	•	•		
Burke-Schumann Diffusion Flames	•			
Capillary Flow	•			
Multiphase Flow	•		•	•
Experiments in Low-G Fire Suppression and Extinguishment Effectiveness	•		•	
Solidification Phase Change			•	
Cryogen Nitrogen Transfer		•		
Pool Boiling		•		

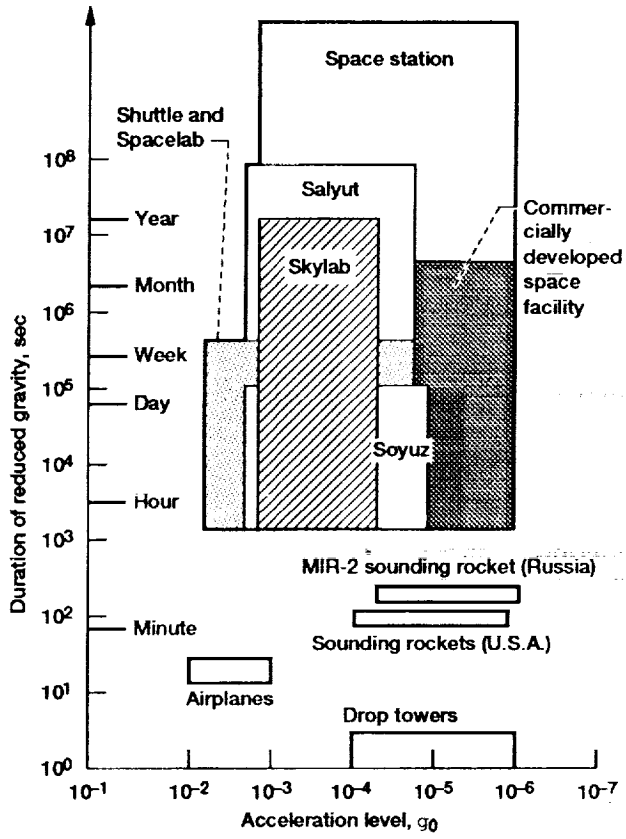

Figure 1.-Characteristic times and acceleration levels of reduced-gravity laboratory facilities.

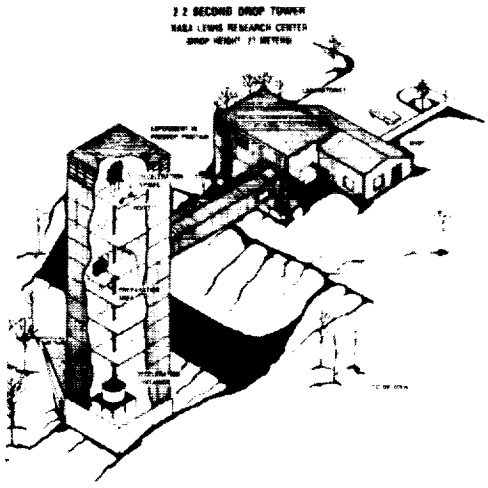

Figure 2.-Cutaway rendering of the LeRC 2.2 Second Drop Tower.

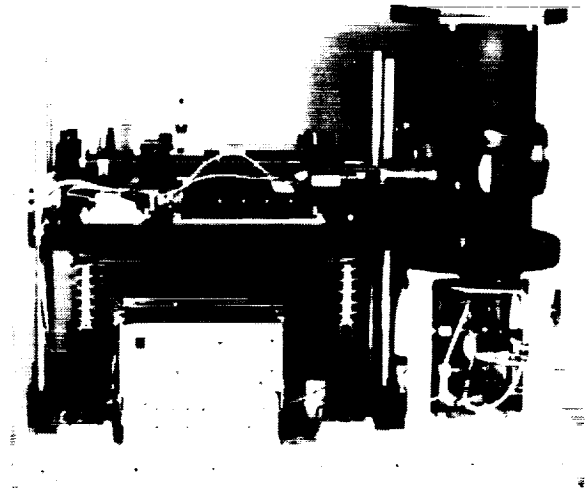

Figure 3.-2.2 Second Drop Tower package (Combustion Diagnostics Laser Rig).

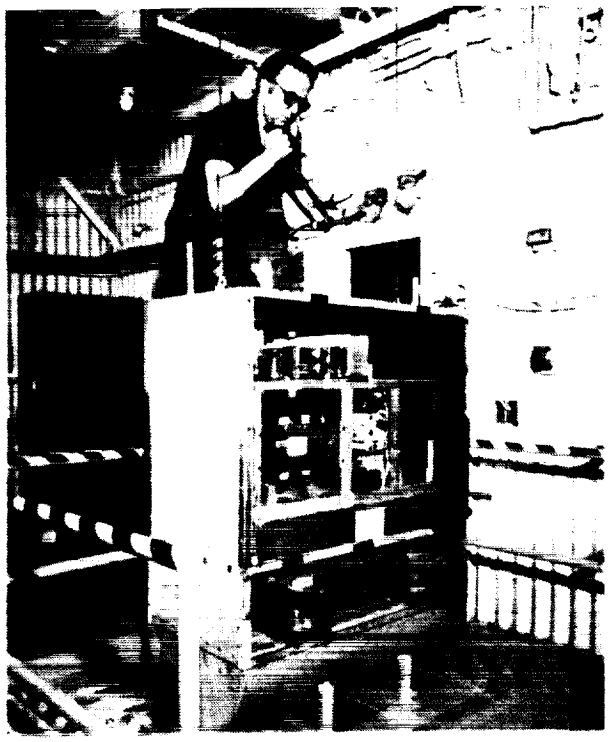

Figure 4.-Drop Tower experiment package drag shield assembly.

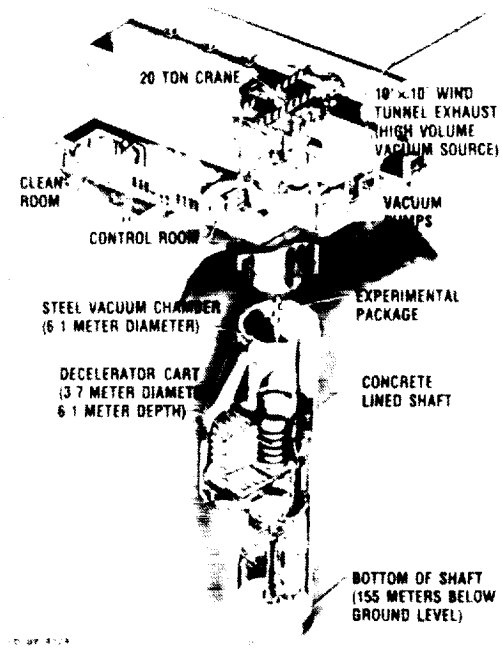

Figure 5.-Cutaway rendering of the LeRC Zero-Gravity Research Facility.

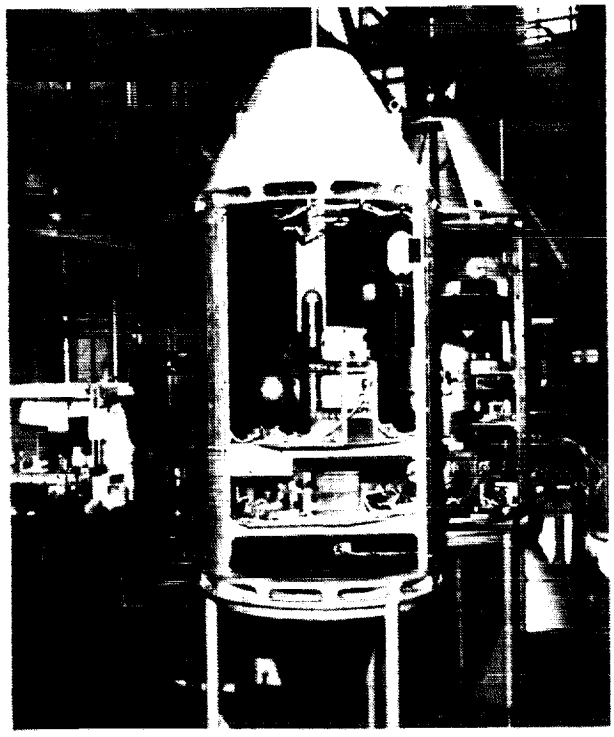

Figure 6.-Cylindrical experiment vehicle utilized in the LeRC Zero-Gravity Research Facility.

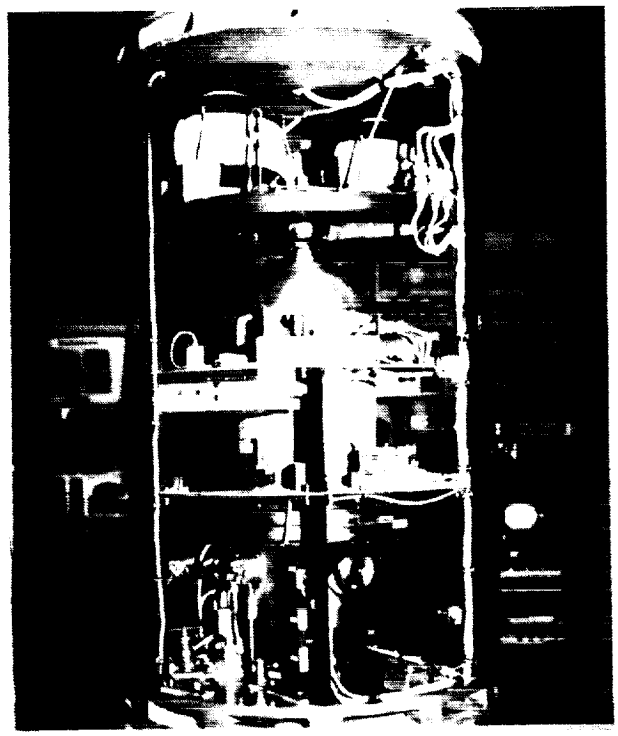

Figure 7.-Test section of cylindrical experiment vehicle outfitted with a multipurpose combustion chamber.

Figure 8.-LeRC Learjet cabin with experiment hardware.

Figure 9.-JSC KC-135 cabin with multiple experiments.

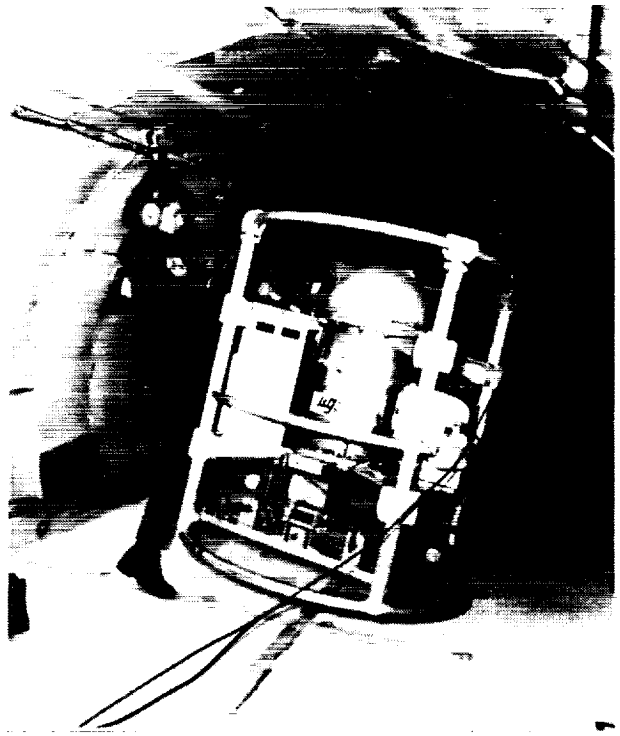

Figure 10.-Free-float experiment aboard the JSC KC-135.

CAPABILITIES AND CONSTRAINTS OF COMBUSTION DIAGNOSTICS IN MICROGRAVITY

N93-20185

Paul S. Greenberg
NASA Lewis Research Center
Cleveland, Ohio 44135

I. Introduction

A significant scientific return from both existing and proposed microgravity combustion science experiments is substantially dependent on the availability of diagnostic systems for the collection of the required scientific data. To date, the available diagnostic instrumentation has consisted primarily of conventional photographic media and intrusive temperature and velocity probes, such as thermocouples and hot wire anemometers. This situation has arisen primarily due to the unique and severe operational constraints inherent in reduced gravity experimentation. Each of the various reduced gravity facilities is accompanied by its own peculiar envelope of capabilities and constraints. Drop towers, for example, pose strict limitations on available working volume and power, as well as autonomy of operation. In contrast, hardware developed for space flight applications can be somewhat less constrained in regards to the aforementioned quantities, but is additionally concerned with numerous issues involving safety and reliability.

The Microgravity Combustion Diagnostics (MCD) group exists to provide diagnostic systems of greater sophistication. The group is located within the Microgravity Combustion Science Branch at NASA-Lewis Research Center, and is funded by NASA Headquarters through the Advanced Technology Development Program. Collocation within this branch helps to assure that the focus of the development efforts are consistent with the scientific objectives of both in-house and sponsored investigators. Although the laboratory staff is frequently involved with the design of diagnostic systems for flight project applications, the MCD program operates on an independent basis, and is not responsible for the design of hardware critical to the development schedule of the space flight projects. The personnel presently supporting this area represent the disciplines of instrumentation and optical systems design, spectroscopy, and computer science.

For a variety of reasons, predominant emphasis has been placed on the development of optical diagnostic techniques. Principal among these is the relative fragility of reduced gravity combustion phenomena as compared to their 1-g counterparts. The action of buoyancy induced convection is vigorous compared to the dominant mechanisms affecting reduced gravity combustion, such as thermal and concentration driven diffusion. The essentially nonperturbative nature of optical measurement techniques is, therefore, well suited to this application. In addition, optical techniques are, in general, amenable to the acquisition of multi-dimensional data fields (i.e. imaging). This is an important consideration in the present state of microgravity combustion science, since a clearer understanding of basic phenomenology, including the verification of fundamental length and time scales and dominating physical mechanisms is still being developed. The ability to simultaneously acquire multi-dimensional data is also an important consideration in the conduct of reduced gravity experimental investigations, since many of the facilities (e.g. drop towers and aircraft) provide periods of only limited duration. Space-borne payloads, in contrast, can provide longer operating times, but are restrictive in terms of repeated access to the investigator, in the amount of power and expendables that may be consumed, and in the total amount of combustion products that can be generated and released into the air.

The process of developing diagnostic systems appropriate for microgravity combustion research does not end in the 1g laboratory. There are a number of reasons why this should be the case, the most significant of which is the differing behavior exhibited by most combustion phenomena under reduced gravity conditions. This is most easily seen in the example of qualitative imaging techniques. In one such example, results indicating an apparent threshold for ignition were later revealed to be an actual threshold in sensitivity of the imaging device under consideration. Differences in mixing and transport phenomena impact overall temperature distributions, population yields of individual species, and resulting temporal and spatial scales. Attempts to duplicate all or part of these observations in the laboratory using such tactics as reduced pressures or varying oxygen concentrations have been marginally successful at best. Thus, the true figure of merit for a given technique requires, in the majority of cases, the

transition from the laboratory into one of the various reduced gravity facilities. This transition unfortunately carries with it complications of its own. The MCD group at LeRC, for example, attempts to initially deploy hardware in the drop tower facilities whenever possible. This decision is affected primarily by reasons of timely access, rapid turnaround, and cost. Utilization of this particular facility, however, carries with it many of its own peculiarities that are completely removed from where the instrument may ultimately reside. The available working volume and electrical power, in addition to the severe shock loads that occur at the termination of the drop, are among the most difficult constraints that can be encountered. These constraints would not be as significant an issue in the design of a space borne instrument, but result from the decision to pursue the course of development in this specific facility.

The specific experimental parameters of concern are similar to those of interest in terrestrial combustion science laboratories. It is most often desirable to precede detailed and precise quantitative measurements with qualitative flow visualization methods. This provides the investigator with a global picture of the complete process, and serves to guide or refine the specific requirements for the quantitative measurements that are to follow. For this purpose, the MCD group has utilized conventional photographic media, conventional and intensified solid-state imaging devices, ultraviolet and infrared sensitive solid-state devices, reactive seeding methods, and schlieren imaging. The quantitative determination of temperature, species concentration, and velocity fields comprises a significant portion of the diagnostic development efforts. The characterization of droplets and particles are also represented. As will be discussed, the particular constraints associated with reduced gravity experimentation motivate approaches that are often unique to these applications. Recent advances in solid-state laser and detector technologies, however, are rapidly changing, and are placing us in a position more closely resembling those in progress in industrial and academic research laboratories.

II. Physical Constraints

Each of the venues available to the reduced gravity experiment investigator is accompanied by its own unique collection of physical and operational constraints and available utilities. [1] It should be noted, however, that a concern for diagnostic amenities is most often not a major factor in the determination of the appropriate vehicle for any given experiment. The dominant emphasis is justifiably placed on the accommodation of the combustion phenomenon itself, involving factors such as duration, required g-levels, attendant expertise, storage of consumables, thermal and combustion product generation, and safety. While the specifics concerning the available power, volume, etc. of the various reduced gravity facilities have been discussed in the preceding presentations, a number of additional observations are in order.

While affording the most ready access to reduced gravity experimentation, drop towers are unquestionably the most challenging of the facilities in regards to the constraints that they present. Particularly in the case of the 2.2 second facility, the available working volume and electrical power are severely limited. The 5.18 second facility is somewhat more generous, but still limited in comparison with aircraft facilities. The latter has the added complication of being operated under vacuum conditions. An example of the problems that this can create is seen in the behavior of some photographic films, which become brittle and can shatter upon impact. Pressurized experiment canisters have been constructed, but are an additional inconvenience to operate and maintain. Drop towers do not permit tended operation of the package, and are problematic due to impact loading during deceleration. This brings to bear questions not only of survivability of individual components, but of inordinate optical diagnostic realignment requirements subsequent to each test. The MCD group has successfully demonstrated a system for the reduction of deceleration loads. This system is consistently yielding impact accelerations of only 30 to 40 g's, and appears capable of considerable improvement below this level. The free travel required by this system, however, creates the need for a certain amount of free volume. This represents a substantial tax against an already restrictive condition.

Tethers in the drop tower facilities have been used for purposes of data and power transmission. A multi-mode fiber optic system now used routinely offers video-based image transmission. The 100 micron fiber and its protective sheath have negligible effect on the trajectory of the roughly 500 kilogram package/drag shield assembly. This system facilitates real-time viewing of the experiment package, both prior to and during the drop, and also permits the use of off-line analog and digital storage capabilities. A 110 VAC tether has also been employed for power transmission. The substantially larger cable size has proven to be somewhat unwieldy and is seldom used. A near-

IR diode absorption spectrometer presently being constructed under contract by Southwest Sciences, Inc. will be completely coupled via fiber optic tether, and will have one multi-mode transmission fiber and eight distinct single-mode detection fibers. This tethering not only isolates sources and detectors from impact loads, but permits power supplies, signal conditioning, and data logging electronics to be remotely located, thereby freeing up valuable power and volume on the package itself. The transmission of substantial amounts of laser power, particularly in pulsed laser applications, through the required lengths of fiber is still somewhat impractical. Several schemes have been proposed for relaying higher laser powers to the experiment package by allowing an expanded beam to freely propagate through space. Due to the essentially straight trajectory of the package, some schemes appear tractable, but have as yet not been implemented.

Reduced gravity aircraft are in some ways the most forgiving from the standpoint of diagnostic systems. Available utilities and working volume are considerably more generous in comparison to the drop tower facilities. Although the hardware must be capable of withstanding 9-g loads (as required by flight safety), this is modest relative to the drop towers. The possibility of tended operation is also a distinct advantage. While safety related flight-worthiness reviews are mandated, they do not approach the rigor encountered in space flight reviews. The primary pitfall associated with the reduced gravity aircraft is the relatively poor g-levels that are available. This fact alone presents an untenable situation for many investigators. Nonetheless, aircraft remain excellent platforms for the demonstration and trouble shooting of diagnostic instrumentation. Some tests aimed at attaining lower residual g-levels by free floating experiment packages within the aircraft have been conducted. This scenario results in significantly shorter run times, and power and data lines must be replaced with tethers, similar to those described above.

Although sounding rockets have not yet been used by our group, they are under consideration as a carrier for several experiments. From the standpoint of physical constraints, sounding rockets form an intermediary between drop towers and reduced gravity aircraft. Provisions for power and working volume are comparable to those in the 5.18 sec facility, although the geometry of the payload package is somewhat peculiar (long and narrow). While launch loads are considerably less than the impacts encountered in the towers, experiment hardware is subject to pre-flight vibration testing of 50g each axis, over a 20 to 2000 Hz bandwidth. Bi-directional telemetry is available, permitting a limited degree of opportunity for command and control functions

Actual space flight applications carry with them their own unique issues. As discussed in detail elsewhere, available volume and utilities vary significantly, depending on the specific carrier and location under consideration. Operations are tended, but it must be kept in mind that one is always operating through the "eyes, ears, and hands" of the flight crew. As capable as they are, there is always a reasonable limit to the degree of expertise that can be expected. They will never be as intimate with every facet of a given instrument as are those who developed it. Unquestionably the most significant issue for experimenters that is encountered in inhabited spacecraft activities is that of proof of safety under worst case assumptions. The resulting constraints placed on allowable materials, configurations, and procedures can be extremely restrictive. Creativity and perseverance on the part of the payload developer are ultimately balanced by the forces of time and cost.

III. Techniques Under Development

The MCD group has tried to provide nominal coverage of all of the experimental parameters demanded by the current microgravity investigators. Initial priority has been given to qualitative visualization methods, followed by temperature, species concentration, and velocity measurements. Particle (i.e. soot) and droplet measurements are a more recent addition. Prioritization within each area is influenced to a degree by the schedules of both ground-based and flight projects under development. While our group does not have direct involvement in producing flight-worthy systems, acknowledgement must be given to the issues that will ultimately be involved, such as available power and mechanical stability requirements. The following paragraphs provide brief summaries in each of these areas.

Advanced techniques being employed for qualitative visualization include intensified solid-state imaging arrays (including the use of band-filters), infrared imaging, reactive seeding, and Rainbow Schlieren imaging. Microchannel plate image intensifiers provide a net photon gain on the order of 10^3, and have demonstrated adequate sensitivity for all of the processes that have been encountered to date, which includes dilute premixed gas combustion, low pressure gas jet diffusion flames, low pressure droplet combustion, and solid fuels under quiescent conditions. In

the case of dilute premixed hydrogen combustion, [2] prior experiments required the use of halon dopants to render them visible. The addition of extraneous chemicals was a matter for concern, particularly as near-limit phenomena were being investigated. The gain afforded by these devices allows the use of narrow bandwidth spectral filters, either to isolate particular emission bands such as that from CH radicals, or to mask the influence of extraneous emissions, such as soot radiation. Photocathodes sensitive in both the visible spectrum and in the UV are being utilized. These devices have been employed on both of the reduced-gravity aircraft, [2,3] but have not yet been deployed in the drop towers. Data on the performance of the impact isolation system mentioned above is encouraging, and will most likely result in the deployment of intensified arrays in drop tower facilities in the near future. These arrays are also slated for inclusion in several flight projects presently under development.

A platinum silicide array has recently been obtained for imaging applications in the near to mid-IR. Suitable sensitivity has been demonstrated in the laboratory to visualize extremely weak flames, even in the presence of narrow bandwidth IR filters. This opens the possibilities for performing two-dimensional temperature field measurements of known emissivity radiators, such as soot or grids of thin (15 micron) ceramic fibers suspended in the flame. These types of fibers are already being utilized in the LeRC 2.2 sec drop tower for the qualitative assessment of temperature distributions in droplets and gas jet diffusion flames. Radiative thermometry can be accomplished by digitizing the output of the array and fitting the response as measured to the Planck distribution function. Point and line measurements of this type have been widely reported; [4] the extension to two-dimensions appears reasonably straightforward.

A more complex characterization of the IR emission spectrum may enable, in certain cases, the determination of major product species concentrations and temperatures. For simple fuels, resolving the spectrum through an appropriate series of bandpass filters may be sufficient, whereas more complex systems may require a more elaborate approach, such as imaging FTIR. A predictive code [5] is presently being utilized to calculate IR spectra for selected flames. The objective is to invert the procedure: the measured emission spectra serving as the input for the calculation of the emitting species and their temperatures.

Rainbow schlieren [6] imaging is also being utilized as a visualization method. Through the use of a continuous color-based filtering scheme, gradients in the refractive index field appear as variations in color. The eye is quite sensitive to these variations in color, much more so than to the grey scale variations provided by conventional knife-edge methods. In addition, the multi-colored images that result are more readily interpreted than the fringe shifts provided by interferometric methods. Several compact optical systems have been designed and constructed, [7] providing the capability for using this method in the drop towers and aboard the reduced gravity aircraft. A method for quantifying the resulting ray deflections has been developed, providing the ability to determine refractive index distributions with a measurement sensitivity comparable to interferometric methods. [8] The resulting instrument is far simpler and mechanically robust than phase sensitive interferometers, and more readily adapted to large fields-of-view.

The MCD group is also providing capabilities to support the acquisition, manipulation, and display of image based data. [9] A dedicated PC-based workstation is available for image processing and analysis, as well as for hardware and software development. Amenities are available for image transfer and archiving among various formats, including 16 mm motion picture film, still photography, and direct digital imaging. Network access has been established, linking this facility to the diagnostics laboratory, photographic laboratory, computer services laboratory, and a variety of PC and Unix workstations serving individual users. A number of analysis routines have been developed, including automated feature tracking and color characterization.

An effort has been initiated very recently to perform two-dimensional (i.e. planar) laser-based temperature and species concentration measurements. The specific techniques under development include molecular Rayleigh scattering, laser-induced fluorescence, and degenerate four-wave mixing. Techniques of this type were not initially included in the scope of the MCD program due to the impracticality associated with the requisite laser sources. Rapid advances in solid-state laser technology have significantly impacted this situation, bringing about the availability of tuneable, pulsed lasers that can be credibly utilized in the reduced gravity facilities. A development contract is presently being negotiated for a pulsed, line-narrowed Nd:YAG/Ti:Al_2O_3 laser with the capability for frequency doubling, tripling, and mixing to access a number of species of interest. This laser is intended to be

compatible with the constraints of the reduced gravity aircraft. Several strategies for beam delivery in the drop towers have been proposed, but are not presently scheduled for implementation.

An alternate technique for species concentration and temperature measurements via absorption spectroscopy is also in progress. This system is being developed by Southwest Sciences, Inc., and utilizes high frequency FM modulation and detection to obtain high sensitivity using inexpensive, near-IR laser diode sources. In the initial configuration, a 1.31 micron diode laser will be utilized to detect absolute concentrations of methane and water vapor, as well as the temperature of the latter. The use of high frequency modulation techniques results in shot-noise limited detection, providing a minimal detectable fractional absorbance of 3×10^{-4}. Fiber optic coupling will allow the system to be used in the drop towers; one multi-mode fiber will be employed for transmission, and eight separate single-mode fibers for detection. This multi-channel arrangement will enable the inversion of axisymmetric distributions from line-of-sight data by tomography. Through the substitution of appropriate source and detector combinations numerous other species can be accessed, including CO, CO_2, O_2, OH, NH_3, and NO_x.

Two techniques are being developed for velocity field measurements: particle image velocimetry (PIV) and laser doppler velocimetry (LDV). Both require the addition of seed material to the flow to serve as scattering centers. The specific PIV method being employed has been developed by the Optical Measurement Systems Branch of the Instrumentation and Control Technology Division at LeRC, and employs direct recording from video-based image sensors (as opposed to the utilization of an intermediary photographic recording). [10] This method has been successfully used in several liquid phase studies, including the recent flight of the Surface Tension Driven Convection Experiment aboard STS-50. It has also been demonstrated in high speed gas phase flows. [11] An extremely compact pulsed Nd:YAG laser is presently being constructed to provide the capability for performing these measurements aboard the reduced gravity aircraft. Lower velocity liquid-phase flow measurements can be performed using relatively low-power laser sources, and are scheduled to be performed in the 2.2 sec drop tower within the coming year. A compact laser doppler velocimeter is also under construction, [12] and utilizes a temperature stabilized laser- diode source operating at 780 nanometers and a solid-state avalanche silicon photodiode detector. The complete unit measures 65 mm in diameter and 175 mm in length, and is quite rugged. Laboratory experiments are presently being configured using two similar units obtained on loan from the Department of the Navy. An effort is also in progress in the design of a compact and robust signal processor. [13]

Measurement techniques applicable to the study of particles (i.e. soot) are also under development. Soot size distributions measurements are being performed both in the laboratory and in the 2.2 sec drop tower using a pneumatically actuated thermophoretic sampling probe. [14] Small transmission electron microscopy (TEM) grids are rapidly inserted into the flame to collect soot and then withdrawn. TEM images are then analyzed to provide information regarding the primary particles as well as the aggregated clusters. Size distribution measurements via multi-angle light scattering have been performed in the laboratory, but are not presently scheduled for reduced gravity implementation due to the relatively long integration times that are required. In addition, scattering measurements do not provide information regarding the primary particles directly. The probe measurements are complemented by light attenuation measurements to provide mass fraction and number density. This measurement is being implemented in an imaging configuration, wherein threshold sensitivity is exchanged for overall spatial yield. This is a reasonable tradeoff for the present measurements being performed in the 2.2 sec drop tower, where the limited duration of the experiments do not facilitate point-by-point scanning of the soot field.

The vaporization of isolated fuel droplets is being investigated through the application of exciplex fluorescence. [15] The addition of particular dopants permits the formation of liquid phase complexes which exhibit fluorescence at longer wavelengths relative to the monomer state of the dopant material. In addition to providing the ability to distinguish between liquid and vapor phase concentrations, thermometry can be performed from the ratio of these temperature dependent fluorescent intensities. A complementary study is being conducted under contract by United Technologies Research Center [16] for the measurement of flow fields both internal to the droplet and in the surrounding gas-phase. In addition to exciplex fluorescence, the techniques of planar laser-induced fluorescence, gas-phase flow tagging, and particle image velocimetry will be investigated.

A summary of the overall program in diagnostics development can be found in Table 2 of Reference 17. Shown along with each particular method under development is the present status, as well as the currently envisioned plans

for incorporation in the various reduced gravity facilities. It should be emphasized that the list of activities undertaken by the MCD group and its associated contractors has a certain flexibility. The results of ongoing investigations, as well as new areas of interest advocated by the scientific community will continue to expand and refine the complement of diagnostic capabilities that are available.

References

1. Lekan, J., "Constraints and Capabilities of Drop Tower and Aircraft Facilities," Proceedings of the Second International Microgravity Combustion Workshop, Sept. 1992.
2. Whaling, K.N., Abbud-Madrid, A., Ronney, P.D., "Structure and Stability of Near-Limit Flames with Low Lewis Number," Fall Technical Meeting of the Combustion Institute, Western States Section, LaJolla, CA, Oct 16-19, 1990.
3. Weiland, K.J., "Intensified Camera Imaging of Solid Surface Combustion aboard the NASA Learjet," AIAA Paper 92-0240, Jan. 1992; also available as NASA TM-105361.
4. Vilimpoc,V., Goss, L.P., Sarka, B., "Spatial Temperature-Profile Measurements by the Thin-Filament-Pyrometry Method," *Optics Letters* 13, 93 (1988).
5. Bernstein, L.S., Wormhoudt, J.C., and Conant, J.A., "The Aerodyne Radiation Code (ARC): Physical Assumptions and Mathematical Approximations," Aerodyne Research, Inc., ARI-RR-173, July 1979.
6. Howes, W.L., "Rainbow Schlieren and its Applications," *Applied Optics*, 23, 2449-2460 (1984).
7. Buchele, D.R., Griffin, D.W., "A Compact Color Schlieren Optical System," submitted to *Applied Optics*.
8. Greenberg, P.S., Klimek, R.B., Buchele, D.R., "Quantitative Rainbow Schlieren Deflectometry," In preparation for submission to *Applied Optics*.
9. Klimek, R.B., Paulick, M.J., "Color Image Processing and Object Tracking Workstation," NASA TM-105561, April 1992.
10. Wernet, M.P., Edwards, R.V., "New Space Domain Processing for Pulsed Laser Anemometry," *Applied Optics*, 29, 3399-3417 (1990).
11. Wernet, M.P., "Particle Displacement Tracking Applied to Air Flows," Proceedings of the Fourth International Conference on Laser Anemometry and Applications, Cleveland, OH, Aug. 5-9, 1991.
12. NASA Contract C-76847-R; EG&G Canada. Ltd.
13. Edwards, R.V., Toole, P.M., "Optimal Signal Processing for the Laser Doppler Velocimeter," Submitted to the Optical Society of America Topical Meeting on Photon Correlation and Scattering, Boulder, CO, Aug 24-26, 1992.
14. Dobbins, R.A., Megaridis, C.M., "Morphology of Flame Generated Soot as Determined by Thermophoretic Sampling," *Langmuir*, 3, 245 (1987).
15. Melton, L.A., "Quantitative Use of Exciplex-Based Vapor-Liquid Visualization System (A Users Manual)," Final Report for Contract DAAL03-86-K-0082 (1988).
16. NASA Contract NAS3-26547, United Technologies Research Center.
17. Ross, H.D., "NASA's Microgravity Combustion Science and Fire Safety Programs," Proceedings of the Second International Microgravity Combustion Workshop, Sept. 1992.

PRIORITIES FOR MICROGRAVITY COMBUSTION RESEARCH AND GOALS FOR WORKSHOP DISCUSSIONS

N93-20186

Gerard M. Faeth
Department of Aerospace Engineering
The University of Michigan
Ann Arbor, Michigan 48109-2140

Introduction

Several concerns motivate fundamental combustion research: combustion-generated pollutants are re-emerging as a major problem, new combustion technologies are needed for effective energy utilization, municipal and hazardous waste incineration are needed to replace landfills and storage, new combustion technologies are needed for advanced aircraft and spacecraft propulsion systems, and current understanding of fires and explosion hazards is limited — particularly for space-craft environments. Thus, it is of interest to determine how experimentation using microgravity facilities can advance research relevant to these problems.

Effects of buoyancy have had an enormous negative impact on the rational development of combustion science. Thus, microgravity (μg) offers a potential breakthrough in combustion research capabilities that could be comparable to the impact of laser diagnostics and numerical computations in recent years. On the other hand, human operations in spacecraft involve fire-safety issues at μg that largely are unexplored. Thus, μg offers both unusual opportunities and unusual challenges to combustion science. The objectives of this paper are to highlight the intrusion of buoyancy on fundamental combustion studies, the current priorities of microgravity combustion program and the goals of this workshop. The present discussion is brief, see several recent reviews of aspects of μg combustion research for more details [1-6].

Intrusion of Buoyancy

The intrusion of buoyancy is a greater impediment to combustion than most other areas of science because density changes caused by chemical reaction initiate buoyant flows that vastly complicate both the execution and interpretation of measurements. Thus, the presence of gravity prevents some fundamental phenomena — most laminar one-dimensional premixed and diffusion flames, low Reynolds number heterogeneous flames, flame spread in dispersed heterogeneous media, etc. — from being observed at all. Perversely, problems of buoyancy are greatest for fundamental laboratory experiments where good temporal and spatial resolution are needed; few practical combustion phenomena are dominated by effects of buoyancy.

The limitations of buoyancy on combustion studies have been quantified using phenomenological theories [4-6]. For example, for effects of buoyancy to be small in a motionless combustion environment at atmospheric pressure, the dimensions of the flame should be no larger than 100 μm; unfortunately, it is not possible to resolve experiments on such scales using either existing or anticipated combustion apparatus and instrumentation [4-6]. Experiments at subatmospheric pressures can increase allowable flame sizes, and this has been exploited in the past, however, the available range is limited due to low reaction rates leading to extinction at low pressures, see [6] and references cited therein.

Experiments in the presence of flow velocities offer a way of circumventing buoyancy effects, however, relatively large velocities must be used causing spatial resolution problems similar to those just discussed, and problems with approaching limiting conditions where either combustion rates or flow velocities are small. Thus, for effects of buoyancy to be small for premixed flames, at atmospheric pressure, laminar flame speeds should be greater than 1 m/s [4-6]. This prevents approaching flammability limits without effects of buoyant motion, which is problematical because premixed flames are unusually responsive to stretch induced by gas motion near limits [7]. Similarly, nonpremixed flames should have characteristic Reynolds numbers of 100 or more to avoid effects of buoyancy at atmospheric pressure [4-6]. This prevents approach to the low Reynolds number Stokes flow regime that has been invaluable for understanding fluid mechanics.

The effect of buoyancy is so ubiquitous that we generally do not appreciate the enormous negative impact that it has had on the rational development of combustion science. For example, aside from limited exploratory work at μg conditions, we have never observed the most fundamental processes of combustion without substantial disturbances of buoyancy. This includes simple one-dimensional configurations and low Reynolds number flows that have been invaluable in other areas of science. Thus, buoyancy prevents the rational merging of theory, where buoyancy frequently is of little interest, and experiments, which always are contaminated by effects of buoyancy at normal gravity (ng).

Turbulent flames, one of the most important unresolved problems of combustion science, provides a graphic example of how buoyancy impedes the parallel development of theory and experiment. Three-dimensional time-dependent numerical simulations provide a rational way to study some phenomena of turbulence but the calculations only will be tractable at low Reynolds numbers for some time to come [8]. Unfortunately, such conditions cannot be duplicated in the laboratory at ng because buoyancy immediately accelerates any low-speed initial condition into a high Reynolds number flow. Similar problems abound for other important combustion problems, e.g., the combustion of sprays and particles due to problems of phase separation, etc. With no massive breakthrough in computer technology in the offing, combustion experiments at μg offer the most promising approach toward resolving this theoretical/experimental dichotomy of combustion science.

Spacecraft Fire Safety

The same features that make μg attractive for fundamental combustion experiments introduce hazards of fires and explosions that have no counterpart on earth. The main concern is that virtually all existing information concerning design procedures to control fires and explosions is based on experience at ng. Even current qualification procedures for materials used in space involve tests at ng, justified by rather limited measurements at μg [3]. Since we know that combustion processes are very different at ng and μg, there is little basis for confidence that this practice is correct. Additionally, excessive caution to reflect our poor understanding of μg fire environments can unduly restrict our capabilities for exploiting space [3].

Addressing spacecraft fire safety concerns at μg will require a substantial research effort. Curiously, an alternative that could eliminate many of these concerns has not received much attention. This involves the use of fire-safe atmospheres in spacecraft, similar to the methods used to avoid fires in undersea systems [9]. This potential exists because fire-related phenomena tend to be functions of the *fractional* amount of oxygen in the atmosphere while human comfort and performance mainly depend on the *absolute* amount of oxygen in the atmosphere. Thus, it may be possible to find a composition for spacecraft atmospheres that will not support combustion but will support normal human activities indefinitely. However, available information concerning fire-safe atmospheres — combustion properties at μg, the performance and health of humans and other biological systems, and potential impacts on spacecraft design and operation — are woefully

inadequate in view of the importance of this selection. Thus, fire-safe atmospheres appear to merit a broad-based interdisciplinary research program due to their potential impact on future human activities in space.

Current Priorities for Microgravity Combustion Research

An objective of this workshop is to identify priority areas within combustion science where microgravity-based investigations are needed. Based on the results of the First International Microgravity Combustion Workshop, the Discipline Working Group (DWG) that advises NASA in the area of microgravity combustion science has set the following priorities: (1) turbulent reacting flows; (2) heterogeneous combustion such as droplets, particles, slurries, solid fuels and pools of liquid fuels; and (3) laminar homogeneous combustion phenomena such as ignition, flameholding, flammability limits, flame instabilities, and diffusion flames. Prioritization also was made with respect to applications, with spacecraft fire safety selected as the single most important application area.

The current microgravity combustion science program only reflects these priorities with respect to relevance to spacecraft fire safety, with the bulk of the work associated with heterogeneous combustion. This status is summarized in Table 1. In this table, flight studies denote investigations that are candidates for experimentation in space. Other studies either use ground-based μg facilities, such as drop towers and aircraft flying parabolic trajectories, or are theoretical studies. The relatively few studies of turbulent combustion is surprising in view of the current high priority of this area. In contrast, seven flight studies and 18 total studies are related to spacecraft fire safety, implying a strong response to this priority area following the last NASA Research Announcement (NRA) in 1989.

Table 1 Current Microgravity Combustion Science Program

Priority	Area	Flight Studies	Total Studies
1	Turbulent Reacting Flows	1	3
2	Heterogeneous Combustion	7	19
3	Laminar Homogeneous Flames	2	6

Goals for Workshop Discussions

As the microgravity combustion science program develops both the priorities and the focus of the research program will change. Thus, an objective of the workshop is to highlight areas where changes should be encouraged. Some questions that might be addressed during the discussions are as follows:

1. Are the areas and priorities selected by the DWG appropriate?

2. Are there new areas, e.g., combustion synthesis, metal combustion, etc., that merit emphasis in the next NRA?

3. What should be done to improve the content and balance of the flight and ground-based programs, and of experimental and theoretical programs?

4. Should a major interdisciplinary research program on spacecraft fire-safe atmospheres be recommended and what should be the combustion component of any such program?

5. Does the present program adequately address fundamental research issues relevant to spacecraft fire safety?

Funding is competitive within the microgravity combustion science program, and perhaps more importantly, between this program and other research areas of interest to NASA and other government agencies. Thus, an active high-quality microgravity combustion science program is required to assure continuing funding levels — much less increases. This workshop is one step in developing such a program; therefore, lively and productive discussions here will be a valuable service to the field of combustion.

Acknowledgements

Helpful inputs from the NASA Microgravity Combustion Science Discipline Working Group are gratefully acknowledged.

References

1. "Microgravity Combustion Science: A Program Overview;" NASA TM 101424, 1989.

2. "Microgravity Combustion Science: Progress, Plans and Opportunities," NASA TM 105410, 1992.

3. Sacksteder, K., *Twenty-Third Symposium (International) on Combustion*, The Combustion Institute, Pittsburgh, 1990, pp. 1589-1596.

4. Law, C.K., AIAA Paper No. 90-0120, 1990.

5. Faeth, G.M., AIAA/IKI Microgravity Science Symposium, Moscow, AIAA, Washington, 1991, pp. 281-293.

6. Law, C.K. and Faeth, G.M., "Opportunities and Challenges of Combustion in Microgravity," in preparation, 1992.

7. Kwon, S., Tseng, L.-K. and Faeth, G.M., Combust. Flame, Vol. 90, 1992, pp. 230-246.

8. Pope, S.B., *Twenty-Third Symposium (International) on Combustion*, The Combustion Institute, Pittsburgh, 1990, pp. 591-612.

9. Gann, R.G., Stone, J.P., Tatem, P.L., Williams, F.W. and Carhart, H.W., Combust. Sci. Technol., Vol. 18, 1978, pp. 155-163.

COMMENTS

Question (Takashi Kashiwagi, NIST): (1) I am not sure that a flame-limited, atmospheric approach removes fire problems in a spacecraft entirely. Smoldering under certain conditions, such as well insulated and preheated cases, can continue even in several percent of O_2. It seems to me as long as there is manned flight there are fire safety issues.

(2) I should like to see clearly defined policy in which the combustion research areas related to fire research could be considered in Microgravity Science Program.

Answer: Fire-safe atmospheres to eliminate conventional unwanted fires would represent a substantial improvement of fire safety in spacecraft. Whether this can be achieved, and the conditions needed to prevent smoldering in microgravity, are open issues at this time that clearly merit further study. Your second comment relates to NASA policy issues, however; my understanding is that relationship of studies in the microgravity combustion program to spacecraft fire safety is a strong point in establishing the relevance of the research.

Question (Fred Dryer, Princeton University): My comment deals with prioritization of microgravity science to practical fire safety problems. Fire safety standards regarding the permissible concentrations of flammable gases and liquids are typically referred to about 10% of the lean limit, a value which apparently will change little from absence or presence of gravity. This does not mean that the science of flammability limits is not important to understand, only that its outcome may have little impact in the fire safety arena. On the other hand, limiting oxygen index apparently changes by as much as a factor of 2, an absolute change of substantial consequence to defining (fire) inert atmospheres. Finally, on Earth there is no experience with the flammability characteristics of wide-range polydisperse aerosols, a likely aerosol character in microgravity conditions.

In addition to the smoldering problem (which must be materials-controlled and studied), the latter two areas of microgravity combustion science would appear to me to be much higher priority than flammability limits.

Answer: My reference to flammability limits, in connection with fire-safe atmospheres, was meant to be generic and not related to a specific criterion like the lean flammability limit or the limiting oxygen index. Your point is well taken that the criteria to be used will influence the definition of fire-safe atmospheres. Clearly, the research issues in this area must involve both the nature and criteria for fire-safe atmospheres.

Question (A. Gomez, Yale University): One of the identified priority areas is that of turbulent reacting flows. Would you agree that before this research area can benefit from microgravity experimentation, we should wait for substantial improvement on available diagnostic techniques?

Answer: No, I see no reason to wait for improved diagnostics in order to address problems of turbulent reacting flows. First of all, available instrumentation at this point is equivalent to methods used to develop much of our understanding of turbulent flames. Next, the environment itself, which allows turbulent-like flame processes to proceed at much smaller velocities than on Earth, provides new potential for conventional experimental methods. Finally, I hesitate to exclude the possibility of some new approach being developed from available technology.

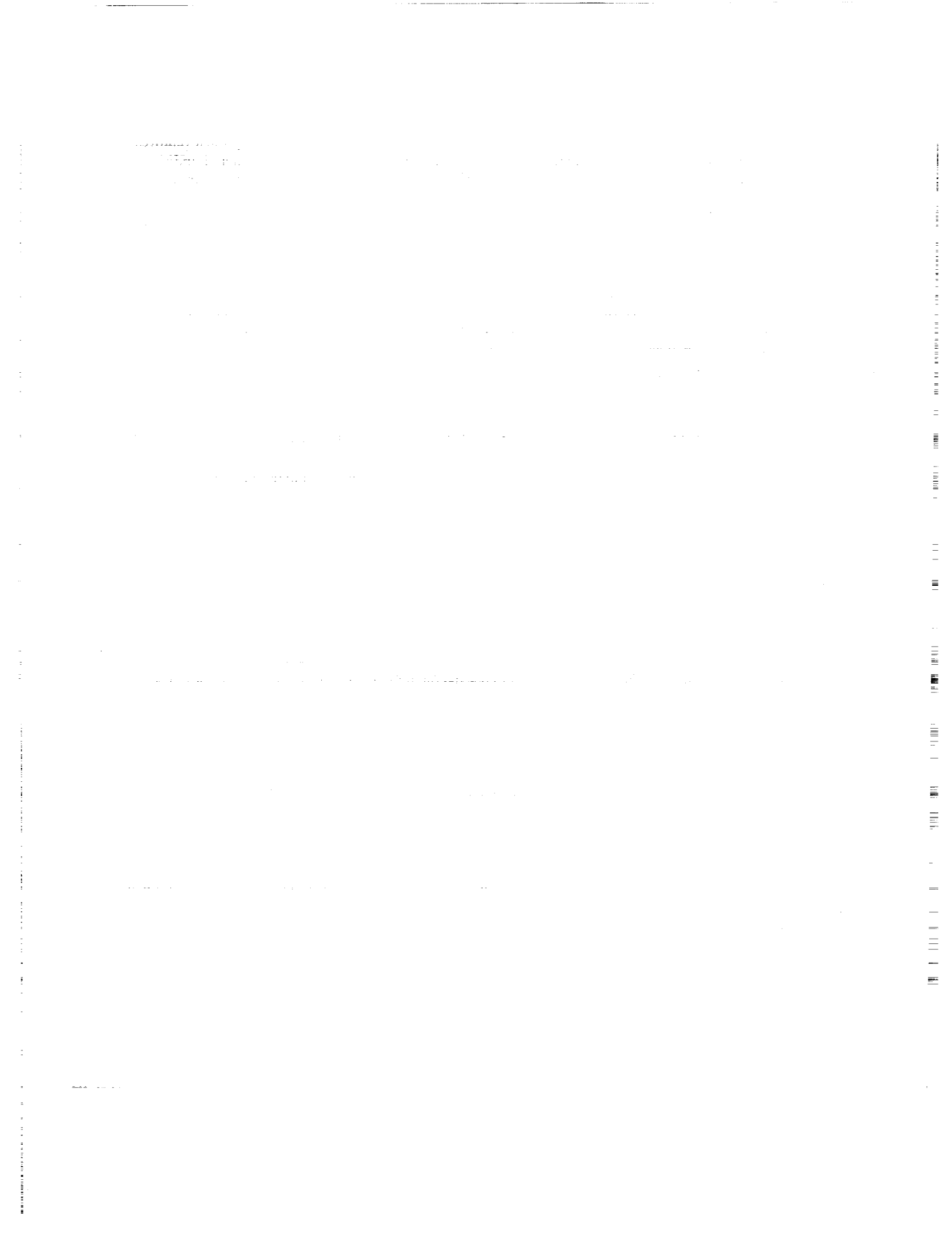

FULLERENES FORMATION IN FLAMES

Jack B. Howard
Department of Chemical Engineering
Massachusetts Institute of Technology
Cambridge, Massachusetts 02139

Introduction

Fullerenes are composed of carbon atoms arranged in approximately spherical or ellipsoidal cages resembling the geodesic domes designed by Buckminster Fuller, after whom the molecules were named[1]. The approximately spherical fullerene, which resembles a soccer ball and contains sixty carbon atoms (C_{60}), is called buckminsterfullerene. The fullerene containing seventy carbon atoms (C_{70}) is approximately ellipsoidal, similar to a rugby ball. Fullerenes were first detected in 1985, in carbon vapor produced by laser evaporation of graphite[1]. The closed shell structure, which has no edge atoms vulnerable to reaction, was proposed to explain the observed high stability of certain carbon clusters relative to that of others at high temperatures and in the presence of an oxidizing gas.

The proposed structure remained unconfirmed until 1990, when samples large enough for spectroscopy were produced by vaporization of graphite rods with resistive heating under inert atmosphere[2]. This method was quickly adopted in several research groups[3-5] and in small new companies. Fullerene samples soon became available, and the pace of research accelerated to an intense level. The interest rapidly expanded to include a still growing list of molecular and crystalline properties of fullerenes, as well as fullerenes with metals and other elements inside the cages, and fullerenes with hydrogen, oxygen, methyl, methylene, phenyl, or other functional groups or cross-links.

The suggested potential applications for fullerenes include superconductors, lubricants, catalysts, high energy fuels, polymers and biomaterials. The chemistry of fullerenes formation is being studied to provide a basis for the design and operation of fullerene synthesis reactors, and for the identification of new fullerene types and derivatives.

The possibility that fullerenes may be formed in sooting flames was suggested[6-9] early in fullerenes research. Zang et al.[6] considered the possible role of carbon shell structures in the formation and morphology of soot. Kroto and McKay[7] described a carbon nucleation scheme involving quasi-icosahedral spiral shell carbon

particles, and suggested it may apply to soot. Curl and Smalley[8] suggested that carbon nets in the form of spiral structures may be important to soot formation in flames. Recent reviews of these concepts are given by Kroto et al.[10-12]

All-carbon ions having charge/mass ratios similar to those reported for fullerenes in graphite vaporization were observed by Homann et al.[13-15] using on-line molecular beam/mass spectrometric probing of low-pressure premixed benzene-oxygen and acetylene-oxygen flames. Iijima[16] published an electron micrograph of a soot particle in which a circular feature was interpreted to be evidence of a fullerene. Malhotra and Ross[17] using field ionization mass spectrometry studied several soots from pyrolysis and combustion processes but found no peaks corresponding to fullerenes.

The presence of C_{60} and C_{70} fullerenes in substantial quantities was reported from spectroscopic analysis of samples collected from low-pressure premixed benzene-oxygen flames at MIT[18,19]. The presence and group behavior of high molecular weight compounds having molecular-weights up to about 1000 g/mole in benzene-oxygen flames had been studied earlier at MIT using molecular-beam sampling with on-line mass spectrometry[20,21] as well as probe collection of condensible material including soot with subsequent analysis by solvent extraction and other methods[22]. Intriguing but inconclusive evidence of the presence of fullerenes had been seen from both on-line mass spectra[21,23] and exploratory fast atom bombardment mass spectra of collected samples[23]. The presence of fullerenes in these flames was finally established[18,19], soon after the discovery[2] and early implementation[3-5] of the graphite vaporization process for producing macroscopic quantities of fullerenes. The same solvent extraction and spectroscopic techniques employed in the graphite vaporization studies were applied successfully in the study of the flame samples.

The knowledge of fullerenes formation in flames has grown significantly during the short time since this process was first established. The effects of combustion conditions on the distribution and yields of C_{60} and C_{70} fullerenes have been studied and the amount of fullerenes formed at different distances or times through the reaction zone of selected flames has been measured. Flame synthesis is found to offer not only an alternative method for large scale fullerenes production, but an ability to control the distribution of products (e.g., the C_{70}/C_{60} ratio) over a larger range than previously realized. Also, a range of fullerenes including metastable isomers can be produced in flames[24]. Plausible mechanisms of fullerenes formation in flames have been proposed and subjected to preliminary kinetics testing against data[25]. These advances are summarized below.

Current Knowledge

Fullerenes can be synthesized in substantial quantities in flames. Most of the research on fullerenes formation in flames has been performed with subatmospheric pressure, laminar, premixed flames of benzene and oxygen, with or without an inert

diluent gas, but acetylene has also been used successfully. The following conclusions about yields and products refer to the use of benzene fuel.

The largest yields of fullerenes are produced in sooting flames, but not under the most heavily sooting conditions. The largest conversion of carbon to soot is about 12% in fullerene forming flames, but the largest yields and production rates of fullerenes are observed when about 2-3% of the carbon is converted to soot. Small yields of fullerenes are formed in nonsooting flames near the critical conditions for impending soot formation.

The largest yield of $C_{60}+C_{70}$ as a percentage of soot is 20%, observed at a pressure of 37.5 torr, a C/O atomic ratio of 0.959 and 25% helium. The largest $C_{60}+C_{70}$ yield on a basis of percentage of carbon fed is about 0.5%, and the largest $C_{60}+C_{70}$ production rate (g/hr) was observed at a pressure of 69 torr, a C/O ratio of 0.989 and 25% helium.

The C_{70}/C_{60} molar ratios observed under different flame conditions are in the range 0.26-8.8, compared to 0.02-0.18 for the graphite vaporization method. The ratio is typically 1.5 to 1.8 for the flame conditions of largest $C_{60}+C_{70}$ production rates and yields. The largest values of this ratio are observed under conditions where the fullerene yields and production rates are relatively low.

The ability to promote the yield of certain products by adjustment of flame conditions apparently extends to larger fullerenes, based on exploratory work with solvents suitable for large fullerenes.

Isomers of fullerene C_{60} are produced in varying amounts in flames under different conditions. Although the isomers' structures are not yet known in detail, they necessarily must include abutting five-membered rings, which have previously been assumed to be avoided because of their high strain energy. Many of the isomers are thermally metastable, the C_{60} isomers having a half-life of 1 hr in toluene at 111°C.

Flame derived fullerenes also include isomers of C_{70}, $C_{60}O$, $C_{70}O$, C_{76}, C_{84}, C_{90} and C_{94}, and many hydrogen-containing complexes such as $C_{60}H_2$, $C_{60}H_4$, $C_{70}H_2$, $[C_{60}(CH_2)(H_2)]$ or $[C_{60}(H)(CH_3)]$, and others.

Fullerenes in flames are formed in the presence of hydrogen and oxygen as well as carbon. The formation of fullerenes is the net result of formation and destruction reactions, and the fullerenes concentration profile exhibits a peak at lower C/O ratios but become monotonically increasing with distance from the burner as the C/O ratio is increased. The formation of fullerenes in sooting flames occurs several milliseconds later than soot formation.

Fullerenes formation in flames is a molecular weight growth process analogous to the formation of PAH and soot but involving curved and hence strained structures.

A detailed mechanism of the formation of C_{60} and C_{70} fullerenes in flames has been constructed based on the types of reactions already used in describing PAH and soot growth, but including intramolecular rearrangements and other reactions needed to describe the evolution of the unique structural features of the fullerenes.

Potential for Microgravity Research

Potential topics for microgravity research include fullerenes formation in both diffusion premixed and laminar premixed flames. In the case of diffusion flames, experiments under microgravity conditions would complement measurements at 1 g in determining the effect of laminar flame structure on the extent of production of the well known C_{60} and C_{70} fullerenes, and on the formation of novel fullerenes. In addition, the measurements would permit preliminary projections of the prospects for fullerenes synthesis in turbulent diffusion flames. Measurements in premixed flames under microgravity conditions would allow the extent of C_{60} and C_{70} formation and the formation of novel fullerenes to be studied under conditions where the behavior is already well known except for the effect of gravity.

Acknowledgements

The author is grateful to M.K. Chung, A.G. Dietz III, L.M. Giovane, D.G. Goldenson, M.E. Johnson, R.J. Juba, Jr., A.L. Lafleur, Y. Makarovsky, S. Mitra, M.D. Nyström, C.J. Pope, L.W. Theiss, and T.K. Yadav for valuable collaboration and/or laboratory work; to the Division of Chemical Sciences, Office of Basic Energy Sciences, Office of Energy Research, U.S. Department of Energy, for financial support under grant No. DE-FG02-84ER13282; and to the National Institute of Environmental Health Sciences for analytical support under Center Grant EHS-5P30-ES02109-10 and Program Grant EHS-5P01-ES01640-11.

References

1. Kroto, H.W., Heath, J.R., O'Brien, S.C., Curl, R.F., and Smalley, R.E.: Nature 318, 162 (1985).

2. Krätschmer, W., Lamb, L.D., Fostiropoulos, K., and Huffman, D.R.: Nature 347, 354 (1990).

3. Taylor, R., Hare, J.P., Abdul-Sada, A.K., and Kroto, H.W.: J. Chem. Soc., Chem. Commun., 1423-1425 (1990).

4. Ajie, H., Alvarez, M.M., Anz, S.J., Beck, R.D., Diederich, F., Fostiropoulos, K., Huffman, D.R., Krätschmer, W., Rubin, Y., Schriver, K.E., Sensharma, D., and Whetten, R.L.: J. Phys. Chem. 94, 8630 (1990).

5. Haufler, R.E., Conceicao, J., Chibante, L.P.F., Chai, Y., Byrne, N.E., Flanagan, S., Haley, M.M., O'Brien, S.C., Pan, C., Xiao, Z., Billups, W.E., Ciufolini, M.A., Hauge, R.H., Margrave, J.L., Wilson, L.J., Curl, R.F., and Smalley, R.E.: J. Phys. Chem. 94, 8634 (1990).

6. Zhang, Q.L., O'Brien, S.C., Heath, J.R., Liu, Y., Curl, R.F., Kroto, H.W., and Smalley, R.E.: J. Phys. Chem. 90, 525 (1986).

7. Kroto, H.W. and McKay, K.: Nature 331, 328 (1988).

8. Curl R.F. and Smalley, R. E.: Science 242, 1017 (1988).

9. Kroto, H.W.: Science 242, 1139 (1988).

10. Kroto, H.W., Allaf, A.W., and Balm, S.P.: Chem. Rev. 91, 1213 (1991).

11. Kroto, H.W.: J. Chem. Soc. Faraday Trans. 87 (18), 2871 (1991).

12. Kroto, H.W.: Angew. Chem. Int. Ed. Engl. 31, 111 (1992).

13. Gerhardt, Ph., Löffler, S., and Homann, K.H.: Chem. Phys. Lett. 137, 306 (1987).

14. Gerhardt, Ph., Löffler, S., and Homann, K.H.: Twenty-Second Symposium (International) on Combustion, p. 395, The Combustion Institute, 1989.

15. Löffler, S. and Homann, K.H.: Twenty-Third Symposium (International) on Combustion, p. 355, The Combustion Institute, Pittsburgh, 1991.

16. Iijima, S.: J. Phys. Chem. 91, 3466 (1987).

17. Malhotra, R. and Ross, D.S.: J. Phys. Chem. 95, 4599 (1991).

18. Howard, J. B., McKinnon, J.T., Makarovsky, Y., Lafleur, A.L., and Johnson, M.E.: Nature 352, 139 (1991).

19. McKinnon, J.T., Bell, M.W., and Barkley, R.M.: Combustion and Flame 88, 102 (1992).

20. Bittner, J.D. and Howard, J.B.: Eighteenth Symposium (International) on Combustion, p. 110, The Combustion Institute, 1981.

21. Howard, J.B. and Bittner, J.D.: Soot in Combustion Systems and Its Toxic Properties (J. Lahaye and G. Prado, Eds.), pp. 57-91, Plenum, 1983.

22. McKinnon, J.T.: Ph.D. Thesis, MIT (1989).

23. Pope, C.J.: M.S. Thesis, MIT (1988).

24. Anacleto, J.F., Perreault, H., Boyd, R.K., Pleasance, S., Quilliam, M.A., Sim, P.G., Howard, J. B., Makarovsky, Y., and Lafleur, A.L.: Rapid Communications in Mass Spectroscopy 6, 214 (1992).

25. Pope, C.J.: Thesis, MIT (in preparation).

COMMENTS

Question (G.M. Faeth, University of Michigan: You mostly discussed Fullerenes formation in premixed flames. Have there been corresponding studies in nonpremixed flames?

Answer: I know of no published studies of Fullerenes formation in diffusion flames. Such studies would be of much interest, given the contrasts between the diffusion and premixed flame structures.

PRINCIPLES OF GAS PHASE PROCESSING OF CERAMICS DURING COMBUSTION

N93-20188

Michael R. Zachariah
Chemical Science and Technology Laboratory
National Institute of Standards and Technology
Gaithersburg, Maryland 20899

Introduction

In recent years, ceramic materials have found applications in an increasingly wider range of industrial processes, where their unique mechanical, electrical and optical properties are exploited [1]. Ceramics are especially useful for applications in high temperature, corrosive environments, which impose particularly stringent requirements on mechanical reliability. One approach to provide such materials is the manufacture of submicron (and more recently nanometer scale) particles, which may subsequently be sintered to produce a material with extremely high mechanical integrity. However, high quality ceramic materials can only be obtained if particles of known size, polydispersity, shape and chemical purity can be produced consistently, under well controlled conditions. These requirements are the fundamental driving force for the renewed interest in studying particle formation and growth of such materials.

Flames have most commonly been viewed as a means for generating energy; however, under some circumstances, they have also been used as an environment for chemical synthesis. The most notable industrial examples are the synthesis of carbon black, titanium dioxide and silica [2]. Some of the earliest work on the characterization of particle formation of refractories in flames was conducted by Ulrich [3]. Their work focused on the agglomeration processes following the formation of silica particles. More recently Calcote and his coworkers have used a generic novel halogen-alkali metal exchange reaction to generate a combustion environment in which the products are either a bare metal or a ceramic (and the halogen-alkali metal salt) [4].

For multi-component compounds where chemical stoichiometry is particularly important, aerosol decomposition is favored. Here, solutions containing the components are reacted within each aerosol droplet, precluding the necessity of controlling multi-component nucleation. Zachariah and Huzarewicz have shown that one can produce high Tc superconductors in a flame by this method [5].

The objective of this paper is not to review the field but to highlight from this authors prospective the most important areas features/factors affecting the growth of ceramic/semiconductor materials from the vapor. In this paper I will review the work on going at NIST on the vapor phase synthesis (gas phase chemistry/nucleation) of submicron and nano-phase particles from the prospective of the fundamental controlling factors and how they might be manipulated to obtain optimum properties.

Ideal Powder Characteristics for Advanced Ceramics

Based on current understanding the most important features in a powder are listed [6]:

- Particle size below 1 μm diameter; nanophase powders < 100 nm.
- Broad particle size distribution for greater packing density and less sintering shrinkage.
- Equiaxed particle shape for highest packing density
- Chemical and Phase purity/stability
- **No Powder defects** (e.g. agglomerates)
  They negate all the above benefits!

From the prospective of "ideal" powder processing, agglomeration is the most serious issue which must be addressed in any synthesis process.

Model System Studies of Vapor Phase Synthesis in Combustion

In order to better understand the controlling factors underlying the vapor phase formation of ceramic compounds we have undertaken to study one model system in great detail. The system chosen was the formation of SiO_x particles. Here particles are formed from silane and silane like precursors in a counter propagating diffusion flame reactor, illustrated in Fig. 1. The details of the reactor geometry can be found elsewhere [7,8]. The two impinging jets create a classical stagnation plane, offset from which (on the oxidizer side) a flame can be stabilized. The flame acts as a heat and radical source to aid in the pyrolysis and oxidation of the precursor (added to the fuel stream). The advantage of this geometry, in a similar fashion to other more traditional combustion studies is that along the stagnation streamline the flow may be described as one dimensional, greatly simplifying the data analysis and modeling complexity.

Studies of the Particle Phase

In-situ light scattering studies in conjunction with aerosol dynamics modeling have been employed to characterize particle growth under a wide variety of process conditions (temperature, precursor concentration, strain rate, etc) [7,9].
The basic conclusions to be reached from these studies were that:

- Precursor concentration was the primary variable for controlling particle size.

- Under most operating conditions the particles formed are chained agglomerates composed of primary particles in the 10-30 nm regime.

- In-situ particle characterization based on light scattering showed average agglomerate sizes which ranged from as low as 50 nm up to 150 nm.

- Temperature was the primary variable for controlling particle morphology. Increasing flame temperature resulted in particle sintering and therefore more spherical shapes. At the highest flame temperatures used (T > 2500K) particles were completely coalesced with mean sized in the 50-100nm range. Sintering could be observed to occur from both light scattering and TEM studies.

- Modeling of particle growth employed both moment and sectional aerosol dynamics [10]. By using a temperature dependent source rate for the monomer (SiO_2) and applying a bi-collider kinetic scheme, one can without having to resort to classical nucleation theory adequately model the overall features of particle growth. Fig 2. shows a comparison of experiment and theory for both particle size and number density. It is clear that one can, using a kinetically constrained approach, model both the size and number density. The calculation also shows a good prediction of the onset of nucleation. Particle size distribution can be significantly perturbed from self-preserving during the early stages of particle growth when the monomer generation rate is high, but quickly evolves to the self-preserving distribution during the relevant flow times of most flames.

Studies of the Gas Phase

In any materials syntheses, morphology (size, shape) is only a part of the final characteristics that need to be controlled. Issues related to phase, chemical composition and crystallinity are also of interest. In order to address these issues it is necessary to develop or borrow methods for chemical characterization and modeling relevant to understanding the chemistry/nucleation that might occur. Characterization of the gas phase has been conducted using in-situ optical probes throughout the reactor during particle formation, for temperature (thermocouple, OH fluorescence), and gas phase/cluster species (laser induced fluorescence (LIF) and resonantly enhanced multi-photon ionization (REMPI)) [11-13].

These measurements have been made in conjunction with a chemical model, which includes gas phase hydrogen-oxygen chemistry, silane pyrolysis and oxidation chemistry (proposed). The gas phase portion of the mechanism contains at the present time 38 chemical species and 128 reversible chemical reactions. In addition, there are 31 nucleation reactions which remove species from the gas phase, through what amount to monomer reactions (e.g. $SiO_2 + SiO_2$ monomer). Added to this, 23 species undergo surface chemistry

directly from the gas phase onto the growing aerosol, via a CVD type mechanism (e.g. SiO_2 + surface) [14]. The chemical kinetics are solved in conjunction with a model for the counter flow geometry developed by Smooke et al [15]

Measurement of gas phase species made by either LIF or REMPI include Si, SiH3, SiO and OH [11,14]. As an example, we show in Fig. 3 concentration profiles for SiO made by LIF for various levels of silane loading. Also shown is the stagnation plane as defined by the steep decline in the scattered light from particles. To the right of the stagnation plane (ie where no particles are present) the SiO concentration is independent of the silane concentration initially used. This behavior is accounted for by considering that as the temperature is increasing for particles approaching the stagnation point, the equilibrium vapor pressure of SiO over a solid is also increasing. At the stagnation point, when all particulate surfaces are removed, the remaining gas phase SiO diffuses across the stagnation plane and is therefore independent of the silane concentration used. Of more interest to us is the region where SiO is sensitive to the amount of silane injected. This region also corresponds to the particle forming zone in the flow field. It is clear that the SiO concentration goes up with increased silane concentration. In addition, the appearance of SiO occurs later in the flow with increased addition of silane.

The mechanism has been tested against measurements of the OH radical made by LIF and allow us some confidence in the reliability of modeling the general features of the flame. The calculated SiO profiles are shown in Figure 4. The results show that the location and magnitude of the SiO concentration can be calculated quite well. The dominant channels (as determined from post-processing the simulation) for the chemistry are shown in Figure 5. The primary consumption route for silane is the unimolecular pyrolysis to silylene ($SiH_4 = SiH_2 + H_2$), which in turn may react with silane to form di, tri silanes. This process occurs under experimental conditions when silane is injected in the larger quantities (>0.25 mole %). It is also the manner in which silicon particles are observed to nucleate in silicon CVD reactors. On the oxidation side of our mechanism we know from our simulations that no molecular oxygen remains in the particle forming zone, having been consumed by the flame. Furthermore, we know from our OH measurement (not shown here) that OH is not in sufficient quantity in the particle zone to participate in significant oxidation. We are therefore left with concluding that H_2O is the primary donor of oxygen to silicon. The most likely candidate is SiH2. In order to address this point we have recently undertaken ab-initio molecular orbital (MO) calculations to show that water will insert to yield both the silicon analogues of methanol and formaldehyde (H3SiOH, H2SiO) [16]. RRKM analysis has been used to obtain rates from these calculations which indicate (see Fig 5) that these channels will be important. Once we have H2SiO, the large concentration of H atoms created in the flame and which have diffused into the particle forming zone successively dehydrogenate to produce SiO or alternatively undergo unimolecular decomposition to SiO and H2.

One of the interesting points regarding nucleation is that SiO2 is not formed in the gas phase and that solid formation must proceed through the polymerization of SiO, HSiOOH, and H3SiOH with subsequent oxidation in order to achieve full oxygenation. We have recently shown through MO calculation that the polymerization of SiO is highly exothermic and proceeds without an activation barrier, however subsequent oxidation to yield full oxidation is slow. This presents opportunity to make oxides with variable stoichiometry. It is this multicomponent nature of gas to particle conversion that is the key to controlled synthesis of nano-scale materials.

Another issue of importance is the dominant mode of particle growth. Based on the model calculation we can show that heterogeneous growth of gas phase species will play only a minor role in the growth of particles. This results from the fact that flame systems act as pulsed sources of monomer (due to the large gradients in temperature) which do not provide sufficient time for CVD growth to existing particles. This means that particle formation will always be dominated by new particle births in flames and will require greater emphasis on quenching to prevent agglomeration [17]

Studies of the Cluster Phase and Nano-Phase Materials

The bridge between gas phase species and the bulk solid is what is euphemistically termed clusters. What separates clusters from bulk species is that they have size dependent properties which can differ substantially from the corresponding property in the bulk. Depending on the property of interest (melting temperature, optical properties, coordination number, etc.) the critical cluster size to obtain bulk properties

will in general be different. One interesting aspect of this is that one has the potential to tailor make materials with a desired property, assuming one knows the size-property relationship and can control the formation/collection of these structures.

In order to understand the growth of this class of materials we have undertaken molecular dynamics studies of cluster growth processes [**18**]. The basic idea is to solve the classical equations of motion for an assembly of atoms based on known interaction potentials. Because the interaction potential surface is quite well known for silicon, our studies to date have been limited to pure silicon clusters.

A representative example result of these calculations are presented in Fig 6. for the case of two 15 atom silicon clusters (equilibrated with an internal temperature of 1850 K) colliding with a relative velocity of 2400 K. The oscillation of the relative velocity of the cluster results from the two body attractive and three body repulsive parts of the interaction potential producing the initial stages of an **agglomerate**. The potential energy curve shows the time evolution of the newly formed 30 atom cluster from the agglomerate through to the coalesced sphere. The potential well at 0.2 ps corresponds to an agglomerate of the two clusters. By climbing an energy barrier the clusters gain a tremendous amount of configuration stabilization and thus much lower potential energy.The temperature profile is essentially a mirror image of the potential curve, showing the large self-heating of the cluster as the cluster finds a more stable configuration.

The relevance to nano-scale materials processing become clear when one realizes that the primary objectives are to make small structures that have little or no agglomeration. This can be accomplishes by either, (for very small particles) forcing particles to cross over the barrier or (for larger particles) trapping them in the agglomerate potential well by rapid cooling.

Potential for Microgravity Processing

Microgravity combustion environments provide the possibility to:

1. Increase residence time
2. Decrease the extent of thermal mixing

These two characteristics have the potential for providing processing conditions not easily achieved on the ground and which in principle at least can be considered to provide an opportunity for further development.

Increased residence time could be applied to the problem of growth of very large particles (microns) which have importance in catalysis. One of the problems encountered in the growth of large particles is the requirement of large residence times in order to vapor deposit onto the existing particle rather than continuously forming new particles via homogeneous nucleation. The increased residence time will allow for extended periods where heterogeneous chemistry CVD can take place under slow chemistry conditions.

The decrease in thermal mixing rates due to the lack of buoyancy driven flows has some potential in the formation of extremely fine particles (nanometer scale). As revealed from the experimental and molecular dynamics models previously discussed, temperature plays a key role in the kinetics of agglomerate formation/coalescence. Increasing temperature can cause complete or partial sintering given sufficient time. Therefore with a judicious choice of time-temperature history, nanophase particles could be made to form and then quickly quenched so that the agglomerates that are made are only weakly bound. Because of the absence of buoyancy, thermal boundary layers can be maintained with steeper gradients for longer times, allowing particles in a flame to be transported by electrophoretic or thermophoretic transport to a much colder quench layer. In this way one can separate nucleation from agglomeration.

Conclusions

Combustion synthesis has established its credentials as a practical method for the synthesis of fine ceramic particles. Its future contribution will be determined by the ability to develop strategies for the formation of particles with specific requirements for size, morphology and chemical composition.

References

1. Sanders, H.J., Chem. Eng. News, July 9, (1984)
2. Ulrich, G.D., Chem. Eng. News, August 6 (1984)
3. Ulrich, G.D., and Subranmanian, Combust. Sci. Tech. **17**, 119, (1977)
4. Calcote, H.F., and Felder, W., Twenty-Fourth Symposium (International) on Combustion, (1992)
5. Zachariah, M.R., and Huzarewicz, S., J. Mater. Res. Soc. **6**, 264, (1991)
6. Messing, G.L., "Critical POwder Characteristics for Advanced Ceramics" to appear in Fortschrittsberiichte der Deutschen Keramischen Gesselschaft.
7. Zachariah, M.R., Chin, D., Semerjian, H.G., and Katz, J.L., Combust. Flame, **78**, 287 (1989).
8. Zachariah, M.R., Chin D., Katz, J.L., and Semerjian, H.G., Applied Optics, **28**, 530 (1989)
9. Zachariah, M.R., and Semerjian, H.G., High. Temp. Sci., **28**, 113, 1990
10. Zachariah, M.R. and Semerjian, H.G., AIChE J. **35**, 2003 (1989)
11. Zachariah, M.R., and R.G. Joklik, J. Appl. Phys. **68**, 311 (1990)
12. Zachariah, M.R., and Burgess, D., "Stratagies for Laser Excited Fluorescence During Particle Formation" Submitted to J. Aeros. Sci.
13. Zachariah, M.R., Ceramic Powder Science III, Ed. Messing, G., **12**, 283 (1990)
14. Zachariah, M.R., "Chemistry of Silane Oxidation and Pyrolysis During Particle Formation: Comparison with In-Situ Measurements", Western States Section of the Combustion Institute, March (1991)
15. Smooke, M.D., Puri, I.K., and Seshadri, K., Twenty-first Symposium (International) on Combustion, pp. 1783. (1986)
16. Zachariah, M.R., and Tsang, W. "Ab-Initio Molecular Orbital Calculations of some Important Reactions and Polymerizations in the Si-O System"., Proceedings of the Materials Research Society, Boston, MA 1992
17. Zachariah, M.R., and Dimitriou, P., J. Aeros. Sci. Tech., **13**, 413 (1990)
18. Blaisten-Barojas, E., and Zachariah, M.R., Phys. Rev. B., **45**, 4403, (1992)

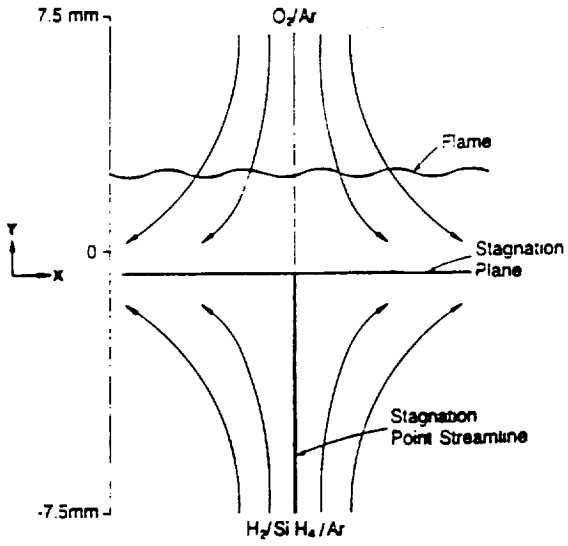

Figure 1. Schematic of counter flow diffusion flow field; Particles formed below stagnation plane. Laser diagnostics along stagnation streamline.

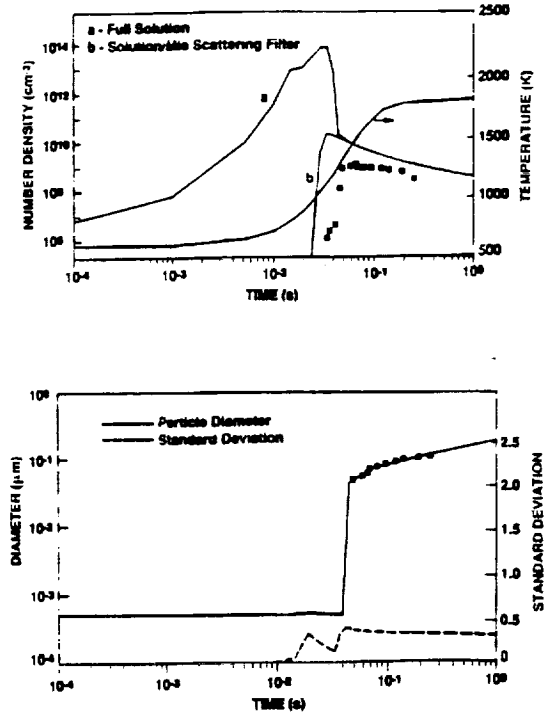

Figure 2. Comparison of model and experiment of SiO2 particle formation in a flame.

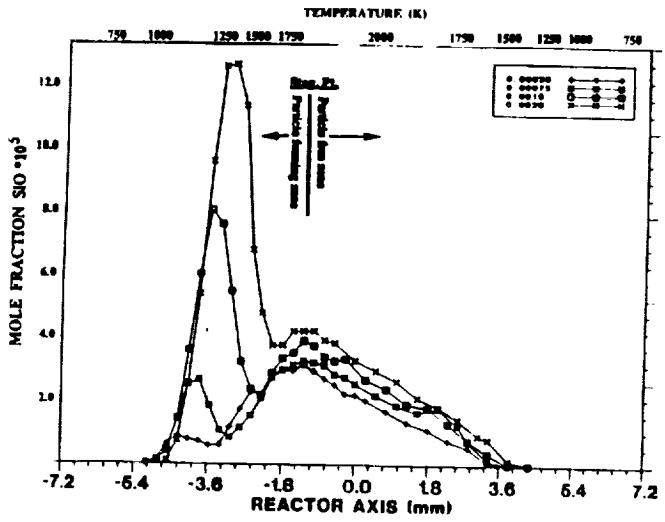

Figure 3. LIF concentration measurement of SiO as a function SIH4 mole fraction. Particles form to the left of the stagnation plane.

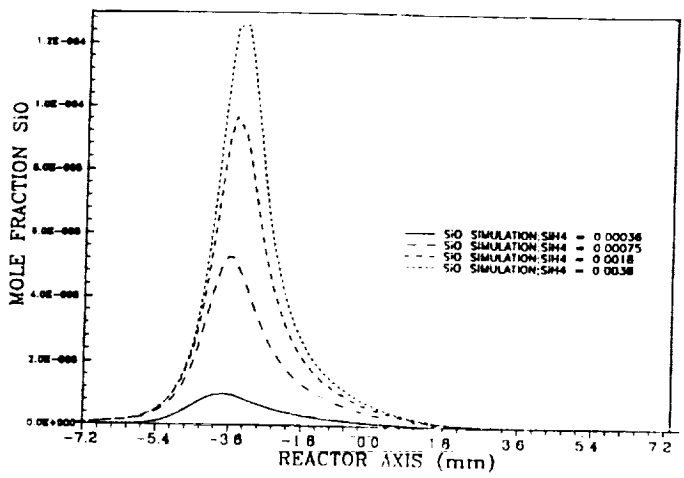

Figure 4. Model predictions of SiO concentration.

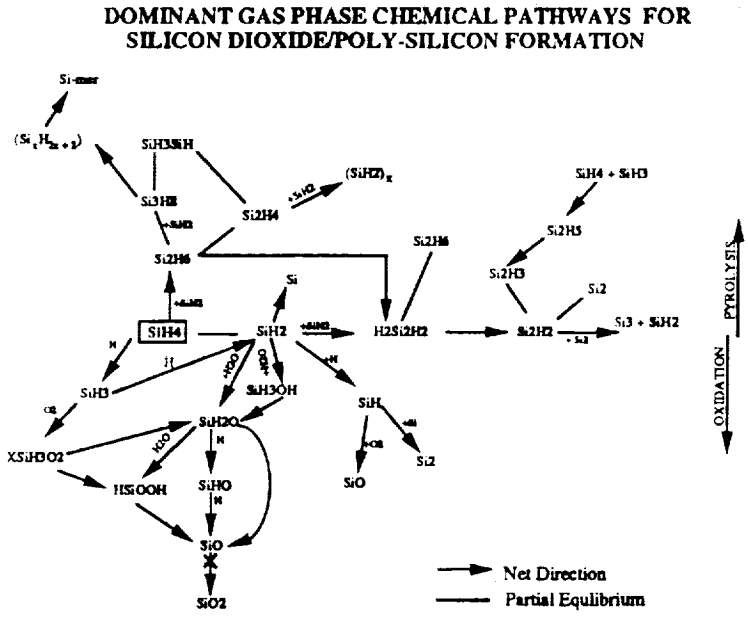

Figure 5. Dominant pathways computed from model calculations for silane oxidation/pyrolysis

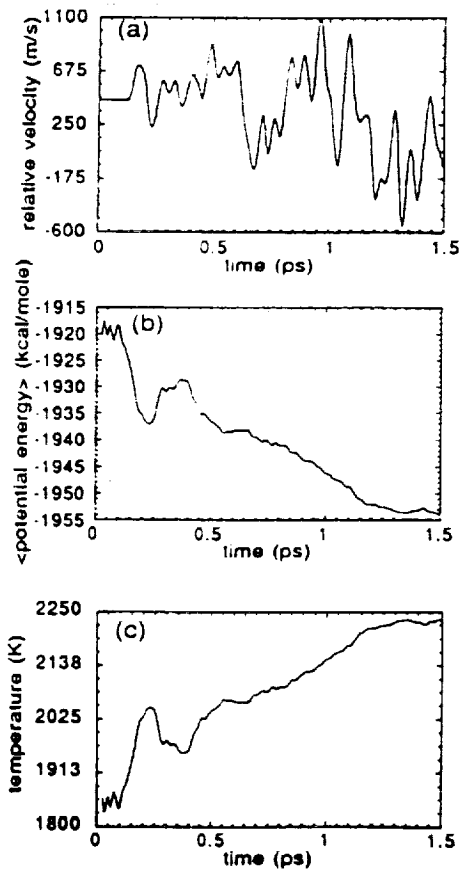

Figure 6. Results from molecular dynamics computation for the collision of two 15 atom silicon clusters for the relative (center of mass) velocity, potential energy and temperature.

COMMENTS

Question (Michael Frenklach, Penn State University): In addition to combustion synthesis in "regular" flames (like laminar premixed or diffusion flames), one can employ a "combined" flame environment. For example, using a microwave-assisted combustion, we were able to synthesize diamond particles in the gas phase.

Answer: I would agree completely that augmented flames can provide a more flexible environment for synthesis. Your diamond synthesis is a fine example of that principle. However, we should not lose sight of the one great advantage "regular" flames provide over other synthesis schemes -- "simplicity" -- which translates into cost-effectiveness, the driver for most process development. As we move to augmented flames through addition of energy (laser, RF, etc.) we transgress into a much more complicated synthesis environment, and into direct competition with the myriad of other processing techniques that may provide a similar result at comparable or lower cost.

SESSION C - Diffusion Flames and Diagnostics

(Chair, Robert Santoro)

88

C-2

EFFECTS OF BUOYANCY ON LAMINAR, TRANSITIONAL, AND TURBULENT GAS JET DIFFUSION FLAMES*

M. Yousef Bahadori†
Science Applications International Corporation
Thermal Sciences Division
Torrance, California 90501-1724

Dennis P. Stocker,‡ David F. Vaughan,†† and Liming Zhou**
NASA Lewis Research Center
Cleveland, Ohio 44135

and

Raymond B. Edelman§
Rockwell International Corporation
Rocketdyne Division
Canoga Park, California

Introduction

Gas jet diffusion flames have been a subject of research for many years. However, a better understanding of the physical and chemical phenomena occurring in these flames is still needed, and, while the effects of gravity on the burning process have been observed, the basic mechanisms responsible for these changes have yet to be determined. The fundamental mechanisms that control the combustion process are in general coupled and quite complicated. These include mixing, radiation, kinetics, soot formation and disposition, inertia, diffusion, and viscous effects. In order to understand the mechanisms controlling a fire, laboratory-scale laminar and turbulent gas-jet diffusion flames have been extensively studied, which have provided important information in relation to the physico-chemical processes occurring in flames. However, turbulent flames are not fully understood and their understanding requires more fundamental studies of laminar diffusion flames in which the interplay of transport phenomena and chemical kinetics is more tractable. But even this basic, relatively simple flame is not completely characterized in relation to soot formation, radiation, diffusion, and kinetics. Therefore, gaining an understanding of laminar flames is essential to the understanding of turbulent flames, and particularly fires, in which the same basic phenomena occur. Figures 1 and 2 show, respectively, the processes occurring in a laminar jet diffusion flame and the three regimes of flames (i.e., laminar, transitional, and turbulent). In order to improve and verify the theoretical models essential to the interpretation of data, the complexity and degree of coupling of the controlling mechanisms must be reduced. If gravity is isolated, the complication of buoyancy-induced convection would be removed from the problem. In addition, buoyant convection in normal gravity masks the effects of other controlling parameters on the flame. Therefore, the combination of normal-gravity and microgravity data would provide the information, both theoretical and experimental, to improve our understanding of diffusion flames in general, and the effects of gravity on the burning process in particular.

---

* Paper presented at the Second International Workshop on Combustion Science in Microgravity, September 15-17, 1992, Cleveland, Ohio. This work is supported by NASA Lewis Research Center under Contracts NAS3-22822 ("Effects of Buoyancy on Laminar Gas Jet Diffusion Flames," End Date: April 1, 1992) and NAS3-25982 ("Gravitational Effects on Transitional and Turbulent Gas Jet Diffusion Flames," Start Date: November 11, 1991) with Science Applications International Corporation.

† Senior Scientist, Author for Correspondence; 21151 Western Avenue, Torrance, CA, 90501-1724.

‡ NASA Project Scientist.

†† Research Assistant, Baldwin-Wallace College, Berea, Ohio.

** Post-Doctoral Resident Research Associate from University of California, Berkeley.

§ Co-Investigator, formerly of Science Applications International Corporation.

The overall objective of this effort is to gain a better fundamental understanding of the behavior and characteristics of gas-jet diffusion flames in the absence of buoyancy. Diffusion flames are selected because they are easy to control, and embody mechanisms important in many combustion processes such as fires and practical combustion systems. The specific objectives of these microgravity studies are to characterize the transient phenomena of flame development following ignition, steady-state flame behavior, effects of soot, radiative characteristics, and if any, extinction phenomena. These objectives are being accomplished through measurements of the microgravity flame size and development, observations on flame color and luminosity, temperature measurements, global and local flame-radiation measurements, and species measurements. In addition, the tests provide the effects of buoyancy as well as Reynolds number, nozzle size, fuel reactivity and fuel type, oxygen concentration, pressure, and other global characteristics of gas-jet diffusion flames over the entire range of laminar, transitional, and turbulent regimes. Comparisons are also being made with the characteristics of the normal-gravity counterparts of these flames to determine the effects of buoyancy on these jet diffusion flames. Analytical and numerical studies are also underway to provide comparisons between the measured and predicted flame phenomena.

In the following sections, we present the experimental and theoretical efforts conducted to date, in addition to the important findings of this program. More information is available from the cited references [1-10]. For a comprehensive review of the past efforts on laminar diffusion flames, see [1].

Experimental Effort

Tests on laminar diffusion flames of methane and propane were conducted in the 2.2-Second Drop Tower and the 5.18-Second Zero-Gravity Facility of the NASA Lewis Research Center. The oxidizing environment consisted of 15% to 50% oxygen in nitrogen at pressures of 0.5 to 1.5 atm. In addition, a preliminary series of tests were conducted in the KC-135 research aircraft. Various nozzle sizes (0.051 to 0.0825 cm in radius) and volume flow rates (1.0 to 5.0 cc/sec for methane and 0.3-1.5 cc/sec for propane) were used. The jet Reynolds numbers for the laminar phase of these studies were in the range of 20-200, based on the nozzle radius and fuel properties.

The 2.2-second tests [2, 4, 6] were conducted to obtain information on the laminar-flame behavior and characteristics, and to define the matrix for the longer-duration, 5.18-second tests. The flames were ignited in microgravity.

Figure 3 shows a schematic of the hardware for the 5.18-second tests [3, 7, 9]. The experimental chamber had a volume of 0.087 m^3. Two movie cameras recorded the laminar flame development and behavior. A wide-view-angle, thermopile-detector radiometer was used to measure the global flame radiation over the range of 0.2-9.0 μm. During the drop, a 3x3 rake of thermocouples measured the temperature both inside and outside the flame at fixed locations.

In the KC-135 tests, both attached and free-float configurations of the package were used, and flame visualization through photography was conducted.

Tests are currently underway [e.g., 10] in the 2.2-Second Drop Tower for studying high-Reynolds-number laminar flames in addition to transitional and turbulent flames of methane, ethylene, ethane, propylene, and propane to obtain the effects of fuel type and Reynolds number, as well as observations of blow-off and other features of these flames. Nozzle sizes are in the range of 0.025 to 0.050 cm in radius. The flames are studied in air at ambient pressure. Flame radiation, temperature, and species measurements are planned, in addition to future tests in the 5.18-Second Zero-Gravity Facility and the KC-135 aircraft.

Theoretical Studies

An analytical model was developed for transient, axisymmetric laminar diffusion flames in the absence of buoyancy [5]. The model incorporated the effects of axial diffusion, and was an extension of the classical model for gas-jet diffusion flames. In addition, a comprehensive numerical model which incorporated the effects of gravity, diffusion, inertia, viscosity, combustion, multi-component diffusion, and radiation, was upgraded and utilized for comparisons with the laminar-flame data. The model is steady-state and two-dimensional (rectangular or cylindrical), with the partial differential equations for mass, momentum, energy, and species in their boundary-layer form. The governing equations are solved using an explicit finite-difference scheme. Details of the flow field including velocity, temperature, and species fields, radiative contributions, flame shape and dimensions, and other characteristics of the flame are predicted and compared with experimental results [e.g., 4].

In addition, a numerical model for turbulent flames is currently under development which incorporates the effects of buoyancy on both mean flow and generation of turbulent kinetic energy (manifested through the correlation of velocity and temperature fluctuations). Also, analytical models are being developed for the effects of disturbances and associated vortex interactions with flame front to better characterize the behavior of transitional and turbulent diffusion flames under microgravity conditions.

In the following sections, some of the important findings of this program on diffusion flames are presented. The first section presents the observations, experimental data, and predictions for laminar diffusion flames. In the second section, the results obtained to date on the transitional and turbulent flames are presented. The efforts have shown unique and unexpected phenomena in microgravity diffusion flames.

Laminar Diffusion-Flame Data and Analysis

Laminar diffusion flames of hydrocarbons under microgravity conditions have shown distinct characteristics relative to normal-gravity flames [1]. Flames are taller (up to twice), rather globular (up to four times in diameter), and sootier in microgravity. This is due to the significant reduction in the buoyant force, which makes diffusion the dominant mechanism of transport. As a result, increased residence time, enhanced soot formation, radiative cooling due to the larger flame size, and the possible onset of a chemical-kinetics limitation on the heat-release process are responsible for the very different characteristics of these flames compared to those in normal gravity. Under the influence of buoyancy, the flame is pencil-like due to the steep gradients of oxygen, which is caused by buoyant convection and associated entrainment. These flames are generally yellow due to soot emission and burn-off. In addition, normal-gravity flames burning in quiescent oxidizing environments flicker with a frequency of 10-20 Hz due to hydrodynamic instability. Under microgravity conditions, flame flicker disappears, the flame becomes larger, and shows colors ranging from orange to red to entirely blue, depending on the fuel, pressure, and composition of the oxidizing atmosphere. In addition, absence of buoyancy makes the gradients of oxygen much more shallow compared to those in normal gravity. The continuous formation and accumulation of the combustion products at the microgravity flame front which are transported primarily by diffusion with some contribution from the initial (and rapidly decreasing) jet momentum are responsible for a larger microgravity flame. This process dramatically affects flame radiation, soot behavior, residence time, flow field characteristics (such as temperature, velocity, and species distributions), fuel pyrolysis, approach to steady state, and (possibly) even kinetics.

Figure 4 shows laminar methane and propane diffusion flames under both normal-gravity and microgravity conditions. As mentioned before, microgravity environment has a strong effect on these flames where, for example, the color, size, and other features of the flame are affected. The yellow, luminous zone indicates the thermal emission of burning carbon particles. This luminous zone becomes orange, then red, and finally, dark red toward the boundary of the visible region, as the temperature of the unburned soot decreases. The orange/reddish color of the flame in microgravity is due to the soot at cooler temperatures that would be expected for typical burn-off conditions. The normal-gravity flames of methane and propane show similar characteristics such as flame flicker and a luminous yellow color due to buoyancy. However, the microgravity flames are completely different. The methane flame shows a closed tip whereas the propane flame has an open tip with quenched soot escaping through the tip. This underventilated-like behavior is attributed to the effects of pyrolysis, soot formation and quenching, extensive radiative loss, and possible thermophoretic effects.

Microgravity tests have shown that laminar flames need longer time to reach their near-steady state compared to the flames in normal gravity. In the presence of buoyancy, times of the order of 0.5 second are needed for the flame to establish and reach steady state following ignition. In microgravity, due to the lack of entrainment caused by buoyancy, the flame needs longer time (as shown in Figure 5) for approach toward steady state. The accumulation and slow transport of the combustion products in the absence of buoyancy contributes to this transient flame development.

Pressure and oxygen concentration effects are much more significant in microgravity than in normal gravity. Laminar flame characteristics, color, luminosity, sooting behavior, and as will be seen later, radiation are strongly affected by various combinations of pressure and oxygen concentration in the environment of the microgravity flame. Sooting was eliminated at 18% O_2 - 0.5 atm, and the flames were weak, entirely blue and soot-free, whereas their normal-gravity counterparts were yellow, luminous, and very similar to normal-gravity flames under atmospheric, or even high-pressure/high-oxygen-concentration conditions. This has an impact on fire detection in microgravity environments. For example, particulate detectors may not respond to blue, non-sooting flames in low gravity. Figure 6 shows a blue microgravity flame typical of low-pressure/ low-oxygen-concentration flames. Massive

sooting has been observed at high oxygen concentrations in microgravity flames. Figure 7 shows a propane flame with 30% oxygen in the environment. Although the flame is stronger in luminosity compared to lower-oxygen microgravity flames, still soot quenching and breakthrough at the tip has been observed, even at 50% oxygen which showed a column of quenched soot emerging through the tip. Figure 8 shows the effects of oxygen concentration on methane flame heights in microgravity and normal gravity. In general, the lower the oxygen concentration, the taller the flame, with a stronger effect in microgravity flames, as predicted.

Figures 9 and 10 show microgravity laminar flame heights of propane burning in air at different pressures and Reynolds numbers. It appears from this data that the flame height correlates linearly with Reynolds number, but reaches an apparent minimum between 0.5 atm and 1.5 atm. The flame height in all of these tests was based on the location where red soot changes color into dull red, indicating local flame extinction. Experimental studies [11] have shown that soot ceases to burn near 1300 K. The red to dull-red transition seems to roughly correspond to this temperature. The non-monotonic behavior of flame height with pressure may be attributed to the competitive, oxygen- and pressure-dependent rates of fuel pyrolysis and particle inception, agglomeration and burn-off. Figure 11 shows the soot quench length (red region at the flame tip) as a function of pressure and Reynolds number.

Tests conducted in the 5.18-Second Zero-Gravity Facility have shown that radiative loss from microgravity laminar flames is approximately an order of magnitude larger than the corresponding normal gravity flames. This is primarily due to the accumulation of the combustion products, as well as larger flame size and increased soot. Figure 12 shows a typical set of data (in mV) for flame radiation in both normal-gravity and microgravity environments. Examination of the data also shows that radiation does not reach steady state (unlike the normal-gravity flame) in 5 seconds of microgravity. This is due to the accumulation and slow transport of combustion products (particularly water vapor and carbon dioxide) in the vicinity of the flame. Visualization of these flames (through photography) has shown that the flame does not appear to significantly increase in size with time near the end of the drop test. However, the diffusion of non-luminous hot gases in the surrounding causes the volume of the gas to increase, which is reflected through the continuous increase in radiation. This has a direct impact on the approach toward quasi-steady-state in microgravity flames. Figure 13 shows the effects of fuel volume-flow rate (i.e., Reynolds number for fixed nozzle diameter) on flame radiation. The figure also shows that because in normal gravity, a large fraction of heat release is removed via the convection of hot products of combustion, the contribution of energy loss due to radiation from the flame is reduced. In microgravity, practically all of the released heat is accumulated around the flame through the combustion products, causing radiative losses of up to an order of magnitude higher compared to normal-gravity condition.

Pressure and oxygen concentration also show a significant effect on radiative loss in microgravity. Figure 14 shows radiation from methane flames under different conditions of pressure and oxygen level. The normal-gravity data show little sensitivity to the environmental condition, whereas radiation levels from microgravity flames are strongly affected by pressure and oxygen concentration. The results have also shown that low-pressure/low-oxygen-concentration flames in microgravity (which are entirely blue, unlike those in normal gravity) approach near-steady-state levels of radiation by the end of the available 5 seconds of microgravity. However, high-pressure/ high-oxygen-concentration flames show a continuous increase in radiative loss throughout the drop period, and do not reach steady state in the available time. Also, blue microgravity flames, which are apparently soot-free, have shown appreciable amounts of radiation, indicating that contributions from the water vapor and carbon dioxide bands are quite significant. These experiments represent the first time flame radiation was measured in microgravity environments.

Figure 15 shows the results of temperature measurements for a typical flame in both normal-gravity and microgravity environments. The position of the thermocouple rake with respect to the flame is also shown. The microgravity flame shape in this figure corresponds to the condition prior to the deceleration of the package. The initial overshoot in the data is due to the presence of excess fuel at ignition. The normal-gravity data show that the temperature drops quickly to the ambient value immediately outside the flame front between radial locations of 0.75 and 2.75 cm. This is due to entrainment. In addition, the strong buoyancy-driven portion of the flame causes the three thermocouples near the centerline to show roughly equal temperatures, which essentially reach steady state approximately 3 seconds after the start of the experiment. However, the microgravity data show that far above and away from the flame, the gas is still experiencing a temperature rise. This figure also shows that the gas temperature does not reach a steady value anywhere in the field during the 5 seconds of microgravity, again due to the continuous dilution and heating of the environment caused by the combustion products. In addition, large temperature gradients are observed in the axial direction for the microgravity flame, and the variation of temperature in the radial direction is significant all the way to the far field. The data suggest that although the flame appeared to have reached steady state (verified through visualization), 5 seconds of microgravity is not sufficient to obtain information on the flame structure, since the field is approaching steady state but is still changing in the available time of 5 seconds.

The modeling effort has been an ongoing development process aided by these experiments, and has proven to be a critically important element contributing to the interpretation of experimental results. Figure 16 shows a comparison between the measured and predicted microgravity flame heights for a series of fuels. Figure 17 shows the centerline velocity as a function of axial distance for different gravity levels, using the numerical model discussed previously. As seen in this figure, under microgravity condition, the gas velocity is highest at the nozzle exit and drops immediately upon expansion of the jet in the absence of buoyancy. The normal-gravity flame shows a significant increase in the centerline velocity due to the influence of buoyancy and the behavior of the streamlines. The intermediate gravitational levels show that the effects of buoyancy become negligible at 10^{-4} g. Figure 18 shows the predicted flame heights as a function of gravity level and their comparison with the available normal-gravity and microgravity flame height measurements. The results are in excellent agreement, and again, it is shown that effects of buoyancy are not important for jet diffusion flames for gravity levels less than 10^{-4} g. Figure 19 shows the predicted shapes of these flames. Figure 20 shows the predicted radial distribution of the axial velocity at two heights (near the middle and the tip of the flame) as a function of gravitational level. The significant effect of buoyancy appears in this figure, in addition to the observation that the tip of the microgravity flame is almost at stagnation. The comparisons of predictions with data are quite encouraging. As data becomes available on other parameters, comparisons of theory with these data will further substantiate the accuracy of the theoretical model being developed.

Transitional/Turbulent Diffusion-Flame Data and Analysis

The investigation of microgravity laminar jet diffusion flames is currently being extended to transitional and turbulent regimes. Several important and unexpected results have already been obtained on this new effort.

The behavior of gas-jet diffusion flames in normal gravity as a function of the fuel Reynolds number was shown in Figure 2. In the laminar regime, the variation of flame height is linear with Reynolds number (or fuel volume flow rate) for a fixed tube diameter. As the Reynolds number increases, the laminar flame undergoes a transitional behavior, in which, instabilities start to develop at the tip of the flame with a brush-type characteristic, and the flame height starts to decrease due to enhanced mixing (see Figure 2). As the Reynolds number is further increased, the boundary of the brush-type region moves upstream, and results in further reduction of flame height. A Reynolds number is finally reached at which the entire flame is fully turbulent and the height no longer changes with increase in jet momentum (see Figure 2). Further increase in Reynolds number will ultimately lead to blow-off. This overall behavior is shifted to larger flame heights with increasing tube diameter, and the blow-off limit also moves to higher Reynolds numbers.

In order to study the effects of microgravity on the different regimes of jet diffusion flames, tests were conducted in the 2.2-Second Drop Tower with propane and propylene flames; tests for other fuels such as methane, ethane and ethylene are underway.

Figure 21 shows the variation of flame height with (cold jet) Reynolds number for propane/air diffusion flames. The normal-gravity flames of the laminar regime show a linear variation of height with Reynolds number, as is expected from the classical behavior. These flames flicker due to hydrodynamic instability, as discussed before, and the flicker range increases with increasing jet momentum. The laminar flames are generally yellow with a small blue base. As the jet momentum increases, the (average) flame height undergoes a transitional regime with a dip which is not a characteristic of typical transitional flames [12]. However, other studies [e.g., 13] have shown that relatively low-momentum flames exhibit this type of behavior and, indeed, the flame height in the turbulent regime can be larger than that in the transitional regime. As the normal-gravity laminar flame goes through transition, lift-off beings, and a large blue base is formed followed by a yellow brush-type flame which both flickers and wavers from side to side. This behavior persists throughout the turbulent regime. Blow-off occurs somewhere near Re = 6,000.

The microgravity flames, on the other hand, show significantly different behavior compared to those in normal gravity. In the laminar regime, the flame is flicker-free, and as discussed before, is much wider than the normal-gravity flame, has an open tip with flame colors changing from blue at the base to yellow, then orange, then red and finally dark red toward the flame tip. The flame color and shape indicate soot quenching and its subsequent escape through the tip, which resembles an underventilated-type behavior. However, as the jet momentum increases toward the transitional regime, the width of the flame tip decreases. In addition, the gap between the microgravity and (average) normal-gravity flame heights increases with increasing Reynolds number. The microgravity flames of Figure 21 show a monotonic flame height variation, indicating that transition from the laminar to turbulent regime may occur quite smoothly, unlike the classical normal-gravity behavior. However, somewhere in the transition

regime, the flame tip closes, and large-scale, slow-moving structures develop which do not look like a brush-type behavior, as in the normal-gravity flames, but rather a wrinkled structure. The flame lifts off the nozzle tip, although the stand-off distance is almost half of that for the normal-gravity flame. Tip flicker was not observed for any of the microgravity flames. The flame slowly increases in height up to a Reynolds number of 4400, and then increases further in height, where the tip of the flame unfortunately falls out of the camera field of view. It is anticipated (as discussed later) that the height will increase in this region with increasing Reynolds number. The microgravity flame height in this regime is almost twice that of the corresponding normal-gravity flame.

Figure 22 shows the behavior of propylene flames under both normal-gravity and microgravity conditions. The (average) normal-gravity height shows the typical classical behavior, similar to Figure 21. The microgravity flame did not drop in height in the transition regime, and again, beyond a Reynolds number of approximately 4400, the flame tip fell outside the camera field of view.

Figure 23 shows the shapes of microgravity and normal-gravity propylene flames in both low- and high-Reynolds-number laminar regimes. In addition, it shows the shapes of transitional and fully developed turbulent flames of normal gravity, and their corresponding microgravity flames. Careful examination of these flames has revealed fundamental differences between the flames of microgravity and those in normal gravity. Under normal gravity, as discussed before, transition is initiated at the tip of the flame and, with increase in Reynolds number, the instability moves downward closer to the flame base. However, in microgravity, transition initiates with the appearance of disturbances that form at the base of the flame and are convected downstream. These disturbances are intermittent in nature, that is, during the 2.2-second available time and at a critical transition Reynolds number, only one disturbance is observed which is convected along the flame boundary and moves toward the flame tip. At a slightly higher Reynolds number, two or three of these disturbances appear during the 2.2-second time, and in between successive disturbances, the flame is completely laminar in nature (i.e., undisturbed). As the jet Reynolds number increases, the frequency of occurrence of the disturbances also increases, until a train of disturbances (with a measured frequency of occurrence of approximately 15 Hz) is formed in the region which corresponds to the normal-gravity turbulent regime.

The differences between normal-gravity and reduced-gravity transition of diffusion flames arise due to the strong influence of buoyancy on the flow field under normal-gravity conditions. With gravity, the flow exiting the nozzle is accelerated, whereas without gravity, the velocity drops with downstream. The numerical model described previously shows that this behavior is indeed related to the velocity field. The predicted centerline velocities for typical normal-gravity and microgravity flames were shown in Figure 17. The velocity in the normal-gravity flame attains its maximum value at the tip of the flame due to the influence of buoyancy, resulting in convergence of streamlines. In microgravity, the maximum velocity is the jet exit velocity, which then drops sharply due to the expansion of the gas caused by the absence of buoyancy. Therefore, instability initiates at the tip of the normal-gravity flame and at the base of the microgravity flame due to this behavior in the velocity field.

The results shown in Figures 21 and 22 also indicate that the transitional behavior of the microgravity flames may be extended well beyond the critical range of Reynolds numbers associated with the normal-gravity flames. In normal gravity, the transition to fully developed turbulent regime is accelerated due to the presence of buoyancy generated turbulence. However, in microgravity, the flame does not have any kinetic energy source associated with buoyancy. As a result, transition to turbulence may occur over a substantially longer range of Reynolds number. It is quite possible that at sufficiently high jet Reynolds numbers, the microgravity flame will ultimately have characteristics identical to a fully developed turbulent flame in normal gravity. In addition, due to the reduction in flame stand-off distance in microgravity, it is possible that the flame may show a higher blow-off Reynolds number compared to that in normal gravity. Quantifying these phenomena in addition to the other characteristics of transitional and turbulent jet diffusion flames in microgravity represents the focus of this research.

Conclusions and Future Plans

The studies conducted to date in this program have provided unique and new information on the behavior and characteristics of gas jet diffusion flames in microgravity environments. Significant differences have been observed between the normal-gravity flames and those under reduced-gravity conditions. The goal of this research is to extend these observations in order to fully characterize the influences of buoyancy on the structure of, and physico-chemical processes occurring in, microgravity gas jet diffusion flames over the entire range of laminar, transitional, and turbulent regimes.

References

1. Edelman, R. B. and Bahadori, M. Y., "Effects of Buoyancy on Gas-Jet Diffusion Flames," Acta Astronautica, Vol. 13, No. 11/12, pp. 681-688, 1986.

2. Bahadori, M. Y. and Stocker, D. P., "Oxygen-Concentration Effects on Microgravity Laminar Methane and Propane Diffusion Flames," Paper presented at the Eastern States Meeting of The Combustion Institute, Albany, New York, October/November 1989.

3. Bahadori, M. Y., Edelman, R. B., Sotos, R. G., and Stocker, D. P., "Measurement of Temperature in Microgravity Laminar Diffusion Flames," Paper presented at the Eastern States Meeting of the Combustion Institute, Orlando, Florida, December 1990.

4. Bahadori, M. Y., Edelman, R. B., Stocker, D. P., and Olson, S.L., "Ignition and Behavior of Laminar Gas-Jet Diffusion Flames in Microgravity," AIAA Journal, Vol. 28, No. 2, pp. 236-244, 1990.

5. Bahadori, M. Y., "An Analytical Solution for Transient, Cylindrically Symmetric Laminar Diffusion Flames in the Absence of Buoyancy," Paper presented at the Central States Meeting of The Combustion Institute, Cincinnati, Ohio, May 1990.

6. Bahadori, M. Y., Stocker, D. P., and Edelman, R. B., "Effects of Pressure on Microgravity Hydrocarbon Diffusion Flames," Paper AIAA-90-0651, AIAA 28th Aerospace Sciences Meeting, Reno, Nevada, January 1990.

7. Bahadori, M. Y., Edelman, R. B., Sotos, R. G., and Stocker, D. P., "Radiation from Gas-Jet Diffusion Flames in Microgravity Environments," Paper AIAA-91-0719, AIAA 29th Aerospace Sciences Meeting, Reno, Nevada, January 1991.

8. Bahadori, M. Y. and Edelman, R. B., "Combustion of Gaseous Fuels Under Reduced-Gravity Conditions," Paper LB-038, in press in Proceedings of The Second Symposium on Lunar Bases, Lunar and Planetary Institute, Houston, Texas, 1992.

9. Bahadori, M. Y., Edelman, R. B., Stocker, D. P., Sotos, R. G., and Vaughan, D. F., "Effects of Oxygen Concentration on Radiative Loss from Normal-Gravity and Microgravity Methane Diffusion Flames," Paper AIAA-92-0243, AIAA 30th Aerospace Sciences Meeting, Reno, Nevada, January 1992.

10. Bahadori, M. Y., Vaughan, D. F., Stocker, D. P., Weiland, K. J., and Edelman, R. B., "Preliminary Observations on the Effects of Buoyancy on Transitional and Turbulent Diffusion Flames," Paper presented at the Central States Meeting of The Combustion Institute, Columbus, Ohio, April 1992.

11. Kent, J. H. and Wagner, H. Gg., Combustion Science and Technology, Vol. 41, pp. 245-269, 1984.

12. Hottel, H. C. and Hawthorne, W. R., Third Symposium on Combustion, pp. 254-266, Williams and Wilkins Co., Baltimore, 1949.

13. Wohl, K., Gazley, C., and Kapp, N., Third Symposium on Combustion, pp. 288-300, Williams and Wilkins Co., Baltimore, 1949.

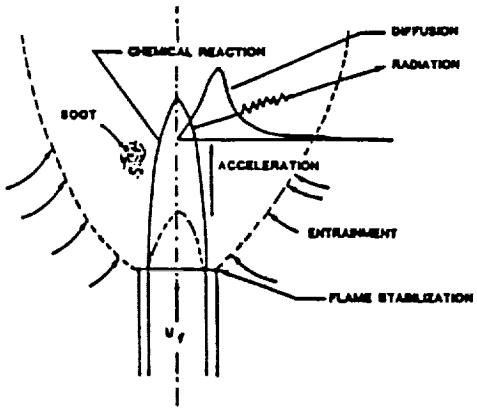

Figure 1.— Schematics of a laminar gas jet diffusion flame in normal gravity.

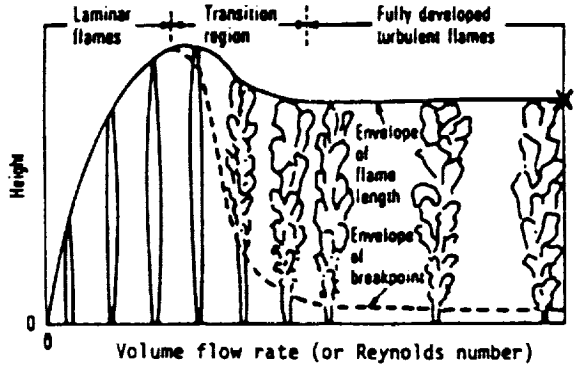

Figure 2.— Change in flame height and behavior with increase in volume flow rate for a gas jet diffusion flame in normal gravity; x indicates blow-off.

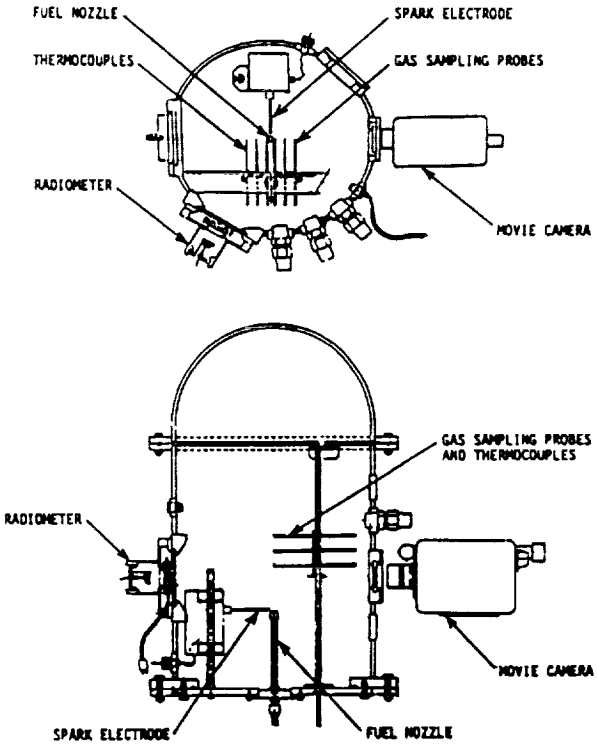

Figure 3.— Schematics of the experiment package for the 5.18-second tests.

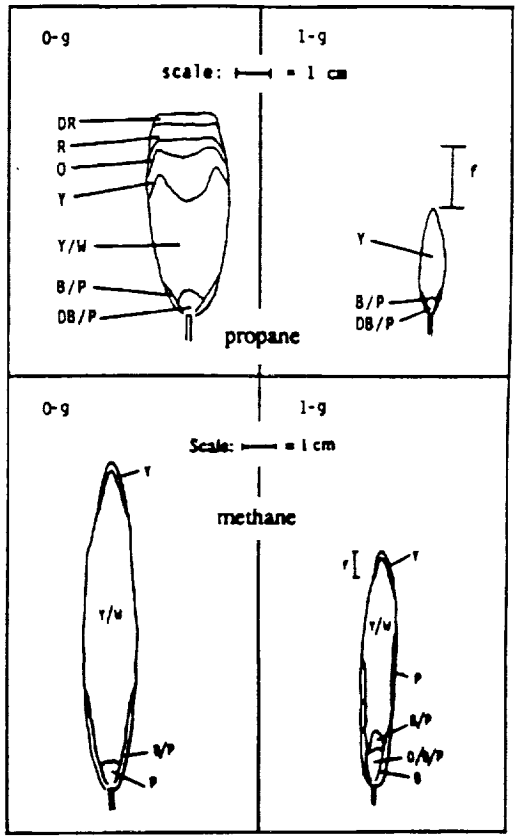

Figure 4.— Typical normal-gravity and microgravity flames of methane and propane in the laminar regime; nozzle radius = 0.048 cm for methane and 0.0825 cm for propane; volume flow rate = 5.25 cc/sec for methane and 1.0 cc/sec for propane; air at 1 atm is the oxidizer. The bars show the range of normal-gravity flame flicker (f). The various colors indicated in the diagram are as follows: B (blue), D (dark), DB (dark blue), DP (dark pink), O (orange), P (pink), R (red), W (white), and Y (yellow); reproduced from [2] and [7].

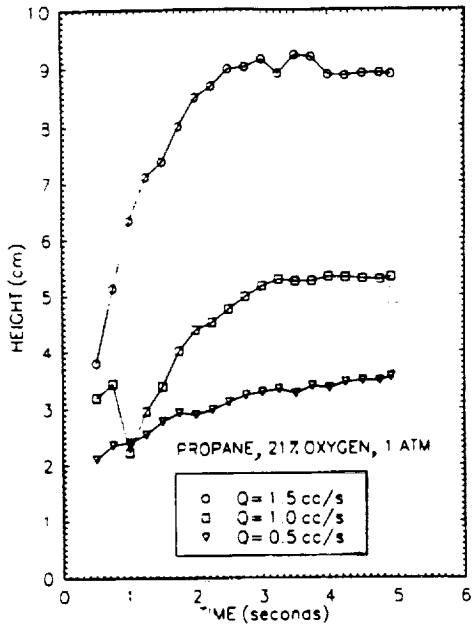

Figure 5.— Ignition and development of a series of microgravity propane diffusion flames.

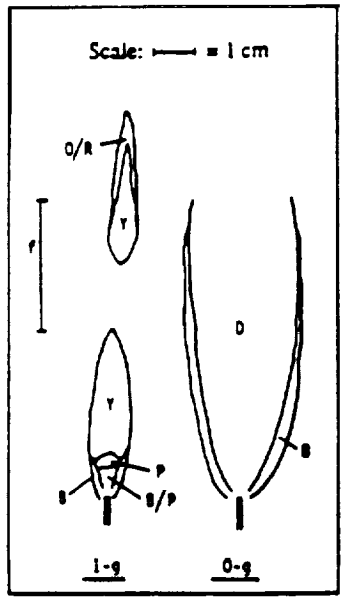

Figure 6.— Effects of low oxygen concentration on a laminar propane diffusion flame; 18% oxygen, 1.0 atm, volume flow rate = 1 cc/sec, and nozzle radius = 0.074 cm; for the definition of colors, see Fig. 4; f is the normal-gravity flicker range; reproduced from [2].

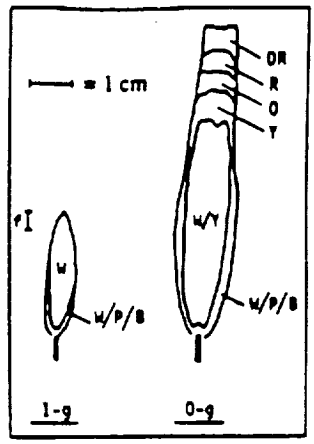

Figure 7.— Effects of high oxygen concentration on a laminar propane diffusion flame; 30% oxygen, 1 atm, volume flow rate = 1 cc/sec, and nozzle radius = 0.048; see Fig. 4 for the definition of colors; f is the flicker range; reproduced from [2].

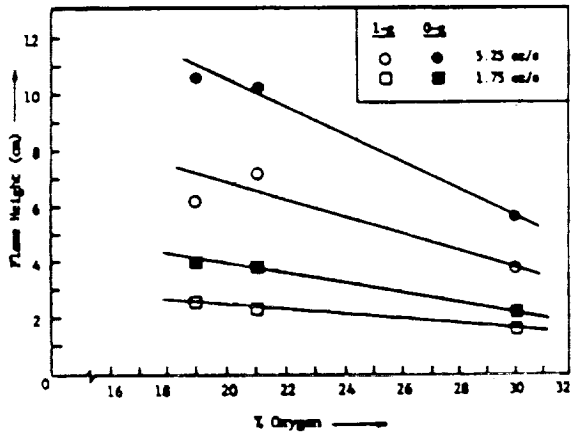

Figure 8.— Effects of oxygen concentration on methane diffusion flames at 1 atm; nozzle inner radius = 0.048 cm and P = 1 atm; reproduced from [2].

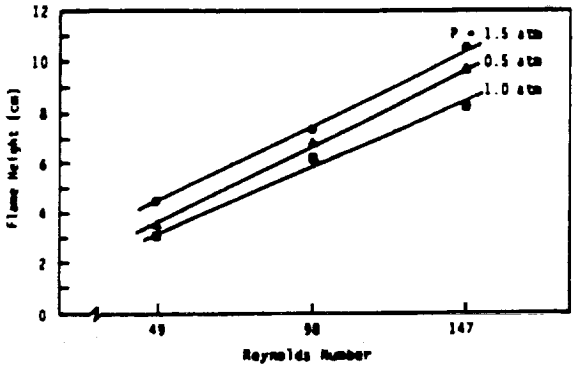

Figure 9.— Microgravity propane-air flame heights vs. Reynolds number for different pressures; reproduced from [6].

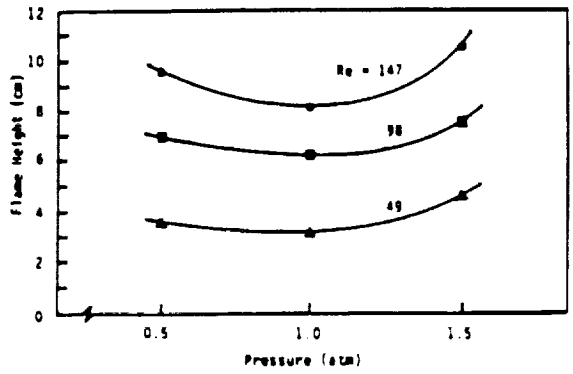

Figure 10.— Microgravity propane-air flame heights vs. pressure for different Reynolds numbers; reproduced from [6].

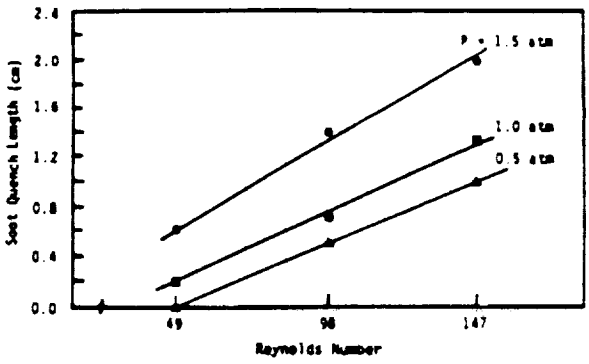

Figure 11.— Soot quench length vs. jet Reynolds number as a function of pressure for microgravity propane air flames; reproduced from [6].

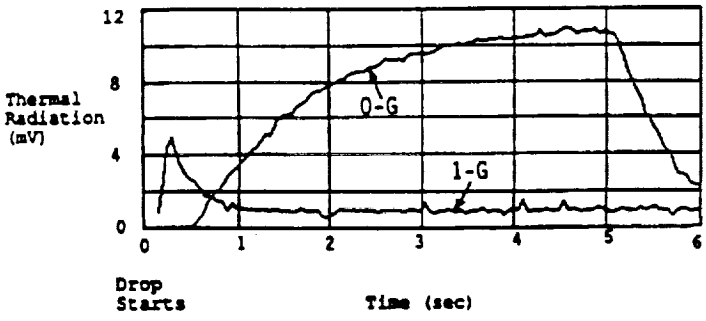

Figure 12.— Radiometer response from a propane flame burning in quiescent air at 1 atm; flow rate = 1.5 cc/sec and nozzle radius = 0.0825 cm; reproduced from [7].

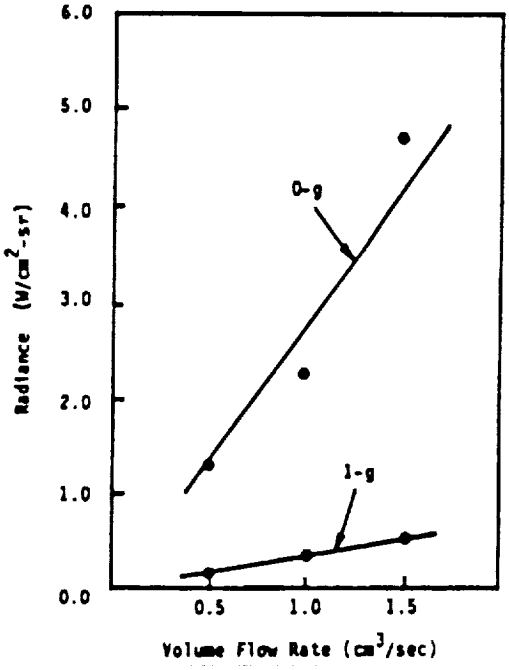

Figure 13.— Effects of fuel flow rate on radiation from laminar propane-air diffusion flames at 1 atm. The radiation data for microgravity flames are the average values between 4.0 and 5.0 seconds after ignition; reproduced from [7].

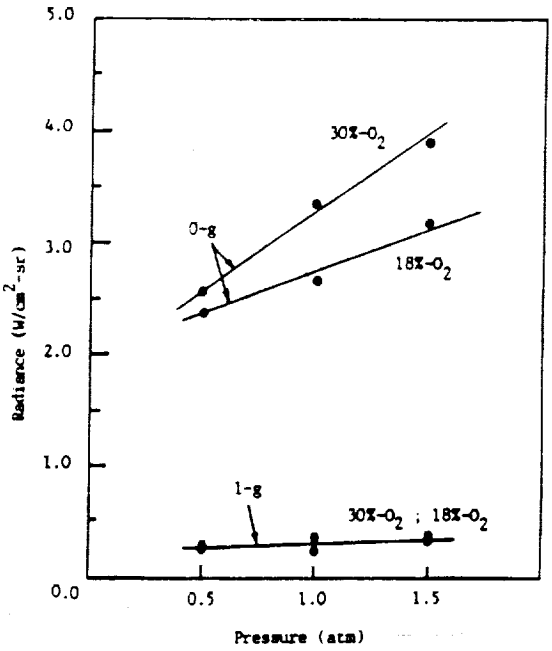

Figure 14.— Effects of oxygen concentration and pressure on radiative loss from methane flames at a fixed mass flow rate (corresponding to 3 cc/sec at 1 atm); nozzle radius = 0.0825 cm.

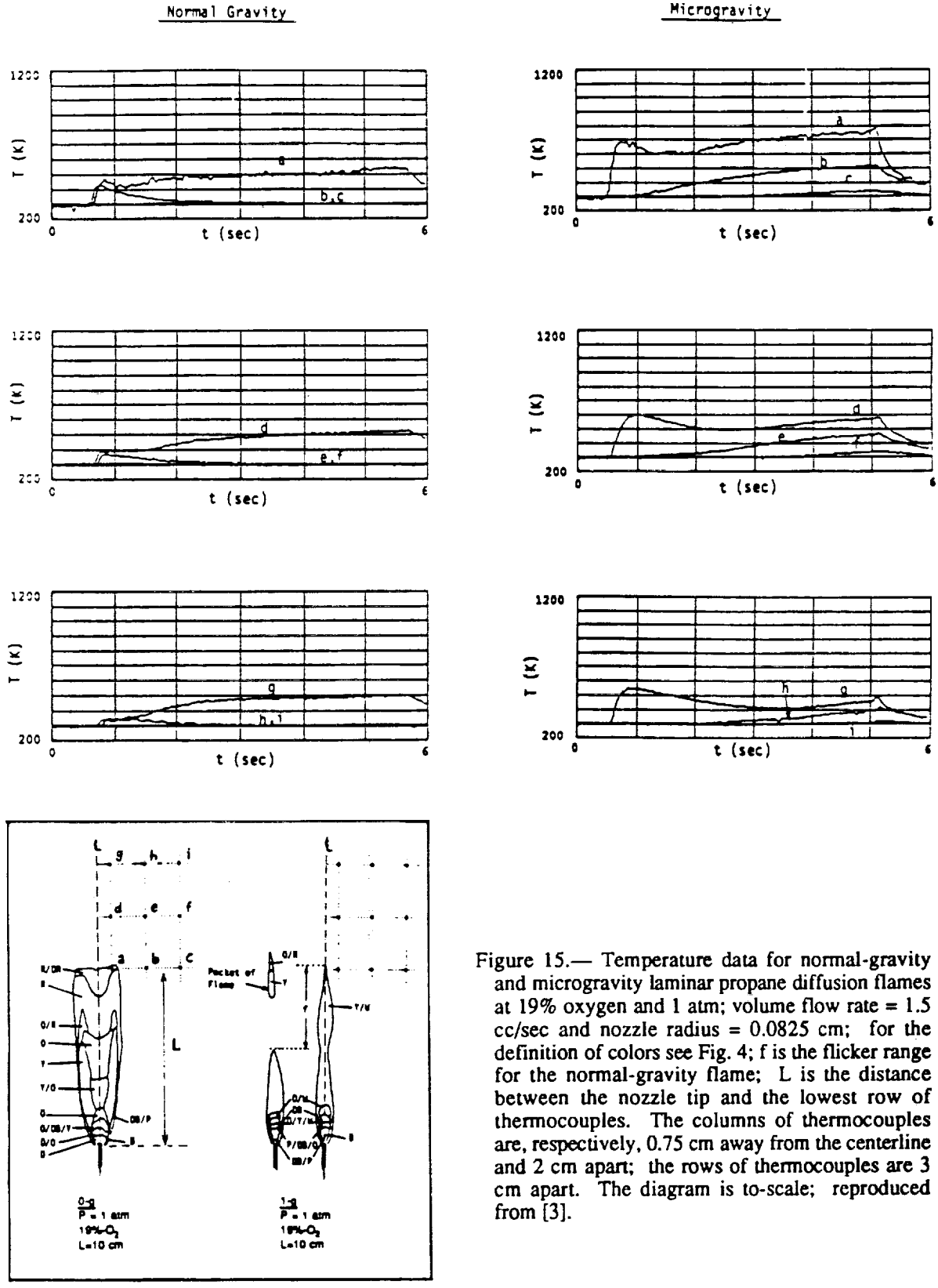

Figure 15.— Temperature data for normal-gravity and microgravity laminar propane diffusion flames at 19% oxygen and 1 atm; volume flow rate = 1.5 cc/sec and nozzle radius = 0.0825 cm; for the definition of colors see Fig. 4; f is the flicker range for the normal-gravity flame; L is the distance between the nozzle tip and the lowest row of thermocouples. The columns of thermocouples are, respectively, 0.75 cm away from the centerline and 2 cm apart; the rows of thermocouples are 3 cm apart. The diagram is to-scale; reproduced from [3].

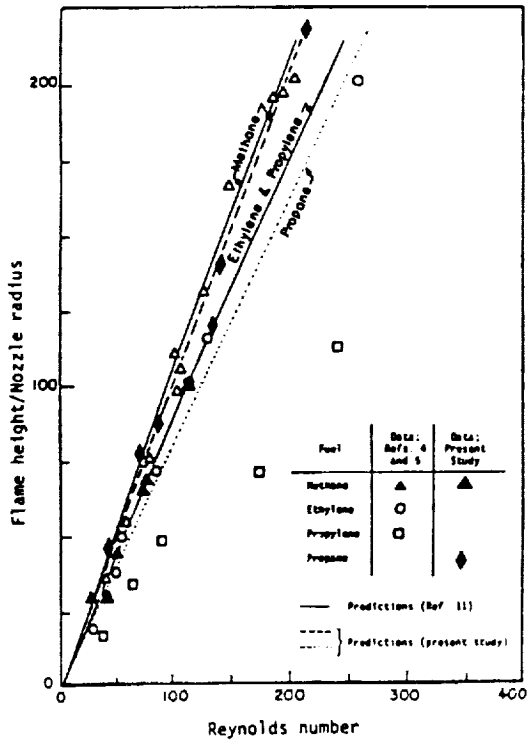

Figure 16.— Measured and predicted microgravity flame heights for different fuels; for the references cited in this figure, see [4].

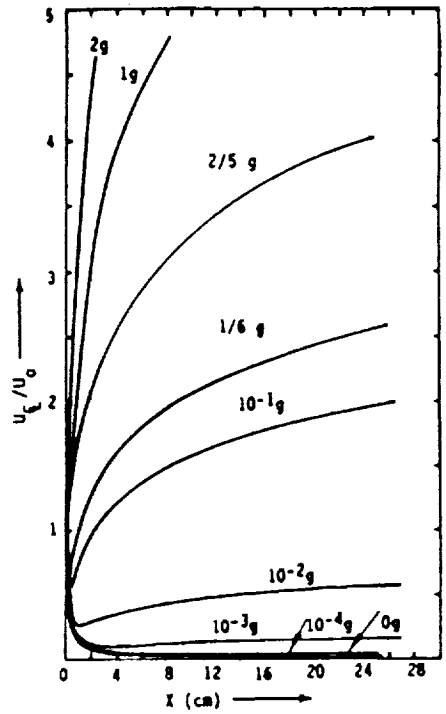

Figure 17.— Predicted non-dimensional centerline velocity (with respect to jet exit velocity) vs. axial distance along the jet; methane/air flames; nozzle radius = 0.0825 cm, fuel flow rate = 1 cc/sec, pressure = 1 atm; reproduced, with modifications, from [1].

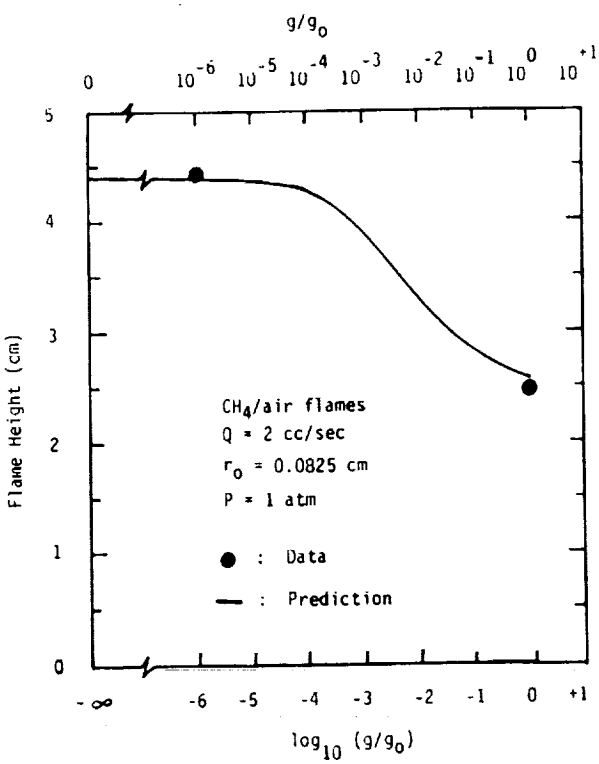

Figure 18.— Predicted flame height as a function of gravity level and comparisons with experimental data; methane-air flames, volume flow rate = 2 cc/sec, nozzle radius = 0.0825 cm, P = 1 atm.

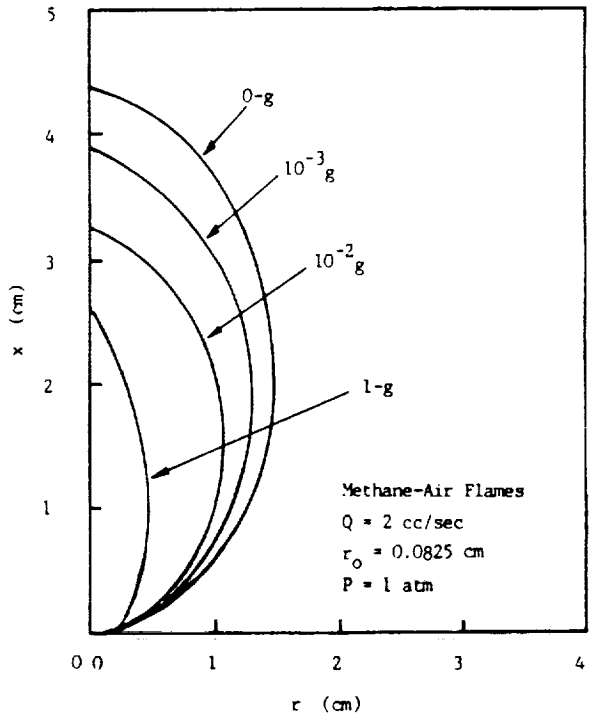

Figure 19.— Predicted flame shapes as a function of gravity level; methane-air flames, volume flow rate = 2 cc/sec, nozzle radius = 0.0825 cm, P = 1 atm.

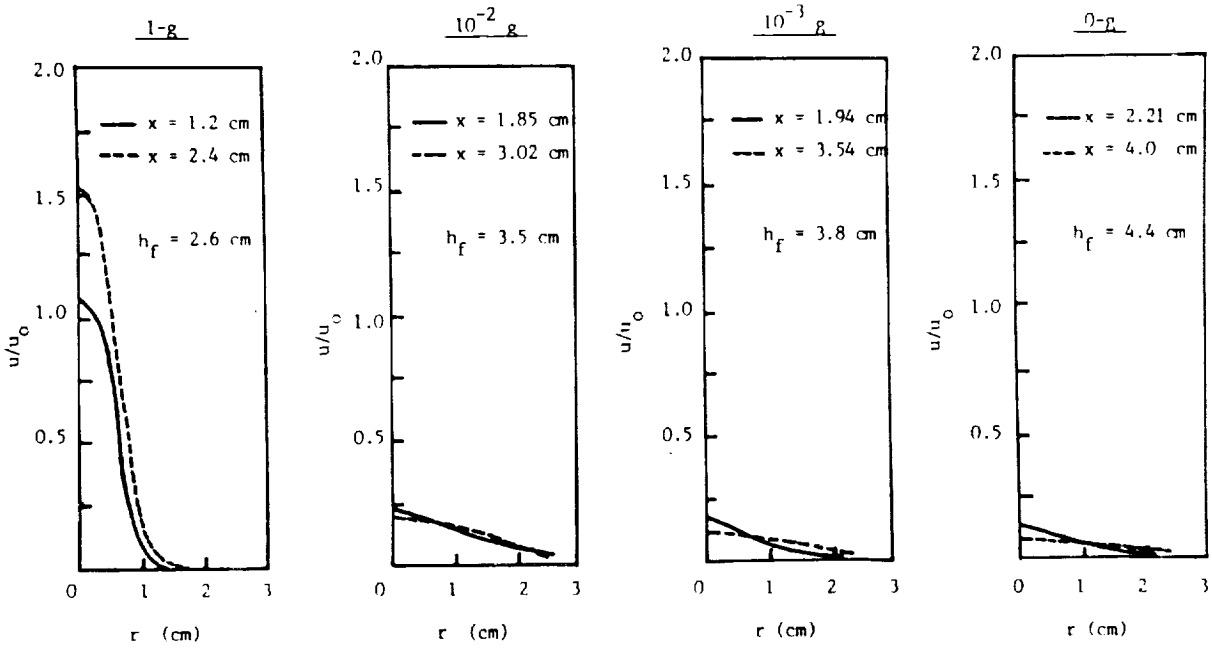

Figure 20.— Predicted axial velocity distributions at different axial locations for flames under different gravitational levels; methane-air flames; p = 1 atm, flow rate = 2 cc/sec, nozzle radius = 0.0825 cm, and jet exit velocity = 93.5 cm/s.

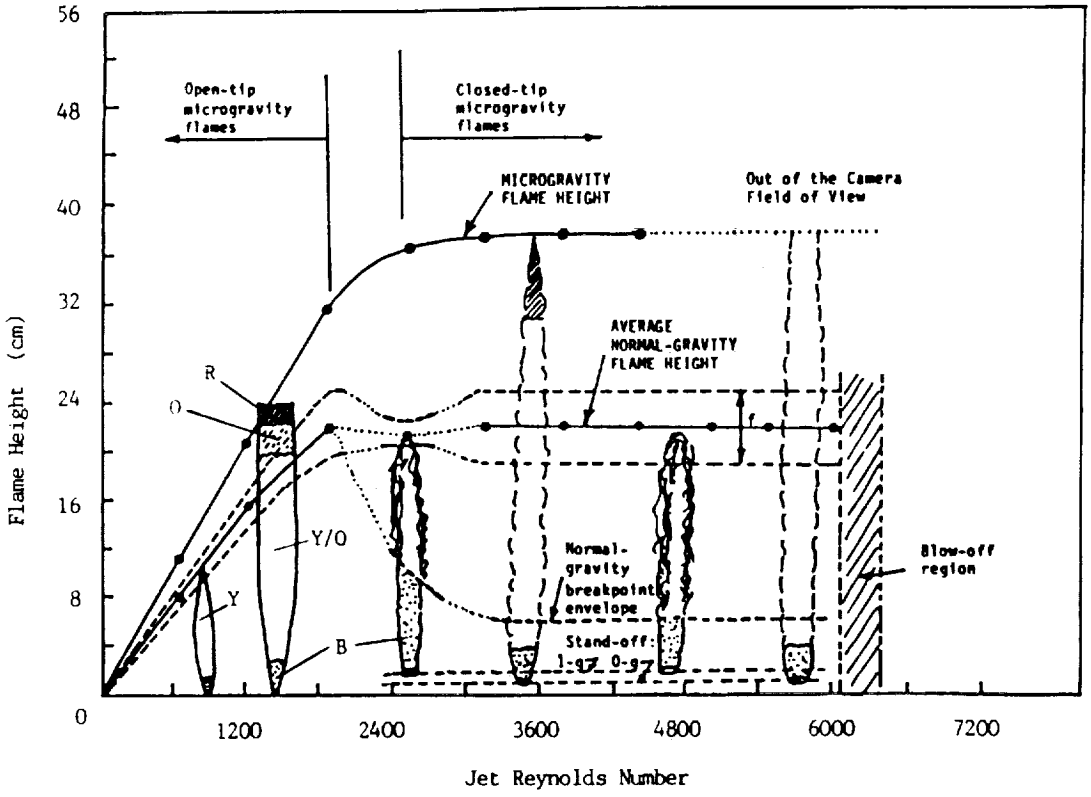

Figure 21.— Normal-gravity and microgravity heights of propane flames burning in quiescent air at 1 atm, as a function of the jet Reynolds number (based on the fuel properties and nozzle diameter); for the color symbols, see Fig. 4. The dotted line in the normal-gravity plots indicates uncertainty in the trend which is currently under investigation. The circles show the particular flames studied in this work; f is the flicker envelope for the normal-gravity flames; reproduced from [10].

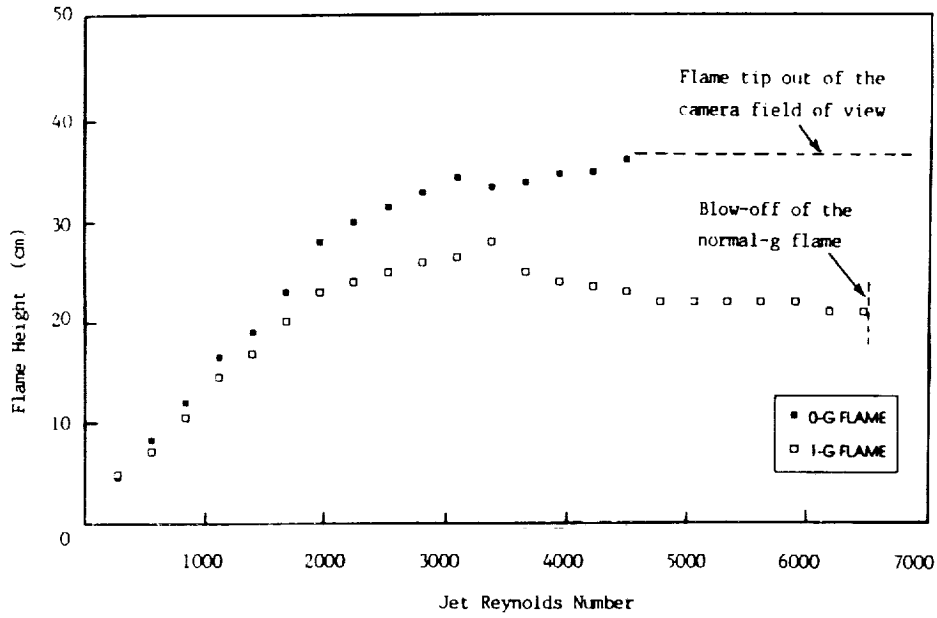

Figure 22.— Microgravity and (average) normal-gravity heights of propylene flames burning in quiescent air at 1 atm, as a function of the jet Reynolds number (based on the fuel properties and nozzle diameter).

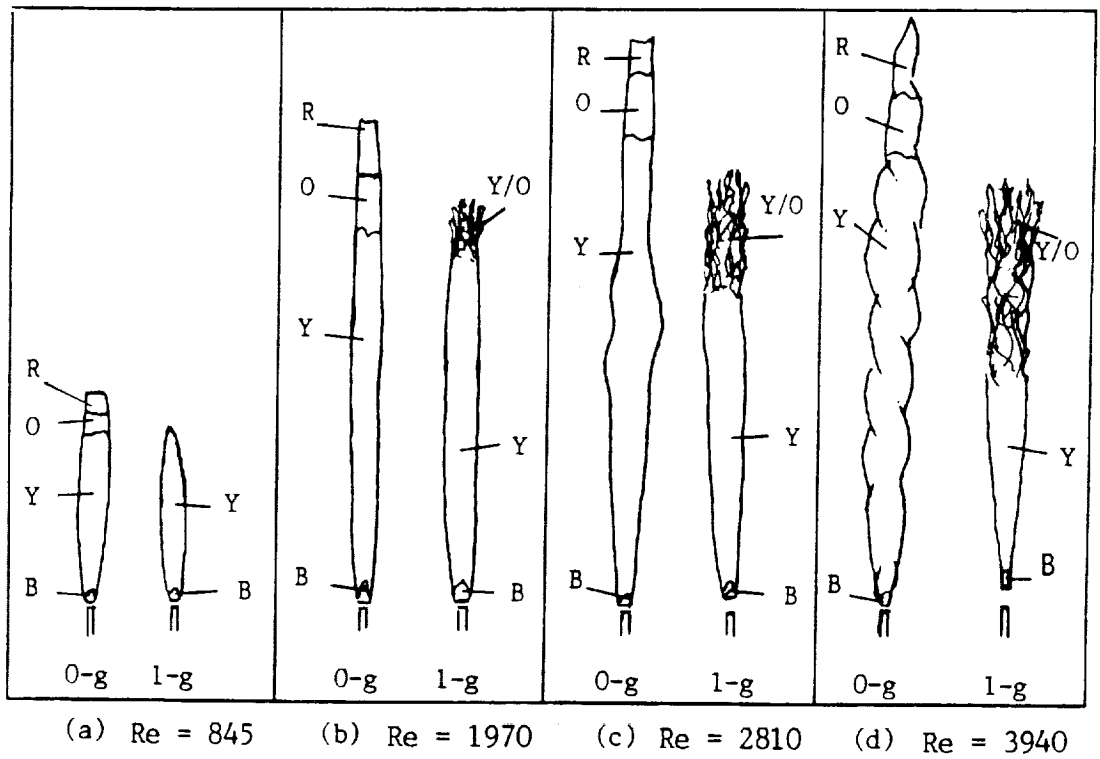

Figure 23.— Normal-gravity and microgravity flames of propylene; (a) low-Reynolds-number laminar flame, (b) high-Reynolds-number laminar flame, (c) beginning of transitional behavior with a single disturbance in microgravity, and (d) fully transitional flame with a train of disturbances in microgravity. The colors are as follows: B (blue), O (orange), R (red), Y (yellow); f is the flicker range for the normal-gravity flame; scale: ⊢——⊣ = 10 cm.

COMMENTS

Question - (Jerry Ku, Wayne State University): For low flow rates (e.g. 1.5 cc/sec), zero-g flames are much taller, wider, and open-tipped. At higher flow rates (e.g. 350 cc/sec), zero-g flames are not much wider and close-tipped. Is there a good explanation for this observation?

Answer: In general, the microgravity laminar flames (including the 350 cc/sec) are taller and wider than their normal-gravity counterparts, and have open tips. At higher Reynolds numbers (i.e., in the transitional and turbulent regimes) the flames are still taller and wider than those in normal gravity, but show a closed tip. The flame-tip closing may be attributed to enhanced transport.

Question (G. Faeth, University of Michigan: It requires some distance to develop the flow in tubes. What was the burner passage length-to-diameter ratio of your experiments?

Answer: The ratio of length to diameter is larger than 100.

Question (S. Raghu, State University of New York at Stony Brook): The Reynolds numbers of the flames you mentioned in your talk is based on the "cold flow" conditions. One has to be cautious in interpreting the fluid dynamic phenomena of stability, transition and turbulence of the flames based on this fictitious cold flow Reynolds number. Are there any details about the exit mean velocity profiles (parabolic or top-hat), and the nozzle shape (contraction ratio, nozzle tip thickness) measured for your setup?

Answer: The cold-fuel Reynolds number was selected to compare the flame behavior with the classical works on this subject. We do realize that the Reynolds number based on local flow properties may significantly deviate from the jet exit Reynolds number. In our opinion, however the latter remains a useful parameter in describing the observed flow phenomena as has been done in the past. As such, we fail to understand what is meant by a "fictitious" Reynolds number. We used circular nozzles in the range 0.5-1.0 mm inner diameter. Although no velocity measurements were conducted, the large length-to-diameter ratio (larger than 100) indicates that the flow is fully developed at the nozzle exit. The nozzle tip was tapered, and the inside had no contraction.

STRUCTURE AND SOOT PROPERTIES OF NON-BUOYANT LAMINAR ROUND-JET DIFFUSION FLAMES

N93-20190

Saeed Mortazavi, Peter B. Sunderland, Jongsoo Jurng, and Gerard M. Faeth
Department of Aerospace Engineering
The University of Michigan
Ann Arbor, Michigan 48109-2140

Introduction

The structure and soot properties of nonbuoyant laminar diffusion flames are being studied experimentally and theoretically in order to better understand the soot and thermal radiation emissions from luminous flames. The measurements involve weakly-buoyant flames at low pressures in normal gravity (ng) and nonbuoyant flames at normal pressures in microgravity (μg).

Earlier measurements of the structure of nonbuoyant laminar diffusion flames have used drop towers [1-7]. Measurements have been limited to flame lengths, finding good agreement between predictions based on the conserved-scalar formalism and measurements, although flame length is not a very sensitive indicator of model performance. Additionally, limited instrumentation and test time capabilities of drop towers have inhibited detailed studies of soot processes.

Buoyant laminar diffusion flames have received significant attention [8-20]. However, buoyancy causes soot to be confined to a narrow soot layer that is difficult to resolve experimentally, while the path that soot follows as it grows and oxidizes is completely different in buoyant and nonbuoyant flames [18]. This limits the value of findings from buoyant diffusion flames because nonbuoyant flames are of greatest practical interest. Additionally, Glassman [17] questions the existence of a global property like laminar smoke point flame lengths for nonbuoyant diffusion flames, analogous to buoyant flames, because they have residence times independent of flame length under the boundary layer approximation. Clearly, the mechanism causing practical nonbuoyant flames to emit soot is not understood.

Finally, detailed simulations of chemical kinetics have been successful for methane/air flames where soot concentrations are low [19,20] but analogous methods for soot-containing flames will require substantial advances in the understanding of fuel decomposition and soot chemistry. An alternative approach is possible, however, because gas species concentrations in soot-containing flames are largely functions of the mixture fraction, yielding state relationships that could be used with the conserved-scalar formalism (the laminar flamelet approach). However, this approach has not been tested.

Thus, the objectives of the present investigation are to study the differences of soot properties between nonbuoyant and buoyant diffusion flames, and to evaluate predictions based on the laminar flamelet approach.

Experimental Methods

Normal-Gravity Tests. Detailed measurements of flame properties are being undertaken at ng, exploiting the fact that buoyancy scales like p^2g in laminar flames, where p = pressure (atm.) and g

= normal gravitational acceleration [18]. Thus, flames at pressures of O(0.1 atm.) have effective gravitational levels of O(0.01 g) and are weakly-buoyant if they are not too large. Present measurements were carried out in a windowed chamber using burners having diameters of 3-10 mm with nearly fully-developed laminar pipe flow at the exit. A continuous inflow of fuel and oxidant, and outflow of combustion products, allows unlimited test times. Thus far, measurements include dark-field photography for flame shapes, fine-wire thermocouples for temperature distributions, laser extinction for soot volume fractions, thermophoretic sampling for soot structure, and wide-band radiometry for radiative heat loss fractions, see [8-15] for descriptions of these methods.

Low-Gravity Tests. Tests at μg were carried out to measure the laminar smoke point flame lengths of nonbuoyant laminar jet diffusion flames at pressures of 0.5-2.0 atm. This involved the NASA KC-135 aircraft facility using a test chamber that was designed at NASA-Lewis with burner diameters of 1.6, 2.7 and 5.9 mm, and fully-developed laminar pipe flow at the exit. Measurements were limited to video and film motion pictures of the flames to find laminar smoke point flame lengths.

Theoretical Methods

The following approximations were used to analyze flame structure: steady, laminar, axisymmetric flow; laminar flamelet approximation, which implies equal binary diffusivities of all species, negligible thermal diffusion, unity Lewis number and attached flames; uniform ambient environment; ideal gas mixture with a constant Prandtl/Schmidt number; and constant radiative heat loss fraction of the available chemical energy release. This yields the following governing equations:

$$\nabla \cdot (\rho \mathbf{u}) = 0 \tag{1}$$

$$\nabla \cdot (\rho \mathbf{u}\mathbf{u}) = \rho g - \nabla p + \nabla \cdot (\mu (\nabla \mathbf{u} + \nabla \mathbf{u}^T)) \tag{2}$$

$$\nabla \cdot (\rho \mathbf{u} f) = \nabla \cdot (\mu \nabla f)/\sigma \tag{3}$$

where ρ = density, $\mathbf{u}$ = velocity vector, μ = viscosity, f = mixture fraction, σ = Prandtl/Schmidt number and superscript T denotes the transpose of a tensor. State relationships giving the composition, temperature, density and viscosity as a function of mixture fraction were found from correlations of measurements in laminar flames for combustion in air [12-14].

Results and Discussion

Flame Structure. Figure 1 is an illustration of predicted and measured flame lengths, L, normalized by the burner diameter, d, as a function of burner exit Reynolds number, Re. These results involve ethylene/air flames at atmospheric pressure, with measurements from Haggard and Cochran [2]. Similar to other evaluations of flame lengths for moderately sooting fuels, the comparison between predictions and measurements is excellent. Flame shapes and temperature distributions provide a more sensitive evaluation of predictions and have been studied using low-pressure flames. Predicted and measured flame shapes for ethylene/air flames at 0.125 and 0.250 atm. are illustrated in Fig. 2 for d = 3 mm, with z and r denoting streamwise and radial directions. The measurements denote the boundary of the blue portion of the flame, and are terminated where yellow soot luminosity prevents observation of the blue boundary. The small change of flame shape as the pressure varies shows that effects of buoyancy are small. The comparison between predictions and measurements is reasonably good, including lengths, widths and the tendency of the flames to attach below the burner exit, for a range of burner exit Reynolds numbers. Predicted

and measured temperature distributions of ethylene/air flames at 0.25 atm. and z/d = 39.2 are illustrated in Fig. 3. Temperatures were measured with thermocouples corrected for radiation errors. The comparison between predictions and measurements is good except for a slight overestimation of peak temperatures and underestimation of flow widths.

It is useful to consider flame residence times, t_r, defined as the time for a fluid parcel to convect along the axis from the burner exit to the flame sheet, in order to interpret smoke point flame lengths. Predictions of t_r for nonbuoyant flames as flame lengths are varied for a particular burner diameter are illustrated in Fig. 4. They show that t_r is proportional to L, which differs from behavior when the boundary layer approximations apply, considered by Glassman [17], due to effects of streamwise diffusion. Similar predictions when the burner diameter is varied for a particular flame length appear in Fig. 5. They show a progressive increase of t_r with burner diameter, which differs from ng conditions where t_r is relatively independent of burner diameter [14]. Another feature of these results is the large residence times of nonbuoyant flames in comparison to buoyant flames of comparable size (an order of magnitude larger) which implies rather different soot reaction conditions.

Soot Properties. A typical example of soot volume fraction distributions in nonbuoyant jet diffusion flames is illustrated in Fig. 6. These results are for an acetylene flame with an ambient oxygen mass fraction of 0.75, d = 3 mm, Re = 250 and p = 0.25 atm. An annular soot layer is evident near the burner exit with soot building up near the axis as the flame tip (ca. z/d = 9.35) is approached. Soot oxidation extends to the axis beyond the flame tip with soot concentrations becoming small far from the burner exit for this nonsooting flame. The breadth of the soot-containing region provides unprecedented spatial resolution in comparison to buoyant flames.

Laminar Smoke Points. Laminar smoke point flame lengths, L_s, were measured for ethylene/air and propane/air flames at pressures of 0.5, 1.0 and 2.0 atm. Some typical results for propane/air flames at atmospheric pressure at μg, and at ng from [14,16], are as follows:

d (mm)	1.6 (μg)	2.7 (μg)	5.9 (μg)	10.0 (ng)
L_s (mm)	42	38	42	162-169

Findings for ethylene/air flames were similar. There are several interesting features about the comparison between observations at μg and ng. First of all, the nonbuoyant flames exhibit laminar smoke point flame lengths, in contrast to the conjecture of Glassman [17], because their residence times vary with flame length as discussed earlier. Secondly, varying d at μg has little effect on L_s even though residence times vary appreciably. Additionally, the L_s are roughly four times shorter at μg than ng. Finally, residence times at the laminar smoke point are appreciably larger at μg than ng, 200-1500 ms in comparison to 40-50 ms. The different soot paths in nonbuoyant and buoyant flames, and the extended oxidation region of nonbuoyant flames, undoubtedly play a role in this behavior, although the specific mechanisms are unknown. These results clearly highlight the substantial differences between the global sooting properties of frequently studied buoyant diffusion flames and the nonbuoyant diffusion flames of greater practical importance.

Conclusions

Thus far, the major conclusions of the study are as follows: (1) the laminar-flamelet approach appears to be attractive for predicting the structure of soot-containing laminar diffusion flames; (2) residence times of nonbuoyant laminar diffusion flames (L/d < 20-30) increase proportional to burner diameter and flame length, with the latter behavior being caused by effects of streamwise diffusion; (3) nonbuoyant diffusion flames exhibit much broader soot-containing regions and

larger soot-oxidation regions in comparison to buoyant diffusion flames; and (4) the properties of laminar smoke point flame lengths and residence times of nonbuoyant laminar diffusion flames have little resemblance to those of more widely studied buoyant laminar diffusion flames.

Acknowledgements

This research was sponsored by NASA Grant No. NAG3-1245, under the technical management of D. Urban of the Lewis Research Center.

References.

1. Cochran, T.H. and Masica, W.J., *Thirteenth Symposium (International) on Combustion*, The Combustion Institute, Pittsburgh, 1970, pp. 821-829.
2. Haggard, J.B. Jr. and Cochran, T.H., Combust. Flame, Vol. 5, 1972, pp. 291-298.
3. Edelman, R.B. et al., *Fourteenth Symposium (International) on Combustion*, The Combustion Institute, Pittsburgh, 1972, pp. 399-412.
4. Klajn, M. and Oppenheim, A.K., *Nineteenth Symposium (International) on Combustion*, The Combustion Institute, Pittsburgh, 1982, pp. 223-235.
5. Bahadori, M.Y., Edelman, R.B., Stocker, D.P. and Olson, S.L., AIAA J., Vol. 28, 1990, pp. 236-242.
6. Bahadori, M. Y., Stocker, D. P. and Edelman, R. B., AIAA Paper No. 90-0651, 1990.
7. Bahadori, M.Y., Edelman, R.B., Stocker, D.P., Sotos, R.G. and Vaughan, D.F., AIAA Paper No. 92-0243, 1992.
8. Santoro, R.J., Semerjian, H.B. and Dobbins, R.A., Combust. Flame, Vol. 51, 1983, pp. 203-218.
9. Santoro, R. J., Yeh, T. T., Horvath, J. J. and Semerjian, H. G., Combust. Sci. Tech., Vol. 53, 1987, pp. 89-115.
10. Dobbins, R.A. and Megaridis, C.M., Langmuir, Vol. 3, 1987, pp. 254-259.
11. Megaridis, C.M. and Dobbins, R.A., Combust. Sci. Tech., Vol. 66, 1989, pp. 1-16; *Ibid.*, Vol. 77, 1990, pp. 95-109.
12. Gore, J.P. and Faeth, G.M., *Twenty-First Symposium (International) on Combustion*, The Combustion Institute, Pittsburgh, 1986, pp. 1521-1531.
13. Gore, J.P. and Faeth, G.M., J. Heat Trans., Vol. 111, 1988, pp. 173-181.
14. Sivathanu, Y.R. and Faeth, G.M., Combust. Flame, Vol. 81, 1990, pp. 133-149.
15. Sivathanu, Y.R. and Faeth, G.M., Combust. Flame , Vol. 82, 1990, pp. 211-230.
16. Schug, K.P., Manheimer-Timnat, Y., Yaccarino, P. and Glassman, I., Combust. Sci. Tech., Vol. 22, 1980, pp. 235-250.
17. Glassman, I., *Twenty-Second Symposium (International) on Combustion*, The Combustion Institute, Pittsburgh, 1988, pp. 295-311.
18. Faeth, G.M., *Proceedings of AIAA/IKI Microgravity Science Symposium*, AIAA, Washington, 1991, pp. 281-293.
19. Dixon-Lewis, G. et al., *Twentieth Symposium (International) on Combustion*, The Combustion Institute, Pittsburgh, 1984, pp. 1893-1903.
20. Rogg, B., in *Mathematical Modeling in Combustion and Related Topics* (C.-M. Brauner and C. Schmidt-Laine, eds.), Martinus Nijhoff Publishers, Amsterdam, 1988, pp. 551-560.

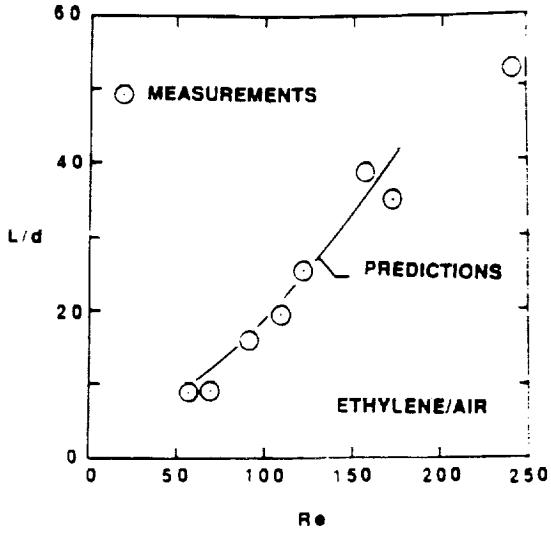

Fig. 1 Predicted and measured flame lengths of nonbuoyant ethylene/air jet diffusion flames. Measurements from Haggard and Cochran [2].

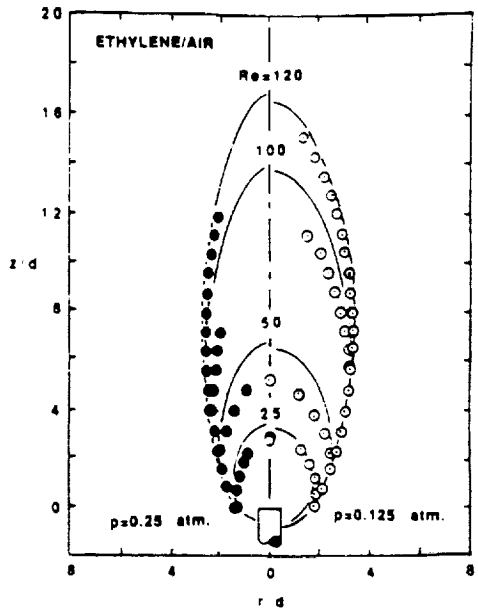

Fig. 2 Predicted and measured flame shapes of weakly-buoyant ethylene/air jet diffusion flames.

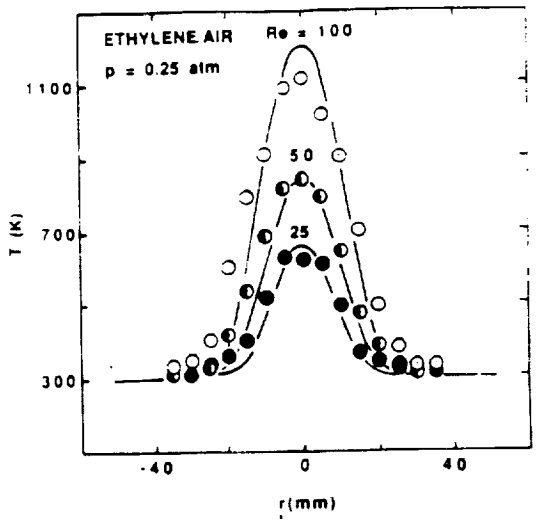

Fig. 3 Predicted and measured temperature distributions in weakly-buoyant ethylene/air diffusion flames.

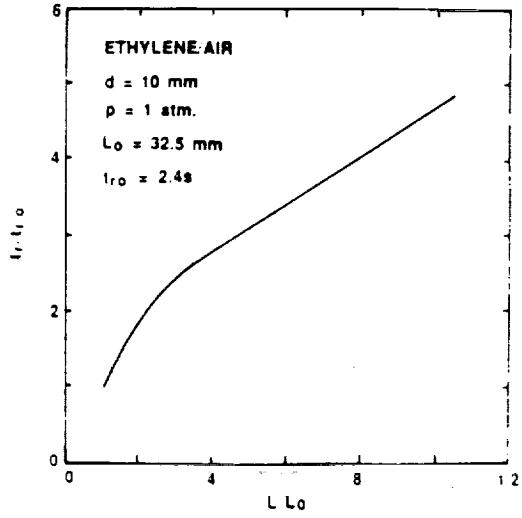

Fig. 4 Predicted flame residence times as a function of flame length for nonbuoyant ethylene/air diffusion flames.

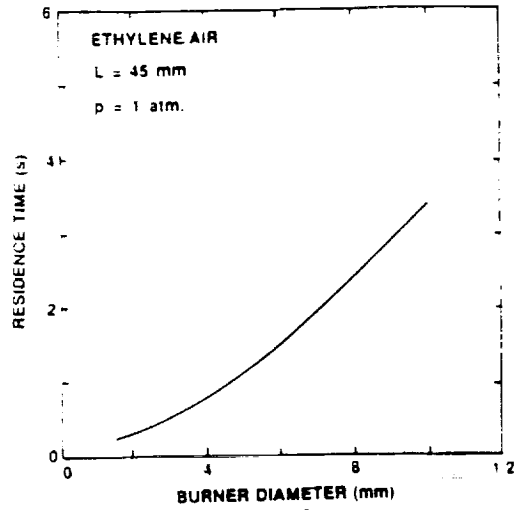

Fig. 5 Predicted flame residence times as a function of burner diameter for nonbuoyant ethylene/air diffusion flames.

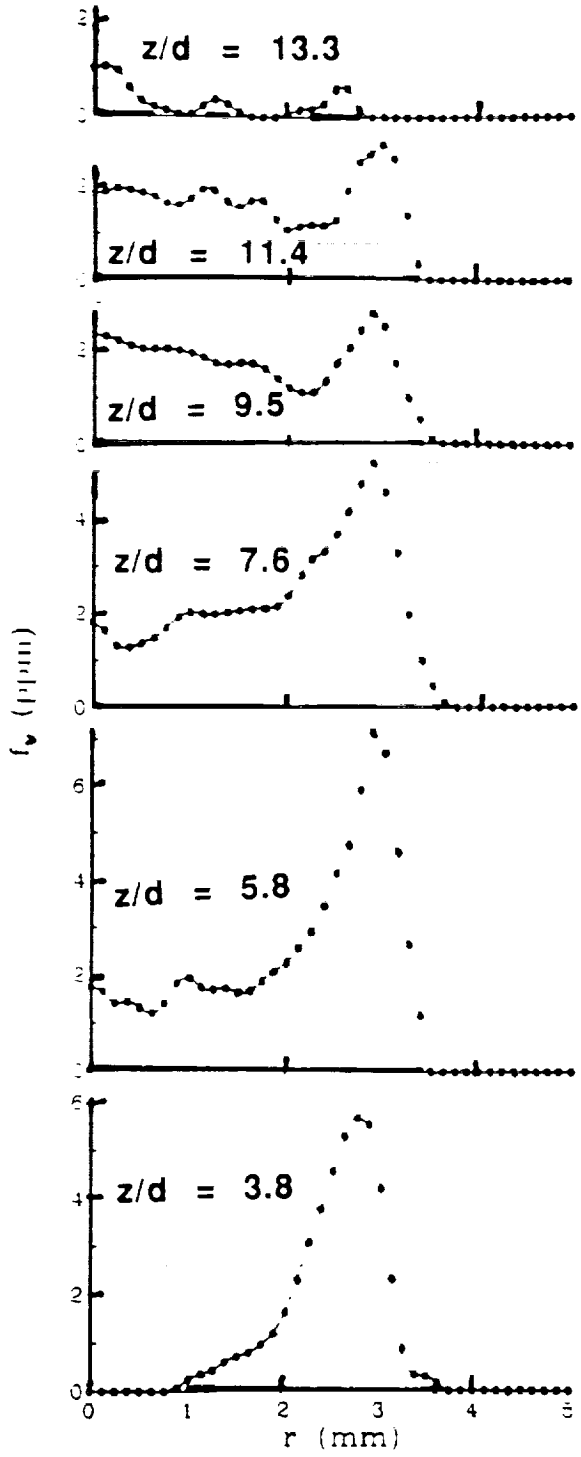

Fig. 6 Measured soot volume fraction distributions for weakly-buoyant acetylene/oxygen/nitrogen diffusion flames: d = 3 mm, Re = 250, p = 0.25 atm. and ambient oxygen mass fraction = 0.75.

COMMENTS

Question: (Osamu Fujita, Hokkaido University): (1) Are there any reasons why you choose ethylene as a fuel?

2) Are the flames you showed in the presentation steady-state or not? According to our results, width or diameter of butane flame become larger with increase in microgravity time, especially when the gas injected speed is low.

Answer: Our experiment currently involves ethylene and acetylene flames because they have been studied extensively in the past - particularly ethylene. Future work will address effects of fuel type over a broader range.

The low-pressure weakly-buoyant flames we are studying in the laboratory are all steady; we can operate them indefinitely and accumulate data over periods of hours. The low-gravity tests using the NASA KC-135 facility last 15-20 seconds, which yields stable flame lengths in the absence of disturbances, but are marginal as steady-state flames due to limited development times and disturbances. This is the best we can do prior to space-based tests at microgravity, but we don't believe that this compromises the major conclusions about differences of laminar smoke-point properties for nonbuoyant and buoyant flames.

Question (C.T. Avedisian, Cornell University): Can you comment on sensitivity of your predictions to uncertainties in physical property values?

Answer: Our predictions are sensitive to estimates of the radiative heat losses from the flames due to the strong variation of transport properties with temperature. Thus, we currently are working on additional measurements of the distribution of radiative heat losses from the flames to reduce these uncertainties. Computations for ad hoc variations of properties have been carried out to a limited degree, and suggest that reduced diffusivities yield proportional increases of flame lengths.

AN EXPERIMENTAL AND THEORETICAL STUDY OF RADIATIVE EXTINCTION OF DIFFUSION FLAMES

Arvind Atreya, Indrek Wichman, Mark Guenther,
Anjan Ray, and Sanjay Agrawal
Department of Mechanical Engineering
Michigan State University
East Lansing, Michigan 48824

INTRODUCTION

In a recent paper on "Observations of candle flames under various atmospheres in microgravity" by Ross et al. (ref. 1), it was found that for the same atmosphere, the burning rate per unit wick surface area and the flame temperature were considerably reduced in microgravity as compared with normal gravity. Also, the flame (spherical in microgravity) was much thicker and further removed from the wick. It thus appears that the flame becomes "weaker" in microgravity due to the absence of buoyancy generated flow which serves to transport the oxidizer to the combustion zone and remove the hot combustion products from it. The buoyant flow, which may be characterized by the strain rate, assists the diffusion process to execute these essential functions for the survival of the flame. Thus, the diffusion flame is "weak" at very low strain rates and as the strain rate increases the flame is initially "strengthened" and eventually it may be "blown out". The computed flammability boundaries of T'ien (ref. 2) show that such a reversal in material flammability occurs at strain rates around 5 sec^{-1}.

At very low or zero strain rates, flame radiation is expected to considerably affect this "weak" diffusion flame because: (i) the concentration of combustion products which participate in gas radiation is high in the flame zone, and (ii) low strain rates provide sufficient residence time for substantial amounts of soot to form which is usually responsible for a major portion of the radiative heat loss. We anticipate that flame radiation will eventually extinguish this flame. Thus, the objective of this project is to perform an experimental and theoretical investigation of radiation-induced extinction of diffusion flames under microgravity conditions. This is important for spacecraft fire safety.

PROJECT DESCRIPTION:

For the experimental and theoretical investigation of radiation-induced extinction two simple geometries are chosen: [Note: this project started in April 1991]

(i) *A spherical diffusion flame supported by a low heat capacity porous gas burner*: This is considered suitable for the μg experiments and modeling because all the soot formed is trapped between the burner and the high temperature reaction zone. Here, flame radiation will be enhanced by soot oxidation which will occur as soot crosses the high temperature reaction zone. To examine the radiative extinction limit, the following parameters will be varied: (i) Fuel type (chemical structure) and concentration; (ii) Ambient oxygen concentration; (iii) Fuel injection velocity; (iv) Ambient pressure. Temperature and radiation measurements made under these conditions will then enable us to understand the radiative extinction phenomenon. These experiments will soon begin in the NASA Lewis 2.2 sec μg drop tower. A schematic of the test apparatus for these experiments is shown in Figure 1a and 1b.

(ii) *An axis-symmetric low strain rate counterflow diffusion flame:* This geometry is adopted for the ground-based experiments and modeling because it provides a constant strain rate flow field which is one-dimensional in temperature and species concentrations. The strain rate is directly related to the imposed flow velocity and the one-dimensionality of this flame simplifies experimental measurements and analysis. Also, there are no solid boundaries which may quench the flame prior to extinction caused by low or high strain rates. Experiments on counterflow diffusion flames are currently being performed to determine the soot particle formation and oxidation rates. Two types of flames are being investigated: (a) A low strain rate diffusion flame which lies on the oxidizer side of the stagnation plane. Here, as shown in Figures 2a and 2b, all the soot produced is convected away from the flame toward the stagnation plane. (b) A low strain rate diffusion flame which lies on the fuel side of the stagnation plane. Here, as shown in Figures 3a and 3b, all the soot produced is convected into the diffusion flame. This enhances flame radiation as the soot is oxidized. This geometry is especially relevant to the μg experiments described above. The results of the ground-based experiments are being used in a transient model to predict the radiative extinction limit and the conditions under which it occurs.

PROGRESS TO DATE

Although this project started in April 1991, we have made considerable progress on the following items:

μg experiments: The test apparatus has been designed to produce a spherical diffusion flame using a low heat capacity spherical burner constructed from porous alumina. A schematic of this apparatus is shown in Figure 1a. It consists of a drop frame that contains the test chamber, ignition system, batteries, electrical control system, and high-speed motion-picture camera. The diffusion flame is supported by the burner inside a cylindrical test chamber. This test chamber can be evacuated and filled with any desired gas mixture from below atmospheric pressure to 5 atm. A 5" clear lexan window enables the camera to photograph the spherical diffusion flame. The fuel flow system, shown in Figure 1b, consists of a fuel supply line from the gas cylinder that is controlled by a metering valve and turned on and off with a solenoid valve. The porous, spherical burner and other drop rig apparatus components have been successfully tested in normal gravity conditions. Microgravity testing will begin early in September and will continue through December of 1994.

1-g experiments: The supporting ground-based experiments have already started. Figures 2(a,b) and 3(a,b) show the two types of flames being investigated. Since the flame on the fuel side of the stagnation plane is directly related to the spherical microgravity flame, it is being investigated first. Figure 4 shows the measured soot volume fraction and the temperature distribution inside this flame. The fuel and oxidizer concentrations and the strain rate for this flame are 22.9%, 32.6% and 8 sec^{-1} respectively. Figure 5 shows the measured concentrations of stable gases inside this flame. It is extremely interesting to note that only CO and H_2 exist after the luminous flame zone. These are later burned in the blue flame above the luminous flame. Also, the CO concentration is greater than 2% and is substantially larger than the corresponding flame on the oxidizer side of the stagnation plane. This may be an important source of CO in building fires.

Theoretical investigation: To investigate the extinction limits of diffusion flames, the work of Linan (ref. 3 & 4) was reviewed and the simple case of a one-dimensional, diffusion flame with flame radiation is being examined. This model corresponds to the ground-based experiments described above. As a first step we have assumed zero gravity, no convection, constant properties, one-step irreversible reaction and unity Lewis number. These equations are being numerically integrated to examine the conditions under which radiation-induced extinction occurs. The soot formation and oxidation rates will be obtained from the counterflow diffusion flame experiments.

FUTURE PLANS

In the near future we plan to focus our attention on the following items:

1. Perform microgravity experiments on spherical diffusion flames for different fuels and under various atmospheres.

2. Continue our work on supporting ground-based experiments at low strain rates to quantify soot formation and oxidation rates and flame radiation for the same fuels and atmospheres used in the μg experiments.

3. Complete our theoretical model for zero strain rate (no flow) flames in microgravity and identify conditions under which radiation-induced extinction occurs.

4. To analyze the experimental results and develop an appropriate theoretical model for spherical diffusion flames with flame radiation.

REFERENCES

1. *Ross, H. D., Sotos, R. G. and T'ien, J. S.*, Combustion Science and Technology, Vol. 75, pp. 155-160, 1991.
2. *T'ien, J. S.*, Combustion and Flame, Vol. 80, pp. 355-357, 1990.
3. *Linan, A.*, Acta Astronautica, Vol. 1, pp. 1007-1039, 1974.
4. *Linan, A., Crespo, A.*, Combustion Science and Technology, Vol. 14, pp. 95-117.

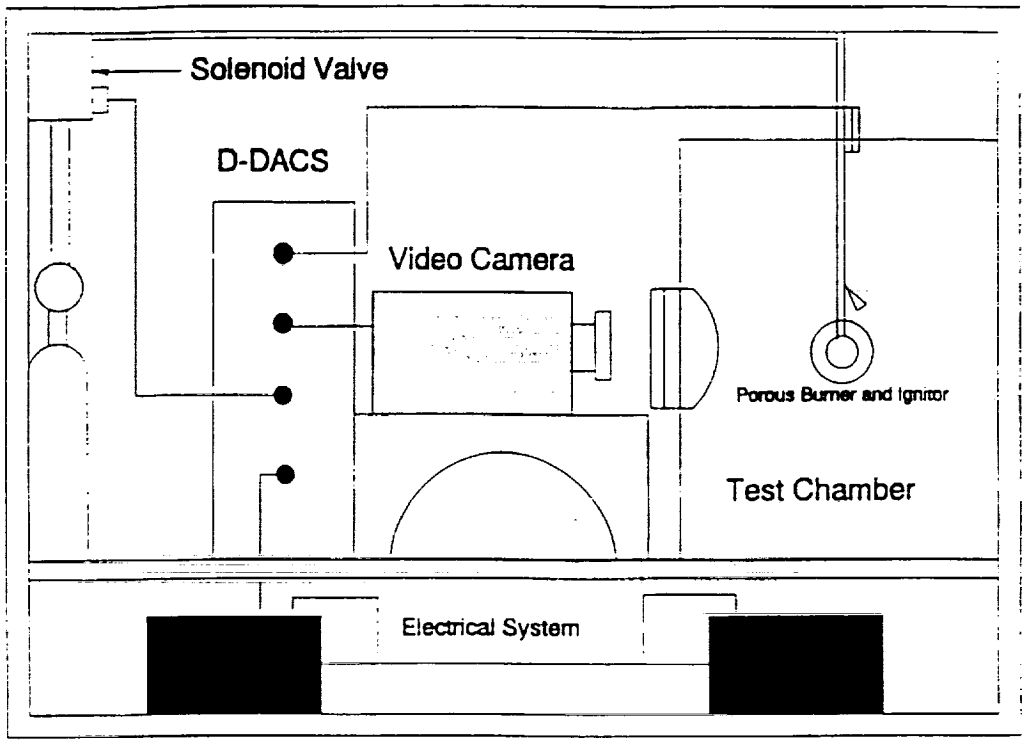

Fig. 1a. Drop Rig Apparatus

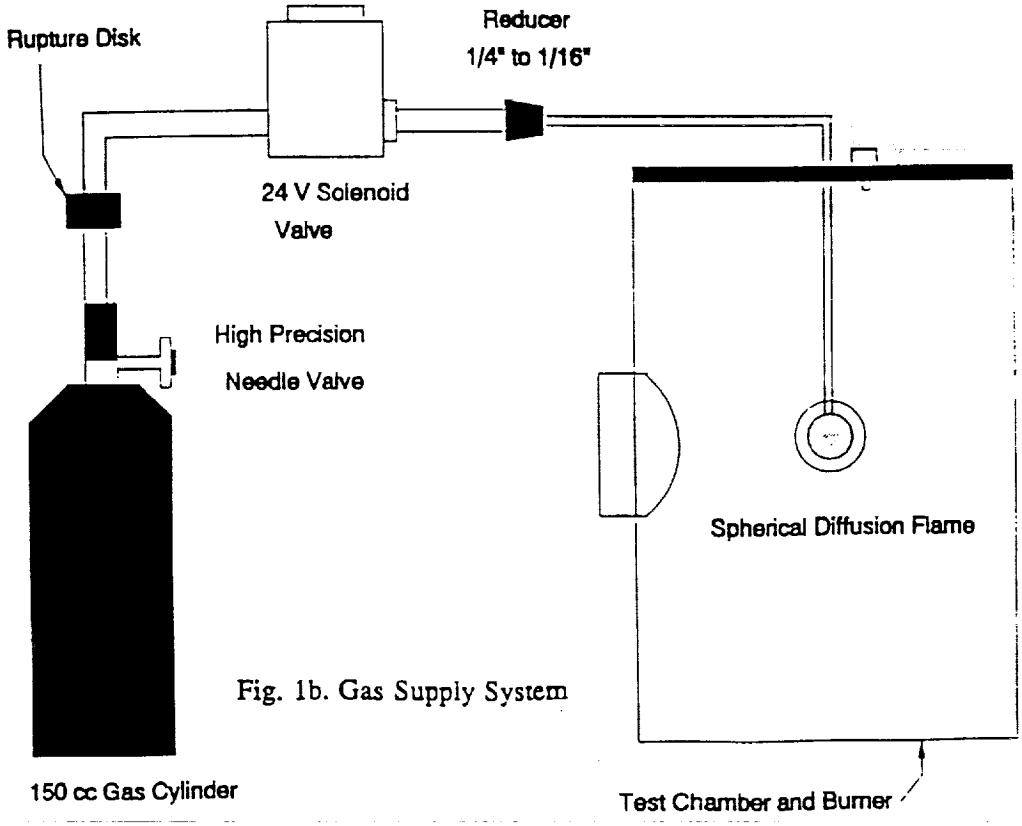

Fig. 1b. Gas Supply System

Fig. 1a. and 1b. Microgravity spherical diffusion flame apparatus for 2.2 second drop tower.

Fig. 2a. Low strain rate, sooty counterflow diffusion flame on the oxidizer side of the stagnation plane

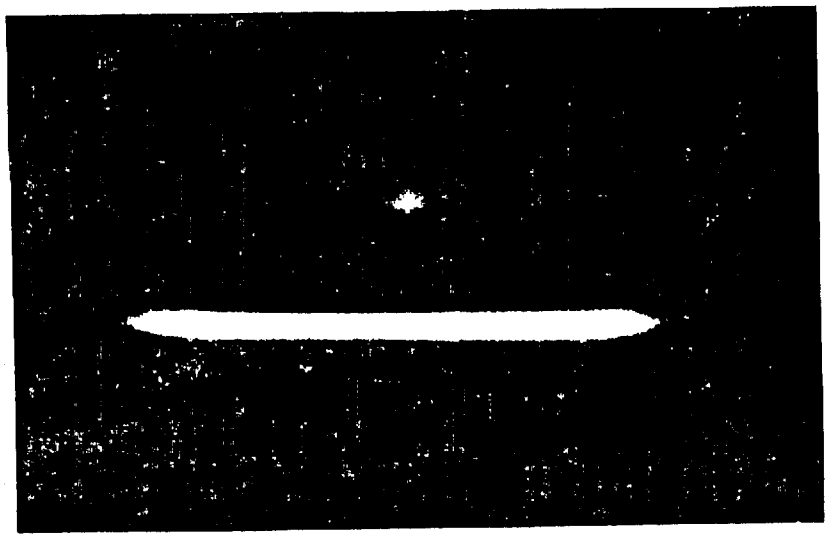

Fig. 2b. Same as Fig. 2a. The $TiCl_4$ streak shows the location of the stagnation plane

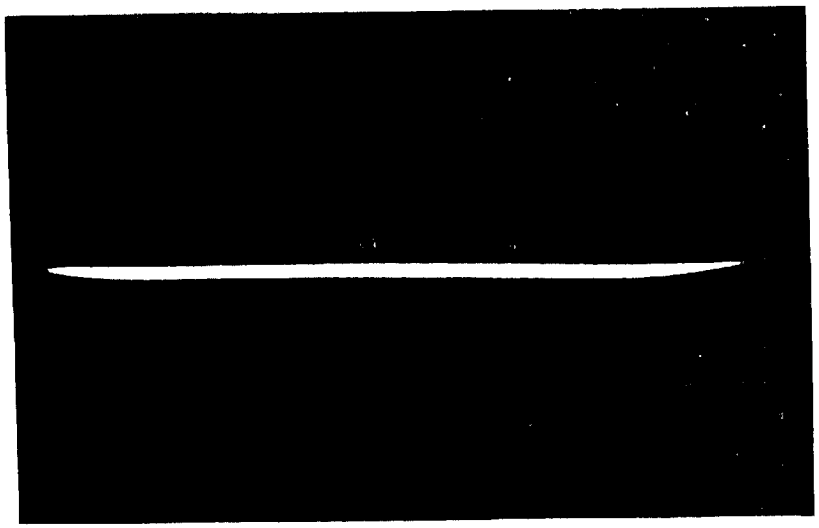

Fig. 3a. Low strain rate, sooty counterflow diffusion flame on the fuel side of the stagnation plane

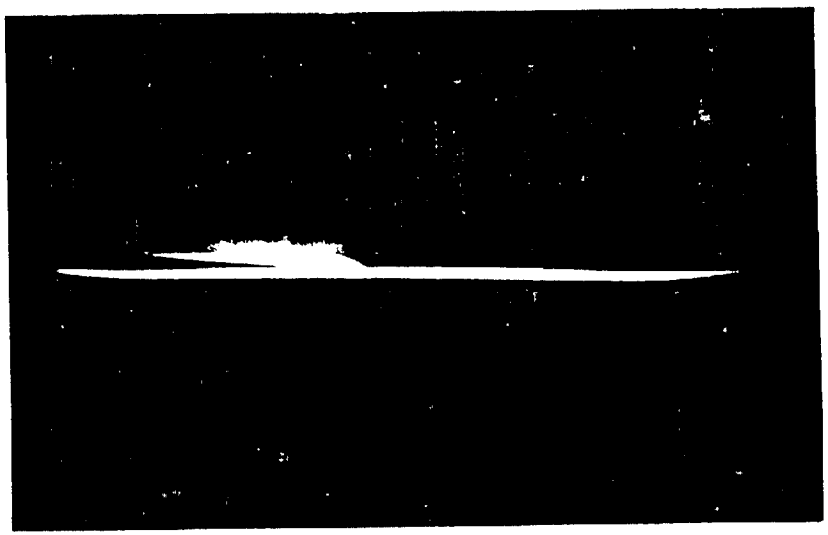

Fig. 3b. Same as Fig. 3a. The $TiCl_4$ streak shows the location of the stagnation plane

See Color Plate C3

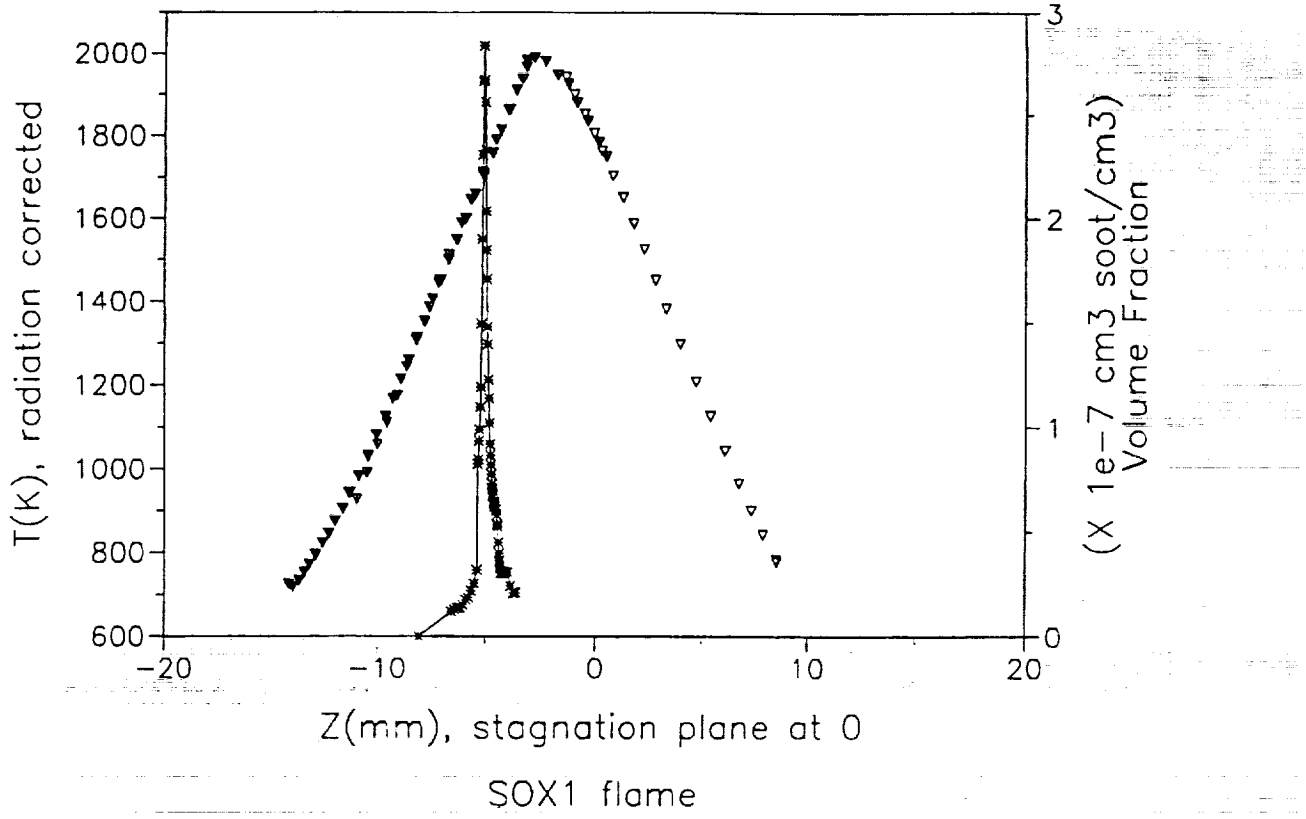

Fig. 4. Soot Particle Volume Fraction and Temperature Profile

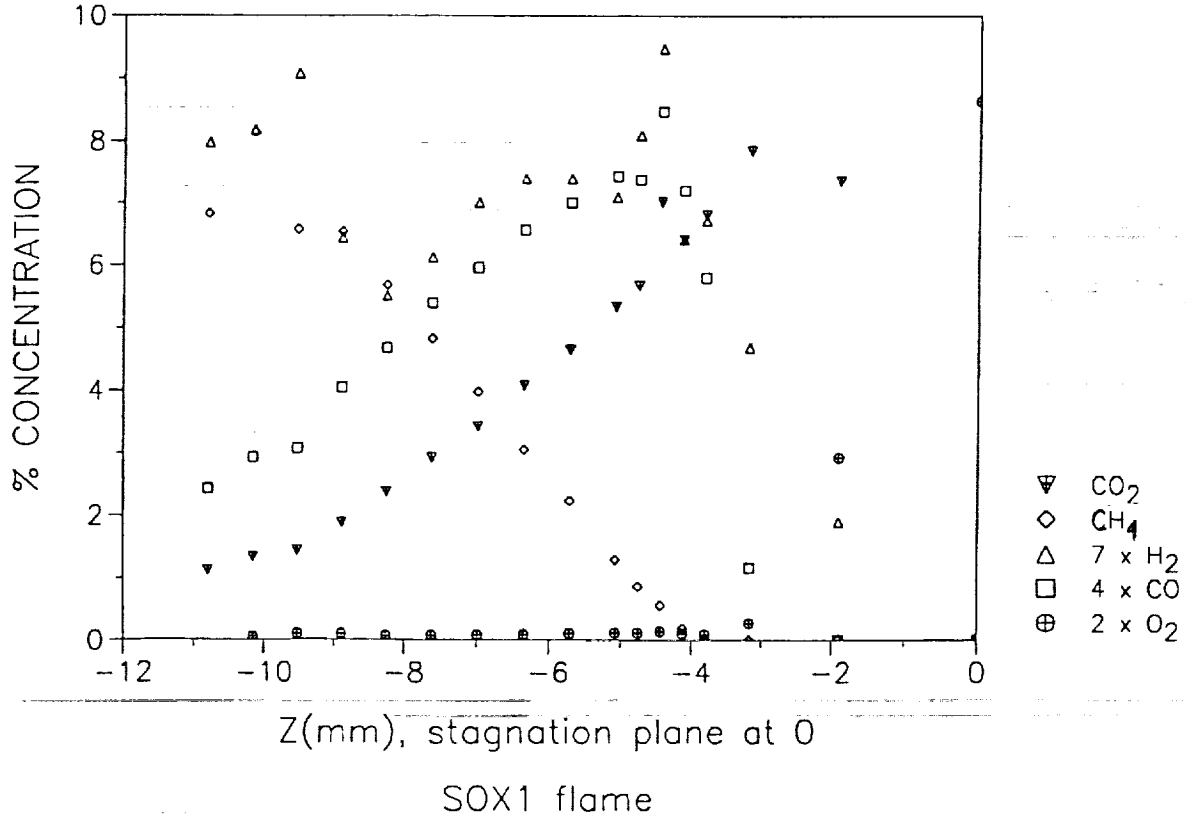

Fig. 5. Concentration Profiles of Stable Gases

SOOT FORMATION AND RADIATION IN TURBULENT JET DIFFUSION FLAMES UNDER NORMAL AND REDUCED GRAVITY CONDITIONS

Jerry C. Ku, Li Tong, and Jun Sun
Wayne State University
Detroit, Michigan 48202

Paul S. Greenberg
NASA Lewis Research Center
Cleveland, Ohio 44135

Devon W. Griffin
Sverdrup Technology, Inc.
Brook Park, Ohio 44142

Introduction

Most practical combustion processes, as well as fires and explosions, exhibit some characteristics of turbulent diffusion flames. For hydrocarbon fuels, the presence of soot particles significantly increases the level of radiative heat transfer from flames. In some cases, flame radiation can reach up to 75% of the heat release by combustion (ref. 1). Laminar diffusion flame results (ref. 2) show that radiation becomes stronger under reduced gravity conditions. Therefore, detailed soot formation and radiation must be included in the flame structure analysis. A study of sooting turbulent diffusion flames under reduced-gravity conditions will not only provide necessary information for such practical issues as spacecraft fire safety, but also develop better understanding of fundamentals for diffusion combustion.

Experimentally, full-field laser light transmission and thermophoretic soot particle sampling techniques will be used to measure flame soot particulate size and number density. Flame temperature will be measured using full-field two-color pyrometry and fine-gage thermocouples. These experiments are conducted in a drop tower.

On modeling, the focus is on complete coupling of flame structure, soot formation, and radiation. The conserved scalar approach based on Favre-averaged governing equations, k-ε-g turbulence model, and an assumed probability density function is used to predict flow field and gaseous species mole fractions profiles (refs. 3 and 4). A soot formation model developed by Syed et al. (refs. 5 and 6) will be modified to predict soot particle volume fraction and number density. The energy equation is incorporated to provide a full coupling between flame structure and radiation. The radiative heat flux is calculated from the radiative transfer equation (RTE) for a finite axisymmetric cylindrical enclosure, which will be solved by the P_3 spherical harmonics approximation (ref. 7).

In this paper, a summary of the work to date and of future plans is reported.

Experimental Results

Experiments are conducted using a 2.2-second drop rig. The rig is now instrumented for thermophoretic soot particle sampling and full-field laser light transmission measurements. Thermocouple and two-color pyrometry measurement are planned. Details for experiments are reported in another paper in this workshop (ref. 8).

Results were collected for laminar flames first to validate our setup and procedure. The nozzle has a diameter of 1.7 mm. Propane and ethylene at 1.0 and 1.5 cc/sec are tested. Micrographs of soot aggregates in 1.5 cc/sec propane-air diffusion flames are shown in Fig. 1. The significant difference in aggregate size (or number of primary particles per aggregate) between normal and reduced gravity conditions is noted, and this has been observed for all fuel and flow rate combinations.

Fig. 2 shows the mean diameter of primary soot particles as a function of height above nozzle exit. The size distribution, deduced from more than 100 particles per sample, agrees well with the normal distribution and 95% of the population falls in ±10 nm range. Incipient soot particles are larger under 0-g. This seems to support the argument that incipient soot starts as liquid droplets, whose dynamics is affected by the relative dominance of surface tension. Under 0-g, the oxidation stage seems to be much weaker for the 1.5 cc/sec case, so flames may smoke (i.e., release soot particles). It is therefore concluded that rates of nucleation, growth, coagulation, and oxidation are very different between 1-g and 0-g. 0-g data are needed for determining these rate constants in models. Larger aggregate and primary particle sizes mean that radiation heat transfer is even more significant under 0-g (ref. 9).

The full-field laser light transmission experiment has been tested for a 1-g flame. Soot volume fraction for a section as tall as 4.5 cm was measured instantaneously using a CCD camera. Results agree well with point-by-point measurements.

Modeling of Turbulent Jet Diffusion Flame

Following the conserved scalar approach, the structure of an axisymmetric turbulent diffusion flame is modeled using Favre-averaged boundary layer flow equations for conservation of mass, momentum, and mixture fraction described by Bilger (ref. 10), and a k-ε-g turbulence model proposed by Lockwood and Naguib (ref. 11). The governing equations can be written in a general form as (refs. 12)

$$\frac{\partial}{\partial x}(\bar{\rho}\tilde{u}\phi)+\frac{1}{r}\frac{\partial}{\partial r}(r\bar{\rho}\tilde{v}\phi)=\frac{1}{r}\frac{\partial}{\partial r}\left(r\mu_{\mathit{eff},\phi}\frac{\partial\phi}{\partial r}\right)+S_\phi \quad , \tag{1}$$

where ϕ = 1 (continuity), $\tilde{u}$ (axial velocity), $\tilde{f}$ (mixture fraction), k (turbulence kinetic energy), ε (turbulence dissipation), or g (mixture fraction variance). Favre-averaged (mass weighted) quantities are defined as $\tilde{\phi}=\overline{\rho\phi}/\bar{\rho}$, whereas an overbar represents conventional time-averaging. Details for $\mu_{\mathit{eff},\phi}$ (effective viscosity) and S_ϕ (source term) can be found in the references. Buoyancy effects will only be considered in the mean flow equation, neglecting buoyancy-turbulence interactions.

Assuming all instantaneous scalar properties are functions of the mixture fraction only, termed the state relationships, the Favre-averaged mean and variance of scalar properties can be determined from an assumed probability density function (pdf). The mixture fraction is described as the mass fraction of fuel atoms anywhere in the flame and by virtue of its definition it is invariant with chemical reaction (so it is a conserved scalar). This allows the fluid mechanics to be decoupled from chemical reactions, and it is a good approximation if the rate of chemical reaction is limited by turbulent mixing and not by chemical kinetics (i.e. fast chemistry at equilibrium) and the diffusivities of all species and heat are equal.

The system represented by Eq. (1) is solved using a block-tridiagonal code written by Chen (ref. 13). Major gaseous species concentrations are then calculated based on the state relationships constructed from thermodynamic equilibrium (adiabatic flame) calculations using STANJAN (ref. 14) and a β-pdf. This has been found accurate for nonluminous and fuel-lean regions of luminous flames, but fails for rich regions of luminous flames. For better accuracy, the laminar flamelet approach (refs. 15 and 16), with the state relationships constructed from laminar flame data, may be used.

Modeling of Soot Formation and Oxidation

Compared to gaseous specious, soot inception is a much slower reaction, and soot particles have very different diffusivities. In addition, soot particles are subjected to turbulent mixing, thermophoretic forces, and strong radiation heat transfer effects. The structure analysis outlined above has been extended to model soot formation and oxidation. Magnussen and Hjertager (ref. 17) introduced rate equation models for both nucleation (based on number density) and surface-growth (based on mass concentration) stages. They used an energy equation in the form of Eq. (1), with the source term for radiation, which is calculated using a two-flux model. Gore and Faeth (ref. 4) constructed state relationships for soot volume fractions from laminar flame data, and for temperature from equilibrium combustion calculation with a fixed fraction of chemical energy release lost by radiation. Kent and Honnery (ref. 18) found that the state-relationship approach for soot volume fractions may work in the top oxidation portion of the flame, where turbulent mixing dominates, but not the lower inception portion, where chemical kinetics dominates. They calculated the temperature from an energy equation with a radiation term of $[-\varepsilon\sigma(T^4 - T_\infty^4)/\ell]$.

It is believed that the rate-equation model approach is more accurate for predicting soot formation and oxidation. Kennedy et al. (refs. 19 and 20) applied Eq. (1) for soot volume fraction in laminar diffusion flames. The soot volume fraction source term was replaced by rate equation models derived for nucleation, growth, and oxidation with an assumed average number density. An energy equation similar to that in Kent and Honnery (ref. 18) was used. The model predicts peak soot volume fractions fairly accurately, but not their radial distributions. We adopt a two-equation model, derived by Moss et al. (ref. 6) and Syed et al. (ref. 5), for soot number density (N) and volume fraction (f_v). The model agrees well with measured flat (Wolfhard-Parker) diffusion flame data. The model has been modified (ref. 21) to couple with reduced

chemical reaction mechanisms, and successfully predicted radiation heat transfer from a turbulent reacting jet in a cross-wind (ref. 22).

Since the model applies Eq. (1) to describe the transport of soot particles in terms of Favre-averaged number density and volume fraction, it can be easily incorporated into the reacting turbulent free-shear flow code. Rate equation models, representing nucleation, surfaced growth, coagulation, and oxidation, are used in source terms as

$$S_\phi = \overline{\alpha} - \overline{\beta}\,\overline{\rho}^2\left(\frac{N}{\rho n_0}\right)^2 - n_0^{1/3}\overline{\chi}\,\overline{\rho}\left(\frac{\rho_s f_v}{\rho}\right)^{-1/3}\left(\frac{N}{\rho n_0}\right)^{4/3}, \quad \phi = \frac{N}{\rho n_0}; \tag{2}$$

$$S_\phi = n_0^{1/3}(\overline{\gamma} - \overline{\chi})\overline{\rho}\left(\frac{\rho_s f_v}{\rho}\right)^{2/3}\left(\frac{N}{\rho n_0}\right)^{1/3} - C_\delta\overline{\alpha}, \quad \phi = \frac{\rho_s f_v}{\rho}; \tag{3}$$

where $n_0 = 6\times10^{26}$ is Avogadro's number and ρ_s is the mass density of solid carbon (typically $1.8\text{-}2.0 g/cm^3$). The rate constants α, β, γ, and χ are modeled in terms of mixture density $\overline{\rho}$, activation temperatures T_α and T_γ, and fuel mole fraction X_c, as

$$\alpha = C_\alpha \overline{\rho}^2 T^{1/2} X_c \exp(-T_\alpha/T), \tag{4}$$

$$\beta = C_\beta T^{1/2}, \tag{5}$$

$$\gamma = C_\gamma \overline{\rho}\, T^{1/2} X_c \exp(-T_\gamma/T), \tag{6}$$

$$\chi = C_\chi T^{1/2} X_{ox} \exp(-T_\chi/T), \tag{7}$$

wherein coefficients and temperatures are determined from experimental data. In Eq. (7), $X_{ox} = X_{OH}$ if $f \geq 0.064$ (fuel-rich), and $X_{ox} = 0.045 X_{O_2}$ if $f < 0.064$ (fuel-lean). The effective viscosities are given in the form of

$$\mu_{eff,\phi} = \frac{\mu_t}{\sigma_\phi} = \frac{\overline{\rho}\, C_\mu k^2/\varepsilon}{\sigma_\phi}, \tag{8}$$

where σ_ϕ are determined from experimental data and C_μ is the same as that for $\tilde{u}$.

Flame Radiation Heat Transfer Calculation

Radiation is fully coupled with flame structure analysis through an energy equation given in the form of Eq. (1) with $\phi = \tilde{H}$ (total enthalpy) and $S_\phi = -\nabla\cdot\vec{q}_{rad}$. Turbulence-radiation interactions are neglected. Gore et al. (ref. 23), using a multi-ray method to calculate the radiative heat flux $\vec{q}_{rad}$, showed that the coupled analysis predicts more accurately than the uncoupled one. However, their work neglected the scattering by soot particles, but accounted for the effects of turbulence-radiation interactions.

The radiative transfer equation (RTE) for axisymmetric finite cylindrical enclosures such as for jet diffusion flames can be expressed as (ref. 7)

$$\left[\frac{1}{\beta}\left(\xi\frac{\partial}{\partial r} - \frac{\eta}{r}\frac{\partial}{\partial\phi} + \mu\frac{\partial}{\partial z}\right) + 1\right] I(r,\theta,\phi,z) = (1-\omega) I_b[T(r,z)]$$

$$+\frac{\omega}{4\pi}\int_0^{2\pi}\int_0^{\pi} I(r,\theta,\phi,z)\,\Phi(\theta,\phi,\theta',\phi')\sin\theta'\,d\theta'\,d\phi' \ . \qquad (9)$$

Here, the subscript λ denoting spectral quantities has been left off, I is intensity (with subscript b for blackbody), β is the extinction coefficient, ω is the single scattering albedo, ξ,η, and μ are direction cosines, and Φ is the phase function. Both β and ω are functions of position (r, z) for axisymmetric diffusion flames.

Menguc and Viskanta (ref. 7) derived a solution using the P_3 spherical harmonics approximation with the delta-Eddington approximation for the phase function. For soot agglomerates, the phase function can be better approximated by a third order Legendre polynomial series (ref. 9) given as

$$\Phi(\theta,\phi,\theta',\phi') = 1+\sum_{n=1}^{3} a_n P_n(\cos\psi) \ , \qquad (10)$$

where ψ is the scattering angle and $\cos\psi = \xi\xi' + \eta\eta' + \mu\mu'$, and coefficients a_n are to be determined. Applying the spherical harmonics approximation, the model equations are obtained by employing the following integrations

$$\int_0^{2\pi}\int_0^{\pi} [\text{Equation (9)}]Y_n^{m^*}\sin\theta\,d\theta\,d\phi \ , \qquad (11)$$

for $n = 0, 1, \cdots N$ and $m = -n, -n+1, \cdots n$, with N being the order of the P_N approximation. The spherical harmonics Y_n^m (superscript * denotes the complex conjugate) can be replaced with multiples of direction cosines. Define the moments of intensity as

$$I_0(r,z) = \int_0^{2\pi}\int_0^{\pi} I(r,\theta,\phi,z)\sin\theta\,d\theta\,d\phi \ , \qquad (12a)$$

$$I_{ij\cdots k}(r,z) = \int_0^{2\pi}\int_0^{\pi} (\ell_i\,\ell_j\cdots\ell_k)\,I(r,\theta,\phi,z)\sin\theta\,d\theta\,d\phi \ , \qquad (12b)$$

where each of the direction cosines ℓ_i, ℓ_j, and ℓ_k is ξ,η, or μ . Physically, the zeroth moment is the total incident radiation, whereas the first moments are radiative heat fluxes along the coordinate axis. The divergence of radiative heat flux vector, which appears in the energy equation, can then be calculated from

$$\nabla\cdot\vec{q}_{rad} = \beta(1-\omega)\{4\pi I_b[T(r,z)] - I_0(r,z)\} \equiv S(r,z) \ . \qquad (13)$$

After some manipulations, results obtained from Eq. (11) can be combined into four coupled elliptical partial differential equations for I_0, I_{11}, I_{33}, and I_{13}. The model equation for is given as

$$\left[4B_3(\Gamma_{rr}+\Gamma_{zz}) + \frac{1}{r}(4B_3+7B_1)\Gamma_r + \frac{1}{r^2}(-16B_3+14B_1) + \frac{70}{3}B_2\tau^2\right]I_0 = -\frac{35}{3}\tau^2\frac{S}{\beta} + A_1 \ , \qquad (14)$$

where B's are functions of a_n and ω, $\tau = \beta r_0$, A_1 is a function of B, τ, I_{11}, I_{33}, and I_{13}, and Γ is the derivative operator. These model equations, together with 16 Marshak's boundary conditions derived for diffusely emitting and reflecting opaque boundary, are solved numerically using a solver called ELLPACK (ref. 24).

To incorporate radiation calculations into the overall flame structure analysis, there are two major difficulties to be overcome. First is that equations for the moment of intensity such as Eq. (14) are elliptical, whereas equations represented by Eq. (1) are parabolic. It seems impossible to solve both systems simultaneously. An alternative, which we are testing now, is to iterate between these two systems until the results numerically converged. The second difficulty is on modeling the spectral radiative properties for integrating the RTE over the spectral range. We will first follow the wide-band approach used by Song and Viskanta (ref. 25).

Preliminary Results and Discussion

We first tested the flame structure and soot formation/oxidation predictions against results in Kent and Honnery (ref. 18) for an ethylene-air turbulent diffusion flame (nozzle diameter $D = 3$ mm, exit velocity $U_0 = 52$ m/sec, $Re_D = 9615$). Good agreement was found for mixture fractions. Fig. 3 shows the comparison for the temperature along the centerline and radially at $x/x_m = 0.4, 0.7$ ($x_m = 115D$). The dashed curve is from adiabatic combustion calculation, and the solid curve from a correction (ref. 21)

$$T = T_{ad}\left[1 - \beta\left(\frac{T_{ad}}{T_{max}}\right)^4\right], \tag{15}$$

where T_{ad} is the adiabatic temperature, T_{max} is the maximum adiabatic temperature, and $0.09 < b < 0.15$. Even Eq. (15) still over-predicts at the flame tip and outer edge. This demonstrates the importance of including the energy equation and detailed radiation heat transfer calculations.

Fig. 4 shows that the soot formation/oxidation model predicts soot volume fraction accurately. The over-prediction near the outer edge is caused by that of temperature. Fig. 5 shows the temperature and soot volume fraction contours, calculated using the same rate coefficients, for one of our test conditions ($Re_D = 536$, $Re_L = 7400$). The temperature contour shows a much taller and wider 0-g flame, as expected. The 0-g flame soot volume fraction contour is obviously unreasonable, since different rate constants are needed as concluded from laminar flame data. A reasonable prediction is possible by decreasing the level of oxidation for 0-g, which agrees with laminar flame results. 0-g measurements are needed for determining the rate constants.

The implementation of a iterative process between the RTE and the flame structure solvers has not been completed. Some numerical problems have been experienced, which are believed to be caused by zero β in part of the cylindrical enclosure where there is no flame. Fig. 6 shows the results of a forward calculation of the terms in the energy equation. Referring to Eq. (1) with $\phi = \bar{H}$ and $S_\phi = -\nabla \cdot \vec{q}_{rad}$, those two terms on the left are convection terms, and the first term on the right is conduction with the last term being radiation. The first three terms are calculated using total enthalpy from the adiabatic combustion calculation for 1-g. The last term is calculated using the temperature from Fig. 5 with an assumed uniform soot volume fraction of 10^{-8}. It is clear that all these terms are of about the same magnitude, and the radiation

term depends strongly on location. This confirms the importance of incorporating detailed radiation calculation into the flame structure analysis.

The modeling can be improved by accounting for interactions between turbulence and radiation (refs. 12 and 25), and between turbulence and buoyancy (ref. 22). The latter should be an important factor between 1-g and 0-g conditions.

Acknowledgments

The authors are indebted to J.-Y. Chen of UC/Berkeley for providing the solver code for turbulent reacting free-shear flows and John Roma of Baldwin Wallace College for electron microscopy and size analysis works.

References

1. H. A. Becker and D. Liang, "Soot Emission, Thermal Radiation, and Laminar Instability of Acetylene Diffusion Flames," Comb. Flame, Vol. 52, 247-256, 1983.
2. R. B. Edelman, M. Y. Bahadori, S. L. Olson, and D. P. and Stocker, "Laminar Diffusion Flames Under Micro-Gravity Conditions," AIAA-88-0645, AIAA 26th Aerospace Sciences Meeting, Reno, Nevada, 1988.
3. S.-M. Jeng and G. M. Faeth, "Species Concentrations and Turbulent Properties in Buoyant Methane Diffusion Flames," J. Heat Transfer, Vol. 106, 721-727, 1984.
4. J. P. Gore and G. M. Faeth, "Structure and Spectral Radiation Properties of Turbulent Ethylene/Air Diffusion Flames," 21st Symp. (Int.) Comb., 1521-1531, 1986.
5. K. J. Syed, C. D. Stewart, and J. B. Moss, "Modeling Soot Formation and Thermal Radiation in Buoyant Turbulent Diffusion Flames," 23rd Symp. (Int.) Comb., 1533-1541, 1990.
6. J. B. Moss, C. D. Stewart, and K. J. Syed, "Flow field Modeling of Soot Formation at Elevated Pressure," 22nd Symp. (Int.) Comb., 413-423, 1988.
7. Menguc, M. P., and Viskanta, R., 1986, "Radiative Transfer in Axisymmetric, Finite Cylindrical Enclosures," J. Heat Transfer, Vol. 108, 271-276.
8. D. Griffin and P. S. Greenberg, "Selected Microgravity Combustion Diagnostics Techniques," 2nd Int. Microgravity Comb. Workshop, Cleveland, Ohio, 1992.
9. J. C. Ku and K.-H. Shim, "Optical Diagnostics and Radiative Properties of Simulated Soot Agglomerates," J. Heat Transfer, Vol. 113, 953-958, 1991.
10. R. W. Bilger, "Turbulent Jet Diffusion Flames," Prog. Energy Comb. Sci., Vol. 1, 87-109, 1976.
11. F. C. Lockwood and A. S. Naguib,, "The Prediction of the Fluctuations in the Properties of Free, Round-Jet Turbulent Diffusion Flames," Comb. Flame, Vol. 24, 109-124, 1975.
12. G. M. Faeth, S.-M. Jeng, and J. Gore, "Radiation from Fires," ASME HTD-Vol. 45 Heat Transfer in Fire and Combustion Systems, 137-151, 1985.

13. J.-Y. Chen, W. Kollmann, and R. W. Dibble, "Numerical Computation of Turbulent Free-Shear Flows Using a Block-Tridigonal Solver for a Staggered Grid System," 18th Annual Pittsburgh Conf. Modeling and Simulation, 1987.

14. W. C. Reynolds, "The Element Potential Method for Chemical Equilibrium Analysis: Implementation in the Interactive Program STANJAN," Department of Mechanical Engineering, Stanford University, 1986.

15. R. W. Bilger, "Reaction Rates in Diffusion Flames," Comb. Flame, Vol. 30, 277-284, 1977.

16. S. K. Liew, N. C. Bray, and J. B. Moss, "A Flamelet Model of Turbulent Non-Premixed Combustion," Comb. Sci. Tech., Vol. 27, 69-73, 1981.

17. B. F. Magnussen and B. H. Hjertager, "On Mathematical Modeling of Turbulent Combustion with Special Emphasis on Soot Formation and Combustion," 16th Symp. (Int.) Comb, 719-729, 1976.

18. J. H. Kent and D. Honnery, "Soot and Mixture Fraction in Turbulent Diffusion Flames," Comb. Sci. Tech., Vol. 54, 383-397, 1987.

19. I. M. Kennedy, W. Kollmann, and J.-Y. Chen, "A Model for Soot Formation in a Laminar Diffusion Flame," Comb. Flame, Vol. 81, 73-85, 1990.

20. I. M. Kennedy, W. Kollmann, and J.-Y. Chen, "Predictions of Soot in Laminar Diffusion Flames," AIAA Journal, Vol. 29, 1452-1457, 1991.

21. K. M. Leung, R. P. Lindstedt, and W. P. Jones, "A Simplified Reaction Mechanism for Soot Formation in Nonpremixed Flames," Comb. Flame, Vol. 87, 289-305, 1991.

22. M. Fairweather, W. P. Jones, and R. P. Lindstedt, "Predictions of Radiative Transfer from a Turbulent Reacting Jet in a Cross-Wind," Comb. Flame, Vol. 89, 45-63, 1992.

23. J. P. Gore, U.-S. Ip, and Y. R. Sivathanu, "Coupled Structure and Radiation Analysis of Acetylene/Air Flames," J. Heat Transfer, Vol. 114, 487-493, 1992.

24. J. R. Rice and R. F. Boisvert, Solving Elliptic Problems Using ELLPACK, Springer-Verlag, New York, 1985.

25. T. H. Song and R. Viskanta, "Interaction of Radiation with Turbulence: Application to a Combustion System," J. Thermophysics, Vol. 1, 56-62, 1987.

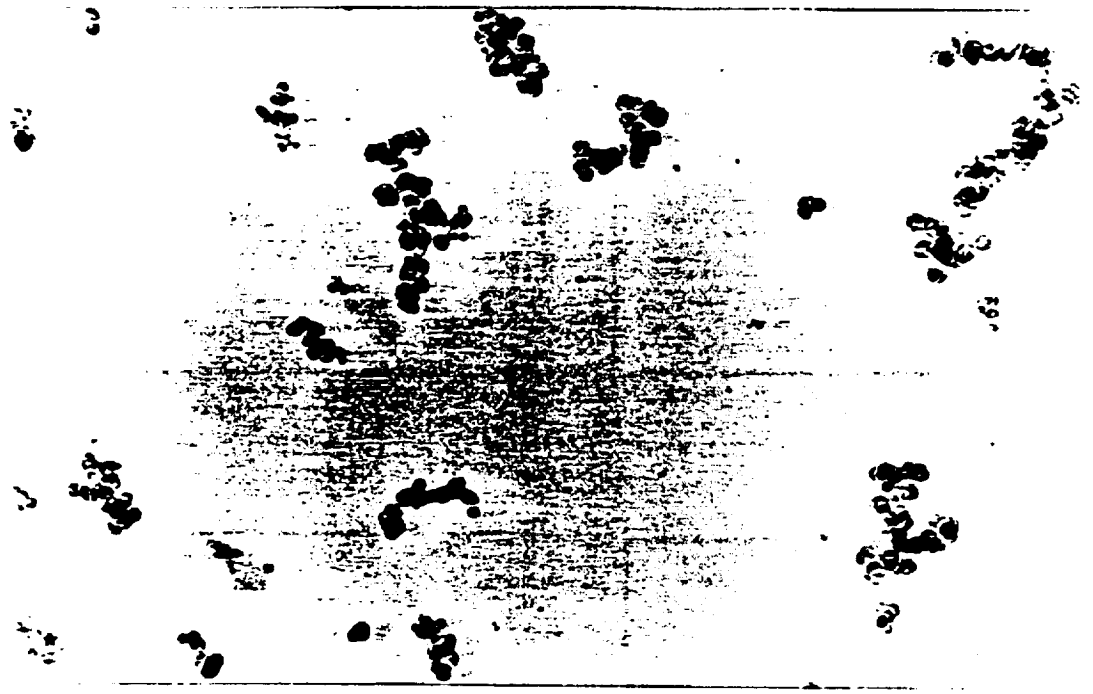

(a) 1-g flame, 40 mm HAB

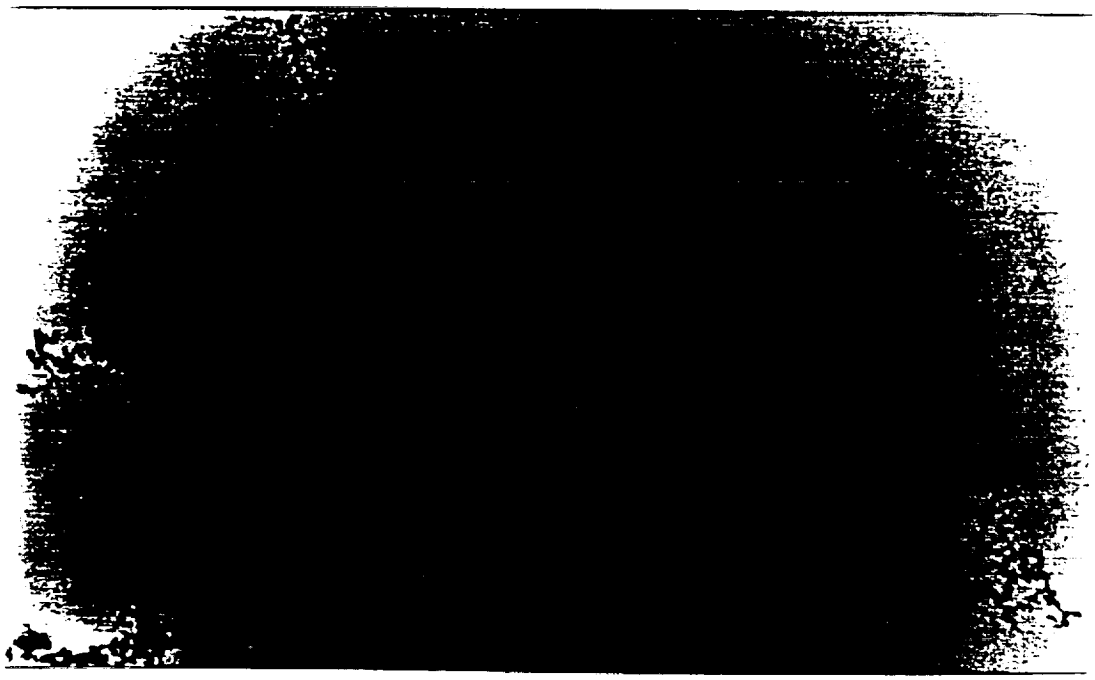

(b) 0-g flame, 80 mm HAB

Figure 1. Micrographs of soot aggregates in 1.5 cc/sec propane-air laminar diffusion flames under (a) normal, and (b) reduced gravity conditions. (1.7 mm nozzle dia.)

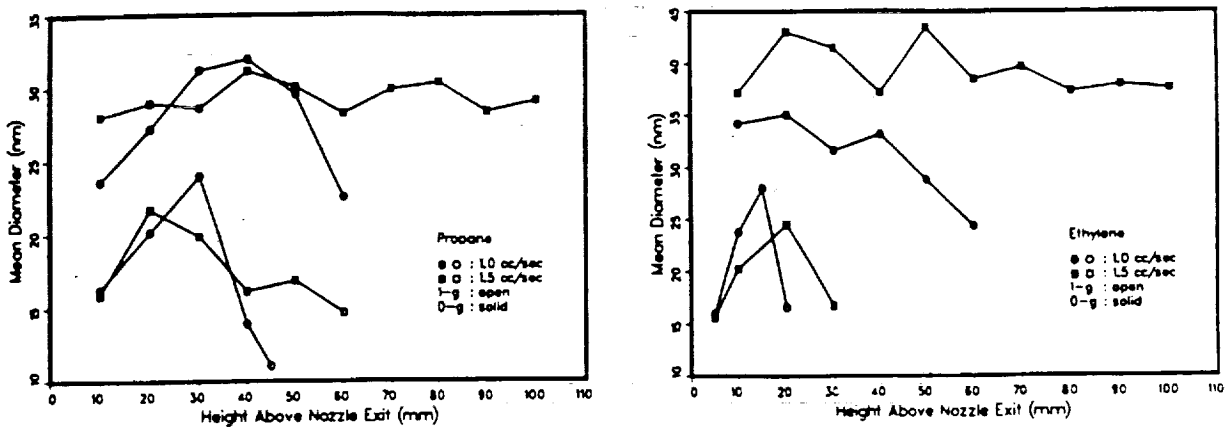

Figure 2. Mean diameter of primary soot particles in laminar diffusion flames.

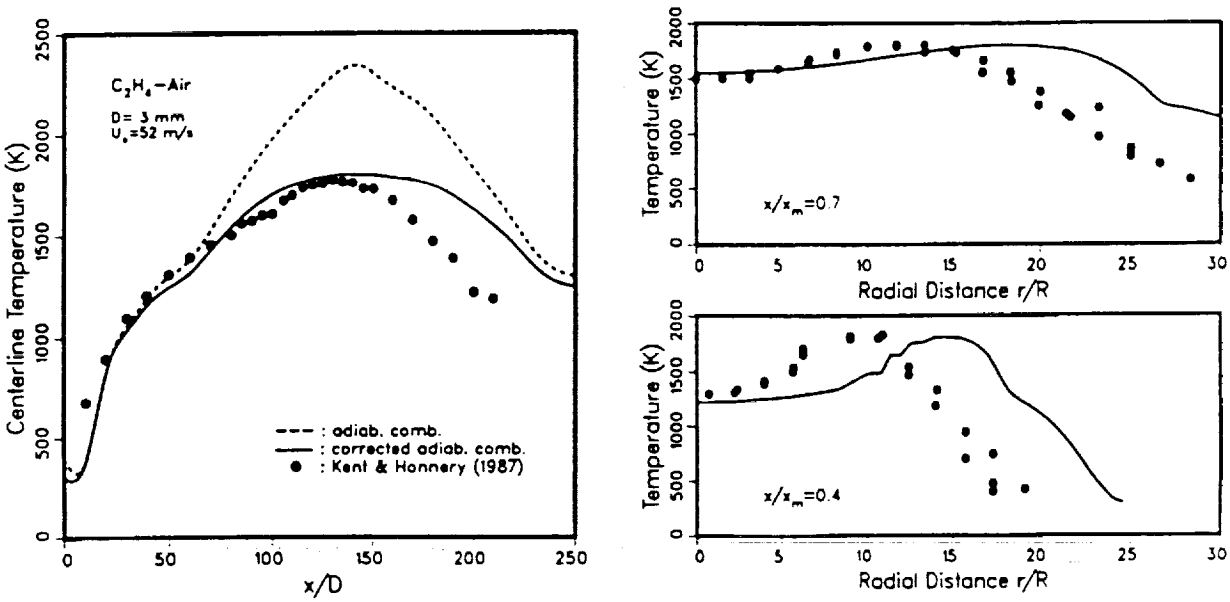

Figure 3. Comparisons of predicted and measured turbulent flame temperatures.

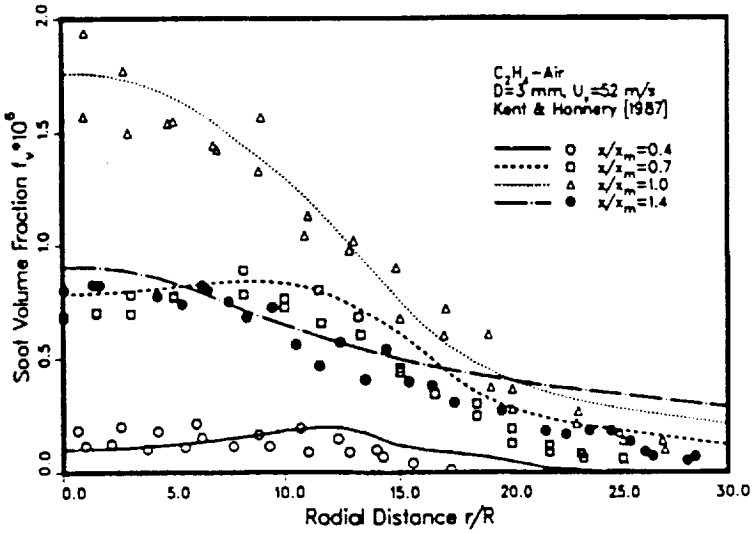

Figure 4. Predicted and measured turbulen' flame soot volume fractions.

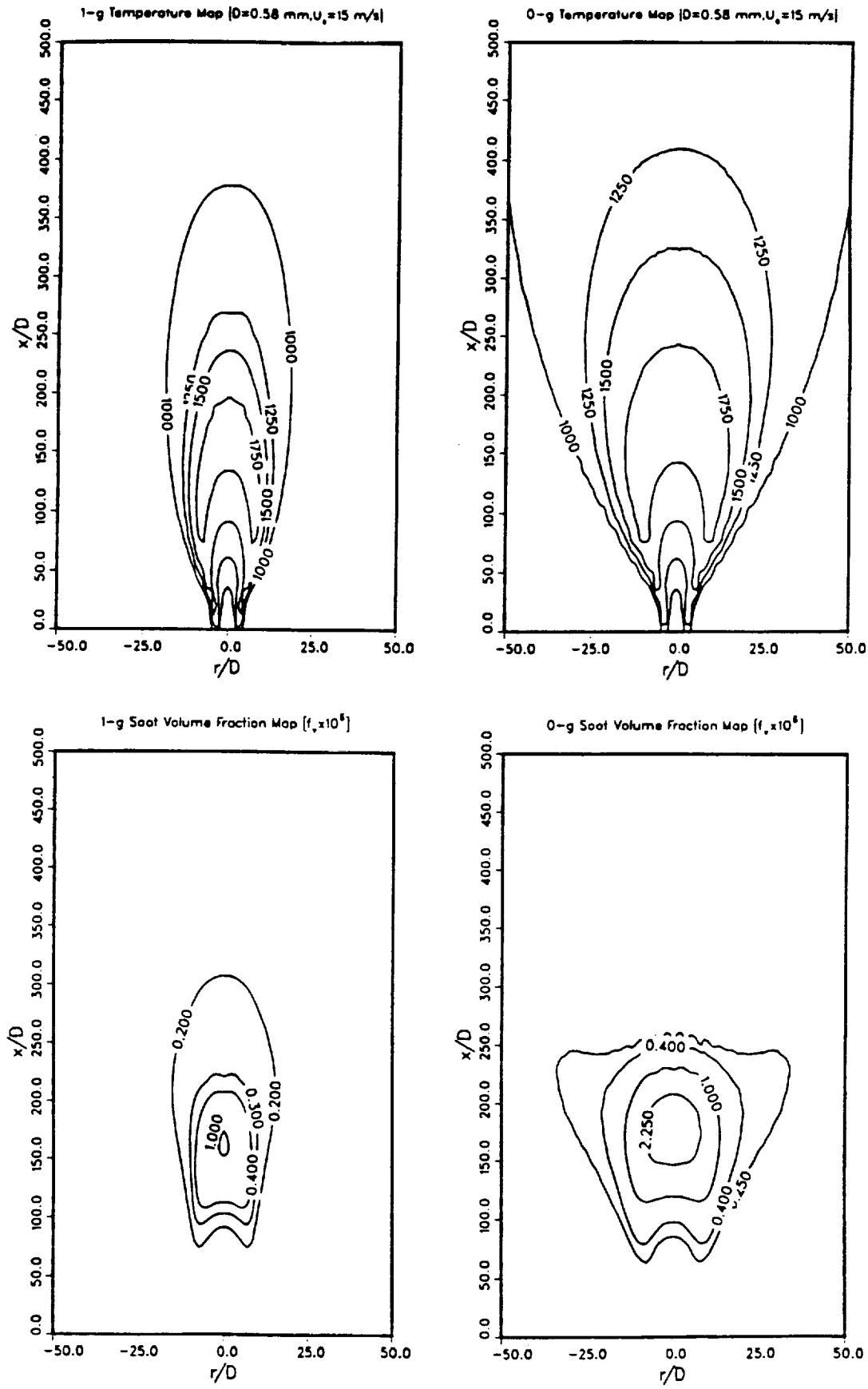

Figure 5. Normal- and reduced-gravity ethylene-air turbulent diffusion flames.

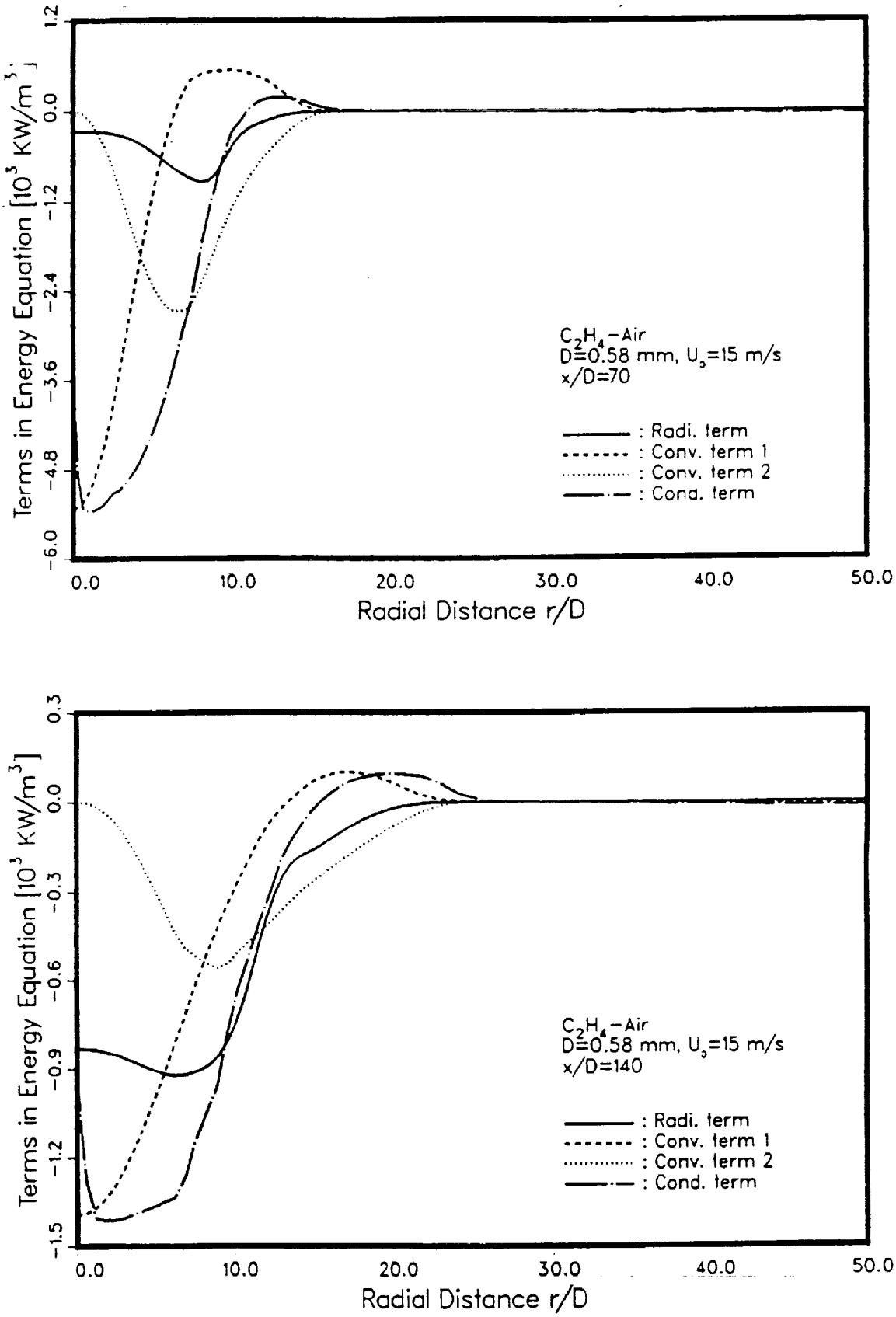

Figure 6. Estimated values of various terms in the energy equation with radiation.

COMMENTS

Question (J.P. Gore, Purdue University):

(1) What is the magnitude of turbulence-radiation interactions, and what is the justification for neglecting this effect in preference to scattering? Scattering is more important in optical diagnostics in the visible rather than in the thermal radiation term in energy equations.

(2) The effects of joint probability distribution functions between mixture fraction and enthalpy are important. Do you plan to model these?

(3) Are the soot volume fraction data from Kent and Honnery (1987) path-integrated equivalent measurements? If so, how is the comparison with predictions made?

(4) Chemical equilibrium calculations are not in agreement with measurements on the fuel-rich side. Should the model be improved in this aspect?

(5) In your verbal response you mentioned that there are other uncertainties such as refractive indices of soot. However, work reported in the literature has shown that items (1), (2) and (4) above have a very strong (even order of magnitude) influence on radiation heat loss. In my opinion, these need to be addressed with priority.

Answer: (1) There is no attempt at this point to model or estimate the magnitude of turbulence-radiation interaction, or to justify that it is negligible. The turbulence-radiation interaction is not included due to its complexity and the lack of definitive information about its effects. On the other hand, the scattering effects have been shown to be significant (Ref. 9) and can be dealt with in our radiation heat transfer calculations.

(2) We agree that the effects of joint pdf between mixture fraction and enthalpy are important and should be included in the model. However, this will not be our focus. Instead, we plan to follow works in existence, such as those by the commentator (Ref. 23), and those developed in the future.

(3) We believe that soot volume fraction data in Kent & Honnery (Ref. 18) are local values, instead of path-integrated. The last sentence in the second paragraph in Experimental Procedure states that horizontal traversing and Abel inversion were applied to extract local extinction data.

(4) Yes. We will improve this aspect of the model by using the laminar flamelet model, as indicated in the paper.

(5) One may argue that soot refractive index data are fairly accurate in the visible wavelengths, even though we are not perfectly convinced of that. However, it is fair to say that data in the infrared are highly questionable. Since there is no directly related analysis on the effects of this uncertainty, we plan to investigate this aspect more quantitatively.

Question: (Ivan Catton, UCLA): In transport processes, one is usually interested in number density and a mean diameter. Your electron micrographs show shapes as far from spherical, and one has to wonder what the "mean diameter" represents.

Answer: We consider soot particulates as aggregates of near-spherical primary particles. The shapes, as referred to in the question, are shapes of aggregates. The mean diameters, as referred to in the paper, are mean diameters of the near-spherical primary particles.

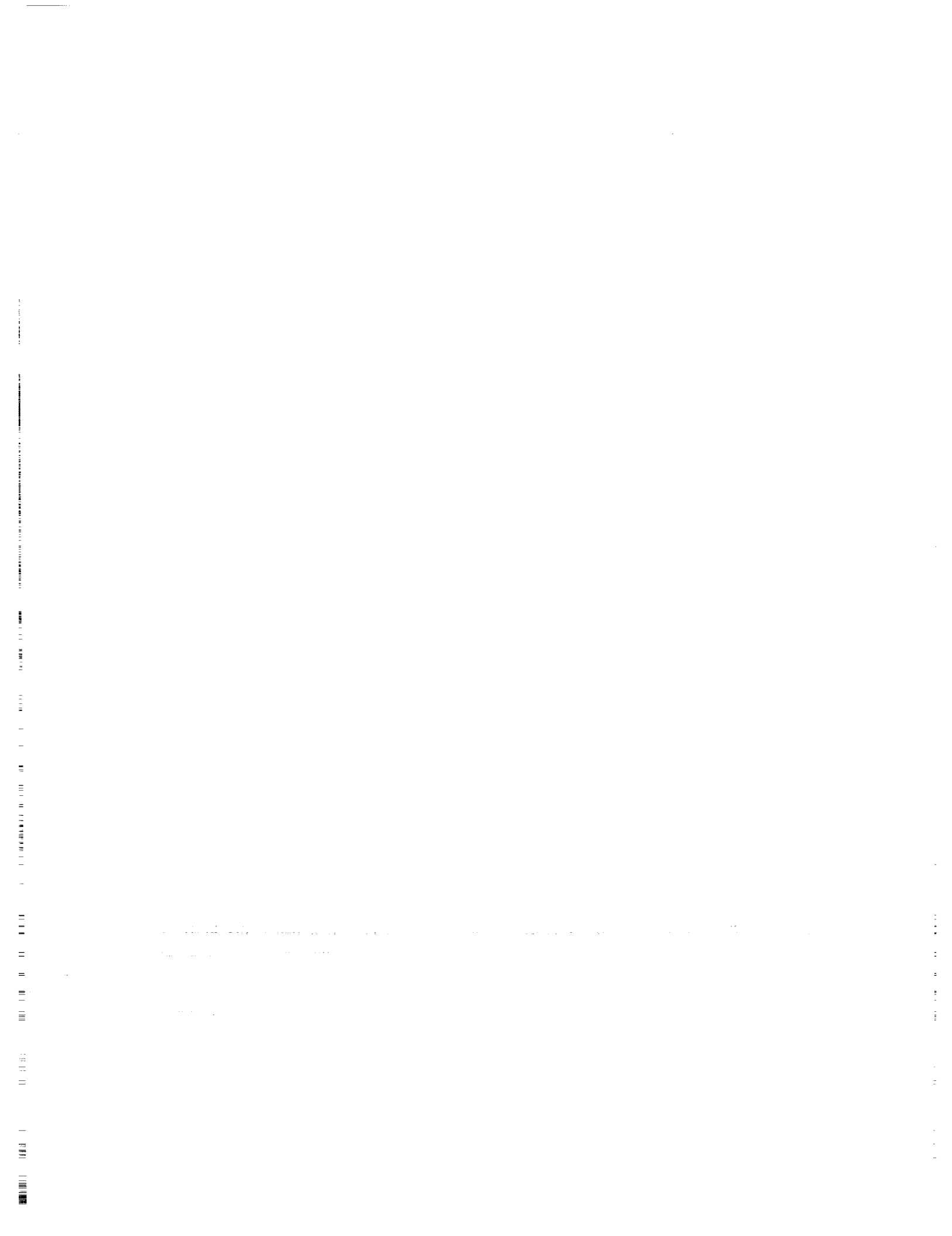

VISUALIZATION AND IMAGING METHODS FOR FLAMES IN MICROGRAVITY

N93-20193

Karen J. Weiland
NASA Lewis Research Center
Cleveland, Ohio 44135

Introduction

The visualization and imaging of flames has long been acknowledged as the starting point for learning about and understanding combustion phenomena. It provides an essential overall picture of the time and length scales of processes and guides the application of other diagnostics. It is perhaps even more important in microgravity combustion studies, where it is often the only non-intrusive diagnostic measurement easily implemented. Imaging also aids in the interpretation of single-point measurements, such as temperature, provided by thermocouples, and velocity, by hot-wire anemometers. This paper outlines the efforts of the Microgravity Combustion Diagnostics staff at NASA Lewis Research Center in the area of visualization and imaging of flames, concentrating on methods applicable for reduced-gravity experimentation. Several techniques are under development: intensified array camera imaging, automated object tracking hardware and software, reactive Mie scattering, infrared emission imaging and two-dimensional temperature and species concentrations measurements. A brief summary of results in these areas is presented and future plans mentioned.

Qualitative Visualization

In many microgravity combustion studies, the systems of most interest lie near the limits of flammability, ignition, or stability, and typically have a dim, blue flame. Difficulties in detecting and imaging these flames using conventional photographic media or video cameras motivate the examination and demonstration of advanced imaging techniques. One approach we have explored is the use of intensified array cameras based on both charge injection device (CID) and charge coupled device (CCD) arrays. The camera contains a microchannel plate intensifier consisting of a photocathode, which converts the photons entering it from the lens into electrons; a microchannel plate, which multiplies the number of electrons; and a phosphor anode, which converts the electrons back into photons. The luminous sensitivity of the camera is increased thereby as much as four orders of magnitude and allows a faceplate illuminance of 10^{-6} to 10^{-5} lux to be detected. Photocathodes sensitive in the visible to near-infrared from 400 to 900 nm and in the ultraviolet from 250 to 650 nm are in use. The output from the camera is available as a RS-170A video signal.

Intensified array cameras have been demonstrated in our 1-g laboratory by imaging several combustion systems, specifically, dilute premixed hydrogen flames, low-pressure gas jet diffusion flames, premixed Bunsen-type flames, solid surface, and low-pressure droplet burning. Results have been obtained using both the visible to near-infrared and ultraviolet photocathodes. Examples of some of these flames are shown in Fig. 1 and 2. Dilute mixtures of hydrogen and air (7% hydrogen) have been imaged by both cameras without the addition of a Halon colorant, previously needed to detect the flames using photographic film. . The image shown in Fig. 1, obtained with the visible to near-infrared camera, is stronger than that obtained using the ultraviolet camera. The cameras are detecting light from different emitters: the visible to near-infrared detects the emission in the near-infrared from the hot water produced in the flame, but the ultraviolet camera detects light from the OH radical centered at 308 nm.

The camera is also able to detect a small, laminar, hydrogen gas jet diffusion flame burning at a total pressure of 100 Torr, which is invisible to the eye. Both cameras have also imaged premixed Bunsen-type methane flames with bandpass filters. Several images of this flame are shown in Fig. 2.

In a reduced-gravity demonstration, an intensified CID camera imaged weakly luminous flames spreading over thermally thin paper samples aboard the NASA Learjet [1]. The camera observed the flames for ashless filter paper samples and laboratory wiper samples burning in quiescent, 21 and 18 percent oxygen environments. Most of the flames would have been difficult to detect using film. Attempts in 1-g to use lower pressure and higher oxygen concentrations to emulate the reduced-gravity combustion were not successful as the flames burned much brighter in 1-g, pointing out the dramatic changes which occur upon greatly reducing buoyant convection. In another reduced-gravity use, premixed hydrogen gas mixtures similar to those in Fig. 1 were imaged using an intensified CCD camera aboard the NASA KC-135A [2]. Heretofore unseen and unpredicted flame structures and behaviors were observed. The use of such a camera is now being planned for a proposed space-flight experiment to further study these flames.

Another type of qualitative visualization which provides an indication of the location of the reaction zone in a flame is reactive Mie scattering [3]. Laser light scattering centers are created *in situ* by seeding the flame with a reactive compound, such as titanium tetrachloride. This material reacts with water produced in the reaction zone to produce particles of titanium dioxide. The light scattered from a laser light sheet by the particles can be imaged onto a detector. This technique was tried in 1-g for small methane and hydrogen gas jet diffusion flames having flow rates typical of those used in previous microgravity studies. With an argon ion laser for the light sheet source, a narrow-band interference filter at 488 nm, and a intensified CID camera, a significant amount of seed, ~0.1% of the total fuel flow of 160 sccm, was required to obtain an acceptable signal. A change in flame color suggested an effect on flame chemistry, although flame emission spectra were not quantified. Others have used this technique for the visualization of transitional and turbulent flame structures. Those flames had much higher total flow rates, and were only slightly perturbed by the production of the particles and hydrogen chloride, as evidence by a 60 K depression in the stoichiometric temperatures [3]. The formation of hydrogen chloride and subsequent problems with corrosion and venting will likely preclude the use of this technique in the reduced-gravity facilities, although the use of titanium isopropoxide, which does not produce HCl, is being considered. The use of a pulsed laser source for the light sheet is also being explored, as a means to reduce the background flame emission by gating of the camera to match the laser pulse length.

A major advancement in our capability to use non-optimum film or video images has been the development of a system for the automatic and semiautomatic tracking of objects on film or video tape using a color image processing and object tracking workstation [4]. The system components include a 16-mm film projector, a lens system, a video camera, an S-VHS tapedeck, a frame grabber, and computer-based storage and output devices. Tracking software has been developed to control the system via a computer. The program controls the projector or tapedeck frame incrementation, grabs a frame, image processes it, locates the feature of the object being tracked, and stores the coordinates in a file. The image processing that can aid in the analysis include selective thresholding, gradient and Laplacian filtering for edge detection, line histogram equalization to eliminate an uneven background, and multi-frame averaging. Applications of the system include tracking the propagation of a flame front over condensed-phase materials in microgravity and tracking the movement of a liquid-gas interface from a nearly invisible meniscus. The system also can be used for objective color characterization, such as that exhibited by the different color regions in a methane diffusion flame.

Infrared Emission Imaging

As mentioned above, many of the interesting flames found in microgravity studies are too weakly luminous in the visible portion of the spectrum to be easily seen by conventional film-based or video cameras. Although flames are not in complete thermal equilibrium, a large portion of their radiant energy is emitted as infrared radiation [5], which may be detected by infrared-sensitive devices. Visibly-clear flame gases emit in an infrared spectrum of discrete bands from hot combustion products. The mid-infrared emission occurs primarily from carbon dioxide at 2.8 and 4.3 microns and from water at 1.8 and 2.7 microns. The intensities and shapes of the bands depend on the temperature and composition of the combustion products. Measurements of temperature and concentration contours are desirable for making a comparison between the observed flame and model calculations. Fuel-rich mixtures also may contain soot, which emits broad-band radiation.

Until recently, the most common infrared cameras have been either single element or linear array detectors. For best detectivity, the detector element is cooled to cryogenic temperatures. The detector element may be combined with scanning optics to provide an expanded field-of-view and spatially-resolved images. These cameras possess some disadvantages for combustion diagnostics. For example, they contain moving parts in the scanning optics, which often produce a smeared image of a moving object. In addition, they are useful primarily for thermography of solids or liquids such as pools, which have known or measured emissivities, and not as useful for the detection of gas phase emissions because of the non-grey-body emissivities. They often give data output in temperature units rather than the intensities needed for spectral data analysis.

Newly developed cameras such as those based on platinum silicide or indium antimonide possess many qualities making them suitable for application to combustion diagnostics. They are sufficiently sensitive in the near- and mid-infrared spectral region of 1 to 5 microns to detect the infrared emissions and are true two-dimensional, solid-state, staring arrays. The output may be digital or a RS-170 video format suitable for display on a monitor, digitizing by a frame grabber, or recording on videotape for immediate playback or future analysis.

A low-resolution (128 x 128 pixels) platinum silicide camera has been used for our laboratory studies, although cameras with higher pixel counts are available at a significantly higher cost. The camera has a 100 mm focal length lens and an integration time of 1/30 sec. The bandpass filter supplied with the camera transmits wavelengths from 3 to 5 microns. An image obtained of a methane diffusion flame is shown in Fig. 3. The flame height as visible to the eye is 5 cm, but the camera is able to detect the structure of the invisible hot gases rising several cm above the flame.

Experimental work to obtain spatially- and spectrally-resolved infrared images has occurred in two areas. First, a monochromator having an infrared grating and detector has been acquired and will be used to acquire an infrared emission spectrum of the flame in order to identify the wavelength regions of interest. Some bandpass filters have already been identified and will be used to obtain spectrally-filtered images. Second, a contract under the Phase I Small Business Innovative Research program has resulted in the design and construction of an infrared imaging spectrometer. The spectrometer has demonstrated the ability to resolve wavelengths from 3 to 5 microns with 15 nm resolution for a propane/air torch flame.

The inversion of spatially- and spectrally-resolved infrared images to obtain species concentrations and temperature profiles still remains a major effort. It involves two parts: computerized image reconstruction using tomographic algorithms, and the analysis of infrared emission spectra. The medical industry has advanced the development of tomographic algorithms, which are being applied to combustion data [6]. Two main classes of algorithms, Fourier transform and iterative, are used. The analysis of infrared emission spectra is complicated by the fact that infrared emitting species also absorb and the path of the light from the emitter to the detector must be considered. Computer codes, such as the Aerodyne Radiation Code (ARC), have been developed to predict infrared spectra [7]. The

ARC calculates the infrared spectral signatures of rocket and aircraft exhaust plumes along a line-of-sight and includes molecular and particulate emission and absorption and chemiluminescent emission. Such codes may be useful for microgravity combustion. One of the goals of this research is to investigate combining code such as this with tomographic algorithms for simple combusting systems to obtain three-dimensional species and temperature profiles.

The acquisition of images of known emissivity radiators, such as soot or thin ceramic fibers placed in the flame, offers another possibility for obtaining temperature field measurements. The emission as seen through two or more narrow-band filters is fit to a Planck distribution function to yield a ratio temperature. Soot measurements have been studied extensively in the past and a body of literature exists for reference. Point and line measurements using thin ceramic fibers have been reported using fast response, near-infrared linear arrays [8]. Ceramic fiber grids are already being used successfully in the drop tower for the qualitative assessment of the temperature distribution in gas-jet diffusion flames and an individual fiber is being used as a tether and temperature indicator for an isolated, combusting droplet.

Two-dimensional Temperature and Species Measurements Using a Solid-State Laser Source

Two-dimensional measurements of temperature and species concentrations in combusting systems are of special value [9]. While various single-point (in time and space) methods have received considerable attention, knowledge of the instantaneous overall flow field is preferable, especially in turbulent or rapidly-evolving flow fields. The acquisition of many single data points does not always allow reconstruction of the flow field and is restricted in microgravity combustion studies by the limited experimental time and/or laboratory availability. Both molecular Rayleigh scattering and planar laser-induced fluorescence (LIF) have been used as imaging techniques and to provide temperature and species concentrations measurements.

Rayleigh scattering is an elastic scattering process, whose signal depends on the incident laser frequency, the molecular composition, and the number of scatterers. As the frequency of the light detected from all scatterers is the same as that of the incident laser light, the technique lacks species specificity. It suffers from interference from scattered laser light and Mie scattering from particles, but has a relatively high signal strength compared to other laser-based diagnostics. Rayleigh scattering is used for total density measurements, which can be related to temperature. LIF is used to detect an atom or molecule detecting fluorescence from an excited electronic state following the absorption of laser light. Species specificity is provided by tuning the laser wavelength to an absorption transition and selecting the observation wavelength, which may be the same as or shifted from the laser wavelength. Key combustion intermediates found near the flame front in the parts per thousand to parts per million, such as OH and CH, can be imaged using a planar light sheet. Quantitative measurements can be made but are more difficult. LIF can be used to measure temperatures by scanning the laser over several rotational transitions originating from different rotational levels having temperature-dependent populations.

Both techniques benefit from a laser source with a short pulse length and high peak power. LIF requires a tuneable laser source in the blue and ultraviolet. Rayleigh scattering measurements also benefit from a tuneable source, since the wavelength may be tuned away from flame emissions. Most currently-available laser sources used for laboratory-based, two-dimensional measurements are unsuitable for low-gravity and space flight applications for a variety of operational and safety reasons. Dye lasers use flammable solvents and toxic laser dyes which have only a finite lifetime. Excimer lasers use corrosive gases such as hydrogen chloride or fluorine, which must also be changed regularly. These lasers are also quite large and require much operator interaction.

The rapid development of pulsed, solid-state lasers based on titanium:sapphire offers a probable solution to the problems outlined above. Laser action in the titanium:sapphire crystal was first reported in 1982

and the material was developed rapidly into a laboratory device [10]. Continuous-wave lasers have been available from several vendors for several years and, recently, pulsed laser systems were introduced. The titanium:sapphire laser is broadly tuneable from 700 to 1000 nm. The production of blue and ultraviolet light useful for combustion diagnostics from such a laser by frequency conversion was demonstrated under a Phase I SBIR contract monitored by NASA Lewis in 1990 [11].

Acquisition of a laser system capable of performing the diagnostic measurements described above is in progress. Development and demonstration of these techniques using this laser source is an important step towards bringing the level of diagnostics commonly available to microgravity combustion research up to that available in other government, university, and industrial laboratories. The system will serve as a prototype for the future and will place the development of microgravity combustion diagnostics at the forefront of this rapidly evolving technological area.

References

1. Weiland, Karen J., "Intensified Array Camera Imaging of Solid Surface Combustion Aboard the NASA Learjet," AIAA Paper 92-0240, Jan. 1992; also NASA TM-105361.

2. Ronney, Paul D., "Studies of Premixed Laminar and Turbulent Flames at Microgravity," Proceedings of the Second International Microgravity Combustion Workshop, Cleveland, OH, Sept. 15-17, 1992.

3. Chen, L.-D., Seaba, J. P., Roquemore, W. M., and Goss, L. P., "Buoyant Diffusion Flames," Twenty-Second Symposium (International) on Combustion, The Combustion Institute, Pittsburgh, PA, 1988, pp. 677-684.

4. Klimek, Robert B., and Paulick, Michael J., "Color Image Processing and Object Tracking Workstation," NASA TM-105561, April 1992.

5. Gaydon, A. G., Flames. Their Structure, Radiation, and Temperature, 3rd ed., Chapman and Hall Ltd., London, 1970, p. 215.

6. Santoro, R. J., Semerjian, H. G., Emmerman, P. J., and Goulard, R., "Optical Tomography for Flow Field Diagnostics," *Int. J. Heat Mass Transfer*, Vol. 24, No. 7, 1981, pp. 1139-1150.

7. Bernstein, Lawrence S., Wornhoudt, Joda C., and Conant, John A., "The Aerodyne Radiation Code (ARC): Physical Assumptions and Mathematical Approximations," Aerodyne Research, Inc., ARI-RR-173, July 1979.

8. Vilimpoc, V., Goss, L. P., and Sarka, B., "Spatial temperature-profile measurements by the thin-filament-pyrometry technique," *Optics Letters*, Vol. 13, No. 2, 1988, pp. 93-95.

9. Eckbreth, Alan C., Laser Diagnostics for Combustion, Temperature, and Species, Abacus Press, Cambridge, MA, 1988, p. 362.

10. Moulton, P., "Spectroscopic and laser characteristics of Ti:Al_2O_3," *Journal of the Optical Society of America B*, Vol. 3, No. 1, 1985, pp. 125-132.

11. Rines, Glen A., and Moulton, Peter F., "Performance of Gain-switched Ti:Al_2O_3 Unstable-Resonator Lasers," presented at the OSA Topical Meeting on Advanced Solid State Lasers, Salt Lake City, UT, March 5-7, 1990.

Figure 1. Image of a 7% hydrogen in air premixed flame obtained using a visible to near-infrared intensified array camera. The image is at 0.2 sec following spark ignition in a closed vessel.

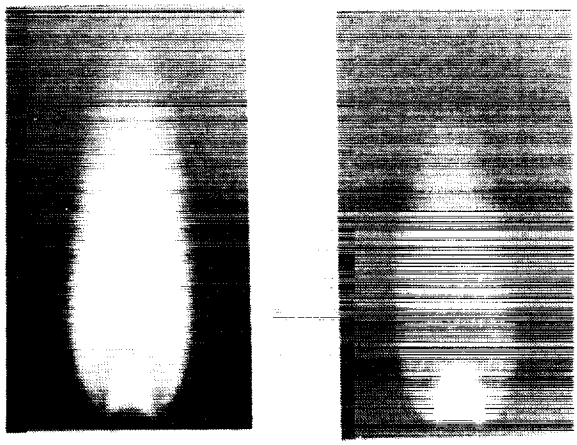

a) b)

1 cm

Figure 2. Images of a Bunsen-type, methane/air jet flame using an ultraviolet to visible intensified array camera. The images are obtained using interference filters centered at a) 307 nm and b) 431 nm and having a bandpass width of 10 nm before the camera.

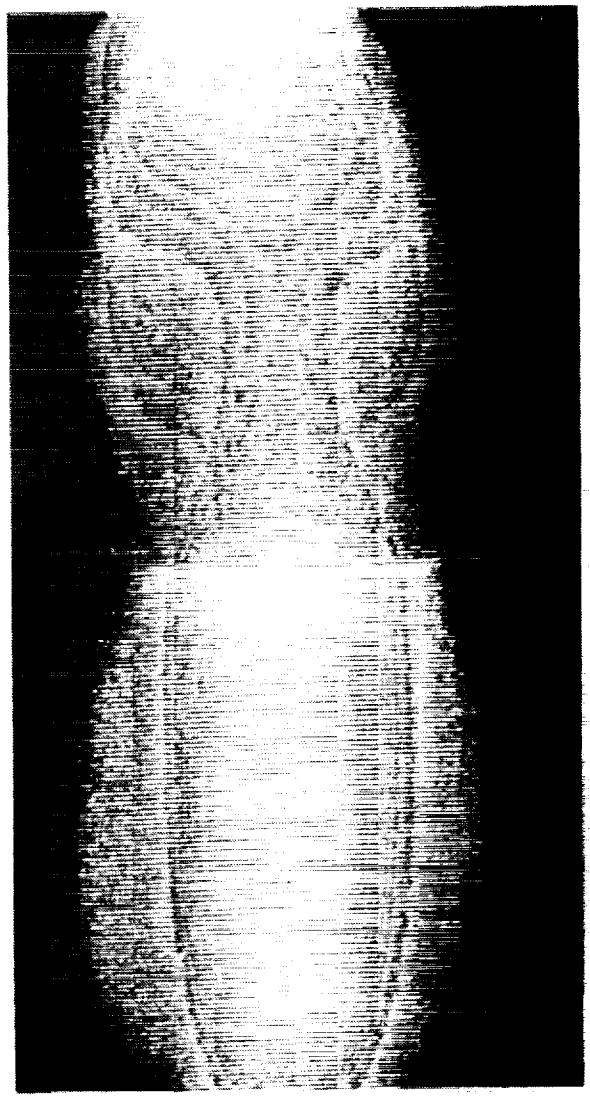

1 cm

Figure 3. Image of a methane gas jet diffusion flame obtained using a platinum silicide infrared array camera.

SELECTED MICROGRAVITY COMBUSTION DIAGNOSTIC TECHNIQUES

DeVon W. Griffin
Sverdrup Technology, Inc.
Brook Park, Ohio 44142

Paul S. Greenberg
NASA Lewis Research Center
Cleveland, Ohio 44135

Abstract

During FY 1989-1992, several diagnostic techniques for studying microgravity combustion have moved from the laboratory to use in reduced-gravity facilities. This paper discusses current instrumentation for rainbow schlieren deflectometry and thermophoretic sampling of soot from gas jet diffusion flames.

I. Rainbow Schlieren Deflectometry

Knowledge of the temperature field surrounding a combustion event is typically desired, particularly in microgravity combustion studies, to assess the relative importance of buoyancy. While temperature information may be obtained by intrusive devices such as thermocouples, this can significantly perturb a reduced gravity flame. Therefore, optical methods are preferred, with interferometry the most common approach. Interferometry is not without its drawbacks: temperature must be calculated from refractive index data, which are not always available, optical elements, paths and path lengths must remain fixed to a high degree of accuracy and visualization is difficult. One method of addressing the latter problem is the use of a grey-scale schlieren system, but the eye is relatively insensitive to grey scale differences. By replacing the Schlieren knife-edge with a color bar filter continuously varying in hue and the typical monochromatic source by a white light, gradients in the refractive index field are displayed as colors in the final image[1-2]. Howes has shown[3-4] this technique is as sensitive as Mach-Zehnder interferometry. Greenberg[5] et al, utilize computer generation of filters and processing of the image to obtain accuracies as good as those available with interferometry with the added benefit that requirements on optical path length and element stability are greatly relaxed. While the final information is given in terms of a refractive index, some knowledge of the combustion constituents and products allows calculation of temperature profiles. Due to these advantages, we have pursued development of this technology.

A schlieren optical system featuring off-axis parabolas (OAP's) is detailed in Figure 1. Due to the nature of schlieren optics, the collimating/decollimating mirrors are larger than the field of regard. As the field is increased, the cost of OAP's can rise dramatically. In addition, they present interesting alignment challenges. While the aforementioned difficulties do not necessarily preclude the use of OAP's, we have also pioneered the development of schlieren systems whose collimating mirrors are rotationally symmetric but are tilted with respect to the optical axis passing through the test section.[6] The primary mirrors may have either a spherical or parabolodial figure while catalog lenses correct the tilt-induced aberrations. All lenses have a broadband antireflection coating due to the large number of air/glass interfaces present.

Final complications in the design of these systems relate to the spatial and spectral properties of the fiber-optically coupled arc lamp that is used as a light source. With the sensitivity of a Rainbow Schlieren device proportional to the focal length, our systems had a F number as high as 30; most fibers emit light into an F-cone of roughly 2.5. Therefore, in one of our systems we place the fiber at the front working distance of a well-corrected microscope objective, which converts the F number to approximately 20, conserving sufficient throughput for the system to function properly.

Quantitative color hue measurements require a rugged source that is spectrally stable with time and has a uniform spectral intensity. We use a fiber-optically coupled arc lamp from ILC Technology. In this device, a feedback-stabilized xenon arc placed at one focus of an ellipse is coupled into a cylindrical sapphire waveguide at the other focus. The output end of the waveguide is polished to a radius

of curvature that produces a focus with a numerical aperture that matches most fibers, although the spot produced is less than optimal. This lamp has the unwanted property of generating large amounts of infrared radiation relative to the amount of visible light, which mandates attention be given to thermal loading in the arc lamp housing. We have experienced failure of the fiber coupler on one of our experimental rigs due to extreme heat loads.

Hue stability of the source is directly related to calibration requirements of the instrument. Since we interpret hue shifts as a ray deviation from a refractive index gradient, a change in the color output with time increases the amount of deviation required to observe a change in hue greater than the RMS noise. Our source tends to exhibit long-term drift over a period of approximately four hours. Therefore, any calibration older than roughly four hours exhibits somewhat decreased accuracy.

The concept of calibration ties together two issues: filter linearity in hue shift and filter fabrication. In the optimal case, a change in position of a ray striking the filter relates linearly to a change in hue as interpreted by the optical system. We represent color via utilization of the tri-stimulus values of red, green and blue in a Hue Saturation Intensity (HSI) model. Throughout its range, the filter changes hue continuously while remaining fully saturated. In fabricating a filter, we begin at one edge with red and progress around the HSI cone, while remaining at a constant intensity and saturation level. Due to the circular nature of the model, colors on the extreme ends of the filter are the same. When the hue has completed a full cycle, saturation is gradually reduced until all three colors contribute an equal amount producing a white band which appears on both ends of the filter. We use two methods to produce a filter. The pattern may be photographed on 35 mm slide film from the display of a high-resolution computer monitor. When taken as a single exposure, the background is black, which acts as a low-pass filter, reducing resolution in the final image. A double exposure which creates a clear background eliminates that problem. Alternatively, we can create digital set of values to describe the filter and from this set, a computer group at Lewis can produce slides.

The preceding discussion deals only with the fabrication of a filter in an ideal system. When such a filter is placed in an actual device with an empty test section, the non-uniform film sensitivity combined with uneven source and instrumental spectral transmission profiles result in a nonlinear variation of hue. To correct this problem, the filter is placed in the actual system and a spot is scanned across the filter and the hue recorded as a function of position. Our custom software then transforms the prescription for the original filter to one that, while irregular in an absolute sense, creates a linear hue variation when used in that specific system. An added complication is that the light source varies spectrally over the period of a few hours and exhibits long-term drift. While this reduces the accuracy of the measurements, we resolve gradients to roughly 0.2%. Given other uncertainties in the system, errors produced from source drift are rarely the limiting factor. However, new filters can and should be fabricated at regular intervals of lamp usage and when the lamp is replaced.

The final image of a rainbow schlieren system may be stored on video tape for later viewing and also as a data source for programs which invert the data and produce a quantitative refractive index field. We do not find the noise floor of the video system to be the limiting factor in the accuracy of the data. Video tape decreases the spatial resolution available, but does not have a large effect on the signal-to-noise ratio. We also observe that the CCD camera and transmitter generate no measurable increase in the noise floor.

In the use of a rainbow schlieren system, the size of the filter must be chosen to match the expected ray deflections. As the magnitude of the refractive index gradient grows, the ray displacement in the filter plane increases as well. Typically, we measure angular deviations on the order of two milliradians, which determine the size of the filter. While some researchers request angular deviations as large as eleven degrees, this is generally not a realistic number for a rainbow schlieren system for two reasons. First, filter size, generation and mounting become difficult, if not impossible. Second, the accuracy of the measurements can be severely degraded due to the presence of coma in the system. Rays parallel to the optical axis suffer only from spherical aberration, while those propagating at some angle with respect to the optic axis are generally affected by other aberrations, the magnitude of which varies

with the correction included in the optical design and fabrication tolerances. As coma is introduced, accuracy suffers because coma may be thought of as a variation of focal length across the field. Since knowledge of the focal length is required to calculate the refractive index distribution, the effects of coma must be considered.

Finally, we use filters somewhat larger than that required by the predicted ray deviations. As rays approach the edge of the filter, care must be taken to avoid interpreting the cutoff region as data. To avoid this problem, we reject any data close to the edge.

II. Soot Diagnostics

Diagnostic efforts in the study of soot have been directed toward determining size distribution and number density of soot within gas jet diffusion flames. To this end, we have demonstrated thermophoretic sampling in both 0 and 1 G laboratories and have performed imaging light extinction in 1 G.

Thermophoretic sampling is well established as a useful method for studying soot[7-11] in numerous types of flames. This technique consists of inserting Transmission Electron Microscopy (TEM) grids in the sooting region of a flame long enough to allow no more than ten percent of the surface to be covered with soot. TEM Photos of the aggregates are then digitized and computer processed to determine primary size distribution and aggregate dimensions. We implement this technique in a rig utilized in the 2.2 second drop tower at the NASA Lewis Research Center.

A simulated microgravity diffusion flame is illustrated in Figure 2 with a flow directed axially along the burner. In the region above and to the side of the flame, two thin stainless steel probes are shown, both of which support carbon-coated TEM grids. As implemented in our rig, the probes are thermally isolated from the flame using a thin aluminum plate with a slit oriented along the axis of the burner, with the probes attached to a pneumatically-activated support. The burner nozzle, probe support structure, and accompanying electrical and gas delivery systems are located in the combustion chamber at one end of the diagnostics rig (shown as Figure 3 in reference 12.) During a typical drop test, electronics within the rig sense the release of the package into free-fall and immediately ignite the flame. Approximately 1.4 seconds after ignition, the thermophoretic probes enter the soot shell and remain for roughly 40 milliseconds. We have found this is long enough to collect a sufficient amount of soot without violating the ten percent criterion.[10-11]

Following the drop, probes are removed from the rig and the grids photographed using the TEM. These negatives are then backlit and the image digitized using commercial CCD arrays and frame-grabber boards. A mix of in-house and commercial software allows us to measure primary size distribution as a function of height, radial position in the flame and maximum aggregate length. In addition, an intensity histogram, when correlated with the grey-scale background cutoff, gives the number of soot pixels in the two-dimensional image. This in turn yields the total 2-D projected area of the 3-D aggregate through use of an approximation.[10,11,13] We have found the size of primaries to be approximately a factor of two larger in low gravity and the aggregates as much as twenty times longer. While the approximation is thought to hold for aggregates of 2500 primaries or less, Köylü and Faeth[11] use it for slightly larger agglomerates. Due to the large size of our aggregates, we are also forced to extrapolate beyond the assumed limit. To date, we have measured only one aggregate with more primaries than the largest of Köylü and Faeth. We intend to examine the model[13] of Meakin, et al. in greater detail to adapt it to our larger aggregates.

A graph plotting the log of the estimated number of total particles versus the log of the maximum aggregate length divided by the average particle diameter, similar to those from References 10 and 11 is shown in Figure 3. The soot is sampled 10 mm above and 8 mm radially from the nozzle of an ethylene diffusion flame with a burner diameter of 2.29 mm and a flow rate of 1 cc/sec. While current data is somewhat sparse as of this writing, fractal numbers are 1.46 ± 0.12 for normal gravity and 1.93 ± 0.16 for reduced gravity, indicating the possibility of different aggregation processes.

The foregoing analysis produces a reasonable indication of soot size distributions within the flame. On the other hand, thermophoretic sampling does not yield information about the total quantity of soot

present in the flame. Therefore, the drop tower rig is also configured for imaging absorption, shown schematically in Figure 4. Light from a He-Ne laser is spatially filtered, expanded and collimated, following which it passes through the test section. As this light encounters the soot shell, it is absorbed or scattered. By making grey scale measurements of the background before the test and comparing those values to the reduced values seen while the flame is burning, quantitative data are obtained describing the total amount of soot present. We implement this procedure in our laboratory and have begun the process of incorporating it into the aforementioned rig used in the 2.2 second drop tower. The largest problem to date is a shifting of the spatial filter and/or laser beam when the package is released into freefall. A hardened spatial filter assembly is now in place and renewed tests should begin shortly.

IV. References

1. Settles, G.S., "Colour-coding schlieren techniques for the optical study of heat and fluid flow," Int. J. Heat and Fluid Flow, **6**, 3-15 (1985).

2. Vasil'ev, L.A., *Schlieren Methods*, (Israel Program for Scientific Translations, LTD) New York (1971).

3. Howes, W.L., "Rainbow Schlieren and its Applications," Applied Optics, **23**, 2449-2460 (1984).

4. Howes, W.L., "Rainbow Schlieren vs. Mach-Zehnder Interferometer: A comparison," Applied Optics, **24**, 816-822 (1985).

5. Greenberg, P.S., Klimek, R.B. and Buchele, D.R., "Quantitative Rainbow Schlieren Deflectometry," In preparation for submission to Applied Optics.

6. Buchele, D.R. and Griffin, D.W. , "A Compact Color Schlieren Optical System," submitted to Applied Optics.

7. Samson, R.J., Mulholland, G.W. and Gentry, J.W., "Structural Analysis of Soot Agglomerates," *Langmuir*, 3, 272 (1987).

8. Dobbins, R.A. and Megaridis, C.M., "Morphology of Flame-Generated Soot as Determined by Thermophoretic sampling," *Langmuir*, 3, 245 (1987).

9. Megaridis, C.M., "Thermophoretic Sampling and Soot Aerosol Dynamics of an Ethene Diffusion Flame," Ph.D. Dissertation, Brown University (1987); also available as NBS report NBGCR-87-532.

10. Megaridis, C.M. and Dobbins, R.A., "Morphological Description of Flame-Generated Materials," *Combustion Science and Technology*, **71**, 95 (1990).

11. Köylü, Ü. Ö. and Faeth, G.M., "Structure of Overfire Soot in Buoyant Turbulent Diffusion Flames at Long Residence Times," *Combustion and Flame*, 89, 140 (1992).

12. Lekan, J. et al, "Constraints and Capabilities of Drop Tower and Aircraft Facilities," Proceedings of the Second International Microgravity Combustion Workshop, 1992.

13. Meakin, P., Donn, B., and Mulholland, G.W., "Collisions between Point Masses and Fractal Aggregates," *Langmuir*, **5**, 510 (1989).

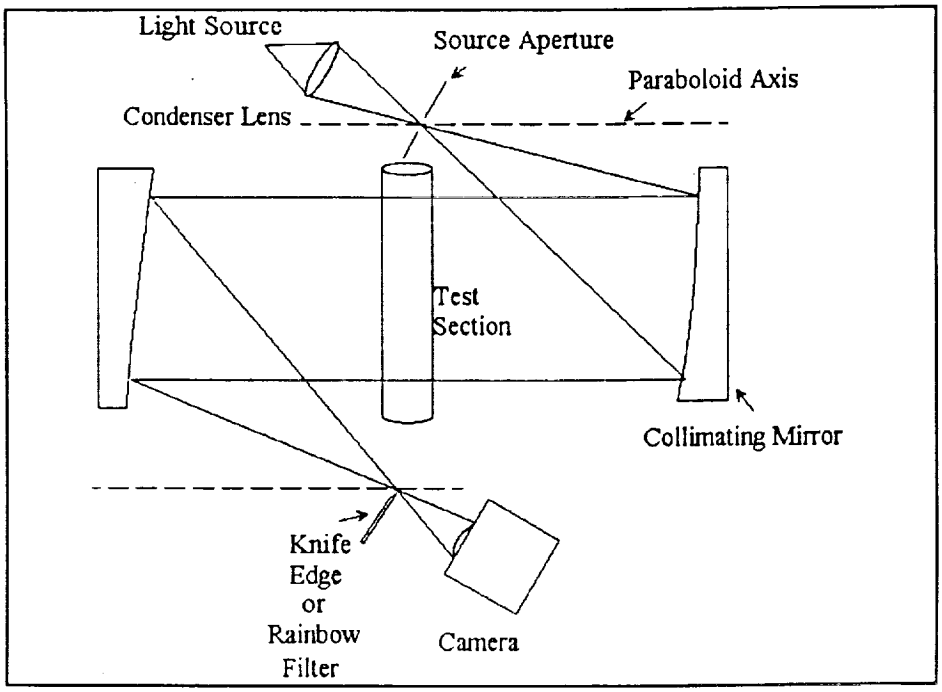

Figure 1
Typical Schlieren Optical System

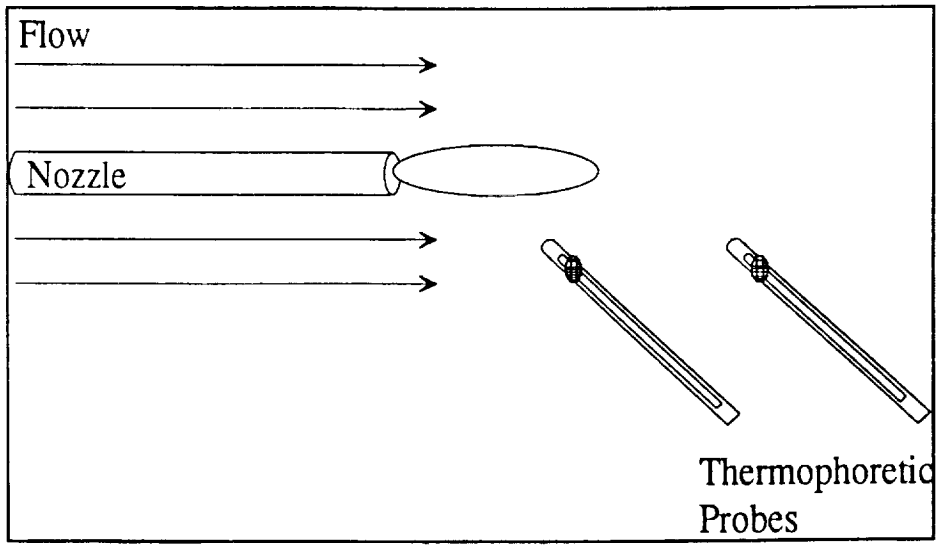

Figure 2
Thermophoretic Soot Sampling Geometry

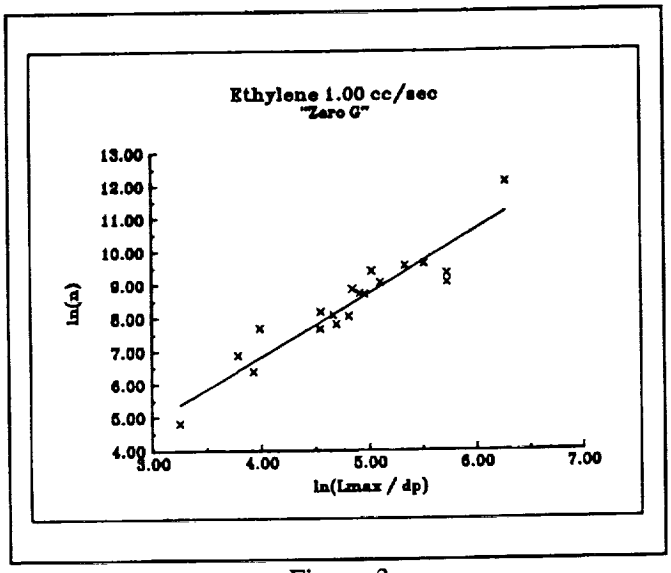

Figure 3
Analysis of Ethylene Aggregates

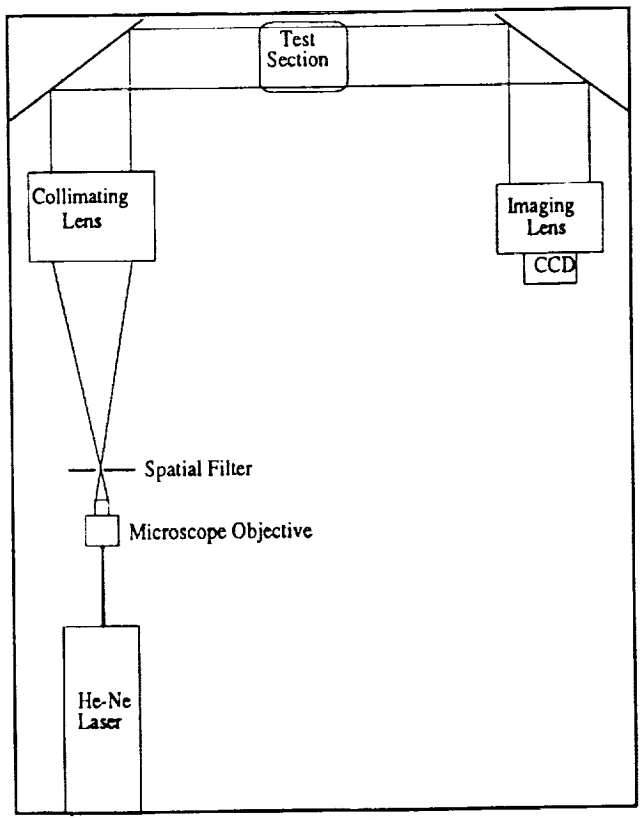

Figure 4
Imaging Absorption Geometry

COMMENTS

Question (Dr. Michael Winter, UTRC): What degree of temperature accuracy is available in the liquid- and gas-phase measurement using the rainbow schlieren technique?

Answer: Accuracy in using the rainbow schlieren technique for either gas or liquid phase temperature measurements depends on several quantities. First, the path length in which the refractive index changes must be known to a high degree of accuracy. This is much easier to determine for liquids with fixed boundaries or general axisymmetric distributions. In addition, the sensitivity of the system increases with the focal length of the decollimating lens. Finally, the quantity calculated is not temperature, but the refractive index distribution. Therefore, knowledge of the constituent substances and the dependence of their index on temperature is required before an accurate determination of the temperature can be made.

The foregoing begs the initial question (i.e., what temperature accuracies are available). We have measured liquid-phase temperatures with a full-field difference of 1 K and a resolution within that field of 0.2 K. While we have reconstructed refractive index profiles for gas-phase distributions, we have not yet performed temperature calculations, but expect to do roughly an order of magnitude worse.

Question (A. Gomez, Yale University): Thermophoretic sampling used to capture aggregates as large as 12 mm may suffer from some biasing with respect to particle size, since you operate in the continuous regimes (Kn approximately 10^{-2} to 10^{-1}). On the other hand in the free-molecular regime (Kn greater than 1), which is typical of n-gravity flames, there is no size-dependent effect on sampling. Could you comment on this complication?

Answer: Thermophoretic sampling of soot is a well-established technique for the study of soot produced in varying flames. [1-3] These studies were performed under normal gravity conditions. This question is directed specifically toward sample biasing due to operation in the continuum regime for large aggregates present in reduced gravity. A recent paper by Rosner, Mackowski and Garcia-Ybarra[4] has shown that even in this extreme, the maximum sampling bias will be at most approximately 20 percent. Therefore, the influence on population samples, morphologies or light scattering properties should be small. Since the fractal number is calculated using the slope of the best-fit line when plotting number vs. normalized size, this quantity should be imperceptibly affected.

REFERENCES:

1. Dobbins, R.A.and Megaridis, C.M. "Morphology of Flame-Generated Soot as Determined by Thermophoretic Sampling," Langmuir, 3, 254-259 (1987).

2. Megaridis, C.M. and Dobbins, R.A., "Morphological Description of Flame-Generated Materials," Combustion Science and Technology, 71, 95-109 (1990).

3. Koylu, U.O., and Faeth, G.M., "Structure of Overfire Soot in Buoyant Turbulent Diffusion Flames at Long Residence Times," Combustion and Flame, 89, 140-156 (1992).

4. Rosner, D.E., Mackowski, D.W., and Garcia-Ybarra, P., "Size- and Structure-Insensitivity of Thermophoretic Transport of Aggregated Soot Particles in Gases," Combustion Science and Technology, 80, 87-101 (1991).

LASER DIAGNOSTICS FOR MICROGRAVITY DROPLET STUDIES

Michael Winter
United Technologies Research Center
East Hartford, Connecticut 06108

N93-20195

ABSTRACT

Rapid advances have recently been made in numerical simulation of droplet combustion under microgravity conditions, while experimental capabilities remain relatively primitive. Calculations can now provide detailed information on mass and energy transport, complex gas-phase chemistry, multi-component molecular diffusion, surface evaporation and heterogeneous reaction, which provides a clearer picture of both quasi-steady as well as dynamic behavior of droplet combustion.[1] Experiments concerning these phenomena typically result in pictures of the burning droplets, and the data therefrom describe droplet surface regression along with flame and soot shell position. With much more precise, detailed, experimental diagnostics, significant gains could be made on the dynamics and flame structural changes which occur during droplet combustion. Since microgravity experiments become increasingly more expensive as they progress from drop towers and flights to spaceborne experiments, there is a great need to maximize the information content from these experiments. Sophisticated measurements using laser diagnostics on individual droplets and combustion phenomena are now possible. These include measuring flow patterns and temperature fields within droplets,[2] vaporization rates and vaporization enhancement,[3] radical species profiling in flames[4] and gas-phase flow-tagging velocimetry.[5] Although these measurements are sophisticated, they have undergone maturation to the degree where with some development, they are applicable to studies of microgravity droplet combustion. This program begining in September of 1992, will include a series of measurements in the NASA Learjet, KC-135 and Drop Tower facilities for investigating the range of applicability of these diagnostics while generating and providing fundamental data to ongoing NASA research programs in this area. This program is being conducted in collaboration with other microgravity investigators and is aimed toward supplementing their experimental efforts.

INTRODUCTION

Measurement Needs

Droplet Internal Flow

While modeling efforts of droplet combustion under microgravity conditions have been expanded to include transport and chemistry,[1] experiments are providing data on droplet surface regression rates along with flame and soot shell position. Even these limited data disagree with theory,[6] possibly as the result of gas-phase convection around the droplet and liquid-phase convection within it. The internal flows may largely be residual from the droplet deployment process in which a droplet is suspended on a hypodermic needle which is rapidly retracted. To understand the results of the experiment, it is necessary to characterize these droplet flow patterns and determine if they can be dissipated over some time delay period.

Gas-Phase Flow

Gas-phase motion over the surface of a droplet can have a profound impact on the droplet burning rate. Droplet deployment can leave droplets with a residual drift on the order of 1-2 mm/sec and as high as 10 mm/sec. Relative gas-phase motion of just a few mm/sec can result in a significant change in the droplet burning rate.[6] The effect of spark ignition can be a dramatic effect; it introduces a perturbation in the gas-phase flow resulting in a second source of residual gas/droplet motion. Techniques for anchoring a droplet in place using either fiber suspension or electrodynamic levitation certainly warrant investigation. These techniques alone, however, may not be adequate without assessing the gas-phase flow, possibly using a flow tagging or velocimetry imaging approach.

Flame Front Position

Knowing the position of the reaction front is important for anchoring computer models. Currently, an approximation of this position is obtained from back illumination images and natural light imaging on a second camera; these characteristics are not likely to be able to be related directly to predicted model parameters in a quantitative fashion. These can be difficult to interpret, since they are a line of sight measurement on a spherical body. Planar laser-induced fluorescence of OH could at least provide representative flame front positions[4]-even if only performed qualitatively. On the lean side of the flame, OH would prove reasonable as a flame front marker. Performed in a time resolved manner, these measurements could provide information on combustion unsteadiness regarding not only flame position relative to the droplet but also the structure of the flame.

Liquid-Phase Thermometry

Droplet combustion can be characterized as a generic gas phase diffusion flame with curvature but no flame stretch. The flame structure is, however, to some degree rate limited by evaporation; the transfer of heat into the droplet is therefore an important influence on the burning rate. Measuring the liquid phase temperature distribution could further the understanding of the flame behavior, particularly for multi-component droplet combustion.

Diagnostic Capabilities

Optical flow diagnostics offer several advantages over physical probes because they permit multi-point measurements non-intrusively. Non-intrusive measurements are of particular importance for droplet combustion and transport in microgravity environments where physical contact would introduce perturbations. The resolution of these diagnostics can also isolate transport to length-scales much smaller than the droplet diameter. These techniques can be configured to instantaneously map an entire flow field in two and three dimensions, providing either qualitative or quantitative information on the distribution of a desired scalar.

Internal Circulation and Quenched Fluorescence

The capability for measuring flow patterns within individual droplets[7] using oxygen quenching of laser-induced fluorescence has been demonstrated. Decane doped with naphthalene was used for the initial experiments. Droplets from a droplet-on-demand generator fall a short distance into a chamber filled with nitrogen and a variable amount of oxygen. A thin sheet of ultra-violet light from the fourth harmonic of a Nd:YAG laser at 266 nm illuminates single droplets. A magnified image of the naphthalene fluorescence is recorded digitally using a two-dimensional vidicon detector interfaced to a laboratory computer. Since oxygen is a strong fluorescence quencher, any liquid volume element which has been exposed to it by surface contact or diffusion will suffer a reduction in fluorescence intensity. Convection from the surface due to internal circulation and diffusion cause oxygenated image regions to appear darker. Oxygen-free experiments provide a baseline case for comparison. These data are shown in Fig. 1. This diagnostic can be used to describe flow patterns within droplets, and for determination of relaxation times for the motion to dissipate.

Exciplex Thermometry

Temperature measurements have been performed within droplets as a function of ambient temperature using two color detection.[2] The temperature measurement technique used is exciplex fluorescence thermometry, which exploits the fluorescence at two different wavelengths resulting from the reaction of an excited dopant molecule to form an excited-state complex or exciplex.[8] The technique was used to measure the temperature along a meridian plane of the droplets. An exciplex system is formed using naphthalene/TMPD in decane. At higher temperatures, the system monotonically shifts to increase monomer selective concentration and monomer fluorescence (blue/violet) dominates, hence, the ratio of monomer fluorescence over exciplex fluorescence (green) and the intensity ratio can yield the temperature. The resulting fluorescence from the droplet is imaged in two dimensions at both wavelength regions. The pixel-to-pixel ratio of these two images can be used, after calibration, to obtain the temperature. This measurement would be especially important for combusting multi-component droplets but due to the sensitivity to oxygen quenching has been used to date in non combusting systems. As will be described below, microgravity droplet combustion may present an ideal opportunity for implementation of this approach since the symmetric envelope flame may preclude oxygen from contacting the droplet fluid.

Levitation and Suspension of Droplets

The aforementioned diagnostic techniques rely on a droplet occupying a known position to allow the laser beam to "slice" through a central plane precisely . The droplet surface acts like a lens, bending the incident rays toward the center of the droplet. The light will appear to not fill the circumference (top and bottom) of the droplet if the illumination sheet is not incident on a great circle, slicing exactly through the center of the droplet. In typical microgravity experiments, slight drifts in droplet position are unavoidable. These drifts may be due to either droplet relative motion within the test chamber,

or, g-jitter which is typical of microgravity environments on aircraft. These drifts, however, can be compensated for by either an electrodynamic levitator or an extremely small fiber to tether the droplet.

Producing and supporting a droplet on a thin fiber or filament can be achieved repeatedly with automated deployment. A droplet-on-demand generator can produce a single droplet which is brought into contact with the fiber filament. When the filament has a slight material bead or buildup at some position along its length, the droplet becomes anchored and supported at that position. This arrangement is shown in Fig. 2. The diameter of the fiber and roundness of the bead require careful attention relative to the droplet diameter so as not to change the surface contour of the droplet at the wetting surface of the fiber. With careful consideration, these criteria are easily met. Droplets supported in this manner can be used for experimentation even in the presence of g-jitter. It should be noted that while the g-jitter effects the data quality, it will not effect the success of the experiments.

Flame Front and Gas-Phase Velocimetry

An additional research requirement would be detailing the gas-phase flow field and position of the flame front. This can be achieved using Planar Laser-Induced Fluorescence (PLIF) of OH[4] which is typically performed by tuning a laser to the OH molecular absorption and recording the emitted radiation with a two-dimensional detector. Laser sources and detection systems capable of operating under the power and shock environments typical of drop tower conditions may be available, however, some development is likely to be required. An alternative approach would be to provide laser-induced fluorescence from a diagnostic seed included in the liquid-phase fuel which would be consumed at the flame front. This, in principle, would be easier, and lower risk since the diagnostic capabilities and instrumentation already exist. The main advantage to this approach would be that the wavelength of the molecular absorption involved can be chosen to coincide with convenient laser wavelengths than lasers can be configured to access OH. The details of this approach will be given under the project description.

Gas-phase flow tagging is capable of defining the flow field around the droplet and can be performed in a number of different ways. For post-combustion gas conditions, photodissociating water vapor in known spatial locations and subsequently recording the PLIF of OH yields gas phase velocities.[5] This approach is probably beyond the scope of microgravity applications due to its complexity and instrumentation requirements. An alternative approach would be to use laser-induced phosphorescence, by writing lines in a pre-seeded flow and subsequent imaging the convection of triplet-state excited molecules. In this way, gas-phase velocities and flame positions could be measured.

Particle Image Velocimetry (PIV) holds the potential for recording two-components of velocity in a two-dimensional plane. Conventional techniques like Laser Doppler Velocimetry would not be appropriate because it is a point technique and would not provide information related to the global flow field. PIV uses lasers to illuminate a seeded fluid with two short, properly-timed pulses. In this way, each particle in a sheet of laser light can be illuminated and imaged twice in a frame of an imaging device such as a CCD camera. With this information, spatially resolved maps of two components of velocity can be determined. The proper selection of image magnification, pulse timing, particle size and seed rate, allow a two-dimensional velocity field to be acquired instantaneously. Video acquisition systems and computer software are used to process the images and manipulate them to produce the vector field.

PROJECT DESCRIPTION

Program Plan

The objective of this program is to perform a series of measurements to investigate the range of applicability of advanced laser diagnostics to microgravity applications while generating as much fundamental data to ongoing NASA microgravity research programs as possible. Through consultation with NASA personnel, and other researchers in the field of microgravity droplet transport and combustion, priorities will be established with respect to measurement parameters. The measurement parameters currently under consideration are:

(1) droplet internal flow
(2) relative gas-phase flow around droplets
(3) flame front position
(4) liquid-phase thermometery.

An integrated diagnostic unit, capable of performing these measurements will be assembled. All of the major components such as lasers, detectors and data systems are currently available and allocated to this effort. A self-contained miniature nitrogen-pumped dye laser system and two-dimensional intensified diode-array imaging system will form the core of the unit.

The testing program will proceed with ever more challenging environments proceeding from the laboratory, to flight based tests, and finally, to drop tower facilities. The diagnostic approaches and instrumentation would be verified in a laboratory setting. Experiments with the intent of reducing the risks associated with high impact and droplet drift would be conducted on either the Learjet or KC-135 Aircraft with fiber suspended droplets. Measurements will be performed on droplet internal flow patterns and the applicability of liquid phase thermometry in a burning droplet. Investigations will be made into performing PLIF measurements of OH or a diagnostic seed material to describe flame front position. Gas-phase flow dynamics will be determined by velocity measurements using particle image velocimetry.

Risk Reduction - Flight Experiments

Initial experiments are designed to reduce the risks associated with high impact and droplet drift. Experiments of droplet combustion under microgravity conditions are best if carried out in either the NASA LeRC 2.2-Second Drop Tower, or the 5.18-Second Zero-Gravity Facility, to provide a "clean" set of experimental conditions. Two aspects of these facilities and the environment they provide present the greatest challenges to laser diagnostic implementation. First, the impact at the bottom of the tower can range from 60 -70 g's. Designing advanced instrumentation to sustain these impacts is quite difficult. A risk reduction step is to perform a test sequence aboard the NASA Aircraft Microgravity Facilities. Although the aircraft do not provide as "clean" a microgravity environment, ($\sim 10^{-2}$ g), the diagnostic could be developed while still providing quality data. These experiments would be followed by measurements in the LeRC 2.2-Second Drop Tower.

Isolate Droplet Motion

The second challenge to diagnostic implementation is the droplet drift present in all previous microgravity droplet experiments. As described above, droplet deployment is always accompanied by some initial velocity which is imparted on the droplet. The relative motion of the droplet to the ambient gas can result in significant change in the burning behavior. Furthermore, this motion complicates the diagnostics. To alleviate these problems the experiments can be performed on droplets supported on a thin fiber, or supported in an electrodynamic trap. Fiber support is relatively simple, however, detailed measurements of the effect of the fiber boundary on droplet internal flow patterns would still need to be understood. The operation of electrodynamic traps becomes considerably simplified at low gravity due to the reduced forces on the droplet.

An automated deployment system will be coupled to thin filament suspension. A droplet-on-demand generator will produce a single droplet which is brought into contact with the fiber filament. The filament will have a slight material bead or buildup at some position along its length so that the droplet becomes anchored and supported at that position as is shown in Fig. 2. The diameter of the fiber and roundness of the bead will receive careful attention relative to the droplet diameter so as not to change the surface contour of the droplet at the wetting surface of the fiber. Droplets supported in this manner will be used for experimentation even in the presence of g-jitter. It should be noted that even though the g-jitter effects the quality of the data relative to combustion due to the gas-phase fluctuations, it will not effect the success of the experiments.

Internal Flow Patterns

Initial measurements are directed toward describing the internal flow patterns of droplets in a non-combusting environment. The convection of oxygen dissolved into the surface fluid of an isothermal, non-burning droplet will be detected by the quenching of laser-induced fluorescence. The fluorescence images will be recorded in two dimensions from a laser sheet, provided by a compact nitrogen laser, which slices through the interior of the droplet. This measurement can be performed in a time-phased manner with the introduction of a time delay to evaluate temporal evolution. These experiments could potentially answer questions relating deviations between current experiments and theory.

Liquid-Phase Thermometry

An extension of the flow measurement techniques will provide liquid-phase thermometry using the same apparatus. Laser-induced exciplex thermometry can be employed in a burning droplet, if it could be shown that no oxygen permeated into the measurement regions. This would be expected in microgravity conditions where a symmetric envelope flame surrounds the droplet and consumes oxygen prior to dissolution in the liquid-phase. This assumption is easily verified by repeating the flow pattern measurements on burning droplets. Liquid-phase thermometry would qualitatively confirm modeling assumptions while providing quantitative temperature data.

Flame Front Measurements

Development of the UTRC diagnostic system will be directed toward PLIF of OH. Potentially minor modifications to the nitrogen laser system may allow it to operate on excimer gases such as XeCl, thus providing a means of directly exciting the OH molecule. Alteratively, arc lamp illumination could be used. This would provide image data on

the position of the flame front around a burning droplet. A second alternative approach would be to perform laser-induced fluorescence from a diagnostic seed included in the liquid-phase fuel which would be consumed at the flame front. This, in principle, would be easier and the diagnostic capabilities and instrumentation already exist. The main advantage to this approach would be that the molecular absorption wavelength can be chosen to coincide with more-easily-accessed laser wavelengths than those of OH. Several diagnostic materials are available with readily available absorptions, high fluorescence yields, and flammability limits similar to typical fuels, i.e., biacetyl in methanol. For these studies, the nitrogen laser will be used in conjunction with the dye laser tuned to the appropriate wavelength.

Gas-Phase Flow

Particle Image Velocimetry (PIV) holds the potential for recording two-components of velocity in a two-dimensional plane. PIV will be performed using two pulses from the nitrogen laser to illuminate the gas surrounding the droplet after it is seeded with aerosol particles. In this way, each particle in a sheet of laser light can be illuminated and imaged twice in a frame of the imaging system. With this information, two components of the velocity vector will be determined. The proper combination of image magnification, pulse timing, particle size and seed rate, provide instantaneous two-dimensional velocity fields. Computer software to process these images and manipulate them to produce the vector field is currently in use at UTRC.

Conclusions

This research program provides measurements investigating the range of applicability of these advanced diagnostics while generating fundamental information relevant to ongoing NASA programs in microgravity droplet combustion. Using a progressive approach, advanced laser diagnostics will be transported from laboratory, to flight experiments, and ultimately to drop tower facilities. In this way, these diagnostics can be developed, while providing fundamental data on droplet transport and combustion at an early date. The experiments and measurement parameters suggested here, reflect the needs of other researchers in this area. Dissemination of the results of this program throughout the community will effect their research directly. At the conclusion of this program, the technology demonstrated herein will be applicable to future ground based research, as well as space based operation aboard future Shuttle, Space Lab or Space Station Freedom laboratory modules. The facility and techniques demonstrated would serve as a stepping stone for future programs. Development and demonstration of this technology at this time, is a prerequisite for these far reaching goals.

References

1. Cho, S. Y., Yetter, R. A. and Dryer, F. L.; A Computer Model for One-Dimensional Mass and Energy Transport in and Around Chemically Reacting Particles, Including Complex Gas-Phase Chemistry, Multicomponent Molecular Diffusion, Surface Evaporation and Heterogeneous Reaction, Journal of Computational Physics, 1991.
2. Winter, M.; Temperature Measurements Inside A Falling Droplet, ILASS, May 1990.
3. Anderson, T. J. and Winter, M.; Measurement of The Effect of Acoustic Disturbances on Droplet Vaporization Rates, AIAA Aerospace Sciences Meeting, Reno Nevada, 1992.
4. Hanson, R. K.; Combustion Diagnostics: Planar Imaging Techniques, Twenty-First Symposium (International) on Combustion, p. 1677, 1986.
5. Boedeker, L. R.; Velocity Measurement By H_2O Photolysis and Laser-Induced Fluorescence of OH, Optics Letters, Vol. 14 p. 473, 1989.
6. Williams, F. A.,Dryer, F. L.; Preliminary Science Requirements Document For The Droplet Combustion Apparatus, NASA LeRC, 1991
7. Winter, M. and Melton, L. A.;Measurement of Internal Circulation in Droplets Using Laser-Induced Fluorescence, Applied Optics, Vol. 29, No. 31, p. 4574, 1990 .
8 Murray, A. M., and Melton, L. A.; Fluorescent Methods for Determination of Temperature in Fuel Sprays, Appl. Optics, Vol. 24, p. 2783, 1985.

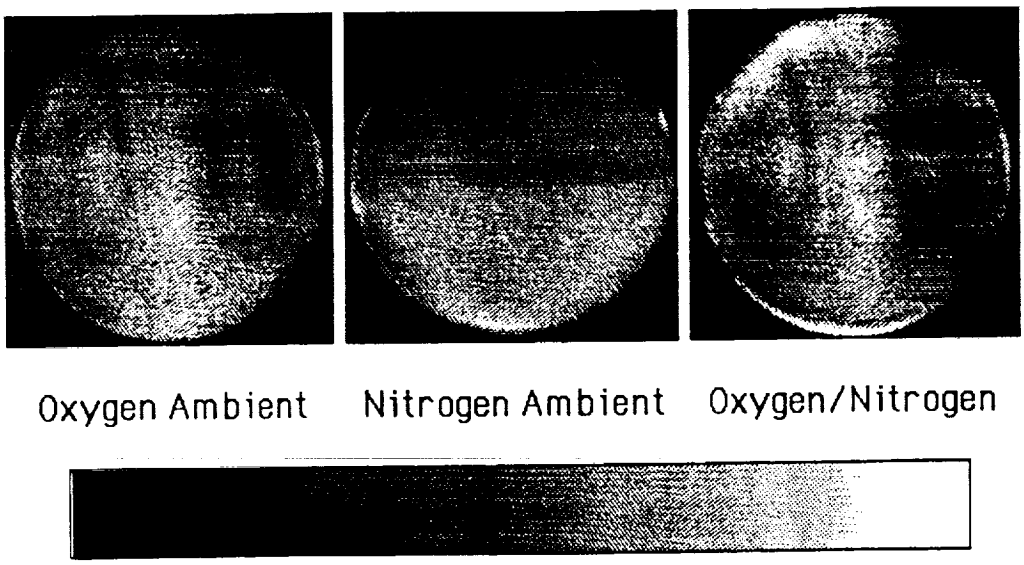

Fig. 1 Measurement of internal circulation from within droplets using fluorescence quenching.

See Color Plate C-7a

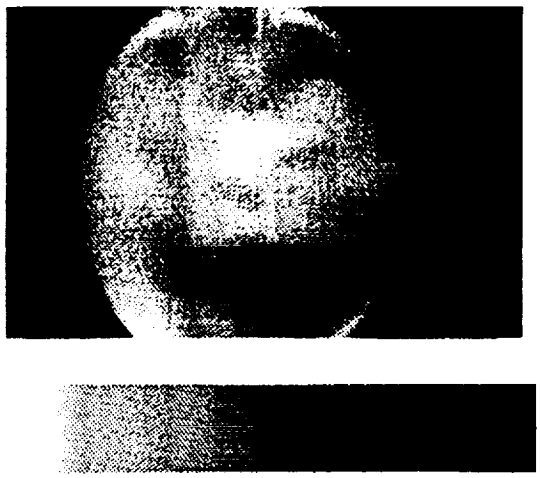

Fig. 2 Surface fluorescence quenching from a droplet supported on a fiber.

See Color Plate C-7b

COMMENTS

Question (A. Gomez, Yale University): In an electrodynamic balance, typically, a DC field is used to counterbalance gravity and AC field is used to provide lateral stability. In the microgravity experiments the g-field is highly variable. Have you thought about a feasible feedback system to accurately change your DC voltage over several orders of magnitude?

Answer: The electrodynamic balance can be operated with a DC field, an AC field, or a superposition of both. In one-g, the gravitational influence is typically offset with the DC field, and the AC field is applied to provide lateral stability. The levitator can, however, be operated stably with just the AC field even at one-g, eliminating the need to actively adjust the DC voltage for changes in gravitational field or droplet mass. Since the AC field provides a force towards equilibrium corresponding to an opposite velocity of the droplet, strong AC fields tend to overdrive the droplets resulting in oscillations. The AC frequency must be tuned for stability, corresponding to a reaction time-constant relating droplet inertia and drag. Our experience has shown that for droplets in the 500 micron diameter range at atmospheric conditions frequencies of the order of 400 Hz are most appropriate.

Question (C.T. Avedisian, Cornell University): How do you plan to "calibrate" your approach for flame diameter measurement based on CH identification? For example, do you plan to compare flame diameter measured from photographs with your laser based flame diameter?

Answer: In hydrocarbon flames, CH radical laser-induced fluorescence is accepted in the literature as the best indicator of most intense chemical reactions. While photographic recording of broadband flame luminosity is often used for indicating flame positions, these measurements suffer from both spatial ambiguity associated with line-of-sight observation, and assumptions related to non-equilibrium chemistry and excited-state radical-species formation. Comparisons will be attempted between luminosity observations and the laser-induced fluorescence flame front indicator to be used in this study, to establish correspondence between the approaches.

SESSION D - PREMIXED FLAMES

(Chair, Mitchell Smooke)

STUDIES OF PREMIXED LAMINAR AND TURBULENT FLAMES AT MICROGRAVITY

N93-20196

Paul D. Ronney
Department of Mechanical and Aerospace Engineering
Princeton University
Princeton, New Jersey 08544

Introduction

The work of the Principal Investigator (PI) has encompassed four topics related to the experimental and theoretical study of combustion limits in premixed flames at microgravity, as discussed in the following sections. These topics include:

- Radiation effects on premixed gas flames
- Flame structure and stability at low Lewis number
- Flame propagation and extinction in cylindrical tubes
- Experimental simulation of combustion processes using autocatalytic chemical reactions

Radiation effects on premixed gas flames

Our previous work has demonstrated the importance of gas radiation in the propagation and extinguishment of premixed gas flames [1, 2]. However, gas radiation is a weak effect and is only a significant influence for very slowly burning flames. These flames can only be observed at μg due to buoyancy effects at one-g. Furthermore, it is not clear whether radiation is a fundamental limit because in very large systems (say, tens of meters) emitted radiation could be reabsorbed within the gas and thus not lost from the system. In this case the propagation rate could actually increase because radiation would augment the usual transport by conduction of heat from the flame front to the unburned gas [3].

To test these hypotheses, we have examined radiation effects by studying flames at μg in gas mixtures to which small quantities of inert, radiant particles have been added. Solid particles emit and absorb radiation across a broad spectrum, unlike gas molecules which are active only in narrow spectral bands. Thus, appreciably more radiation and absorption can be expected in particle-laden gases. Our preliminary experiments [4] have shown that at small particle loadings, burning rates are reduced (Fig. 1), peak pressures in constant-volume combustion are lower (Fig. 1) and thermal decay rates in the burned gases are increased (Fig. 2). This indicates that the significance of radiative loss is enhanced by the addition of particles to the gas. With sufficient seeding, the burning rates are practically the same as those found in particle-free mixtures (Fig. 1), the peak pressures are comparable (Fig. 1) and the thermal decay rate is smaller than particle-free mixtures (Fig. 2). All of these observations are consistent with the hypothesis that at sufficiently high particle loadings, radiation is reabsorbed within the combustible medium, and thus may not constitute a fundamental limit in very large systems. In essence, the presence of particles has made the system "larger" in that the ratio of the system size to mean absorption length of radiation is increased.

Future work will focus on methods of quantifying the particle density, mixture optical thickness, and obtaining results for a variety of mixtures and particle loadings to compare with theory and to determine if flammability limits can be entirely suppressed when radiation losses are eliminated.

Flame structure and stability at low Lewis number

We have found in previous work that the tendency of flames in mixtures with low Lewis numbers, e.g. hydrogen-air, to break up into cells affects the near-limit behavior dramatically [5]. In some cases flame propagation ceases entirely without flame extinction occurring. In these cases stable, stationary spherical flames ("flame balls") seem to exist. Stationary spherical flames have been predicted previously but are predicted to be unstable. Further work has showed that such phenomena seem to occur in all mixtures with sufficiently low Lewis number and near flammability limits, independent of the chemical mechanism [6]. Experiments on the KC-135A aircraft showed that these structures are stable for at least the 20 seconds of low-g available [6]. By comparison with analytical models [7, 8], it has been concluded that radiation from the combustion products, along with diffusive-thermal effects in low-Le mixtures, is probably the stabilization mechanism which allows flame balls to exist at μg.

At one-g, these flames are entirely buoyancy-dominated. Consequently, the flammability limits are much leaner at μg than one-g, for example 3.35% vs. 4.0% H_2 for H_2-air mixtures [6]. This result is in very good agreement with a computational study of flame balls employing detailed chemistry and transport models [9] in which a limit of 3.5% H_2 was predicted.

The g-jitter in the KC-135A experiments (≈ 0.02g) caused substantial motion of flame balls. The drift velocity was found [6] to be proportional to $g^{1/2}$, consistent with bubble theory. This drift also led to the formation of two types of quasi-cylindrical flame structures which we have termed "flame strings" (Fig. 3) [6]. These strings are unstable, in that they eventually break into flame balls, but live much longer than would be expected based on thermal diffusion time scales alone. Consequently, they are almost certainly being supported by chemical reaction. Their existence is curious, because no steady solution is possible for cylindrical flames (unlike spherical flames). It seems then that they would evolve radially given sufficient time, but the axial instability which leads to their breakup manifests itself before radial evolution occurs. Recent theory [10] supports this suggestion.

Another type of flame string, not directly related to that discussed above, has been observed in H_2-O_2-SF_6 and CH_4-O_2-SF_6 mixtures, particularly at high pressures [6]. These strings are different in that they are uncorrelated with buoyancy effects and seem to form much faster than any conventional diffusional or hydrodynamic timescale would allow. We conjecture that these are a result of reabsorption of emitted radiation, which is most likely to occur in SF_6-diluted mixtures and at high pressures because the Planck mean absorption length (L_p) is much shorter in SF_6 than CO_2 or H_2O and is inversely proportional to pressure; at 300K and 2 atm, L_p for SF_6 is only 0.13 cm!.

A flight experiment is under development to determine if the apparent stability of flame balls can be confirmed in experiments where both the duration of μg is long (unlike drop-tower experiments) and the quality is significantly better than that in aircraft tests. Also, the presence or absence of flame strings will be studied to determine the role buoyancy plays in their formation. In addition to addressing development issues in support of the development of flight hardware, future work will stress the role of reabsorption of emitted radiation on these flame structures using high-pressure tests and particle-laden mixtures. It is possible that the presence of particles will influence transport of thermal energy (see above) but should not influence mass transport, leading to a radiation-influenced Lewis number which may be higher than the particle-free value, thereby inhibiting the cellular instability.

Flame propagation and extinction in cylindrical tubes

The standard apparatus for measuring flammability limits of premixed gases at earth gravity is the Standard Flammability Limit Tube, or SFLT. This is a tube 5 cm diameter and 200 cm long which is filled with combustible gas and ignited at one end. The mixture is defined to be flammable if it supports propagation throughout the tube. Despite many years of study, the mechanisms of flame extinction in the SFLT is not well understood. The relative importance of

buoyancy, flame stretch, heat loss to the tube wall, radiation loss, etc. have not been assessed.

Most theories of flammability limits predict the flame propagation rate at the limit ($S_{b,lim}$). Hence, measurement of $S_{b,lim}$ enables comparison with theories. We have conducted such experiments at earth gravity in tubes of varying diameter, at varying pressures and with mixtures having varying fuels, inerts, and Lewis numbers (Le). We have found that the characteristics of the limits can be described in terms of the effect of the Grashof number $Gr \equiv gd^3/\alpha^2$ on the limit Peclet number $Pe \equiv S_{b,lim}d/\alpha$, where g is gravity, d the tube diameter and α the thermal diffusivity at room temperature. Figures 4 and 5 show the results for upward and downward propagation, respectively. In each case, at low Gr the results are consistent with theoretical predictions [11] for flame extinguishment by conduction loss to the tube walls, namely Pe = constant ≈ 40. At higher Gr, results are consistent with buoyancy-induced extinction mechanisms, in the upward propagating case $Pe \sim Gr^{1/2}$ [12] and in the downward case $Pe \sim Gr^{1/3}$. Because of the difference in extinction mechanisms, we have found that the flammability limit can actually be wider for downward propagation than upward propagation (though for most commonly-studied values of Gr and Le, this is not the case).

In the upward case, at $Gr > 2.0 \times 10^8$ (corresponding to a pipe-flow Reynolds number of 2000) turbulent flow is exhibited; the flame behavior can be either flamelet-like or distributed-like depending on Gr and Le. Downward turbulent propagation at the limit is also possible, but would require $Gr \approx 40 \times 10^9$ according to our scaling analysis, and is beyond the limits of our apparatus.

Our scaling analyses indicate that radiation losses cannot be significant at earth gravity for any experimentally realizable conditions; either conduction losses or buoyancy effects will dominate. Of course, radiation can be the dominant extinction mechanism in large tubes at μg. We are initiating a study of this extinction process for comparison to our previous results in a constant-volume chamber with central ignition (which produces spherically expanding flames.)

Experimental simulation of premixed flames using autocatalytic chemical reactions

The PI has introduced the use of aqueous autocatalytic propagating chemical fronts (in particular, the arsenous acid-iodate system) for the experimental simulation of premixed combustion in nonuniform and unsteady flows [13]. These fronts more nearly match the assumptions made by most relevant theoretical models that do gaseous flames. These assumptions include that of constant density. The role of density change (due to heat release) in gaseous premixed flame propagation has been a continuing source of controversy, especially in turbulent flows. It has not even been established whether density changes result in an increase or decrease in the turbulent flame propagation rate (S_T) [13]. Consequently, it is desirable to compare front propagation in gaseous flames and aqueous autocatalytic fronts to study effects of density change.

A limitation on the utility of aqueous fronts is that even the small fractional density change across the aqueous front leads to significant buoyancy influences at one-g because of the very low planar front propagation rate (S_L). Only when the imposed disturbance intensity (u′) is much greater than buoyancy-induced flow velocities can buoyant effects be neglected. Gaseous flames with $u' >> S_L$ cannot be observed because of quenching which results from the hydrodynamic strain at high $U \equiv u'/S_L$; this makes it impossible to compare the aqueous and gaseous front propagation at the same U, and thereby assess the role of density changes. High U is also inaccessible to computational studies because of numerical difficulties, especially when density changes are included.

This discussion indicates the need for studying aqueous fronts at μg to eliminate buoyancy influences, enabling the study of front propagation at low U and thereby allowing comparison of front propagation in aqueous and gaseous fronts at the same u'/S_L.

We have studied these autocatalytic propagating fronts in a Taylor-Couette flow, i.e. in the annulus between two rotating concentric cylinders. This flow was chosen because (1) the flow is homogeneous in the direction of front

propagation (axially), so that a quasi-steadily propagating front can be studied, and (2) well-characterized disturbances are generated even at very low Reynolds numbers (and thus low u'). When only the inner cylinder is rotated, pairs of counter-rotating toroidal vortex pair (Taylor vortices) fill the annulus. Fig. 4 shows the measured [13] effect of u'/S_L on S_T/S_L in the Taylor-vortex regime and the predictions of a theoretical model [13]; agreement is good. (Data were taken up to $u'/S_L \approx 10{,}000$, but only the lower values of u'/S_L are of interest to this study in that they may be affected by buoyancy).

Our scaling analysis has shown that in a space experiment, it is possible to study aqueous fronts with $U \approx 7$ at $g = 10^{-4}g_o$ (a typical figure for space experiments) without buoyant convection, whereas $U \approx 140$ is the lowest possible U at $g = g_o$ without buoyant convection. It is possible to study $U = 7$ in gas combustion without quenching, whereas $U = 140$ is not possible. Thus, space experiments would enable us to study the aqueous fronts at values of U accessible to gas combustion experiments and numerical simulations, enabling us to create a "bridge" between studies of fronts with and without substantial density changes.

References

*1. Ronney, P.D., "On the Mechanisms of Flame Propagation Limits and Extinction Processes at Microgravity," *Twenty Second Symposium (International) on Combustion*, Combustion Institute, 1988, pp. 1615-1623.

*2. Abbud-Madrid, A., Ronney, P. D., "Effects of Radiative and Diffusive Transport Processes on Premixed Flames Near Flammability Limits," *Twenty Third Symposium (International) on Combustion*, Combustion Institute, 1990, pp. 423-431.

3. Joulin, G., Eudier, M. *Twenty-Second Symposium (International) on Combustion*, Combustion Institute, 1988, p. 1579.

**4. Abbud-Madrid, A., Ronney, P. D., "Effects of Particulate Radiation on Premised Gas Flames," AIAA 31st Aerospace Sciences Meeting, Jan. 11-14, 1993, Reno, NV (to be presented.)

*5. Ronney, P. D., "Near-Limit Flame Structures at Low Lewis Number," *Combustion and Flame* 82, 1-14 (1990).

**6. Ronney, P. D., Whaling, K. N., Abbud-Madrid, A., Gatto, J. L. Pisowicz, V. L., "On Stationary Premixed Flames in Spherical and Cylindrical Geometries," submitted to *Proceedings of the Royal Society (London) Series A* (1992).

**7. Buckmaster, J. D., Joulin, G., Ronney, P. D., "Structure and Stability of Non-adiabatic Flame Balls: II. Effects of Far-Field Losses," *Combustion and Flame* 84, 411-422 (1991).

**8. Buckmaster, J. B., Gessman, R., Ronney, P. D., "The Three-Dimensional Dynamics of Flame Balls," *Twenty-Fourth International Symposium on Combustion*, 1992 (to appear in the Proceedings).

9. Buckmaster, J. D. and Smooke, M. "Analytical and Numerical Modelling of Flame-Balls in Hydrogen-Air Mixtures," submitted to *Combustion and Flame*.

10. Buckmaster, J. D., *Combust. Sci. Tech.* 84, 163 (1992).

11. Spalding, D. B., *Proc. Roy. Soc. (London)* A240, 83 (1957).

12. Levy, A., *Proc. Roy. Soc. (London)* A283, 134 (1965).

**13. Shy, S. S., Ronney, P. D., Buckley S. G., Yakhot, V., "Experimental Simulation of Premixed Turbulent Combustion Using Aqueous Autocatalytic Reactions," *Twenty-Fourth International Symposium on Combustion*, 1992, (to appear in the Proceedings).

Other work supported by the NASA-Lewis:

*Farmer, J. N., Ronney, P. D., "A Numerical Study of Unsteady Nonadiabatic Flames," *Combustion Science and Technology* 73, 555-574 (1990).

*Buckmaster, J. D., Joulin, G., Ronney, P. D., "Effects of Heat Loss on the Structure and Stability of Flame Balls," *Combustion and Flame* 79:381-392 (1990).

*"Effects of Ambient Atmosphere on Flame Spreading and Extinction," Workshop on Spacecraft Fire Safety Risk Analysis Assessment, Oct. 31 - Nov. 1, 1991, Los Angeles, CA (Invited presentation).

*"New Premixed Gas Combustion Phenomena," Gordon Research Conference on Gravitational Effects in Physico-Chemical Systems, June 16-21, 1991, Plymouth, NH. (Invited Presentation).

**Ronney, P. D., "An Investigator's Suggestions for Effective use of the NASA-JSC Reduced Gravity Program KC-135A Aircraft," in: *JSC Reduced Gravity Program User's Guide*, NASA JSC-22803, July 1991.

**Buckmaster, J. D., Lee, C. J., Joulin, G., Ronney, P. D., "Modelling of Microgravity Ignition Experiments," in: *Recent Advances in Combustion Modelling* (B. Larrouturou, ed.), Series in Advances in Mathematics for Applied Sciences, Vol. 6, pp. 1-18, World Scientific Press, Teaneck, NJ, 1991.

*Work supported by NASA-Lewis under grant NAG3-965
**Work supported by NASA-Lewis under grant NAG3-1242

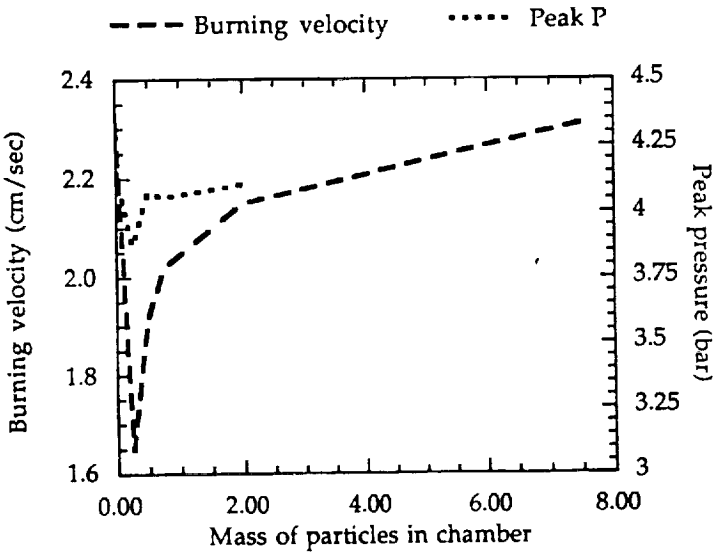

Figure 1. Propagation rates and peak pressures of particle-laden flames. Mixture: 5.25% CH_4 in air.

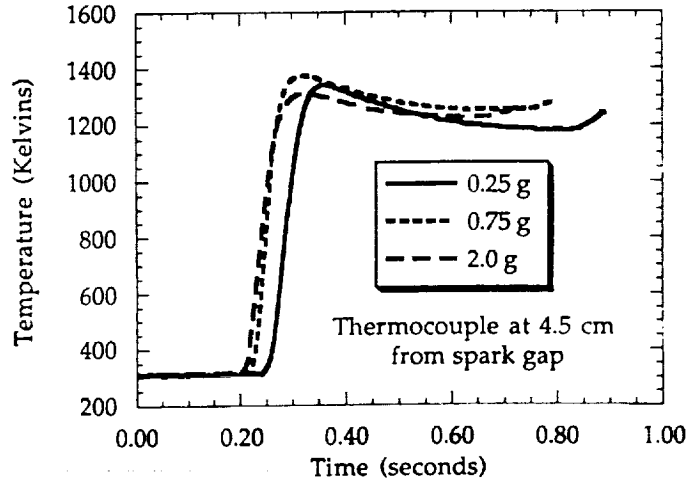

Figure 2. Thermal characteristics of flames in particle-laden mixtures. Mixture: 5.25% CH_4 in air.

Figure 3. IR image of "flame string" at μg. Mixture: 5.5% H_2 in air.

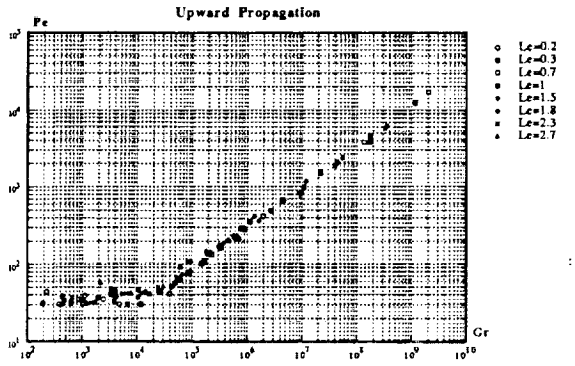

Figure 4. Limit Peclet number versus Grashof number for upward-propagating flames in tubes.

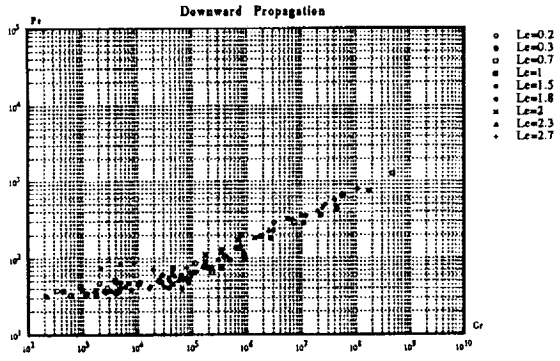

Figure 5. Limit Peclet number versus Grashof number for downward-propagating flames in tubes.

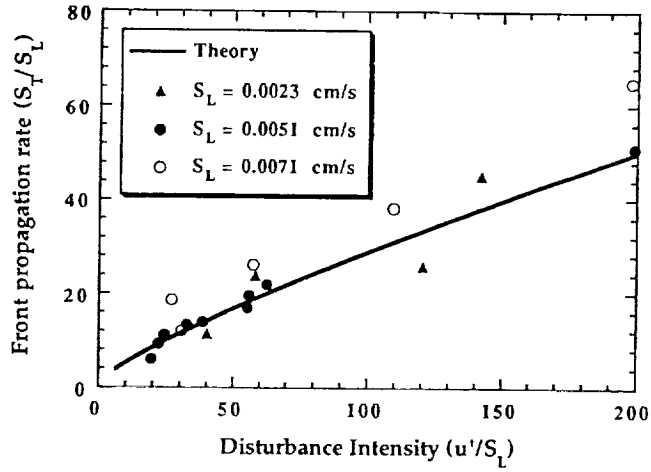

Figure 6. Effect of disturbance intensity on front propagation rate in aqueous autocatalytic system.

MODELING OF MICROGRAVITY COMBUSTION EXPERIMENTS

John Buckmaster
University of Illinois
Urbana, Illinois 61801

N93-20197

Introduction

Modeling plays a vital role in providing physical insights into behavior revealed by experiment. The program at the University of Illinois is designed to improve our understanding of basic combustion phenomena through the analytical and numerical modeling of a variety of configurations undergoing experimental study in NASA's microgravity combustion program. Significant progress has been made in two areas: (i) flame-balls, studied experimentally by Ronney and his co-workers [1]; (ii) particle-cloud flames studied by Berlad and his collaborators [2]. Additional work is mentioned below. NASA funding for the U. of Illinois program commenced in February 1991 but work was initiated prior to that date and the program can only be understood with this foundation exposed. Accordingly, we start with a brief description of some key results obtained in the pre - 2/91 work.

Flame Balls - Results Prior to 2/91

Flame-balls are stationary, premixed spherical flames observed in certain near-limit mixtures [1]. They have zero flame-speed. Their study is likely to lead to an improved understanding of flammability limits. The configuration is sketched in Fig. 1.

Reference [3], *The structure and stability of non adiabatic flame-balls,* provides the first description of mathematically stable flame-balls. The stabilizing mechanism is heat loss by thermal radiation. The analysis assumes that the Lewis number (Le) is significantly less than 1. Only for such mixtures are flame-balls observed.

Reference [4], *The structure and stability of non adiabatic flame-balls: II. Effects of far-field losses,* is an extension of Ref. [3]. For physical flames there will be losses in the near-field (in and near the burnt gas) and the far-field. Dealing simultaneously with both leads to technical (mathematical) difficulties and these are dealt with here. Differences in the effects of the two losses are revealed by Fig. 2. Near-field losses can generate a three-dimensional instability (the upper thick portion of curve A), far-field losses do not. The lower thick portions of both curves define regions of one-dimensional instability. Note that for curve B this includes a portion of the top solution branch.

Flame-balls are only observed if Le is sufficiently small (≤ 0.5?) In Ref. [5], *The structure and stability of flame-balls: A near-equidiffusional flame analysis,* it is shown that radiation is not stabilizing when $Le = 1$ and there is a critical Lewis number Le_C (< 1) such that stability requires $Le < Le_C$. The closer Le is to Le_C the smaller is the range of parameter values for which stable solutions exist.

Flame-balls can be stabilized by heat loss other than by radiation. Convective heat losses generated by weak shear or straining flows are discussed in Ref. [6], *Flame balls stabilized by suspension in fluid with a steady linear ambient velocity distribution.* These are far-field losses. As noted earlier, a key difference between near-field and far-field losses is that the former can give rise to three-dimensional instabilities, the latter do not (see Ref. [9], discussed below).

Flame-Balls - Post 2/91 Results

In flame-ball experiments carried out in the KC-135 (see Ronney, this proceedings), unsteady flame-strings have been observed. A straight flame-string is a cylindrical counterpart to the spherical flame-ball. Flame-strings display a sausage or peristaltic instability. These instabilities are analyzed in Ref. [7]. For perturbations $\sim e^{\alpha t+ikx}$ where x is distance measured along the cylinder axis, Fig. 3 shows the manner in which α varies with the wave-number k. The flame structures must have a minimum length if they are to support unstable waves, i.e. short cylinders are stable.

Reference [8], *Influence of boundary-induced losses on the structure and dynamics of flame-balls*, shows that conductive heat losses to a cold wall can stabilize flame-balls. Configurations of this kind might well be important for space experiments designed to examine the structure of a stationary flame-ball.

The results of Ref. [3], [4] imply the response sketched in Fig. 4. This shows the maximum temperature in a flame-ball as a function of mixture strength. The stable region lies between points A and B. The implication is that insufficiently reactive mixtures can not support flame balls (static quenching at A' or dynamic quenching at A); and that overly reactive mixtures will lead to non-spherical flame-balls. These conclusions are consistent with experiment.

The point B is a neutral stability point for three-dimensional instabilities and a transcritical bifurcation analysis can be carried out, valid in the neighborhood of B, which describes unsteady three-dimensional, weakly-nonlinear deformations of the flame-ball. In Ref. [9], *The three-dimensional dynamics of flame-balls,* an equation for the flame-ball shape is derived:

$$\frac{x^2}{1+\frac{42}{4}.\frac{\delta K}{(t_c-t)}}+\frac{(y^2+z^{2)}}{1-\frac{21}{4}.\frac{\delta K}{(t_c-t)}}=1 \qquad (1)$$

where δK is a positive parameter that vanishes at B, and t_c is a critical time at which 'blow-up' occurs. Equation (1) describes the first observable manifestation of the instability, and corresponds to an elongating prolate spheroid. Prolate spheroids have been observed by Ronney. The experimental spheroids, once they become long enough, neck and split. We believe that this is due to the flame-string instability discussed in Ref. [7].

The analytical work of Ref. [3] - [9] has been remarkably successful in providing a description of flame-balls that agrees, qualitatively, with the experimental observations. Quantitative comparisons are only meaningful with detailed numerical simulations, and a program of this kind has recently been embarked upon in collaboration with M. Smooke. Figure 5 shows the variations of maximum temperature with mixture strength described in Ref. [10], *Analytical and numerical modeling of flame-balls in H_2/air mixtures.* This work predicts a static flammability limit of 3.5% H_2 by volume. This is close to the experimental value. Predicted flame-ball sizes

are consistent with observations but precise comparison is not possible at this time since the nature of the experimental image is uncertain.

It is clear that at this time an unusually strong synthesis of experiment, theory and numerical work has elucidated the physics of flame-balls.

Flame-Balls - Future Plans

In all the work completed to date radiation losses are only accounted for within the framework of an optically thin field. There is reason to believe that this is not always correct, and a more general approach is under development.

Additional numerical work is planned. It would be appropriate to construct steady solutions for the various mixtures that have been used experimentally. Moreover, because of the importance of the stability boundaries in defining the existence of flame-balls it is important to identify them numerically. This would not be excessively difficult for the one-dimensional stability boundary, but the three-dimensional boundary is a different matter. Reduced chemistry schemes might be useful in this connection.

Particle Cloud Flames

Reference [2] describes experiments on flames propagating in particle-air mixtures. A mixture of lycopodium and air in a tube that is open at one end, closed at the other, is ignited at the open end. For some mixture strengths and flame locations unsteady propagation is observed which, we believe, is driven by an acoustic instability. Reference [11], *An acoustic instability theory for particle-cloud flames,* contains a mathematical description of a plausible mechanism. Because of slip (thermal and kinematic) between the two phases, an acoustic wave generates fluctuations in the mixture flux fraction entering the flame; there are time dependent fluctuations in the difference between the particle velocity and the gas velocity relative to the flame. These fluctuations generate variations in the heat generated by combustion, and these can drive the acoustic wave *via* the well-known Rayleigh criterion. Apart from the inclusion of slip the flame model is similar to that of Seshadri *et al* (this proceedings).

Additional theoretical aspects are briefly discussed in Ref. [12], *The structure and stability of laminar flames.* It is well known that a classical (gaseous) unbounded deflagration can support a pulsating instability if *Le* is large enough, but this constraint demands exotic mixtures. However, modifications to the flame configuration can move the domain of instability and make it accessible to certain everyday mixtures. Heat loss to a burner is such a modification. Supplying the fuel in particle form is another. It is possible, therefore, that the instability observed by Berlad *et al* is intrinsic in nature, albeit modified by the acoustic constraints, rather than the acoustic creature discussed in Ref. [11]. These and related aspects are presently being explored. However, the termination of the experimental program limits the progress that can be expected in our understanding of these flames. In view of the importance of particle cloud burning, and recognizing that the microgravity environment is exceptionally congenial for its study, this author believes that a new initiative in the area would be most valuable, preferably one tied closely to modeling efforts.

Self-Extinguishing Flames

Self-extinguishing flames (SEFs) are generated by the point ignition of certain near-limit mixtures [13]. An essential characteristic of a SEF is that it extinguishes at a radius of several centimeters after the release of chemical energy several orders of magnitude greater than the spark initiation energy. Because of this disparity one might expect that the final behavior of these flames is independent of the spark energy, but that is not the case. A SEF which extinguishes after releasing

energy equal to 10^3 times the spark energy can be converted to a non-extinguishing flame by doubling the spark energy. We have been engaged in attempts to understand this sensitivity by the use of simple asymptotic treatments. In Ref. [14], *The effects of confinement and heat loss on outwardly propagating spherical flames,* asymptotic methods are used to derive a model equation for the evolution of the spherical flame:

$$\frac{dV}{dR} = \frac{2V}{R} - L + V^2\left[\frac{1}{3}kR^3 - \ln V\right], \quad \frac{dR}{dt} = V. \tag{2}$$

Here R is the flame radius, t is time, L is a heat-loss parameter that accounts for radiative losses, and k is a confinement parameter that accounts for the pressure rise in the fixed volume chamber.

Solutions to equation (2) can display extreme sensitivity to the initial data, as exemplified by Fig. 6. However, we are not prepared to claim that confinement effects are significant in Ronney's experiments, but merely present these results as a simple example of sensitivity.

Acknowledgment

The work described here was supported by the NASA-Lewis Research Center, and by AFOSR. It owes its genesis to the unusual intellectual generosity of Paul Ronney. After discovering flame-balls in the laboratory, he came to the opinion that radiation plays a key role in their existence and invited me to Princeton and asked me if I thought that it would be possible to do some modeling. That question, his videotapes, and his physical insights, have fueled this endeavor.

References

[1] Ronney,P. *Combust. Flame*, 82, 1990, 1-14 .
[2] Berlad,A., Ross,H., Facca,L., and Tangirala,V. *Combust. Flame*, 82, 1990,448-450.
[3] Buckmaster,J., Joulin,G., and Ronney,P. *Combust. Flame*, 79, 1990, 381-392.
[4] Buckmaster,J., Joulin,G., and Ronney,P. *Combust. Flame*, 84, 1991, 411-422.
[5] Lee,C., and Buckmaster,J. *SIAM J. Appl. Math.*, 51, 1991,1315-1326.
[6] Buckmaster,J., and Joulin,G. *J. Fluid Mech.*, 227, 1991, 407-427.
[7] Buckmaster,J. *Combust. Sci. and Technol.*, 84, 1992, 163.
[8] Buckmaster,J., and Joulin,G. *Combust. Sci. and Technol.*, in press.
[9] Buckmaster,J., Gessman,R., and Ronney,P. *24th Symposium,* in press.
[10] Buckmaster,J., and Smooke,M. Submitted. Some results from this paper were presented in a poster session at the 24th Symposium, and are recorded in the book of abstracts.
[11] Buckmaster,J., and Clavin,P. *24th Symposium,* in press.
[12] Buckmaster,J. Article in *Annual Review of Fluid Mechanics*, Vol. 25, to appear,1993.
[13] Ronney,P. *Combust. Flame*, 62, 1985, 121.
[14] Buckmaster,J., and Lee,C. *24th Symposium,* in press.

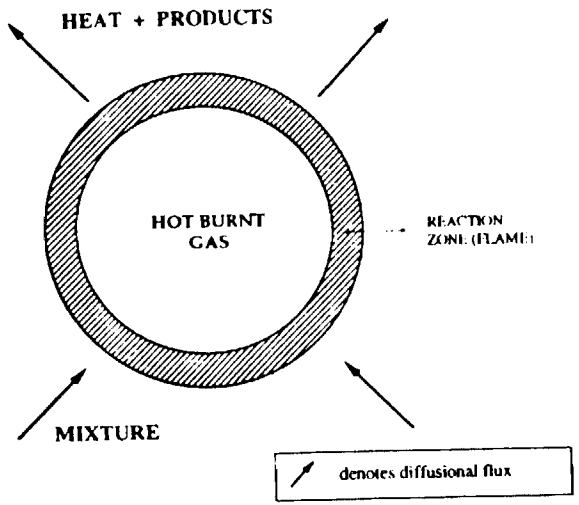

Fig.1. Stationary flame ball. The flame-speed is zero and mixture reaches the reaction zone by diffusion.

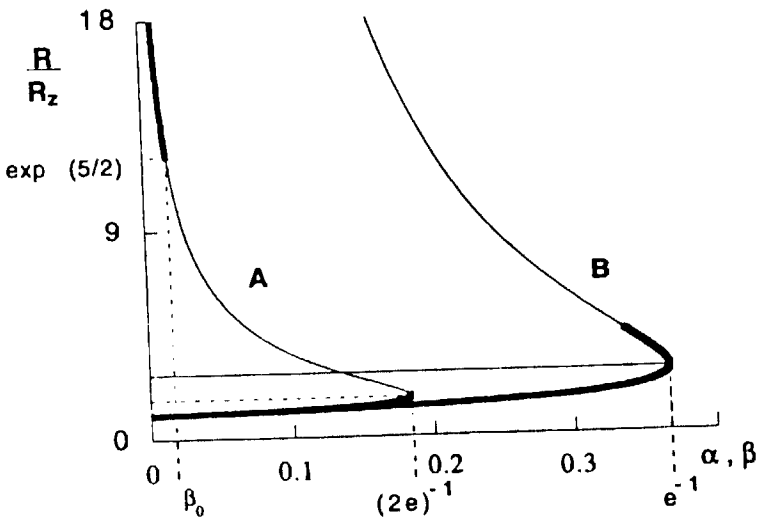

Fig.2. Flame-ball radius vs. heat loss. Curve A is appropriate for near-field losses, cuve B for far-field losses.

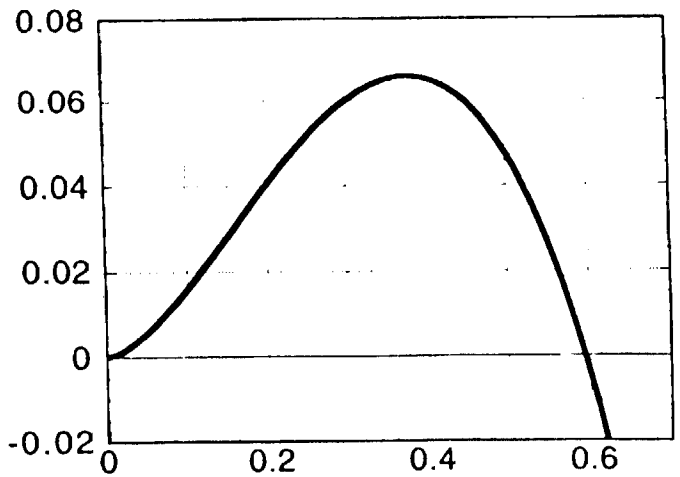

Fig.3. Growth rate α vs. wave-number k for flame-cylinders. Short cylinders will be stable.

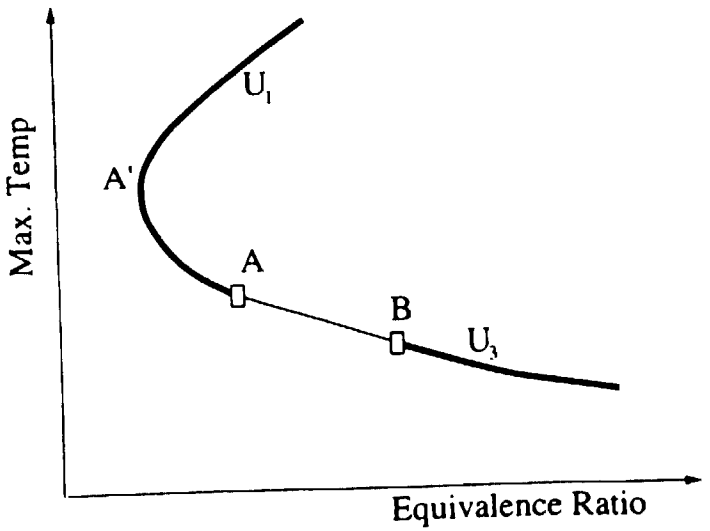

Fig.4. Flame-ball response showing a stable region between the points A and B.

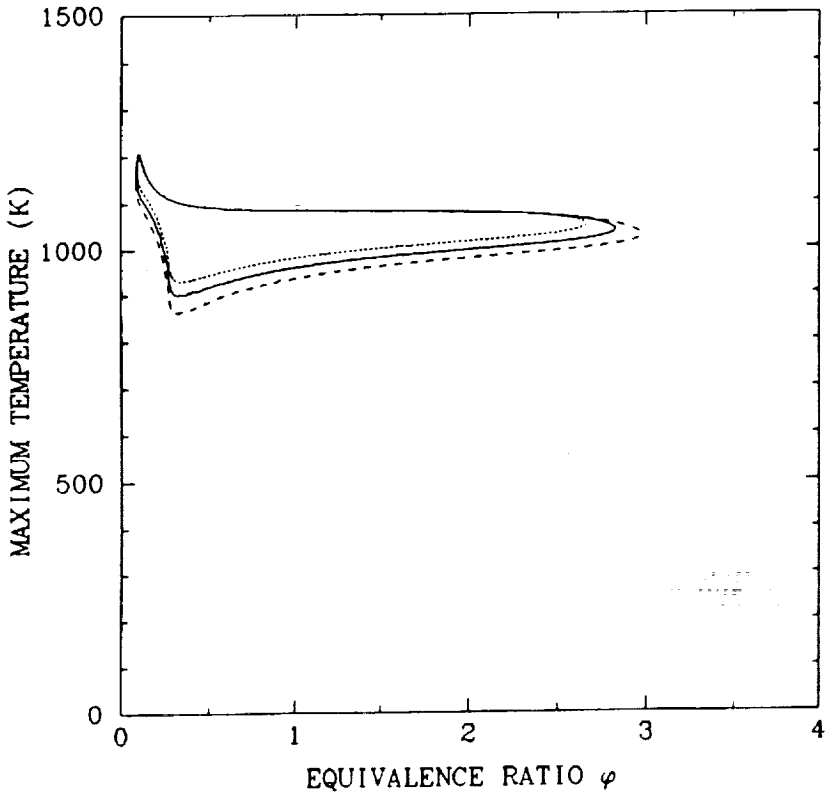

Fig.5. Numerical results for flame-balls in hydrogen/air mixtures, showing the maximum temperature vs. equivalence ratio (solid line).

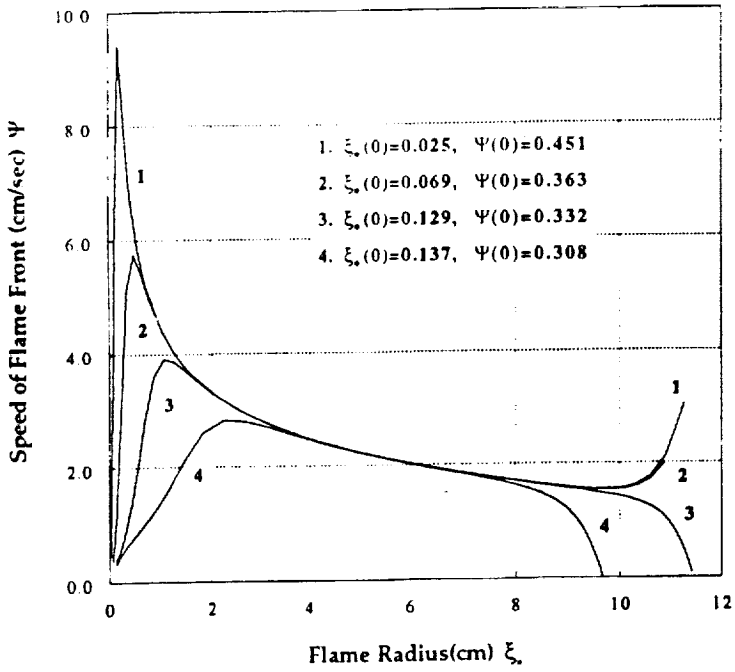

Fig.6. Flame front speed vs. flame radius for different initial conditions showing sensitivity when confinement effects are accounted for. At first the curves come together, but their final fate depends on the initial data.

STRUCTURE AND DYNAMICS OF PREMIXED FLAMES IN MICROGRAVITY

K. Kailasanath
Naval Research Laboratory
Laboratory for Computational Physics & Fluid Dynamics
Washington, D.C. 20375

and

G. Patnaik
Berkeley Research Associates
Springfield, Virginia 22150

Introduction

In this report we describe the research performed at the Naval Research Laboratory in support of the NASA Microgravity Science and Applications Program over the past three years with emphasis on the work performed since February 1992, the beginning of the current project. The focus of our research has been on investigating fundamental combustion questions concerning the propagation and extinction of gas-phase flames in microgravity and earth-gravity environments. Our approach to resolving these fundamental questions has been to use detailed time-dependent, multidimensional numerical models to perform carefully designed computational experiments. The basic questions we have addressed, a general description of the numerical approach, and a summary of the results are described in this report. More detailed discussions are available in the papers published which are referenced herein.

A systematic study which isolates the various processes that could lead to flame instabilities and extinction is needed to gain a better understanding of flammability limits and flame dynamics in microgravity. Numerical simulations, in which the various physical and chemical processes can be independently controlled, can significantly advance our understanding of flame instabilities and flammability limits on earth and in a microgravity environment. In the past three years, we have addressed a number of basic issues aimed at resolving some of the important aspects of flame structure and propagation. Some of the issues we have addressed using our numerical simulations are: the effects of heat losses and buoyancy forces on the structure and stability of flames(both burner-stabilized and flames in tubes), the existence of flammability limits in the absence of external losses or buoyancy forces in the system, and the extinguishment process at the downward-propagation limit.

Computational Tools

Two computational models developed at NRL, FLIC2D and FLAME1D, have been used in the work reported here. Both the numerical models are time-dependent and solve the multispecies coupled partial differential reactive-flow equations. These models include a detailed chemical kinetics mechanism coupled to algorithms for convection, thermal conduction, viscosity, molecular diffusion, thermal diffusion, and external forces. The external force, gravity, can be in any direction relative to flame propagation and can have a range of values. Energy sources and sinks may also be prescribed as a function of time. All of the chemical and physical processes are solved sequentially and then coupled asymptotically by timestep splitting [1].

FLIC2D, a two-dimensional model, has been used extensively to study cellular flames [2,3], the effects of gravity and heat losses on the structure and dynamics of lean hydrogen-air flames [4-8]. FLAME1D has been applied to various studies of flame phenomena including calculations of burning velocities, minimum ignition energies and quenching distances, effects of curvature and dilution, and flammability limits [9-11]. This one-dimensional model is generally used to test new sub-models such as for radiation and chemistry before implementing them in the multidimensional model. It is also used to study physical and chemical phenomena in which multidimensional effects are secondary. Space restriction does not allow the elaboration of the models here but details can be found in previous reports [9,12]. These models are also continuously evolving. Some of the recent additions to the models are the inclusion of wall effects and radiation, heat losses to a burner, moving adaptive grids and a parallel implementation of chemistry solver.

Summary of Research

Our recent research can be broadly divided into four categories: (a) dynamics of cellular flames [3], (b) effects of gravity, heat losses and viscosity on flame instabilities and structure[4-6], (c) extinguishment process at the lean-flammability limit[7,8] and (d) instabilities near the rich-flammability limit[13]. Each of these categories are briefly discussed below.

Dynamics of Cellular Flames

Our initial simulations [2] of cellular flames were in qualitative agreement with experimental observations on the stability of flames in lean and rich hydrogen-oxygen-nitrogen mixtures [14] and were also able to identify the thermo-diffusive instability mechanism as the primary mechanism responsible for the formation of cellular flames in hydrogen-oxygen-nitrogen mixtures in most systems. We then used the simulations to investigate the cell-split limit phenomena observed in the NASA drop tower [15] experiments.

We simulated the structure and dynamics of flames in a series of mixtures with 15% or less hydrogen in air. We observed brisk formation of cells and their subsequent splitting in lean mixtures with more than 11% hydrogen. In leaner mixtures with 9.5-11% hydrogen, the formation and splitting of cells is less vigorous. For mixtures with 9% or less hydrogen, a single cell is formed which does not split at all. For these mixtures, even calculations for very long times (0.4 seconds) in larger systems (10.2 cm channel width) did not show any indications of cell-splitting.

Heat losses have been postulated as a mechanism that can cause a cell-split limit. However, the simulations in this study do not include any loss mechanism; yet such a limit is still observed. This suggests that external loss mechanisms are not required and that the cell-split limit is actually an intrinsic feature of the lean hydrogen-air mixture itself. However, the actual mixture at which cell splitting ceases may be affected by losses.

Effects of Gravity, Heat losses and Viscosity on Flame Instabilities and Structure

We have performed a systematic series of investigations to isolate and study the role of gravity, heat losses and viscosity on the structure and stability of flames. In the first series, we isolated the effects of gravity by comparing upward- and downward-propagating flames to zero-gravity flames in idealized two-dimensional systems in which the effects of viscosity and heat losses to the wall can be ignored [4,5].

These simulations showed that the effects of gravity become more important as the lean flammability limit is approached. In mixtures with 12% or more of hydrogen in air, gravity plays only a secondary role, with the stability and structure of the flame controlled primarily by the thermo-diffusive instability mechanism. However, in leaner hydrogen-air mixtures gravity becomes more important. Upward-propagating flames are highly curved and evolve into a bubble rising upwards in the tube. Downward-propagating flames are flat or even oscillate between structures with concave and convex curvatures. The zero-gravity flame shows only cellular structures. Cellular structures which are present in zero gravity can be suppressed by the effect of buoyancy for

mixtures leaner than 11% hydrogen. These observations have been compared to theoretical and experimental observations [4] and have been explained on the basis of an interaction between the processes leading to buoyancy-induced Rayleigh-Taylor instability and the thermo-diffusive instability. These results also indicate that the instability mechanisms can interact in a quite complex manner, and even though one mechanism can mask the other, in certain regimes, both can be equally important.

In many practical applications as well as in the determination of flammability limits, flames are confined. Heat and radical losses will occur to the confining walls and the flow will also have to come to rest at the surface of the walls. Our simulations indicate that viscous effects play only a secondary role when the walls are assumed to be isothermal. However, heat losses to the walls play a dominant role resulting in the formation of additional cellular structures near but slightly displaced from the walls.

We also investigated how gravity modifies the structure and dynamics of flames in an isothermal, two-dimensional channel [6]. Heat losses are found to significantly modify upward- and downward-propagating flames. In the upward-propagating case, instead of a single bubble rising in the tube, a two-fingered flame is observed. This flame has some features similar to experimentally observed flames in lean hydrogen-air mixtures. The downward-propagating flame is also quite different when the effect of heat losses are considered. In this case, a flame is "visible" only in the central portion of the channel(see figure). Again, this flame is qualitatively similar to some near-limit flames in experiments. Therefore, we decided to do further simulations including the effects of heat losses to isothermal walls to gain some insight into the dynamical behavior observed experimentally in flames near extinguishment.

Extinguishment Process at the Lean-Flammability Limit

The experimentally observed flammability limit is between 9 and 10% for downward flame propagation in lean Hydrogen-air mixtures. Therefore further simulations including the effect of wall heat losses were carried out for flames in 10%, 9.75%, 9.5% and 9% hydrogen-air mixtures. The computational results show that a downward propagating flame in an isothermal channel has a flammability limit of around 9.75%. The details of the extinguishment process in this mixture has been analysed and found to be in excellent agreement with experimental observations.

In experiments, the flame is first observed to halt its downward propagation and then actually move back up into the burnt products[16]. From the simulations we can understand the reason for this observed behavior. The simulations indicate that the flame is quenched at the walls and tongues of colder gases, comprised mainly of burnt products flow down the sides. At the same time, there is an upward motion of the gases at the center of the channel, causing the flame to rise up into the burnt products. Further simulations also indicate that the dilution of the unburnt mixture with the products of combustion is an essential step in the extinguishment

Our earlier simulations have shown that a flame can propagate downward in a 9% mixture in a channel with adiabatic walls and cellular flames occur in this mixture in a zero-gravity environment. These observations taken in conjunction with our current simulations indicate that both heat losses and gravity are simultaneously required to cause the observed limit. A general conclusion from this work is that detailed numerical simulations that include wall heat losses can adequately simulate the dynamics of the extinguishment process in downward-propagating flames [8]. At the upward-propagation limit, the flames are highly three-dimensional and therefore must await the development of a three-dimensional model for a complete description.

Instabilities Near the Rich-Flammability Limit

A fundamental question that has not yet been fully resolved is the existence of an intrinsic flammability limit in a zero-gravity environment. In the absence of buoyancy forces, there are many competing factors such as preferential diffusion, flame chemistry, conductive and radiative heat

losses, the aerodynamics of burnt gases, and flame stretch that can cause or modify flammability limits. Numerical simulations provide an ideal way to systematically isolate and evaluate the role of various factors.

We have conducted a systematic study of flames in rich hydrogen-air mixtures[13]. Because these flames are nearly one-dimensional, we conducted these investigations with the FLAME1D code. The numerical simulations indicate that a steady burning velocity is not obtained for very rich hydrogen-air mixtures. As the amount of hydrogen is increased, at first a damped oscillation is observed in the flame and burning velocities, and then with further increase in the amount of hydrogen, an undamped oscillation with a complex set of frequencies is observed. Simulations with a simplified one-step irreversible chemical reaction do not show these oscillations, suggesting that chemical kinetics plays a strong role in inducing these oscillations. Further analysis shows that the oscillations are due to a competition for H atoms between chain branching and chain-terminating reactions. However, the limiting mixture predicted by these simulations is beyond the experimentally observed limit. These differences may be because of the neglect of phenomena such as stretch and radiative heat losses.

Simulations of spherically expanding flames suggest that stretch effects (due to curvature) will cause the oscillations to occur in less rich mixtures than that observed for planar flames. Further calculations including multidimensional effects and radiative and conductive heat losses are needed to quantitatively determine the flammability limits in zero-gravity as well as to more fully understand the significance of the instability induced by chemical kinetics.

Work in Progress

The calculations discussed above have lead to a better understanding of the structure and propagation of flames. We now understand the reasons for some of the observed differences in the structure of upward and downward propagating flames. We also have a detailed description of the extinguishment process in downward-propagating flames and rich hydrogen-air flames. However, these simulations have also brought up a number of unresolved issues which need to be examined. Four major issues which need to be addressed are: (1) What is the role of radiation in near-limit flame phenomena, especially for hydrocarbon flames ? (2) Will the extinguishment process and the relative importance of various instability mechanisms be the same for hydrocarbon flames as for hydrogen flames ? (3) Are burner-stabilized flames significantly different from freely propagating flames ? and (4) How does three-dimensionality modify the observations from the two-dimensional simulations ?

These are the issues that we are currently focussing on in our research efforts. We have implemented a sub-model that accounts for radiation from water in our one-dimensional flame code. Simulations using this model indicate that for the wide range of hydrogen-air mixtures (from lean to rich), radiative loss plays only a minor role in modifying the flame properties. A sub-model to account for radiation losses from CO_2 is being developed for inclusion in our studies of hydrocarbon flames.

Detailed reaction mechanisms are available for some hydrocarbons but the cost of including such mechanisms in time-dependent, multidimensional simulations is very high. The solution of the chemical rate equations would take a significant portion of the computer time because of the large number of species and the large number of rate equations involved in a mechanism consisting of hundreds of elementary reactions. The major advances being made in parallel computing will probably be the crucial factor enabling us to simulate the hydrocarbon flames to the same level of detail as we do with the hydrogen flames. Currently, we are working on a parallel-processing approach for doing our multidimensional flame simulations. Meanwhile, continuing efforts are also being made to reduce the cost of doing detailed multidimensional simulations.

One approach to reducing the cost of multidimensional flame simulations is to use a greatly simplified reaction mechanism. However, some important phenomena may be missed by using a

overly simplified mechanism. An intermediate approach is to use a skeletal mechanism [17, 18] which retains many characteristics of the detailed reaction mechanism. Results from using such a skeletal mechanism can then be compared to those using the more reduced reaction mechanisms to evaluate their validity and performance. With this approach in view, we are implementing and testing the skeletal mechanism for methane in FLAME1D. After this, we plan to incorporate the hydrocarbon chemistry along with the radiation model in FLIC2D and use it to simulate the structure and dynamics of multidimensional flames in hydrocarbons.

Currently, we have also begun to simulate burner-stabilised flames in order to address the effects of the burner on the structure and stabiity of cellular flames. Preliminary results indicate that the tendency to cellular structure can be significantly affected by the presence of the burner. A freely-propagating flame exhibiting vigorous cell-splitting can be stabilised at an inflow velocity lower than the normal burning velocity to suppress the formation of cells. Factors such as the details of the boundary-conditions imposed at the burner and the inflow velocity appear to play a significant role on the observed flame dynamics.

Many other interesting flame phenomena observed in microgravity are fully three-dimensional. The development of simplified but validated radiation and chemistry models along with advances in parallel computing of reacting flows are required to simulate the detailed dynamics of such flames.

References

1. Oran, E.S., and Boris, J.P., Numerical Simulation of Reactive Flow, Elsevier, New York, 1987.
2. Patnaik, G., Kailasanath, K., Laskey, K.J., and Oran, E.S., *22th Symposium (International) on Combustion*, pp. 1517-1526, The Combustion Institute, Pittsburgh, PA, 1989.
3. Patnaik, G. and Kailasanath, K., AIAA Paper No. 90-0041, AIAA, Washington, D.C., 1990.
4. Patnaik, G., Kailasanath, K., and Oran, E.S., AIAA Paper No. 89-0502, AIAA, NY, 1989. (also see AIAA Journal, Vol. 29, pp. 2141-2148, 1991.)
5. Patnaik, G. and Kailasanath, K., *Proceedings of the 23rd Symposium (International) on Combustion*, pp. 1641-1647, The Combustion Institute, Pittsburgh, PA, 1990.
6. Patnaik, G. and Kailasanath, K., AIAA Paper No. 91-0784, AIAA, Washington, D.C., 1991.
7. Patnaik, G. and Kailasanath, K., AIAA Paper No. 92-0336, AIAA, Washington, DC,1992.
8. Patnaik, G. and Kailasanath, K., *Proceedings of the 24th Symposium (International) on Combustion*, The Combustion Institute, Pittsburg, PA., 1992.
9. Kailasanath, K., Oran, E.S., and Boris, J.P., NRL Memorandum Report No. 4910, Washington, D.C., 1982.
10. Kailasanath, K., Oran, E.S., and Boris, J.P.,*Combust. Flame.* 47: 173–190 (1982).
11. Kailasanath, K., and Oran, E.S., *Prog. Aero. and Astro.* 105, Part 1, 167-179, 1986.
12. Patnaik, G., Laskey, K.J., Kailasanath, K., Oran, E.S. and Brun, T.A., NRL Memorandum Report 6555, Naval Research Laboratory, Washington, D.C., September 1989.
13. Kailasanath, K., Ganguly, K. and Patnaik, K., Proceedings of the 13th International Colloquium on the Dynamics of Explosions and Reactive Systems, Nagoya, Japan, July 1991.
14. Mitani, T., and Williams F.A., *Combust. Flame.* 39: 169–190 (1980).
15. Ronney, P., AIAA Paper No. 89-0157, AIAA, NY, 1989.
16. Jarosinski, J., *Prog. Energy Combust. Sci.*, 12: 81-116 (1986).
17. Paczko, G., Lefdal, P.M., and Peters, N., *Proceedings of the 21st Symposium (International) on Combustion*, pp. 739-748, The Combustion Institute, Pittsburg, PA., 1988.
18. Rogg, B., *Combust. Flame.* 73: 43–65 (1988).

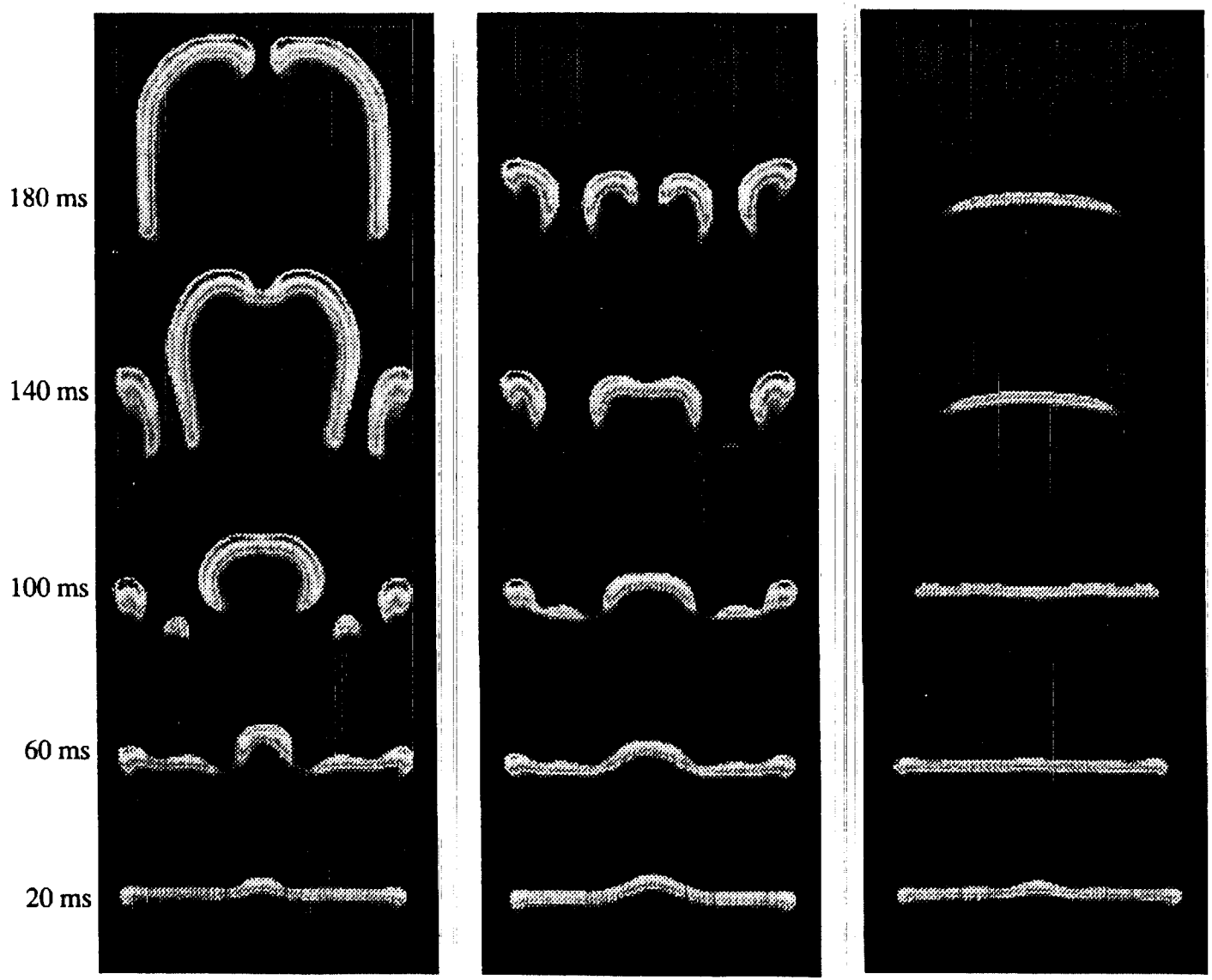

Comparison of OH concentration in upward-, zero-gravity and downward- propagating flames with heat loss to walls.

See Color Plate D-3

ON THE STRUCTURE AND STABILIZATION MECHANISMS OF PLANAR AND CYLINDRICAL PREMIXED FLAMES

James A. Eng, Delin Zhu, and Chung K. Law
Department of Mechanical and Aerospace Engineering
Princeton University
Princeton, New Jersey 08544

Introduction

The configurational simplicity of the stationary one-dimensional flames renders them intrinsically attractive for fundamental flame structure studies. The possibility and fidelity of studies of such flames on earth, however, have been severely restricted by the unidirectional nature of the gravity vector. To demonstrate these complications, let us first consider the premixed flame. Here a stationary, one-dimensional flame can be established by using the flat-flame burner (Fig. 1a). This flame, however, is inherently nonadiabatic because it is stabilized through heat loss to the burner surface. Furthermore, radicals generated at the flame potentially can also diffuse back to the burner surface and become deactivated. Such loss processes have introduced uncertainties in the study of flame chemistry. Furthermore, even an adiabatic planar flame can be produced by using the counterflow burner (Fig. 1b), where two symmetrical planar flames are formed in the stagnation field of two opposed jets of premixed gases, the flame is aerodynamically strained by the nonuniform flow field. The associated flame stretch effects can significantly modify the flame properties from the idealized one-dimensional flame in the doubly-infinite domain [1].

A class of one-dimensional flames that has the potential of eliminating heat loss and stretch effects is the cylindrical and spherical flames, where a premixed gas flows through a porous cylindrical (or spherical) burner and the resulting flame is formed at some distance from the burner, as shown in Figs. 1c and 1d. Since the flame is stationary and the flow velocity is in the radial direction and thereby normal to the flame surface, it is curved but not stretched [1]. Furthermore, while the flame can be stabilized by heat loss to the burner, the divergent nature of the flow offers an additional stabilization mechanism. That is, as the flow rate is continuously increased the flame recedes from the burner and heat loss can be eventually reduced to become negligible as compared to the heat generated at the flame. At this point the flame temperature is almost equal to the adiabatic flame temperature. Further increases in the flow rate can be accommodated by an increase in the flame standoff distance to a position where the flame speed again balances the flow velocity. Thus, the cylindrical geometry offers a unique advantage for the study of adiabatic, one-dimensional, stretch-free flames that is not present in other commonly used experimental systems. It is, however, also clear that because of the distorting nature of the buoyant flow, such a flame can only be established, and studied, in a microgravity (μg) environment.

We next consider nonpremixed flames. First it may be noted that in an unbounded gravity-free environment, the only stationary one-dimensional flame is the spherical flame. Indeed, this is a major motivation for the study of microgravity droplet combustion, in which the gas-phase processes can be approximated to be quasi-steady because of the significant disparity between the gas and liquid densities for subcritical combustion. However, recent studies [2] have shown that because of initial conditions, the combustion response such as the droplet burning rate and the flame location still vary significantly with time. Such complications can be avoided by using the spherical porous burner of Fig. 1d, in which a truly steady spherical flame can be generated in μg by steadily feeding either a gaseous or a liquid fuel through the burner.

In view of the above considerations, an experimental and theoretical program on cylindrical and spherical premixed and nonpremixed flames in microgravity has been initiated. For premixed flames, we are interested in (1) assessing the heat loss versus flow divergence as the dominant stabilization mechanism, (2) determining the laminar flame speed by using this configuration, and (3) understanding the development of flamefront instability and the effects of flame curvature on the burning intensity. For nonpremixed flames, we are interested in the state of extinction and the properties of the soot layer formed in the inner region to the flame, as observed in microgravity droplet experiments [3]. For both premixed and nonpremixed flames the detailed dynamic, thermal, and chemical structures of the flame will also be studied through laser-based instrumentation and computation with detailed chemistry.

As a starting point for the present program, we have performed a computational and normal-gravity (ng) experimental investigation of the planar premixed flame over the flat flame burner, which serve as a calibrating and referencing system for the study of cylindrical flames. We have also performed theoretical, computational and μg experimental investigations of the cylindrical flame, and will present comparisons between the planar and cylindrical flames.

Asymptotic Analysis and Qualitative Behavior

The nondimensional conservation equations for the reactant mass fractions Y_i and temperature T can be expressed for the cylindrical flame as

$$\left[\tilde{m}\frac{d\tilde{Y}_F}{d\tilde{r}} - \frac{1}{Le_F}\frac{d}{d\tilde{r}}\left(\tilde{r}\frac{d\tilde{Y}_F}{d\tilde{r}}\right)\right] - \left[\tilde{m}\frac{d\tilde{Y}_O}{d\tilde{r}} - \frac{1}{Le_O}\frac{d}{d\tilde{r}}\left(\tilde{r}\frac{d\tilde{Y}_O}{d\tilde{r}}\right)\right] = 0 \tag{1}$$

$$\left[\tilde{m}\frac{d\tilde{Y}_F}{d\tilde{r}} - \frac{1}{Le_F}\frac{d}{d\tilde{r}}\left(\tilde{r}\frac{d\tilde{Y}_F}{d\tilde{r}}\right)\right] + \left[\tilde{m}\frac{d\tilde{T}}{d\tilde{r}} - \frac{d}{d\tilde{r}}\left(\tilde{r}\frac{d\tilde{T}}{d\tilde{r}}\right)\right] = 0 \tag{2}$$

$$\tilde{m}\frac{d\tilde{Y}_F}{d\tilde{r}} - \frac{1}{Le_F}\frac{d}{d\tilde{r}}\left(\tilde{r}\frac{d\tilde{Y}_F}{d\tilde{r}}\right) = -\frac{\Lambda}{\varepsilon^2(\tilde{\beta}_O - 1)}\tilde{r}\tilde{\rho}^2\tilde{Y}_F\tilde{Y}_O\exp\left[\frac{\tilde{T}_f}{\varepsilon}\left(\frac{\tilde{T} - \tilde{T}_f}{\tilde{T}}\right)\right] \tag{3}$$

In the above the nondimensional quantities are $\tilde{r} = r/r_S$, $\tilde{m} = mc_P/2\pi\lambda$, $\tilde{Y}_F = Y_F/\beta_F$, $\tilde{Y}_O = Y_O/\mu_O\beta_O$, $Le_i = \lambda/c_P\rho_S D_i$ is the Lewis number of the ith specie, $\tilde{T} = c_P T/q_F$, $\tilde{\rho} = \rho/\rho_f$, $\tilde{\beta}_O = \beta_O/m_O\beta_F$, Λ is the burning rate eigenvalue, and $\varepsilon = \tilde{T}_f^2/\tilde{T}_a$ is the small expansion parameter, where T_a is the activation temperature. Furthermore, r is the radial coordinate, r_S the burner radius, β_i the mass flux fraction of the ith specie at the burner surface, μ_O is the stoichiometric mass ratio between oxygen and fuel, ρ the density, c_P the mixture specific heat, λ the thermal conductivity, D_i the mass diffusivity of the ith specie, q_F the energy release per unit mass of fuel consumed, and m the mass flow rate per unit burner length. The boundary conditions are

$$\tilde{r} = 1: \quad \tilde{T} = \tilde{T}_S \qquad \tilde{m}\tilde{Y}_F - \frac{1}{Le_F}\tilde{r}\frac{d\tilde{Y}_F}{d\tilde{r}} = \tilde{m} \qquad \tilde{m}\tilde{Y}_O - \frac{1}{Le_O}\tilde{r}\frac{d\tilde{Y}_O}{d\tilde{r}} = \tilde{m}\tilde{\beta}_O \tag{4}$$

$$\tilde{r} \to \infty: \quad \tilde{T},\ \tilde{Y}_i \text{ bounded} \tag{5}$$

where T_S is the burner surface temperature. The analysis was restricted to a fuel lean system with a one-step irreversible reaction. The problem is now well defined, and the analysis proceeds using the standard techniques of asymptotic analysis [4], with ε as the small expansion parameter.

The proper independent variable for the system is the mass flow rate m, with the overall flame response being the flame temperature, the standoff distance from the burner, and the heat loss to the burner. The analysis yields the following expressions relating the nondimensional flame temperature $\tilde{T}_f$, flame radius $\tilde{r}_f$, and burner heat loss $\tilde{L}$ to the normalized mass flow rate $M = \tilde{m}/\tilde{m}^o$ for the cylindrical geometry,

$$M = \frac{\tilde{m}}{\tilde{m}^o} = \tilde{r}_f \frac{\tilde{T}_f}{\tilde{T}_{ad}} \exp\left[\frac{1}{2}\tilde{T}_a\left(\frac{1}{\tilde{T}_{ad}} - \frac{1}{\tilde{T}_f}\right)\right] \tag{6}$$

$$\frac{\tilde{T}_f}{\tilde{T}_{ad}} = 1 - \frac{1}{\tilde{T}_{ad}}\left(\frac{1}{\tilde{r}_f^{\tilde{m}}}\right) \tag{7}$$

$$\tilde{L} = \frac{\tilde{m}}{\tilde{m}^o}\left(\tilde{T}_{ad} - \tilde{T}_f\right) = \frac{\tilde{m}}{\tilde{m}^o}\left(\frac{1}{\tilde{r}_f^{\tilde{m}}}\right) \tag{8}$$

where T_{ad} is the adiabatic flame temperature and $m^o = 2\pi r_s \rho_s S_u^o$ is a reference flow rate based on the laminar flame speed. Note that due to divergence M can have a value greater then one. The nondimensional heat loss is $\tilde{L} = L/m^o \beta_F q_F$, where L is the heat transfer to the burner, and can be interpreted as the energy transferred to the burner per unit reference energy of the mixture.

Figures 2 to 4 are graphs of the heat loss $\tilde{L}$, flame standoff distance $\Delta = r_f - r_s$, normalized flame temperature $\bar{T}_f = \tilde{T}_f / \tilde{T}_{ad}$ and heat loss per unit mass as a functions of M. In order to present the results for the planar and cylindrical geometries on the same graph, the standoff distances are normalized by the laminar flame thickness $\delta^o = \lambda/c_p \rho_s S_u^o$, rather than by the burner radius. Figures 2 and 3 show that the standoff position and the total heat loss rate display a dual response behavior in that the heat loss has a maximum and the flame standoff position has a minimum. This behavior has been observed experimentally [5,6] and explained theoretically [7] for the planar flame.

For the planar case M is bounded by one, at which the flame moves to infinity, the heat loss to the burner vanishes, and the flame speed is S_u^o. On the other hand, for the cylindrical flame M can be increased beyond one due to flow divergence. Consequently, the flame is located at a finite standoff position even after the heat loss has become vanishingly small. The stabilization mechanism has therefore changed from heat loss to flow divergence. Comparing the results of the two cylindrical flames with different burner radii, the flame with the smaller burner is stabilized closer to the burner because of the larger divergence effect of the smaller burner.

It is also of interest to examine the mass flux through the reaction zone and compare it with the reference laminar flame value. An expression for this can be obtained by normalizing the mass flow by a reference mass flow rate based on the reaction zone area, $m_f^o = 2\pi r_f \rho_s S_u^o$. The resulting expression is

$$\frac{\tilde{m}}{\tilde{m}_f^o} = \frac{\tilde{T}_f}{\tilde{T}_{ad}} \exp\left[\frac{1}{2}\tilde{T}_a\left(\frac{1}{\tilde{T}_{ad}} - \frac{1}{\tilde{T}_f}\right)\right] \tag{9}$$

This equation shows that when T_f approaches T_{ad} the mass flux at the reaction zone approaches the laminar flame value such that the burned velocity S_b is equal to S_b^o. Consequently, the unburned velocity S_u must exceed the laminar flame speed S_u^o. This effect is due entirely to flow divergence.

Computational and Experimental Studies - Methodology

Methane/air/inert mixtures were used in the studies. In the numerical simulation a version of the Sandia premixed flame code was used, with modifications to ensure strict mass conservation in the divergent flow field. The kinetic mechanism used was that developed by Egolfopoulos et al [8].

The experimental flat flame burner was made of a 5.1 cm diameter porous bronze disk with 20μm pore size and embedded cooling coils. Thermocouples were positioned inside the porous plug at known distances from the surface to measure the temperature gradient at the burner surface, from which the heat loss rate can be determined. During the experiments, the burner surface temperature was held at a constant value by varying the coolant flow rate. The inner and outer edges of the luminous zone of the flame were measured visually using a microscope. For detailed comparison, temperature profile through the flame was measured by using both thermocouples and Laser-Raman Spectroscopy. Experiments with the flat-flame burner were conducted under normal gravity conditions.

The cylindrical burner was made of a porous bronze tube with 5μm pore size, 1.25 cm diameter, and 3.76 cm active length. Due to the small burner size and the limited duration of the microgravity experiments, no cooling was used for the burner. A thermocouple was inserted inside the burner wall to record burner temperatures. Experiments were performed under microgravity conditions at the NASA-Lewis 2.2 second drop tower. Mass flow rates were measured using sonic flow nozzles and pressure transducers to record upstream pressures during the experiment. A video camera was used to record flame shapes and standoff distances.

Computational and Experimental Studies - Results

For the planar flame, Fig. 5 shows the optically-measured and computed temperature profiles across a ϕ=0.75 methane/air flame with a mass flow rate of 0.015 gm/cm^2-s. The comparison is fairly close, especially for the final temperature. This could imply that radiative heat loss, which is not included in the numerical calculations, is probably indeed unimportant for the weak flame investigated. The horizontal shift between the experimental and calculated profiles is about 0.25 mm. Since the flame location and thereby the temperature profile are fairly sensitive functions of the surface temperature, this shift could be due to a slight inaccuracy in the measured surface temperature.

Figure 6 compares the experimental and calculated flame standoff position and burner heat loss rate. For the numerical calculations the flame location was defined to be the position of maximum CH radical mole fraction, since this is the major species contributing to the flame luminosity. It is seen that the calculated flame standoff distance is smaller than the experimental values, with a correspondingly larger calculated heat loss rate. The overall level of agreement, however, can be considered to be satisfactory in view of the independent nature with which the calculation and experiments were conducted.

For the cylindrical flames, mixtures of $CH_4 + 2O_2 + 7.52\ N_2 + 5.665$ He, with an effective Lewis number of 2.2, were used for the experiments; helium was added to enhance flamefront stability [9]. The adiabatic flame temperature for the unburned mixture temperature of 300 K is 1885 K, and the calculated laminar burning rate is 17.1 cm/s, or 0.0135 gm/cm^2 s.

Figure 7 compares the calculated and measured flame standoff distance as a function of normalized mass flow M. Since the flames were not strictly cylindrical, the vertical bars of the experimental data show the range of the flame positions. The numerical results show that there is no heat loss to the burner at the flow rates shown in the figure. The comparison shows that for

high mass flow rates the calculated results are higher than the experimental values. The cause for this disagreement needs further study.

Summary

Microgravity cylindrical and spherical flames offer well-controlled flame configurations for fundamental studies of the structure and response of premixed and nonpremixed flames. Preliminary analytical, computational, and experimental studies demonstrate the viability of this approach.

Acknowledgments

This research was supported by the microgravity combustion program under NASA sponsorship. We appreciate the generous technical advice and assistance from K. Sacksteder and D. Dietrich at NASA-Lewis, and at Princeton University C. J. Sung and J. Liu.

References

1 Law, C. K. (1988). Dynamics of Stretched Flames. Twenty-Third Symposium (International) on Combustion, 1381.
2 Law, C. K. (1982). Recent Advances in Droplet Vaporization and Combustion. Prog. Energy. Combust. Sci. 8, 169.
3 Choi, M. Y., Dryer, F. L. and Haggard, J. (1991). Observations on a Slow Burning Regime for Hydrocarbon Droplets: n-heptane/Air Results. Twenty-Third Symposium (International) on Combustion, 1597.
4 Buckmaster, J. D. and Ludford, G. S. S. (1982). Theory of Laminar Flames. Cambridge Univ. Press, New York.
5 Ferguson, C. R. and Keck, J. C. (1979). Stand-Off Distances on a Flat Flame Burner. Combust. Flame 34, 85.
6 Spalding, D. B. and Yumlu, V. S. (1959). Experimental Demonstration of the Existence of Two Flame Speeds. Combust. Flame 3, 553.
7 Chao, B. H. and Law, C. K. (1988). Duality, Pulsating Instability, and Product Dissociation in Burner-Stabilized Flames. Combust. Sci. Tech. 62, 211.
8 Egolfopoulos, F. N., Zhu, D. L. and Law, C. K. (1990). Experimental and Numerical Determination of Laminar Flame Speeds: Mixtures of C_2-Hydrocarbons with Oxygen and Nitrogen. Twenty-Third Symposium (International) on Combustion, 471.
9 Matalon, M. and Matkowsky, B. J. (1983). Flames in Fluids: Their Interaction and Stability. Combust. Sci. Tech. 34, 295.

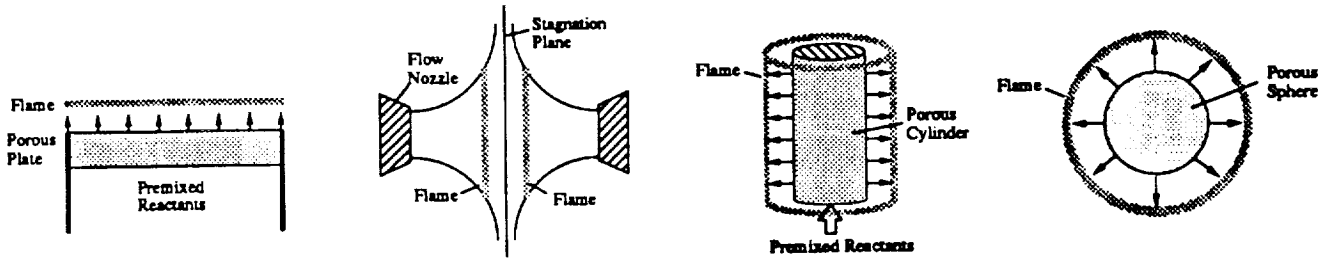

a) Flat Flame Burner b) Counterflow Burner c) Cylindrical Burner d) Spherical Burner

Figure 1

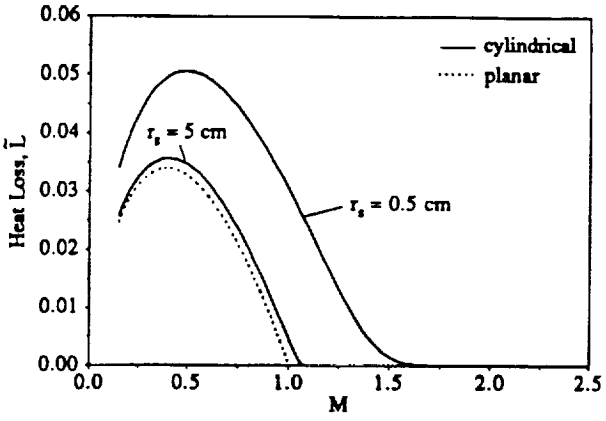

Figure 2

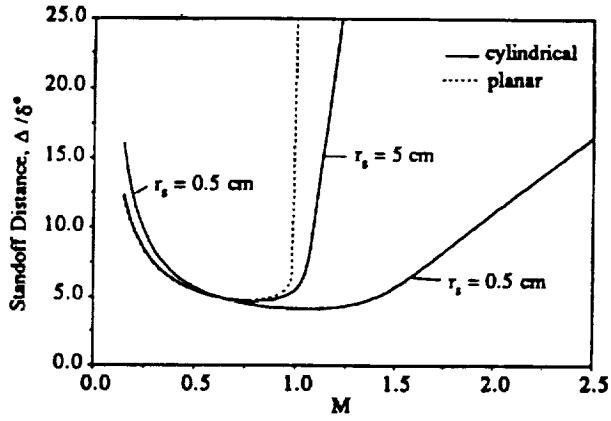

Figure 3

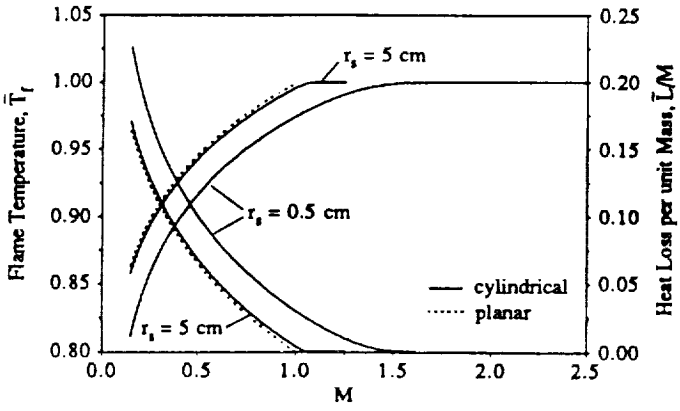

Figure 4

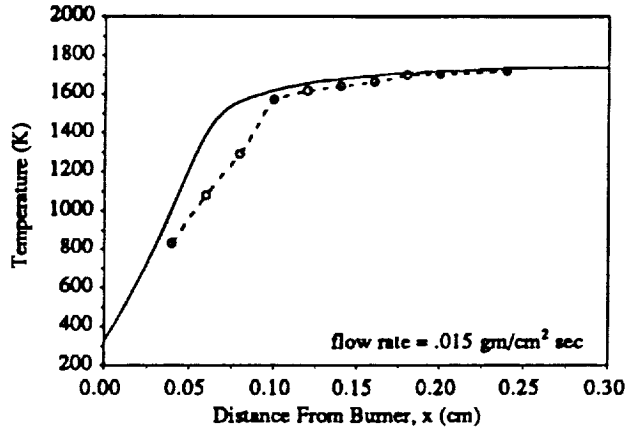

Figure 5

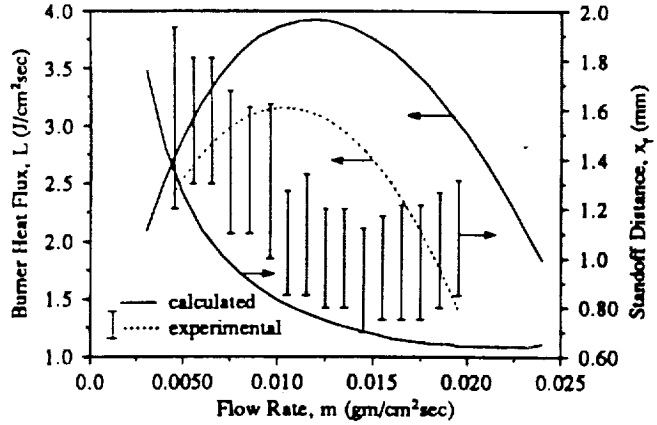

Figure 6

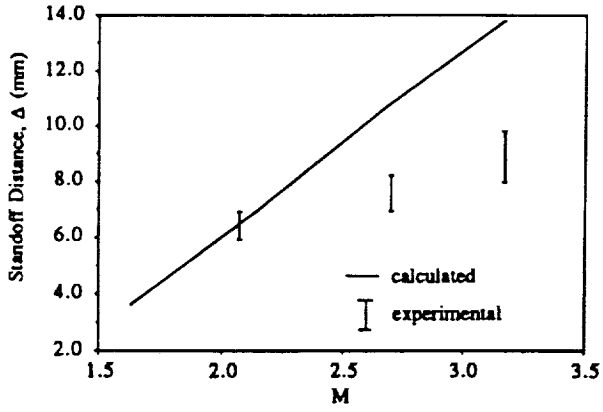

Figure 7

C-3

THE EFFECTS OF GRAVITY ON WRINKLED LAMINAR FLAMES

L.W. Kostiuk, L. Zhou, and R.K. Cheng
Lawrence Berkeley Laboratory
Energy & Environment Division
Berkeley, California 94720

N93-20200

Introduction

The effects of gravity are significant to the dynamics of idealized unconfined open premixed flames. Moderate to low turbulence Reynolds number flames, i.e. wrinkled laminar flames, of various unconfined geometries have been used extensively for investigating fundamental processes of turbulent flame propagation and to validate theoretical models. Without the wall constraints, the flames are free to expand and interact with surrounding ambient air. The flowfield in which the flame exists is determined by a coupling of burner geometry, flame orientation and the gravity field. These complex interactions raise serious questions regarding the validity of comparing the experimental data of open flames with current theoretical and numerical models that do not include the effects of gravity nor effects of the larger aerodynamic flowfield. Therefore, studies of wrinkled laminar flame in microgravity are needed for a better understanding of the role of gravity on flame characteristics such as flame orientation, mean aerodynamics stretch, flame wrinkle size and burning rate.

To date, most studies of microgravity combustion have concentrated on investigating laminar flames. The primary diagnostic used is high speed movies of flame luminosity to observe gross flame properties changes. For example, Durox et al. [1] reported flame tip motion of rich laminar Bunsen flames under microgravity and analyzed the motion by a flame instability model. However, the study of premixed turbulent flames under microgravity requires more sophisticated diagnostics. But there are also many experimental constraints. The short duration of microgravity experiments in drop towers or onboard parabolic flights precludes detailed statistical investigation of velocity and scalar fluctuations. The lack of a high power laser source prohibits the use of many established techniques to measure parameters such as flame crossing frequencies and mean scalar length scales suitable for direct comparison with theoretical models such as the one developed by Bray et al. [2].

Our approach to characterize and quantify turbulent flame structures under microgravity is to exploit qualitative and quantitative flow visualization techniques coupled with video recording and computer controlled image analysis technologies. The experiments will be carried out in the 2.2 second drop tower at the NASA Lewis Research Center. The longest time scales of typical wrinkled laminar flames in the geometries considered here are in the order of 10 msec. Hence, the duration of the drop is sufficient to obtain the amount of statistical data necessary for characterize turbulent flame structures.

Diagnostics and apparatus

Schlieren visualization was widely used in early studies of premixed turbulent combustion. Because it is a line-of-sight technique, it has been superseded by laser planar imaging techniques in recent years. Schlieren's most appealing aspects for microgravity work are that it require relatively low power light source, the optics are relatively simple and it is easy to align. When using a laser source coupled with modern CCD cameras with high shutter speeds (up to 1/10000 sec), new video recording and analysis technologies, laser schlieren can provide qualitative information of the flame flowfield and quantitative information such as flame angles and perhaps flame wrinkle size.

The schlieren system developed for our microgravity experiments uses a 0.5 mW He-Ne laser light source and two 75 mm diameter schlieren lenses. The lenses' diameter is also the effective field-of-view of the system. Due to the constraints of the drop package size, the two lenses are of different focal length. The transmitting lens has

This work is supported by NASA Microgravity Sciences and Applications Division. Technical support is provided by NASA Lewis Research Center under contract No. C-32000-R. Project Scientist is Dr. Karen J. Weiland.

a relatively short focal length of 300 mm and the converging lens has a focal length of 1000 mm to maintain a sensitive system. An opaque spot etched on a glass window is used as the schlieren stop. This arrangement produces a reverse field image (i.e., dark background), and regions of high density gradients appear bright.

A CCD camera and video recorder are used to record the schlieren images with the shutter speed varied from 1/60 to 1/10000 sec. The system has an effective framing rate of 60 Hz even though standard play-back speed is 30 Hz. Each frame is made up of two interlaced fields (i.e., separate images) recorded 1/60 sec. apart. Individual fields can be displayed on the S-VHS deck during freeze-frame operation or the images can be digitized and the fields separated using a computer controlled image processing system. The digitized images can be stored and analyzed by standard image processing software.

A conical Bunsen type burner is used for the first set of experiments. The burner is made of aluminum and has a 25 mm diameter outlet supplied by a converging nozzle mounted on a cylindrical settling chamber. The converging nozzle is designed to produced laminar flows with uniform velocity distribution across the exit. The flame is stabilized by a ring fitted to the exit of the burner to enable stabilization of lean flames. Turbulence is generated by a perforated plate placed 20 mm upstream of the exit. The laser, optics, burner, flow control and supply systems, and onboard computer are mounted inside a standard 3' x 3' x 1.5' drop package frame for the NASA Lewis Research Center 2.2 second drop tower (Fig. 1).

Normal gravity studies

As a necessary prerequisite to the microgravity experiments, we have conducted a parametric study to determine the mixture and flow conditions at which the effects of gravity on flame characteristics are most prominent. Schlieren images of laminar and turbulent conical flames subjected to +g (upwards) and -g (downward) forces are compared. In addition to schlieren visualization, selected flames are investigated in detail by the use of two-component laser Doppler anemometry (LDA) to determine the coupling between the flowfield (encompassing the reactants, flame, and surrounding gases) and the flame characteristics.

Figure 2 shows a typical schlieren image of a +g laminar conical flame. The flame is shown by the triangular silhouette above the burner exit. In addition, the interfaces formed between the hot products and the ambient air are also visible. This product/air interface is unstable and is characterized by the formation of bulges reminiscent of the roll-up of torroidal vortices. A comparison of two time sequences of +g and -g schlieren images of a laminar methane/air flame (ϕ = 0.6 and incident flow velocity U = 0.7 m/s) is shown in Fig. 3. The development of the roll-up vortex like structure in the unstable product/air shear interface is apparent. The video also shows that the flame tip moves up and down synchronously with this shear layer disturbance. Subjecting the flame to -g changes the flame shape and turns the product/air interface into a stable envelope of hot gases, so the flame is much more stable than in the +g case.

The flame tip motion being fully synchronous with the unsteady product/air interface is also observed in the +g turbulent cases. Figure 4 shows a typical sequence. The flame wrinkles are either stretched larger or compressed smaller during the cycle. This implies a direct flowfield effect on the turbulent burning rate.

Durox et al. [1] also reported and analyzed flame tip motion in their rich laminar flames under normal and microgravity. By only observing flame luminosity, they were not aware of the significance of the product/air interface. The flame tip motion in their study was attributed to flame instability developed at the burner rim. To estimate if their results are consistent with the present data, the schlieren videos are analyzed to determine the fluctuation frequencies of the product/air interface. The width of the product/air interface silhouette at the mean height of the flame tip are determined for 60 fields (1 sec total time). The results are fitted with a cubic spline and analyze by Fast-Fourier-Transform. All flames show primary fluctuation frequencies between 8 to 13 Hz (Fig. 5). These frequencies are about the same as those reported by Durox et al. Therefore, it seems that the flame tip motion observed by Durox et al. are also induced by the instability of the product/air interface.

The unstable product/air interface also induces flow fluctuations in the approach flow. The velocity spectra obtained at the centerline about 4 mm upstream of a laminar flame tip clearly show a dominant fluctuation frequency (Fig. 6) and higher harmonics of this primary frequency also exist. This is a strong evidence of the coupling between the flowfield and flame front dynamics. Velocity spectra obtained in a turbulent flame also

show the dominant fluctuation frequency (Fig. 7) though the relative energy containing in this frequency is diminished by the turbulent kinetic energy associated with the grid turbulence. This observation strongly suggests that the unstable product/air interface has a significant influence on flame propagation and is the avenue through which gravity affects turbulent flame characteristics. These results have been presented at the poster session of the 24th International Combustion Symposium [3].

Planned activities and diagnostic development

The microgravity work will be carried out at NASA Lewis Research Center in September, 1992. The experiments will be concentrated on methane/air laminar and turbulent flames with equivalent ratio from 0.5 to 1.0 and mean flow exit velocity from 0.5 to 1.0 m/s. These are the conditions found to be most affected by the change in the direction of the gravitation forces. Schlieren will be the primary diagnostic and the results will be analyzed as outlined above to obtain the changes in the flame shape, and the fluctuation frequencies of the flame tip and of the product/air interface. The videos will also provide qualitative information on the changes in the flame wrinkle sizes.

The second phase of the microgravity experiments will involve the use of other flame configurations such as rod-stabilized v-flames. The development of quantitative diagnostics for measuring flame wrinkle characteristics is also planned. The single beam schlieren technique will be exploited for measuring the flame crossing frequencies at a point. The deflection of a He-Ne laser beam traversing the flame zone can be quantified by the use of a diode. Fast Fourier transform of the diode output will produce a spectrum of the flame crossing frequency that is directly related to the flame wrinkle sizes. Refinement of the technique will rely on comparing the results with those obtained from the Mie scattering from oil droplet method that is normally used in laboratory experiments. The comparison will also help to establish the proper data interpretation method.

References

1. Durox, D., Baillot, B., Scoufflaire, P. and Prud'homme, R. "Some Effects of Gravity on the Behavior of Premixed Flames", Combustion and Flame, Vol. 82, 1990, p. 66.
2. Bray, K.N.C., Libby, P.A., and Moss, J.B., "Unified Modeling Approach for Premixed Turbulent Combustion - Part I: General Formulation", Combustion and Flame, Vol. 61, 1985, p. 87.
3. Kostiuk, L. W., Zhou, L. and Cheng, R. K., "The Effects of Gravity on Wrinkled Lamianr Flames", Poster paper 102, 24th Internation Symposium on Combustion, July 5-11, Sydney, Australia 1992.

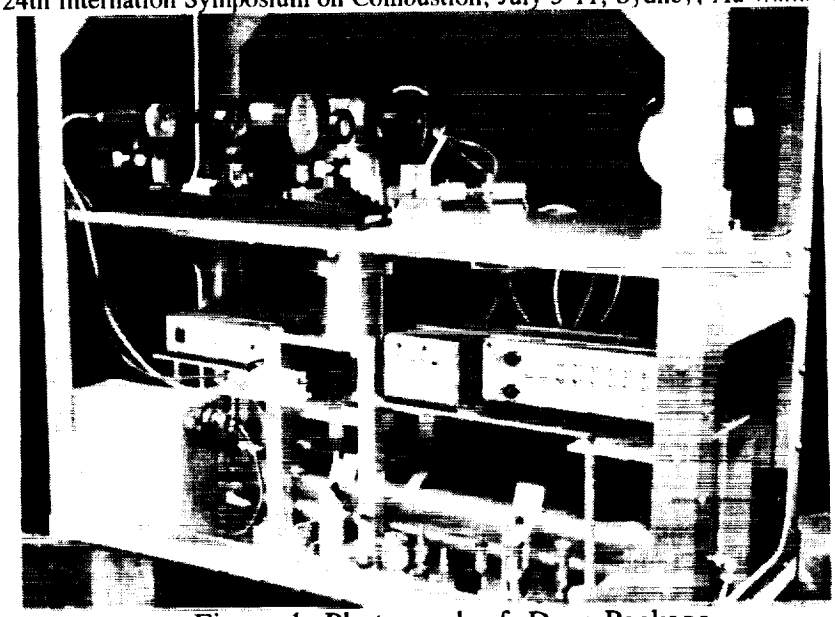

Figure 1: Photograph of Drop Package.

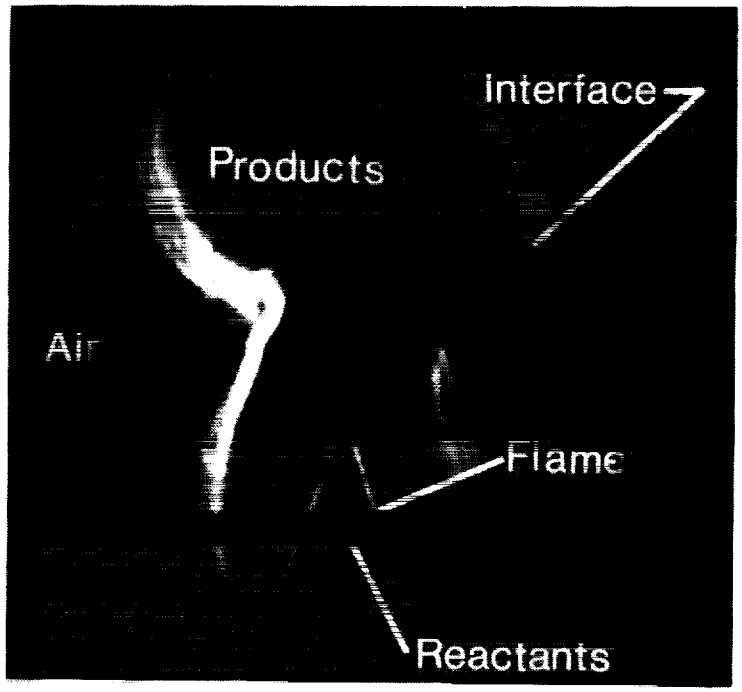

Figure 2: Typical Schlieren Image of Premixed Laminar Bunsen Flame.

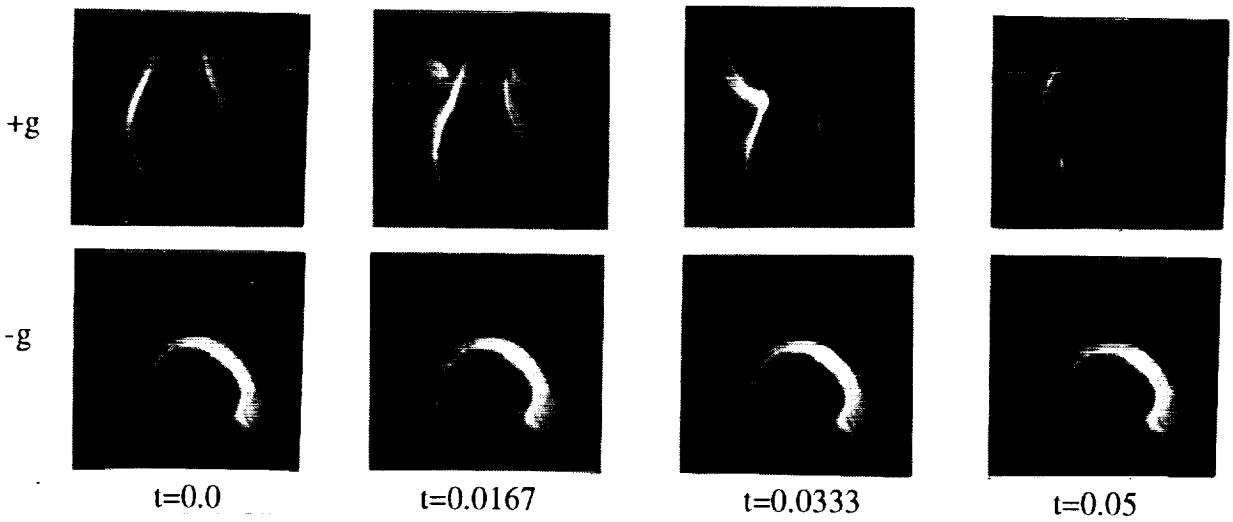

Figure 3: Time Sequence of Schlieren Images for Laminar Flame.

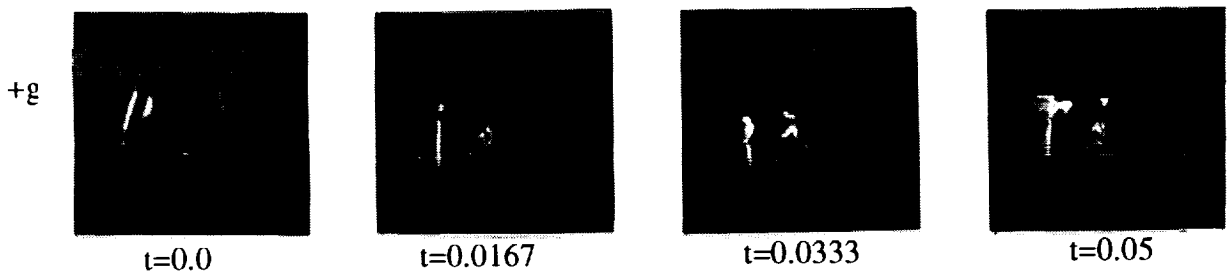

Figure 4:Time Sequence of Schlieren Images for Turbulent Flame.

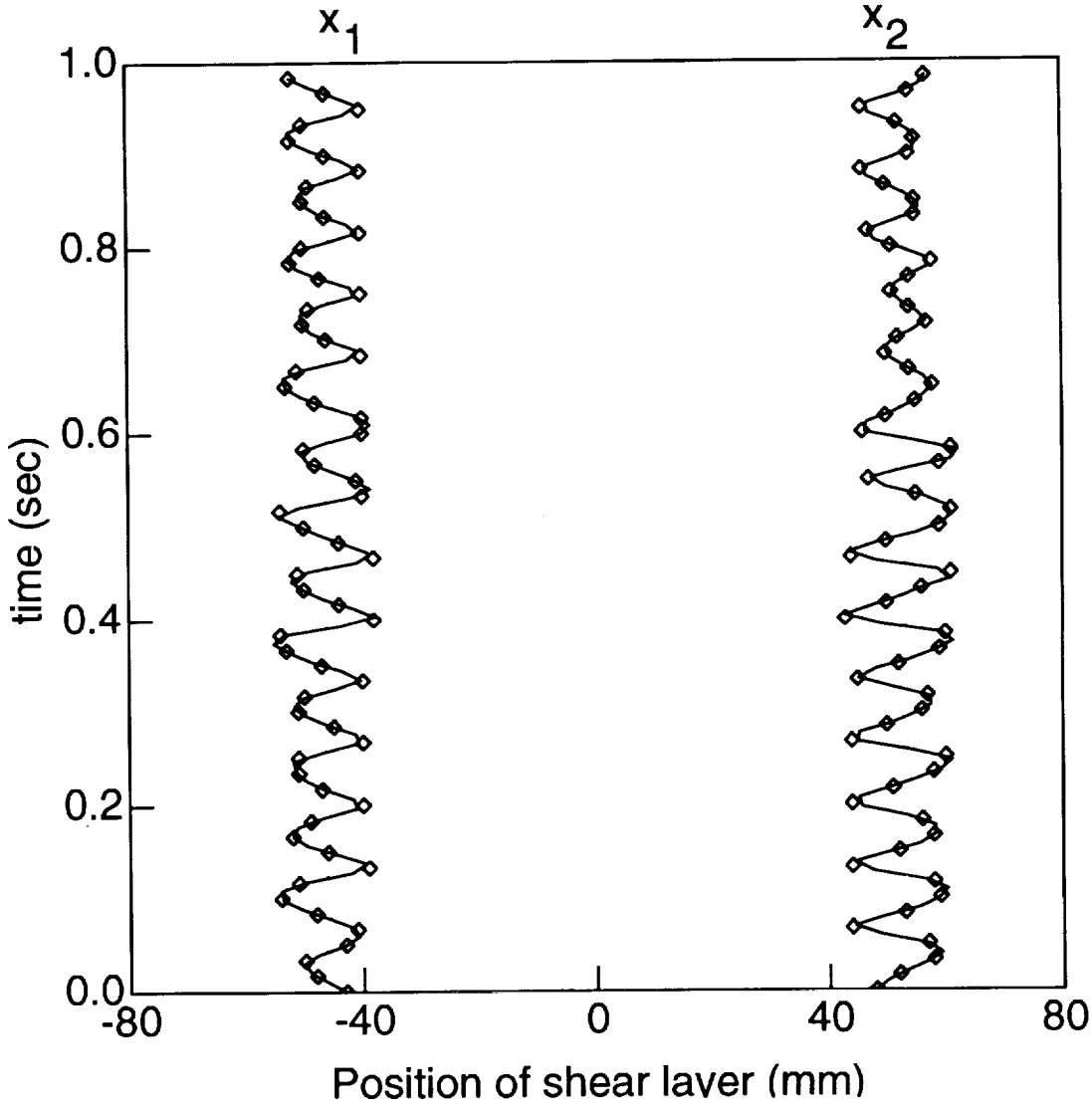

Figure5: Radial Position of Air/Product Interface.

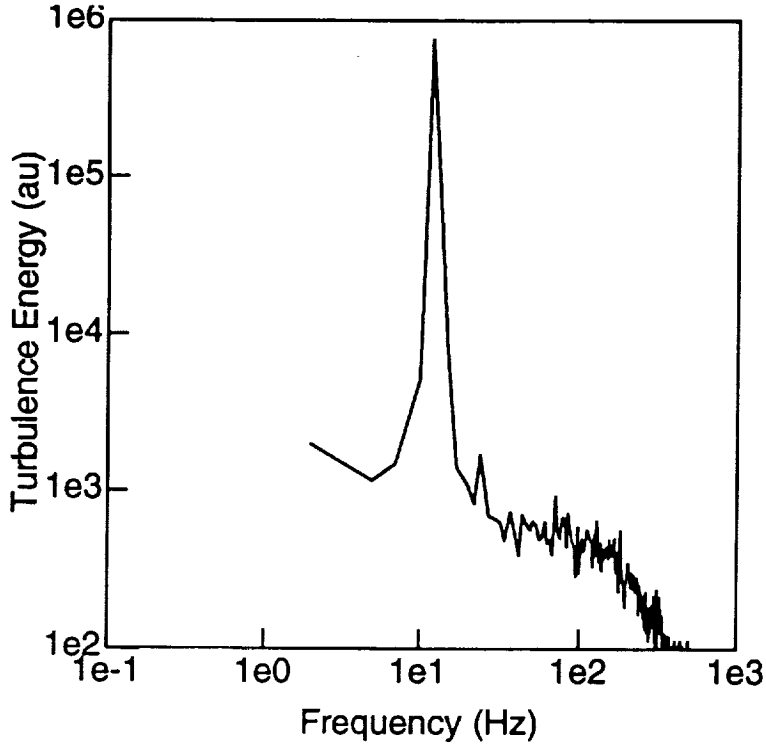

Figure:6 Velocity Spectra of Laminar Flame.

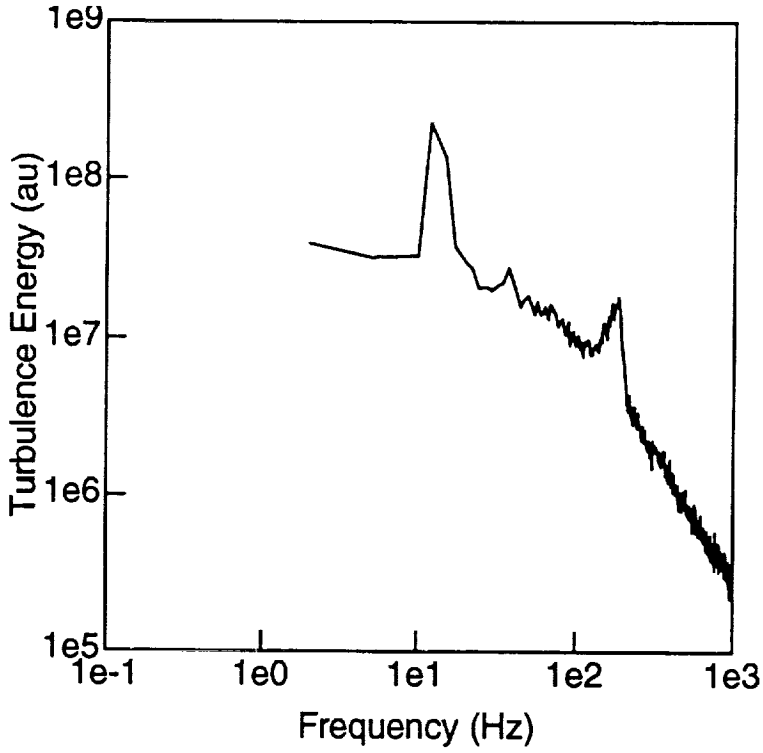

Figure7: Velocity Spectra of Turbulent Flame.

MICROGRAVITY COMBUSTION OF DUST SUSPENSIONS

John H.S. Lee, Olivier Peraldi, and Rom Knystautas
Department of Mechanical Engineering
McGill University
Montreal, Canada

Introduction

Unlike the combustion of homogeneous gas mixtures, there are practically no reliable fundamental data (i.e., laminar burning velocity, flammability limits, quenching distance, minimum ignition energy) for the combustion of heterogeneous dust suspensions. Even the equilibrium thermodynamic data such as the constant pressure volume combustion pressure and the constant pressure adiabatic flame temperature are not accurately known for dust mixtures. This is mainly due to the problem of gravity sedimentation. In normal gravity, turbulence, convective flow, electric and acoustic fields are required to maintain a dust in suspension. These external influences have a dominating effect on the combustion processes. Microgravity offers a unique environment where a quiescent dust cloud can in principle be maintained for a sufficiently long duration for almost all combustion experiments (dust suspensions are inherently unstable due to Brownian motion and particle aggregation). Thus, the microgravity duration provided by drop towers, parabolic flights, and the space shuttle, can all be exploited for different kinds of dust combustion experiments. The present paper describes some recent studies on microgravity combustion of dust suspension carried out on the KC-135 and the Caravelle aircraft. The results reported are obtained from three parabolic flight campaigns; NASA KC-135 (March and July 1992) and ESA Caravelle (April 1992).

General Considerations

Pioneering studies of microgravity combustion of lycopodium dust clouds have been carried out by Berlad, Ross and co-workers at NASA LeRC [1,2]. Acoustic waves from a speaker at one end of a 5 $cm \times 30\ cm$ flame tube was used to lift a uniform layer of dust initially placed along the horizontal tube. An inflatable balloon at the other end of the tube maintains more or less constant pressure combustion. Chattering or pulsating flames were observed which were credited to the non-uniform stratified distribution of the dust by the acoustic field [3]. However, vibrating flames are typical for flame propagation in tubes due to flame-pressure wave interactions. Laminar burning velocities

were deduced based on an estimate of the complex flame shapes. Adhesion of the dust to the tube wall was found to be a problem.

Although the laminar burning velocity and the temperature profile in the reaction zone provide more important information on the flame propagation mechanism, we consider it important to first obtain some thermodynamic data on dust combustion in microgravity. The standard combustion experiment for dust suspension is constant volume burning where the peak pressure and the maximum rate of pressure rise are determined. Standard apparatus and procedures have been developed (e.g., the Hartmann bomb, the spherical 20 liter bomb of Siwert, the 1 m^3 vessel of Bartknecht) by the dust explosion community. In all these apparatus, a given sample of dust is first dispersed by a strong turbulent jet and the subsequent suspension is then introduced into the partially evacuated combustion chamber. A key parameter is the so-called dispersion turbulence which decays rapidly with time. However, in normal gravity, dust sedimentation occurs when the dispersion turbulence decays and it is necessary to carry out the burning at a high level of turbulence in the dust suspension. Strong turbulence tends to stratify the dust in the eddies beside having a quenching effect on the combustion processes (especially for the slower burning rates of heterogeneous dust mixtures). Furthermore, turbulence also strongly influences the transport and hence burning rate. Therefore, the rate of pressure rise is strongly influenced by the dispersion turbulence and perhaps more so than by the chemical and physical properties of the dust cloud itself. Thus far, it has not been possible to obtain accurate data even on the thermodynamic combustion parameters for dust suspensions. In microgravity, where sedimentation is absent, it is then possible to wait till the dispersion turbulence has decayed prior to ignition. In this manner, more fundamental information can be obtained that is characteristic of the dust cloud and not the apparatus and procedure. We judge that this is an appropriate first step towards the understanding of dust cloud combustion.

Apparatus

Experiments were carried out during the nominal 20 *sec* duration of μg of parabolic flights of the NASA KC-135 and ESA's Caravelle. The spherical combustion chamber used is 5.4 liters in volume ($\sim$ 20 *cm* diameter) and is essentially a 1/4-scaled down version of the standard 20 liter spherical bomb of Siwert [4]. The dust sample is placed inside a small cylindrical dust cup which is connected to a small pressure vessel of about 0.2 liter in volume via an electrically operated solenoid valve. When the valve is activated, the high pressure air from the 0.2 liter chamber discharges into the dust cup and disperses the dust sample. The resulting dust suspension then flows into the spherical combustion chamber through numerous small jets ($\sim$ 1 *mm* diameter) spaced about 1 *cm* apart around the inner radius of a tubular ring inside the spherical vessel. The spherical vessel is initially evacuated to some sub-atmospheric pressure so that after the dust dispersion, the final pressure in the chamber is atmospheric. Ignition is via a small pyroelectric match-head and the time delay between dispersion (activation of the

solenoid valve) and ignition is controlled by a time delay generator. A schematic of the apparatus is shown in Fig. 1. To carry out the experiments on board the KC-135, a self-contained system comprising the vacuum and compressed gas supply, data acquisition system and the various electrical equipment, and control valves is required. This system is shown schematically in Fig. 2. The dust used is aluminum and two mean particle sizes are used (AMPAL 637 ($d_{32} = 5\ \mu m$) and AMPAL 615 ($d_{32} = 20\mu m$). Electron micrograph analysis of these dusts indicate a far from spherical morphology. Instead, the geometries of the particles are highly irregular. Two pressure transducers (PCB 113A24) with heat shields are used as the main diagnostics and a matrix of light absorption probes are used to monitor the dust concentration inside the vessel. The concentration-time measurements are taken without combustion in the vessel. After each experiment, the burnt products are evacuated to outside the aircraft and the bomb is opened to clean the residual deposits.

Results and Discussion

Figure 3 compares the pressure-time curves (for the 5 μm dust) for both the normal and μg experiments. For short delay times (i.e., 0.2 m/s), the normal and μg results are practically identical, indicating that the dispersion turbulence dominates the early time combustion processes inside the chamber. As the turbulence decays both the peak overpressure as well as the rate of the pressure rise decreases for the normal gravity experiments. The decrease in peak overpressure with delay time for the initial period can be credited to both turbulent quenching and wall deposits as the dust jets impact on the wall. It should be noted that the duration of the dispersion process (i.e., pressurized air discharging from the 0.2 liter vessel) is about 500 ms. Thus, the turbulence level is still fairly intense for the first few seconds after the start of the dispersion process. The slower decrease of the peak pressure (as well as the rate of pressure rise) for the longer delays of 10 *sec* and 15 *sec* could be due to gravity sedimentation. For the microgravity case, we note that the pressure-time profile appears to reach an asymptotic limit without the gravity sedimentation. The rate of pressure rise remains the same for different delay times, indicating that the influence of the dispersion turbulence is essentially negligible after about the first 5 *sec*. For both the normal and the μg experiments, the optimum peak overpressures (corresponding to a time delay of 200 ms) is about 6.2 atm. as compared to the theoretically computed constant volume explosion overpressure for aluminum of 11.6 atm. Incomplete voiding of the dust from the dust dispersion system into the vessel, adhesion of the dust to the wall, as well as heat losses and quenching as the flame reaches the copper wall of the spherical vessel could account for this. From the microgravity gravity results, an asymptotic value of the peak overpressure of about 4 atm is obtained, corresponding to only about 10% of the dust that is actually burnt in terms of energetics. Hence, instead of the global nominal dust concentration, of 500 gm/m^3 based on the total account of dust divided by the volume of the bomb, only about 10% remains in suspension after the dynamic process has subsided. The actual amount of dust may be higher since heat losses to the wall and the dispersion ring may

be significant. Assuming a thin spherical flame, one can also deduce the laminar burning velocity from the pressure-time curve [5]. The laminar burning velocity corresponding to the asymptotic pressure-time history from the microgravity experiment is found to be about 0.25 ms based on the peak overpressure of 4 atm observed experimentally. This is quite a reasonable value.

The peak overpressure versus time delays for the 5 μm and 20 μm dusts are shown in Fig. 4. The continuous decrease in the peak overpressure with time in normal gravity after the dynamic dispersion processes have subsided can be attributed to gravity sedimentation. The microgravity results show an asymptotic limit of about 4 *bars* after a delay time of about 5 *sec* where most of the initial dispersion turbulence processes have decayed. However, for the large particle size case, both the microgravity and normal gravity experiments are similar, i.e., the initial dynamic processes completely control the combustion. An optimum peak overpressure (at 200 ms delay) of only 4 *bars* (as compared to 7 *bars* for the 5 μm dust) indicating that substantial amounts of dust are not discharged from the dispersion ring. When dispersed, the larger particles also do not follow the recirculation turbulent flow and hence more losses to the wall occur due to particle impact result. For large particles, the standard method of dispersion is not suitable and perhaps the simpler (but perhaps less uniform) method as used in the Hartmann bomb may give better results.

Conclusion

The preliminary experiments so far have demonstrated the feasibility of obtaining a quiescent dust cloud for fundamental flame propagation studies in microgravity. The major problem that has been identified is the initial generation of the dust suspension and its introduction into the combustion chamber. Higher shear rates from an intense turbulent jet is found necessary to break up an agglomerated dust sample, yet a low velocity laminar flow is needed to introduce the suspension into the combustion chamber to avoid turbulent stratification and high speed impact and subsequent adhesion of the dust to the chamber wall. These are technical problems that can best be resolved by more manned experiments on the KC-135 (or equivalent). Once the dust dispersion problem has been resolved, fundamental experiments on flame propagation, structure, quenching distance and flammability limits, minimum ignition energy can readily be designed. Theoretical modelling is considered to be of vital importance in design of the experiments due to the large number of variables involved in dust combustion. The limited diagnostic that can be effectively used for optically thick dust flame in the restricted space lab environment also necessitates the use of theoretical models for interpretation of the experimental results obtained.

Acknowledgement

This work is supported by the Canadian Space Agency through contract #9F007-1-

8022/01-SW. Technical assistance by Champlain Landry, Pedro Gregorio, Debbie Soriano are gratefully acknowledged.

References

1. Berlad, A.L., "Combustion of Particle Clouds in Combustion Experiments in a Zero Gravity Laboratory", Ed. T.H. Cochran, AIAA Progress in Astronautics and Aeronautics, Vol. 73 (1981), p. 91.

2. Berlad, A.L. and Tangirala, V., "Reduced Gravity Combustion of Particle Cloud", NASA CR Rept. 182299 (1989).

3. Ross, H., Facca, L, Berlad, A., Tangirala, V., "Feasibility of Reduced Gravity Experiments involving Quiescent Uniform Particle Cloud Combustion", NASA Tech. Memo 101371 (1989).

4. Bartknecht, W., "Explosions", Springer-Verlag, N.Y. (1980).

5. Lee, J.H.S., Pu, Yi-Kang and Knystautas, R., "Influence of Turbulence on Closed Volume Explosion of Dust-Air Mixtures", Archivum combustionis, Vol. 7, No. 3/4 (1987) pp. 280-297.

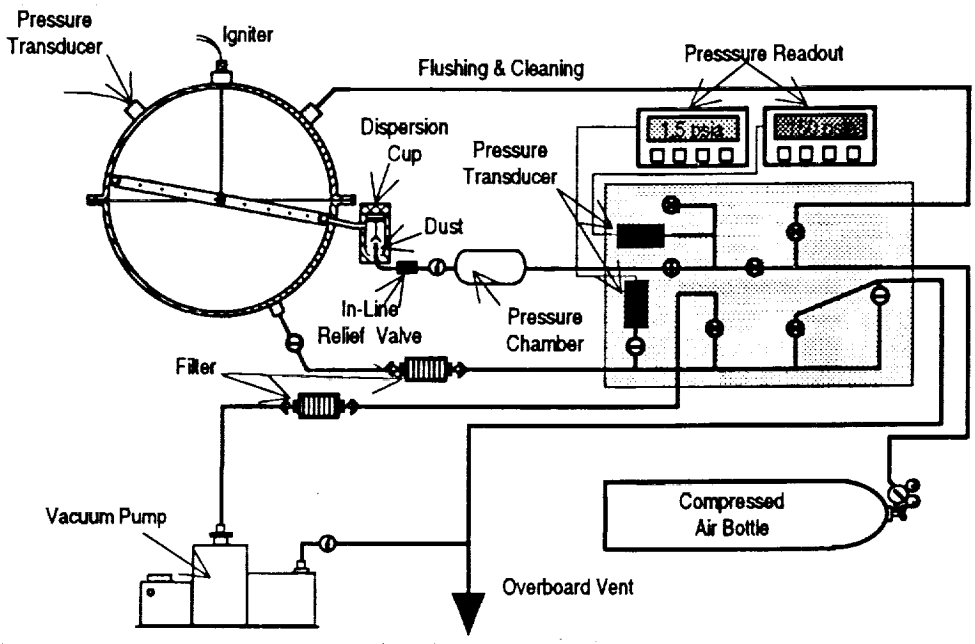

Figure 1 : Schematic diagram of the experimental apparatus.

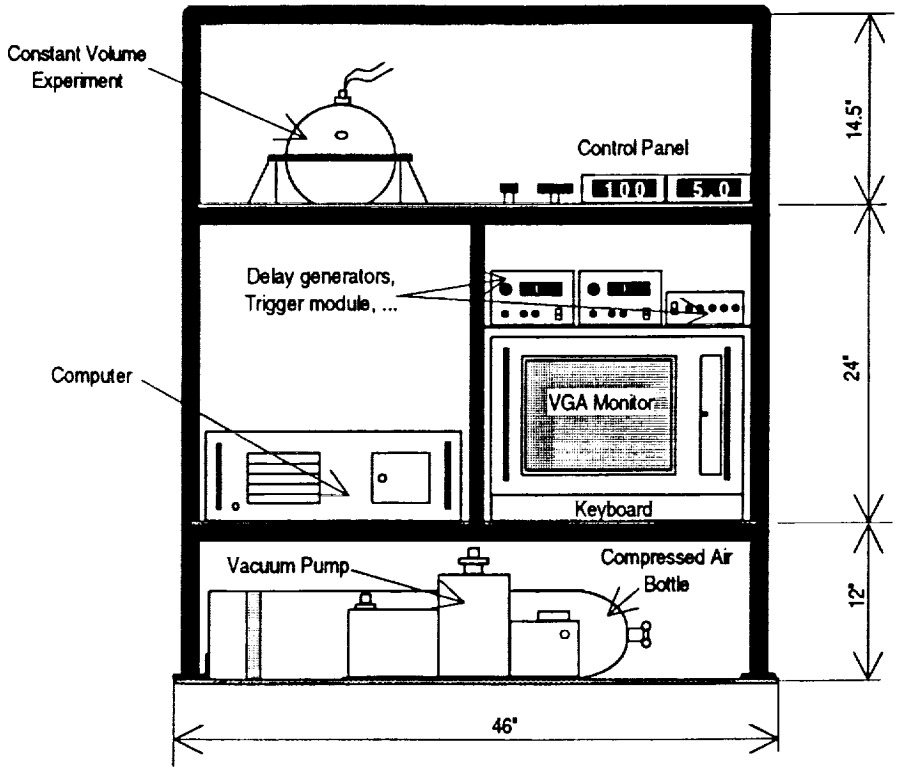

Figure 2 : Microgravity Experimental Package.

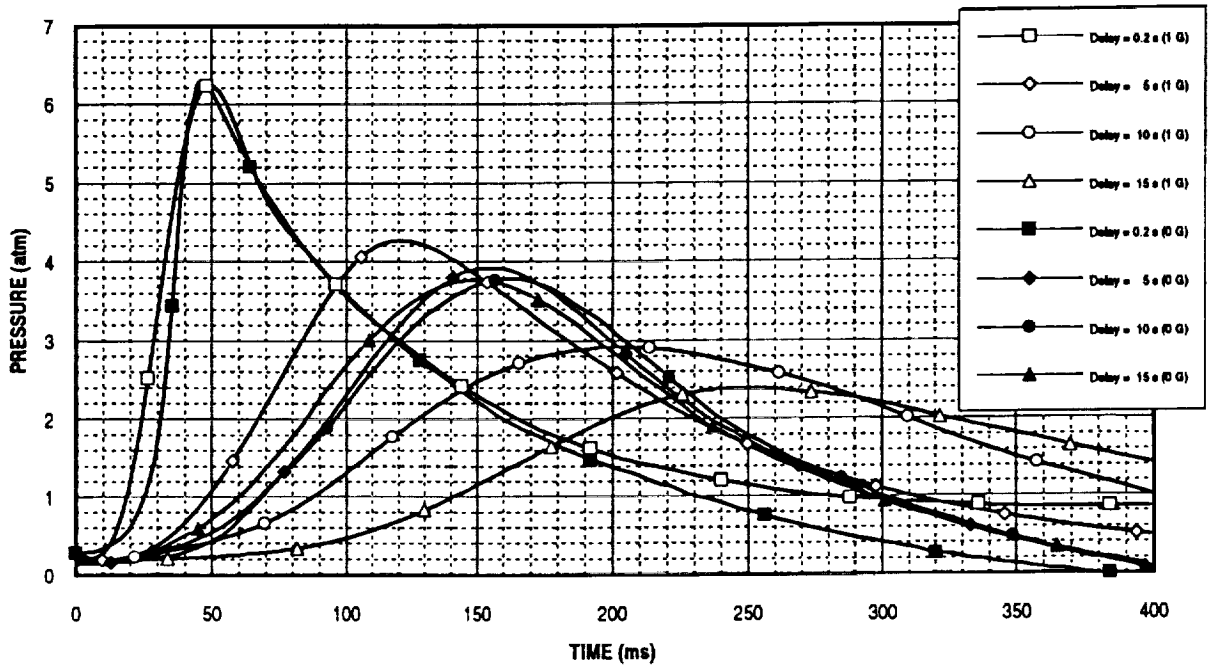

Figure 3 : Pressure rises for different delay times between dispersion and ignition in 1-g and μ-g.

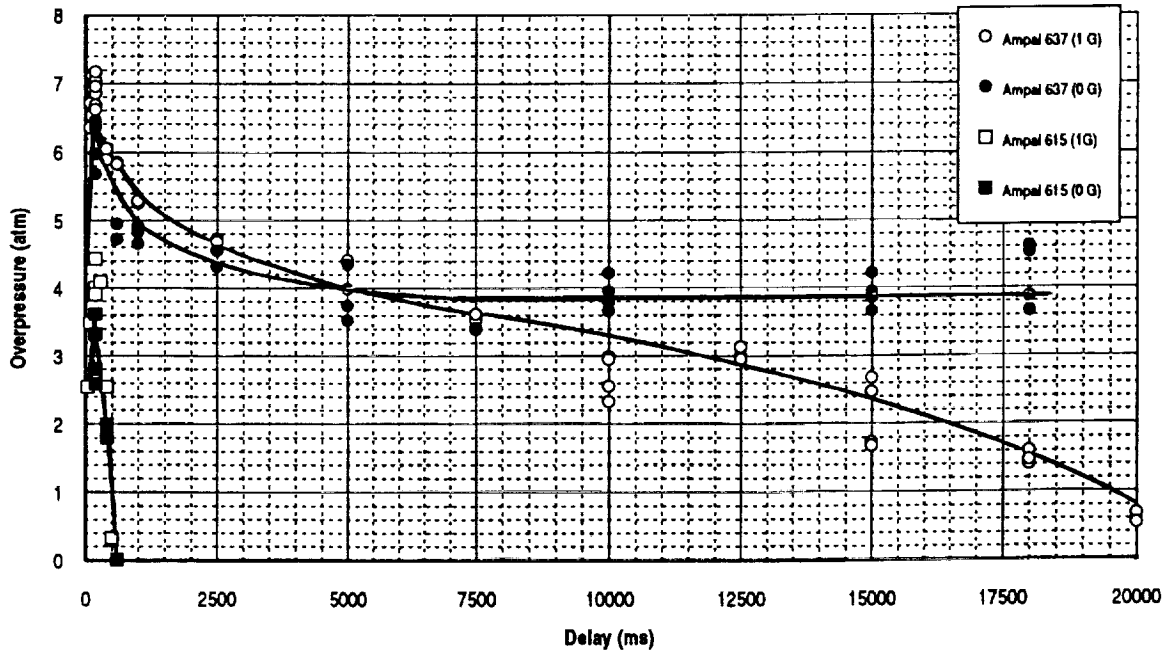

Figure 4 : Variation of peak constant volume explosion pressure with delay time between dispersion and ignition in 1-g and μ-g.

THE STRUCTURE OF PARTICLE CLOUD PREMIXED FLAMES

K. Seshadri
Department of Applied Mechanics and Engineering Sciences
University of California - San Diego
La Jolla, California 92093

1. Introduction.

The aim of this study is to provide a numerical and asymptotic description of the structure of planar laminar flames, propagating in a medium containing a uniform cloud of fuel-particles premixed with air. Attention is restricted here to systems where the fuel-particles first vaporize to form a known gaseous fuel, which is then oxidized in the gas-phase. This program is supported for the period September 14, 1991 to September 13, 1992. Some results of the study is shown in Ref. 1. The work summarized in Ref. 1 was initiated prior to September 14, 1991 and was completed on February 1992. Research performed in addition to that described in Ref. 1 in collaboration with Professor A. Linan, is summarized here.

The model developed here is built on previous asymptotic analysis structure of premixed particle-cloud flames [1]. In this previous analysis the vaporization rate of the fuel-particles was presumed to be proportional to $T_s^{1.33}$, where T_s is the temperature of the fuel-particles. Hence, the activation temperature in an Arrhenius-type rate law for the vaporization process is not large. For simplicity, the temperature of the fuel-particles was presumed to be equal to the gas temperature. The analysis was performed for values of $\phi_u > 1.0$, where ϕ_u is the equivalence ratio based on the gaseous fuel available in the particles. For given values of ϕ_u the analysis yields results for the burning velocity and ϕ_g, where ϕ_g is the effective equivalence ratio in the reaction zone [1]. The analysis shows that even though $\phi_u > 1.0$, for certain cases the calculated value of ϕ_g is less than unity.

A two-temperature model is described here, where the temperature of the fuel-particles is different from the temperature of the gas. However the size of the fuel-particle is assumed to be small enough so that its velocity is nearly equal to the gas velocity. A general treatment of flame propagation supported by volatile fuel-particles should consider both radiative and molecular transport mechanisms, the temperature difference and the differences in velocity between the gas and the particulates, the nonadiabaticity of combustible systems of finite size, as well as the detailed kinetics of oxidation and the kinetics of vaporization pyrolysis. This work has the somewhat limited aim of examining the interplay of vaporization kinetic and oxidative kinetic processes for cases where nonadiabatic and radiative transport mechanisms are not substantial.

2. Formulation.

A model is developed to describe steady, one-dimensional, planar flame propagation in a combustible mixture consisting of uniformly distributed fuel-particles in air. The initial number density of the particles, n_u (number of particles per unit volume) and the initial radius a_u are presumed to be known. All external forces including gravitational forces effects are assumed to be negligible. The kinetics of vaporization of a fuel-particle is represented by the expression

$$\dot{m} = 4\pi a^2 A \exp\left(-\frac{T_{av}}{T_s}\right) = -\frac{4}{3}\pi \frac{d(a^3)}{dt}\rho_s, \tag{1}$$

where $\dot{m}$ represents the mass of gaseous fuel vaporized per unit time from the fuel-particle, a and ρ_s are the instantaneous radius and density respectively of a fuel- particle. The rate parameters A and T_{av} which respectively represent the frequency factor and the activation temperature of the vaporization process are presumed to be known. The ratio T_{av}/T_s is presumed to be a large quantity.

Consider a vaporizing fuel-particle in an ambient atmosphere. The balance equation for the mass fraction of the gaseous fuel vaporizing from the fuel-particle Y_F, and the energy balance equation can be written as,

$$\frac{\dot{m}}{4\pi r^2}\frac{\partial Y_F}{\partial r} - \frac{1}{r^2}\frac{\partial}{\partial r}\left(r^2 \frac{k}{c_p L_F}\frac{\partial Y_F}{\partial r}\right) = 0, \tag{2}$$

$$\frac{\dot{m}}{4\pi r^2}\frac{\partial (c_p T)}{\partial r} - \frac{1}{r^2}\frac{\partial}{\partial r}\left(r^2 k \frac{\partial T}{\partial r}\right) = 0, \tag{3}$$

where r is the radial coordinate. For the gas mixture k is the thermal conductivity, c_p the heat capacity, and T the temperature. The quantity $L_F = k/(\rho c_p D_F)$ is the Lewis number of the gaseous fuel which is presumed to be a constant and D_F is the diffusion coefficient of the gaseous fuel. Boundary conditions for Eqs. 2 and 3 far from the surface of the fuel-particle, and at the surface of the fuel-particle can be written as,

$$\begin{aligned} &T = T_\infty,\ Y_F = Y_{F,\infty} \text{ as } r \to \infty, \\ &T = T_s,\ \dot{m}(1 - Y_F) = -\frac{4\pi k r^2}{c_p L_F}\frac{\partial Y_F}{\partial r} \text{ at } r = a. \end{aligned} \tag{4}$$

The values of T_∞ and $Y_{F,\infty}$ will be determined from the solution of the equations governing the structure of the laminar flame. The temperature of the fuel-particle T_s can be calculated from the energy balance equation

$$q_g = \left(4 \pi r^2 k \frac{\partial T}{\partial r}\right)_{r=a} = \dot{m} L_v + \frac{4}{3} \pi a^3 \rho_s c_s \frac{dT_s}{dt}, \tag{5}$$

where t represents the time, c_s represents the heat capacity of fuel-particle, and L_v represents the heat required to vaporize unit mass of vapor from a fuel-particle. The values of c_p and c_s are presumed to be constant. If the value of k is also presumed to be constant, then from integration of Eqs. 2 and 3, using Eq. 4 to determine the constants of integration, the profiles of Y_F and T can be expressed as

$$Y_F = 1 - (1 - Y_{F,\infty}) \exp\left(-\frac{\dot{m} c_p L_F}{4 \pi k r}\right), \tag{6}$$

and

$$T = T_s - \frac{q_g}{c_p \dot{m}} + \left(T_\infty - T_s + \frac{q_g}{c_p \dot{m}}\right) \exp\left(-\frac{\dot{m} c_p}{4 \pi k r}\right) \tag{7}$$

Introducing the definition,

$$\lambda = \left(\frac{\dot{m} c_p}{4 \pi k r}\right)_{r=a}, \tag{8}$$

from Eqs. 5 and 7 it follows that

$$\frac{4 \pi a k \lambda (T_\infty - T_s)}{\exp(\lambda) - 1} = \frac{4 \pi a k L_v \lambda}{c_p} + \frac{4}{3} \pi a^3 \rho_s c_s \frac{dT_s}{dT}. \tag{9}$$

The term on the left side of Eq. 9 denotes the rate of heat transfer from the gas to the fuel-particle, with the effective Nusselt's number denoted by $\lambda/[\exp(\lambda) - 1]$. The first term following the equality sign on the right side of Eq. 9 denotes the latent heat required to vaporize the fuel-particle, and the second term denotes the sensible heat required to raise the temperature of the fuel-particle. It follows from Eqs. 1, and 8 that

$$\lambda = \frac{a c_p}{k} A \exp\left(-\frac{T_{av}}{T_s}\right). \tag{10}$$

Let T_v denote a characteristic value of the temperature of the fuel-particle for which the value of λ evaluated from Eq. 10 is of order unity. For $T_s < T_v$, the vaporization rate and consequently the value of λ, is exponentially small. In the limit of small values of λ, $\lambda/[\exp(\lambda) - 1] = 1$. Hence the first term on the right side of Eq. 9 can be neglected in calculating the value of T_s. For $T_s = T_v$, λ is of order unity. If the value of T_s is allowed to increase beyond T_v, then the value of λ would become exponentially large and the term on the left side of Eq. 9 would become exponentially small, consequently the rate of heat transfer from the gas-phase to the solid, will be small. Therefore, for values of T_s beyond T_v, the value of the derivative dT_s/dt will be negligibly small, so that the value of λ remains of order unity. For simplicity, it is presumed that $\dot{m} = 0$

for $T_s < T_v$ and the value of T_s does not increase after it attains the value T_v.

The governing equations for the structure of the flame can be written as,

$$V = \rho_u u_u + \frac{4}{3}\pi \rho_s n_u u_u \left(a_u^3 - a^3\right), \tag{11}$$

$$\frac{d(V Y_F)}{dx} - \frac{k_u}{c_p L_F}\frac{d^2 Y_F}{dx^2} = \frac{n_u \rho_u u_u}{V}\dot{m} - w_F \frac{\rho_u}{\rho}, \tag{12}$$

$$\frac{d(V Y_{O_2})}{dx} - \frac{k_u}{c_p L_{O_2}}\frac{d^2 Y_{O_2}}{dx^2} = - w_{O_2}\frac{\rho_u}{\rho}, \tag{13}$$

$$\frac{d(V c_p T)}{dx} - k_u \frac{d^2 T}{dx^2} = \frac{n_u \rho_u u_u}{V} q_p + Q_R w_F \frac{\rho_u}{\rho}. \tag{14}$$

Here the subscript u denotes conditions in the ambient reactant stream. The subscript ∞ has been dropped from the quantities Y_F, Y_{O2} and T appearing in Eqs. 12-14. The quantities w_F and w_{O2} denote the rate of consumption of gaseous fuel and oxygen per unit volume, and Q_R is the heat released per unit mass of gaseous fuel consumed. The independent variable x is related to the spatial coordinate x' as,

$$x = \int_0^{x'} \left(\frac{\rho}{\rho_u}\right) dx'. \tag{15}$$

In the regions where $T_s < T_v$, the vaporization rates are assumed to be negligibly small hence the radius of the fuel-particle does not change and its temperature T_s and the quantity q_p can be calculated from the relations,

$$a_u^2 \frac{\rho_s c_s V}{\rho_u}\frac{dT_s}{dx} = \frac{3 k_u}{2 T_u}\left(T^2 - T_s^2\right), \tag{16}$$

and

$$q_p = - \frac{4}{3}\pi a_u^3 \rho_s c_s \frac{V}{\rho_u}\frac{dT_s}{dx}. \tag{17}$$

When the value of the temperature of the fuel-particle reaches T_v, they begin to vaporize and the increase in their temperature is negligibly small. The radius of the fuel-particle and the quantity q_p can be calculated from the expressions,

$$a\frac{da}{dx} = - \frac{k_u \rho_u}{T_u c_p \rho_s V}\left[T - T_v + \left(T_v - \frac{L_v}{c_p}\right)\ln\left(1 + \frac{c_p(T - T_v)}{L_v}\right)\right], \tag{18}$$

and,

$$q_p = \dot{m}\left(c_p - L_v\right), \dot{m} = - \rho_s \frac{4}{3}\pi \frac{V}{\rho_u}\frac{d(a^3)}{dx}. \tag{19}$$

In deducing the system of equations 12-19 the product ρk was presumed to be a constant. The chemical reaction between the gaseous fuel and the oxidizer is presumed to occur by a one-step process. The system of equations 12-19 were solved numerically.

3. Results

For purpose of illustration calculations were performed assuming that the gaseous fuel that evolves from the fuel-particle is methane. The chemical kinetic rate parameters characterizing the gas-phase oxidation were chosen such that the burning velocity for stoichiometric mixture of gaseous methane and air is 37 cm/s. The values of some of the parameters used in the calculations are k_u = 0.00035 cal/(cm s K), ρ_u = 0.001135 g/cm^3, ρ_s = 1.0 g/cm^3, T_u = 300 K, T_v = 600 K, L_v/Q_R = 0.01. Results of some of these calculations for values of a_u equal to 0.0007 cm, 0.0010 cm, and 0.0015 cm are shown in Figs. 1 and 2. Figure 1 shows the the burning velocity u_u, as a function of the equivalence ratio ϕ_u, calculated based on the gaseous fuel available in the fuel-particles. Figure 1 shows that steady flame propagation is possible in fuel-rich combustible mixtures. In Fig. 2 the structure of the flame is plotted at a value of ϕ_u = 1.89 and a_u = 0.0010 cm. The various non-dimensional quantities appearing in this figure are defined as,

$$z = \frac{\rho_u u_u c_p}{k_u} x, \quad \theta = \frac{T - T_u}{T_b - T_u}, \quad \theta_s = \frac{T_s - T_u}{T_b - T_u},$$
$$\alpha = \frac{a}{a_u}, \quad y_F = \frac{4 Y_F}{Y_{O_2 u}}, \quad y_{O_2} = \frac{Y_{O_2}}{Y_{O_2 u}}. \tag{20}$$

where T_b is the adiabatic flame temperature. Interpretations of results similar to those shown in Fig. 1 and 2 are currently in progress.

4. Future Research.

Future research is directed toward performing numerical calculations using the system of equations 12-18 over a wide parametric range. Asymptotic description of the flame structure will also be attempted.

5. References.

1). Seshadri, K., Berlad, A. L., and Tangirala, V., *The Structure of Particle-Cloud Flames*, Combustion and Flame **89**: 333-342 (1992)

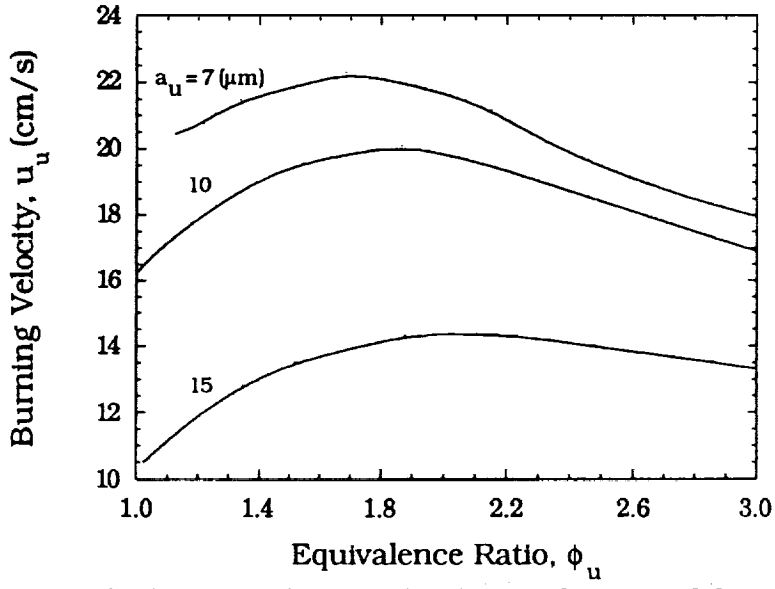

Figure 1. The burning velocity u_u (cm/s) as a function of the equivalence ratio ϕ_u, for various values for the initial radius of the fuel-partical a_u.

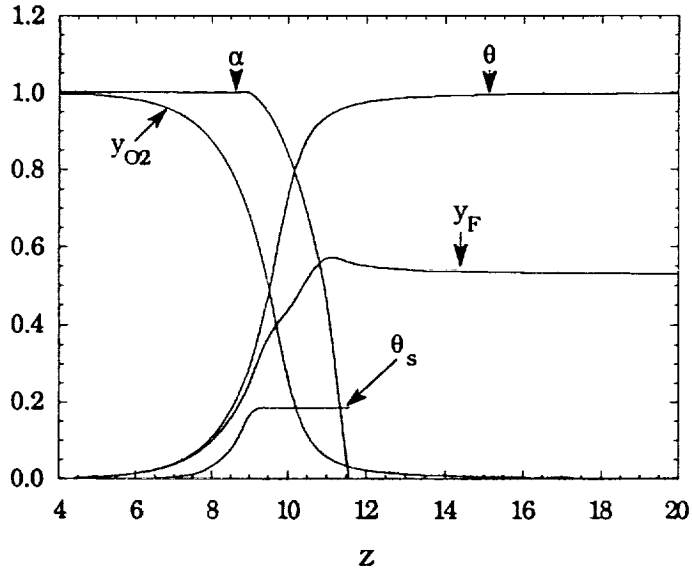

Figure 2. The structure of the flame for ϕ_u = 1.89 and a_u = 0.0010 cm.

COMBUSTION SYNTHESIS OF CERAMIC AND METAL-MATRIX COMPOSITES

N93-20203

John J. Moore, Heng J. Feng, and Kevin J. Hunter
Department of Metallurgical and Materials Engineering
Colorado School of Mines
Golden, Colorado 80401

and

David G. Wirth
Coors Ceramics Company
Golden, Colorado 80401

Introduction

Combustion synthesis or self-propagating high temperature synthesis (SHS) is effected by heating a reactant mixture, to above the ignition temperature (Tig) whereupon an exothermic reaction is initiated which produces a maximum or combustion temperature, Tc. These SHS reactions are being used to produce ceramics, intermetallics, and composite materials.[1] One of the major limitations of this process is that relatively high levels of porosity, e.g., 50%, remain in the product. Conducting these SHS reactions under adiabatic conditions, the maximum temperature is the adiabatic temperature, Tad, and ΔH (Tad) = 0, Tad = Tc. If the reactants or products go through a phase change, the latent heat of transformation needs to be taken into account,

$$\text{i.e. } \Delta H(Tad) = \Delta H(To) + \int_{To}^{Ttrans} CpdT \pm \Delta H(trans) + \int_{Ttrans}^{Tad} Cpdt = 0 \quad (6)$$

where To is the initial or starting temperature, eg. 298 K. Ttrans is the phase transition point of a reactant -ΔH(trans) or a product +ΔH(trans) and ΔH(trans) is the corresponding heat of transformation. Tad can be determined from equation (6) or graphically as indicated in Figure 1.

Experimental Reaction Systems

Several model composite systems have been investigated in which an excess amount of Al is used both as a reductant in the reaction and as the metal component of the ceramic-metal composite.[3-6]

ie.

$$3TiO_2 + 3C + (4+x)Al = 3TiC + 2Al_2O_3 + xAl \quad (1)$$
where x was varied between 0 to 9.[2]

$$3TiO_2 + 3B_2O_3 + (10+x)Al = 3TiB_2 + 5Al_2O_3 + xAl \quad (2)$$
where x was varied between 0 to 17.[3]

$$3ZrO_2 + 3B_2O_3 + (10+x)Al = 3ZrB_2 + 5Al_2O_3 + xAl \quad (3)$$
where x was varied between 0 and 13.[4]

$$2B_2O_3 + C + (4+x)Al = B_4C + 2Al_2O_3 + xAl \quad (4)$$
where x was varied between 0 and 3.[5]

The excess amount of liquid Al, created by the combustion synthesis reaction, is allowed to simultaneously infiltrate the pores produced in the ceramic composite thereby taking advantage of this major limitation in the SHS process, and hence improve the relative density of the composite produced. Incorporating a ductile metal into a brittle ceramic composite matrix has considerable potential for substantial improvements in fracture toughness. A variation of reaction (1) is given in reaction (5) in which the excess Al is used to reduce TiO_2 and generate an excess amount of Ti.[6]

$$(3 + x)TiO_2 + 3C + (4 + 4/3x)Al = 3TiC + (2 + 2/3x)Al_2O_5 + xTi \quad (5)$$

The enthalpy-temperature plots for these five reaction systems have been examined and that for reaction (1) is given in Figure 1 in which Xr and Xp refer to the respective reactant and product H-T plots associated with the corresponding excess amount of aluminum used in the reaction. The corresponding melting and boiling points of reactants and products are indicated in Figure 1 and Table I.

Experimental Procedure

The reactant powders (Table 1) were thoroughly mixed using porcelain ball milling for a minimum of six hours, and pressed to various green densities with varying values of x, into cylindrical compacts of 0.5 inches (12.7mm) in diameter and 1 inch (25.4mm) in length. These pellets were dried for 1 hour at 110°C in an oven and were subsequently ignited in the propagating mode using a heated tungsten wire in an argon atmosphere as described in an earlier publication.[2] The ignition temperatures, Tig, were determined using a Pt-Pt/10%Rh thermocouple and the combustion temperatures, Tc, were determined using an Ircon Mirage Two Wavelength Infrared Pyrometer. A video camera was used to record the propagation of the combustion front. In this way, it was possible to assess the stability of the combustion wave and also its rate of propagation. The ceramic-metal composites produced were examined using optical and scanning electron microscopy (SEM) interfaced with an energy dispersive spectroscopy (EDS) facility and also by x-ray diffraction (XRD). The density of the products was determined using an immersion in water technique.

Results and Discussion

A maximum of 75% theoretical density could be achieved in the composites produced in reactions (1), (2) and (3) while an expanded or foamed ceramic-metal composite was produced in reaction (4). Reaction (3) also produced a large volume of Al_2O_3 whiskers while reaction (2) produced a small amount of Al_2O_3 whiskers present in the pores of the composite. SHS reaction stability diagrams were constructed for each of the reactions (1)-(5) as shown in Figure 2-5. A stable combustion front was observed for each level of excess Al used in reaction (4), i.e. x = 0, 1, 2 and 3. Increasing excess Al and green density eventually resulted in decreased stability of the combustion front and possible quenching out. This is almost certainly the result of increased heat losses from the SHS reaction on account of increased thermal conductivity (increased green density) and latent heat of fusion (increased excess Al). There is a slight increase in thermal conductivity of the green pellet on increasing the excess amount of Al or Ti and increasing the green density.[2-6] This increased thermal conductivity could have two opposing effects: (i) the heat from the reaction front is more efficiently transferred to the reactants ahead of the reaction front and (ii) the heat lost from the reactants ahead of the reaction front is increased. Even though the velocity of the reaction front is considered to be high [typically 0.2cm s^{-1} for reaction (1),[2] and (5)[6] and 2cm s^{-1} for reaction (2),[3] 7cm s^{-1} for reaction (3)[4] and 5cm s^{-1} for reaction (4)],[5] it is more likely that (ii) will prevail in the small reactant pellet systems used. In each reaction system studied, except reaction (4), the aluminum becomes liquid (melting point 660°C) before the ignition temperature is reached, ie. Tig for reaction (1) >900°C,[3] for reaction (2) >850°C,[4] for reaction (3) >900°C,[5] for reaction (4) >600°C.[6] for reaction (5) of >950°C. The typical values of Tc achieved in each system were 1600-2000°C for reaction (1),[2] 1550-2300°C for reaction (2),[3] 2000-2400°C for reaction (3),[4] 1850-2050°C for reaction (4),[5] and 2000-2300° for reaction (5).[6]

Reaction systems (1), (2) and (5) produced considerable increases in product density with increased excess Al as expected, eg. from 45% (x = 0) to 75% (x = 9) relative densities. However, unlike reaction (1), the maximum density in the ceramic-metal product for reactions (2) and (3) were obtained at low to intermediate green densities, while reaction (4) expanded 400% in length producing a maximum density of 35%. This is most likely due to the high volatility of B_2O_3 used in these reactions. The calculated vapor pressures of the reactant and product species in reactions (1) to (5) (presented in Figure 3) indicate that the combustion temperatures produced in reaction (3) resulted in considerable volumes of both B_2O_3 and Al gases which resulted in Al_2O_3 whisker formation from a vapor-liquid-solid mode of synthesis (Figure 4). Al_2O_3 whiskers were also produced in pores in the TiB_2-Al_2O_3-Al composite produced by reaction (2). However, these whiskers were far less numerous than those produced by reaction (3). Since the Tc achieved in reaction (2) produces a high vapor pressure (eg. >1 at) of B_2O_3 vapor and only a moderate vapor pressure of Al gas (ie. from 10^{-5} to 10^{-1} at). Both these reaction systems (2) and (3) resulted in improved product densities with excess Al provided that lower green densities were maintained, i.e., using a compaction pressure of 1.6 x 10^7 kg/m^2 or below. The lower Tc value in reaction (4) would result in a low vapor pressure of Al ie. typically 10^{-3} to 10^{-2} at., but the large vapor pressure of B_2O_3 produced by this Tc (ie. >1 at) and the larger reaction mass of B_2O_3 in reaction (4) compared with those in reactions (2) and (3) has resulted in a large volume of B_2O_3 at 1 atmosphere pressure or higher. This high pressure, high volume B_2O_3 gas is able to push or expand the reactant materials ahead of the combustion

front in the vertical direction, thereby producing an expanded or foamed ceramic-metal composite which exhibited ≥65% uniform porosity (Figure 5) and an expansion of up to 400%. The more readily predicted behavior of product densities in reactions (1) and (5), ie. increased product densities with increased green density and excess Al, is readily explained in the absence of any major volatile species. However, reaction (5) was able to produce a semi stable combustion front up to at least a value of x = 50 due to the fact that the exothermicity of reaction (5) increases with xTi. The effect of density-driven fluid flow of liquid Al was also evident in these products (Figure 6).

Conclusions

Although reaction systems (1) to (5) use the same concept of synthesizing ceramic-metal composites, the different physical properties of the reactants and products, eg melting and boiling points, thermal conductivity, and combustion temperatures achieved in each system result in different product formations, morphologies, microstructures and relative densities. The presence and extent of liquid and gaseous species appear to have a significant influence over these product microstructures and densities. Incorporating an excess amount of metal within the combustion synthesis reaction in which no significant gaseous phases are generated increased the composite relative density from 45% to 75% without the application of pressure. The prospect of synthesizing reinforcing whiskers in-situ from gaseous species generated within the combustion synthesis reaction to produce a ceramic-metal composite without the problem of handling these hazardous materials is extremely attractive. The concept of producing stability diagrams has been introduced for these ceramic-metal combustion synthesis reactions that indicate how the process parameters can produce stable propagating reaction fronts. Also the effect of green density and excess Al on the composite product density is dependent on the character and extent of the liquid and gaseous species present at the reaction front. The concept of producing expanded or foamed ceramic and ceramic-metal composites by utilizing a high volume of a volatile specie at the reaction front has been introduced. These materials could find considerable applications varying from catalyst support systems to filters to ultra light weight structural materials. The effect of gravity on density driven fluid flow and vapor transport is likely to be significant in producing tough, dense ceramic-metal composites with uniform microstructures and properties.

Acknowledgements

The authors are grateful for partial support of this work from NASA, through the Microgravity Science Division - Code SN.

References

1. Z. A. Munir, Ceramic Bulletin, 67(2) (1988) 342.
2. H.J. Feng, J.J. Moore, D.G. Wirth, "The Combustion Synthesis of Ceramic-Metal Composites: The TiC-Al_2O_3-Al System", accepted for publication in Met. Trans.
3. H.J. Feng, J.J. Moore, D.G. Wirth, "Combustion Synthesis of TiB_2-Al_2O_3-Al Composite Materials" published in proceedings of Symposium on Developments in Ceramic and Metal Matrix Composites, TMS Annual Meeting, San Diego, March 1-5, 1992. Pub by TMS, pp 219-239.
4. H.J. Feng, J.J. Moore, D.G. Wirth, "Combustion Synthesis of Ceramic Metal Composite Materials: The ZrB_2-A_2O_5-Al System" to be published in proceedings of the International Symposium on Self-Propagating High Temperature Synthesis (SHS), Alma-Ata, USSR, Sept 23-28, 1991; pub by Soviet Academy of Sciences.
5. H.J. Feng, J.J. Moore, D.G. Wirth, "The Combustion Synthesis of B_4C-Al_2O_3-Al Composite Materials" to be published in proceedings of Symposium on Synthesis and Processing of Ceramics: Scientific Issues, MRS Fall Meeting, Boston Dec 2-6 1991; pub by MRS.
6. K. J. Hunter, J. J. Moore, D. G. Wirth, Proceedings of 6th International Titanium conference, San Diego, CA, June 28- Aug. 2, 1992, pub. by TMS.

Table I. Physical Properties of Reactants and Products in Reactions (1)-(5)

Material	TiO_2	C	Al	TiC	Al_2O	B_2O_3	TiB_2	ZrO_2	ZrB_2	B_4C	Ti
Mpt°C	1830		660	3140	2050	450	2900	2715	3000	2450	1660
Bpt°C	3000		2467	4820	2980	1860		5000		3500	3287
SG*	4.26	2.25	2.70	4.93	3.97	2.46	4.50	5.60	6.09	2.52	4.54
Size (μm)	-44	-44	-44			-75		-44			

*Specific Gravity

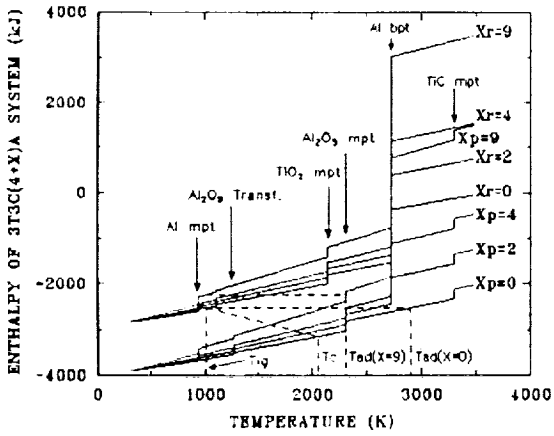

Figure 1 Enthalpy-temperature plots for reactants (Xr) and products (Xp) for various amounts of excess Al for Reaction (1)

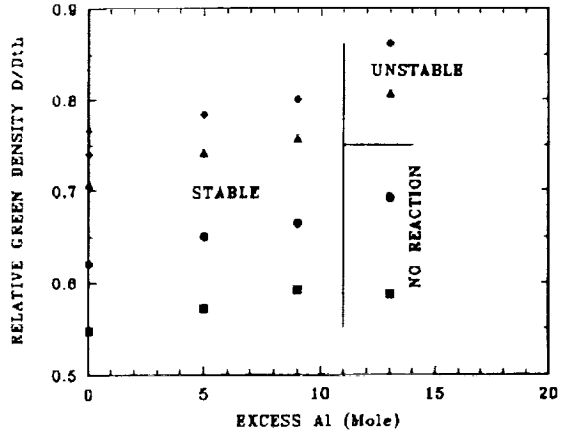

Figure 2 Effect of excess Al and relative green density on the stability of the propagating combustion wave for Reaction (1).

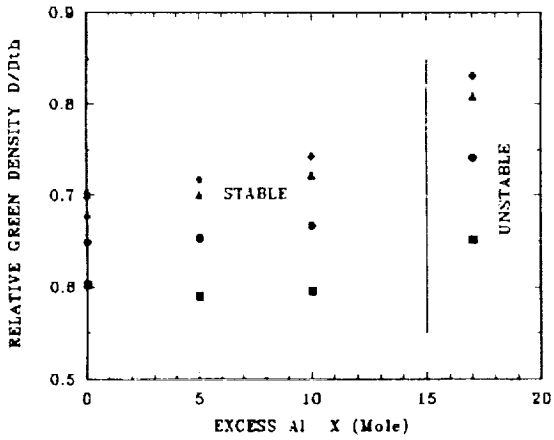

Figure 3 Effect of excess Al and relative green density on the stability of the porpagating combustion wave for Reaction (2).

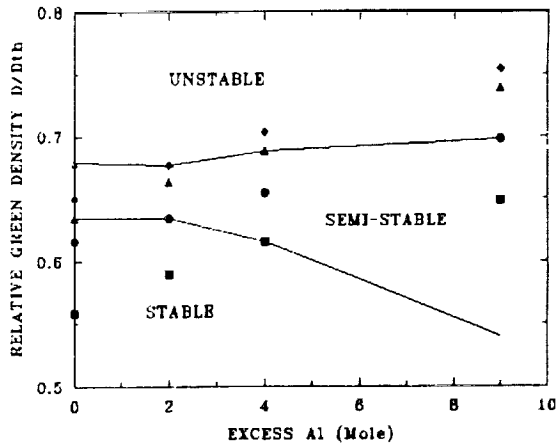

Figure 4 Effect of excess Al and relative green density on the stability of the propagating combustion wave for Reaction (3).

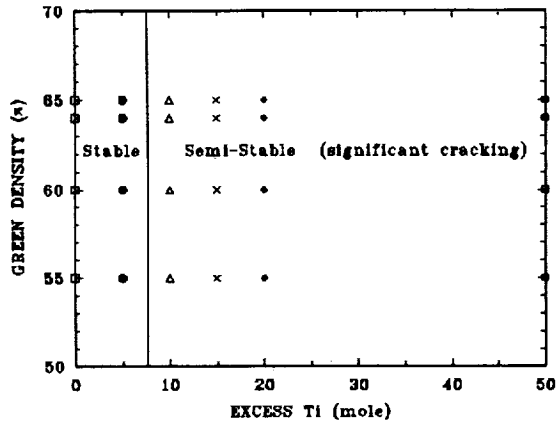

Figure 5 Effect of excess Ti and relative green density on the stability of the propagating combustion wave for Reaction (5).

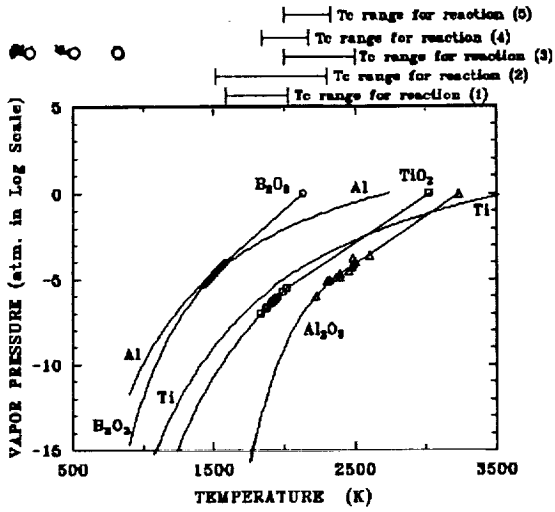

Figure 6 The effect of temperature on the calculated vapor pressues of species present in Reaction (1) to (4).

Figure 7 Al_2O_3 whisker formation during Reaction (3).

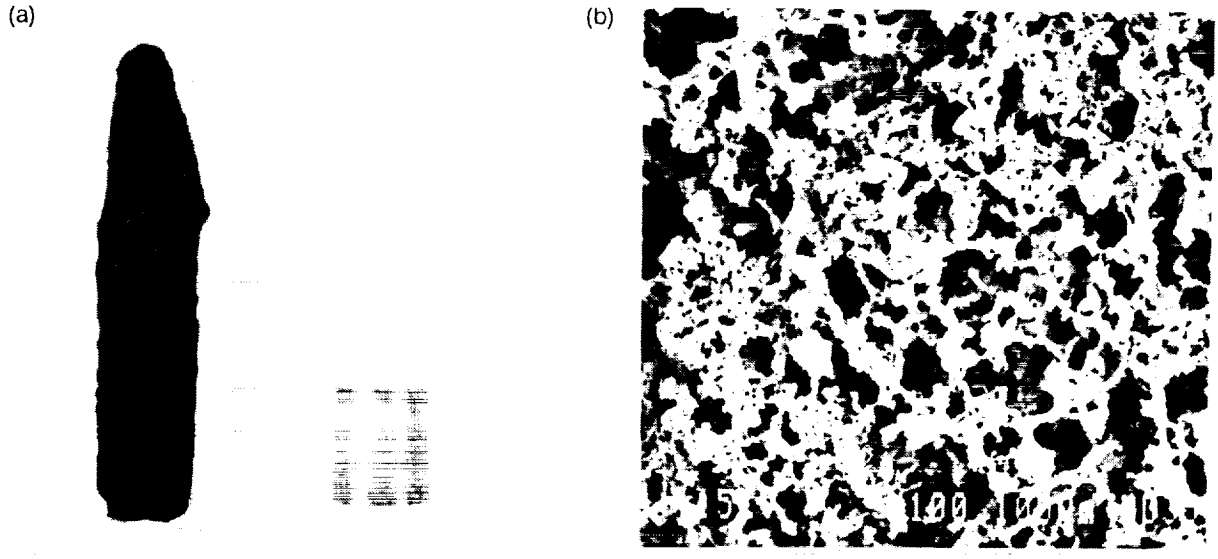

Figure 8 (a) Expanded or foamed ceramic and ceramic-metal composites produced by reaction (4) comparison of reacter (left) with unreacted (right) green pellet; (b) scanning electron photomicrograph of (a) for x = 0.

Figure 9 Optical photomicrograph of TiC-Al_2O_3-9Al composite, indicating gravity-driven fluid flow of the liquid Al to the bottom half of the coposite.

COMMENTS

Question (Prof. Bernard J. Matkowsky, Northwestern University): You referred to experiments in the former Soviet Union, in which the sample produced by S.H.S. is significantly expanded (i.e., its porosity is significantly increased). I presume you are referring to the experiments of A. Shteinberg. First, in his experiments the increase in porosity was due to gas being liberated, rather than consumed, in the reaction. Was this true in your experiments as well? Second, he observed that the degree of increase in porosity was different if the sample was arranged (1) horizontally or (2) vertically in normal gravity, and (3) in microgravity. I understand that you have not yet done the experiments in microgravity, but did you observe similar differences between horizontal and vertical arrangements in normal gravity.

Finally, you described the propagation of the combustion wave as being either (1) stable, by which you mean that it propagated with a planar front with a constant velocity, or (2) unstable, by which you mean that propagation ceased. However, in addition to the stable mode of propagation, there have been observations of pulsating propagation, in which a planar front propagates with an oscillatory velocity, and spinning propagation, in which a hot spot (or spots) moves in a helical fashion. Did you observe either of these modes of propagation?

Answer: The increase in porosity was due to gaseous species both liberated and consumed. For example, in combustion synthesis reactions involving B_2O_3, which has a boiling point slightly in excess of 1800 degrees C, the combustion temperature was well above this point, and, therefore, generated B_2O_3 gas of 1 atmosphere pressure. At the same time, the B_2O_3 gas was also consumed in the reaction to produce compounds such as TiB_2 with $TiBO_2$ reactant or B_4C with graphite as the reactant. In certain combustion synthesis reactions that we studied, the combustion temperature was sufficient to produce a significant volatility (i.e., partial pressure of aluminum gas). In this respect, the aluminum gas and the B_2O_3 gas reacted to produce Al_2O_3 whiskers. In our experiments, the very large levels of porosity (e.g., greater than or equal to 75%) were produced when there was only one major gaseous species produced (i.e., B_2O_3 gas).

Yes, I was referring to Professor Alex Shteinberg's work in Russia. Most of our experiments were conducted in which the pellet was ignited at the bottom of the cylindrical pellet and the major expansion occurred in the vertical direction against gravity.

We defined a stable combustion front as one which propagated a steady rate down through the pellet, wherein an unstable combustion front was one which eventually quenched out. Our definition of a semi-stable combustion front was one that slowed down, almost extinguished, and then picked up speed again, probably going through two or three of these cycles. In one or two occasions we did observe a spinning mode of propagation, which we defined as semi-stable front.

SESSION E - PLENARY DINNER

(Chair, Robert Rhome)

FIRE SAFETY PRACTICES IN THE SHUTTLE AND THE SPACE STATION FREEDOM

N93-20204

Robert Friedman
NASA Lewis Research Center
Cleveland, Ohio 44135

ABSTRACT

The Shuttle reinforces its policy of fire-preventive measures with onboard smoke detectors and Halon 1301 fire extinguishers. The forthcoming Space Station *Freedom* will have expanded fire protection with photoelectric smoke detectors, radiation flame detectors, and both fixed and portable carbon dioxide fire extinguishers. Many design and operational issues remain to be resolved for *Freedom*. In particular, the fire-suppression designs must consider the problems of gas leakage in toxic concentrations, alternative systems for single-failure redundancy, and commonality with the corresponding systems of the *Freedom* international partners. While physical and engineering requirements remain the primary driving forces for spacecraft fire-safety technology, there are, nevertheless, needs and opportunities for the application of microgravity combustion knowledge to improve and optimize the fire-protective systems.

INTRODUCTION

Fire safety in spacecraft has been cited as one practical motivation for advancing microgravity combustion research (ref. 1). Current spacecraft fire protection, however, is based largely on established fire-safety practices used in enclosed compartments, such as aircraft (ref. 2). The application of fundamental, quantitative information from microgravity combustion research could promote greater efficiency in the design and operation of protective systems, lessen restrictions on the use of materials and operations in space-based hardware, and reduce excessive safety factors and false alarms. Certainly, the advent of the complex, permanently orbiting Space Station *Freedom* offers an opportunity for novel and improved spacecraft fire-safety techniques derived from a thorough understanding of fire behavior in low gravity (ref. 3).

This paper is thus a review to acquaint the microgravity combustion research community with current and proposed fire-safety practices and critical issues for U.S. human-crew spacecraft and to suggest relevant fields where microgravity combustion research may promote spacecraft fire safety.

HAZARD ANALYSES FOR SPACECRAFT

General Strategies

The major emphasis in spacecraft fire safety is on fire prevention through control, if not elimination, of one of the three elements necessary for fire, *i. e.*, fuel, ignition, and oxygen (ref. 4). For the first element, the control is based on a policy of qualifying acceptable materials for spacecraft use through tests of the resistance to upward (in normal-gravity) flame spread following exposure to promoted ignition. Of course, many necessary spacecraft items fail this test (including articles made from paper and fabrics). Usage of these materials is permitted in limited quantities under prescribed conditions of fire-safe storage. For the second element, control of ignition is through standard practices of electrical grounding, circuit breakers, pressure containment, and the like. There is no control of the third element, oxygen. The Shuttle atmosphere is sea-level air, which is enriched to 30% oxygen at a reduced total pressure of 72 kPa for prebreathing prior to an extravehicular activity. The use of fire-resistant, reduced-oxygen atmospheres for human support in submarines and other enclosed

habitats has been investigated (ref. 5). For the Shuttle and the initial phases of the Space Station *Freedom*, however, design and operational considerations eliminate the consideration of other than conventional atmospheres (ref. 4).

Fire Scenarios

Absolute fire prevention is impossible and perhaps not even desirable if possible. Spacecraft fire safety must address the tradeoff of minimum risk against operational practicality, where a minimum, residual risk level can be defined as the consequences of a worst-case fire that causing possible component damage that can suspend some operations temporarily but no human injuries (ref. 6). For the Shuttle, plausible fire-initiating scenarios are electrical breakdowns (shorts, overloads, and arc tracking) or electromechanical overheating (motors, rotating equipment, heaters). For *Freedom*, potential fire-causing scenarios are more numerous. W. Fuller and M. Halverson (cited in ref. 7) conducted a qualitative risk assessment for the station with initiating fire scenarios covering electrical shorts, faults in electrolysis units, oxygen leaks, chemical reactions, faulty experiments, or improper crew or ground actions.

A complete strategy of fire protection in spacecraft thus proceeds from the assumption that fires or their precursors will have a finite probability of occurrence. Onboard fire safety in current and proposed spacecraft must then concentrate on fire detection, suppression, and post-fire restoration. The description and evaluation of these fire-responsive techniques are the primary scope of this review.

BRIEF HISTORY OF U.S. SPACECRAFT FIRE SAFETY

The atmosphere in the early spacecraft, Mercury, Gemini, and Apollo, was 100% oxygen, an atmosphere in which no common organic material can truly resist fire spread. This failing was emphasized by the disastrous Apollo 204 fire in 1967, occurring during ground testing at sea-level total pressure. The investigation of the Apollo fire led to the development of new plastic materials, the adaptation of the present flammability-assessment methods, and the use of a diluted oxygen atmosphere for ground operations.

The development of fire-responsive techniques in spacecraft has been slower than that of fire-prevention measures (ref. 2). In the simple configurations of Mercury, Gemini, and Apollo, the crew members could observe the complete interior of the pressurized modules. Hence, the senses of the human crew were adequate to detect the initiation of a fire. The water gun for food reconstitution was designated for use as an emergency fire extinguisher. The Apollo spacecraft system added dedicated foam-agent fire extinguishers. It was not until the introduction of the first U.S. space station, Skylab in 1973 to 1974, however, that instrumented fire detection was incorporated in a spacecraft. The Skylab system used 30 line-of-sight ultraviolet flame detectors, placed throughout the station.

The Skylab space station also provided the environment for a pioneering test of low-gravity flammability, until recently the only quantitative study of fire behavior under low gravity. The Skylab study was an observation of the time-dependent flame front in the combustion of practical materials, including aluminized Mylar, Nylon, neoprene-coated Nylon, polyurethane foam, and paper. The materials were ignited in the Skylab atmosphere of 65% oxygen in nitrogen at 36 kPa total pressure. The flame-spread rate was calculated from comparisons of the flame-front position on successive motion-picture frames. Kimzey (ref. 9 and Appendix C of ref. 10) discussed the Skylab low-gravity and corresponding normal-gravity results and made the following key observations:

- Flame-spread rates are always lower in microgravity, with comparative rates ranging from .15 to .60 those in normal gravity.
- The visibility of a flame is significantly reduced in microgravity.

- Extinguishment by vacuum is effective, and the flame is extinguished when the available oxygen decreases sufficiently. A significant side effect is the flame intensification that develops during the initial phase of venting.
- Extinguishment by water is possible provided the application is controlled and adequate. If insufficient water strikes a burning material, it always causes a flareup that can scatter burning material.

The Skylab conclusions established the safety factor underlying the use of NASA normal-gravity flammability test assessments. That is, the material-acceptance criterion assumes that any item passing an upward-spreading normal-gravity test would be no more "flammable" in low gravity.

Recently, Pogue, one of the Skylab crew members, summarized his conclusions based on first-hand observations of the flammability study (ref. 11). Pogue also noted that flame-spread rates always are lower in low gravity than under corresponding normal gravity. However, he warned of some qualifications to be considered in interpreting the low-gravity flame-spread data for fire-prevention, detection, and extinguishment applications:

- Porous materials may capture oxygen within items to enhance microgravity flammability.
- Local agitation or displacement of air may occur from the thermomechanical response of burning materials.
- Local air flow may be induced by the usual cabin ventilation and air circulation systems.
- Local air flow may be induced by fire extinguishing.

FIRE PROTECTION FOR THE SHUTTLE

The early U.S. human-crew spacecraft were designed to meet specific mission objectives. The Shuttle, on the other hand, is a component of a complete Space Transportation System (STS). As originally conceived, the STS was to become the sole system for launching, maintaining, and retrieving orbiting satellites and space probes. For practical and economic reasons, the inclusion of all space activities into the human-crew STS has not occurred. Currently, world-wide launch operations use non-crewed expendable launch vehicles (ELV), and the U.S. retains a mix of the STS and ELV space transportation.

Fire Detection and Suppression Subsystem

The Shuttle normally has a pressurized atmosphere only in the front cabin, and the fuselage payload bay is exposed to the vacuum of space. For the increasing number of Shuttle missions dedicated to microgravity research, such as USML-1, the "payload" is the laboratory connected to the cabin by an air lock and tunnel. The pressurized laboratory shares its life-support system with the Shuttle cabin.

Fire protection for the Shuttle cabin and any pressurized laboratory is provided through a Fire Detection and Suppression Subsystem, which is a component of the Shuttle Environmental Control and Life Support System (ECLSS). The Shuttle cabin and its pressurized laboratories use ionization-type smoke detectors. Two units are located in each of three electronics bays for redundancy (a single-fault tolerant system). The smoke detectors are identical in principle to ionization detectors in common use in buildings and aircraft, although they have particular adaptations for spacecraft use (ref. 12). An integral fan creates a flow across entrance port to the ionization chamber to bypass larger, high-momentum particles, assumed to be dust, not smoke. The fan flow also insures adequate sampling in the absence of natural convection. Unfortunately, the bypass system may reject larger smoke agglomerates, possibly characteristic of a microgravity fire, reducing the detector sensitivity. The set points, determined by normal-gravity smoke-chamber calibrations, are established at very sensitive levels, however, well below those associated with visible smoke.

Fig. 1 shows the flight deck fire-protection panel, which has indicators for smoke-detector alarm status and actuators for the fixed fire extinguishers installed in the Shuttle cabin and in its payload-bay laboratory. These extinguishers, as well as additional portable extinguishers, are charged with Halon 1301 (bromotrifluoromethane). The manufacture and commercial use of Halon 1301, which is recognized as having a potential to deplete ozone in the stratosphere, is to be eliminated by international protocol in the next decade. There are no immediate plans for replacement of the Halon 1301 agent on the Shuttle. While Halon 1301 is a very effective agent for many fires, it can generate halogen acid gases, which are toxic and corrosive. Shuttle mission rules call for an immediate termination of the mission and return to Earth following discharge of a fire extinguisher.

Shuttle Mission Experience

Several minor incidents with fire-causing potential have occurred on Shuttle missions (ref. 13). On two reported occasions, the crew detected a smoke odor, and subsequent examination showed overheated components. In the first incident, on STS-6, April 1983, an odor was caused by the fusing of overheated wires near a space-processing unit. No degradation products were found in an atmospheric sampling; presumably, the carbon filter in the Shuttle ECLSS was effective in removing the trace compounds contributing to the odor. In the second incident, on STS-35, December 1990, the crew reported a smoke odor and a one-ampere current surge, before the failure of an overheated resistor in an elapsed-time circuit of a digital display unit shut off power to the unit. No atmospheric changes were otherwise noted. Recently, the STS-50 crew (July 1992) reported an odor and the failure of a medical apparatus, which was later traced to a blown electrical capacitor.

An incident of potentially greater consequence occurred on STS-28, August 1989, when a cable strain and insulation failure caused an electrical short circuit at a teleprinter unit. The crew observed sparks and 4 or 5 glowing embers during a period of about one to two seconds at the vicinity of the cable. One of the smoke detectors showed an increased particle-concentration level of 158 $\mu g/m^3$ for about 60 sec, with a momentary peak at 180 $\mu g/m^3$, levels well below the alarm set point of 2000 $\mu g/m^3$. Based on the observed mass of pyrolyzed material released from the burned wire insulation, calculations showed that the air-borne particle concentration could have exceeded the set-point concentration (C. Asuncion and B. Harkness, Rockwell International, internal letter, October 1990). Several reasons for the low observed smoke-concentration level reading were suggested:

- Some pyrolyzed mass was in particles larger than 50 μm (as observed by the crew) that bypassed the detector chamber.
- Some mass was in particles adsorbed on surfaces.
- Some mass was produced as gases rather than as aerosols.

The Shuttle mission experience confirms that breakdowns threatening incipient fires have finite probabilities. At the same time, the fire-protective systems and the alertness of the crew have been shown to be effective in recognizing and responding to these minor incidents.

FIRE PROTECTION FOR THE SPACE STATION *FREEDOM*

The proposed Space Station *Freedom* will not be the first permanently inhabited satellite system of this kind. *Freedom*, however, represents the first completely original approach to this space community, rather than a derivative assemblage with adapted components from earlier missions. *Freedom* will provide greatly expanded accommodations for life science studies, microgravity science and technology, earth observations, space probe launching, and satellite servicing. Obviously, potential hazard situations and consequent fire-protection demands will increase considerably over the proposed 30 years of continuous operations, compared to those for the short-duration missions of the Shuttle.

Preliminary Assembly and Atmospheres

Eventually, the Space Station *Freedom* assembly will evolve into a complex truss, module, and attachment assembly, the configuration usually publicized. The immediate concern of fire safety, however, is in the protection of the Man-Tended Configuration (MTC). The MTC is the minimum assembly of components necessary to sustain human activities within the station, a state anticipated to be completed in about six Shuttle-tended assembly operations, perhaps a year or so after the date of the first element launch (fig. 2). The working volume of the MTC consists of three pressurized modules: a laboratory, resource node, and docking adapter (ref. 14). The module atmosphere will have a composition of 30% oxygen in nitrogen at a total pressure of 72 kPa to permit ready egress for space-suited extravehicular activities, without the need for prebreathing to avoid decompression sickness (ref. 15). Clearly, this enriched-oxygen atmosphere increases the potential fire hazard over that of standard air. *Freedom* will be occupied by the crew only during the Shuttle-tended periods from the MTC until the final configuration of the Permanently Manned Capability. The pressurized atmosphere will be retained in the modules during the untended periods between assembly phases.

Fire-Protection Principles

The designs for the Space Station *Freedom* fire protection follow the principles established for the Shuttle. Again, flammability testing will screen out many materials and components from use. The Fire Detection and Suppression subsystem (FDS) is a component of the Environmental Control and Life Support System (ECLSS). The key requirements for fire detection and suppression (H. Kolnsberg, Boeing, unpublished presentation, Nov. 1991) are summarized as

- independent FDS in each module or element,
- fire protection of untended locations without need for monitoring by onboard or ground personnel,
- data management system to provide a remote signal indicating a fire and fire location,
- automatic and manual means of fire suppression,
- nontoxic extinguishing agents compatible with the ECLSS, and
- single-failure-tolerant designs for the FDS.

These common-sense requirements have proven to be very difficult to meet, however, because of the severe limitations on mass, volume, and power in the station. The ability of current designs in achieving the desired goal of efficient FDS operation in the confined quarters of *Freedom* remains to be demonstrated.

Freedom Fire-Detection Designs

The interior of the cylindrical Space Station *Freedom* modules has a central core surrounded by banks of racks along the walls, ceiling, and floor for installation of equipment for experiments, flight monitoring, life support, and housekeeping (fig. 3). The basic configuration of a standard rack, constructed of graphite-epoxy composite materials, is illustrated in fig. 4. Powered racks, those with utilities and electricity, are to be protected with a smoke detector in the internal ventilating-air return collector and a solenoid-activated signal-flag alarm indicator. In the proposed *Freedom* smoke-detector, shown in concept in fig. 5, smoke particles in the air stream attenuate and scatter a laser beam. Radiation sensors in the detector provide an analog signal proportional to the smoke-particle concentration. Prototype smoke detectors are now being evaluated in *normal-gravity* tests for smoke response, mechanical characteristics, and electrical performance.

The single-point-failure tolerance specification stated in the preceding section implies the redundancy that, upon the failure of a primary system, protection will be retained through an equally reliable secondary system. Initial *Freedom* designs offered redundancy by duplicate photoelectric smoke and thermal detectors in each powered rack and additional smoke detectors in the common module air-supply ducting. Design simplifications, however, eliminated the thermal detectors (which are

probably ineffective for early warning, anyhow) to save mass and eliminated the common ducting in favor of individual fans for distributed ventilation systems in each powered rack. New approaches to guarantee single-failure tolerance in the current ECLSS designs are still under consideration.

Fire detection in the central module core, in contrast to that in the powered racks, is provided by flame detectors, sensing radiation from overheating components or incipient flames. The proposed Space Station *Freedom* flame detectors incorporate three sensors in each unit, tuned to ultraviolet, visible, and infrared wavelength bands. Built-in test equipment in the form of internal light sources offer periodic operational checks. While this detector concept has the advantage of multiple-response logic from three signals to distinguish a potential fire from stray radiation, appropriate alarm set points are not yet established. These definitions require information on microgravity flame temperatures, spectral qualities, and their time variations.

Fig. 6 is a sketch of the end cone of the laboratory module, identifying several of the many components mounted on, or passing through, the end cone. The proposed flame detector is shown, installed for a line of sight into the central model core. Since a corresponding detector will be mounted on the opposite end cone, the two detectors, observing in effect the same volume, satisfy the single-failure-tolerant design requirement.

While the smoke and flame detectors discussed are the fire-detection systems currently specified for the *Freedom* MTC configuration, alternative concepts are under study. An obvious method of promise is the use of atmospheric gas sampling, already considered for ECLSS quality monitoring (ref. 16). The most sensitive indication of pyrolysis and combustion of almost all organic materials is carbon monoxide evolution, although effective sampling systems must be devised for improved response times if gas-sampling applications to fire detection are considered (ref. 13).

Freedom Fire-Suppression Designs

For the Space Station *Freedom*, the designated fire-suppression agent is carbon dioxide, which offers environmental and logistic advantages over the current Shuttle agent, Halon 1301. The selection of carbon dioxide is justified by the results of several system trade-off studies (summarized in ref. 8) and normal-gravity evaluations (ref. 17). The removal of excess carbon dioxide, at least in modest quantities, is within the capabilities of the Space Station *Freedom* ECLSS.

The *Freedom* fire-suppression designs must meet specified requirements (M. Gard, NASA Marshall, unpublished presentation, March 1992). Foremost among these are

- confirmation of a fire prior to automatic suppressant release,
- allowable CO_2 leakage to the general module to be no greater than a maximum concentration, to be specified,
- CO_2 supply in any module sufficient for at least two releases into the largest enclosed volume (powered rack),
- two portable fire extinguishers located in separate areas in each module,
- each portable fire extinguisher capable of extinguishing a fire in the largest enclosed volume, and
- inadvertent CO_2 release prevented by two-failure tolerant designs.

The proposed fire-suppression system, which is a derivative of the current Shuttle technology, consists of a combination of fixed and portable extinguishers. In brief, the logic, shown in a simplified representation in fig. 7, offers choices of no action, manual suppression, or automatic suppression in response to an apparent fire alarm. The automatic system is a centralized delivery system with remotely operated release valves at each powered rack. A conceptual sketch of the proposed system is shown in fig. 8. The portable fire extinguishers will be accessible at each end-cone location, as shown in fig. 6.

The *Freedom* fire-suppression system is sized to deliver suppressant to achieve a 50%-vol. concentration in the largest powered rack (with excess pressure venting as necessary) within one minute of agent release. The designers prefer to avoid two-phase flow in the delivery system; hence, the system is limited in capacity, because the carbon dioxide storage must be at less than the saturation pressure at ambient temperatures, *i.e.*, as a superheated gas (ref. 18).

Freedom Fire-Suppression Problems

It is evident that there are serious problems to be resolved in the design and operation of the *Freedom* fire-suppression system. The most important issues are

- non-conformity to the general requirements for the FDS,
- lack of commonality among international program partners, and
- prescribed agent that is unacceptable for use in the Hyperbaric Air Lock.

Despite the requirement limiting the maximum atmospheric leakage concentration of carbon dioxide, the designation of this agent as meeting the "nontoxic" requirement may be questioned. In addition, the redundancy for the single-failure-tolerance has not been achieved. Original design proposals called for backup suppression by venting the atmosphere to the vacuum of space. At present, the objections to venting are that the venting flow temporarily enhances the burning rate in microgravity (ref. 9), the final total pressure for guaranteed fire suppression is unknown, and the stores of makeup atmospheres for reconstitution after venting are limited.

The Space Station *Freedom* is an international program, with Japan and the European Space Agency (ESA) each contributing pressurized laboratory modules in the final space-station configuration. The international laboratories will be assembled after the MTC, but their development is now underway. The FDS designs for the international modules are derived independently of the corresponding U.S. subsystems, but the subsystems interconnect through common data-management systems and intermodule ventilation flows. All three international partners now agree on a carbon dioxide system for fire suppression, with many details equivalent in principle to those established for the U.S. modules. There are, however, some primary design and operational differences. Most of these variations do not affect safety, but one discrepancy is of concern. Because of possible system icing and limited pressure-relief capacity, the suppressant-flow system cannot deliver the required quantity of carbon dioxide in one minute in the ESA module. A maximum release-time specification of 30 minutes was requested, an unreasonable delay time for fire suppression in a closed environment. A compromise goal of 10-min delivery time is now under consideration, a delay that still is regarded as unsatisfactory by safety specialists.

The Hyperbaric Air Lock (HAL) is a chamber within one of the modules, sized to accommodate a patient and a medical attendant for treatment of decompression sickness and for other medical activities. While the HAL is not a component of the MTC assembly, its fire protection is actively under development. The HAL will have an atmosphere of 21% O_2 in nitrogen at a maximum total pressure of 340 kPa. If carbon dioxide is released to extinguish a fire in the HAL, the medical specialists fear that the resulting partial pressure of carbon dioxide at the proposed suppression concentration in the HAL will be highly toxic.

A recent communication (S. Pool, NASA Johnson, unpublished letter, April 1992) discussed alternative fire-prevention and suppression approaches for the HAL, although none of these are ready for development. The HAL proposal is to retain the common fire-detection system of the U.S. laboratory module, but to install a separate, dedicated fire-suppression system. The proposed fire-suppression concept includes nitrogen purging of electrical and instrument racks within the HAL for first-order fire prevention. Primary fire suppression will be furnished by a portable nitrogen extinguisher, which is a method that has no design counterpart in conventional fire-extinguisher technology. In

addition, a fixed nitrogen-suppression system will release nitrogen to dilute the HAL atmosphere after extinguishment to prevent reignition.

CONCLUDING REMARKS

This paper discussed the features of fire protection incorporated into current and proposed U.S. human-crew spacecraft. In general, there is a strong reliance on preventive measures along with use of proven detection and suppression techniques. The experience with minor "near-fires" on Shuttle missions has shown that the crew response is the major factor in alleviating danger, but designed safety provisions offer an adequate backup.

For the future Space Station *Freedom*, dependence on human response will not be sufficient, and reliable automated fire protection is essential. The difficulties facing the *Freedom* environmental- and safety-design specialists must be appreciated. The principal drivers for the designs and operations are the stringent and sometimes conflicting (and often changing) specifications, to be met within the severe restrictions on material and component mass, volume, power, quality control, and cost. Certain alternatives, such as those for multiple-failure-tolerant features, await new inventions well beyond the present state-of-the-art. In addition, the fire-safety provisions must advance the goal of full utilization of *Freedom*, must allow for the long-duration conduct of a varied crew, and must satisfy the individual safety approaches of international partners tied into the common safety network.

While it would appear that microgravity combustion research plays a secondary role in spacecraft fire-protection strategies, effective and trustworthy fire protection can benefit greatly from fundamental scientific knowledge. The microgravity combustion research community has much to offer advanced spacecraft fire safety. Already spacecraft fire safety is guided by preliminary information on microgravity ventilation effects and radiant flame (non-flickering) characteristics. Examples of other important needs that may be addressed by microgravity combustion research are the assessment and prediction of material flammability, the physical and radiant characteristics of fires, gaseous and aerosol emissions from fires, the physical and chemical actions of extinguishment, and the long-duration toxic and corrosive effects of combustion and extinguishment products.

REFERENCES

1. Law, C., Combustion in Microgravity: Opportunity, Challenges, and Progress. AIAA Paper 90-0120, Jan. 1990.
2. Friedman, R., and Olson, S., Fire Safety Applications for Spacecraft, in "Aircraft Fire Safety", AGARD Conf. Publ. No. 467, Oct. 1989, pp. 15-1 to 15-15.
3. Rodney, G., Critical Safety Assurance Factors for Manned Spacecraft — A Fire Safety Perspective. IAF Paper 90-555, Oct. 1990.
4. Friedman, R., and Sacksteder, K., Fire Behavior and Risk Analysis in Spacecraft. NASA TM 100944, Nov. 1989.
5. Knight D., Medical Guidelines for Protecting Crews with Flame-Suppressant Atmospheres. SAE Tech. Paper 891596, July 1989.
6. Peercy, R., and Raasch, R., Threat-strategy Technique: A System Safety Tool for Advanced Design. *Jour. Spacecraft*, vol. 23, no. 2, 1986, pp. 200-206.
7. Kaplan, S., Safety Risk Assessment in the Space Station *Freedom*. AIAA Paper 90-3771, Sept. 1990.
8. Friedman, R., Sacksteder, K., and Urban, D., Risks, Designs, and Research for Fire Safety in Spacecraft. NASA TM 105317, Nov. 1991.
9. Kimzey, J., Skylab Experiment M479 Zero Gravity Flammability, in "Skylab Results", *Proc. Third Space Processing Symp.*, NASA MSFC M-74-5 (NASA TM X-70252), vol. 1, Jan. 1974, pp. 115-130.

10. Youngblood, W., and Vedha-Nayagam, M., Advanced Spacecraft Fire Safety: Proposed Projects and Program Plan, NASA CR 185147, Oct. 1989.

11. Pogue, B., Skylab Mission, in Baugher, C., ed., "Space Station *Freedom* Toxic and Reactive Materials Handling", NASA CP 3085, July 1990, pp. 5-1 to 5-7.

12. Thomas, E., Microgravity Fire Detection Problems — Fact or Fiction, SAE Tech. Paper 901215, July 1990.

13. Limero, T., James, J., Cromer, R., and Beck, S., A Combustion Products Analyzer for Contingency Use During Thermodegradation Events in Spacecraft. SAE Tech. Paper 911479, July 1991.

14. Sendral, E., Overview and Status of Space Station *Freedom* Modules. AIAA Paper 92-1307, March 1992.

15. McCarthy, K., and Green, J., The Effect of Reduced Cabin Pressure on the Crew and Life Support System. SAE Tech. Paper 911331, July 1991.

16. Sonnenschein, R., and Hienerwadel, K., Evaluation of the Suitability of CO Measurements for Fire Detection in Space. SAE Tech. Paper 901285, July 1990.

17. Sircar, S., and Dees, J., Evaluation of the Fire Extinguishants for Space Station *Freedom*. NASA JSC White Sands Test Facility Doc. TR-650-001, Mar. 1992.

18. Gedke, J., Mohamadinejad, H., and Gard, M., Preliminary Analyses of the CO_2 Fire Suppressant Distribution System for Space Station *Freedom*. SAE Tech. Paper 911473, July 1991.

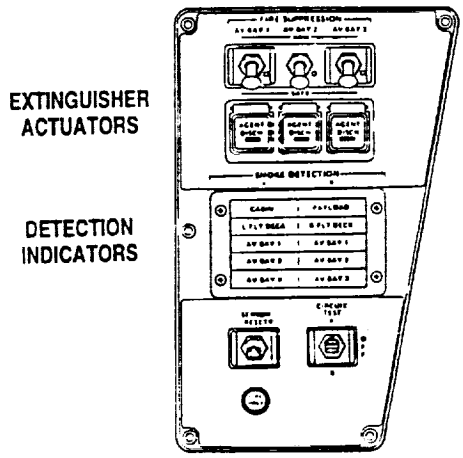

Figure 1. - Shuttle Fire Detection and Suppression Panel

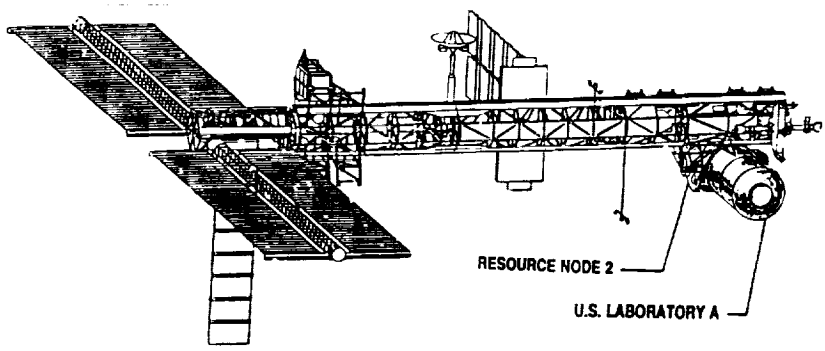

Figure 2. - Sketch of the Man-Tended Configuration of Space Station Freedom

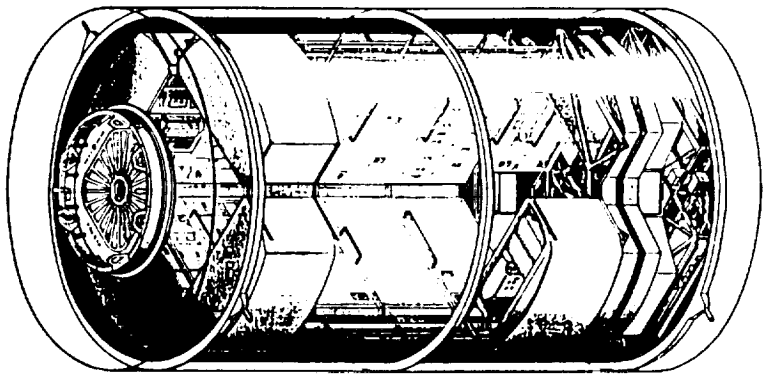

Figure 3. - Phantom view of the U.S. Laboratory Module for *Freedom*, showing central core and rack arrangement (Boeing design).

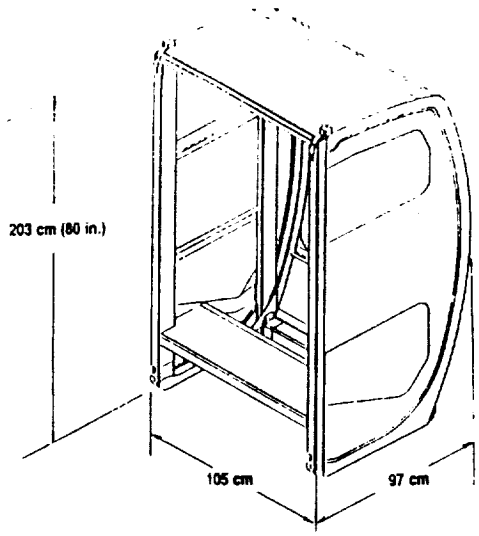

Figure 4. - Typical rack design for the Space Station *Freedom*.

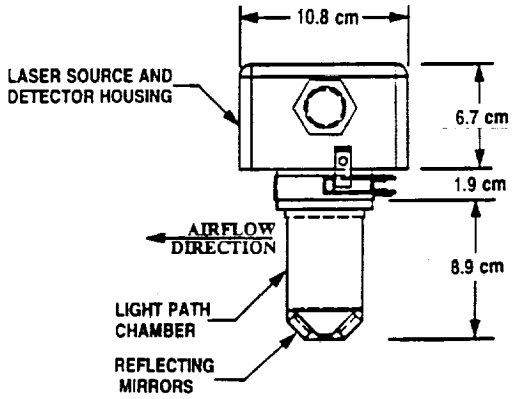

Figure 5. - Concept of photoelectric smoke detector proposed for *Freedom* racks (Allied Signal design).

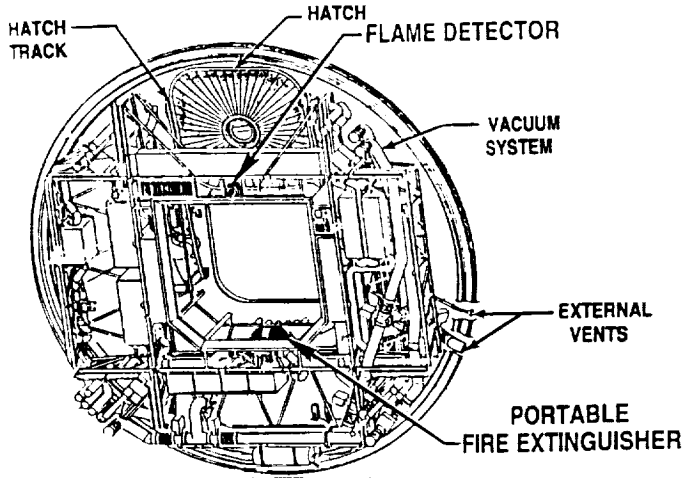

Figure 6. - End-cone arrangement of *Freedom* Laboratory Module

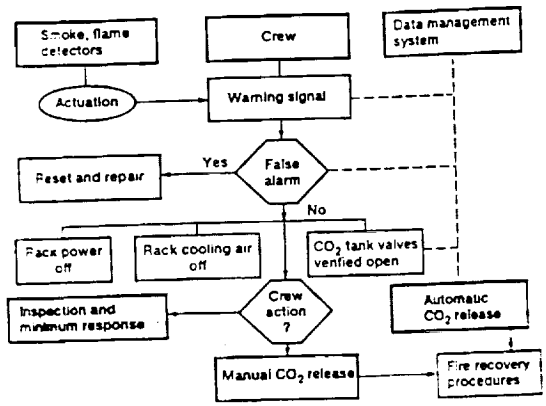

Figure 7. - Fire detection and suppression response logic for *Freedom*.

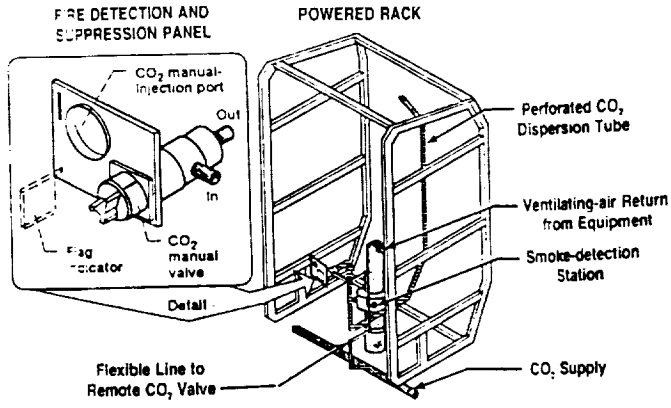

Figure 8. - Proposed Space Station *Freedom* carbon dioxide suppression system.

SESSION F - IGNITION, SMOLDER, AND FLAME SPREAD OF CONDENSED PHASE FUELS

(Chair, Raymond Friedman)

IGNITION AND SUBSEQUENT FLAME SPREAD OVER A THIN CELLULOSIC MATERIAL

N93-20205

Kazuyoshi Nakabe,* Howard R. Baum, and Takashi Kashiwagi
Building and Fire Research Laboratory
National Institute of Standards and Technology
Gaithersburg, Maryland 20899

Introduction

Both ignition and flame spread on solid fuels are processes that not only are of considerable scientific interest but that also have important fire safety applications. Both types of processes, ignition and flame spread, are complicated by strong coupling between chemical reactions and transport processes, not only in the gas phase but also in the condensed phase. In most previous studies, ignition and flame spread were studied separately with the result that there has been little understanding of the transition from ignition to flame spread. In fire safety applications this transition is crucial to determine whether a fire will be limited to a localized, temporary burn or will transition into a growth mode with a potential to become a large fire. In order to understand this transition, the transient mechanisms of ignition and subsequent flame spread must be studied. However, there have been no definitive experimental or modeling studies, because of the complexity of the flow motion generated by buoyancy near the heated sample surface. One must solve the full Navier-Stokes equations over an extended region to represent accurately the highly unstable buoyant plume and entrainment of surrounding gas from far away. In order to avoid the complicated nature of the starting plume problem under normal gravity, previous detailed radiative ignition models were assumed to be one-dimensional (ref.1) or were applied at a stagnation point (ref.2). Thus, these models cannot be extended to include the transition to flame spread. The mismatch between experimental and calculated geometries means that theories cannot be compared directly with experimental results in normal gravity.

To overcome the above difficulty, theoretical results obtained without buoyancy can be directly compared with experimental data measured in a microgravity environment. Thus, the objective of this study is to develop a theoretical model for ignition and the transition to flame spread and to make predictions using the thermal and chemical characteristics of a cellulosic material which are measured in normal gravity. The model should take advantage of the microgravity environment as much as possible in the gas phase instead of modifying a conventional normal-gravity approach. A thermally-thin cellulosic sheet is considered as the sample fuel, which might ignite and exhibit significant flame spread during test times available in NASA's drop towers or in the space shuttle, without requiring a pilot flame. This last situation eliminates many complicating parameters such as pilot flame location, temperature, and size (ref.3).

---

* Guest researcher from Osaka University, Osaka Japan.

2. Theoretical Model

2.1 Gas Phase Model

The absence of gravity (microgravity is approximated to be zero gravity) removes the buoyancy-induced vorticity generation mechanism. The small scale of the planned experiment, together with the slow external flow (less than 10 cm/s), simulating the ventilation flow level in a spacecraft, implies a low Reynolds number flow domain. When surface pyrolysis is present, the thermally-induced surface blowing velocity must be taken into account, even at low Reynolds numbers. Both these concepts can be accommodated by assuming the velocity field to be a potential flow. The only loss is the no-slip boundary condition which is already relaxed in the classical Oseen approximation to low Reynolds number phenomena. This approximation is adopted and is implicit in the analysis. The conservation equations of mass, energy and species in the gas phase under low Mach number combustion and heat transfer conditions can be written as:

$$\frac{D\rho}{Dt}+\rho\nabla\cdot\vec{v}=0 \quad , \quad \rho\frac{D\int_0^T c_p dT}{Dt}-\nabla\cdot(k\nabla T)=\Delta H\dot{m}_f+\dot{q}_R$$

$$\rho\frac{DY_{ox}}{Dt}-\nabla\cdot(\rho D\nabla Y_{ox})=-\nu\dot{m}_f \quad , \quad \rho\frac{DY_f}{Dt}-\nabla\cdot(\rho D\nabla Y_f)=-\dot{m}_f \tag{1}$$

We assume that the reaction is represented by a global one step Arrhenius reaction and its kinetic constants are selected. Equations (1) are supplemented by an equation of state, taken in a form appropriate for low-Mach-number flows. Now multiply the first of Eqs. (1) by enthalpy, h, and add it to the second. The result is:

$$\rho_\infty h_\infty\nabla\cdot\vec{v}-\nabla\cdot(k\nabla T)=\Delta H\dot{m}_f+\dot{q}_R \tag{2}$$

Equation (2) is the fundamental equation for determining the velocity field $\vec{v}$. Since $\vec{v}$ is a vector field it can be decomposed into the gradient of a potential ϕ and a solenoidal field $\vec{u}$.

$$\vec{v}=\nabla\phi+\vec{u} \quad , \quad \nabla\cdot\vec{u}=0 \tag{3}$$

Substitution of Eq. (3) into Eq. (2) yields:

$$\nabla^2\phi=\frac{1}{\rho_\infty h_\infty}(\Delta H\dot{m}_f+\dot{q}_R+\nabla^2\psi) \quad , \quad \psi=\int_{T_\infty}^{T}k(T)\,dT \tag{4}$$

Note that the third term on the right hand side of the first equation of Eq. (4) can be eliminated by introducing a particular solution ϕ_P as:

$$\phi_P=\frac{\psi}{\rho_\infty h_\infty} \tag{5}$$

Moreover, it is convenient to introduce another particular potential $\phi_{P\infty}$ representing the effects of the external wind velocity u_∞. Then, introducing a remainder potential Φ, ϕ may be expressed in the

$$\phi = \phi_P + \phi_{P\infty} + \Phi \quad , \quad \nabla^2 \Phi = \frac{\Delta H \dot{m}_f''' + \dot{q}_R}{\rho_\infty h_\infty} \tag{6}$$

nf

Equations (5) and (6) relate the potential field to the temperature distributions in the gas phase. In the calculation the sample is irradiated and auto-ignited at the center by continuous thermal radiant flux with a Gaussian distribution. Far from the surface, ϕ, T and Y_i must decay to their ambient initial values. T and Y_i decay exponentially to their ambient values. However, the potential field decays slowly away from the heated region. Thus, putting ϕ or its gradient equal to zero at the computational boundary would introduce unacceptable error into the calculation. These errors are avoided by using the analytical solution to Eq.(6) subject to the boundary condition at the sample surface to generate accurate values for ϕ on the computational boundary (ref.4). Then, Eqs.(1) are solved by a time-splitting algorithm.

2.2 Condensed Phase Model

It is assumed that the condensed phase is a thermally thin sheet of cellulosic material, and uniform in composition through its depth. The thermal degradation of the cellulosic sheet is described by two global thermal degradation reactions and a char oxidation reaction (ref.5). They are; (1) endothermic global pyrolysis reaction which degrades the cellulosic sheet to gases and a char, (2) weakly exothermic global thermal oxidative reaction which degrades the cellulose sheet to gases and a char, (3) highly exothermic global char oxidation reaction which degrades the char to gases and ash. Here, it is assumed that the reactivity of the char with oxygen formed from the above two reactions with oxygen is the same. In the above global reactions combustible gases represent hydrocarbons and CO and non-combustible gases represent CO_2 and H_2O. Here, it is assumed that the combustible gases formed from each reaction above are the same. Although these reactions are crudely approximated compared to the actual, extremely complex degradation reactions, their accuracy is comparable to the global one-step gas phase oxidation reaction for the combustible gases, which is used for the gas phase reaction in this study.

The reaction rate of each reaction above, RR_i, is approximately expressed by the following Arrhenius-type equations:

(1) $RR_p = A_p(\rho_s Y_f/\rho_{s0})^{np}\exp(-E_p/RT)$
(2) $RR_{ox} = A_{ox}(\rho Y_{ox}/\rho_{0,ox})^{nox}(\rho_s Y_f/\rho_{s0})^{nf,ox}\exp(-E_{ox}/RT)$
(3) $RR_{char} = A_{char}(\rho Y_{ox}/\rho_{0,char})^{no2,char}(\rho_s Y_{char}/\rho_{s0})^{nchar}\exp(-E_{char}/RT)$

Values for the above kinetic parameters together with the heats of reaction, ΔH_i, for a black cellulosic paper have been measured; the details are given in Ref.5.
The equations for the condensed phase are given as follows.
Conservation of solid mass:

$$\partial(\rho_s/\rho_{s0})/\partial t = -(1 - \nu_{char,p})RR_p - (1- \nu_{char,ox})RR_{ox} - (1-\nu_{ash,char})RRchar \tag{7}$$

Conservation of initial cellulosic material: $\partial(\rho_s Y_f/\rho_{s0})/\partial t = -RR_p - RR_{ox}$ (8)

Conservation of char:

$$\partial(\rho_s Y_c/\rho_{s0})/\partial t = \nu_{char,p}RR_p + \nu_{char,ox}RR_{ox} - RRchar \tag{9}$$

Conservation of energy:

$$\delta\cdot\partial(\rho_s c_s T)/\partial t = (-\Delta H_p RR_p - \Delta H_{ox} RR_{ox} - \Delta H_{char} RR_{char})\cdot\rho_{s0}\delta + (1-r)\dot{q}_{ex} - \varepsilon\sigma(T_s^4 - T_0^4) + k\partial T(r,0,t)/\partial z \quad (10)$$

where δ is the half-thickness of the paper. The mass flux of evolved combustible gases from the surface is given by the following expression:

$$\dot{m}_s = [(1-\nu_{char,p})RR_p+(1-\nu_{char,ox})RR_{ox}+(1-\nu_{ash,char})RR_{char}]\cdot\rho_{s0}\delta \quad (11)$$

The cellulosic material used in the present study is a $0.38\text{x}10^{-4}$ m thick sheet.

3. Results and Discussion

Four different cases are being studied: (1) heat transfer with the degradation of the paper sheet irradiated by the external radiation at the center of the paper in an axisymmetric configuration, no gas phase reaction; no external flow, (2) ignition and subsequent flame spread in an axisymmetric configuration; no external flow, (3) heat transfer with a slow external flow in a three-dimensional configuration, and (4) ignition and subsequent flame spread with a slow external flow in a three-dimensional configuration. Since the results in the first case were published in ref.4, they are not discussed here due to space limitations.

3.1 Quiescent axisymmetric configuration

A maximum external radiant flux of 5 W/cm^2 (continuously on during computation) at 21%, 30% and 50% oxygen concentrations was used in the calculation. The results indicate that ignition is observed for 21% and 30% oxygen concentrations but the transition to flame spread does not occur. However, in 50% oxygen the transition is achieved as shown in Fig.1 which plots the gas phase temperature distribution at 1.0s after initiation of the external radiation. Each temperature isotherm line is a 100°K interval starting from 350°K. There are two high temperature regions;one is behind the flame front and the other is at the center where the external radiation continuously irradiates the sample. The results at later time show that there are two separate flames; the primary flame propagates radially outward, while the secondary flame stays at the center and becomes gradually weaker and disappears. Eventually one ring-like flame appears to continue its spread radially outward. The distribution of velocity vectors at the same time is shown in Figs.2. The large expansion flow motion near the flame front is clearly seen in Fig.2. The large mass addition near the center is caused by the continuously applied external radiation. Since the sample was nearly completely converted to char at the center, little mass is added there. The distribution of oxygen and fuel concentration indicates that the flame near the traveling front is a premixed flame followed by a diffusion flame behind the flame front. The energy balance at the sample surface at 1.0s is shown in Fig.3, where Q_{ex} is the external radiant flux, Q_{rad} is the re-radiation loss, Q_{rr} is the net heat balance of the three solid degradation reactions and Q_{fcon} is the convective/conductive heat transfer from the gas phase to the sample. A high energy feedback rate of nearly 6 W/cm^2 is calculated as opposed to the nearly 1 W/cm^2 for the 21% oxygen concentration case at 1.6s after initiation of the external radiation as shown in Fig.4. This difference in energy feedback rate is mainly caused by differences in flame temperature (about 1400°K for 21% vs 2000°K for 50%) and also in the location of the peak gas phase reaction rate (closer to the sample surface in 50% oxygen concentration).

The previous experiment in a quiescent microgravity environment showed that the flame spread limit is about 20% oxygen for a light paper towel (Kimwipes paper) (ref.6). Thus, unsuccessful transition to flame spread in 21% and 30% oxygen predicted in this study does not agree with successful transition observed in the experimental work. Also, the predicted flame spread rate in 50% oxygen concentration is about 19 cm/s which is roughly five times faster than the experimentally-measured rate using the drop tower (ref.6). In the calculation the only uncertainty is the kinetic constants for the gas phase oxidation reaction. Since

there are no data available on the degradation products of the paper, the accuracy of the selected values is questionable. Since there are significant differences between the experimental setup and the calculation, for example, a two-dimensional experimental configuration vs. an axisymmetric calculation and piloted ignition in the experiment vs. auto-ignition, no attempt is made to adjust the kinetic constants of the gas phase reaction to match with the experimental data. These constants will be measured in the future.

3.2 Three-dimensional Calculation

Although preliminary results on ignition in the three dimensional configuration with a slow external flow have been obtained, more time is needed to determine their accuracy and correctness. It is hoped that the results will be presented at the meeting. Here, the results for the three dimensional heat transfer problem are briefly discussed. In this problem either a thermally thin or thick non-reactive condensed material is irradiated by continuously applied external radiation with a Gaussian flux distribution. Typical examples of the distributions of velocity vectors relative to the ambient flow and temperature contours in the gas phase for a thermally thick non-reactive material are shown in Figs. 5 at 8s after the initiation of an external radiant flux of 4 W/cm^2 with an external velocity of 2 cm/s (from left to right). The left corner figure in Figs. 5 represents the front view (looking in the downstream direction) distribution. The top rectangular figure represents the side view of the distribution and the lower rectangular figure represents the top view of the distribution. The distribution of velocity vectors represent the flow motion generated by heat addition from the irradiated surface. This flow is smaller than the external flow of 2 cm/s. Its center is located at a short distance upstream from the center of the external irradiation (x=0). This indicates that the steepest temperature gradient occurs at the upstream location due to downward pushing of the heated layer by the ambient flow. At a short distance downstream from x=0, there is a sink of flow due to the steep temperature gradient due to heat loss from the hot gas stream to the cold surface. Since the temperature gradient drives the flow, the flow generated by the external radiation is limited to a region near the irradiated surface area at an early time.

4. Future plans

1. Complete development of the three-dimensional ignition and flame spread code.
2. Conduct parametric study to determine which parameters affect ignition, the trnsition, and flame spread.
3. Measure global gas phase oxidation reaction rate for the degradation products of the paper.
4. Modify the codes to include piloted-ignition.

Reference

1.Kashiwagi,T, "A Radiative Ignition Model of a Solid Fuel", *Combustion Science and Technology*, 8, 1974, pp.225-236.

2.Amos,B. and Fernandez-Pello,A.C., "Model of the Ignition and Flame Development on a Vaporizing Combustible Surface in a Stagnation Point Flow: Ignition by Vapor Fuel Radiation Absorption", *Combustion Science and Technology*, 62, 1988, pp.331-343.

3.Tzeng,L.S., Atreya, A., and Wichman,I.S., "A One-Dimensional Model of Piloted Ignition", *Combustion and Flame*, 80, 1990, pp.94-107.

4.Kushida,G., Baum,H.R., Kashiwagi,T. and di Blasi, C., "Heat and Mass Transport from Thermally Degrading Thin Cellulosic Materials in a Microgravity Environment", *Journal of Heat Transfer*, 114, 1992, p.p484-502.

5.Kashiwagi,T. and Nambu,H., "Global Kinetic Constants for Thermal Oxidative Degradation of a Cellulosic Paper", *Combustion and Flame*, 88, 1992, pp.345-368.

6.Olson,S.L., Ferkul,P.V., and Tien,J.S., "Near-Limit Flame Spread Over a Thin Solid Fuel in Microgravity", *Twenty Second Symposium (International) on Combustion*, The Combustion Institute, Pittsburgh, PA, 1988, pp.1213-1222.

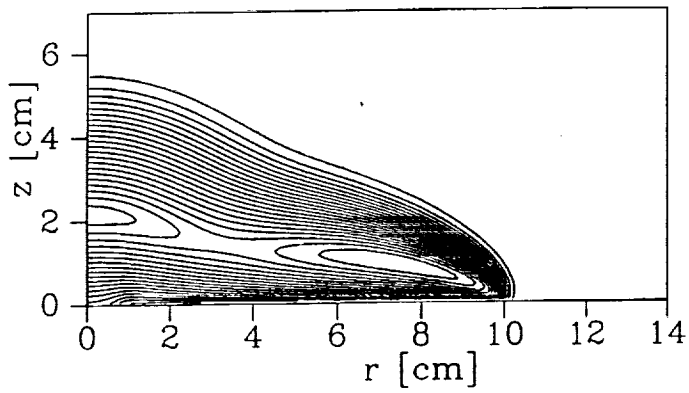

Fig. 1 Temperature contour in the gas phase

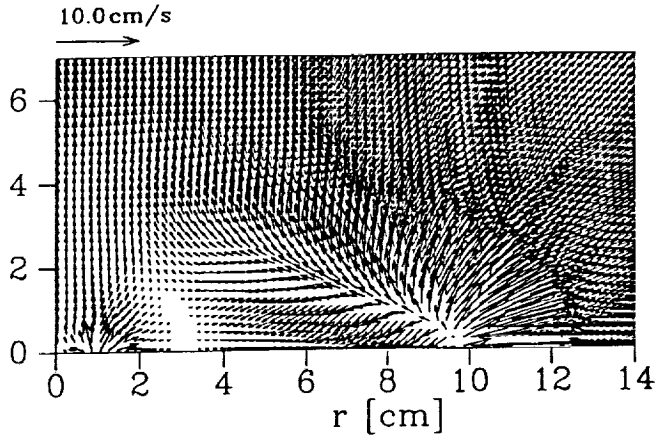

Fig. 2 Velocity vector

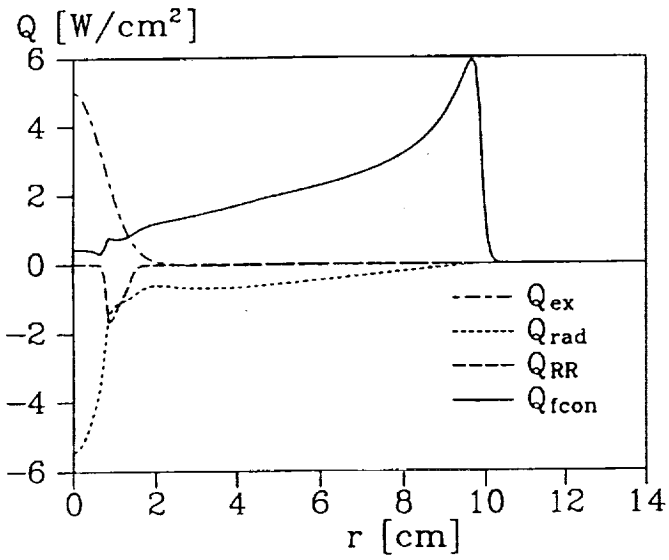

Fig. 3 Energy balance at the surface 50% oxygen

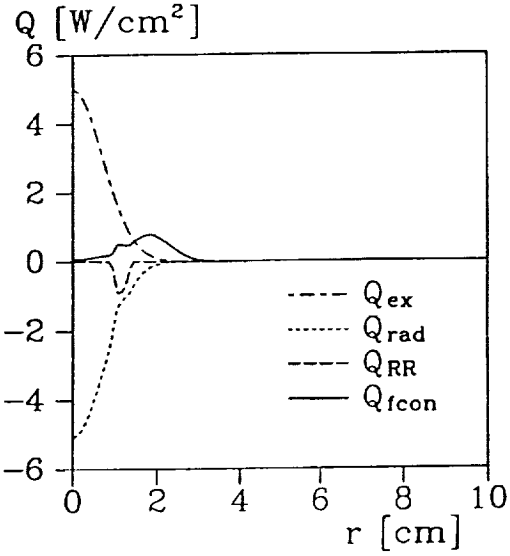

Fig. 4 Energy blanace at the surface in air

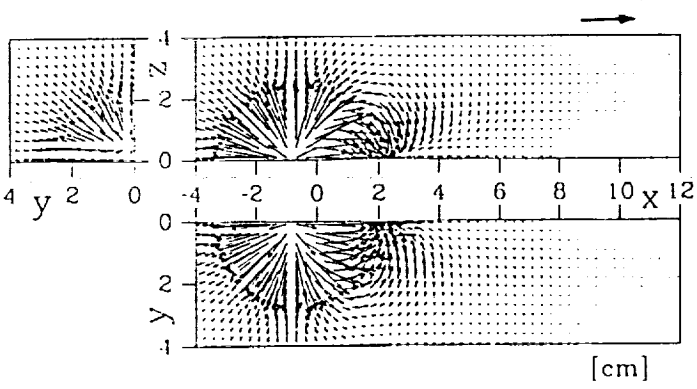

Fig. 5 Velocity vector in 3D flow

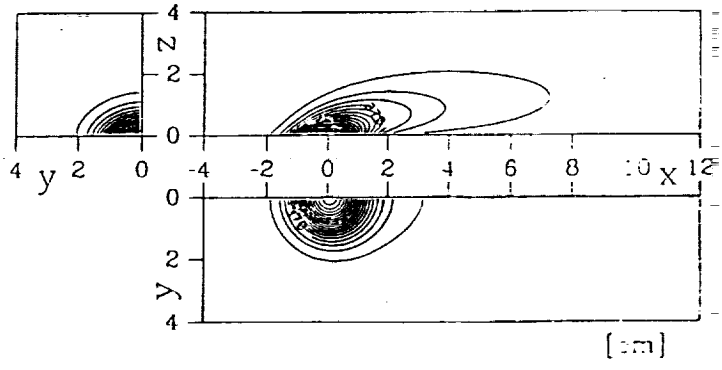

Temperature contour in 3D flow

COMMENTS

Question (David Schiller, U.C. Irvine): I have two questions regarding your numerical technique:

(1) In your paper, you state that you use a time-splitting algorithm to solve the governing equations. I have tried using different time steps for transport and chemical kinetics in my model of flame spread over liquid fuel pools. I have found that significant errors are introduced if the solution of the chemical kinetic and transport conditions are decoupled in this manner. Will you please describe your time-splitting algorithm in more detail and also tell me what you've done (if anything) to show that your time-splitting algorithm is "time step independent" and/or gives the same results as you would get if no time-splitting was used?

(2) It appears ignition occurs very close to the solid fuel surface. Is your solution grid independent? How fine a mesh was required in the gas just above the fuel surface (I use delta-y_g of about 50 microns at the gas/liquid interface in my problem. Do you incorporate a partially or fully adaptive grid scheme to provide fine resolution near the flame leasing edge as the flame propagates?

Answer: The algorithm employed in the computations is not time-split in the sense suggested in the question. It is a member of a class analyzed by Wichman (1). Basically, for a single-step reaction model of the kind used in many combustion studies (including this one) the reaction is almost always either much slower than or much faster than the local diffusion-convection balance. Under these circumstances, it is possible to show analytically that the species and energy equations can be advanced by splitting the time step in the following way: first the species in each computational cell are allowed to react as if the system were spatially homogeneous for the duration of the time step. The resulting temperature and species distributions are then initial conditions for the diffusion-convection problem, which is solved implicitly for the same time step. A stiff ODE solver is used for the first part of the calculation. The solver may require many internal steps to calculate the homogeneous reaction. The error is first order in the time-step if the reaction time is comparable to or greater than the diffusion-convection time and is smaller than this by a factor of the time-scale ratio when the reaction is fast. These statements are true for any scheme which is itself stable for the convection-diffusion problem.

The scheme has been tested by numerically computing solutions to the three-dimensional time-dependent heat transfer problem with an Oseen flow in the same geometry that has also been solved exactly analytically. The computer temperatures agree with the analytical results to better than 1/2 percent for the grid used. The ODE solver is a package with its own internal error controls, with a tolerance that can be set by the user. We require convergence in temperature to less than 0.5 degrees Kelvin in our computations. No adaptive grid schemes is employed. The gas phase grid is one millimeter on a side and a time step of 4×10^{-4} seconds is employed. This is certainly sufficient to put the flame in approximately the right place, although details of the flame structure might be lost. However, if fine structure in the flame leading edge is wanted, a considerably more sophisticated reaction scheme is also required. Such a study in the context of a three-dimensional transient problem is well beyond the current state-of-the-art.

Question (Subrata Bhattacharjee, San Diego State): (1) How do you justify the flow being potential as well as creeping?

(2) In the absence of imposed convection, could the gas phase (combustion product) radiation cause significant flame cooling?

Answer: The velocity field that is used to evaluate the convection term in the diffusion-convection balance at low Reynolds numbers is a potential flow in almost all of the existing fluid flow, heat transfer, and combustion literature. As a simple example, the "Oseen flow" of any quantity at low Reynolds number is the leading order approximation to the solution for that quantity everywhere for a constant property fluid. The flow field that is used in the convection terms is a uniform flow which is trivially a potential flow. The approximation is correct even when the quantity being convected is the fluid vorticity! Indeed, this is exactly how the classical low Reynolds number drag, heat transfer, and combustion results are obtained. The actual velocity fields are far more complex, but additional detail is not needed if only the quantities that satisfy the Oseen equations are required. For further explanation and additional references see Kushida, et. al. (2).

The major role of radiation is in cooling the condensed phase surface. Its importance in the gas phase is unclear, in part because the precise nature of the gaseous combustion products is not yet well understood. We intend to investigate this further in the future.

REFERENCES:

(1) Wichman, I.S., "On the Use of Operator Splitting Methods for the Equations of Combustion", Combustion and Flame, Vol. 3, pp. 240-252, (1991).

(2) Kushida, G. Baum, H.R., Kashiwagi, T., and di Blasi, C., "Heat and Mass Transfer from Thermally Degrading Thin Cellulosic Materials in a Microgravity Environment", J. Heat Transfer, Vol. 114. 494-502, (1992).

OPPOSED-FLOW FLAME SPREADING IN REDUCED GRAVITY

N93-20206

Robert A. Altenkirch
Department of Mechanical and Nuclear Engineering
Mississippi State University, Mississippi State, Mississippi 39762

Subrata Bhattacharjee
Department of Mechanical Engineering
San Diego State University, San Diego, California 92182

Sandra L. Olson and Kurt Sacksteder
NASA Lewis Research Center
Cleveland, Ohio 44135

Introduction

Experimental results obtained in drop towers and in Space Shuttle based experiments coupled with modelling efforts are beginning to provide information that is allowing an understanding to be developed of the physics of opposed–flow flame spread at reduced gravity where the spread rate and flow velocity are comparable and of the role played by radiative and diffusive processes in flame spreading in microgravity [1–6]. Here we describe one Space Shuttle based experiment on flame spreading in a quiescent environment, the Solid Surface Combustion Experiment, SSCE [7], one planned microgravity experiment on flame spreading in a radiatively–controlled, forced opposing flow environment, the Diffusive and Radiative Transport in Fires Experiment, DARTFire [8], modelling efforts to support these experiments, and some results obtained to date.

SSCE Apparatus

The SSCE apparatus consists of a sealed container, approximately 0.039 m^3 in volume, that is filled with a mixture of specified O_2 and N_2 percent by volume at a prescribed pressure. The test specimens are either ashless filter paper (thin fuel), 0.165 mm thick, 10 cm long, and 3 cm wide, or polymethylmethacrylate (PMMA; thick fuel), 0.318 cm thick, 2 cm long, and 0.635 cm wide. One end of the sample is ignited using an electrically–heated nichrome wire.

For the thin fuel, three 0.127 mm Pt/Pt–Rh thermocouples are positioned along the sample centerline. The first is embedded in the sample 5 cm from the ignition end of the sample, the second is located 2.3 mm above the sample but 2.54 cm farther from the ignitor, and the third is located 7.0 mm above the sample directly over the first. For the thick fuel, one one thermocouple is positioned in the gas, and two in the solid, one at the surface and one in depth. Two orthogonal views of the experiment are recorded using 16 mm cine–cameras operating at 24 frames/s.

SSCE Results

Four experiments for the ashless filter paper samples have been run to date, three

at 50%O_2/50%N_2 by volume at 1.5 atm (STS–41, October 1990), 1.0 atm (STS–40/SLS–1, June 1991), 2.0 atm (STS–43, August 1991), and one at 35%O_2/65%N_2 at 1.5 atm (STS–50/USML–1, July 1992). Figure 1 shows four frames from the side–view film for 50% O_2 at 1.5 and 1.0 atm. Just after the ignitor wire is heated, ignition from nitrocellulose on the wire results in a bright orange flash that subsides once the flame spreads away from the ignitor wire. The flame is spreading from left to right, and the time for each frame is the time after the first flame–like image appears on the film.

As the flame spreads, the soot radiation level in the tail of the flame decreases in both flames, and the lower pressure flame becomes entirely blue. Additionally, the flame elongates early in the spread process as the leading edge propagates faster than the trailing edge. Even though the soot radiation changes with time and the flame elongates just following ignition, the leading–edge spread rate is almost fixed immediately after the flame leaves the ignitor. The spread rates for the first three experiments are 0.358, 0.454, and 0.547 cm/s for 1.0, 1.5, 2.0 atm, respectively, at 50% O_2, and for the 35% O_2 experiment it is 0.092 cm/s at 1.5 atm.

Thermocouple traces, as a function of location in the flame, for the surface and gas temperatures, and the net heat flux to the solid [6] are shown in Fig. 2. The leading edge of the flame is at x=0, which is fixed at the location of the peak net heat flux. The surface temperature increases rapidly as the flame is approached and then reaches a relatively steady temperature, which indicates the region of pyrolysis. The temperature then rises, and as the tail of the flame passes the thermocouple, the temperature quickly decreases until the residual char increases in temperature again as fresh oxygen, which diffuses to the surface while products diffuse away, results in surface oxidation.

Steady–State Modelling

Flame spread modelling is used to support the experimental effort. A comprehensive, steady–state, mathematical model developed along with the experimental program has been presented elsewhere [3,4]. The conservation equations in the gas for mass, fuel, oxygen, x and y momentum, and energy, including finite–rate chemistry, and the energy and mass conservation equations in the solid, including finite–rate, endothermic pyrolysis, are solved for the steady–state spread rate and distribution of field variables. For the thin fuel, radiation from CO_2 and H_2O is considered [4], but the radiation fed back to the surface is generally assumed to balance that reradiated from the surface so that a direct radiative coupling between the gas and the solid is not presently considered [5].

Some computed results are compared to experimental results for the 50% O_2, 1.5 atm experiment in Fig. 3. The character of the gas–phase temperature at the leading edge of the flame is predicted well, but the trailing edge of the flame is too far from the surface, with little or no curvature toward the surface, to provide agreement with experiment. Because the leading edge of the flame is responsible for establishing the spread rate, reasonable agreement between measured and predicted spread rate is obtained, the measured values, given above, for the 50% O_2 experiments being 0.358, 0.454, 0.547 cm/s for 1.0, 1.5, 2.0 atm, respectively, compared to predicted values of 0.360, 0.417, 0.450 cm/s. Both the measured and predicted spread rates increase with

pressure; without gas–phase radiation, the predicted spread rate, which is approximately a factor of two higher than experiment (0.704 cm/s) at 1.0 atm, is almost independent of pressure, although it declines slightly with an increase in pressure.

For thin fuels, radiative effects are important at low opposing flow velocities, decreases in flow velocity causing a decrease in spread rate and possible extinction [9]. As the flow velocity is increased, the effects of radiation become unimportant, with extinction at high flow velocities occurring via blowoff. While thick fuel experiments have not been completed yet, modelling of flame spread over thick fuels has progressed, although the effects of radiation have been confined to surface reradiation [10]. For these fuels, surface radiative effects are important for all flow velocities because as the flow velocity is increased from very low values to very high values, the radiative effects compared to the conduction effects do not decrease as they do for thin fuels.

DARTFire Experiment

Experimental and modelling results, obtained in conjunction with the SSCE, show that radiative effects are important in low–velocity, opposed–flow flame spreading at reduced–gravity. Although in the SSCE the opposing flow is not controlled, because the environment is quiescent, it is, in flame–fixed coordinates, the spread rate. In the DARTFire experiment, which is described in a recently–developed Science Requirements document [8], the fuel surface is subjected to various levels of an external radiative flux, and the flame spreads into a low–velocity, forced–flow boundary layer. Such a configuration will allow determination of those environments that lead during flame evolution to sustained spreading or extinction and development of a clear understanding of the interaction between the flow and radiation fields at reduced gravity.

Unsteady Modelling

More recently, the steady–state model has been extended to include unsteady effects [11,12] that allows flame characteristics to be computed from ignition onward. While the spread rates measured in the SSCE are steady, which is understandable because the flow field around the leading edge of the flame is established by the flame itself and is relatively fixed independent of flame location, the trailing edge of the flame exhibits some unsteady behavior. For DARTFire, the flame spread is inherently unsteady because the flame spreads into a thinning boundary layer in which the flow field changes with flame position.

Conclusions

Results of gas and surface temperature and spread rate measurements in flame spread over a thin cellulosic fuel in a 50% O_2/50% N_2 quiescent environment obtained aboard recent missions of the Space Shuttle show steady spreading, and, when coupled with steady–state modelling, the importance of radiation. Spread rate increases with pressure through the effects of pressure on gas radiation, the optical depth of the lower pressure flames and the attendant heat loss being greater than at higher pressure. Computed results agree with experimental results near the leading edge of the flame, but additional refinement of the model is needed in order to describe accurately the trailing edge of the flame and more accurately the coupling of gas and surface radiative processes. Development of an experiment in which the radiative and flow environment will be carefully controlled is proceeding as well as the development of unsteady flame

spread models.

Acknowledgements

Support for the SSCE effort is provided through NASA contract NAS3–23901 with starting date December 1984, and for DARTFire through NASA contract NCC3–221 with starting date June 1991.

References

1. Olson, S.L. (1991). *Combust. Sci. Technol.* **76**, 233–249.

2. Bhattacharjee, S., Altenkirch, R.A., Olson, S.L., and Sotos, R.G. (1991). Heat Transfer to a Thin Solid Combustible at Zero–Gravity, *Journal of Heat Transfer* **113**, 670–676.

3. Bhattacharjee, S. and Altenkirch, R.A. (1991). *Combust. Flame* **84**, 160–169.

4. Bhattacharjee, S. and Altenkirch, R.A. (1991). *Twenty–Third Symposium (International) on Combustion*, The Combustion Institute, Pittsburgh, pp. 1627–1633.

5. Bhattacharjee, S. and Altenkirch, R.A. (1992). A Comparison of Theoretical and Experimental Results in Flame Spread over Thin Condensed Fuels in a Quiescent, Microgravity Environment, *Twenty–Fourth Symposium (International) on Combustion*, The combustion Institute, Pittsburgh, to appear.

6. Bhattacharjee, S., Altenkirch, R.A. and Sacksteder, K. (1992). Implications of Spread Rate and Temperature Measurements in Flame Spread Over a Thin Fuel in a Quiescent, Microgravity, Space–Based Environment, *Combust. Sci. Technol.*, to appear.

7. Altenkirch, R.A. (1985). Science Requirements Document for the Solid Surface Combustion Experiment, NASA Contract NAS3–23901 Report.

8. Altenkirch, R.A., Olson, S.L. and Bhattacharjee, S. (1992). Science Requirements for the Diffusive and Radiative Transport in Fires Experiment, NASA Contract NCC3–221 Report.

9. Altenkirch, R.A. and Bhattacharjee, S. (1990). *AIAA Prog. Astro. Aero.* **130**, 723–740.

10. West, J., Bhattacharjee, S. and Altenkirch, R.A. (1992). Surface Radiation Effects on Flame Spread over Thermally Thick Fuels in an Opposing Flow," *ASME/AICHE National Heat Transfer Conference.*

11. Bullard, D.B. (1992) Modeling Unsteady Flame Propagation over Thermally Thick Solid Fuels in a Microgravity Environment, MS Thesis, Mississippi State University.

12. Bullard, D.B., Tang, L., Altenkirch, R.A. and Bhattacharjee, S. (1992). Unsteady Flame Spread over Solid Fuels in Microgravity, *Committee on Space Research World Space Congress*, also *Advances in Space Research*, submitted.

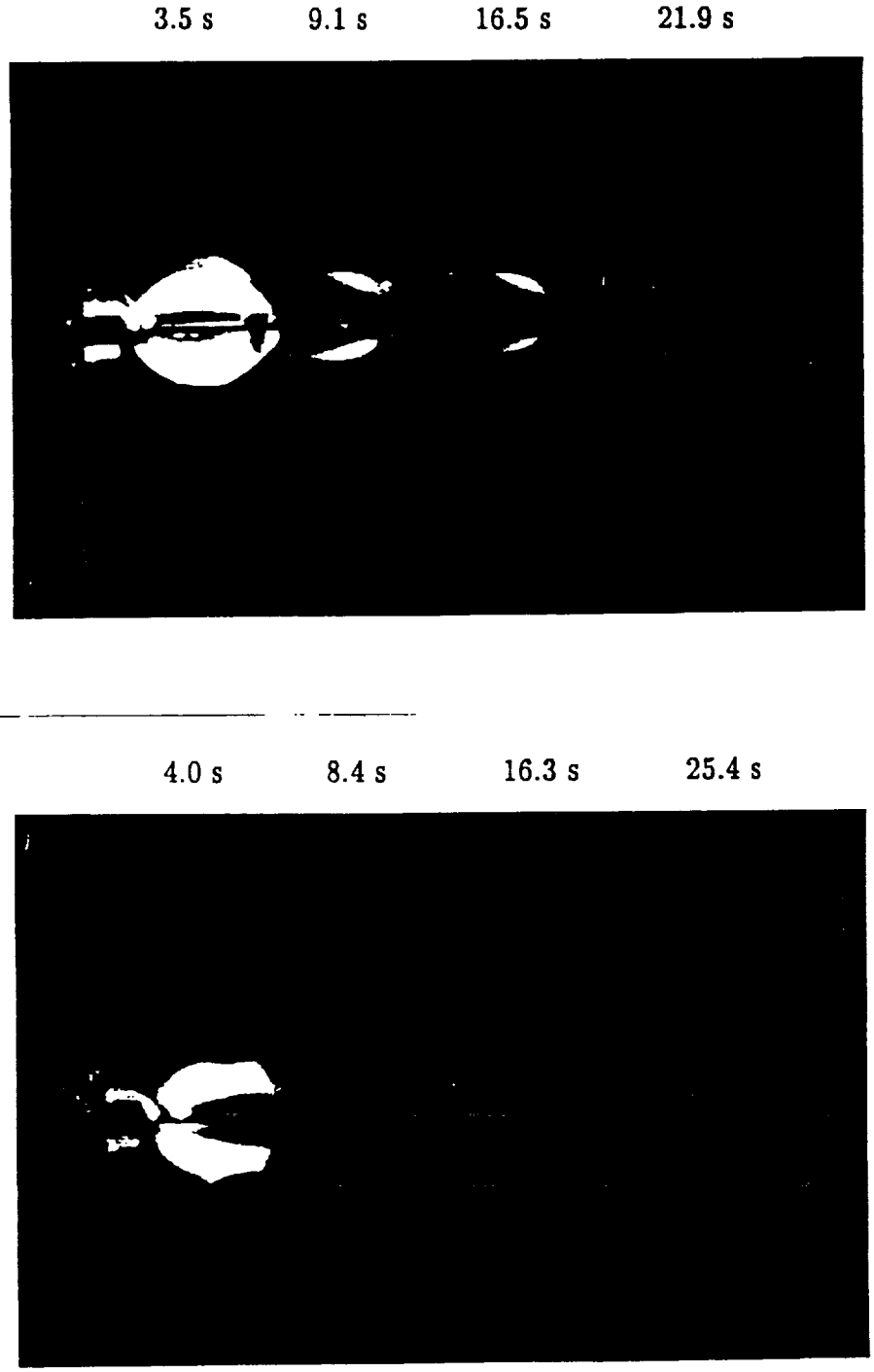

Fig. 1. Four frames from 16 mm film of flame spread over ashless filter paper in the SSCE at 50% O_2 at 1.5 atm (top) and 1.0 atm (bottom). Times are time from the first appearance of a flame–like image on the film.

See Color Plate F-2

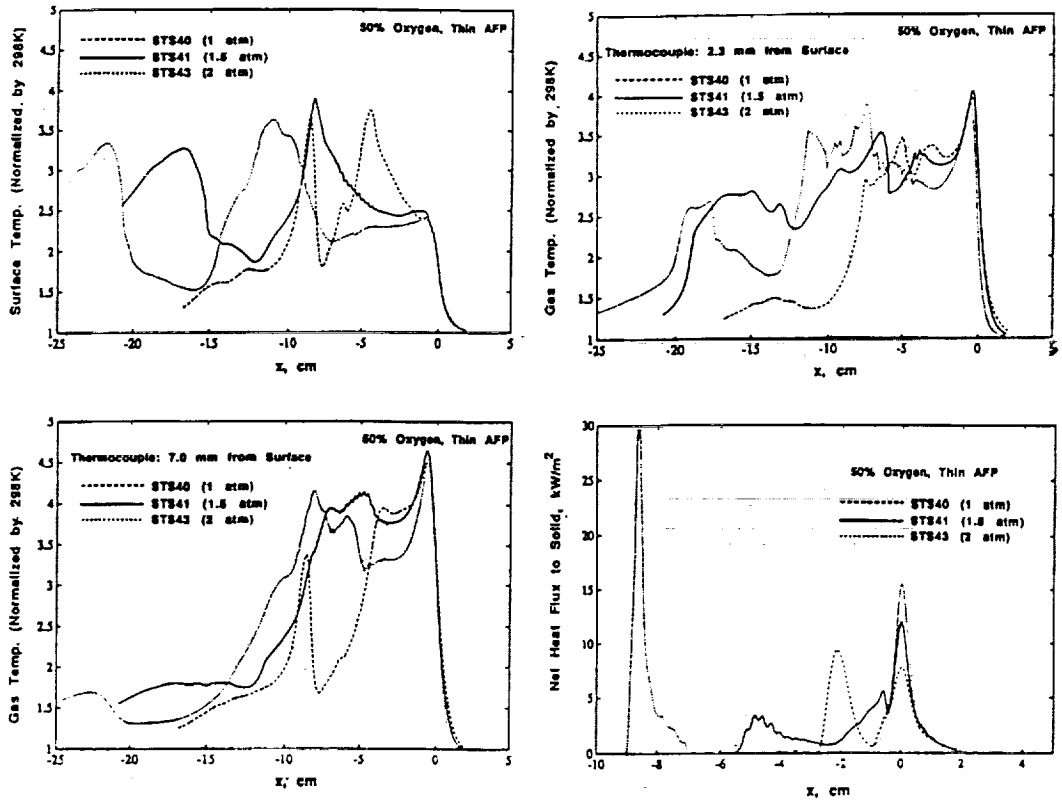

Fig. 2 Measured temperature and heat flux profiles for spread over ashless filter paper in the SSCE at 50% O_2.

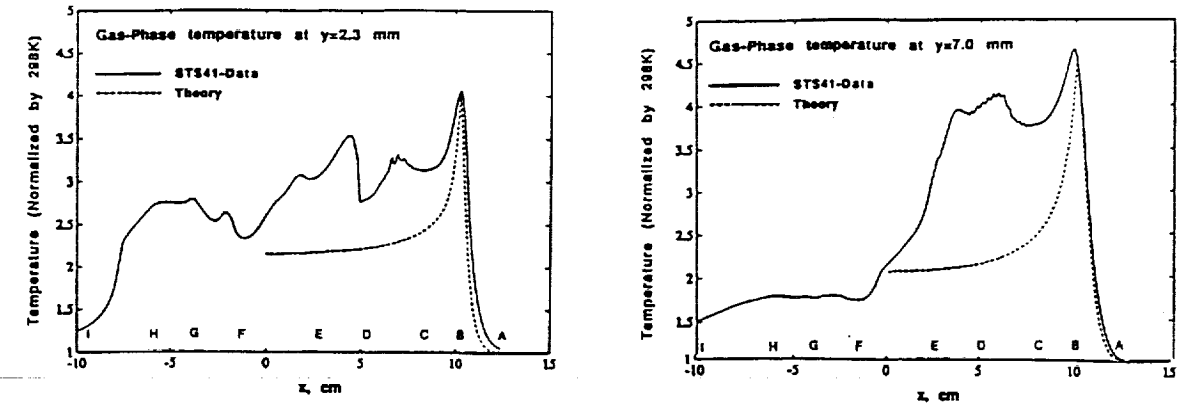

Fig. 3. Comparison between measured and computed temperatures for spread over ashless filter paper in the SSCE at 50% O_2 and 1.5 atm.

COMMENTS

Question (Howard R. Baum, NIST): The role of gas phase radiation in these problems may indeed be important. However, while the local emission can be roughly approximated in a 2-dimensional simulation, the feedback to the condensed phase is inherently 3-dimensional. This is due to the limited width of the fuel sample and the rapid decay of the temperature and combustion product species in the lateral direction.

Answer: Dr. Baum's points are well-taken, and, as he indicates, there are two separate issues to address here. In some earlier preliminary work (1,2), we found that the Planck mean absorption coefficient as defined here is not particularly sensitive to sample width. Values from "two-dimensional" computations, which have a 3-D aspect to them in that lines of sight throughout a 2-pi steradian solid angle are considered in calculating fluxes on the computational domain, do not change much as the sample width is reduced to a range in which we are interested, as long as some physically reasonable temperature and species profiles are used in the lateral direction when radiation loss from the sides of the flame is considered. Consequently, the "two-dimensional" radiation model for the gas-phase emission appears to be a reasonable approximation.

In considering radiation feedback to the surface though, which we have not done here but have rather taken the feedback to balance the surface reradiation, 3-D effects are inherent. While the 2-D model accounts for reasonable overall radiative loss from the gas-phase, the fraction of gas radiation fed back to the surface depends on the details of how the radiation loss though the sides of the flame is treated. We plan to address this inherent 3-D effect in an approximate way in future 2-D computations.

REFERENCES:

1. Altenkirch, R.A. et al. (1991). February through March, NASA Technical Progress Report on NASA Contract NAS3-23901.

2. Bhattacharjee, S. and Altenkirch, R.A. (1991). Three-Dimensional Radiative Effects in Opposed-Flow Flame Spread Modeling, Central States Section Meeting of The Combustion Institute meeting.

COMBUSTION OF SOLID FUEL IN VERY LOW SPEED OXYGEN STREAMS

James S. T'ien,* Kurt R. Sacksteder,† Paul V. Ferkul,* and Gary D. Grayson*
*Case Western Reserve University, Cleveland, Ohio 44106
†NASA Lewis Research Center, Cleveland, Ohio 44135

1. Introduction

In reduced gravity, the combustion of solid fuel in low-speed flow can be studied. The flame behavior in this low-speed regime will fill a void in our understanding of the flow effect on combustion. In addition, it is important for spacecraft fire safety considerations. In this work, modeling and experimental work on low-speed forced-concurrent-flow flame spread are carried out. In addition, experiments on reduced-gravity buoyant-flow flame spread are performed.

2. Low Speed Forced Flow

2.1 Concurrent-Flow Flame Spread Model [1]

The model considers two-dimensional, steady flame spread in concurrent flow over a thin solid. Because of its thinness, the fuel bed can burn through. The flame could therefore reach a constant length provided that a constant (and equal) flame tip velocity, pyrolysis front velocity, and fuel burnout rate, can be obtained in the low-speed concurrent flow environment.

The flame is assumed to be laminar because of its small size and low velocity. The gas-phase fluid mechanical treatment is more comprehensive than most works in the past. In the flame base region (where the upstream flow is seen first), streamwise heat and mass diffusion is included. This, together with finite-rate, gas-phase chemical kinetics, enables us to examine the question of flame stabilization and extinction. The elliptic treatment of this flame stabilization zone entails the full Navier-Stokes equations. On the other hand, to save computational time, a boundary layer approximation is employed in the downstream region. The two zones are coupled at an appropriate gas-phase location. They are also coupled indirectly through the solid by energy exchange. A simplified solid fuel model is used. The solid is assumed to be thermally thin and to pyrolyze according to a one-step Arrhenius law with no char and tar formation. A solid-surface radiative-loss term is included which becomes critically important in the low-speed flammability limit. Because of the coupling between elliptic and parabolic regions and between the gas and solid phases, the numerical solutions require many iterations and are computationally intensive; they are carried out using the Cray X-MP Supercomputer at the NASA Lewis Research Center.

Although the model has been formulated for a mixed forced and buoyant flow, extensive computations have been performed for purely forced flow only, using oxygen mole fraction and free-stream velocity as parameters. Fig. 1 gives all the points calculated and the extinction boundary. Some of the important results are summarized below.

- The extinction boundary consists of a quenching and a blowoff branch similar to those in stagnation-point flow [2] and in opposed-flow flame spreading [3]. The quenching limit is due to the surface radiative loss. Without radiative loss, the model predicts no low-speed limit. Fig. 2 shows the maximum computed flame temperatures. In all cases, the maximum temperature decreases with flow velocity, especially near the quench limit. The flame spread rate decreases monotonically with flow velocity, as expected (Fig.3).

- Flames quench at low speed by shrinking in size. Near-limit flames remain stabilized in the fuel burnout region, as shown in Fig. 4. This fixed stabilization is in contrast to flame blowoff at higher

speed where the flame cannot be stabilized in the fuel burnout region. Extinction is reached when the flame is blown downstream. This illustrates one of the distinctions in flame extinguishment between quenching and blowoff. This difference becomes clear in a two-dimensional analysis but is obscure in one-dimensional stagnation-point flames. The reactivity contours shown in Fig. 4 resemble the visible blue flame seen in experiment (take $w=10^{-4}$ g/cm^3/sec for example), which will be discussed in the next section.

- Using finite-rate kinetics enables us to examine the integrated flux of fuel vapor crossing any vertical plane. Far downstream, the fuel-flux stops changing (because the reaction becomes frozen), providing a measure of fuel escaping the flame. The fraction of fuel not consummed in the flame increases dramatically at lower speeds because of the increased importance of flame-tip quenching. Additionally, the variation of escaped fuel vapor is not monotonic with flow velocity.

2.2 Forced Concurrent Flow Flame Spread Experiments [4]

Low-speed concurrent-forced-flow experiments were conducted at Lewis Research Center's 5-second drop tower using thin tissue paper Kimwipe) as the solid fuel. The relative flow was generated using a sample translation device in a total of twenty-seven drop tests. In these tests, the flow velocity was varied from less than 1 cm/s to 5 cm/s and the oxygen concentration in nitrogen (at normal atmospheric pressure) from 30% down to extinction. Color cine films were made of the flames.

While in most tests the leading edge of the fuel receded steadily as it was burnt following the ignition transient, the downstream flame tip propagation was unsteady. Flames grew in length (after the ignition transient) at higher oxygen concentrations and relative flow velocities, but shrunk at lower concentrations and velocities. In higher-speed flows, in normal gravity, flame length has always been observed to grow after ignition [5]. The shrinking flames observed in these microgravity tests could be quenching, but the slow evolution of the flame length in the 5 second test time did not allow enough time to observe their eventual fate. Alternatively, the small, slowly evolving flames may be indicative of near-steady configurations of flames in very-low-speed concurrent flows. Fig. 6 (the color photos are grouped together) shows a comparison of flames at approximately 5 cm/sec relative concurrent flow at three different oxygen concentrations. The shape of the 15% oxygen concentration case can also be compared favorably with the computed reaction contours (e.g. 10^{-4} g/cm^3/sec) shown in Fig. 4 for the same test condition.

The measured spread rates of the flame base, the leading edge of the fuel at which burnout occurs, are similar to the computed values shown in Fig. 3. However, spread rates at high oxygen concentrations and high relative-flow velocities are lower experimentally at the end of the drop while the rates at low oxygen concentrations and low relative-flow velocities are higher experimentally. These observations are consistent with the suggestion that the flames might not have had sufficient time to reach their final configuration in the available 5 seconds.

A flammability map, based upon the status of flames at the end of 5 seconds of microgravity, has been drawn and is similar to Fig. 1. No detailed comparison can be made because steady flames have not been achieved experimentally. It is clear that even for a thin fuel such as Kimwipes, which provide ample steady flamespread data in opposed-flow configurations, longer microgravity duration is needed to satisfactorily determine flame spread rates and extinction limits in concurrent flow.

3. Buoyant-Flow Flame Spread in Reduced-Gravity Experiments

Flame spread in buoyant flow under reduced-gravitational conditions has been observed using the NASA KC-135 aircraft flying parabolic trajectories at approximately 1/3rd, 1/6th, and 1/10th normal earth gravity levels. The test apparatus includes provisions for controlled ignition energy, color-schlieren flame imaging and three dimensional measurements of the local acceleration levels. Tests were conducted in O_2/N_2 mixtures from 18% oxygen down to extinction (of the same thin Kimwipe tissues used in our other tests) at normal and reduced pressures for upward (concurrent flow) flame propagation; and at normal pressure for downward (opposed flow) propagation.

3.1 Downward Flame Spread and Extinction

Schlieren images of flames spreading in buoyant, opposed flow showed steady propagation in oxygen concentrations below the normal-gravity flammability limit. At each oxygen concentration (18, 16, and 15% oxygen) spread rates decrease with increasing acceleration, though the difference between 1/10th g and 1/6th g is small. Tests conducted at 14% oxygen showed flame propagation at 1/10th g, and a blowoff extinction was observed during the aircraft pullout maneuver to approximately 2g. Flames at higher acceleration levels and 14% oxygen did not appear to survive the ignition transient. Fig. 5 shows a flammability map using acceleration level and normal-atmospheric-pressure oxygen concentration as parameters. The solid line gives the high-g blowoff boundary. The low-g extinction boundary, which cannot be determined accurately in the aircraft experiment, is indicated by the shaded curve. Fig. 7 shows schlieren images of the downward spreading flames at 15% oxygen at two reduced-gravity levels.

3.2 Upward Flame Spread

Schlieren images of flames spreading in buoyant, concurrent flows show propagation of flames down to normal-atmospheric-pressure oxygen concentrations of 12%, in both 1/6th and 1/3rd g. A single test at 1/10th g did not result in a propagating flame at 12% oxygen, while another at 14% did.

At normal atmospheric pressure, the upward spreading flames were characterized by thermal/flame plumes that become unsteady downstream of the flame stabilization zone. The tissue-paper fuel tended to curl, particularly in the normal pressure tests, disturbing the bottom of the flame. Fig. 8 a and b show two parts of an upward propagating flame at 15% oxygen in 1/6th g as they passed by the single schlieren window. In Fig. 8a, the unsteady/unstable plume is shown, while in Fig. 8b, the bottom of the flame is shown stabilized near the lowest point on the fuel surface.

Tests were conducted at reduced pressure and showed the existence of low-pressure limits. In the small number of tests conducted, the pressure limits were not determined with precision. At reduced pressure the flame plumes were more laminar and the fuel deformed more slowly during burning. Fig. 8c shows the downstream plume of a 15% oxygen, 0.5 atmosphere pressure flame at 1/6th g. Below, in Fig. 8d, the stabilized bottom of the same flame is shown.

4. Future Plans

Although surface radiative loss is included in the current model and has proven to be important in low-speed flows, gaseous radiation has been neglected. In stagnation point flow, gas radiation is found to alter the low-speed quenching limit for one-dimensional stationary flames. In concurrent flow gaseous radiation is likely to be more important because the flame is longer. Comparison with experiment also shows that without gas radiation the model overpredicts the flame length. The inclusion of gaseous radiation in the model is the logical next step and will complete our understanding of radiative effects on flame spreading over solid fuels in low speed flows. At the same time thermally-thick solid fuel needs to be treated in the theory (presently, we have dealt with thermally-thin fuel only). The new elements that need to be added will include solid-phase heat transfer, fuel geometry change and an unsteady flame growth process.

Experimentally we will also begin to test thicker fuels in low-speed flows. Because of the limitations of microgravity time in ground-based facilities, steady state is not expected, even were burnout possible. In order for the results to be useful, a controlled ignition process will be extended to thick fuels. The ignition transient experiments and related modeling will lead to a rational design of a space-based experiment required to obtain concurrent-flow flame spreading data in the very low-speed regime.

Because of the flammability limit data we have obtained for both low-speed forced flow and buoyant flow in reduced gravity, we also hope to contribute to the reevaluation of flammmability test methods for spacecraft materials.

REFERENCES

1. Ferkul, P. V.: A Model of Low-Speed Concurrent-Flow Flame Spread over a Thin Solid Fuel, Ph.D. Thesis, Department of Mechanical and Aerospace Engineering, Case Western Reserve University, Cleveland, Ohio, expected October 1992.

2. T'ien, J. S., Combustion and Flame, 65, 1, pp. 31-34 (1986).

3. Olson, S. L. Ferkul, P. V., and T'ien, J. S., 22nd Sym. (Int.) on Combustion, The Combustion Inst., pp. 1213-1222 (1988).

4. Grayson, G. D.: An Experimental Study of Low-Speed Concurrent Flow Flame Spread over a Thin Fuel, M.S. Thesis, Department of Mechanical and Aerospace Engineering, Case Western Reserve University, Cleveland,Ohio (1991).

5. Loh, H. T. and Fernandez-Pello, A. C.: Flow Assisted Flame Spread over Thermally Thin Fuels, proceedings of the First International Sym. on Fire Science, Hemisphere (1986).

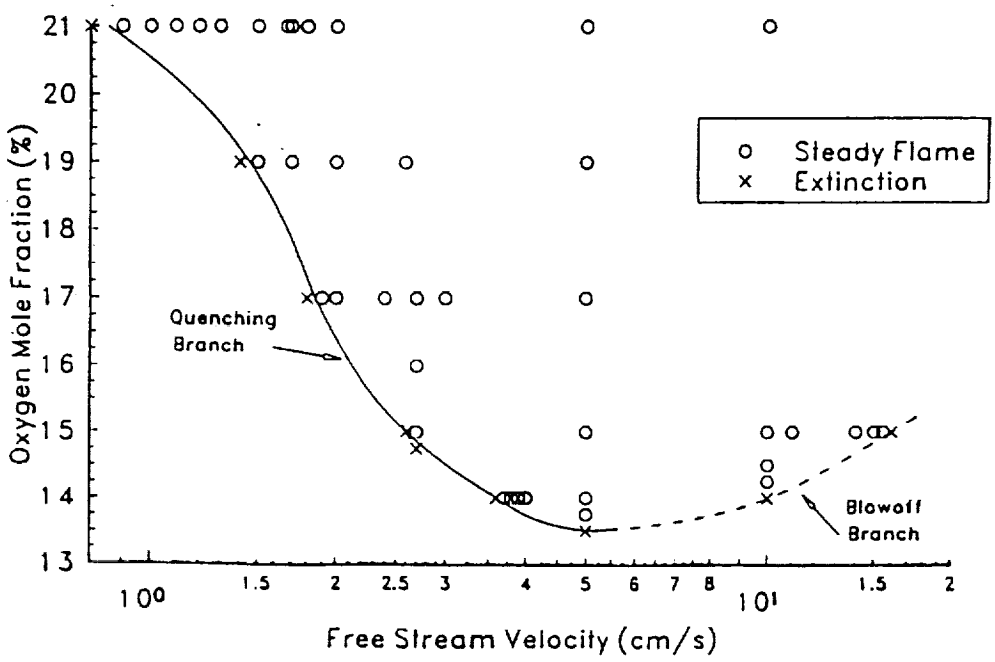

Fig. 1 Extinction Boundary of a Thin Solid Fuel in Concurrent Flow

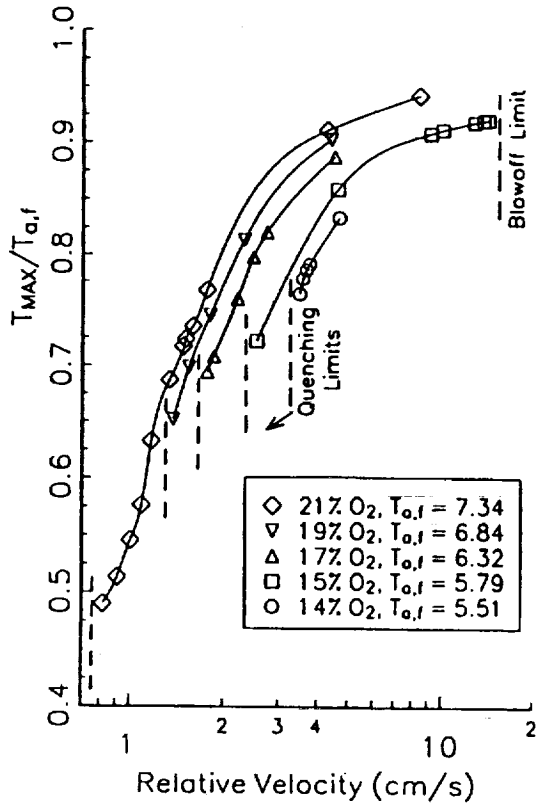

Fig. 2 Maximum Flame Temperature

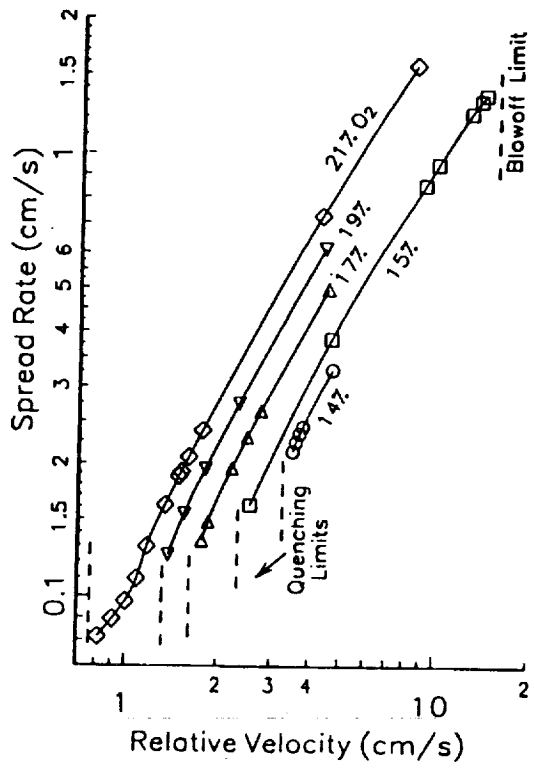

Fig. 3 Flame Spread Rate

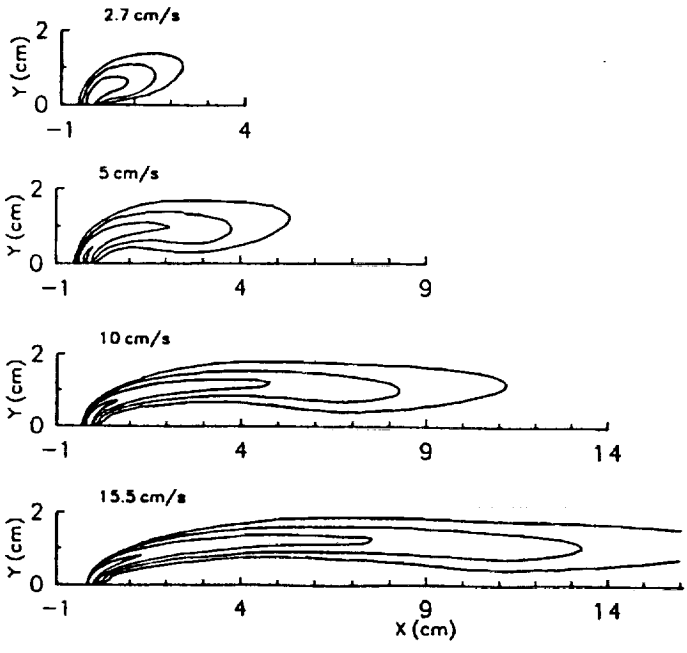

Fig. 4 Reactivity Contours at 15% Oxygen from Quenching to Blowoff (Outermost contour is 10^{-6} g/cm^3/s; a factor of separates contours)

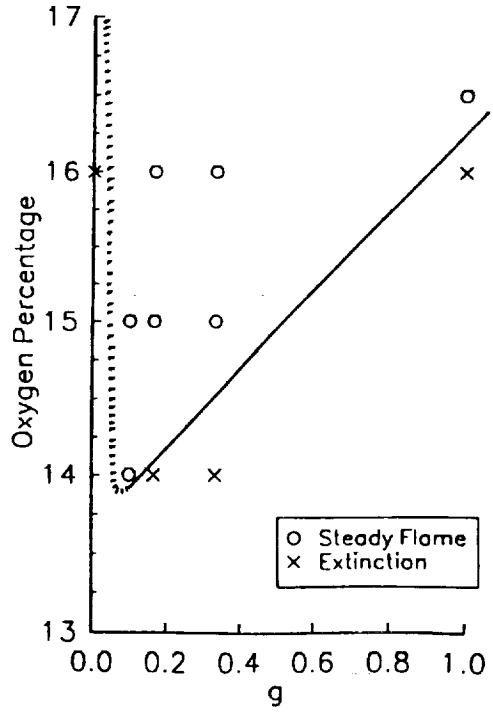

Fig. 5 Extinction Boundary for Kimwipe in Buoyant Opposed Flows (earth: g = 1)

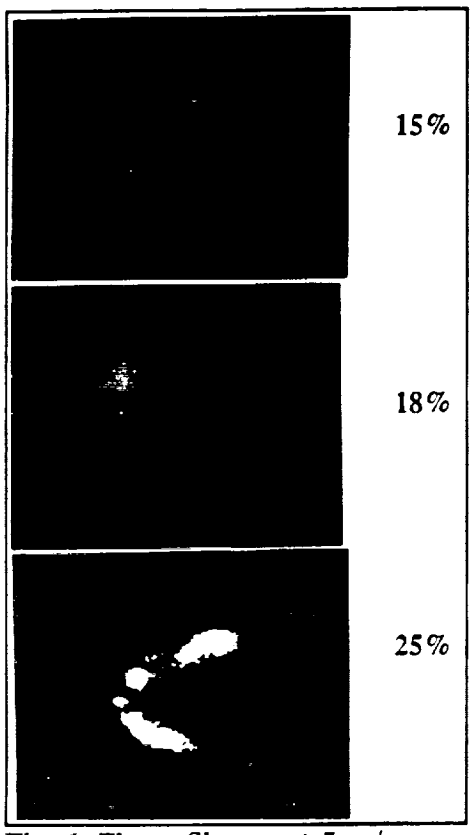

Fig. 6 Flame Shapes at 5cm/sec Relative Concurrent Flow

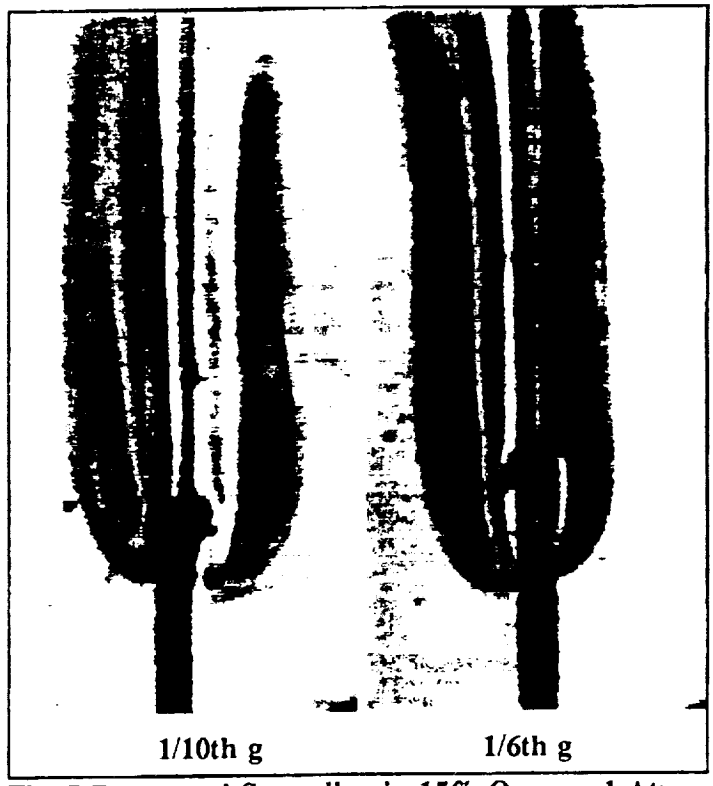

Fig. 7 Downward Spreading in 15% Oxygen, 1 Atm

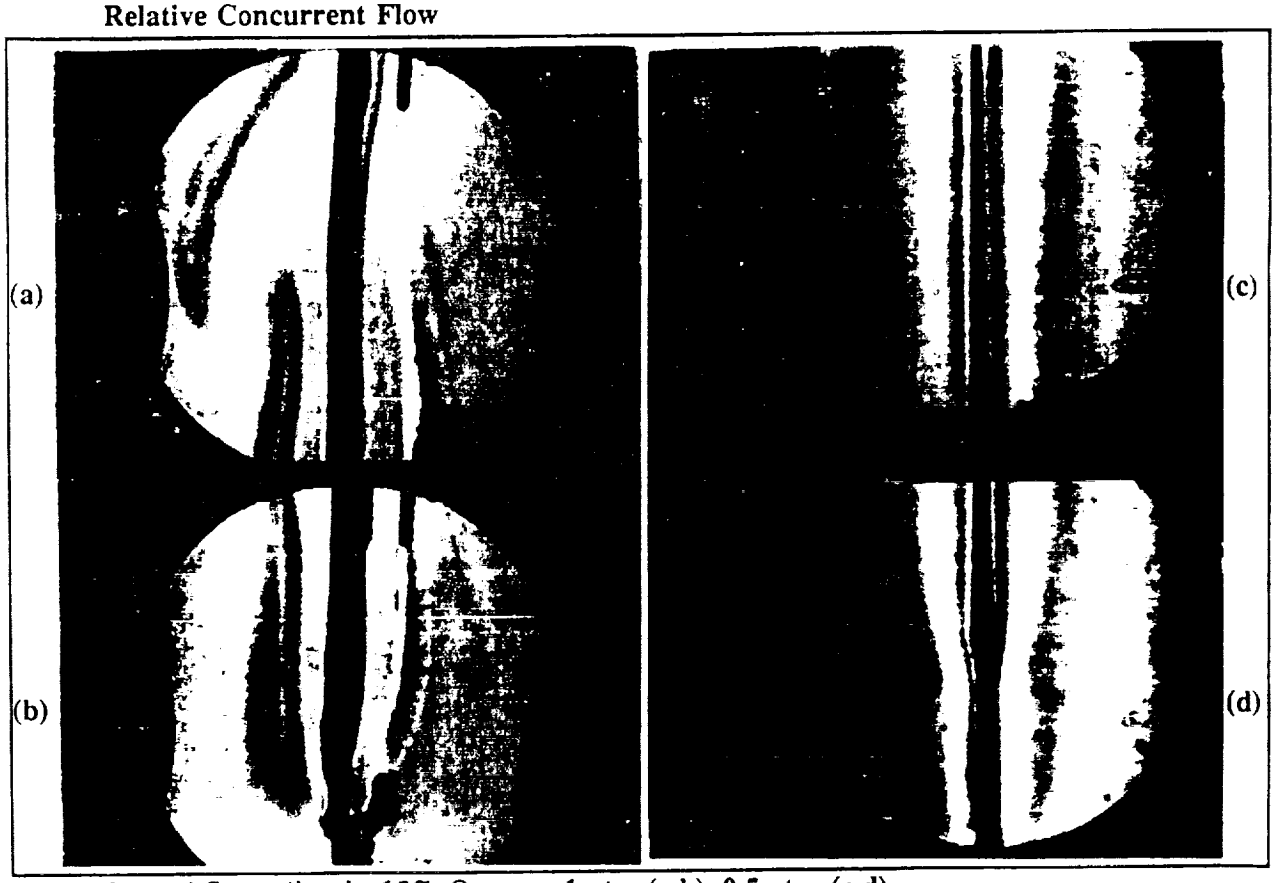

Fig. 8 Upward Spreading in 15% Oxygen, 1 atm (a,b), 0.5 atm (c,d)

See Color Plate F-3

A FUNDAMENTAL STUDY OF SMOLDERING COMBUSTION IN MICROGRAVITY

N93-20208

Carlos Fernandez-Pello, Principal Investigator
Patrick J. Pagni, Co-Principal Investigator
Department of Mechanical Engineering
University of California
Berkeley, California 94720

ABSTRACT

A research program is being conducted to study smoldering combustion in microgravity. The program's final objective is to design and conduct smolder experiments in a space based laboratory, which will complement normal gravity ones, and that will help to: increase the current fundamental understanding of smoldering; predict smolder behavior in a space-based installation; and prevent and control smolder originated, ground or space based, fires.

I. INTRODUCTION

Smoldering is defined as a non-flaming, surface combustion reaction, that propagates through the interior of porous combustible materials. The propagation of the smolder reaction is a complex phenomena involving processes related to the transport of heat and mass in a porous media, together with surface chemical reactions. Smoldering is a weakly reacting phenomena, and generally propagates very slowly. The products of smoldering combustion are, however, often toxic and consequently hazardous. Smoldering can also play an important role in the initiation of unwanted fires because of the potential rapid transition from the slow smoldering reaction to the flaming combustion of the material. Furthermore, smoldering is often difficult to detect and suppress because it may take place in the material interior and the porosity of the material may prevent the access of the extinguishing agent to the reaction zone. Thus, understanding of the physical and chemical mechanisms controlling smoldering is important not only because smoldering is a fundamental combustion process, but because such understanding can be critical to the prevention and control of unwanted fires.

Gravity influences smoldering by affecting the transport controlling propagation mechanisms, the stability of the propagation front, the structure of the porous material and the flow of particulates through the material. Conducting smolder experiments in microgravity will simplify the study of the phenomena by eliminating some of these effects. Furthermore, to date there is no experimental information about smoldering behavior in microgravity. This is important since such information and complementary theoretical

foundation are necessary to asses the fire risk of a space based installation.

The project's overall objective is the understanding and prediction of smoldering combustion under normal and microgravity conditions. This is accomplished by conducting smolder experiments on the ground and in a space based laboratory, and developing theoretical models of the process.

II. RESEARCH PROGRESS

II.1 Normal Gravity Smoldering:

A series of experiments of forced flow smoldering, opposed and forward, have been conducted. In addition to providing information about smoldering, the experiments have the objective of determining the effect of buoyancy in the smolder process. This is accomplished by comparing the experimental results for upward and downward smoldering, and by comparing the data with the predictions of theoretical models of the process. Measurements conducted in these experiments included the smolder propagation velocity and the reaction zone temperature as a function of some of the parameters that affect them. The data are correlated with non-dimensional parameters that are derived from a theoretical analysis of the problem.

The experimental apparatus consists of a square cross section duct containing the fuel and through which the oxidizer gas flows to produce a one-dimensional, forced flow, smolder, and the supporting instrumentation. The test section containing the porous fuel consists of a 0.3 m long vertical duct with a 0.15 m side square cross section. Metered air flows into the test section through a diffuser and a 50 mm long settling section filled with glass beads. All the tests are conducted with 150mm side cubes of open cell, unretarded, white flexible polyurethane foam. The rate of smolder propagation is obtained from the temperature histories of eight Chromel-Alumel thermocouples 0.8 mm in diameter that are embedded at predetermined positions in the porous fuel with their junction placed in the fuel centerline. The smolder velocity is calculated from the time lapse of the reaction zone arrival to two consecutive thermocouples, and the known distance between the thermocouples. These thermocouples are also used to measure the reaction zone temperature which is characterized by a maximum in the temperature profile.

All the experiments showed that three zones with distinct smolder characteristics can be identified along the foam sample. An initial zone near the igniter where the smolder process is influenced by heat from the igniter, an intermediate zone where smolder is relatively free from external effects, and a third zone near the sample end that is strongly affected by the external environment. The smolder reaction propagation velocity and temperature generally have a direct correspondence and vary in each one of these three zones.

Opposed Smolder: Characteristics results of opposed smolder are presented in Fig. 1, which shows the variation of the downward smolder propagation velocity through the sample length for several representative opposed air flow velocities. Tests were also conducted at other flow velocities, but the results are not presented to avoid crowding of the figure. The data is the average from five tests, and the error bars describe the maximum deviations from the mean. These data plus other obtained with different foam lengths, initial temperature and orientation are correlated in Fig. 2 in terms of a non-dimensional smolder velocity that is derived from a theoretical analysis of the problem previously developed under this grant. The analysis basically balances the energy needed to heat the foam to the smolder temperature and the energy generated by the smolder reaction, which is assumed to be in thermodynamic equilibrium. By assuming that all the oxygen is consumed at the reaction zone (smolder is oxygen limited), the analysis predicts that the smolder velocity is proportional to the mass flux of oxygen at the reaction zone. The mass flux of oxidizer to the reaction zone is obtained in its turn from an analysis of the mixed, forced and free, flow through the porous fuel. From the correlation of Fig. 2 it is seen that the model predicts well the measurements, except at conditions were extinction or transition to flaming occur. In these limiting conditions solid or gas chemical kinetics play an important role, and the smolder velocity is no longer singly controlled by the oxidizer mass flux. An interesting result of correlating the experimental data with the

model prediction is that the effect of buoyancy can be extracted by simply comparing the pure forced flow and mixed flow correlations. Such comparison shows that buoyancy has an influence over the hole range of velocities tested.

These results point out to a smolder process that is controlled by the competition between the supply of oxidizer to the reaction zone and the loss of heat from the reaction zone. For example analyzing the data in zone II of Fig. 1, it is seen that at very low flow velocities (< 0.5 mm/s) the smolder propagation velocity is very small, indicating the presence of a weak smolder reaction. As the air flow velocity is increased, the smolder reaction velocity first increase, reaches a maximum (at approximately 2.5 mm/s), and then start to decrease. The initial increase in the smolder temperature and velocity is due to the increased supply of oxidizer to the reaction zone which enhances the heat production, as predicted by the model. As the air velocity is increased further, the heat generated at the reaction and the convective heat losses eventually balance each other and the smolder reaction velocity reaches a maximum. If the air flow rate is increased even further the heat losses overcome the heat generation and the smolder temperature and velocity start to decrease. For air flow rates larger than 2.8 mm/s, the heat losses dominate and cause the weakening and final extinction of the smolder reaction. The above discussed controlling mechanisms also apply to the other two zones, although the external effects modify somewhat the balance between them.

Forward Smoldering: The measurements show that in this type of smolder, as the flow velocity is increased the smolder velocity increases but the reaction temperature decreases, regardless of the sample location. These trends are the result of the hot post-combustion gases being convected ahead of the smolder front. Although they preheat the virgin material downstream of the reaction favoring the propagation of the smolder reaction, they also dilute the oxidizer ahead of the reaction weakening it and reducing its temperature. The smolder velocity data are also correlated well with the predictions of a theoretical model of this mode of smolder. For upward smoldering, transition to flaming was observed to occur in the char at the zone closer to the sample end and for air velocities of 15 mm/sec or larger. Comparison between upward and downward smoldering also showed that the effect of gravity takes place for air flow rates smaller than 3 mm/sec.

Transition to Flaming: Experiments are currently being conducted to study smoldering in the presence of a gas/solid interface, and the phenomenon of the transition to flaming. The experiments are conducted in a test facility that includes a small scale combustion tunnel and the supporting instrumentation. The tunnel test section is 0.61m long with a cross section 0.15m wide and 0.07m deep, and is vertically oriented. Pre-metered compressed air flows through a settling chamber and a converging nozzle prior to entering the test section. Foam samples with a 0.15m side square cross section and with variable lengths are mounted flush in one of the test section walls. A flat type igniter is mounted in the upstream end of the fuel sample. The experiments show that transition to flaming is very sensitive to sample size, probably because of heat losses to the surrounding ambient. Samples with lengths smaller than 0.15m showed a smolder reaction that would propagate upward at an increased velocity, and that would became hotter and produce considerable amounts of smoke, but that eventually would extinguish itself apparently because of the dilution of the available oxidizer by the post-combustion gases. For samples larger than 0.15 m and at relatively low flow velocities (of the order of 0.3 m/s), transition to flaming is consistently observed initially in the upper part of the foam near the interface, after which the whole sample is rapidly involved in flames and burns completely. A parametric study is currently being conducted to study the mechanisms controlling the transition to flaming.

II.2 Ground Based Microgravity Smoldering:

A series of smolder experiments were conducted at the NASA LeRC 2.2 seconds drop tower to observe trends in the ignition characteristics of the foam, and to attempt to infer how smoldering will behave in microgravity. The parameter analyzed was the time derivative of the smolder reaction temperature, because the temperature itself, or the smolder velocity, do not change enough in 2.2 seconds to observe significant differences. The temperature gradients measured in the foam ahead of the reaction zone

showed that microgravity favors the initial heating of the virgin fuel by the smolder reaction, and that the upper range of flow velocities at which buoyancy plays a significant role on smoldering is around 3 mm/s, in approximate agreement with the normal gravity experiments.

A series of opposed flow, downward and upward, smoldering experiments were also conducted in a NASA KC-135 aircraft (30 s of micro-g for up to 40 parabolas) to observe the effects of the variation of the gravity on the smolder process. The experimental apparatus is a small scale version of that described in the normal gravity forced flow experiments. Although the microgravity period was too short to study steady smoldering in micro-gravity, the tests provided initial information about the process and permitted the observation of smolder trends as the gravity changes. The tests also complement the Drop Tower tests summarized above. As with those tests, the variation of the smolder reaction temperature with time was the parameter used to infer the effect of gravity on the smolder process.

A characteristic example of the measurements made is given in Fig. 3, where the variation with time of the temperature in the three zones of the foam identified above (near igniter, middle, and free end) is plotted together with the gravity level variation. The results show that buoyancy affects the temperature differently according to the location of the measurement with respect to the reaction zone. In the virgin foam ahead of the reaction zone and in the char behind of it, the temperature increases as the gravity is reduced, but the opposite is observed around the reaction zone. This indicates that buoyancy affects both the species transport and transfer of heat to and from the reaction zone. At the reaction zone the former is dominant, which results in a decrease of the smolder temperature in microgravity. Away from the reaction zone the latter is dominant and the temperature increases due to the lack of convective cooling. All these effects are less noticeable as the flow velocity is increased, and as the reaction propagates toward the sample interior confirming that buoyancy is important at low flow velocities and near the sample ends.

II.3 Space Based Experiment:

Work on this aspect of the program has included the design of a small scale smolder experiment that was successfully carried out in the glovebox in Spacelab on USML-1, during the June 25 - July 11, 1992 mission of the Space Shuttle Columbia, and the preparation of the Science Requirement Document and Conceptual Design Review for a larger scale space based experiment to be conducted in the mid-deck or one of the gas-cans of the Space Shuttle in the mid-nineties.

The glovebox experiment hardware consists of four modules each containing an instrumented fuel sample, with an embedded igniter and an internal fan to induce forced convection. The test variables of the experiment are the igniter geometry and the convective environment. Through the use of an axial igniter and a plate igniter, both radial and axial smolder is investigated. For each igniter geometry, a test is conducted with a quiescent environment and with a low velocity flow, for a total of four test conditions. The modules are sealed, lexan boxes, nominally 0.15m by 0.20m, filled with air. A cylinder of open-cell polyurethane foam, 50mm in diameter and 80mm length is positioned in the center of the box. The igniters are resistively heated ceramic elements. The fuel sample is instrumented with 6 thermocouples, located at various positions to measure the smolder reaction temperature and its propagation throughout the sample. The temperature and igniter current measurements are displayed on two digital displays and recorded with a video camera.

Currently we are in the process of analyzing the data from the experiment, and we expect to completed the analysis within the next few months. However, preliminary temperature histories such as that of Fig. 4, which correspond to a test with the axial igniter and the fan on, indicate that although incipient smolder occurred, and seemed to be more intense than in normal gravity, the smolder reaction itself was not self-sustained and did not propagate beyond the vicinity of the igniter. A possible reason for this is that the incipient smolder reaction chokes itself with its own products by diluting the surrounding air. In microgravity, diffusion of oxidizer toward the reaction zone seem to be too slow to counteract this dilution process. Although we believe that for the same igniter conditions the smolder reaction would not propagate

in normal gravity either. we think that this will be due to convective cooling effects and no to chemical reaction effects.

III. FUTURE RESEARCH PROGRAM

The future research program maintains the general guidelines established during the current research program. It contains two major tasks; one that concentrates on the space based experiments; and the other on the ground based experiments, and on the development and verification of theoretical models.

III.1 Ground Based Smoldering Experiments

III.1.1 Effect of Buoyancy on Forced Flow Smoldering

The experiments on the effect of buoyancy on forced flow smoldering will be continued. A parametric study will be made of the influence of parameters such as the fuel type and void fraction, the oxidizer oxygen concentration. ambient temperature and pressure, on the gravity effects. Experiments to study the effects of oxidizer temperature and oxygen concentration will be conducted first. The former will affect the rate of heat losses from the reaction, and the latter the rate of heat release. These are two competing mechanisms that determine the characteristics of the smolder reaction.

III.1.2 Transition Processes in Smoldering

This is a very interesting task of the research program because transition processes such as ignition, flaming and extinction are issues of great importance in the fire safety field. These processes are also interesting as a fundamental combustion problem, and very little information is currently available on them.

The experiments will concentrate initially in the determination of the conditions leading to smolder initiation (or ignition), and to flaming. Smolder ignition is very sensitive to porous fuel type, rate of heat addition, geometry of the experiment and igniter, and temperature, among others, and there is a need to characterize the process. There is also a need to come up with a protocol for the ignition of the foam that is reliable so that an automatized ignition system can be designed for its use in the space experiments. Concerning the transition to flaming, the parametric study currently being conducted will be continued to determine the conditions leading to transition to flaming. As the program progresses drop tower and parabolic flight tests will be planned to study these process under microgravity conditions. Since the characteristic time of the transition process is small (particularly flaming) it is expected that the ground base microgravity experiments will give useful information.

Concurrent with the above experiments, the analyses already developed of forced flow opposed and forward smoldering will be extended to include finite rate kinetics. The objective is to predict those conditions were extinction of the reaction was observed experimentally. The modeling of the transition to flaming both in one-dimensional and smoldering in an interface will also be continued.

III.2 Space Experiments

This task will consist primarily in the interaction with the NASA LeRC engineers in the design and construction of the space based experimental apparatus. Also the data from the USML-1 smolder experiments will be analyzed and compared with the ground data. The results will be used to finalize the design of the large scale space experiments

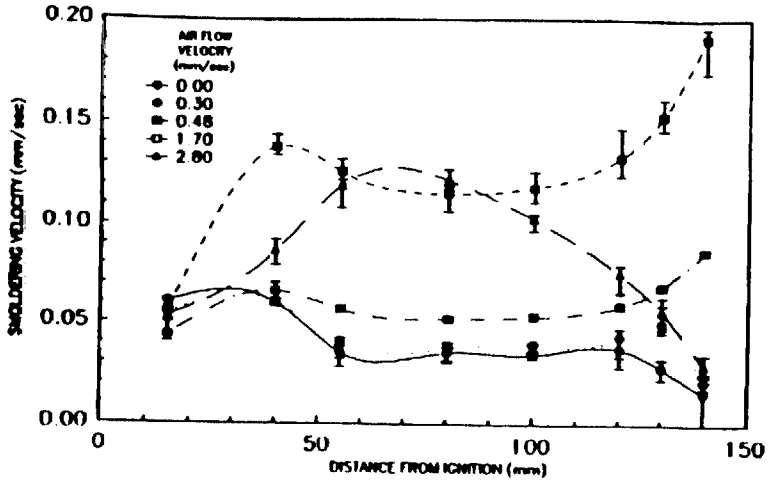

Fig. 1. Variation of the downward smolder velocity along the foam sample for several opposed air flow rates.

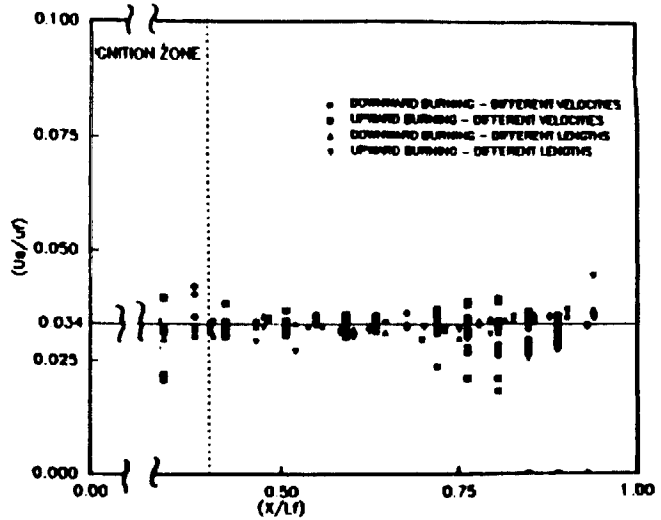

Fig. 2. Correlation of the opposed flow smolder data in terms of the theoretically calculated nondimensional smolder velocity.

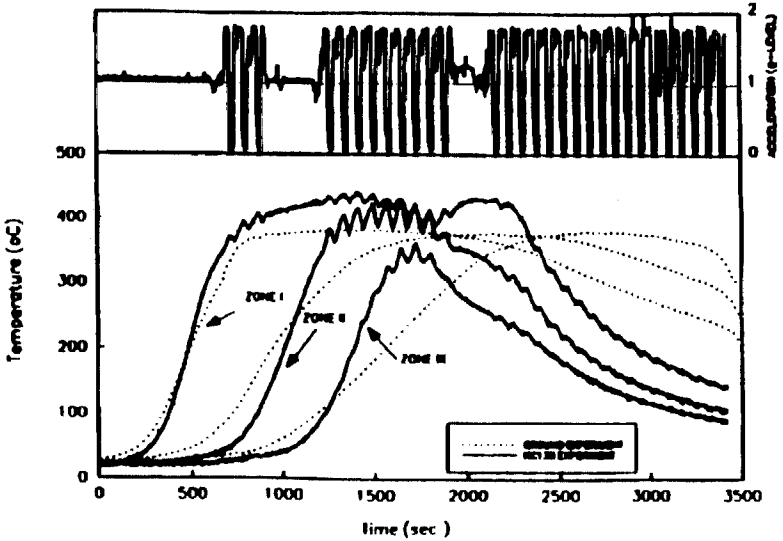

Fig. 3. Foam temperature histories in natural convection, downward smolder from experiments conducted in a KC-135 aircraft (acceleration level is indicated for reference).

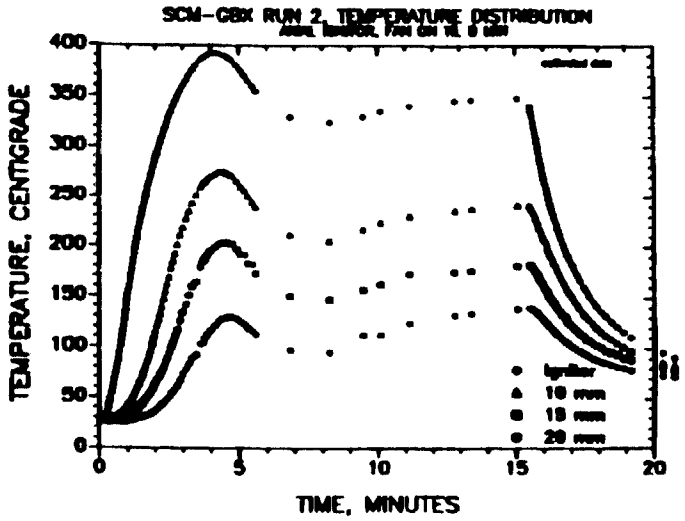

Fig. 4. Temperature histories at several locations of the foam sample from experiment conducted in the USML-1 of the Space Shuttle Columbia.

N93-20209

FLAME SPREAD ACROSS LIQUID POOLS*

Howard Ross (NASA Lewis Research Center), Fletcher Miller (NASA Lewis/Case Western Reserve Unviersity), David Schiller (University of California at Irvine), and William A. Sirignano (University of California at Irvine)

For flame spread over liquid fuel pools, the existing literature [1-9] suggests three gravitational influences: (a) liquid phase buoyant convection, delaying ignition and assisting flame spread; (b) hydrostatic pressure variation, due to variation in the liquid pool height caused by thermocapillary-induced convection; and (c) gas-phase buoyant convection in the opposite direction to the liquid phase motion. No current model accounts for all three influences. In fact, prior to this work, there was no ability to determine whether ignition delay times and flame spread rates would be greater or lesser in low gravity.

Flame spread over liquid fuel pools is most commonly characterized by the relationship of the initial pool temperature to the fuel's idealized flash point temperature, with four or five separate characteristic regimes having been identified [2]. In the uniform spread regime, control has been attributed to: (a) gas-phase conduction and radiation [2]; (b) gas-phase conduction only [10]; (c) gas-phase convection and liquid conduction [11], and most recently (d) liquid convection ahead of the flame [3]. Suggestions were made that the liquid convection was owed to both buoyancy and thermocapillarity. In the pulsating regime, complicated flow structures have been observed in both the gas and liquid phases with circulation around several centers; these flows, were attributed to combined thermocapillary and buoyant effects [1].

Of special interest to this work is the determination of whether, and under what conditions, pulsating spread can and will occur in microgravity in the absence of buoyant flows in both phases. One possible mechanism for pulsating spread in microgravity is if the "premixed gas - diffusive burning" pulsations are due to periodicity between gas-phase conductive and liquid-phase convective control, as suggested in [7]. A second possibility, which will be determined by these investigations, is whether pulsations may be induced in low gravity by the presence of slow, forced, gas-phase, flow.

The approach we have taken to resolving the importance of buoyancy for these flames is: (a) normal gravity experiments with advanced diagnostics; (b) microgravity experiments; and (c) numerical modelling at arbitrary gravitational level.

NORMAL GRAVITY EXPERIMENTS [12]: Most normal gravity flame spread tests were conducted inside a large metal glove box, 1.2 m long x 0.8 m wide x 0.65 m high which served to eliminate drafts from the room. The fuel tray, which was 300 mm long and 20 mm wide, was placed lengthwise in the center of the box and leveled on a platform. By placing aluminum inserts in the tray to raise its bottom, the depth of the tray could be varied from 12.5 mm to 2 mm. The inside walls of the tray were lined with 3 mm thick glass over the entire depth and length to reduce heat losses to the walls (the tray was 20 mm wide with the glass in place). The outer aluminum walls of the tray, as well as the bottom, were hollow, allowing a glycol-water solution to flow between them as a means of heating or cooling the tray. A standard CCD video camera recorded the flame, and the image was later digitized to allow mapping of the flame position vs. time. This semi-automated data conversion technique allowed detailed graphs of flame position vs. time for dozens of runs to be made with relative ease.

Experiments on pool depth effects (where buoyancy might be expected to be important) were carried out between temperatures of 13 °C and 21 °C, at approximately 1 °C intervals. For pools of 1-propanol at T_{Liq} = 17.3 °C, the 10 mm pool shows a slightly higher flame speed than the 5 mm pool (borne out in several runs), and both are well above that shown by the 2 mm deep tray. Furthermore, at this temperature, which is approximately the transition temperature from uniform to pulsating spread, the shallow pool clearly shows regular pulsations, while the others show only small amplitude irregular variations in spread rate. In fact,

* Portions of this paper are reprinted from references 5, 12, and 15.

we found definite, cyclic pulsations at temperatures as high as 18.4 °C for the 2 mm pools, which was thought to be above the transition temperature, but very uniform spread for the deeper pools. This difference in flame spread character with depth provides indirect evidence that there may be a weak liquid phase flow at these conditions that produces pulsations in a shallow fuel layer but yields uniform spread in deeper pools.

Well into the pulsating region, at T_{Liq} = 14.1 °C, all three depths showed regular pulsations, and it is quite clear that the spread rate is dependent on pool depth. Again, the deeper pool shows a higher flame propagation rate, with the difference between 5 mm and 10 mm now somewhat enlarged compared to the 17.3 °C pool. Furthermore, it is clear that the pulsation wavelength is also strongly dependent on pool depth. Deeper pools exhibit much longer wavelength pulsations, in this case 4 pulsations over the 25 cm distance presented for the 10 cm deep pool, compared to 13 for the 2 mm deep pool.

The flame velocity in the "jump" portion of the cycle appears to be constant at about 12.5 cm/sec and therefore not to be a function of the pool depth, while the crawl velocity increased from 1 cm/sec at 2 mm deep to 3 cm/sec for fuel layers 10 mm deep. This indicates that the conditions in the gas phase are similar and controlling *during* a jump. Between jumps, the flame propagation is severely retarded for the shallowest pools, and the flame remains nearly stationary at times. This is most likely due to a hindered development of the subsurface eddy which preheats the liquid enough for the flame to spread further.

As shown by Williams [13], the velocity in the liquid phase, which is of the same order as the flame spread velocity, can be thought of as receiving contributions from both buoyancy and surface tension effects. His scale analysis shows that for shallow pools the dependence of the average flame spread rate should range from between h to h^3, depending on whether the dominant driving mechanism is surface tension or buoyancy, respectively (here, h is the boundary layer depth = pool depth for shallow pools). Experiments in which depth effects were reported only showed dependence from $h^{1/3}$ [9] to at most h [14]. While conceding that more than three depths should be studied to reliably establish a trend, the three depths we used indicate a linear dependence of average flame velocity on depth in the pulsating regime, and a less than linear dependence in the uniform regime. As noted above, there is no depth dependence on the jump velocity; the linearity arises from the increase in crawl velocity with depth. From this it seems that surface tension is the primary driving mechanism in the flow, with liquid-phase buoyancy of lesser importance than is attributed to it in Ref. 3. Further support for this conclusion is that, for shallow or deep pools, no one has witnessed anything approaching a cubic dependency, or even a higher than first-order dependency, on depth.

The pool depth has a strong effect on the pulsation wavelength, but there is no easily discernable temperature dependence. The depth effect may be due to a limitation imposed by the bottom on the size of the liquid circulation zone that slightly precedes the flame leading edge. This zone cannot fully develop in the shallow pools, and the flame catches up more rapidly. Drag on the bottom may also slow down this flow during each cycle, leading to more frequent pulsations but a lower overall velocity. This explanation is consistent with numerical predictions of more frequent pulsations for increasing values of liquid viscosity and/or decreasing surface-tension coefficient [6]. For the 2 mm deep pool, surface deformation may also be significant [8] and lead to the formation of roll cells; these cells could be the cause of the depth effect on pulsation. Future work is needed to resolve the subsurface flow in shallow fuel pools and to confirm this hypothesis.

Recently [15] we examined the temperature field using rainbow schlieren deflectometry (RSD) and the velocity field using particle image velocimetry (PIV) for uniform and pulsating flame spread using propanol and butanol as fuels. The RSD and PIV were recorded with standard CCD video cameras and S-VHS video recorders. The particle tracks, obtained using an 840 nm laser diode light sheet and 12 micron pliolite particles, on the video record were digitized, color coded, and time-averaged to assist analysis.

Figure 1 is a 35 mm still photograph, taken off the video records, of the RSD visualization of the refractive index gradients observed ahead of a left-to-right spreading flame in the pulsating regime. Figure 2 shows

a 35 mm still photograph superposing 10 consecutive frames to reveal a 0.33 sec time-lapse picture of the flow field for the same conditions; in this case the flame moves from right-to-left. In order to determine the direction of the particle movement, the first frame was color coded red and the last frame was color coded blue; a gradual transition between the two was then performed on intermediate frames. The initial initial frame corresponds to when the flame was just visible on the right side of the photograph. Figure 2 suggests that the flow ahead of the flame has multiple, counter-clockwise rotating, centers.

In comparing figs. 1 and 2, notice that the flow penetrates to the full depth of the pool, unlike the temperature field. Thus, as might be expected, the use of methods responding to *thermal* variations, such as RSD or interferometry, to infer the *flow* patterns, can be misleading. From the video records, the flame position never surpassed a surface location of elevated temperature indicated by the color change along the surface. These results are consistent with the findings of Ito et al [3] who used holographic interferometry to determine the temperature field. The distance at which surface flow is seen ahead of the flame exceeded that of the temperature field. The set of measurements implies that the flame advances only to that position where the surface temperature rises to the flash point; however, the flow head clearly surpasses this location and the flame's leading edge throughout the pulsating spread cycle, consistent with the conclusions of refs. 6-7.

Similar measurements were made in the uniform spread regime. The RSD indicates elevated liquid temperatures penetrate less distance both into the pool depth and ahead of the flame. The PIV also shows liquid-phase convection does indeed exist a short distance ahead of the flame. Most likely then convection is the dominant heat transfer mechanism all the way to the flash point even in the uniform spread regime, a conclusion which is consistent with ref. 3.

MICROGRAVITY EXPERIMENTS [5,12]: We performed a series of normal and microgravity (μg) experiments in the NASA Lewis 5.18 second Zero Gravity Facility. A 15 cm diameter, 1 mm deep tray was mounted inside a 113 liter pressure vessel for both safety purposes and to permit the oxygen concentration to be varied. The base of the tray was machined from ceramic material to minimize heat losses and ease ignition from a small nichrome, electrically-heated wire (250 μm diameter) cantilevered over the tray. To provide a reproducible fill level, and to minimize pre-drop evaporation, the pool was filled by gravity just before the drop. Multiple safety systems were employed as described below. The sole instrumentation was top and side view cameras, operating at 24 f/s and 50 f/s, respectively, and a thermocouple to determine the initial system temperature. The slow speed of the cameras was required due to the low luminosity and thinness of the flame. Following the test, the flame spread rate was determined from the visible flame diameter as a function of time through the use of a digitized motion analyzer.

A major problem with μg, fluid experiments is the control of the liquid surface, whose shape is determined by a balance of gravitational and surface tension forces, i.e. the static Bond number, $Bo=\rho^* g^* l^2/\sigma$, where ρ is the liquid density, g is the gravitational acceleration, l is the characteristic vessel dimension, and σ is the surface tension. For propanol, Bo, based on a 7.5 cm radius, is about 1800 in normal gravity and 0.0018 in microgravity. As such, the liquid surface transitions from a "flat" configuration in normal gravity to one of constant curvature, related to its contact angle. Scale analysis and drop tower experiments in both the 2.2 sec and 5 sec facilities were performed in partially and completely filled cylinders to estimate the transition and settling time. For simple comparison to normal gravity results and due to the limited μg time, the surface curvature and transition time needed to be minimized. The use of very shallow (1.6 mm) pools in completely full trays provided such minimization; also the contribution to spread of gas-phase buoyancy was isolated by a comparison of normal and microgravity flame spread characteristics.

Although the leading edges were virtually identical in appearance, the trailing shape of the microgravity flame was nearly parallel to the pool surface, indicating the suppression of buoyancy. For conditions where the corresponding normal-gravity flame spread was uniform, the microgravity spread was also uniform, at rates comparable to the normal gravity flames. The similarity of normal and microgravity spread in the uniform regime indicates that (a) buoyancy-driven motion in either phase had no influence on uniform flame

spread, (b) radiation effects on spread were probably small for this scale experiment (the large change in flame height made no difference), and therefore (c) liquid conduction, gas conduction or thermocapillary-induced liquid motion were the controlling parameters. Normal gravity results described above suggest the latter is the controlling parameter.

In contrast, pulsating flame behavior in microgravity, where buoyant flows in both the liquid and gas phases are negligible, was never observed. Instead, independent of O_2 concentration, fuel or diluent type, the initial conditions which gave rise to pulsating flame spread in normal gravity coincided with those causing extinguishment in a quiescent, microgravity environment. In those cases where the flame did spread to the edge of the tray, the microgravity flame subsequently collapsed "bottom-up," i.e. toward the luminous region farthest from the pool, until the remaining flame was very thin and blue at a distance of 10-15 mm from the pool surface. After this collapse, the flame lifted very slightly away from the pool, and its luminosity steadily diminished, disappearing at low O_2 concentrations before the end of the test.

In a second series of microgravity tests, the fuel tray was changed from being circular to a trough with dimensions 15 cm x 2 cm x 1 cm deep. In this case 1-butanol in air and 1-propanol in 17% O_2 were used as the fuels, since they produce pulsating flames at room temperature. To test whether the extinction condition can be changed and whether pulsating spread can occur in the presence of a forced air flow in microgravity, a series of tests was conducted with a fan providing a slow, opposed flow of 10-25 cm/sec, as measured with a TSI hot wire anemometer. *This flow regime is inaccessible in normal-gravity flame spread due to the induced buoyant flows.* Initial experiments confirmed that the change of tray geometry from a shallow, axisymmetric pool to a deep, linear pool did not affect the previous conclusions regarding microgravity flame spread behavior under quiescent conditions: the aforementioned pulsating/extinction and uniform/uniform correspondence was maintained in the new pool when comparing normal/microgravity behavior. However, with the opposed air flow the flame was sustained in microgravity where under quiescent conditions it had extinguished. This agrees with studies of microgravity flame spread over solids, in which slow, opposed flow lowers the limiting oxygen index [16]. Unlike solids though, the flame stand-off distance remained immeasurably close to the pool surface until extinction. For solids, surface re-radiation has been cited as contributing principally to the extinction [17] , but the low surface temperature of the pool makes this an unlikely mechanism. These differences suggest that other factors, perhaps gas-phase radiative losses [16], conductive losses to the environment or the pool [6], and/or low oxygen transport rates [18], are contributing to flame extinction of liquid pools in microgravity.

The character of the flame spread with opposed flow was unsteady, and to some extent pulsating, with the frequency of the pulsations comparable to those observed in normal gravity. It was determined that the fan swirl was also approximately of this frequency (no flow straightener was used), so a definite statement that classical pulsating spread was observed is not yet justifiable. The flames appeared very responsive to the air flow; when the air flow weakened, so did the flame, to the point that it nearly extinguished. Therefore, the tests showed conclusively that the flame spread behavior was tied to the air flow, furthering proof that subflash microgravity flame spread is not controlled entirely by liquid convection.

NUMERICAL MODELLING: Our recent computational studies have addressed unsteady, axisymmetric and planar open pool configurations. The transient numerical model uses the SIMPLE algorithm [19] with the SIMPLEC modification [20]. This method uses primitive variables (u, v, p, h), a staggered mesh, and the hybrid-differencing scheme. The continuity equation is satisfied by solving the pressure-correction equation in the SIMPLE algorithm. A "phase-split" solution technique is used in that the gas and liquid phases are solved separately. At the gas/liquid interface, Dirichlet-type boundary conditions from the solution of the liquid phase are used for the solution of the gas phase, while Neumann conditions from the gas phase are used for the upper boundary of the liquid phase. Accurate modelling of the reaction zone requires a fine numerical mesh not only in the reaction zone itself, but also in the region between the reaction zone and the liquid surface (to predict accurately the liquid surface heating ahead of the flame). In order to save computer time, a partially-adaptive grid scheme is used to move the fine mesh region along with the spreading flame in the radial direction. Convergence of the governing equations is optimized

by underrelaxation and extra iterations of the pressure-correction equation.

The effects of blackbody radiation, surface tension, gravity level, variable density and thermophysical properties, vaporization, and finite-rate chemical kinetics are included in the computational model. Infinitely-fast chemical kinetics (i.e., the flame sheet approximation) cannot be assumed because the flame leading edge is premixed. The model assumes that the liquid surface remains flat and horizontal at all gravity levels. Solutocapillary forces and recession of the liquid surface due to vaporization are neglected.

It is predicted that at normal gravity, the temperatures in the reaction zone are generally higher and the reaction zone thinner than at microgravity. The flame standoff distance is slightly smaller at normal gravity than at microgravity, but the reason for this is not as clear as with flame spread over solids. Without the effects of surface tension, flame spread rates decrease with increasing gravity level. When surface tension is included, flame propagation is either uniform or pulsating depending on the gravity level and initial pool temperature.

Pulsating spread of the precursor flame in front of the main body of the diffusion flame is caused by the formation of a recirculation cell in the gas phase in front of the flame leading edge (see Figure 3). This recirculation cell is formed by a combination of opposed flow in the gas phase due to buoyancy and concurrent flow in the liquid phase due to thermocapillary forces. At microgravity, a recirculation cell may still form in front of the flame leading edge solely due to the surface-tension-driven shear flow. However, the strength of this recirculation cell is relatively weak compared to that at normal gravity. Therefore, periodic flame pulsations are not predicted at microgravity.

Hot gas expansion plays a significant role in the flame pulsation process by causing the periodic destruction of the gas-phase recirculation cell. Large hot gas expansion velocities oppose the flow of fresh oxygen to the reaction zone. Both a lack of oxygen due to the hot gas expansion and quenching by the liquid surface leads to the extinguishment of the precursor flame. When hot gas expansion is not included in the simulations, small backward and forward pulsations of the precursor flame still occur at normal gravity due to the presence of the recirculation cell in front of the flame leading edge. However, the recirculation cell structure remains intact throughout the pulsation cycle, and the precursor flame is extinguished due to quenching by the liquid surface.

The presence of both opposed flow (e.g., due to buoyancy) and concurrent flow (due to thermocapillarity) in front of the flame is required for periodic flame pulsations to occur. Since the flame spread rate increases with initial pool temperature (due to a larger concentration of fuel vapor in the gas phase), the region of liquid surface heating ahead of the flame decreases. Without appreciable liquid surface flow ahead of the flame, a recirculation cell does not form in front of the flame leading edge; therefore, flame pulsations do not occur for initial temperatures near the flash point.

FUTURE WORK: Numerical simulations to date have used fuel properties of n-decane. In the future, alcohols such as methanol will be simulated to help explain the fundamental differences in flame spread characteristics between hydrocarbon and alcohol fuels. The effects of gas-phase radiation and diluent type will also be investigated.

In normal gravity experiments, we will continue to perform flow and temperature field visualization studies for several pool sizes over a range of temperatures. In addition we plan to do rocket-based microgravity experiments. The three principal areas will be: a. The effects of deeper and longer pools; b. the effects of small levels of forced gas-phase flow, both opposed and concurrent, in both the uniform and pulsating spread regime; and c. the effect of fuel type on flame spread.

REFERENCES

1. Glassman, I. and Dryer, F.: Fire Safety Journal 3, 123 (1980/81).
2. Akita, K.: Fourteenth Symposium (International) on Combustion, p. 1075, The Combustion

Institute, 1973.
3. Ito, A., Masuda, D., and Saito, K.: Comb. Flame 83, 375 (1991).
4. Matsumoto, Y. and Saito, T.: Transactions of the Japan Society of Mechanical Engineers 46(B), 998 (1980) (in Japanese).
5. Ross, H. and Sotos, R.: Twenty-Third Symposium (International) on Combustion, p. 1649, The Combustion Institute, 1990.
6. Schiller, D., and Sirignano, W.: "Ignition and Flame Spread Above Liquid Fuel Pools," Fall Meeting of the Western States Section of The Combustion Institute, Paper No. WSCI 91-96 (1991).
7. Di Blasi, C.: Twenty-Third Symposium (International) on Combustion, p. 1669, The Combustion Institute, 1990.
8. Torrance, K., and Mahajan, R.: Comb. Sci. Tech. 10, 125, (1975).
9. Mackinven, R., Hansel, J., and Glassman, I.: Comb. Sci. Tech. 1, 293 (1970).
10. Glassman, I., comments in Akita, K., in *Fourteenth Symposium (Int'l) on Combustion*, Combustion Institute, Pittsburgh, PA, pp. 1075-1083, (1973).
11. Hirano, T., Suzuki, T., *Combust. Sci. Technol.*, 23: 215-224 (1980).
12. Miller, F. and Ross, H.: Twenty-Fourth International Symposium on Combustion, p. TBD, The Combustion Institute, 1992.
13. Williams, F.: Combustion Theory, 2nd ed., p. 515, Benjamin/Cummings, 1985.
14. Burgoyne, J. and Roberts, A.: Proc. Roy. Soc. A 308, 55 (1968).
15. Miller, F. and Ross, H.: "Liquid-Phase Flow and Temperature Field Measurements of Flame Spread over Laboratory-Scale Alcohol Pools" submitted to the Western States Section Fall, 1992 Meeting of The Combustion Institute.
16. Olson, S., Ferkul P., and T'ien, J.: Twenty-Second Symposium (International) on Combustion, p. 1213, The Combustion Institute, 1988.
17. Altenkirch, R. and Bhattacharjee, S.: AIAA Prog. Astro. Aero. Sci. 130 (1990).
18. Olson, S.: Comb. Sci. Tech. 76, 233 (1991).
19. Patankar, S. V., Numerical Heat Transfer and Fluid Flow, McGraw-Hill, New York, 1980.
20. Van Doormaal, J. P. and Raithby, G. D., "Enhancements of the SIMPLE Method for Predicting Incompressible Fluid Flows, "Numerical Heat Transfer, Vol. 7, pp. 147--163, 1984.

FIGURE 1: RSD Visualization of a butanol-air flame at 23 C. Flame spreads from left to right. The pool depth is 1 cm.

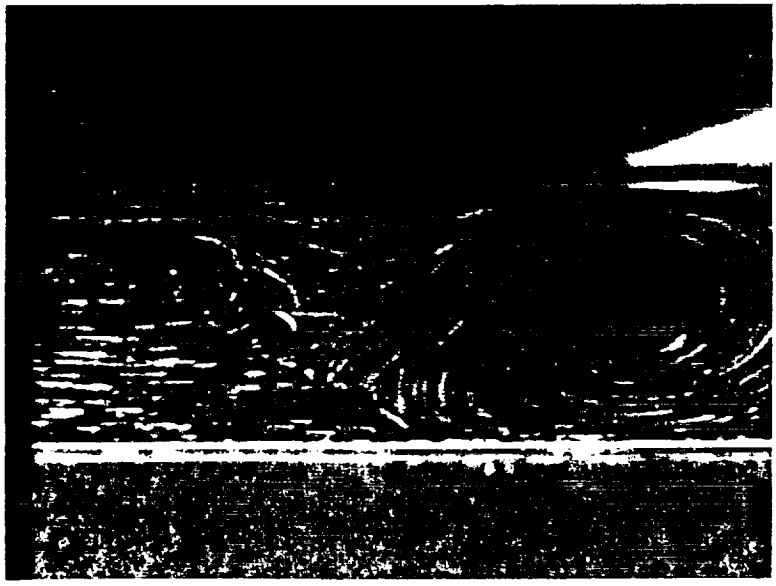

FIGURE 2: PIV of a butanol-air flame at 23 C. Flame spread is from right to left. Time lapse is 0.33 sec. Pool depth is 1 cm; note that the field of view of this picture is different than that of Figure 1.

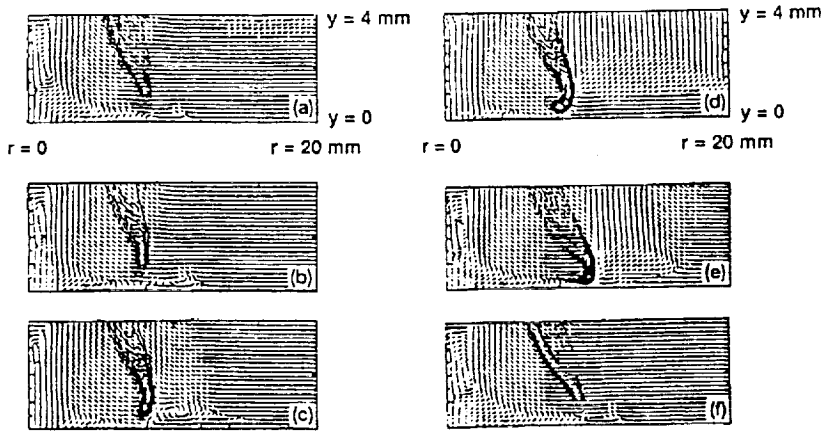

Figure 3.—Flow pattern and flame structure for one flame pulsation at normal gravity. In (d)-(f), the recirculation cell structure in front of the flame leading edge is destroyed during the premixed burning portion of the flame. Hot gas expansion opposes the flow of fresh oxygen to the reaction zone, and the flame moves backwards (as if it were being extinguished). The gas expansion rate decreases after the flame propagates through the premixed region, and, subsequently, the buoyant forces recover to provide fresh oxygen to the reaction zone.

See Color Plate F-5

COMMENTS

Question (Sandra Olson, NASA Lewis Research Center): You commented that there is no consensus as to the effect of pool depth on spread rate. Your data, for pools 2-10 mm deep, agrees qualitatively with literature data for 1-7 mm deep pools (i.e., linear relation). The other two references cited; 2-4 mm and 2-25 mm (I think) show no effect or a 1/3-dependence relation, respectively. Could you comment further on the trend with depth, specifically if it is possible that for the ranges studies each may be valid, which may help interpret controlling mechanisms of flame spread?

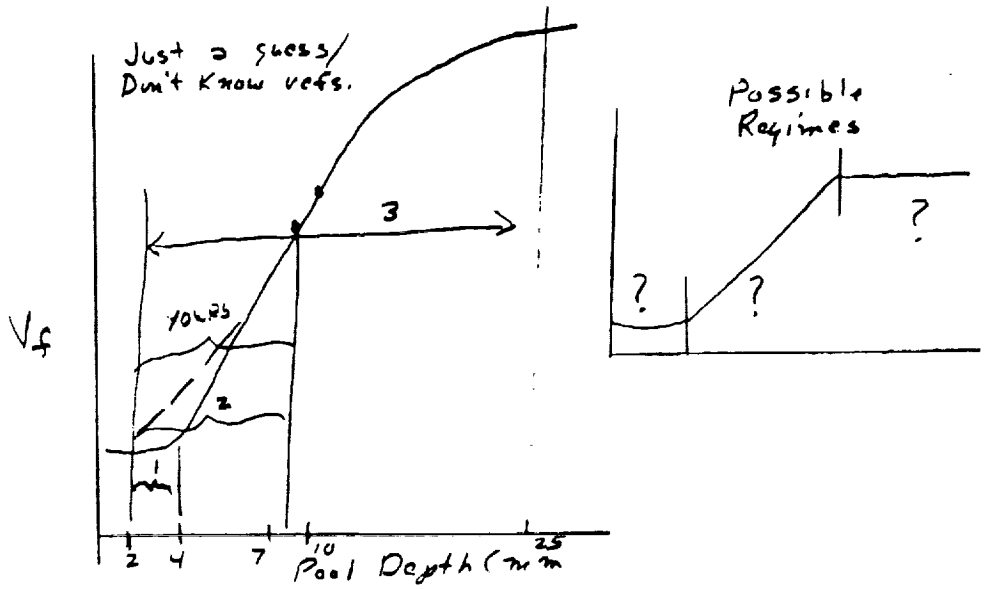

Answer: The question of how flame spread velocity varies with pool depth has been studied by several researchers with mixed results. We believe that the work with very shallow pools missed a depth dependence by collecting too few data points, and then plotting them on a log scale. The linear relation we described was based on 3 data points; we readily conceded in our paper that was insufficient to draw firm conclusions. Eventually one expects the flame spread rate to become independent of pool depth, at least in normal gravity (i.e., the pool could be considered "deep"). Previous work suggested that a pool depth of 1 cm would meet this criterion. It is met based on thermal penetration depth, but not momentum considerations: our PIV showed the vortex reaches the pool bottom.

Question (S. Raghu, SUNY at Stony Brook): In the flow pattern in the liquid resembles that during surface wave propagation have any studies been done from this perspective?

Answer: No one has yet measured quantitatively the extent of surface deformations or waves during flame spread. At the same time, we know they exist. Estimates suggest deformation is on the order of 1 mm, therefore deformation may be quite significant for shallow pools. Our PIV results suggest that some form of surface wave exists and affects the flow pattern in 2 mm deep pools, but not in 10 mm deep pools.

A STUDY OF IGNITION PHENOMENA OF BULK METALS BY RADIANT HEATING

N93-20210

Melvin C. Branch, A. Abbud-Madrid, T.J. Feiereisen, and J.W. Daily
Mechanical Engineering Department
University of Colorado
Boulder, Colorado 80309-0427

Introduction

Early research work on combustion of metals was motivated by the knowledge of the large heat release and corresponding high temperatures associated with metal-oxygen reactions. The advent of space flight brought about an increased interest in the ignition and combustion of metallic particles as additives in solid rocket propellants (Refs. 1 and 2). More recently, attention has been given to the flammability properties of bulk, structural metals due to the number of accidental explosions of metal components in high-pressure oxygen systems (Ref. 3).

The following work represents a preliminary study that is part of a broader research effort aimed at providing further insight into the phenomena of bulk metal combustion by looking at the effects of gravity on the ignition behavior of metals. The scope of this preliminary experimental study includes the use of a non-coherent, continuous radiation ignition source, the measurement of temperature profiles of a variety of metals and a qualitative observation of the ignition phenomena at normal gravity.

The specific objectives of this investigation include: a) a feasibility study of the use of a continuous radiation source for metal ignition, b) testing and characterization of the ignition behavior of a variety of metals and c) building a preliminary experimental database on ignition of metals under normal gravity conditions.

The advantage of using a continuous radiation light source lies primarily on its non-intrusive character and on the nature of its spectral distribution. A short-arc lamp provides broadband radiation in the ultraviolet, visible and near-infrared regions (in the 200-1200 nm range); since the absorptivity of metals increases significantly with decreasing wavelength within this region, this feature will in turn result in a decreased input power requirement. The flexibility, ruggedness and low-weight properties of these lamps make them also very attractive for future experiments on high-speed centrifuges (for elevated gravity environments) and zero-gravity simulators (for reduced gravity experiments).

The metals tested in this investigation, iron (Fe), 1018 carbon steel, titanium (Ti), deoxidized copper (Cu) and aluminum (Al) were selected because of their importance as elements of structural metals and their simple chemical composition (pure metals instead of multi-component alloys to avoid complication in future morphology studies). These samples were also chosen to exemplify the two different combustion modes experienced by metals: heterogeneous, surface oxidation (Fe, 1018 carbon steel, Ti and Cu) and

homogeneous, gas phase reaction (Al). In addition, these specimens exhibit a wide variety of melting temperatures, heats of combustion, oxide formation processes and adiabatic flame temperatures. Copper was selected since no reported cases of copper rod burning were found in the literature. 1018 carbon steel was chosen for comparison purposes since it has an almost identical composition as iron except for a 0.18% carbon content difference (and less than 1% of other elements). The experimental approach consisted in providing temperature profiles, ignition temperature values and a visual record of the heating, ignition and combustion stages of the metal specimen.

Experimental Apparatus and Procedures

The experimental system is shown in Figure 1. The radiation source consisted of a 1000 W xenon short-arc lamp with 250 W of broadband output radiation power (with approximately 42% of output power between 800-1200 nm and the rest between 200-800 nm).

The high-intensity, non-coherent light comes out of the lamp in a collimated beam (4° half-angle) and is then intercepted by an aspheric lens (8 cm diam., 6 cm f.l.) which provides the maximum light collection efficiency for a given focal length under these conditions. The beam is then focused down to a 5 mm spot on the top surface of a metal sample providing approximately a 1 MW/m^2 power density (corrected for transmitting medium absorption). The cylindrical metal specimen is 5 mm in diameter and 5 mm high and rests on top of a circular refractory brick base which isolates the sample from heat conduction to its pedestal. These components are located inside a 4.5 liter stainless steel cylindrical chamber which permits input radiation and visual access through a 10 cm diam., 2 cm thick quartz window. An oxygen environment (99.5% pure O_2) was used in all cases at absolute pressures between 0.4 and 4.0 atm. The chamber pressure was monitored by a solid-state piezoresistive pressure transducer (0-20 atm range). The specimen surface temperature was measured by a Pt-Pt 10% Rh (0.1 mm diam.) thermocouple located at approximately 0.3 mm below the surface. Visual observations were recorded with a black and white Panasonic camera with a #5-density aluminized mylar filter.

Prior to the experimental run, the metal sample was thoroughly cleaned with acetone and placed on top of the refractory firebrick. Care was taken to assure that the thermocouple made good contact with the metal. After closing the combustion chamber, three evacuation and filling cycles were executed to assure a pure oxygen atmosphere inside. The lamp was turned on to full power and the beam was focused on top of the metal specimen. The experiment was monitored throughout by temperature and pressure displays and the video camera. After complete combustion, the sample was allowed to cool down and the final pressure was recorded to quantify oxygen consumption. The chamber was opened and the solid combustion products were stored for future analysis. A minimum of 5 samples of each metal were tested to ensure consistency and experimental repeatability.

Results and Discussion

Initial testing of the short-arc lamp was performed with simple heating and melting experiments with the different metals in air at atmospheric conditions. Melting was successfully achieved in all cases in time periods ranging from 15 to 25 seconds. The lamp was then tested for radiant ignition of metal samples in a pure oxygen atmosphere. All metals except for aluminum exhibited ignition and combustion within the same time period as with the melting tests. The results obtained are summarized in the next three sections.

I) Qualitative observations

A visual record of all successful experimental runs revealed the existence of three important and distinctive phases:

a) The heating period included an initial sudden thermal expansion of the top surface of the specimen after radiation was applied. Surface structure changes were also detected by the variation of the radiation characteristics of the sample. These surface changes are related to the allotropic nature of metals in the solid phase, the oxide layer formation and the solid-liquid phase transition.

b) The ignition phase was characterized by the formation of a liquid metal pool on the top surface of the sample, followed by rapid oxidation and a noticeable increase in energy release evidenced by the intense radiation emitted from the reaction zone.

c) The combustion event, i.e., the self-sustained propagation of the reaction zone was accompanied (in the case of iron, 1018 carbon steel and titanium) by a violent exothermic reaction including outward expelling of small particles that collected in the walls and window of the chamber. The detection of intense luminosity is due to the high temperature (3000-4000 K) obtained in the reaction zone. A marked difference in reaction intensity was observed between the iron and the 1018 carbon steel samples, where the latter exhibited a much higher flux of ejected hot particles probably due to its carbon content. The behavior of copper in the combustion phase had very different characteristics as explained in the Special cases section.

II) Temperature profiles

Temperature records also revealed uniquely the existence of the heating, ignition and combustion stages. Figure 2 shows the temperature histories of titanium, copper, iron and 1018 carbon steel.

All samples showed an increase in temperature with asymptotic approach to a steady-state value in the first few seconds of radiative heating. In the preliminary melting experiments in air the steady-state temperature value (not shown) was fixed by the melting point of the metal due to the constant-temperature phase change. In contrast, a point of inflection was reached on the temperature vs. time plots corresponding to ignition experiments in pure oxygen (see Figure 2). This transition point is identified as the temperature at which the heat generated by the metal oxidation first exceeds the heat lost through conduction, convection and radiation. This temperature is defined in this investigation as the critical ignition temperature of the metal sample. Beyond this point, the metal specimen is driven into a thermal runaway region as a consequence of the exponential dependence of the reaction rate on temperature. The acceleration of the reaction rate ultimately reaches the catastrophic oxidation level which defines the exothermic, self-propagating combustion zone. At this stage, the temperature drastically increases to the vaporization temperature of the metal oxide (approx. 3000-4000 K depending on the metal type) where it stays throughout the combustion phase. As shown in Figure 2, the thermocouples were unable to follow the temperature increase in this last stage because their maximum operating temperature is around 2000K.

Table 1 shows the heat of combustion, melting temperature, ignition temperature, and adiabatic flame temperature of the different metals tested. In the case of iron, 1018 carbon steel, copper and titanium the ignition temperature is always below or in the range of the melting temperature of the metal. This result is typical of metals exhibiting heterogeneous reaction with non-protective oxide layers. In the case of iron and 1018 carbon steel, the temperature profiles and ignition temperatures are very similar due to the almost identical chemical composition. For the titanium run shown in Figure 2, the thermocouple broke before the temperature curve reached the point of inflection corresponding to the critical value for ignition (approx. 1720 K).

III) Special cases

The following cases represent two noteworthy examples of different behavior from the previously mentioned results.

a) Aluminum. All ignition tests performed on aluminum were unsuccessful. This metal proved to be impossible to ignite due to the formation of a thick, extremely resistant, insulating oxide layer that prevented the molten metal inside to come into contact with the surrounding oxygen atmosphere. The existence of this protective aluminum oxide layer has been confirmed by other studies (Refs. 4 and 5). The ignition temperature of aluminum is much higher than the melting temperature of the metal and it actually corresponds to the melting point of the metal oxide (Al_2O_3). Different techniques (including forced mechanical stressing and prolonged radiation heating) were used to induce ignition in the metal sample, but all proved unsuccessful.

b) Copper. A very interesting and unexpected result of this investigation was the ignition and combustion of copper samples. Previous work (Ref. 6) has classified copper as a non-flammable metal due to the sudden extinction of the rod after ignition on upward propagation studies. However, under our experimental configuration, clear evidence of ignition and subsequent indefinite downward propagation of copper specimens was obtained at 0.84 atm. In contrast with iron, 1018 carbon steel and titanium, copper exhibited a smooth combustion phase characterized by a slow regression rate with a low-luminosity reaction zone. This behavior may be due to the low heat of combustion which retards the melting and subsequent oxidation of the metal in the molten surface. This same argument may explain the difficulty of burning copper in the upward propagation mode. Under this configuration, the detachment of the first molten ball from the vertical rod removes the thermal mass that preheats the solid metal in front of it and causes a rapid cooling of the reaction zone (where the low heat of reaction is unable to overcome heat losses) with extinguishment following afterwards. Several tests with different specimen lengths (up to 30 mm) were made to provide unmistakable evidence of self-propagation and complete oxidation of the sample. In addition, all tests showed a noticeable decrease in chamber pressure (2-5%) providing further indication of complete metal oxidation.

Conclusions

This study has demonstrated the effectiveness of using a non-coherent, continuous radiation source for metal ignition. In addition, ignition and combustion tests were performed on different metal specimens, including iron, 1018 carbon steel, titanium and copper. Qualitative observations and temperature profiles have revealed the existence of the heating, ignition and combustion stages. These zones are characterized by well-defined surface structure changes, surface temperature behavior, luminosity and chemical activity. Values of ignition temperatures (defined here as the critical point of inflection in the temperature vs. time curve) were obtained and compared with results of previous investigations (Refs. 4,8,9). Good agreement (+/- 10%) was found considering the differences on ignition temperature definition and experimental technique used among the various studies.

The experimental work is being complemented by modeling studies which include the effects of conduction, convection and radiation heat transfer in the solid specimen and the surrounding gas. The computational model explores the effects of gravity (0.0 g to 10.0 g) and pressure (0.15 atm to 10 atm) on the heating phase of the metal sample under non-oxidizing conditions. Preliminary results indicate that for a constant input heat flux on the specimen, there is an increase in convection heat transfer that asymptotically approaches a constant value both for increasing gravity and for increasing pressure. This limit in convection heat transfer imposes a limit on the minimum steady state specimen temperature

obtained. The heat transfer studies are designed to help evaluate the energy balance on the specimen during heating prior to ignition.

Acknowledgements

This work was supported by the National Aeronautics and Space Administration, Lewis Research Center, Grant NASA-NAG3-1257. The starting date for the research project was May 1, 1991.

References

1. Markstein, G. H., "Combustion of Metals", AIAA Journal, 1, No. 3, 1963, pp. 550-562.

2. Friedman, R. and Macek, A., "Ignition and Combustion of Aluminum Particles in Hot Ambient Gases", Combustion and Flame, 6, 1962, pp. 9-19.

3. Stoltzfus, J. M., Homa, J. M., Williams, R. E., and Benz, F. J., "ASTM Committee G-4 Metals Flammability Test Program: Data and Discussion", Flammability and Sensitivity of Materials in Oxygen-Enriched Atmospheres: Third Volume, ASTM STP 986, D.W. Schroll, Ed., American Society for Testing and Materials, Philadelphia, 1988, pp. 28-53.

4. Nguyen, K., and Branch, M. C., "Ignition Temperature of Bulk 6061 Aluminum, 302 Stainless Steel and 1018 Carbon Steel in Oxygen", Combustion Science and Technology, 53, 1987, pp. 277-288.

5. Merzhanov, A. G., Grigorjev, M. and Galchenko, Y. A., "Aluminum Ignition", Combustion and Flame, 29, 1977, pp. 1-14.

6. Mc Ilroy, K., Zawierucha, R., and Drnevich, R. F., "Promoted Ignition Behavior of Engineering Alloys in High-Pressure Oxygen", Flammability and Sensitivity of Materials in Oxygen-Enriched Atmospheres: Third Volume, ASTM STP 986, D.W. Schroll, Ed., American Society for Testing and Materials, Philadelphia, PA, 1988, pp. 85-104.

7. Brzustowski, T.A., and Glassman, I., "Vapor-Phase Diffusion Flames in the Combustion of Magnesium and Aluminum: II. Experimental Observations in Oxygen Atmospheres", in Heterogeneous Combustion, Wolfhard, H. G., Glassman, I., and Green, L., Jr., (eds.), Academic Press, New York, 1964, pp. 117-158.

8. Grosse, A.V., and Conway, J.B., "Combustion of Metals in Oxygen," Ind. Eng. Chem., 50, 1958, pp. 663-672.

9. Reynolds, W.C., "Investigation of Ignition Temperatures of Solid Metals," NASA TN D-182, 1959.

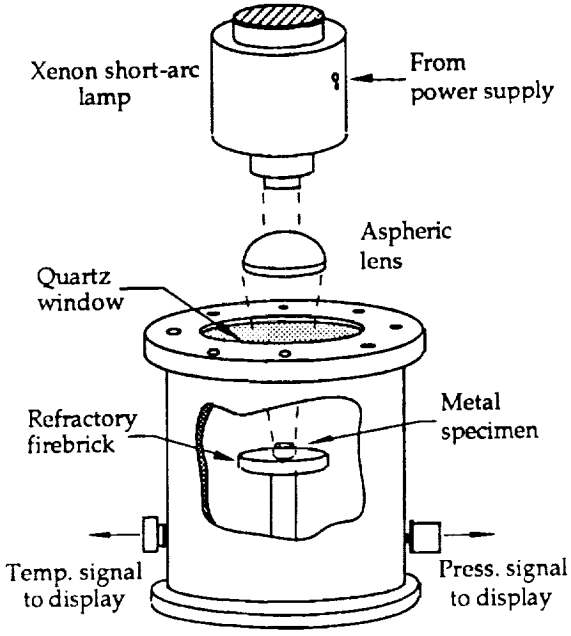

Figure 1. Experimental Apparatus

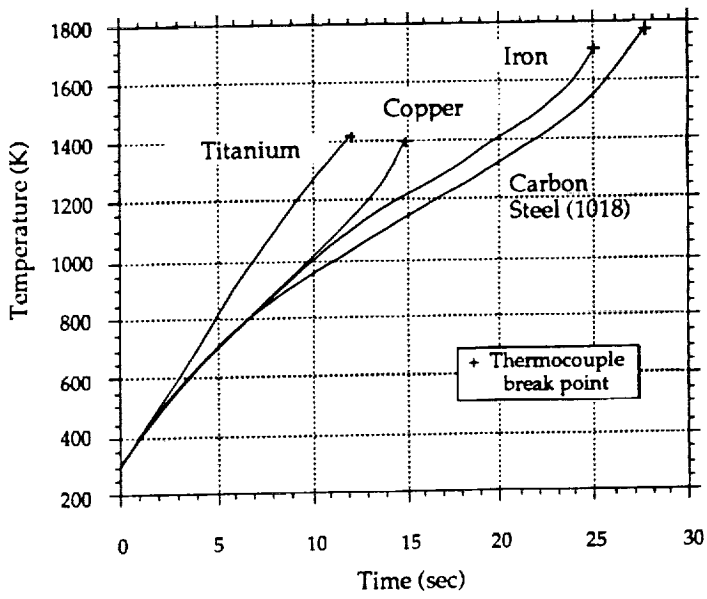

Figure 2. Temperature vs. time behavior of iron, 1018 carbon steel, copper and titanium

Metal Specimen	Heat of Combustion (cal/g)	Melting Temperature (K)	Ignition Temperature (K) [a]	Adiabatic Flame Temp. (K)
Aluminum (Al)	7425	930	2300	3800
Titanium (Ti)	4710	1963	1720	3300
Iron (Fe)	1765	1812	1490	3000
Carbon Steel (1018)	1765	1812	1450	3000
Copper (Cu)	585	1356	1060	1635

[a] From this investigation, except for aluminum from Brzustowski, et. al. [7]

Table 1. Heats of combustion, melting, ignition and adiabatic flame temperatures for the different metal specimens used in this investigation.

COMMENTS

Question (John Moore, Colorado School of Mines): I noticed that you said you did not ignite the aluminum, yet you quote an ignition temperature for aluminum of 2300 K - this is the approximate melting point of aluminum - there must be some connection. Can you please comment?

Answer: In the present investigations of the ignition of metals by a continuous radiation source we were unable to ignite the aluminum specimens. We feel that this is due to the limitation of the power of the radiant ignition source used. In previous studies using a CO_2 laser for ignition (Reference 4 in the paper) we were able to ignite specimens of Al 6061. In those studies the aluminum specimen formed a solid aluminum coating on the surface with molten aluminum in the core of the specimen. The ignition occurred when the oxide coating approached its melting temperature and weakened sufficiently to crack or otherwise expose the molten aluminum to the oxygen. Therefore, there is a connection between the melting temperature of aluminum and the ignition process in the aluminum specimens.

METALS COMBUSTION IN NORMAL GRAVITY AND MICROGRAVITY

Theodore A. Steinberg and D. Bruce Wilson
Lockheed-ESC
White Sands Test Facility, New Mexico

N93-20211

and

Frank J. Benz
NASA
White Sands Test Facility, New Mexico

Introduction and background

The study of the combustion characteristics of metallic materials has been an ongoing area of research at the NASA White Sands Test Facility (WSTF) (ref. 1 and ref. 2). This research has been in support of both government and industrial operations and deals not only with the combustion of specific metallic materials but also with the relative flammabilities of these materials under similar conditions. Since many of the metallic materials that are characterized at WSTF for aerospace applications are to be used in microgravity environments, it was apparent that the testing of these materials needed to proceed in a microgravity environment. It was believed that burning metallic materials in a microgravity environment would allow the evaluation of the validity of applying normal gravity combustion tests to characterize metallic materials to be used in microgravity environments. It was also anticipated that microgravity testing would provide insight into the general combustion process of metallic materials. The availability of the NASA Lewis Research Center's (LeRC) 2.2-second drop tower provided the necessary facility to accomplish the microgravity portion of the testing while the normal gravity testing was conducted at NASA WSTF. The tests, both at LeRC and WSTF, were conducted in the same instrumented system and utilized the standard metal flammability test of upward propagation burning of cylindrical rod samples.

Until this study, microgravity combustion tests did not exist for metals and alloys and there was uncertainty as to whether these materials would support combustion in the absence of gravity. However, nonmetals have been tested under microgravity conditions. Generally it has been found that in microgravity, nonmetals do not burn as well as similar experiments in normal gravity. Normally, the reduction in combustion rate for nonmetals in microgravity has been attributed to the vapor-phase diffusion flame these materials exhibit.

To study the microgravity combustion of metallic materials, a

proposal was written and submitted to the director of Johnson Space Center (JSC). The JSC director funded this work through the JSC Director's Discretionary Fund in 1989 with a duration of two years. With this funding, an experimental program with appropriate instrumentation and facility usage commenced to study the combustion of metallic materials in microgravity. Three subsequent proposals were funded by the NASA WSTF Laboratories Office Chief to continue this work and two proposals are currently under consideration for funding. The results of these test programs and anticipated future work are summarized below.

The use of metallic particles as additives to rocket propellants is normally thought of as the impetus for understanding the combustion characteristics of metallic materials. Since this time, there have been several critical failures of metal components in high-pressure oxygen systems. For these reasons NASA was prompted to initiate programs to better understand the ignition, combustion, and flame spread of metallic materials as well as programs to contrast the similarities and differences of metallic materials combustion as a function of the gravity level.

Unlike nonmetallic materials which burn in a vapor-phase reaction, metallic materials can exhibit a liquid or condensed-phase combustion reaction (ref. 3). The majority of recent testing conducted by WSTF and others involved the combustion of cylindrical rods. In normal gravity, it has been shown that, an increase in rod diameter will be accompanied by a decrease in the regression rate of the melting interface (ref. 2). Experimentation in normal gravity has also shown that a decrease in the ambient oxygen pressure will also result in a decrease in the regression rate of the melting interface (ref. 2).

Experimental

Complete details of the experimental system design, equipment, certification, ignition event, and operation both in normal gravity at WSTF and microgravity at LeRC are given in ref. 4.

The oxygen used at both WSTF and LeRC was 99.5% pure (min.) and the oxygen environment was static at the beginning of a test except for the slight free-convective effects induced by the ignition event. The metals and alloys tested, to date, include rods of iron, 316 stainless steel, 2219 aluminum, titanium, nickel 200, Monel K-500, copper, and tungsten. Thin and thick sheets and meshes of 316 stainless steel were also tested.

Results and Discussion

Figure 1a shows a molten ball, just after detachment, that was formed on the end of a 0.32-cm-diameter cylindrical iron rod burning at 6.9 MPa in normal gravity. The melting interface is the contact area between the solid rod and the formed molten ball (while still attached to the rod). The molten ball grows as energy is transferred from the combustion process to the solid

rod and the melting interface moves upward. This process proceeds, in normal gravity, until the molten ball detaches from the solid rod and a new molten ball is formed. The detachment of the molten ball occurs when the gravitational force exceeds the sum of the adhesion and surface tension forces which hold the molten ball to the solid rod.

As stated, at the beginning of testing it was unclear as to whether metallic materials would support combustion without gravity. It was quickly determined that the metallic materials tested do support combustion under microgravity conditions similar to conditions that support combustion in normal gravity. Figure 1b shows the microgravity combustion of the equivalent experiment shown in Fig. 1a. The 2.2 seconds of microgravity time would have been equivalent to approximately five growth-and-detachment cycles in normal gravity. Instead of detaching in microgravity, the molten ball continues to accumulate mass until impact at the bottom of the drop tower occurred. Upon impact, now in normal gravity, the rod would not extinguish but would continue to burn until completely consumed.

Several differences between the normal gravity and microgravity burning of the metal rods were apparent and include 1) the change in shape of the molten ball from a teardrop to a near perfect sphere, 2) the change in the shape of the melting interface from a circular section to an elliptical section which results in a larger attachment area, and 3) in microgravity the molten ball is often observed to precess around the rod as it burns (equivalent to the instability leading to spinning deflagration).

Calculation of regression rates of the melting interface in normal gravity is accomplished by monitoring the upward movement of the horizontal melting interface from a photographic record of the burning event. In microgravity, the regression rate of the melting interface is calculated by first representing the melting interface by a slanted line with start point and end point defined by the intersection of the molten ball and the solid rod. By monitoring the midpoint of this line as the melting interface progresses up the rod, a value of the regression rate can be obtained. As described in the background, in normal gravity, the regression rate of the melting interface increases with increasing oxygen pressure or decreasing rod diameter. This trend is also true during the microgravity combustion of metallic rods. Though a similar dependency of the regression rate as a function of rod diameter and oxygen pressure is shown between normal gravity and microgravity, there is a significant difference between the absolute regression rates. The regression rate of the melting interface greatly increases, for similar experimental conditions, during microgravity conditions. This increased regression rate, rod diameter dependency, and oxygen pressure dependency, as a function of gravity level, for the iron system, is shown in Fig. 2.

It has also been shown (ref. 5) that the molten ball formed on a

burning iron rod (0.32-cm-diameter) at 6.9 MPa oxygen pressure, in normal gravity, contains excess oxygen above stoichiometric requirements (for the formation of FeO). This result is also true during the microgravity combustion of iron over a pressure range between 1.7 and 8.6 MPa.

The combustion of a 0.32-cm-diameter 2219 aluminum rod shows a combustion zone that is similar in shape, growth, and progression up the rod as seen with the iron rods. It is different with regards to total luminosity (more) and the quantity of volatile products surrounding the combustion zone.

During the microgravity combustion of 316 stainless steel (rods, sheets and meshes), which physically appears to burn identical to the iron, there was a fine olive green powder residue deposited throughout the chamber. This phenomena does not occur during similar experiments in normal gravity. This powder was collected, analyzed by x-ray diffraction, and shown to be chromium oxide (Cr_2O_3). This result suggests that the temperature of the molten ball during microgravity combustion is greater than for combustion in normal gravity and leads to the volatilization of chromium or chromium oxides. As the molten ball grows in microgravity, the molten ball retains more of the heat that is generated by combustion and results in a higher temperature. This increase in temperature is consistent with the increase in the regression rates also exhibited in microgravity.

Different shapes were burned in microgravity to compare configurational effects to similar normal gravity tests. One such test was a thin sheet of 316 stainless steel at 6.9 MPa oxygen pressure which, in normal gravity, extinguishes at this pressure. As the molten mass accumulates in normal gravity it detaches and residual thermal energy is lost at a faster rate than it is generated and so the burning extinguishes. In microgravity, this sample shape burns until the entire sample is consumed since the molten mass does not detach from the sheet. T'ien (ref. 6) has hypothesized the probability of a change in the flammability of a material when the burning event is moved from normal gravity to microgravity, but no experimental evidence, until this study, has verified this hypothesis.

Copper, nickel 200, and Monel K-500 are three materials that have been shown at WSTF to be nonflammable (0.32-cm-diameter rods) in normal gravity up to oxygen pressures of 69.5 MPa. In microgravity, these materials all appeared to burn at oxygen pressures as low as 6.9 MPa, but the test time of 2.2 seconds did not allow adequate time to allow propagation of the burning event for a significant distance along the sample rod. The burning copper rod is shown in Fig. 1c.

Conclusions and future work

Metals and alloys burn readily in microgravity environments which

indicates adequate circulation in the formed molten mass to ensure fuel-oxidizer mixing. Under similar experimental conditions, rods that burn in normal gravity burn faster in microgravity. Sample shapes (sheets) that extinguish in normal gravity burned completely under similar microgravity conditions. Sample materials that do not burn in normal gravity at very high oxygen pressure burn in microgravity at substantially lower oxygen pressure for the 2.2 seconds of test time. A similar dependency between regression rate of the melting interface and oxygen pressure and rod diameter exists in normal gravity and microgravity. 316 stainless steel (rods, meshes, and sheets) produced volatile combustion products when burning in microgravity which does not occur in normal gravity. All of these observations are consistent with the implied observation that the temperature in the molten ball in microgravity is greater than in normal gravity. Excess oxygen, above stoichiometric requirements, is contained in the molten ball formed on iron rods both in normal gravity and microgravity.

There are several areas of emphasis for future work. More configuration testing and new material testing is also needed. The solution of a metals combustion model for iron (condensed-phase burning material) in microgravity is also proceeding which will result in determination of the activation energy, preexponential factor, and other parametric values needed for the characterization of the burning iron system. A stability analysis on the combustion phenomena at both the melting interface and the reaction zone is ongoing. The study of gravity effects on nonmetals which burn with surface flames (Teflon and graphite-filled polymers) is also anticipated future work.

References

1) Stoltzfus, J.M., et. al., in *Flammability and Sensitivity of Materials in Oxygen-Enriched Atmospheres: Third Volume, ASTM STP 986*, D.W. Schroll, Ed., American Society for Testing and Materials, Philadelphia, 1988, pp. 28-53.

2) Steinberg, T.A., et. al., in *Flammability and Sensitivity of Materials in Oxygen-Enriched Atmospheres: Fourth Volume, ASTM STP 1040* (J.M. Stoltzfus, F.J. Benz, and J.S. Stradling, Eds.), American Society for Testing and Materials, Philadelphia, 1989, pp. 54-75.

3) Steinberg, T.A., et. al., *Combust. Flame*, accepted.

4) Steinberg, T.A., Ph.D. dissertation, NMSU, Las Cruces, N.M., May, 1990; Univ. Micro., Inc., Ann Arbor, MI, 91-01023, 51-08B, *Dissertation Abstracts*, p. 4021.

5) Steinberg, T.A., et. al., *Combust. Flame*, 88:309-320 (1992).

6) T'ien, J.S., Presented at the International Microgravity 2Combustion Workshop, LeRC, Cleveland, OH, Jan. 25-26, 1989.

Figure 1.—— Molten ball formed on a burning 0.32-cm-diameter rod in pure oxygen, a) iron in normal gravity (just after ball detachment-6.9 MPa), b) iron in microgravity (6.9 MPa) and, c) copper in microgravity (8.1 MPa). The white lines were added to the photographs to show the boundaries of the rods.

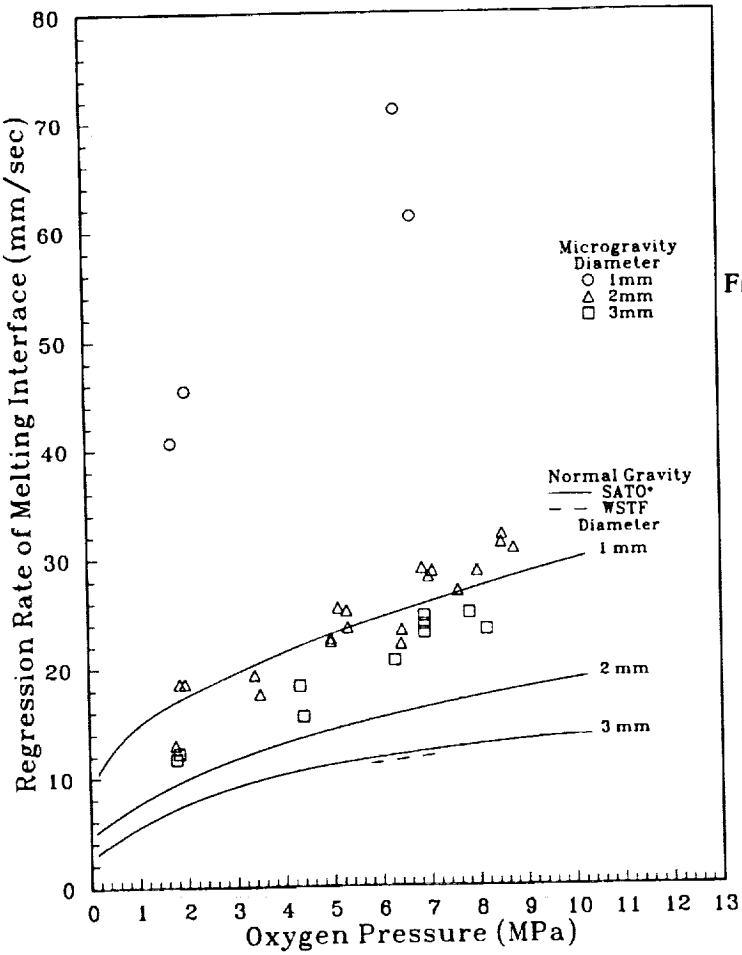

Figure 2.—— Comparison of regression rate of melting interface between normal gravity (mild steel and iron) and microgravity (iron) as a function of oxygen pressure and rod diameter. *From Sato, J. in *Flammability and Sensitivity of Materials in Oxygen-Enriched Atmospheres: Fifth Volume*, ASTM STP 1040 (J. Stoltzfus, F.J. Benz, and J. Stradling, Eds.), American Society for Testing and Materials, Philadelphia, 1989, pp. 162-167.

COMMENTS

Question (R. Friedman, Factory Mutual): What procedure did you use to ignite your sample?

Answer: The microgravity combustion test at LeRC had two different ignition procedures. In the first procedure, the ignition of the test samples occurred before the drop began, in order that the combustion could be observed during a transition from normal gravity to microgravity. The second initiation procedure ignited the test sample after free-fall (microgravity conditions) was established, in order to evaluate a rod's combustion in microgravity alone.

All experiments were ignited by small amounts of Pyrofuze wire wrapped around the bottom of the sample. The Pyrofuze wire was ignited by resistive heating and had a negligible effect on the surroundings.

SESSION G - DROPLET AND SPRAY COMBUSTION

(Chair, Forman Williams)

STUDIES OF DROPLET BURNING AND EXTINCTION

F.A. Williams
Department of Applied Mechanics and Engineering Sciences
University of California, San Diego
La Jolla, California 92093-0310

Introduction

A project on droplet combustion, pursued jointly with F.L. Dryer of Princeton University, has now been in progress for many years. The project involves experiments on the burning of single droplets in various atmospheres, mainly at normal atmospheric pressure and below, performed in drop towers (e.g., ref. 1) and designed to be performed aboard space-based platforms such as the Space Shuttle or the Space Station. It also involves numerical computations on droplet burning, performed mainly at Princeton, and asymptotic analyses of droplet burning, performed mainly at UCSD. The focus of the studies rests primarily on time-dependent droplet-burning characteristics and on extinction phenomena.

The presentation to be given here concerns the recent research on application of asymptotic methods to investigation of the flame structure and extinction of hydrocarbon droplets. These theoretical studies are investigating the extent to which combustion of higher hydrocarbons – heptane, in particular – can be described by four-step reduced chemistry of the kind that has achieved a good degree of success for methane flames. The studies (refs. 2, 3, and 4) have progressed to a point at which a number of definite conclusions can now be stated. These conclusions and the reasoning that led to them are outlined here.

Asymptotic Descriptions of Diffusion Flames

A mixture fraction Z (ref. 5), defined to be zero in the oxidizer and unity in the fuel, serves as an attractive independent variable for analyses of diffusion-flame structures because its adoption enables the problem to be formulated in a universal manner that does not depend on the specific geometrical configuration. However, a unique Z exists only if all relevant Lewis numbers are unity. It has been argued (ref. 3) that for droplet burning, in the transport zones away from the stoichiometric mixture fraction Z_c, Lewis numbers of unity are reasonable approximations, mainly because those for oxygen and products in the outer zone are close enough to unity, while in the fuel zone only the fuel specific heat is relevant (since no other species are transported there), and this is large enough to counteract the small fuel diffusion coefficient, again giving the Lewis number close to unity. It is important to account for Lewis numbers different from unity in the thin reaction zone centered at $Z = Z_c$, but this can be done without difficulty and without affecting the definition of Z, so long as this zone is thin in the mixture-fraction coordinate. Thus, the droplet-burning problem is formulated in terms of the mixture fraction (ref. 2, 3, and 4).

In the mixture-fraction formulation, the simplest asymptotic description is the Burke-Schumann reaction-sheet structure, shown by the straight lines labeled "equilibrium" in figure 1. This limit corresponds to an infinite Damköhler number for one-step, irreversible chemistry and provides

the outer, transport-zone solutions to which the reaction-zone solutions are matched. Figure 1 illustrates that in the reaction zone there is a one-parameter family of solutions, the parameter being χ_c, the value at stoichiometry of the scalar dissipation rate

$$\chi = 2D \mid \nabla Z \mid^2, \tag{1}$$

where D is the (local, variable, common) diffusion coefficient of the outer solutions. As χ_c increases, the peak temperature decreases, and eventually an abrupt extinction is approached, at a critical value of χ_c. Figure 1 illustrates this qualitatively on the basis of activation-energy asymptotics (AEA); after extinction the solution is the frozen one given by the dashed lines.

When the mixture-fraction formulation is employed, the distinction between different geometrical configurations arises only through the expression for the scalar dissipation, χ. For a stagnant mixing layer of thickness, l

$$\chi = 2D/l, \tag{2}$$

while for constant-density counterflow mixing with a normal-component strain rate K_O in the oxidizer stream

$$\chi = (K_O/\pi)/\exp\left\{2\left[\mathrm{erfc}^{-1}(2Z_c)\right]^2\right\} \tag{3}$$

in which erfc^{-1} denotes the inverse (not the reciprocal) of the complementary error function. It has recently been shown (ref. 6) that for small Z_c, the usual case encountered in practice, variable-density effects can be included reasonably by placing on the right-hand side of equation (3) the additional factor

$$f = \left[3(\sqrt{\rho_O/\rho_c}+1)^2\right] / \left[4(2\sqrt{\rho_O/\rho_c}+1)\right], \tag{4}$$

where ρ_O is the density of the oxidizing stream and ρ_c that at the stoichiometric flame sheet. For droplet burning (ref. 2) it is found that

$$\chi = \frac{8D}{d_l^2}\left\{\frac{[ln(1-Z)]^2(1-Z)}{ln(1+B)}\right\}^2 \tag{5}$$

where d_l is the droplet diameter, and B is the transfer number for the droplet combustion process, given in an approximation of constant specific heat c_p by

$$B = \{c_p(T_\infty - T_l) + QY_{O_2\infty}/[(3n+1)W_{O_2}/2]\}/L, \tag{6}$$

where T, W, and Y denote temperature, molecular weight, and mass fraction, the subscript ∞ identifies the ambient atmosphere, L is the energy required to vaporize a unit mass of fuel, Q stands for the heat released per mole of gaseous fuel in combustion, and n represents the number of carbon atoms in the alkane. By use of equation (5) at $Z = Z_c$, the droplet diameter at extinction d_{le}, can be obtained from χ_{ce}, the value of χ_c at extinction, which has been calculated without reference to the specific geometrical configuration.

Figure 2 illustrates how figure 1 is modified by reduced chemistry. This figure pertains to a two-step approximation in which the reaction zone is split into two parts, a fuel-consumption zone and an oxidizer-consumption zone. The asymptotic analyses have addressed flame structures in two-step, three-step, and four-step approximations. Qualitative illustrations of resulting concentration and temperature profiles in physical space are shown in figure 3, in which C_2H_2 is one representative of numerous intermediate fuel species.

Reduced Chemistry

Systematic reductions to four-step mechanisms for alkanes result in the reduced chemistry

$$C_nH_{2n+2} + \gamma H + \left[\beta - (n+1+\frac{1}{2}\gamma)\right] H_2O + \left\{n - \frac{1}{2}\alpha - \frac{1}{2}\left[\beta - (n+1+\frac{1}{2}\gamma)\right]\right\} O_2 \rightarrow \alpha CO + \beta H_2 + (n-\alpha)CO_2, \quad (7)$$

$$CO + H_2O \rightleftharpoons CO_2 + H_2, \quad (8)$$

$$2H + M \rightarrow H_2 + M, \quad (9)$$

$$O_2 + 3H_2 \rightleftharpoons 2H + 2H_2O. \quad (10)$$

Equations (7), (8), (9), and (10) describe the fuel-consumption, water-gas shift (or CO-consumption), radical-recombination, and oxygen-consumption (radical-production) steps, respectively, and they proceed mainly at the rates of the elementary steps

$$C_nH_{2n+2} + H \rightarrow C_nH_{2n+1} + H_2, \quad (11)$$

$$CO + OH \rightleftharpoons CO_2 + H, \quad (12)$$

$$H + O_2 + M \rightarrow HO_2 + M, \quad (13)$$

and

$$H + O_2 \rightleftharpoons OH + O, \quad (14)$$

respectively. The values of the constants α, β, and γ in equation (7) depend on the chemical-kinetic description of the fuel chemistry. Studies (refs. 3 and 4) have shown that theoretical predictions are especially sensitive to the value of γ, the number of radicals destroyed for each fuel molecule that is consumed. It may be expected that the larger γ is, the lower will be the radical concentration and the less robust the flame.

For methane (n = 1), the summation

$$\begin{array}{rcl} CH_4 + H & \rightarrow & CH_3 + H_2 \\ CH_3 + O & \rightarrow & CH_2O + H \\ CH_2O + H & \rightarrow & CHO + H_2 \\ CHO + M & \rightarrow & CO + H + M \\ H + OH & \rightarrow & O + H_2 \\ H + H_2O & \rightarrow & OH + H_2 \\ \hline CH_4 + 2H + H_2O & \rightarrow & CO + 4H_2 \end{array}$$

with the steps dictated by the need to cancel all steady-state species through their fastest reactions results in $\alpha = 1, \beta = 4$, and $\gamma = 2$. Even excluding the second of these steps by assuming (erroneously) that $2CH_3 + M \rightarrow C_2H_6 + M$ is very fast and that ethane chemistry therefore controls the fuel consumption gives only $\alpha = \frac{1}{2}, \beta = 3$, and $\gamma = 1$, that is, the number of radicals consumed is decreased by just a factor of two. Consequently there is relatively little significant uncertainty in step (7) for methane. However, for a larger alkane, such as heptane, there is a large difference, depending on whether the fuel chemistry follows a propene path after step (11), namely,

$$C_7H_{15} \rightarrow CH_3 + 2C_3H_6 \quad (15)$$

(overall), as proposed by Warnatz, or an ethene path,

$$C_7H_{15} \rightarrow CH_3 + 3C_2H_4 \tag{16}$$

(overall) as favored by Dryer. The propene path gives $\alpha = 7$, $\beta = 20$, and $\gamma = 10$, while the ethene path gives $\alpha = 4$, $\beta = 13$, and $\gamma = 2$, a factor of five difference in the number of radicals consumed. This large factor turns out to have a large influence on the scalar dissipation at extinction because the much greater extent of consumption of radicals by fuel in the propene path leads to extinction much earlier. Since uncertainties in the detailed fuel chemistry of higher hydrocarbons do not enable a selection to be made between the propene and ethene paths, for example, at present, it is concluded that further study of elementary steps and mechanisms in alkane fuel chemistry is needed.

In the present work (ref. 4) experimental results on extinction of burning heptane pools were employed along with the asymptotic theory for the four-step description to infer what value of γ is needed to best fit the data. In this manner, it was found that $\gamma = 13$ is close to the optimum selection. This suggests that revisions in equations (15) or (16) or in the propene and ethene consumption mechanisms are needed if agreement with extinction experiments is to be achieved.

Computations were made not only with the four-step mechanism but also with a three-step mechanism, obtained from the four-step description by putting the H atom in steady state, and with a two-step mechanism, obtained from the three-step description by imposing partial equilibrium on step (8). There were large differences in the resulting predictions of heptane flame structures and extinction, much larger than for methane. For example, differences in the scalar dissipation at extinction exceeded a factor of ten, in contrast to being less than a factor of two for methane. It is concluded that the higher hydrocarbons are more sensitive to the kinetic descriptions and that therefore experiments on flame structures and extinction for these fuels may provide information of greater relevance to the chemical kinetics.

Flame Structure and Extinction

In the two-step approximation, the structure is as illustrated in figure 2, with the fuel-consumption zone thin compared with the oxygen-consumption zone, which in turn occupies an asymptotically small range of Z. In the three-step approximation, nonequilibrium of step (8) occurs in a portion of the oxygen-consumption zone adjacent to the fuel-consumption zone, provided that the Damköhler number for this step is large enough, which it is for the propene path but not for the ethene path. If the ethene path without modification is correct (which seems quite unlikely), then an alternative analysis, paralleling that of Bui-Pham, Seshadri, and Williams for the premixed methane flame with slow CO oxidation, will be needed, but it does not appear that the correct fuel chemistry for alkane diffusion flames will require this. In the four-step approximation, the thin fuel-consumption zone itself has substructure. There are two limiting behaviors of this substructure, as illustrated in figures 4 and 5. When H has a strong tendency to achieve steady state, as was found for methane, there is a thin radical-consumption layer within the fuel-consumption layer, as illustrated in figure 4, where the nondimensional thickness of the fuel-consumption layer is δ, and the parameter μ, (ref. 4) involving ratios of reaction rates in the rate-ratio asymptotic analysis (RRA) is large. When this tendency is weak (μ small), the situation illustrated in figure 5 occurs, in which there is a diffusion flame between radicals and fuel within this inner layer – a diffusion flame within the diffusion flame. The results (ref. 4) show heptane to lie strongly in this last regime ($\mu \rightarrow 0$).

Predictions of the location Z_0 and outer-solution temperature T^0 of the inner fuel-consumption zone are of interest. For heptane, contrary to the relative location illustrated in figure 2, the

two-step and three-step descriptions give Z_0 on the oxidizer side of Z_c for most values of χ_c, in particular at extinction. This disagrees with experiment and also with the predictions of the four-step mechanism, which place Z_0 on the fuel side, as illustrated in figure 2, even at extinction. The temperature T^0 of this fuel-consumption zone also is more realistic with the four-step mechanism, as illustrated in figure 6. Thus, in every respect, the four-step description is much better than simpler descriptions for higher hydrocarbons.

From χ_{ce}, equation (5) is used to calculate extinction diameters. Results are shown in figures 7 and 8. Figure 7, for the propene route, clearly shows the large differences obtained with different degrees of reduction of the chemistry. The most reasonable values probably are close to the two-step prediction, fortuitously through cancellations of errors, but until heptane droplet extinction is observed experimentally, this conclusion is not certain. If the four-step predictions in figure 7 are correct, then it is unlikely that droplet extinction can be observed experimentally, because the droplets will become too small. If $\gamma = 13$ in equation (7), then the four-step predictions fall much closer to those shown for the two-step predictions. Comparison of the three-step results shown in figure 8 for the propene and ethene routes shows the extremely large difference in extinction diameters for these two descriptions ($\gamma = 10$ versus $\gamma = 2$); calculations with two-step and four-step chemistry for the ethene route gave essentially zero extinction diameters. It seems likely that many more than two radicals are destroyed for each heptane molecule consumed, but further chemical studies are needed to determine how many.

Future Plans

It is planned to investigate the fuel chemistry further, in an effort to determine better the values of the parameters α, β, and γ. It is also planned to initiate similar asymptotic analyses for alcohol fuel droplets. Finally, microgravity experiments on alkane droplet extinction in different atmospheres are planned, to test predictions.

References

1. Choi, M.Y., Dryer, F.L., Card, J.M., Williams, F.A., Haggard, J.B., Jr., and Borowski, B.A., "Microgravity Combustion of Isolated n-Decane and n-Heptane Droplets," AIAA Paper No. 92-242, January, 1992.

2. Card, J.M. and Williams, F.A., "Asymptotic Analysis of the Structure and Extinction of Spherically Symmetrical n-Heptane Diffusion Flames," Combustion Science and Technology 84 (1992) 91-120.

3. Card, J.M. and Williams, F.A., "Asymptotic Analysis with Reduced Chemistry for the Burning of n-Heptane Droplets," Combustion and Flame, to appear, 1992.

4. Card, J.M., "Asymptotic Analysis for the Burning of n-Heptane Droplets using a Four-Step Reduced Mechanism," Combustion and Flame, submitted, 1992.

5. Williams, F.A., "Combustion Theory," Addison-Wesley, Menlo Park, CA, 1985.

6. Kim, J.S. and Williams, F.A., "Structures of Flow and Mixture-Fraction Fields for Counterflow Diffusion Flames with Small Stoichiometric Mixture Fractions," Combustion Science and Technology, submitted, 1992.

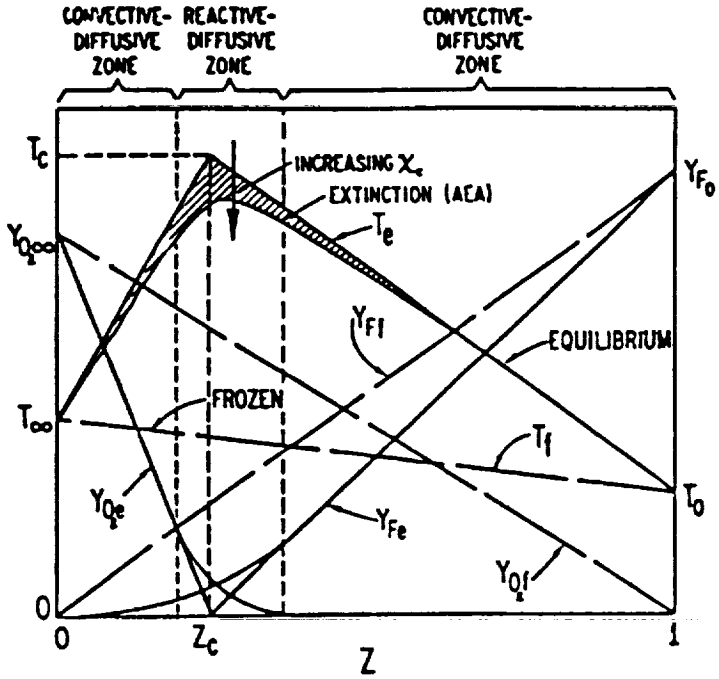

Figure 1.– Schematic diagram of the flame structure in the mixture-fraction coordinate for one-step empirical Arrhenius chemistry, showing fuel (F), oxygen (O_2), and temperature profiles.

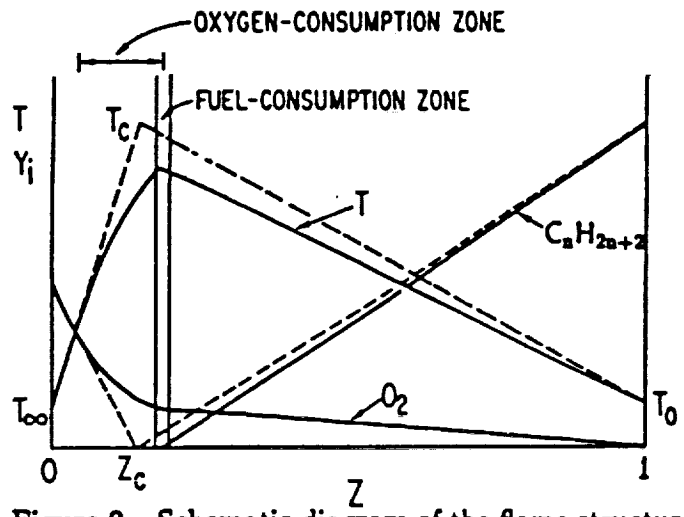

Figure 2.– Schematic diagram of the flame structure in the mixture-fraction coordinate for two-step reduced chemistry.

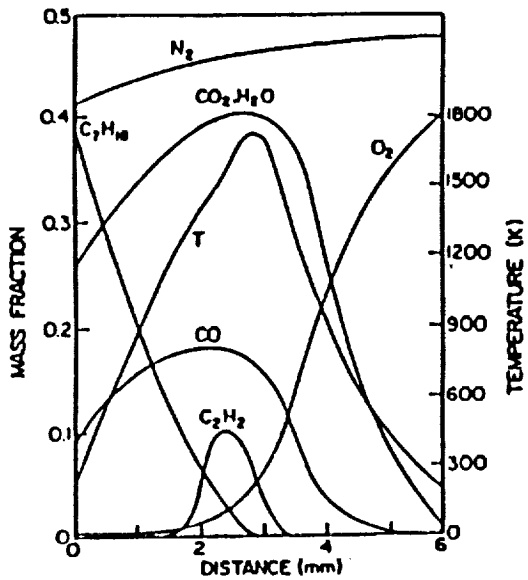

Figure 3.– Schematic illustration of implications of theory concerning heptane flame structure in physical coordinates.

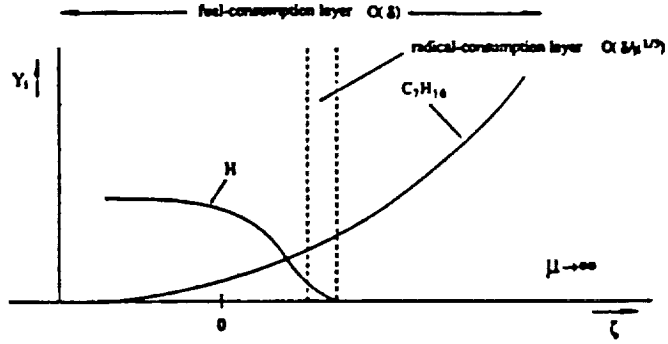

Figure 4.– Schematic illustration of inner-layer structure when there is a strong tendency for H to be in steady state.

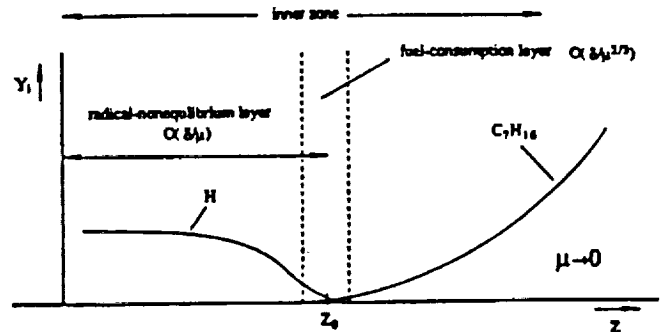

Figure 5.– Schematic illustration of inner-layer structure when there is a weak tendency for H to be in steady state.

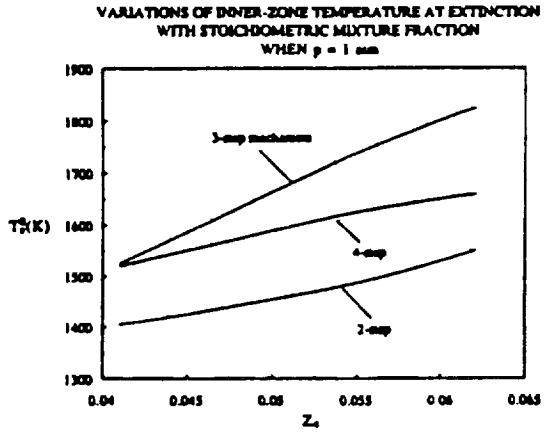

Figure 6.– Dependence of the inner-zone temperature at extinction on the stoichiometric mixture fraction (varied by dilution) for the propene path at normal atmospheric pressure and temperature.

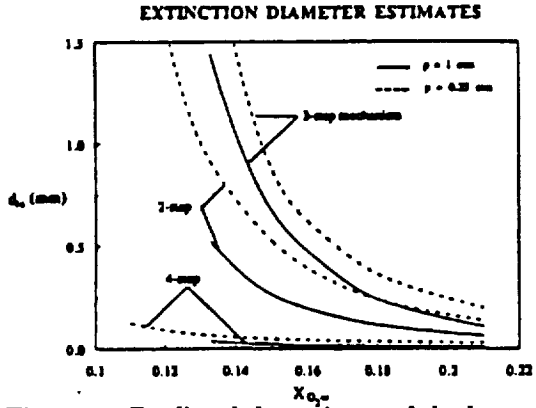

Figure 7.– Predicted dependence of the heptane extinction diameter on the oxygen mole fraction in the ambient gas for the propene path.

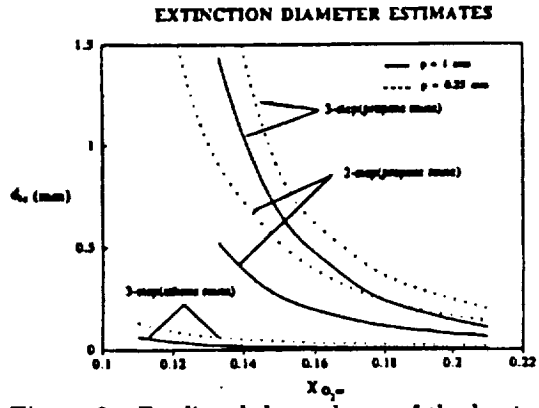

Figure 8.– Predicted dependence of the heptane extinction diameter on the oxygen mole fraction in the ambient gas for both propene and ethene routes.

COMMENTS

Question (Ray Edelman, Rockwell International): I would expect burning rate and extinction, in particular, would depend strongly on soot formation and the attendant radiation loss on reducing temperature. This might be enhanced at high pressures. Could you comment on what your data shows and how you reconcile this with your analyses? Do competing effects balance this with enhanced kinetics at increasing pressure?

Answer: Our studies are at normal atmospheric pressures and at reduced pressures, not at high pressures. For our small single droplets under these conditions, radiant transfer associated with soot formation probably is negligible. At high pressures it will become more important, but temperature reduction through radiant energy loss still could be a perturbation because of the small size.

COMPUTATIONAL/EXPERIMENTAL STUDIES OF ISOLATED, SINGLE COMPONENT DROPLET COMBUSTION

N93-20213

Frederick L. Dryer
Department of Mechanical and Aerospace Engineering
Princeton University
Princeton, New Jersey 08544-5263

Introduction

Isolated droplet combustion processes have been the subject of extensive experimental and theoretical investigations for nearly 40 years. The gross features of droplet burning are qualitatively embodied by simple theories and are relatively well understood (e.g. ref.1). However, there remain significant aspects of droplet burning, particularly its dynamics, for which additional basic knowledge is needed for thorough interpretations and quantitative explanations of transient phenomena. Spherically-symmetric droplet combustion, which can only be approximated under conditions of both low Reynolds and Grashof numbers, represents the simplest geometrical configuration in which to study the coupled chemical/transport processes inherent within non-premixed flames. Microgravity droplet combustion can closely approximate these conditions, while also giving insights as to how coupling of the above processes is affected by the absence of gravitational forces. Advances in both asymptotic and numerical computational abilities allow more recent analyses of droplet burning to include considerably refined descriptions of the transport and chemical effects, particularly if the spherically symmetric assumption can be maintained. While such improvements in theory represent significant promise for future advances, experimental data available for comparison with theory, without corrections for convective effects, remain relatively limited.

The research summarized here, concerns recent results on isolated, single component, droplet combustion under microgravity conditions, a program pursued jointly with F.A. Williams of the University of California, San Diego. The overall program involves developing and applying experimental methods to study the burning of isolated, single component droplets, in various atmospheres, primarily at atmospheric pressure and below, in both drop towers and aboard space-based platforms such as the Space Shuttle or Space Station (e.g. refs. 2-4). Both computational methods (e.g. ref. 5) and asymptotic methods, the latter pursued mainly at UCSD, (see preceding paper), are used in developing the experimental test matrix, in analyzing results, and for extending theoretical understanding. Methanol, and the normal alkanes, n-heptane, and n-decane, have been selected as test fuels to study time-dependent droplet burning phenomena. The following sections summarize the Princeton efforts on this program, describe work in progress, and briefly delineate future research directions.

Methanol

Methanol is thermophysically, thermochemically, and kinetically, the most well characterized of liquid fuels. Methanol burns diffusively without the production of soot and a number of its combustion intermediates and products, notably water and formaldehyde, are highly soluble in the fuel (refs. 2,7,8). As a result, spherically symmetric modeling of methanol droplet combustion is especially amenable to time-dependent, computational studies which include detailed multi-component transport, thermo-chemistry, and chemical kinetics (ref. 6). Thus, methanol is an ideal fuel selection for providing benchmark comparisons of theory and experiment.

Utilizing the Chemically Reacting Flow Model (CRFM) developed at Princeton (ref. 5), computational studies have been performed including multi-component transport (ref.9), and detailed kinetics (ref. 10). Calculations were compared with experimental data generated in the 2.2 second drop tower (ref. 6) and with ground-based laboratory experiments (refs. 2,8). Droplet gasification rate, flame position, and extinction were shown to be affected by species absorption and dissolution into the liquid phase. The non-linear behavior of the square of the droplet diameter with time and the extinction diameter calculated for the combustion of a methanol droplet in 50% helium/50% oxygen mixtures at atmospheric pressure compare well with 2.2 second drop tower experiments. Calculated flame temperature profiles suggest temperature is an insensitive parameter for experimentally defining flame position. However, experimental measurements of gas phase [OH], and [CH2O] profiles would apparently permit accurate determination of the oxidizer and fuel consumption regions (i.e. flame structure) as well as position.

Additional ground-based experimental and computational work is planned on both pure methanol and methanol-water droplets to further develop fundamental understanding and a space-based test matrix. One-g suspended and free droplet studies have been performed at Princeton on methanol-water mixtures which show interesting effects of initial water content on extinction diameter (refs. 2,7,8). Both 2.2 second and 5 second tower studies are scheduled, pending availability of the NASA-Lewis 2.2 second drop-package and the refurbishment of the 5.0 second tower facility. Computational development of full-flight and ground-test matrices for methanol droplet studies (similar to those described below for n-heptane) require further refinement of the detailed chemistry utilized in the model (ref. 10), particularly its pressure-dependent characteristics. Kinetic model refinements are presently underway, based on other recently published studies (refs. 11-13), and a new variable pressure (1-15 atm.) flow reactor study recently concluded in the author's laboratory (ref. 14). Finally, a reduced mechanism for methanol diffusion flames remains to be developed to assist in parallel asymptotic studies.

Normal Alkanes

Normal-heptane and n-decane have been utilized in many prior droplet burning studies, both in earth's gravitational field (e.g. ref. 15) and in droptowers (e.g. ref. 16). Under microgravity droplet combustion conditions, both exhibit significant soot formation and accumulation (by

thermophoresis) within the surrounding diffusion flame (refs. 17,18). The "sootshell" thus formed and the soot agglomerate densities within it are strongly influenced by ambient pressure, oxygen indices, and diluent species (refs. 2,8), as well as by initial droplet size (ref. 19) and relative gas/droplet convection (refs. 8,18). Associated with the formation and presence of the sootshell, is a reduced droplet gasification rate that can be as much as 40% lower than observed in early drop tower measurements at similar drop sizes (no sootshells present). The burning rate data increase with measured relative gas/droplet convection rate (ref.18), and recent experiments (refs. 2,8) show that, contrary to classical theory, the gasification rate is increased significantly by pressure reduction (through reduced sooting). No fundamental theory has been conclusively established for these effects, but it has been suggested that radiation losses from the sootshell, changes in the temperature-averaged transport properties, and changes in gas-phase volume flux due to soot formation are possible sources of effects which change both the surface gasification rate and flame position (refs. 2,18).

Over some ranges of experimental parameters, droplet disruption and dismemberment is also observed to occur early in the droplet burning history (refs. 8,17,18), while over other ranges of conditions, droplet extinction is observed to occur. Speculations for the mechanisms which produce disruption are: deposition of high-molecular-weight soot precursor intermediates in the liquid phase, resulting in multi-component droplet gasification behavior (ref. 17); collapse of the diffusion flame structure into the soot shell, causing intense disturbances from the soot shell ignition.; soot deposition at the liquid surface; and critical electrostatic charge accumulation in the soot shell and/or droplet surface (refs. 2,8). Recent experiments at one-g suggest that deposition of high molecular weight components is insignificant (ref. 2,8), and a clear explanation of the disruption phenomena remains to be established.

Unfortunately, thermophysical, thermochemical, and chemical kinetic properties for these alkanes are not very well defined (ref. 2). Experimental values of thermophysical parameters have been determined only at low temperatures, and theoretical evaluations based on ideal gas properties to guide extrapolations to flame temperatures are in significant disagreement (ref. 2). More importantly, the detailed kinetic mechanisms for large alkanes are only qualitatively understood (ref. 20). A 96 step semi-empirical mechanism has been proposed by Warnatz for predicting laminar pre-mixed flame propagation (ref. 21) for n-heptane-air flames, and this work has formed the basis for several studies on diffusion flames and reduced model development (refs. 4,22). The principal empiricism is the description of n-heptyl radical decomposition into the unlikely products of CH_3 + 2 C_3H_6 (in fixed ratio) rather than the expected mixture of β-scission products, C_2H_4, C_2H_3, C_3H_6, C_4H_8, CH_3, and C_3H_{10} (ref. 20), which are, in fact, evidenced in n-heptane-air diffusion flame structures (ref. 23) and flow reactors (ref. 24). More complex detailed kinetic mechanisms have been developed for autoignition studies in engines (up to 5000 reaction steps), but these mechanism involve considerable uncertainty and low and intermediate oxidation chemistry of little relevance in diffusion flames. However, as a means of developing ground- and space-based experimental test matrices, initial computations have been performed using the CRFM and two step semi-empirical kinetics with reversible CO/CO_2 chemistry (refs. 3,4,8). Numerical constants in the kinetic mechanism were adjusted to reproduce suspended droplet extinction diameter data (ref. 25) of n-heptane at low pressure (no soot formation), and calculations were performed to determine the burning characteristics of isolated n-heptane droplets under various ambient pressures, oxygen indices, diluents (nitrogen, helium), and initial diameters.

Figure 1 is typical of results from parametric calculations in which the ignition energy (magnitude) and (spatial) deposition parameters were varied for droplet burning in helium (refs. 3,4,8). The displayed function represents the minimum droplet size for which any amount of ignition energy specified would not produce ignition. At this droplet size, transport to the ambient and vaporization removed ignition energy from flammable regions at a rate more rapid than the chemical heat release rates anywhere surrounding the droplet region. As the critical ignition diameter increases, the amount of energy required to achieve ignition also increases. At the maximum critical ignition diameters displayed in the figures, no ignition energy could be found which would initiate droplet combustion. Experimentally, the critical ignition diameter must be large in comparison to the calculated extinction diameter. (Critical ignition energy predictions are unique to time-dependent computations.) Figure 2 displays calculated extinction diameter as a function of ambient pressure and oxygen index in helium diluent (refs. 3,4,8). Extinction diameter increases with decreasing pressure and with substitution of helium for nitrogen, i.e. by increasing the diffusivity relative to chemical kinetic conditions. Calculated results are similar to values (within 20%) from asymptotic analyses with 2-step (propene intermediate) reduced chemistry (see preceding paper, this workshop and refs. 3,4,8). Combined with the characteristic times required for various experimental procedures (e.g., droplet growth and deployment), and combustion properties (e.g. controlled sooting by selection of appropriate pressure, diluent, and oxygen indices) a test matrix envelope have been developed for proposing ground- and space-based microgravity experiments, e.g. Fig. 3 (Refs. 3,4,8).

As noted above, soot formation and accumulation effects are important factors in determining the burning characteristics of droplets. No theoretical model presently exists which explicitly includes sooting. Previous investigations have addressed the formation of the sootshell by balancing thermophoretic and viscous drag forces acting on a soot particle (refs. 26,17). However, the lack of detailed information regarding the distribution of the gas-phase transport and thermophysical properties prevented accurate determination of the sootshell position. Using the simplified chemistry for n-heptane described above (with no soot formation mechanism included) and temperature-dependent thermophysical properties, the CRFM model was used to estimate these parameters by calculating the transient gas-phase field distributions between the droplet surface and the flame location (ref. 8).

Once formed in the diffusion flame region, soot particles are acted upon by viscous drag (caused by Stefan flow), diffusion and thermophoresis, i.e. particle transport caused by a temperature gradient in the surrounding gas-phase (ref. 27). Because the sootshell location is much closer to the droplet surface than the flame and mass diffusion should be important only near the flame where the concentration gradients are large, this mode of particle transport can be neglected. Waldman and Schmidt (ref. 28) analyzed the viscous drag and thermophoretic force acting on a small spherical particle by calculating the momentum transferred per unit time to the particle by gas molecule collisions. The resulting force equation, solved at equilibrium, gives the thermophoretic flux, ρV_t, as

$$\rho V_t = \frac{-3\mu \frac{dT}{dr}}{4(1+\pi\alpha/8)T} = f(r) \qquad (Eqn.\ 1)$$

where ρ is the gas density, V_t is the relative velocity experienced by the particle, μ is the viscosity, and α is the thermal accommodation factor which is usually assigned a value of 0.9. Note that thermophoretic flux is independent of particle size for sizes on the order of incipient soot particles (ref. 29), i.e. for particles that are much smaller than the mean free path. For conditions under which soot agglomeration is prevalent, mean particle size may become much larger than the mean free path. The thermophoretic flux formulation is then defined as (ref. 27):

$$\rho V_t = \frac{-2\lambda^2 \sigma \rho \frac{dT}{dr}}{(2\lambda+\lambda_p)P} = f(r) \qquad (Eqn.\ 2)$$

where λ and λ_p are the thermal conductivities of the gas and the particle. The term, σ, is a dimensionless constant that relates the slip velocity at the particle surface and the gas-phase temperature gradient, usually assigned a value of 0.2. The thermal conductivity of soot particles was estimated from the temperature-dependent values for amorphous carbon (ref. 30).

When the surrounding gas-phase produces a Stefan flux, ρV, equal to ρV_t, the forces acting on the particle will be counter-balanced and the particles will accumulate to form the sootshell. Figure 4 displays the modeling results for the Stefan, the small-particle thermophoretic [denoted as SPT, Eqn. 1] and the large-particle thermophoretic [denoted as LPT, Eqn. 2] velocities, plotted versus normalized radius (divided by instantaneous droplet radius) for n-heptane burning in atmospheric pressure air. The time-dependence of mass gasification rate, droplet and flame dimensions and the temperature gradients will cause changes in these profiles. The results presented in Fig. 5 are typical of those produced under the quasi-steady burning conditions. The Stefan velocity near the droplet surface is observed to increase with radial position to a maximum near $r/r_o = 1.5$ and then decrease monotonically. Similar behavior is also observed for the SPT velocity, which matches the Stefan velocity at a normalized radius of 5.5. Considering that the calculated flame standoff ratio is 10 (in comparison to about 8 experimentally), this prediction is quite reasonable. The principal source of the disparity is that the calculated gasification rates are approximately 36% higher than the values measured for the most quiescent n-heptane droplet combustion experiments. Under sooting conditions, the portions of the gasified fuel which forms soot also possess negligible specific volume when compared to that of the gaseous species, which reduces the flame stand-off ratio. Scaling of the Stefan flux by the ratio of the experimental and calculated gasification rates and incorporating the flame contraction effects by reducing the distance between all calculated node locations by a factor of

$$F(t) = \frac{[\frac{d_{flame}}{d_{drop}}]_{(exp,\ t)}}{[\frac{d_{flame}}{d_{drop}}]_{(model,\ t)}}$$

calculations were performed for each droplet combustion time step to determine the location of the Stefan/thermophoretic flux equilibrium. The model-generated soot standoff ratios compare favorably with experimentally measured values (within 10%), see Fig. 5. Similar model calculations were also performed for droplet combustion in higher oxygen indices. For the 30%, 40% and 50% oxygen concentrations in nitrogen, the calculated soot standoff ratios were reduced to 2.65, 2.54 and 2.46, respectively (compared to measured ratios at 40% and 50% oxygen of approximately 2.2). Similar reductions for increasing oxygen indices have also been reported in ref. 31. For all oxygen concentrations, the calculated Stefan velocities were larger in magnitude than the minimum convective velocities required for equilibrium between viscous drag and LPT forces (within region bounded by droplet surface and flame front). This suggests that when larger soot agglomerates form, they should be transported towards the flame and eventually pass through it. This behavior was, in fact, observed in experiments at high oxygen/nitrogen ratios (> 0.4) for both n-decane and n-heptane fuel droplets.

It appears that thermophoretic effects are unlikely to lead to soot particle deposition on the liquid surface (speculated to lead to disruption) since viscous drag dominates very near the droplet surface. The flame would need to regress toward the droplet for a force imbalance to favor thermophoretic soot deposition. Regression of the flame through any part of the soot shell would expose the nascent soot particles to oxygen and lead to violent ignition processes in the gas phase surrounding the droplet. More refined analyses which explicitly include sooting effects will be needed to fully understand the mechanism(s) which result in reduced gasification rates and disruption. Areas of continuing interest also include the analysis of the internal circulation likely introduced by the experimental droplet deployment mechanism, and the small, but finite relative gas-droplet motions produced by all known techniques for droplet deployment and ignition. Improved experimental methods to characterize these attributes, and means to include their effects (as well as those of sooting) in the theoretical analyses, are presently being pursued.

Recently, we have incorporated the 96 step mechanism of Warnatz (ref. 21) in CRFM, along with multi-component transport to investigate unsteady burning behavior of n-heptane droplets, such as droplet heating before and after ignition, variation of the gasification rate and flame standoff ratio under limiting conditions of no droplet heating (infinitesimal heat capacity), conduction-limited heating, and infinite internal heat conduction (rapid liquid mixing). Time dependent calculations were performed for a 1 mm n-heptane droplet burning in ambient air. An initial vaporization period, followed by ignition by imposition of a spherically symmetric hot shell were studied. Initially, the no-droplet heating configuration was studied to investigate non-steady burning characteristics, and then more realistic liquid-phase heat transfer conditions were included. Species profiles are shown for quasi-steady burning in Fig. 6.

The model simulations suggest that the calculated flame stand-off ratio continuously increases even after the gasification rate reaches 99% of the quasi-steady value (for times $t/t_b > 0.1$, t_b = total burning time), see Fig 7. This unsteadiness has been previously suggested to be due to fuel vapor accumulation effects between the droplet surface and the flame (ref. 32). However, after t/tb> 0.1, the rate of fuel accumulation is near zero and eventually becomes negative due to droplet regression and flame contraction. The initial droplet heating period is strongly influenced by internal circulation. However, after initial transient period, the flame stand-off ratio, the gasification rate, the gas phase temperature and species profiles are not affected by the liquid phase heat transfer mechanism, even though the internal droplet temperature distribution may continue to change

(Fig. 8). Flame unsteadiness, is apparently also not related to internal droplet heating and appears to result primarily from a purely transient phenomenon associated with diffusion flame structural changes and the resulting changes in transport properties in the vicinity of the droplet. Further calculations to study the effects of the Warnatz mechanism on extinction diameter predictions are underway.

Future Work

In the near term, areas of theoretical interest include: improvement of the chemical models utilized for both computational and asymptotic approaches, improvement in understanding the effects of soot on droplet burning phenomena, and consideration of the low relative gas/droplet convection (which is inherent in droplet generation, deployment, and ignition), and assessing the effects of internal circulation induced by growth, deployment and ignition methods. Experimentally, additional efforts are underway to further reduce perturbations caused by droplet deployment and ignition methods, and to qualitatively image some of the flame species profiles, specifically, OH. Finally, the thermo-chemical and chemical kinetic foundations for n-heptane combustion need further improvement. As part of another study on autoignition chemistry of internal spark ignition fuels (e.g., see ref. 24), the author's laboratory is developing a homogenous kinetic experimental database on n-heptane oxidation which will be useful in improving and validating a more appropriate chemical mechanism for future use.

Acknowledgements

The work at Princeton was supported by NASA-LeRC of Cleveland, OH. under contract number #NAS3-1231. Contributors to this research include, Dr. S.Y. Cho, Dr. M. Y. Choi, Mr. P. Michniewicz., Mrs. Y. Stein, and Mr. J. Sivo. MYC was partially supported by the NASA Graduate Researcher Fellowship Program from 1988-1991.

References

1. Williams, F.A.: Diffusion Flames and Droplet Burning, Combustion Theory, 2nd Ed., Benjamin/Cummings Publ. Co., Menlo Park, CA, 1985, p. 52.
2. Choi, M.Y., Cho, S.Y. Dryer, F.L., and Haggard, J.B. Jr.: Some Further Observations on Droplet Combustion Characteristics: NASA LeRC-Princeton Results, AIAA/IKI Microgravity Science Symposium, AIAA Conference Proceedings (ISBN 1-56347-001-2), 1991, p. 294.
3. Choi, M.Y., Cho, S.Y., Dryer, and Haggard, J.B. Jr.: Computational/Experimental Basis for Conducting Alkane Droplet Combustion Experiments on Space-Based Platforms, IUTAM Symposium on Microgravity Fluid Mechanics, Bremmen, FRG, (Rath, H. J., ed.). Springer-Verlag, Berlin, 1992, p. 337.
4. Williams, F.A., Dryer, F.L.and Haggard, J.B. Jr.: Preliminary Science Requirements Document for the Droplet Combustion Apparatus, NASA-Lewis Research Center, November 1, 1991.
5. Cho, S.Y., Yetter, R.A. and Dryer, F.L.: Computer Model For Chemically Reacting Flow With Complex Chemistry/Multi-Component Molecular Diffusion/Heterogeneous Processes, Journal Of Computational Physics, 101, 1992. In press.
6. Cho, S.Y., Choi, M.Y. and Dryer, F.L.: The Extinction of a Free Methanol Droplet in Microgravity, Twenty-third Symposium (International) on Combustion, The Combustion Institute, 1990, p.1611.
7. Lee, A., Law, C.K. and Makino, A.: An Experimental Investigation on the Droplet Vaporization and Combustion of Alcohol Fuels, Fall Eastern Section Meeting of the Combustion Institute, Orlando, FL, 1990.
8. Choi, M.Y.: Droplet Combustion Characteristics under Microgravity and Normal Gravity Conditions, PhD Thesis, Dept. of Mechanical and Aerospace Engineering, Princeton University, Princeton, NJ, 1992, Report MAE T-1937.
9. Kee, R.J., Warnatz, J., and Miller, J.A.: TRANS, Sandia National Laboratories, Livermore, CA, 1983, Report No. 83-8209.
10. Norton, T.S. and Dryer, F.L.: Some Observations on Methanol Oxidation Chemistry, Comb. Sci. and Tech., 63, 1989, p.107.
11. Norton, T.S. and Dryer, F.L.: Toward a Comprehensive Mechanism for Methanol Pyrolysis, Int. J. Chem. Kin., 22, 1990, p. 219.
12. Egolfopoulos, F.N., Du, D.X., and Law, C.K.: A Comprehensive Study of Methanol Kinetics in Freely-Propagating and Burner-Stabilized Flames, Flow and Static Reactors, and Shock Tubes, Comb. Sci. and Tech., 83, 1992, p. 33.
13. Grotheer,, H,H,, Kelm, Driver, H.S.T., Hutcheon, R.J., Lockett, R.D., and Robertson, G.N.: Elementary Reactions in the Methanol Oxidation System. Part I: Establishment of the Mechanism and Modeling of Laminar Burning Velocities. Part II.: Measurement and Modeling of Autoignition in a Methanol-Fuelled Otto Engine, Berichte der Bunsengesellschaft, to appear in October, 1992 Issue.
14. Held, T.J.: PhD Thesis, Methanol, Iso-butene, and MBTE Oxidation in a Flow Reactor: the Effects of Ambient Pressure, Dept. of Mechanical and Aerospace Engineering, Princeton University, Princeton, NJ, 1992. In Preparation.
15. Law, C.K. and Williams, F.A.: Kinetics and Convection in the Combustion of Alkane Droplets, Comb. and Flame, 19, 1972, p. 393.
16. Choi M.Y., Dryer, F.L., Card, J.M., Williams, F.A., Haggard, J.B. Jr., and Borowski, B.A.: Microgravity Combustion of Isolated n-Decane and n-Heptane Droplets, AIAA Paper No. 92-242, January, 1992.
17. Shaw, B.D., Dryer, F.L., Williams, F.A. and Haggard, Jr., J.B.: Sooting And Disruption In Spherically-Symmetrical Combustion Of Decane In Air, Acta Astronautica, 17, 1988, p. 1195.
18. Choi, M.Y., Dryer, F.L. and Haggard, Jr., J.B.: Observation of a Slow-Burning Regime for Hydrocarbon Droplets: n-Heptane/Air Results, Twenty-Third Symposium (International) On Combustion, The Combustion Institute, 1990, pg. 1597.
19. Jackson, G.S. and Avedisian, C.T.: Possible Effects of Initial Diameter in Spherically Symmetric Droplet Combustion of Sooting Fuels, Fall Eastern States Technical Meeting, The Combustion Institute, Ithaca, NY, November, 1991.
20. Dryer, F.L.: The Phenomenology of Modeling Combustion Chemistry, Fossil Fuel Combustion (Bartok, W. and Sarofim, A, eds.), Wiley and Sons, NY, 1991.
21. Warnatz, J.: Chemistry of High Temperature Combustion of Alkanes up to Octane, Twentieth Symposium (International) on Combustion, The Combustion Institute, 1984, p. 845.
22. Bui-Pham, M. and Sheshadri, K.: Comparison Between Experimental Measurements and Numerical Calculations of the Structure of n-Heptane-air Diffusion Flames, Comb. Sci. and Tech., 79, 1991, p. 293.

23. Kent, J.H. and Williams, F.A.:Extinction of Laminar Diffusion Flames for Liquid Fuels, Fifteenth Symposium (International) on Combustion, The Combustion Institute, 1974, p. 315.
24. Kennedy, S, Brezinsky, K. and Dryer, F.: Flow Reactor Oxidation Studies of the Extent of Reaction in Heptane/Iso-octane Mixtures as a Function of Octane Number, Eastern Sectional Meeting of the Combustion Institute, Philadelphia, PA, 1985. Also Kennedy, S. BSE Thesis, Dept. of Chemical Engineering, Princeton University, Princeton, NJ, 1986.
25. Law, C.K. and Chung, S.H.: An Experimental Study of Droplet Extinction in the Absence of External Convection, Comb. and Flame, 64, 1986. p. 237.
26. Green, G.J., Dryer, F.L., and Sangiovanni, J.J.: Cenosphere Soot Agglomerates Formed During Low Reynolds Number Combustion Of Isolated Free Droplets, Paper presented at the 1984 Fall Eastern States Technical Meeting of the Combustion Institute, Gaithersburg, MD, 1984.
27 Friedlander, S.K.: Smoke, Dust and Haze, Wiley & Sons, NY, 1977.
28. Waldmann, L. and Schmitt, K.H.: Thermophoresis And Diffusiophoresis Of Aerosols, Aerosol Science, (Davies, C.N. ed.), Academic Press, NY, 1966, Chpt VI.
29. Palmer, H.B. and Cullis, H.F.: The Chemistry And Physics Of Carbon, Marcel Dekker. Vol. 1, 1965, p. 265.
30. Thermophysical Properties Of Matter, (Touloukian, Y.S. and Ho, C.Y. ,eds.), Plenum Press, NY, 1972.
31. Sangiovanni, J.J. and Liscinsky, D.S.: Soot Formation Characteristics of Well Defined Spray Flames, Twentieth Symposium (International) On Combustion, The Combustion Institute, Pittsburgh, 1984, p. 1963.
32. Law , C.K., Chung, S.H., and Srinivasan, N.: Gas Phase Quasi-Steadiness and Fuel Vapor Accumulation Effects in Droplet Burning, Comb. and Flame, 38, 1980, p. 173.

Figures

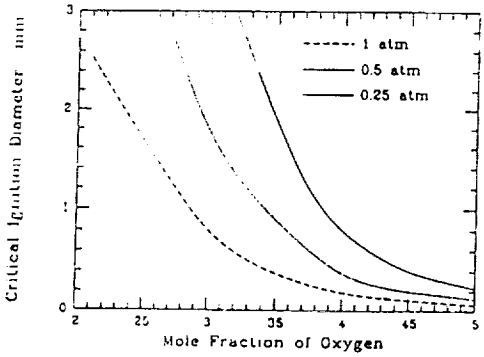

Figure 1. Computed Critical Ignition Diameters for n-Heptane Burning in Oxygen/Helium. (refs. 3,4,8).

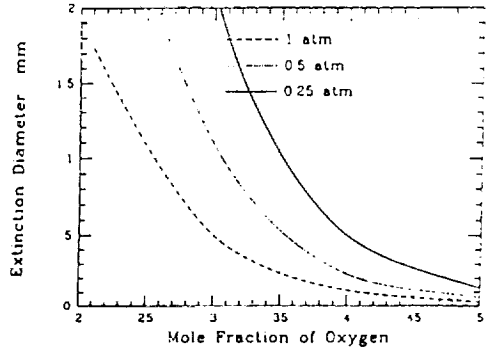

Figure 2. Computed Extinction Diameters for n-Heptane Burning in Helium Diluent. (refs. 3,4,8).

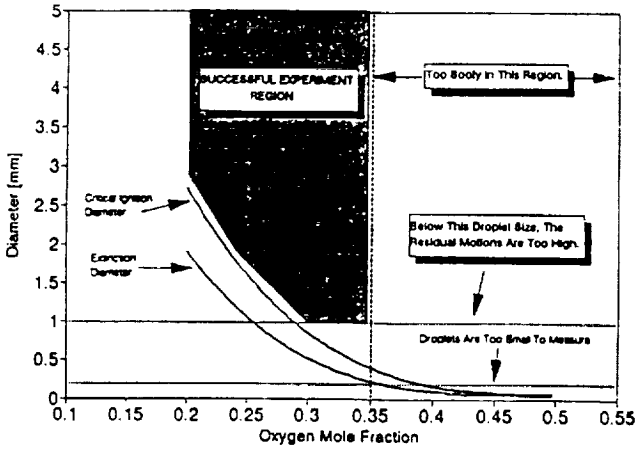

Figure 3. Test Envelope for n-Heptane Droplet Studies in Droptowers and on Space-based Platforms in Helium Diluent. (refs 3,4,8).

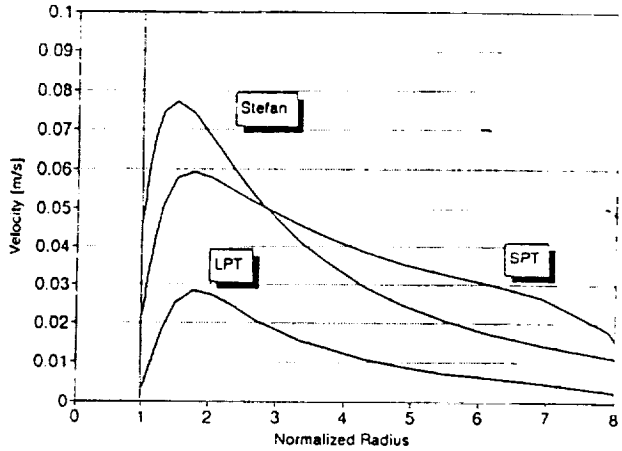

Figure 4. Predicted Stefan, Small Particle Thermophoretic (SPT), and Large Particle Thermophoretic (LPT) Velocity Distributions at Quasi-Steady Conditions for n-Heptane-Air (Nitrogen) Droplet Burning (1 atm.).

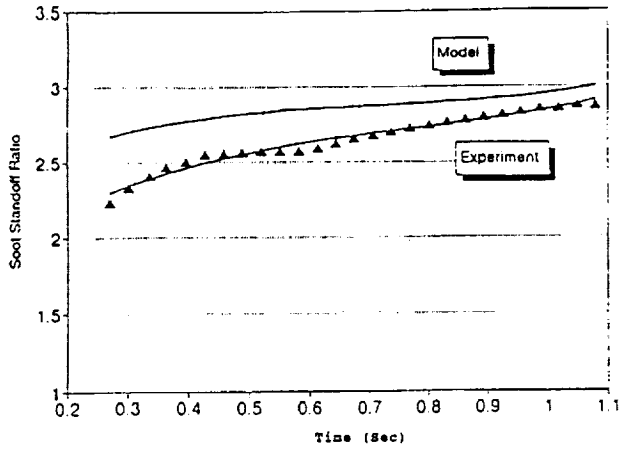

Figure 5. Predicted /Experimental Sootshell Stand-off Ratio for n-Heptane-Air (Nitrogen) Droplet Burning (1 atm.).

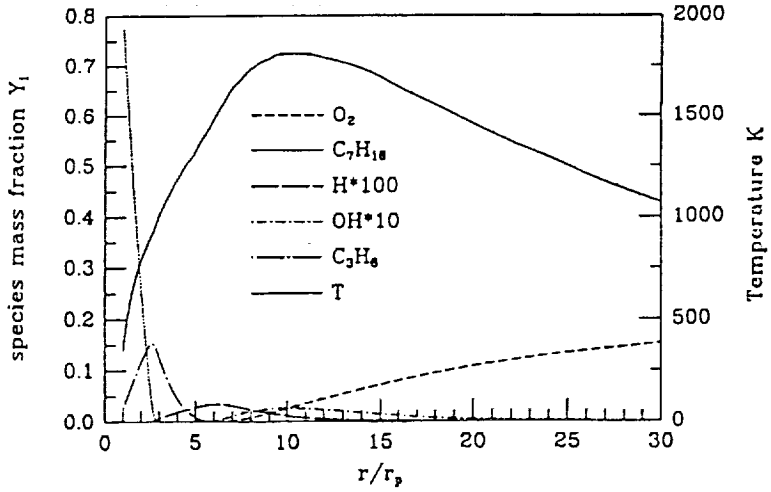

Figure 6. Predicted Species Profiles for Quasi-Steady n-Heptane-Air Droplet Burning (1 atm.) using the Detailed Mechanism of Warnatz (21). No Droplet Heating.

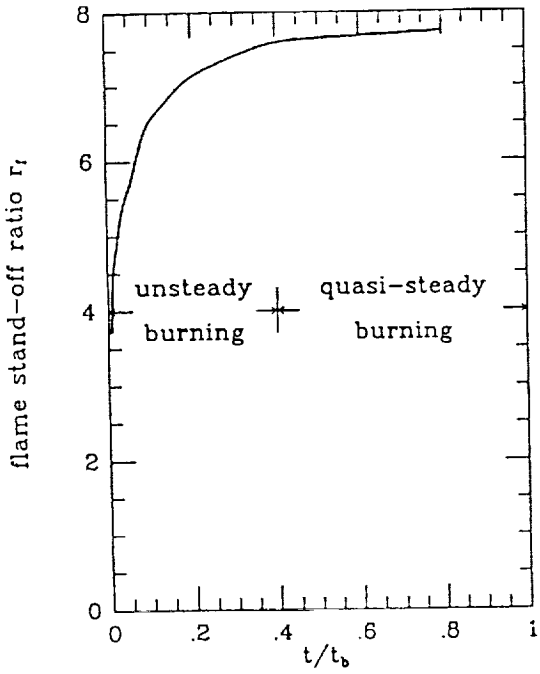

Figure 7. Calculated Flame Stand-off Ratio for n-Heptane-Air Droplet Burning with Mechanism of Warnatz (21). No Droplet Heating.

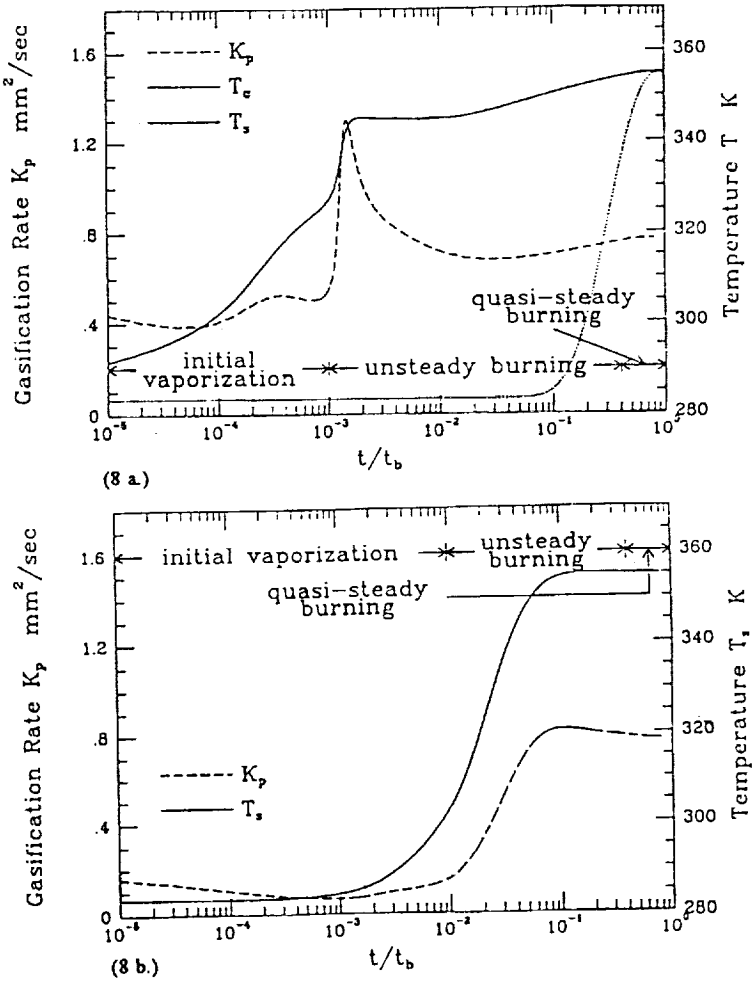

Figure 8. The Temporal Variation of Gasification Rates (K_p), Droplet Surface Temperature (T_s) and Droplet Center Temperature (T_c). (a). Conduction Limit Model. (b). Infinite Heat Conductivity Model ($T_s = T_c$).

COMBUSTION EXPERIMENTS IN REDUCED GRAVITY WITH TWO-COMPONENT MISCIBLE DROPLETS

N93-20214

Benjamin D. Shaw[1] and Israel Aharon[2]
Mechanical, Aeronautical and Materials Engineering Department
University of California
Davis, California 95616

Introduction

The combustion of liquid fuels is a topic worthy of scientific attention on practical and fundamental grounds. Most practical applications of liquid-fuel combustion involve the formation of spray diffusion flames, where droplets frequently burn in groups rather than individually. The combustion is typically complex, with interactions occurring between various physical mechanisms.

Many efforts to understand liquid sprays have focused upon studying isolated droplets. Information gained from these studies is often not directly transferable to spray situations. However, isolated-droplet studies are useful in that they allow certain phenomena (e.g., extinction) to be studied under well-controlled and simplified conditions. When theory and experiment agree for simplified situations, predictions for more complex cases (where accurate experimental data may not exist) may be made with more confidence. The simplest droplet combustion scenario is that of an isolated droplet undergoing spherically-symmetric combustion in an environment of infinite extent. This idealization is approached only when forced and buoyant convection are negligible, the droplet is unsupported, and all foreign objects are far-removed from the combustion zone. Appreciable gravity levels compromise spherical symmetry by inducing buoyant convection.

In practice, liquid fuels are usually multicomponent. It is important to understand the vaporization mechanisms of multicomponent fuels, especially the rates that fuel components with differing properties are vaporized from the liquid phase. This is because gas-phase phenomena depend on the components that have been vaporized, while liquid-phase phenomena depend on the components remaining in the liquid. The simplest multicomponent fuels are (arguably) binary and miscible. Studying binary miscible fuels is useful because they exhibit phenomena which do not appear with pure fuels but which are characteristic of multicomponent blends, for example influences of volatility differences and liquid-phase species diffusion.[3]

Though small droplets are of practical concern (e.g., < 50 μm as found in some spray systems), it is difficult to performed detailed experiments with them. This is because small droplets are difficult to deploy and ignite without significant perturbations, and they may be difficult to resolve photographically. Hence, most detailed investigations into single-droplet combustion have focused upon larger droplets which are easily observed. In this program, reduced-gravity combustion behaviors of miscible binary droplets initially about 1 mm in diameter are studied. Gravity levels significantly less than 10^{-3} g's are required to make buoyancy effects negligible for these size droplets.

Vaporization histories of binary miscible droplets may be significantly different than for pure fuels. When there is a significant volatility difference between droplet components and the lower-volatility component is initially present in small amounts, binary droplets may exhibit a two-staged combustion history where two periods of nearly d-square-law combustion (i.e., where the square of the droplet diameter decreases linearly with time) are separated by an intermediate period where vaporization rates are low and flame diameters decrease significantly. These behaviors are thought to be a result of a sudden buildup of the lower-volatility component at the droplet surface [1,2], necessitating a sudden increase in the droplet surface temperature. While the droplet is heating, the flame contracts because more of the energy transported to

[1]Assistant Professor.

[2]Graduate Research Assistant.

[3]Exceptions do exist for initially-pure fuels. For example methanol droplets may absorb water from the gas phase.

the liquid is used for heating rather than simply for vaporization. Asymptotic analyses of these phenomena are reported in [2]. During the first period of d-square-law vaporization, most of the fuel being vaporized is the higher-volatility component, while during the second d-square-law vaporization period, if liquid-phase species diffusivities are sufficiently small, both liquid components are vaporized at rates that are nearly proportional to their average liquid mass fractions [3]. This mode of combustion, where both liquid components are vaporized at rates that are nearly proportional to their average liquid mass fractions, may be termed the diffusion limit. Recent experiments [4] have suggested that liquid-phase species diffusion may be more rapid than previously thought such that liquid-phase behaviors are intermediate between the diffusion limit and the batch distillation mode. The experiments in Ref. [4] were performed in normal earth gravity and with convective environments, so it is possible that convection may have played a role in promoting liquid-phase transport.

For binary mixture droplets undergoing combustion, the surface concentration of the lower volatility component will generally tend to increase with time. Because liquid species diffusion is typically slow relative to droplet surface regression rates, chemical stratification may occur in the droplet such that the droplet interior has a higher mass fraction of high-volatility component than the droplet surface. During combustion, the temperature at the droplet surface will tend to approach the boiling temperature of the liquid surface mixture. Since Lewis numbers for liquids are typically large relative to unity, the droplet interior may be heated above temperatures required for bubble nucleation and growth. As a result, a bubble may grow and eventually fragment a droplet (the droplet may experience a "disruption" or "microexplosion"). These phenomena have been observed in normal-gravity experiments for multicomponent mixtures [1,5-7]. Disruption has also been observed in reduced-gravity experiments on combustion of unsupported droplets initially composed only of n-decane [8]; similar disruptions of n-decane under normal-gravity conditions appear not to have been reported in the literature. The mechanism behind disruption of n-decane droplets in reduced gravity has not yet been clearly identified, though it has been postulated that disruption may be related to sooting behavior [2,8].

Experiments in reduced gravity should yield insights into the efficiency of liquid-phase species diffusion, since this diffusion may markedly influence combustion behaviors, as described above for the two-staged combustion behaviors. By noting times for flame contraction to occur with mixtures that exhibit two-staged combustion behaviors, calculations for effective liquid-phase species diffusivities may be made (e.g., with the asymptotic theory in [2], or with numerical models). Finally, sooting behavior may be significantly different during the two d^2-law periods since gas-phase compositions may differ significantly. Differences in sooting may be observable photographically by noting behaviors of apparent flame luminosities and soot particles large enough to be observed.

Scientific Objectives

This research focuses on the combustion of binary miscible droplets. Experiments are performed at the NASA Lewis 2.2 sec drop tower in Cleveland, Ohio. Mixtures of n-heptane and n-hexadecane are presently being studied, providing significant variations in component volatilities. The objectives are to gather data on the following:

(1) Transient droplet diameters (including two-staged combustion behaviors and disruption).
(2) Transient flame behaviors (including sudden flame contraction as discussed above, and extinction).
(3) Transport of observable soot particles.

Obtaining these data will be useful in several respects. Knowledge of transient droplet and flame diameters will provide an experimental base from which comparisons between theory and experiment may be made. Working with droplets composed of high-volatility and a low-volatility components, with the latter initially present in small amounts relative to the former, should allow the sudden-flame-contraction behaviors discussed previously to be observed. By noting times for sudden-flame contraction to occur, estimates of liquid-phase species diffusivities may be made. These data will also be useful for development and validation of detailed numerical models.

Work Performed To Date

Digital Image Processing System - A Sun workstation-based digital image processing system has been developed and constructed for analysis of cine films from drop tower experiments. Basic concepts for this system were obtained from Ref. [9], where a PC-based digital image processing system is described. Software for the Sun-based system has been developed with the assistance of Virtual Visions Software[4].

[4]Address: 408 Mountain Laurel Court, Mountain View, CA 94043.

Drop Tower Experiments - During the summer of 1992, experiments with n-heptane/n-hexadecane mixture droplets were performed at the NASA Lewis Research Center 2.2 sec drop tower. An existing droplet combustion apparatus available at NASA Lewis was used for these experiments; this apparatus is described elsewhere [10]. Experiments were attempted both with and without a ceramic support fiber (≈ 10 μm diameter) being present. The ceramic fiber was utilized to prevent significant droplet drift after deployment. The fiber assembly used in the present experiments was developed by D. Dietrich[5]. Twenty-two experiments were performed, both with and without the fiber. Initial droplet compositions, environmental compositions, and pressures were varied in the experiments. Four experiments were successful, with droplets that had low deployment velocities (a few mm/s or less). The other experiments were unsuccessful for various reasons, the most common of which was large residual deployment velocities that caused droplets to quickly leave the camera field of view, even when the fiber was used.

The four successful experiments all utilized the support fiber - data was not obtained for unsupported droplets. Droplets in the successful experiments were burned in air at 1 atm, and involved using initial droplet hexadecane mass fractions of 0, 20, 40 and 60%. In the experiments, two cine cameras with orthogonal fields of view were used to simultaneously record liquid droplet and flame behaviors. Photography of liquid droplets involved backlighting, while flames were photographed without backlighting.

Preliminary analyses of the cine films have been performed with the workstation-based image processing system. Further processing is needed to complete analysis of these films. The image processing system was used to measure droplet diameter histories from the four films, as well as the flame diameter history for one film. Shown in Fig 1. are plots of the squares of the droplet diameters (d^2) vs. time for the four successful experiments. Data are plotted for the time period from spark ignition until the droplets either became too small to image or the drop package hit the bottom of the drop tower. The percentages listed are the initial hexadecane liquid mass fractions. After decay of initial transients, droplet diameter histories appear to show regions where the d-square-law approximately holds. Only the experiment with a 20% hexadecane initial mass fraction appears to clearly show a plateau in the d^2 vs. time plot, indicative of droplet heating. Cine films of the flame behavior for this experiment show the flame to grow, contract, and then grow again over a time period near when the plateau in the d^2 plot in Fig. 1 appears. A sequence of three pictures showing the flame behavior over this time period is shown in Fig. 2. Times in this figure are after ignition, and show the flame prior to contraction, after the flame has contracted (the flame was very dim during this time), and later when it begins to grow in size again. Squares of measured droplet and flame diameters for this experiment are shown in Fig. 3, where it is seen that the onset of flame contraction occurs just prior to the onset of the plateau in the droplet diameter history. Flame diameters in Fig. 3 were measured perpendicular to the fiber.

In the films, it was evident that the fiber was influencing combustion to some extent. For example, soot particles large enough to be seen were sometimes observed to migrate to the fiber and accumulate there. The flames in Fig. 2 are elongated along the fiber, suggesting an influence of the fiber. Shown in Fig. 4. is an image of a droplet, initially 60% hexadecane, 0.39 sec after ignition. The observable soot "shell" is not spherical, though it does appear to be somewhat symmetric about the support fiber axis. In the cine film, soot can be seen to accumulate at the fiber as time progresses. Glowing of support fibers in the hotter portions of the flames was also observed. This is evident in Fig. 2, where the bright, horizontal streaks in each image are actually the glowing fiber. How the radiative heat loss associated with this glowing affects combustion has not yet been evaluated.

Cine films of combustion of a droplet composed initially of 100% n-heptane showed evidence of what appears to be a microexplosion. A sequence of images showing the flame behavior just prior to, during, and after the microexplosion are shown in Fig. 5. This event appears to have caused the droplet to have lost an appreciable amount of mass in a short time period, as is evident in the d^2 plot of Fig. 1 by the "kink" in the data that appears between about 0.3 and 0.4 sec.

Future Plans

Design and Construction of Droplet Combustion Apparatus - A droplet combustion apparatus for use in the NASA Lewis 2.2 sec drop tower is being developed and constructed at UC Davis. This apparatus is projected to be ready for use in late fall 1992. To improve experiment success rates, improvements will be incorporated. For example, it is difficult with the apparatus presently available at NASA Lewis to accurately set the deployment needles and ignition electrodes to desired tolerances, resulting in many failed experiments because of bad droplet deployment or ignition. The new apparatus will incorporate positioning equipment that should allow accurate and repeatable placement of ignition electrodes and deployment needles prior to each experiment. Efforts will also be directed at providing suitably-matched pairs of droplet deployment needles.

---

[5]Current Address: Sverdrup Technology, Inc., 2001 Aerospace Parkway, Brookpark, Ohio 44142.

The new apparatus being constructed is projected to use scanner motor technology previously applied in older versions of the apparatus (for droplet deployment, scanner motors were used to simultaneously retract two opposed deployment needles between which droplets were grown [10]). Preliminary tests by NASA Lewis personnel have suggested that the use of DC motors with retraction speeds significantly higher than scanner motors may result in very small residual droplet deployment velocities and significantly higher experiment success rates. This DC motor technology, still under development, will be considered for use in the apparatus being built at UC Davis.

Drop Tower Experiments - The UC Davis drop apparatus will be used for more experiments with n-heptane/n-hexadecane mixtures. Experiments will be done with different initial environmental compositions and pressures. Initial oxygen mole fractions from about 0.1 to 0.5 and initial pressures from 0.5 to 2 atm will be used. Different inerts will be used in the gas phase to enhance or inhibit certain phenomena. For example, He may be used to increase average gas phase transport properties, promoting extinction and higher burning rates [11], while CO_2 may possibly be used to inhibit soot formation [12].

It may be important to inhibit soot formation in these experiments. Flame contractions and droplet disruptions have previously been observed for n-decane droplets burning in low-gravity environments [8], as well as the n-heptane droplet described above. These behaviors, which were unexpected for single component fuels, have been postulated to result from sooting effects [2,8]. If this is correct, flame contractions and droplet disruptions arising from surface buildup of the less volatile component in a binary fuel droplet may be influenced to an unknown extent by sooting, making interpretation of experimental results difficult. Experiments will be performed to search for conditions where sooting appears to influence combustion negligibly. Alcohol mixtures (which should tend to soot less than hydrocarbons) may also be used, though alcohols may absorb water into the liquid phase.

Image Processing System - Films are currently processed manually with the image processing system. The image processing system will be automated to allow a large number of frames to be rapidly processed from each film strip. In addition, data is presently taken from films by manually setting a threshold corresponding to the perceived droplet diameter. Edge detection algorithms will be incorporated into the image processing program, allowing more repeatable and accurate measurement of droplet diameters.

Computational Modeling - Efforts to provide numerical data for comparison with experimental results have been initiated. Professor H. A. Dwyer of UC Davis is the principal architect of the models presently being utilized. Briefly, the models assume that spherical symmetry exists in the gas and liquid phases. The governing equations are cast in a finite-volume form, and solved numerically for transient liquid- and gas-phase variables. Variable properties in both the liquid and gas phases are allowed. Complex chemical kinetics in the gas phase can be modeled, as well as global one-step reaction schemes. Initial results from this model were not available at the time this paper was written, but are expected to be available in the near future. Calculations are performed using the Sun workstation also used for image processing.

Other - To aid interpretation of experimental efforts, studies of allowable acceleration levels and durations will be performed. Issues such as droplet oscillation amplitudes, oscillation decay times, pre-ignition vaporization, etc., will be considered. In addition to being relevant to drop tower experiments, such studies will be germane to possible future flight experiments involving droplet combustion.

References

1. Wang, C.H., Liu, X.Q., and Law, C.K., "Combustion and Microexplosion of Freely Falling Multicomponent Droplets," Combustion and Flame, 56: pp.175-197 (1984).

2. Shaw, B.D., and Williams, F.A., "Theory of Influence of a Low-Volatility, Soluble Impurity on Spherically Symmetric Combustion of Fuel Droplets," International Journal of Heat and Mass Transfer, 33: pp. 301-317 (1990).

3. Shaw, B.D., "Studies of Influences of Liquid-Phase Species Diffusion on Spherically Symmetric Combustion of Miscible Binary Droplets," Combustion and Flame, 81: pp. 277-288 (1990).

4. Randolph, A.L., Makino, A., and Law, C.K., "Liquid-Phase Diffusional Resistance in Multicomponent Droplet Gasification," Twenty-First Symposium (International) on Combustion, pp. 601-608 (1988).

5. Lasheras, J.C., Fernandez-Pello, A.C., and Dryer, F.L., "Experimental Observations on the Disruptive Combustion of Free Droplets of Multicomponent Fuels," Combustion Science and Technology, 22, pp. 195-209 (1980).

6. Yap, L.T., Kennedy, I.M., and Dryer, F.L., "Disruptive and Micro-Explosive Combustion of Free Droplets in Highly Convective Environments," Combustion Science and Technology, 41, pp. 291-313 (1984).

7. Niioka, T., and Sato, J., "Combustion and Microexplosion Behavior of Miscible Fuel Droplets Under High Pressure," Twenty-First Symposium (International) on Combustion, pp. 625-631 (1988).

8. Shaw, B.D., Dryer, F.L. Williams, F.A., and Haggard, J.D., "Sooting and Disruption in Spherically-Symmetrical Combustion of Decane Droplets in Air," Acta Astronautica, 17: pp. 1195-1202 (1988).

9. Choi, M. Y. and Dryer, F. L., "A Digital Image Processing Technique for Droplet Burning Data," Mechanical and Aerospace Engineering Report #1875, Princeton University (1989).

10. Haggard, J. B. and Kropp, J. L., "Development of a Droplet Combustion Experiment for Low-Gravity Operation," paper AIAA-87-0576 presented at the AIAA Twenty-Fifth Aerospace Sciences Meeting.

11. Cho, S. Y., Choi, M. Y., and Dryer, F. L., "Extinction of a Free Methanol Droplet in Microgravity," Twenty-Third Symposium (International) on Combustion, pp. 1611-1617 (1990).

12. Kadota, T., Hiroyasu, H., and Farazandehmer, A., "Soot Formation by Combustion of a Fuel Droplet in High Pressure Gaseous Environments," Combustion and Flame, 29, pp.67-75 (1977).

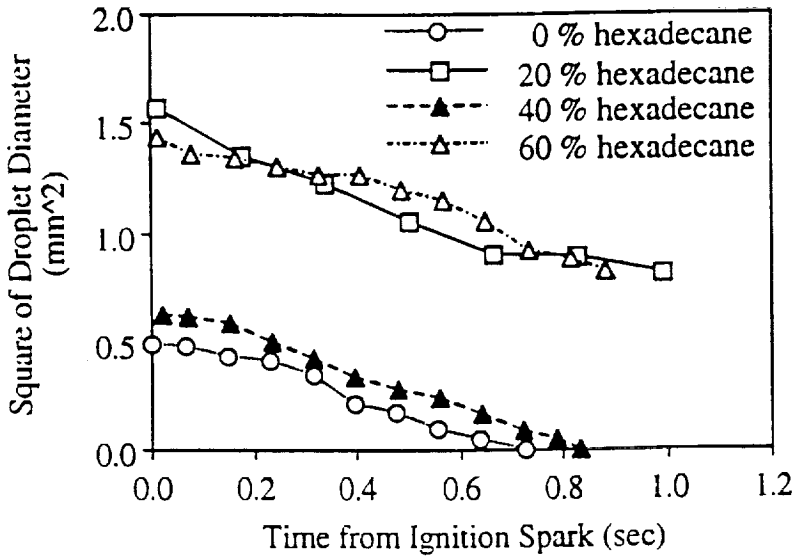

Figure 1.--Plots of squares of measured droplet diameters vs. time.

0.794 sec 0.860 sec 0.990 sec

Figure 2.--Sequence of images showing flame contraction and growth for a droplet composed initially of 20% n-hexadecane and 80% n-heptane. Times are after the ignition spark. Visible flame diameters (measured perpendicular to the fiber) for this droplet are plotted in Fig. 3.

See Color Plate G2A

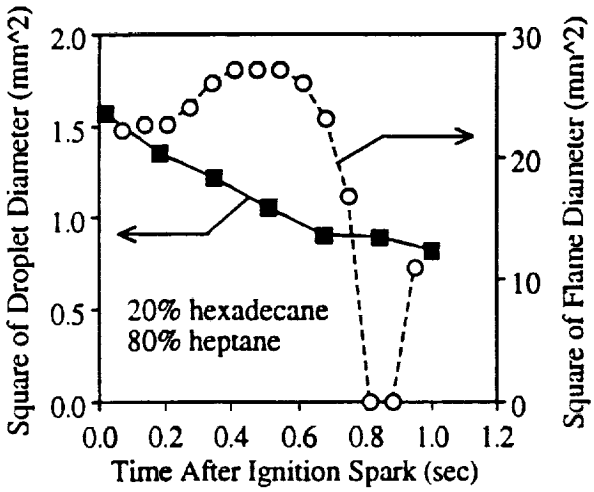

Figure 3.--Plots of squares of droplet and flame diameters for a droplet composed initially of 20% n-hexadecane and 80% n-heptane.

Figure 4.--Image of a droplet (initially 60% n-hexadecane and 40% n-heptane) showing the support fiber and the soot "shell". The droplet diameter is about 1.07 mm.

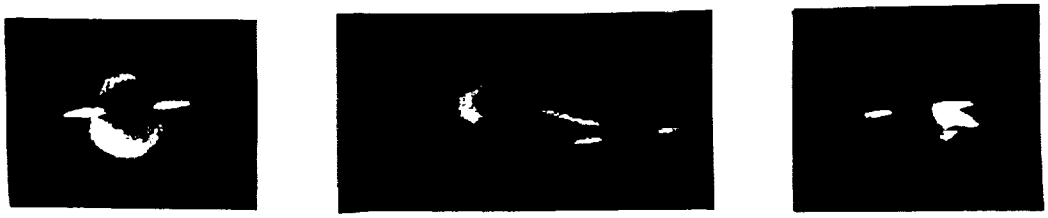

0.324 sec 0.333 sec 0.342 sec

Figure 5.--Sequence of images showing the flame behavior just prior to, during and after what appears to be disruption of a droplet initially composed only of n-heptane. Times are after the ignition spark. For a scale reference, the visible flame diameter at 0.324 sec is about 4.7 mm (measured perpendicular to the fiber).

See Color Plate G2b

STATUS OF THE CNRS-LCSR PROGRAM ON HIGH PRESSURE DROPLET VAPORIZATION AND BURNING

Christian Chauveau and Iskender Gökalp
Centre National de la Recherche Scientifique
Laboratoire de Combustion et Systèmes Réactifs
45071 Orléans cédex 2, France

Introduction

Depending on the surrounding flow and thermodynamic conditions, a single droplet may experience several gasification regimes, ranging from the envelope flame regime to pure vaporization. In practical situations, such as rocket propulsion or diesel combustion, the size distribution of droplets is, at best, bimodal, so that the possibility exists for the simultaneous presence of various regimes. For example, very small droplets are transported by the gas phase with zero relative velocity. This picture validates then the spherical symmetry hypothesis applied to the droplet and to the diffusion flame enveloping it. On the other hand, for larger droplets, a relative velocity exists due to drag forces. The most important influence of forced convection on droplet burning is the possibility to extinguish globally the envelope flame, or to establish a flame stabilized in the wake region. The burning rates of these regimes differ strongly. The characteristic time of droplet gasification is also influenced by the surrounding pressure and temperature. A parametric investigation of single droplet burning regimes is then helpful in providing the necessary physical ideas for sub-grid models used in spray combustion numerical prediction codes.

The CNRS-LCSR experimental program on droplet vaporization and burning deals with these various regimes: stagnant and convective monocomponent droplet burning (refs. 1 and 2); convective mono and bicomponent droplet vaporization (refs. 3 and 4); high temperature convective mono and bicomponent droplet vaporization (ref. 5); burning regimes of hydrazine and hydroxyl-ammonium-nitrate based monopropellant droplets and the vaporization regimes of liquid oxygen droplets. Studies on interacting droplets and on liquid aluminium droplets will start in the near future. The influence of high pressure is a common feature of all these studies. This paper summarizes the status of the CNRS-LCSR program on the effects of high pressure on monocomponent single droplet burning and vaporization, and some recent results obtained under normal and reduced gravity conditions with suspended droplets are presented. In the work described here, parabolic flights of an aircraft is used to create a reduced gravity environment of the order of 10^{-2} g.

Description of the experimental techniques

The High Pressure Droplet Burning Facility

Droplet burning experiments under stagnant and variable pressure conditions are performed in a specially designed facility : High Pressure Droplet Burning Facility (HP-DBF). The HP-DBF is designed to investigate

the gasification regimes of suspended or free-floating droplets under variable pressure conditions, up to 12 MPa. Low pressure droplet burning experiments can also be realized (refs. 6, 7 and 8). HP-DBF can be used during the parabolic flights of an aircraft. This apparatus is articulated around a cylindrical combustion chamber of 11 litres capacity, made of an aluminium alloy (AU4G), and mounted on a support structure with a control panel. Two circular flanges are mounted on the two sidewalls of the octogonally shaped external faces of the chamber. Ten identical openings are positioned on the chamber: two openings on the sidewalls to support the droplet injection and ignition systems, and eight along the octagonal perimeter. Two injection needles are positioned face to face and are connected to an electrical pump, allowing the injection of a fuel amount of 0.5 microliters/min. A droplet is formed between the two retractable injectors. A tiltable (d = 0.2 mm) quartz fibre, mounted on the upper chamber wall, can be positioned between the two needles to hold the droplet in the case of suspended droplet experiments. Depending on the droplet burning experiment type, various ignition systems are used. During normal pressure experiments, the droplet is ignited by one pair of electrodes mounted around one injection needle. The ignition spark is produced by a high tension (10 kV) solenoid under 24 V DC. For high pressure droplet burning experiments, an improved version of the injection system and a heated coil for ignition are used. The sequence of injection and ignition operations is computer controlled

Diagnostics

The principle diagnostic systems we are using are based on the visualization of the droplet vaporization or burning phenomena. For droplet burning experiments, the recording equipment is composed of two systems. A high speed video camera, Kodak-Ektapro 1000, which can record up to 1000 full frames per second, allows detailed analysis of droplet burning. The Ektapro 1000 Motion Analyzer's live, real-time viewing makes possible to follow the investigated phenomena frame per frame. A standard video camera, Sony 8 mm PAL, is used to record the droplet and the flame in true colours, but only at 25 frames per second. A second camera has been added to the Kodak-Ektapro 1000 system, in order to be able to observe simultaneously the droplet and the flame with respective appropriate magnification rates. The digitized images from the Ektapro system are transferred to a microcomputer where the image analyses are performed. Details of the image analysis are fully documented in ref. 6.

For droplet vaporization experiments a different imaging system is used. It is composed of a camera, a data acquisition interface, a time base corrector, a micro-computer, and a TV monitor. The camera is monochromatic and has 256 grey levels and a CCD matrix of 512 x 512 pixels. It is equipped with an electronic shutter with a maximum rate of 1/10000. The camera optics provides a maximum magnification rate of 80. The image digitization is done through of a MATROX PIP 1024 interface (video memory 1 Mo) which allows the digitization of an image of 1024 x 1024 or four images of 512 x 512 . A digital time corrector with 1 ms resolution is added. The digitization rate is 50 Hz. Each pixel is coded on 8 bits, that is 256 levels of grey. The microcomputer has a I486DX 33 MHz processor, a hard disk of 200 Mo, 4 Mo of memory and a S-VGA screen.

Suspended droplets are backlighted; this provides the necessary contrast for direct threshold definition. The time to extract the droplet contour is less then 1/50 s to allow the maximum image acquisition rate (50 Hz). The droplet contour determination is based on dichotomic point research methodology. To optimize the speed of frame grabbing and the size of the image data, we have chosen to take only eighty points along the contour. These data are simultaneously memory saved and displayed on the screen. At the end of the acquisition (750 frames) the complete data sets are transferred to the hard disk. The data analysis consists in calculating the surface area from the contour points and to obtain the droplet equivalent diameter. The droplet diameter and its corresponding time are saved in a synthesized file. The major advantage of the method is its well defined time resolution, characterized by the impressive number of pictures taken into account during a droplet lifetime.

Results and discussion

High pressure low temperature vaporization experiments

Preliminary experiments have been conducted under normal gravity conditions to determine the influence of ambient pressure on the vaporization of n-heptane and methanol droplets in air at 300 K (or Tr = T/Tc = 0.56 and 0.59 respectively). The maximum reduced pressure Pr = P/Pc was 3.6 for heptane and 1.2 for methanol. Droplet initial diameters were between 1 mm and 1.5 mm. The variation with time of $(d/do)^2$ for n-heptane droplets is shown on Fig. 1. These curves are used to determine an average vaporization constant, Kav. The variation of Kav with P/Pc is shown on Fig. 2. Kav decreases strongly for P/Pc < 1 and shows a weakly increasing behaviour for P/Pc > 1. The decrease of Kav for P/Pc < 1 can be explained by the increased ambient gas density which delays the build up of the fuel vapour concentration profile near the droplet surface and its further diffusion into the ambience. The decrease of Kav in the subcritical pressure regime is confirmed by methanol droplet vaporization experiments (Fig. 2). They also show another phenomenon for moderate pressures. The data for pure methanol for P = 0.1 MPa indicates a sequential vaporization behaviour (Fig 3). This behaviour is no more observed for approximately P/Pc > 0.3. The sequential vaporization behaviour of methanol droplets for moderate pressures is to be compared with the observations of refs. 9 and 10. The curves of $d^2(t)$ are also used to determine the instantaneous vaporization rates (Figs. 4a and 4b). For heptane droplets, the largest variation is observed for the atmospheric pressure case. For increasing pressures, K(t) increases during the last quarter of the vaporization lifetime, which may well be an artefact of the influence of the suspension fibre. Except the moderate pressure experiments, K(t) for methanol droplets shows the same behaviour. A quasi-steady state process can thus be assumed to characterize high pressure vaporization of n-heptane and methanol droplets in room temperature air.

High pressure droplet burning experiments

High pressure burning experiments have been conducted with n-heptane and methanol droplets. The experiments with n-heptane droplets were conducted under reduced gravity conditions only up to a maximum pressure of 0.65 MPa. With increasing pressure, they show (ref. 10) a gradual increase of the average burning rate and an increasing non-stationary behaviour of the instantaneous burning rate. n-heptane burning droplet experiments have been continued for higher pressures under normal gravity. Contrary to the results of ref. 11, the vanishing surface tension prevented to increase the pressure above 1.8 MPa. The increased soot formation also prevented the determination of the instantaneous droplet diameter. An average burning rate is then determined by assuming the d^2 law and by using the duration of the flame luminosity as the burnout time. The results are presented on Fig. 5 with error estimate margins. The reduced gravity results are clearly lower than the corresponding normal gravity results. The variation with pressure of the average burning rate in the subcritical regime can be represented with a power law of the form $P^{0.36}$.

Burning experiments of considerably less sooting methanol droplets have been conducted under reduced gravity conditions to be able to detect the instantaneous droplet diameter. These experiments have been conducted between normal atmospheric pressure and a maximum reduced pressure of Pr = 0.63. Two pictures of a burning suspended methanol droplet with d_o = 1.5 mm and for Pr = 0.63 are shown on Plate I. Figure 6 presents the curves of $d^2(t)$ for two pressures. The sequential gasification behaviour is not observed even for the lowest pressure range (see also ref. 12). As shown on Fig. 7, the average burning rate increases with pressure. Three methods have been compared on this figure: the method based on the d^2 law and the droplet lifetime; the method based on the average slope of the $d^2(t)$ curve; and that based on the average value of K(t). As a first approximation, and for the pressure range investigated here, the three methods give comparable values and a quasi-linear increase of the average burning rate with pressure. Figure 8 shows the instantaneous burning rates for high pressure methanol droplet burning experiments. The curve for the highest pressure, P = 5 MPa, is distinguishable from the others by its accentuated non-stationary behaviour.

Future work

The investigation of high pressure effects will be the main focus of the future LCSR work on droplet gazification regimes. The supercritical regime will be approached with the help of a new version of the HP-DBF which is under construction: it will allow to increase the temperature as well as the pressure of the ambient medium. This apparatus will be used to investigate the vaporization and burning of mono and multicomponent fuel droplets in high pressure and high temperature conditions and also to compare normal gravity and reduced gravity experiments to infer natural convection effects. An electrodynamic balance is under development and will be added to the apparatus. It will allow to conduct supercritical vaporization experiments under normal gravity conditions. The parabolic flights of the Caravelle aircraft will be continued to be used for suspended droplet experiments. A new high pressure droplet burning module will be developed to be used during sounding rocket experiments in collaboration with ESA/ESTEC and MBB-ERNO. A major purpose of the following years is the investigation of high pressure vaporization of liquid oxygen droplets. A collaboration is established with the University of Marseille and ONERA to develop the numerical modelling part of this task.

Acknowledgments

The droplet vaporization and burning studies program of the CNRS-LCSR is supported by the Microgravity Office of the European Space Agency, the Centre National d'Etudes Spatiales, the Société Européenne de Propulsion, the Commission of the European Communities, the Joint Research Programme of the European Car Manufacturers, the French Army Research Office, and ONERA.

References

1. Gökalp, I., Chauveau, C., Richard, J.R., Kramer, M. and Leuckel, W., **Twenty-Second Symposium (International) on Combustion**, The Combustion Institute, Pittsburgh, 1988 pp. 2027-2035.
2. Chauveau, C. and Gökalp, I., **Proceedings of 7th. European Symposium on Materials Sciences and Fluid Physics in Microgravity**, ESA-SP-295, 1990, pp. 467-472.
3. Gokalp, I., Chauveau, C., Simon, O. and Chesneau, X., **Combustion and Flame**, vol. 89, 1992, pp. 286-298
4. Gokalp, I., Chauveau, C., Ramos-Arroyo, N.A., Berrekam, H. and Chesneau, X., **Proceedings of the 5th ILASS Americas**, May 18-20, 1992, San Ramon, Ca.
5. Ramos-Arroyo, N.A., Berrekam, H., Chauveau, C. and Gökalp, I., Paper to be presented at the **Fall Meeting of the Western States Section of the Combustion Institute**, October 12-13, 1992, Berkeley, Ca.
6. Chauveau, C., Vaporisation et Combustion des Gouttes Isolées de n-Heptane. Etude en Microgravité et Influence de la Convection Forcée. **PhD. Thesis**, Université d'Orléans, 1990
7. Chauveau, C. and Gökalp, I., **Ann. Chim. Fr.**, vol. 17, 1992, pp. 27-44.
8. Chesneau, X., Chauveau, C. and Gökalp, I., **Proceedings of the First European Symposium on Fluids in Space, ESA SP-353**, 1992, pp. 407-418.
9. Law, C.K., Xiong, T.Y. and Wang, C.H., **Int. J. Heat Mass Transfer**, vol. 30, no. 7, 1987, p. 1435.
10. Cho, S.Y., Choi, M.Y. and Dryer, F.L., **Twenty-Third Symposium on Combustion, The Combustion Institute**, 1990, pp. 1611-1617.
11. Sato, J., Tsue, M., Niwa, M. and Kono, M., **Combustion and Flame**, vol. 82, 1990, pp. 142-150.
12. Yang, J.C., Jackson, G.S. and Avedisian, C.T., **Twenty-Third Symposium on Combustion, The Combustion Institute**, 1990, pp. 1619-1625.

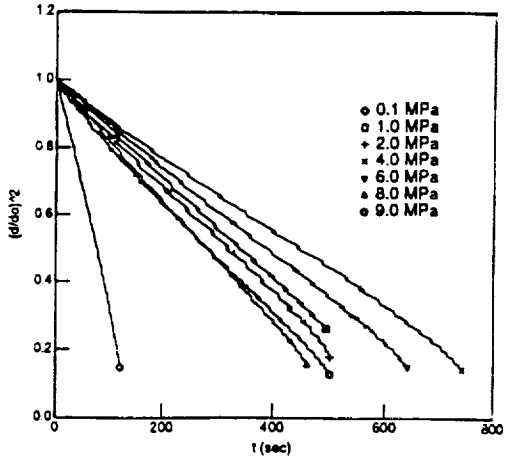

Fig. 1 : Influence of the ambient pressure on the vaporization of n-Heptane droplets.

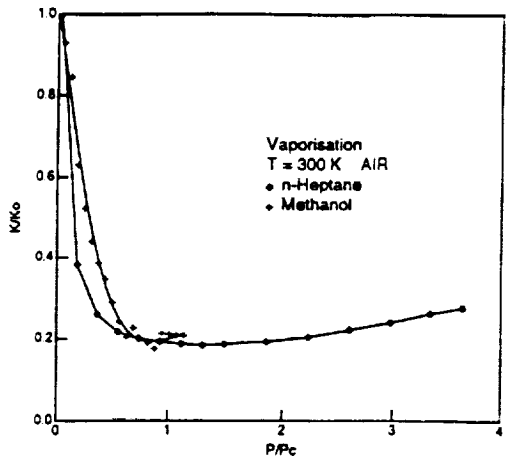

Fig. 2 : Evolution of K/Ko with P/Pc for n-Heptane and Methanol droplets.

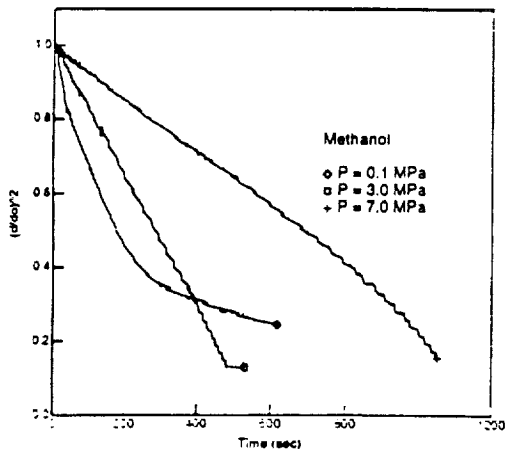

Fig.3 : Influence of the ambient pressure on the vaporization of Methanol droplets.

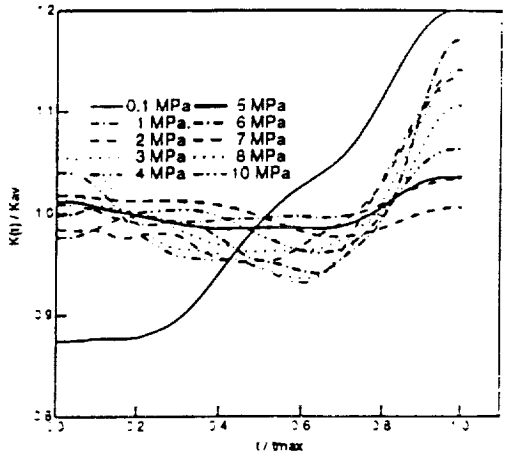

Fig. 4a : Instantaneous vaporization rates for n-Heptane droplets.

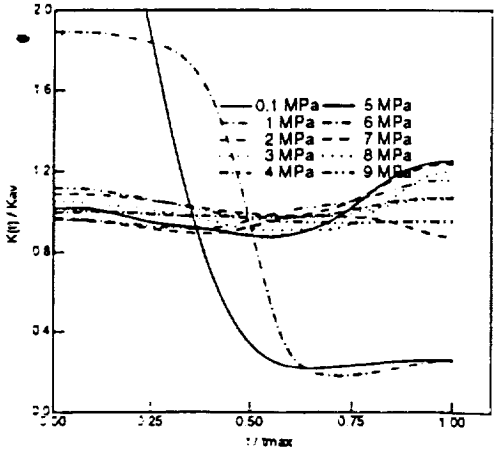

Fig. 4b : Instantaneous vaporization rates for Methanol droplets.

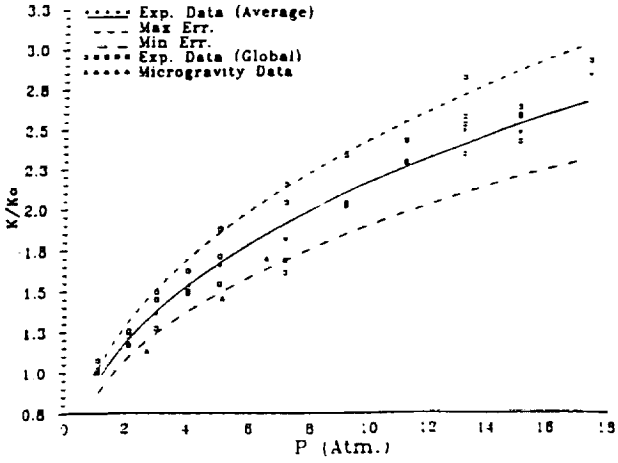

Fig. 5 : Influence of the ambient pressure on the combustion of n-Heptane droplets

(a) t = 520 ms

(b) = 1244 ms

Plate 1 : Pictures of a burning suspended Methanol droplet; P = 5 MPa, g≈ 10^{-2} g_o, d_o=1.5 mm

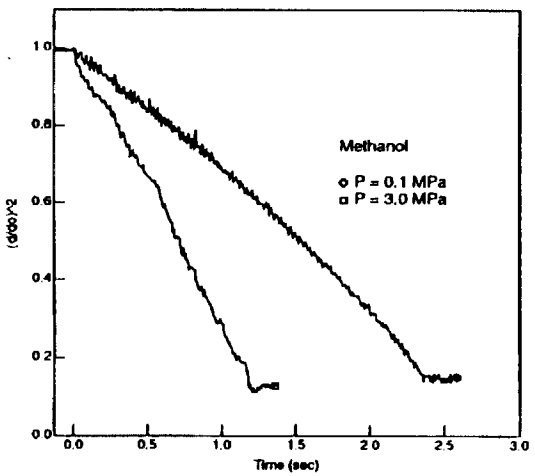

Fig. 6 : Evolution of $(d/do)^2$ with time for Methanol droplet burning in microgravity.

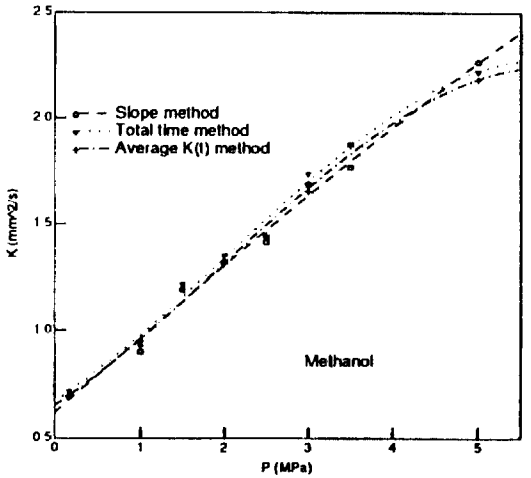

Fig. 7 : Evolution of the average burning rate with the ambient pressure, for Methanol droplets, in microgravity.

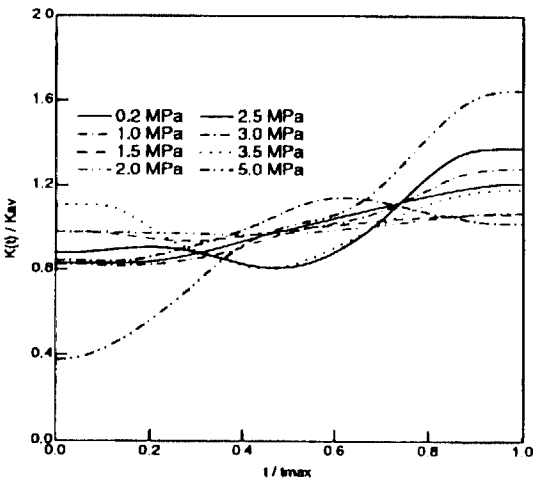

Fig. 8 : Instantaneous burning rate for high pressure methanol droplet burning experiments.

HIGH-PRESSURE DROPLET COMBUSTION STUDIES

M. Mikami and M. Kono
Department of Aeronautics, University of Tokyo
Hongo, Bunkyo-ku, Tokyo 113, Japan

N93-20216

J. Sato
Research Institute
Ishikawajima-Harima Heavy Industries Co., Ltd.
Toyosu, Koto-ku, Tokyo 135 Japan

D.L. Dietrich
Sverdrup Technology, Inc.
NASA Lewis Research Center, Cleveland, Ohio 44135

and

F.A. Williams
Center for Energy and Combustion Research
Department of Applied Mechanics and Engineering Sciences 0310
University of California San Diego, La Jolla, California 92093

Introduction

This is a joint research program, pursued by investigators at the University of Tokyo, UCSD, and NASA Lewis Research Center. The focus is on high-pressure combustion of miscible binary fuel droplets. It involves construction of an experimental apparatus in Tokyo, mating of the apparatus to a NASA-Lewis 2.2-second drop-tower frame in San Diego, and performing experiments in the 2.2-second tower in Cleveland, with experimental results analyzed jointly by the Tokyo, UCSD, and NASA investigators. The project was initiated in December, 1990 and has now involved three periods of drop-tower testing by Mikami at Lewis.

The research accomplished thus far concerns the combustion of individual fiber-supported droplets of mixtures of n-heptane and n-hexadecane, initially about 1 mm in diameter, under free-fall microgravity conditions. Ambient pressures ranged up to 3.0 MPa, extending above the critical pressures of both pure fuels, in room-temperature nitrogen-oxygen atmospheres having oxygen mole fractions X of 0.12 and 0.13. The general objective is to study near-critical and super-critical combustion of these droplets and to see whether three-stage burning, observed at normal gravity, persists at high pressures in microgravity. Results of these investigations will be summarized here; a more complete account soon will be published (ref. 1).

Experimental Apparatus and Procedure

Figure 1 shows a schematic diagram of the experimental apparatus. The pressure chamber has four orthogonal windows that give two views of the combustion process, a backlit view from which the droplet size as a function of time is obtained and a second view which shows

the flame surrounding the droplet. During each test, both of these views were recorded by 16 mm cine cameras. Microgravity conditions were attained by dropping the pressure chamber and associated experimental equipment in a drop tower at NASA Lewis Research Center that provides 2.2 seconds of microgravity ($\sim 10^{-5}$ normal).

Before release of the experimental package, a fuel droplet was formed at the end of a 0.125 mm silica fiber from a high-pressure syringe driven by a stepping motor. Following release, immediately upon entry into microgravity the droplet was ignited. The ignition source was a hot wire (aluminum alloy, 0.2 mm diameter) formed into a 2 mm diameter loop that surrounds the droplet. The hot wire was rapidly removed after ignition, leaving approximately 2 sec of the 2.2 sec to observe combustion. All processes, including droplet dispensing and ignition, were controlled by a microcomputer.

The initial droplet size was approximately 1 mm in diameter.[1] This droplet diameter is nearly an order of magnitude larger than that of the suspending fiber, while also being small enough that complete burning could be observed in the available microgravity time. The ambient gas was a nitrogen-oxygen mixture with oxygen mole fractions, X, being 0.12, except for a small number of tests at X = 0.13. These reduced oxygen concentrations were employed to aid in visualizing the droplet from the backlit view at high pressure. All experiments were performed with the ambient gas and the droplet initially at room temperature.

The binary fuel droplet was composed of n-heptane and n-hexadecane with mass fractions of hexadecane, Y, ranging from 0 (pure heptane) to 1.0 (pure hexadecane). The subject fuels have critical temperatures and pressures of 540 K, 2.74 MPa and 722K, 1.53 MPa for heptane and hexadecane respectively. The pressure in the data reported here varied from 0.4 to 3.0 MPa.

General Combustion Behavior

Figure 2 shows variations of the square of the droplet diameter d with time t at different pressures, both normalized according to theory by dividing by the square of the initial droplet diameter d_o. For fuel mixtures, after the initial transition period and the first stage of linear behavior, another transition period exists (the second stage), after which the square of the droplet diameter again decreases with time almost linearly (the third stage), as seen in Figure 2. The cause of such three-stage burning is as follows: In the first straight segment, the high-volatility fuel, heptane, vaporizes preferentially from the droplet surface since the droplet temperature is relatively low. Since liquid-phase diffusion is slow relative to droplet surface regression, the hexadecane mass fraction gradually increases in the surface region. When the surface concentration of hexadecane reduces that of heptane sufficiently, the vaporization rate decreases and the flame approaches the droplet (the second transition period). After the droplet is heated by the flame enough to allow sufficient hexadecane to vaporize, hexadecane and heptane vaporize vigorously together, in the second straight segment. Figure 3, which shows both normalized droplet diameter and flame diameter as functions of time, illustrates how flame contraction follows the onset of the transition period; this delay is reduced at larger X.

[1] When the droplet is suspended from the fiber, it is not spherical in shape, but is elongated along the fiber due to surface tension. The equivalent spherical droplet diameter is computed as the cubic root of the product of the major diameter (along the fiber) with the square of the minor diameter (perpendicular to the fiber).

As seen in Figure 2, this staged type of burning still exists at the supercritical ambient pressure of 3 MPa. The concentration Y=0.11 in Fig. 2 lies outside the boundary of staged burning reported earlier by Niioka and Sato. The phenomenon may have been present but not observable in the normal-gravity experiments because the duration of the second stage is shortened by the increased rate of heat transfer produced by natural convection, or the gas-velocity and surface-tension variations under natural convection may have promoted internal liquid mixing and thereby narrowed the region of staged burning. Stage burning occurred for all mixtures tested other than pure fuels in the present study.

Homogeneous nucleation is not observed in this experiment. This result is expected because the ambient gas is diluted with nitrogen, reducing the droplet surface temperature, so that the local droplet temperature has less of a tendency to exceed the limit of superheat.

Droplet Lifetime

Figure 4 shows the dependence of the normalized droplet lifetime[2], t_l, at different ambient pressures on the initial hexadecane mass fraction.

This figure shows that the droplet lifetime reaches a maximum at an intermediate hexadecane mass fraction, at all but the highest pressure. For fixed initial hexadecane mass fraction, the droplet lifetime decreases with increasing ambient pressure, except for pure hexadecane. For hexadecane, the droplet lifetime exhibits a minimum value at 2.5 MPa rather than the critical pressure of 1.5 MPa, and the burning-rate constant exhibits a maximum at 2.5 MPa, as described later. Earlier results indicated that in air the burning-rate constant achieves its maximum at the critical pressure. Studies of fuel-droplet evaporation, however, have reported that the evaporation constant reaches its maximum at an ambient pressure above the critical pressure and at higher ambient pressures when the ambient temperatures are lower. Therefore, the occurrence of the minimum droplet lifetime and the maximum burning-rate constant above the critical pressure, rather than near the critical pressure, may be caused by delayed attainment of liquid criticality, associated with the lower temperatures produced by dilution of air in the present experiments. It is noteworthy that minima are not seen for heptane or any of the mixtures. Most of their histories seem dominated by heptane, whose critical pressure is significantly higher; the minima could develop at higher pressures for these droplets.

As shown by Figure 2, the square of the droplet diameter decreases almost linearly with time in the first and third stages. Figure 5 shows the burning-rate constant in the first stage, K_1, and in the third stage, K_3, both here defined from the maximum slope in each segment. While K_1 decreases sharply with increasing initial hexadecane mass fraction at fixed ambient pressure, K_3 increases somewhat. Both increase with increasing pressure, except for pure hexadecane, which exhibits a maximum value at 2.5 MPa, as described above.

Since the first straight segment occupies most of the droplet lifetime for small Y, K_1, which decreases with increasing Y, has a major influence under these conditions. On the other hand, for large Y, since the second straight segment occupies most of the droplet lifetime, K_3, which increases with increasing Y, is dominant.

The burning-rate constant K_1 may be approximated as

$$K_1 = [8\lambda/(\rho c_p)]ln(1 + B) \tag{1}$$

[2]The droplet lifetime is defined as the time from the initial appearance of a luminous flame until the droplet disappears.

where the transfer number B is

$$B = [Y_{C7+} + Y_{O,\infty}\, \nu_{C7}\, W_{C7}/(\nu_O W_O)]/(1 - Y_{C7+}) \tag{2}$$

on the assumption that, in the first straight segment, the droplet surface temperature is nearly equal to the boiling point of heptane, and hexadecane vaporization is negligible for small hexadecane mass fraction. Here, Y_{C7+} is heptane mass fraction in the gas phase at the gas-liquid interface. The heptane mole fraction in the gas phase X_{C7+} is written as

$$X_{C7+} = \alpha X_{C7-} = \alpha(1 - X_{C16-}) \tag{3}$$

by Raoult's law and the Clausius-Clapeyron relation, where $\alpha < 1$, and X_{C7-} and X_{C16-} are heptane and hexadecane mole fractions in the liquid phase at the phase interface. Here Y_i are related to X_i as

$$Y_i = X_i W_i / \Sigma X_j W_j \qquad . \tag{4}$$

From these relations, $dK_1/dY_{C16-} < 0$ can be shown, which is consistent with the decrease in K_1 with increasing initial hexadecane mass fraction.

Similar reasoning could rationalize the K_3 dependence only if heptane vaporization were negligible in the third stage. It seems more likely that, with decreasing Y, the reduced duration of the third stage delays attainment of its maximum K_3.

Onset of the Second Transition Period

Figure 6 shows data for the ratio of the critical volume, V_c, defined as the volume of the droplet at the onset of the second transition period, to V_o, the initial droplet volume. These data also may be interpreted approximately as the volume at the onset of flame contraction, which follows the onset of the transition period as seen Figure 3. Results at an ambient oxygen mole fraction of 0.13 are also shown in Figure 6. The results indicate that the critical volume increases with the initial hexadecane mass fraction and is almost independent of ambient pressure and oxygen content.

Two types of curves are shown in Figure 6 for the critical volumes at 1 MPa generated with different assumptions. The dotted curve is

$$V_c/V_o = Y(\rho_o/\rho) \tag{5}$$

on the assumption that the liquid-phase diffusion is infinitely rapid and hexadecane does not vaporize until the droplet has exhausted all heptane. Here ρ_o is the density of the fuel mixture at room temperature, and ρ the density of hexadecane at the boiling point of heptane. The broken curves are

$$V_c/V_o = [Y/\{Y + 3\epsilon(1 - Y)\}](\rho_o/\rho), \tag{6}$$

which is an equation of Shaw based on the assumption that the liquid-phase diffusion coefficient D is sufficiently small relative to the burning-rate constant K such that $\epsilon = 8D/K << 1$ can be treated as a small parameter, and hexadecane vaporization is negligible. If ϵ is estimated with the assumption that D is the liquid-phase diffusion coefficient of heptane in hexadecane at the boiling point of heptane, and K is the burning-rate constant of heptane, then at 1 MPa, ϵ is about 0.05. The experimental results lie between this result and the infinite-diffusivity result but fall closer to this result at the larger values of Y and closer to the infinite-diffusivity curve at smaller Y. Reasons for this behavior are discussed fully in ref. 1.

Conclusions

The main conclusions can be listed: Staged burning still exists above the critical pressures of heptane and hexadecane. Heptane is dominant in gasification in the first stage and hexadecane in the third even at high pressure. Droplet lifetimes increase with the initial hexadecane mass fraction and reach a maximum value at a mass fraction of about 0.3 for pressures below 2.5 MPa in sufficiently diluted atmospheres. The maximum burning-rate constant in the first stage decreases with the initial hexadecane mass fraction but that in the third stage increases. The droplet volume at the onset of the second transition period is almost independent of the ambient pressure. Although it can be predicted qualitatively from liquid-phase diffusion-controlled theory, quantitative predictions are uncertain because of variations in burning-rate constants and in liquid-phase diffusion coefficients.

Future Plans

In view of the results described above, it would be of interest to test behaviors of these mixtures at higher pressures and at different oxygen-nitrogen ratios, particularly at higher oxygen content, such as in normal air. However, experimental difficulties in observing the droplets cause the success of such investigations to be uncertain. Other plans under consideration involve studying free droplets, testing binary alcohol mixtures at these elevated pressures (but probably not super-critical because of their higher critical pressures), and investigating droplet arrays to obtain information relevant to high-pressure spray combustion. In any event, this successful international cooperation appears to deserve to continue.

References

1. Mikami, M., Kono, M., Sato, J., Dietrich, D.L., and Williams, F.A., "Combustion of Miscible Binary-Fuel Droplets at High Pressure under Microgravity," Combustion Science and Technology, to appear, 1992.

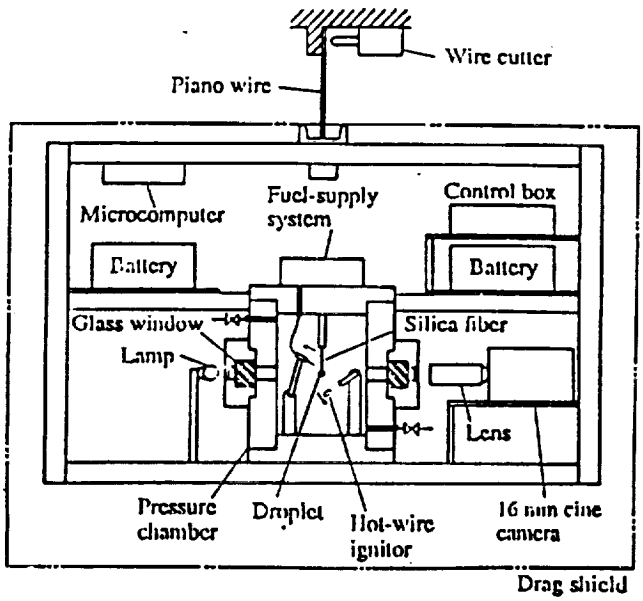

Figure 1. Schematic diagram of the experimental apparatus.

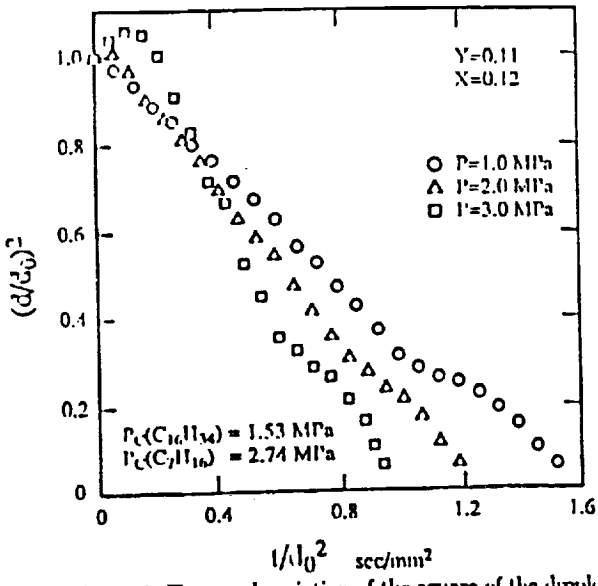

Figure 2. Temporal variation of the square of the droplet diameter, d, with time at different ambient pressures.

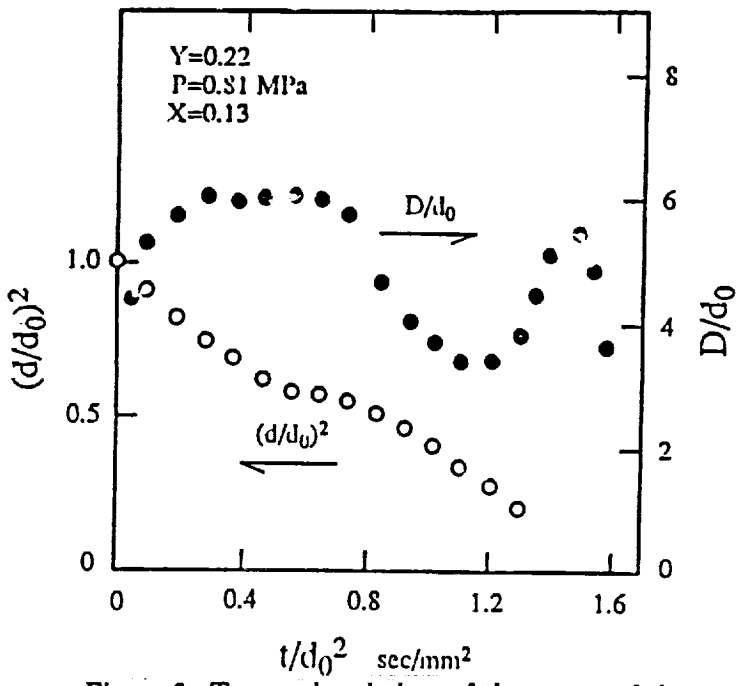

Figure 3. Temporal variations of the square of the droplet diameter, d, and flame diameter, D, with time.

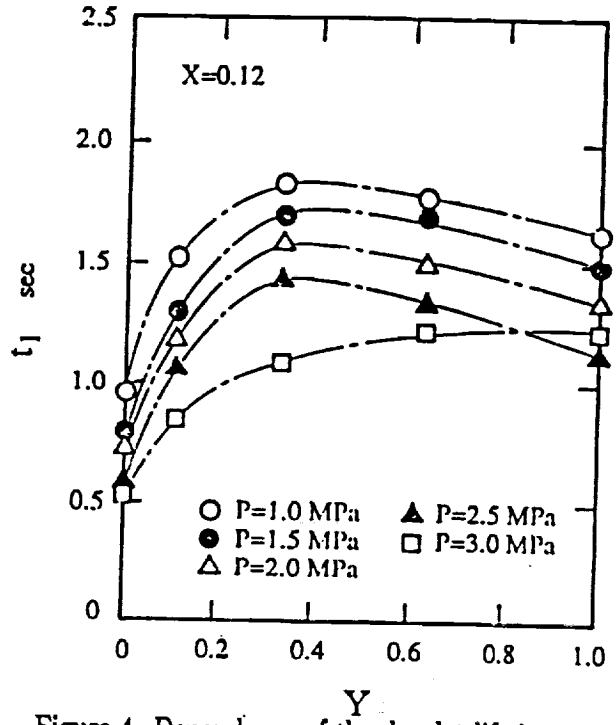

Figure 4. Dependence of the droplet lifetime, t_l, at different ambient pressures on the initial hexadecane mass fraction, Y.

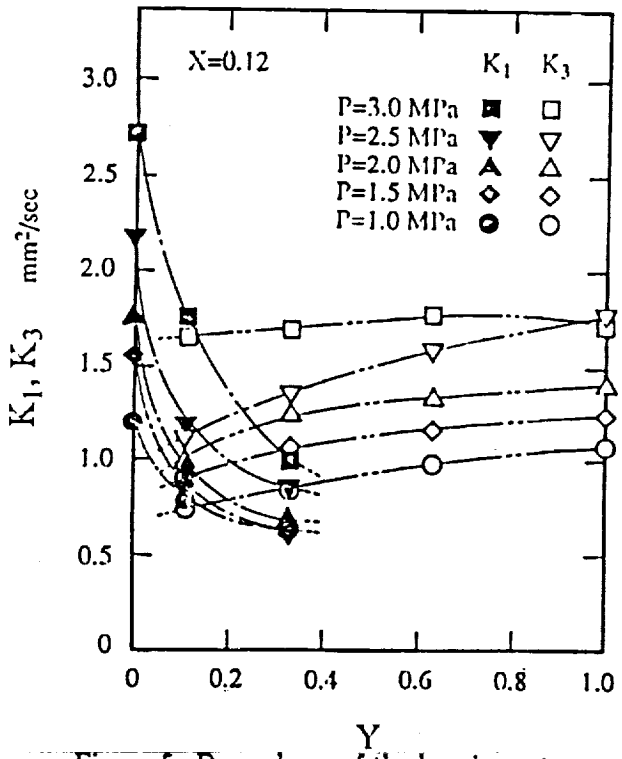

Figure 5. Dependence of the burning rate constant in the first stage, K_1, and in the third stage, K_3, at different ambient pressures on the initial hexadecane mass fraction, Y.

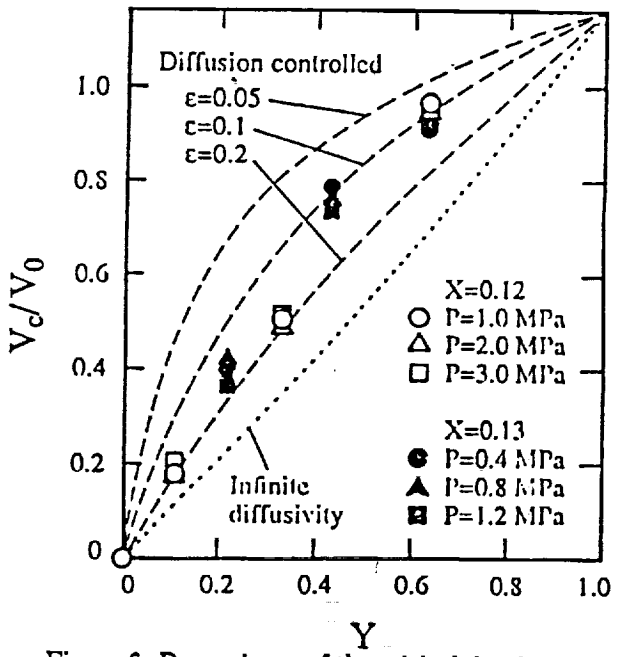

Figure 6. Dependence of the critical droplet volume, V_c, at different ambient pressures on the initial hexadecane mass fraction, Y.

COMBUSTION OF INTERACTING DROPLET ARRAYS IN A MICROGRAVITY ENVIRONMENT*

N93-20217

Daniel L. Dietrich
Sverdrup Technology, Inc.
Cleveland, Ohio 44135

and

John B. Haggard
NASA Lewis Research Center
Cleveland, Ohio 44135

Introduction

This research program involves the study of one and two dimensional arrays of droplets in a buoyant-free environment. The purpose of the work is to extend the database and theories that exist for single droplets into the regime where droplet interactions are important. The eventual goal being to use the results of this work as inputs to models on spray combustion where droplets seldom burn individually; instead the combustion history of a droplet is strongly influenced by the presence of the neighboring droplets.

Recently, Annamali and Ryan (ref. 1) have summarized the current status of droplet array, cloud and spray combustion. While no attempt will be made to duplicate this work here, there are several relevant ideas that should be mentioned. There a number of simplified theories (refs. 2-6), and a small number of detailed numerical studies (refs. 9 and 10) of droplet vaporization/combustion where multiple droplet effects are significant. These theories all neglect the effect of buoyancy. Experimentally, all studies to date show how important the effect of buoyancy is, in fact, it becomes the dominant transport mechanism in the problem. Only the works of Law and co-workers were performed in an environment where buoyancy effects were small (refs. 11 and 12), and the authors were limited to studying combustion in high oxygen index, low pressure ambient environments.

The emphasis of the present investigation is experimental, although comparison will be made to existing theoretical and numerical treatments when appropriate. Both normal gravity and low gravity testing will be employed, and the results compared. The work to date will be summarized in the next section, followed by a section detailing the future plans.

---

* Research initiation date: 4/1/91.

Work to Date

Normal Gravity Droplet Combustion Chamber

As presented in the previous section, normal gravity testing will be employed in this work. Toward this end a combustion chamber to study the burning of single droplets and droplet arrays was designed and built. The chamber can handle absolute pressures from 0 - 1 atm, and is equipped with a gas mixing system so that the ambient pressure and gas composition can be accurately controlled. Inside the chamber, droplet(s) are suspended from 125 μm quartz optical fibers with a precisely controlled[1] 250 μm bead placed on the end. Droplets are placed on the end of the fiber with a hypodermic tube attached to a rotary solenoid. Ignition is accomplished with a length of .010 inch Kanthal (Aluminum alloy) wire heated with a current of approximately 4 amps. The hot-wire is attached to a linear solenoid, and is removed immediately after ignition. Photographic images are obtained by two orthogonal views; one a backlit view from which the droplet size as function of time is obtained, and the other from which the flame dynamics are captured. The entire droplet dispense/ignition and photographic process is controlled with a time delay relay circuit.

One of the first uses of the combustion chamber was to evaluate the suitability of an intensified array camera to image the flame in the ultra-violet region of the spectrum as opposed to the visual image usually obtained. This work is in support of the Droplet Combustion Experiment (M. Vehda-Nayagam, project scientist). Methanol and n-heptane droplets were burned in ambient environments of Helium/Oxygen and Nitrogen/Oxygen at atmospheric and sub-atmospheric pressures. The flame images were recorded with the intensified array camera (UV Nikkor lens, quartz viewing window) and regular black and white video camera. Most of the video with the intensified camera was taken with a 310 nm bandpass filter in place. The purpose was to attempt to image the OH emission and compare that image with the visual image.

Figure 1 shows two images, the one on the right being that obtained with the intensified array camera, and on the left from the black and white video camera at the same time. This was an n-heptane droplet burning in a 35% Oxygen/65% Helium (mole fraction), and a total pressure of 0.75 atm. As is easily seen, the two images are very different, with a measurement of the flame diameter and shape being very different depending on the camera used. At the present time, no definitive conclusions can be drawn from the existing data, as further analysis of the existing data is needed, in addition to more data with a color video camera and possibly more filters.

Single droplets of methanol and n-decane were studied in high oxygen, low pressure ambients. The purpose was to duplicate some of the work of Law and co-workers (refs. 13 and 14). The result of one of these tests is shown in Fig. 2 with the square of the normalized droplet diameter shown as a function of time. "the burning rate constant, defined as the best linear fit between the two dotted lines in Fig. 2, was 0.84 mm^2/sec. This was somewhat lower than the value reported by Chung and Law. As also seen in Fig. 2, flame extinction occurs before the droplet has completely vaporized (fuel was visible on the fiber). The extinction diameter for this droplet was approximately 300 μm. This droplet size was very close to the suspending fiber bead size, however, so fiber interference effects were no doubt important.

For the same oxygen concentration and fuel as shown for the test in Fig. 2, but higher pressures (0.3 atm), microexplosions were observed. A sequence of frames from before, during, and after a microexplosion are shown in Fig. 3. In the beginning, droplet burning was normal, but then the liquid disruption begins and finally the explosion. After the explosion, normal droplet burning

---

1 The ability to accurately control the size of the bead is critical when performing the droplet array studies so that the droplets in the array are as identical as possible (ref. 10).

continued if any liquid remained on the fiber. These microexplosions seem to originate on the fiber indicating fiber interference. Microexplosions also occurred at 0.2 atm, but were less severe, and typically occurred later in the droplet lifetime. No microexplosions were seen at 0.1 atm.

More recently, work has started on burning multiple droplets. Figure 4 shows two droplets initially 1 mm in diameter separated by approximately 6 mm. The fuel was n-decane, and the pressure was 0.1 atm. Three pictures are shown at different times in the droplet lifetime. As expected, early in the burning history, the two flames merge into a single flame, and later in the lifetime the two droplets experience less interactions, and burn individually. Because of the low pressure in the flames in Fig. 4, buoyancy effects were reduced (not eliminated) and the flames were more spherical.

Reduced Gravity Droplet Combustion

Progress in low gravity has been limited by problems with the experimental apparatus. The major development in this area has been utilizing extremely small (10-15 μm) Si-C fibers to suspend droplets. These fibers are an order of magnitude smaller than the fibers used in most suspended droplet studies. Figure 5 shows an n-decane droplet suspended from one of these fibers. This drop was created in low gravity by stringing one of these fibers between the two deployment needles in the droplet combustion facility of the 2.2 second drop tower. As can easily be seen, the deviation from spherical symmetry is very small, with the fiber being barely visible. Figures 5 also shows the backlit view of the same droplet during combustion. One of the major advantages of using these fibers is the potential to perform thermometry measurements in the gas phase of sootless droplet burning (ref. 15). This is particularly useful when studying extinction phenomena; enabling one to identify flame position, change in flame temperature, and flame dynamics at extinction.

Given the encouraging results using these fibers, a new experimental apparatus for the low gravity facilities is being developed. The experiment is designed to study one and two dimensional arrays of droplets suspended by the Si-C fiber. The current status of the rig is that the design and construction are nearly complete. Integration into a drop frame for the 2.2 second drop tower is under way. Initial testing is expected to begin in the beginning to mid-October.

Another accomplishment is the development of an automatic data processing technique to measure droplet size as a function of time from drop tower data. The technique is similar to that of Choi et al. (ref. 16) and involves grabbing a frame from film (or video) and digitizing it. The edge of the droplet is then detected by one of two methods (absolute intensity or intensity gradient), and the area averaged droplet diameter is determined.

Future Work

Work in the remaining 2+ years of the grant will continue in both the normal gravity test cell, and the low gravity apparatus. Several minor improvements will be made to the normal gravity apparatus. The ignition system will modified, possibly even incorporating a spark ignition system; the ultimate goal being to reliably ignite a droplet in the shortest amount of time with as little disturbance as possible. This work will be done in conjunction with the Droplet Combustion Experiment (DCE) science team (F. Williams, F. Dryer, and M. Vehda-Nayagam). The fuel system will be improved to allow accurate delivery of multiple droplets simultaneously. This new fuel system is nearly complete.

Another area of work that will be done in conjunction with the DCE science team, is on improved flame imaging. Further testing will be done with the intensified array video camera, a color and black and white video camera to determine the best method of imaging a droplet flame. For some of these tests, a small Si-C fiber will be strung across the droplet (not supporting the droplet) and

the luminous image of the fiber during combustion will be recorded. The image of the 'glowing' fiber will be compared to the visual flame images obtained with the video cameras.

In addition, work will continue on attempting to obtain temperature measurements from these fibers. Currently, a model is being developed to correct the temperature of the fiber for radiation, conduction and convective losses. The first experimental work will be conducted in the normal gravity facility, and if the results are promising, it will be incorporated into the drop rig. Even if absolute temperature measurements are not possible, these fibers will enable a qualitative measurement of location of the maximum flame temperature, change in flame temperature as a function of time and flame width.

Normal gravity work in the next year will be focussed on studying single droplets and linear droplet arrays. Two fuels will be employed. The first will be methanol, the second n-decane. The major variables will be the inter-droplet spacing, ambient oxygen concentration, pressure and diluent (helium or nitrogen). The results of these studies will be compared to similar tests that will be conducted in the 2.2 second drop tower with the new droplet combustion apparatus.

References

1. Annamalai, K. and W. Ryan. "Interactive Processes in Gasificcation and Combustion. Part I: Liquid Drop Arrays and Clouds," *Progress in Energy and Combustion Science* **18**, 1992, 221.
2. Brzustowski, T.A., E.M. Twardus, S. Wojcicki and A. Sobiesiak. "Interaction of Two Burning Fuel Droplets of Arbitrary Size," *AIAA Journal* **17**, No. 11, 1979, 1234.
3. Labowsky, M. "A Formalism for Calculating the Evaporation Rates of Rapidly Evaporating Interacting Particles", *Combustion Science and Technology* **18**, 1978, 145.
4. Labowsky, M. "Calculation of the Burning Rates of Interacting Fuel Droplets," *Combustion Science and Technology* **22**, 1980, 217.
5. Marberry, M., A.K. Ray and K. Leung. "Effect of Multiple Particle Interactions on Burning Droplets," *Combustion and Flame* **57**, 1984, 237.
6. Samson, R., D. Bedeaux and J.M. Deutch. "A Simple Model of Fuel Spray Burning II. Linear Droplet Streams," *Combustion and Flame* **31**, 1978, 223.
7. Umemura, A., S. Ogawa and O. Nobunori. "Analysis of the Interaction Between Two Burning Droplets", *Combustion and Flame* **41**, 1981, 45.
8. Raju, M.S. and W.A. Sirignano. "Unsteady Navier-Stokes Solution for Two Interacting, Vaporizing Droplets", AIAA-87-0300, AIAA 25th Aerospace Sciences Meeting, Reno, Neveda, 1987.
9. Tal, Reuven and W.A. Sirignano. "Cylindrical Cell Model for the Hydrodynamics of Particle Assemblages at Intermediate Reynolds Numbers", *American Institute of Chemical Engineers Journal* **28**, No. 2, 1982, 233.
10. Miyasaka, K. and C.K. Law. "Combustion of Strongly Interacting Linear Droplet Arrays", *Eighteenth Symposium (International) on Combustion* [The Combustion Institute, 1981, 283.
11. Xiong, T.Y., C.K. Law, C.K. and K. Miyasaka. "Interactive Vaporization and Combustion of Binary Droplet Systems", *Twentieth Symposium (International) on Combustion* / The Combustion Institute, 1984, 1781.
12. Chung, S.H., and C.K. Law. "An Experimental Study of Droplet Extinction in the Absence of External Convection," *Combustion and Flame* **64**, 1986, 237.
13. Law, C.K., S.H. Chung and N. Srinivasan. "Gas-Phase Quasi-Steadiness and Fuel Vapor Accumulation Effects in Droplet Burning", *Combustion and Flame* **38**, 1980, 173.

14. Vilimpoc, V. and L.P. Goss. "SiC-Based Thin-Filament Pyrometry: Theory and Thermal Properties," *Twenty-Second Symposium (International) on Combustion / The Combustion Institute*, 1988, 1907.
15. "Choi, M.Y., F.L. Dryer, J.B. Haggard, M.H. Brace. "Further Observations on Micro-gravity Droplet Combustion in the NASA-Lewis Drop Tower Facilities: A Digital Processing Techniqui for Droplet Burning Data," Third International Colloquium on Drops and Bubbles, Monterey, California, 1988.

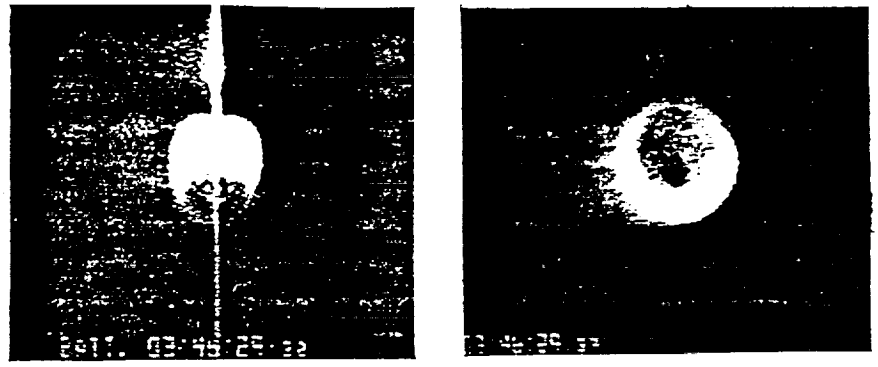

Figure 1. Comparison of images from a black and white video camera (left) and intensified array video camera with 310 nm bandpass filter in place. n-Heptane in a 0.75 atm, 0.35/0.65 Oxygen/Helium (mole fraction) ambient.

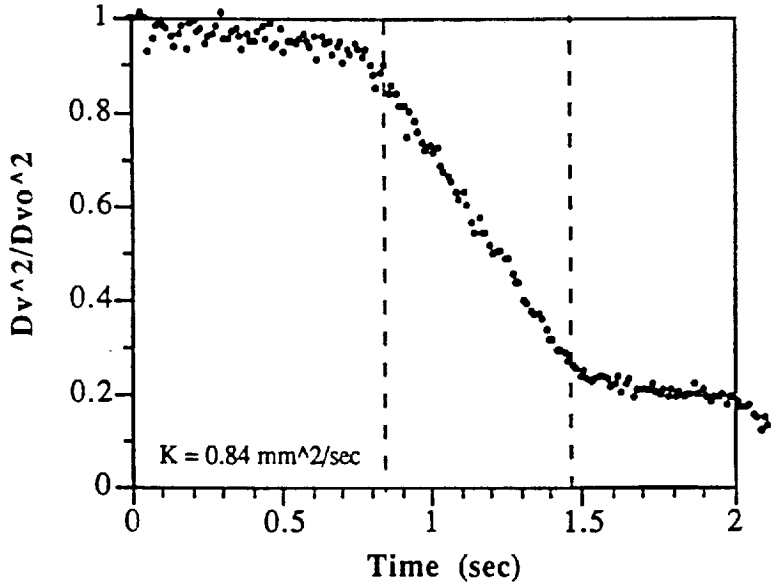

Figure 2. Normalized volume averaged droplet diameter as a function of time for n-decane burning in a 0.1 atm, 0.5/0.5 Oxygen/Nitrogen (mole fraction) ambient.

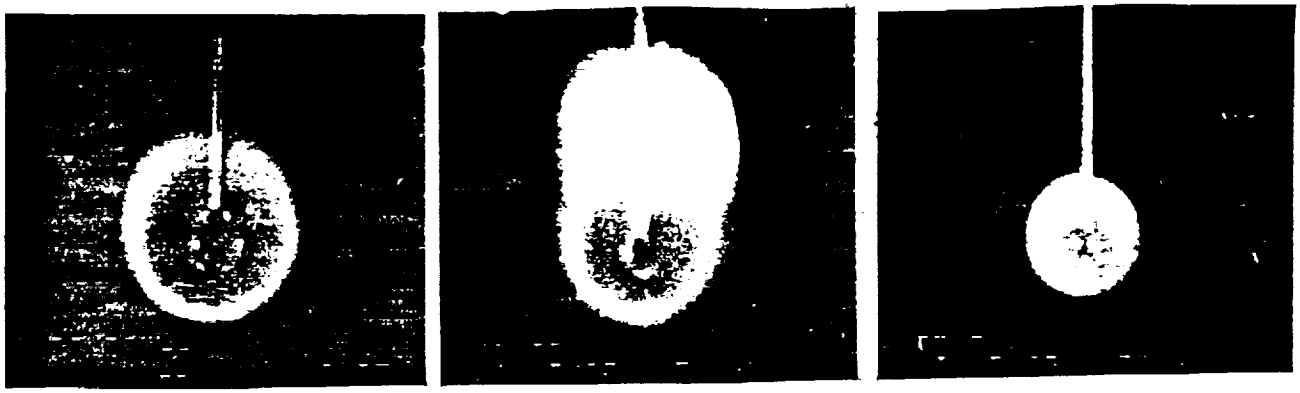

Figure 3. n-Decane in 0.3 atm, 0.5/0.5 Oxygen/Nitrogen ambient, before (left), during (center) and after (right) microexplosion.

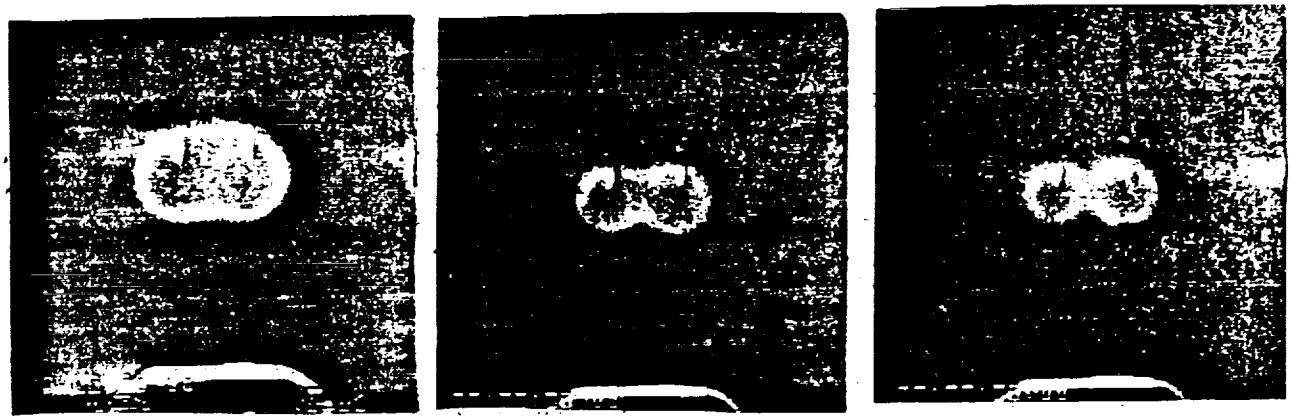

Figure 4. Two n-decane droplets burning in air at 0.1 atm on 125 μm fibers at three times during the burning history.

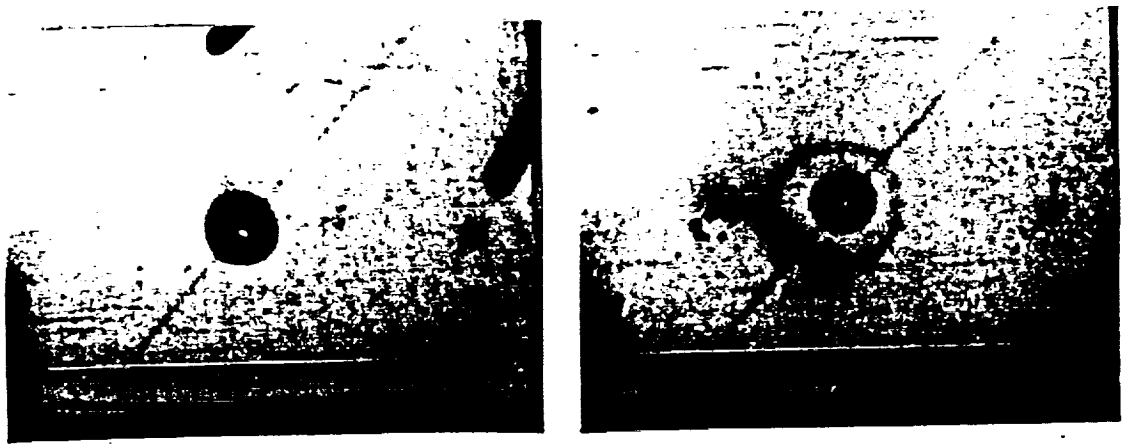

Figure 5. n-Decane droplet in air at 1 atm supported on a 10-15 μm Si-C fiber before (left) and during combustion (right).

COMMENTS

Question (C.T. Avedisian, Cornell University): In looking at your video of the combustion of droplet arrays in microgravity using fiber supported droplets, some work that Brzustowski and co-workers did in the late 70's on unsupported droplet arrays in microgravity came to my mind. Do you intend to include a study of unsupported droplet arrays in your work?

Answer: Not in the immediate future (1 year). We are, however, considering looking at unsupported arrays in the last year of funding.

THE ELECTROSPRAY: FUNDAMENTALS AND COMBUSTION APPLICATIONS

N93-20218

Alessandro Gomez
Department of Mechanical Engineering
Yale University
New Haven, Connecticut 06520

1. Introduction

Liquid fuel dispersion in practical systems is typically achieved by spraying the fuel into a polydisperse distribution of droplets evaporating and burning in a turbulent gaseous environment. In view of the nearly unsurmountable difficulties of this two-phase flow, it would be useful to use an experimental arrangement that allow a systematic study of spray evolution and burning in configurations of gradually increasing levels of complexity, starting from laminar sprays to fully turbulent ones. An Electrostatic Spray (ES) of charged droplets lends itself to this type of combustion experiments under well-defined conditions and can be used to synthesize gradually more complex spray environments. In its simplest configuration, a liquid is fed into a small metal tube maintained at several kilovolts relative to a ground electrode few centimeters away. Under the action of the electric field, the liquid meniscus at the outlet of the capillary takes a conical shape, with a thin jet emerging from the cone tip. This jet breaks up farther downstream into a fine spray of charged droplets (see Fig. 1 and ref. 1). Several advantages distinguish the electrospray from alternative atomization techniques: the self-dispersion property of the spray due to coulombic repulsion; the absence of droplet coalescence; the potential control of the trajectories of charged droplets by suitable disposition of electrostatic fields; and the decoupling of atomization, which is strictly electrostatic, from gas flow processes. Furthermore, as recently shown in our laboratory (ref. 2), the electrospray can produce quasi-monodisperse droplets over a very broad size range (1-100 μm).

The ultimate objective of this research project is to study the formation and burning of electrosprays of liquid fuels first in laminar regimes and then in turbulent ones. Combustion will eventually be investigated in conditions of three-dimensional droplet-droplet interaction, for which experimental studies have been limited to either qualitative observations in sprays or more quantitative observations on simplified systems consisting of a small number of droplets or droplet arrays (refs. 3-6). The compactness and potential controllability of this spray generation system makes it appealing for studies to be undertaken in the next two years on electrospray combustion in reduced-gravity environments such as those achievable at NASA microgravity test facilities.

2. Summary of the Research Activity from 3-1-1991 to 8-31-1992

The project has developed along two parallel avenues: we have performed a variety of cold flow experiments aimed at examining the fundamental mechanism of electrospray atomization and dispersion as well as identifying and characterizing the domain of operating variables under which the generated droplets are quasi-monodisperse. The other focus of the research has been on the combustion of the electrospray in laminar regime: we have constructed a counterflow spray burner, tested it at normal gravity and begun to examine the dynamics of the interaction of droplets and flame. Primary diagnostic tools are: a commercial Phase Doppler Anemometer (PDA), the workhorse of this phase of the project, used to measure distributions of droplet size and either axial or radial velocity component; and a shadowgraph system consisting of a nanosecond flashlamp, a long-range microscope and a CCD camera, capable of capturing and digitizing images of droplet shadows with an overall magnification of up to 1100X. Further details are given in the seven publications (refs. 2, 7-12) that have resulted from the research activity in the first seventeen months of the project.

2.1 Fundamentals of Electrospray Atomization

Research on the fundamentals of electrospray atomization is crucial to develop strategies for optimizing the ES and tailoring it to a particular application. In particular, it is necessary to: define and understand limits of operation of the system; infer scaling laws that would allow to generalize experimental findings and perform scale-up to commercially interesting liquid flow-rates. In this phase of the study we first obtained a phenomenological picture of the atomization and dispersion processes, as sketched in Fig. 1, through flash shadowgraphs of the breakup region (refs. 2 and 10). When narrow size distributions are generated, the liquid exits the cone formed at the outlet of the charged capillary as a thin, stable, thread that persists for a short distance. This ligament then breaks up into droplets of bimodal size distribution, with primary, larger droplets, and satellite ones, on average one third smaller. Farther downstream, droplets in the spray core become nearly monodisperse as the satellites, driven by the electric field, migrate more rapidly away from the spray axis because of higher charge to mass ratio and lower inertia. The core of uniform droplets was found to carry 97% of the total flow rate and 85% of the total current; the remainder is present in a shroud of satellites. We also identified the operating conditions under which the electrospray generates monodisperse droplets. A map of the ES stability domain in the applied-voltage vs liquid flow rate plane was obtained for heptane, doped with the antistatic additive (Stadis 450,

0.3% by weight) to provide electric conductivity. A domain was identified in which monodisperse droplets were generated whose size was primarily controlled by the liquid flow rate and, to a less extent, by the applied voltage (ref. 12). Since the ultimate goal was to evaluate the size and monodispersity of the spray, results are plotted in Fig. 2 as average droplet diameter, measured by the PDA versus applied voltage for several liquid flow rates. For all measurements the droplet standard deviation was less than 10 % of the average diameter, the latter spanning a remarkable range of over two orders of magnitude (1-140 μm). The boundaries of this stability region were found to be determined by the onset of different types of instabilities: at a given flow rate, the minimum voltage was set by the onset of pulsations in the liquid meniscus, whereas the maximum voltage was typically set by the onset of traverse instabilities on the jet issuing from the conical meniscus. The lower flow rate limit was set by diagnostic limitations: the Phase Doppler system cannot, in fact, measure submicron droplets; the upper limit in flow rate was instead determined by the onset of droplet fission, which is achieved when Coulomb repulsion of the electrical charges on the droplet surface overcomes surface tension and the droplet disrupts, as discussed below in greater detail.

We also examined in detail a prototypical ES, operated for diagnostic convenience in conditions resulting in the generation of monodisperse droplets measuring 32 μm in diameter. After detailed scans of the spray in both radial and axial directions, we first observed that droplet velocity and number density profiles are self-similar in the electrospray. Efforts were then focused on the inference of the electric field that is the driving force determining spray formation and dispersion. Such determination is important for spray modelling, it can help the analysis of the complex electro-hydrodynamics in the liquid meniscus and it is also useful to define limits of operation of the system. The electric field was determined indirectly by quantifying through a variety of measurements on the charged droplets the electrostatic force acting on them (ref. 10). To this end, we: a) measured both droplet and gas velocity, droplet size and average interdroplet spacing; b) inferred droplet charge from measurements of the total current carried by monodisperse droplets using a specially fabricated, variable-aperture electrode; and c) solved the equation of motion for an isolated droplet under the action of electrostatic, gravitational and drag forces. We found that droplets, driven by the field, are ejected from the jet at relatively high velocity. They maintain this velocity even though the field is rapidly decreasing because of inertia effects and ultimately decelerate under the action of drag force and a progressively weaker electrostatic force. The net electric field acting on the droplet is due primarily to the external field, except near the break-up region of the spray, where the internal field due to space charge appears also to be important. Indeed, droplet coulombic repulsion plays a crucial role: if only the external field were acting on the droplets, they would predominantly persist in their axial trajectory without dispersing into a spray. Space charge effects, coupled with diverging lines of the external field between capillary and ground electrode ultimately lead to spray dispersion.

2.2 Electrospray Combustion

Spray combustion in a stagnation-point flow configuration has been examined experimentally, numerically and analytically in diffusion flames in a few recent studies (refs. 13-17). The focus of our effort has been to study the effects of the interaction between flow field, flame and droplets on the structure of the counterflow spray diffusion flame (ref. 7). We also found the first evidence in a burning spray of secondary atomization due to Coulomb fission (ref. 11).

The counterflow diffusion flame burner (Fig. 3) has been described elsewhere (ref. 7). Briefly, electrosprayed heptane and a co-flow of N_2 flowed through the bottom half of the burner and oxygen was admitted through the top one. Combustion occurred in a gap between top and lower half of the burner, near the stagnation region between the two impinging streams. Experiments were performed on two heptane flames, both operated at the same overall equivalence ratio of 0.36, and, thus, both having the same adiabatic flame temperature. The first flame, labelled LS, was characterized by a nominal strain rate of 3 s^{-1}, droplet mean diameter and mean velocity near the burner mouth equal to 36.3 μm and 0.63 m/s respectively. In the second flame, labelled HS, strain rate, initial droplet size and droplet relative velocity were increased to 4.3 s-1, 47.3 μm and 1.3 m/s respectively. The ratio of standard deviation and mean droplet size near the burner mouth were 0.09 and 0.13 in the two flames and therefore droplets can be considered quasi-monodisperse, at least initially. Both flames are in a diluted spray regime where droplet-droplet interactions are expected to be negligible (ref. 18). Droplets entered the combustion region with a substantial slip with respect to a host gas velocity of only a few cm/s.

In Fig. 4 the average droplet diameter and gas-phase temperature, measured along the burner axis, are plotted versus the distance from the bottom burner rim, z, for the two heptane flames: open symbols refer to Flame LS (Low Strain rate) and full symbols to Flame HS (High Strain rate). The error bars on the droplet diameter have a width equal to two standard deviations. The temperature was measured with a fine silica coated, Pt-Pt/13%Rh thermocouple. In the case of Flame LS, we observe that as droplets approach the combustion region and the stagnation plane, the temperature begins to rise and droplet mean diameter decreases gently in the first 4.5 millimeters and much more abruptly in the subsequent two millimeters. Droplets disappear at about 5.7 mm from the burner mouth, before reaching the flame that was located at z=7 mm and appeared like a thin, flat sheet, of a blue-violet color. In the case of the higher strain rate heptane flame, HS, the flame had an appearance markedly different from Flame LS and exhibited a more complex structure. We observe a thin blue region, similar to that of Flame LS, at z=7.1 mm, another thin sheet characterized by violet luminescence at z=7.3 mm and a thick orange region between z=7.7 and z=9.6 mm, whose luminosity is presumably due to the presence of soot particles. Some of the droplets penetrated through the blue flame and continued to burn within the oxidizer region where they eventually disappeared in the homogeneously thick orange region. Larger droplets burning individually could be identified by their luminous wake occasionally protruding beyond the uniform orange region. From these measurements one concludes that Flame LS behaves in some respects as a purely gaseous diffusion flame

since droplets never directly interact with the flame but simply provide a source of heptane vapor, which then diffuses towards the oxidizer region. This observation confirms numerical predictions under similar conditions (refs. 14, 17) and is also consistent with visual observations of analogous spray flames (ref. 15, 17). Flame HS on the other hand clearly exhibit a direct interaction of droplets and flame. The dramatically different appearance of the two flames can be explained as follows. First, in the case of Flame HS the droplet mean size and axial velocity component measured close to the burner mouth are 30 % larger and twice as large as compared to Flame LS. The larger size and larger velocity of droplets in HS result in longer lifetime (based on d-square law) and shorter residence time, which accounts for droplet survival over significantly longer distances as compared to Flame LS. Second, inertia effects and the consequent inability of the droplets to follow the host gas are more significant in the higher strain rate flame.

A comparison between the temperature profiles in the two heptane flames (Fig. 4) shows that the flame with the nominally higher strain rate, Flame HS has a substantially broader temperature profile. This finding is in contrast with what expected in purely gaseous diffusion flames on the basis of both theoretical analyses, that predict proportionality between the width of the temperature profile and the inverse of the square root of the strain rate (ref. 19), and numerical predictions (ref. 20). Furthermore, even though the two flames have identical overall equivalence ratios and nearly equal adiabatic flame temperatures, Flame HS has a peak temperature 240 K higher than Flame LS. This difference is probably an effect of the local stoichiometry. Since N_2 was introduced only from the fuel side, the inert concentration is a monotonically decreasing function of z. Thus, droplets cross the blue flame in Flame HS and continue to burn stoichiometrically in an oxygen rich environment while the inert concentration progressively decreases.

The error bars on the droplet diameters in Fig. 3 show that the initially narrow size distribution broadens in the course of evaporation. This effect can be attributed to size-dependent droplet evaporation rate and residence time, as explained in detail in ref. 7. Also noteworthy is the non-monotonic behavior in Flame HS of the mean droplet diameter as function of the axial coordinate, z, which is due to an inertia separation effect (ref. 7).

2.3 Fission of charged Droplet

Measurements of charge and size of droplets generated in electrostatic sprays of heptane operated in the conditions described in Section 2.1 showed that: a) droplet charge-to-volume ratio is a monotonically decreasing function of droplet size; and b) that the larger are the droplets the closer they are to the limiting charge at which they rupture. This limit is attained when the Coulombic repulsion of surface charge overcomes surface tension (ref. 21). Thus, somewhat paradoxically, large droplets with relatively low charge-to-volume ratio are proner to disintegrate than smaller droplets with higher ratios. Exploiting these findings, for the first time we have captured photographically the fission of nearly-monodisperse, charged droplets generated by an electrospray (Fig. 5). Observed fissile patterns show that droplet disintegration is characterized by the formation of a tail, or "cone", reminiscent of the conical liquid meniscus from which the electrospray originates (see Fig. 1). From the tip of this cone, a stream of droplets is ejected, all much smaller in size than the parent droplet and apparently equisized. Consequently, since droplet evaporation time varies with the square of the droplet diameter at typical prevailing conditions, the offspring droplets will vaporize at much faster rate than will the residual "parent" droplet. A phenomenological explanation of the observed dependence of charge density on droplet size has been offered in terms of the relative magnitude of two characteristic times: an electric relaxation time, i.e. a characteristic time for charge motion in the liquid or on the liquid surface; and a characteristic fluid time, i.e. the time over which varicose wave instabilities propagate along the axis of the liquid jet from which the electrospray originates. Some implications of these findings, with particular emphasis to electrospray ionization, a technique widely used in biochemical mass-spectrometry are discussed in (ref. 9).

Experimental evidence of droplet fission was also obtained in the combustion of electrosprays (ref. 11). PDA measurements in the flame labelled LS in Fig. 4 showed in fact a peculiar feature of the size distributions in the vicinity of the flame. Fig. 6 shows one such distribution as measured at z= 5.5 mm. Notice the bimodality of the distribution with the appearance of a secondary peak in correspondence of diameters of 2-3 μm, i.e. one order of magnitude smaller than the mean droplet diameter. No evaporation mechanism can account for this finding, which can be explained only in terms of a disintegration of droplets into finer fragments of consistently much smaller size. Other evidence in support of the existence of secondary atomization is offered by velocity measurements showing that in correspondence with secondary peaks in the size distribution both radial and axial components of the droplet velocity are unusually large, i.e. one or two orders of magnitude larger than the corresponding mean values, which is indicative of the occurrence of an ejection process. This disruption occurs despite the presence of chemi-ions and electrons that are naturally present in the flame and that might have partially or totally neutralized the droplet, as originally suggested by Weinberg (ref. 22). The morphology of the fission process captured in cold flow experiments (Fig. 5) is consistent with the size distribution found in these combustion experiments.

3.0 Future Plans

Task 1- We would like first to characterize as quantitatively as possible the evolution of the spray as the droplets approach the flame. With the measurements of droplet size, velocity and gas-phase temperature, we should to be able to reconstruct the evolution of the droplet size distribution as the droplets approach the flame and to determine the droplet vaporization rate.

Task -2 Further studies are needed to capture droplet fission in combustion environments and to clarify whether disruption is characterized by only 1-2 % liquid mass loss, or whether the mass loss can be substantially higher because of the presence of chemi-ions* . In the first case, the disruption process enhances the evaporation rate of only a small fraction of the liquid supply but it may still aid in the overall stability of the spray flame. In the second case, the advantages of secondary atomization would be far more dramatic. A suitable electrostatic atomizer would generate *directly* large droplets, with the inherent advantage of good penetration of fuel into the oxidizer, and *indirectly* small droplets, via Coulombic fission,with the advantage of rapid evaporation and effective molecular mixing of fuel and oxidizer.

Task 3- Experiments to date have been conducted in a regime of diluted spray, as discussed in Section 2.2. To operate the spray ultimately in a regime of droplet-droplet interaction, we would like to develop strategies to focus electrostatically the spray by manipulating droplet trajectories with electric fields and therefore controlling interdroplet spacing If space charge effects are limiting, partial neutralization of droplet charge by an aerosol neutralizer may be necessary before focusing can be implemented.

Task 4 - Part of the experimental program in the third and fourth year would be implemented at the 2s Drop Tower NASA facility. Efforts will be made to retrofit the current version of the counterflow burner to the drop-package before the end of the current year. The obvious goal is that of studying spray combustion in an environment free of natural convection effects. Buoyancy can generally play a role in displacing the flame in low strain rates flames, as we also observed in purely gaseous flames (ref. 24). In the particular case of spray flames, its role will become very significant in regimes of droplet-droplet interaction, when the characteristic length of the Grashof number is no longer the droplet size but the "spray size." In this context, efforts in task 3 will be crucial.

Task 5- To be able to compare the results of the laminar spray experiments in the counterflow configuration with computations, Prof. M. D. Smooke will develop a model that accounts for the interchange of mass, momentum, chemical species and energy between the gas and liquid phases in a monodisperse spray. Building upon the experience obtained in the investigation of detailed transport/finite rate chemistry models of gaseous premixed and nonpremixed counterflow systems (refs. 20, 25, 26), we plan to solve the complete liquid-gas phase system with a modified version of the algorithm described in detail in the literature (ref. 25), after coupling in the liquid phase by utilizing the ideas of Sirignano and coworkers (ref. 14). This approach will enable us to investigate the effects of droplet size, droplet spacing and the effects of droplet vaporization on flame location, temperature and species distributions. The interaction between modeling and experiments will help in interpreting the experimental findings and in validating the model both at normal and reduced gravity.

Task 6- We plan to complement the measurements of droplet size and velocity with spectroscopic determination at normal gravity of the concentration of major gaseous species as well as of some radicals. This study will be valuable for determining flame location, studying its evolution, evaluating oxidizer penetration into the droplet-laden region and comparing results with numerical predictions. Experiments will be performed in collaboration with Prof. M. B. Long. Major species such as O_2, CO_2, H_2O and N_2 will be detected by spontaneous Raman scattering. For radical such as OH and CH, on the other hand, the laser will be tuned to an absorption line and the fluorescence will be detected at a wavelength shifted from that of the input laser. Point measurements can be performed by using optical filters to reject partially or totally the droplet intense elastic light scattering in combination with a synchronization scheme in which spectroscopic signals will be collected conditionally upon the absence of droplets in the laser probe volume. Since the anticipated interdroplet spacings are in the order of ten droplet diameters and droplet data rate are in the order of a few Hz, this strategy should be easily realizable. We would also like to initiate imaging experiments by combining a CCD detector with a pulsed laser illumination sheet or line and ultimately map the concentrations in a single plane or line intersecting the spray (see for example ref. 27).

Task 7- The last phase of the project will be devoted to turbulent sprays. The same type of measurements performed in laminar sprays will be repeated in carefully selected environments in which turbulence is "injected" in the gaseous stream by synthesizing various turbulent scenarios, characterized by different intensities and scales. Since liquid atomization is achieved strictly by charging, in contrast with aerodynamic atomization mechanisms, the host gas where the liquid is injected can in fact be controlled independently.

4.0 References

1. Zeleny, *J., Phys. Rev.* **10**, p.1 (1917).
2. Gomez, A. and Tang, K., Proceedings of the Fifth International Conference on Liquid Atomization and Spray Systems, ICLASS-91, Gaithersburg, MD, U.S.A., H. G. Semerjian Ed., NIST Special Publication No. 813, p.805 (1991).
3. Twardus, E.M. and Brzustowki, T.A., *Combust. Sci. and Technol.*, **17**, p.215 (1978).
4. Brzustowski, T.A., Twardus, E.M., Wojcicki, S. and Sobiesiak, A., *AIAA J.*, **17**, p.1234 (1979).
5. Sangiovanni, J.J. and Kesten, A.S., *Sixteenth Symposium (International) on Combustion*, p.577, The Combustion Institute (1977).
6. Sangiovanni, J.J. and Labowski, M., *Combust. Flame*, **47**, p.15 (1982).

* Taflin et al. (ref. 23), in fact, reported that in ionized gaseous medium the disruption can differ substantially from that in unionized gases and can be characterized by much larger mass loss.

7. Chen, G. and Gomez, A., "Counterfow Diffusion Flames of Quasi-Monodisperse Electrostatic Sprays," to appear in *Twenty-fourth Symposium (International) on Combustion*, (The Combustion Institute, Pittsburgh, PA, 1992).
8. Gomez, A. and Tang, K., Proceedings of the Fifth International Conference on Liquid Atomization and Spray Systems, ICLASS-91, H. G. Semerjians, Eds., (NIST Special Publication 813, Gaithersburg, MD,USA, p.805, 1991).
9. Gomez, A. and Tang, K., "Fission of Charged Droplets in Electrostatic Sprays", submitted to *Phys. Fluids A* (1992).
10. Tang, K. and Gomez, A.: "On the Structure of an Electrostatic Spray of Monodisperse Droplets", submitted to *Phys. Fluids A* (1992).
11. Gomez, A. and Chen, G., "Secondary Atomization in the Combustion of Electrostatic Sprays," submitted to *Combust. and Flame* (1992).
12. Gomez, A. and Tang, K., "Stability Domain of an Electrospray Generating Monodisperse Droplets in the Size Range 1-140 μm", to appear in *J. Aerosol Sci.* (1992).
13. Greenberg, J.B., Albagli, D. and Tambour, Y., *Combust. Sci. and Tech.*, **50**, p. 255 (1986).
14. Continillo, G. and Sirignano, W.A., *Comb. Flame* **81**, p.325 (1990).
15. Li, S.C., Libby, P.A. and Williams, F.A. "Experimental and Theoretical studies of Counterfow Spray Diffusion Flames," to appear in *Twenty-fourth Symposium (International) on Combustion*, (The Combustion Institute, Pittsburgh, PA, 1992).
16. Chen, N. H., Rogg, B. and Bray, K.N.C., "Modelling Laminar Two-phase Counterflow Flames with Detailed Chemistry and Transport", to appear in *Twenty-fourth Symposium (International) on Combustion*, (The Combustion Institute, Pittsburgh, PA, 1992).
17. Lacas, F., Darabiha, N., Verasevel, P., Rolon, J.C. and Candel, S., "Influence of Number Density on the Structure of Strained Laminar Spray Flames", to appear in *Twenty-fourth Symposium (International) on Combustion*, (The Combustion Institute, Pittsburgh, PA, 1992).
18. Faeth, G.M., *Prog. Energy Combust. Sci.* 9, p.1 (1983).
19. Zeldovich, Ya.B., Barenblatt, G.I., Librovich, V.B. and Makhviladze, G.M.: The Mathematical Theory of Combustion and Explosions, Ch. 8, Plenum (1985).
20. Puri, I.K., Seshadri, K., Smooke, M.D. and Keyes, D.E., *Combust. Sci. and Tech.* **56**, p.1 (1987).
21. Rayleigh, *Philos. Mag.* **14**, p.184 (1882).
22. Thong, K.C. and Weinberg, F.J., *Proc. Roy. Soc. Lond. A* **324**, p.201 (1971).
23. D. C. Taflin, T. L. Ward and E. J. Davis, *Langmuir* **5**, p.376 (1989).
24. Gomez, A. and Rosner, D. E., "Thermophoretic Effects on Particles in Counterflow Laminar Diffusion Flames," to appear in *Combust. Sci. and Tech.* (1992).
26. Giovangigli, V. and Smooke, M. D., *Comb. Sci. and Tech.*, **53**, p.23 (1987).
25. Smooke, M. D., Puri, I. K. and Seshadri, K., *Twenty-First Symposium (International) on Combustion*, p. 1783, The Combustion Institute, 1987.
26. Giovangigli, V. and Smooke, M. D., *Comb. Sci. and Tech.*, **53**, p.23 (1987).
27. Smooke, M. D., Lin, P., Lam, J. K. and long, M.B., *Twenty-Third Symposium (International) on Combustion*, p. 575, The Combustion Institute, 1991.

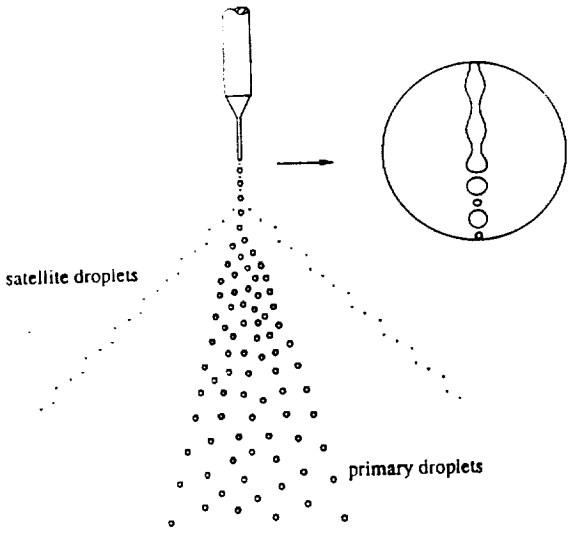

Fig. 1. Schematic of an electrospray.

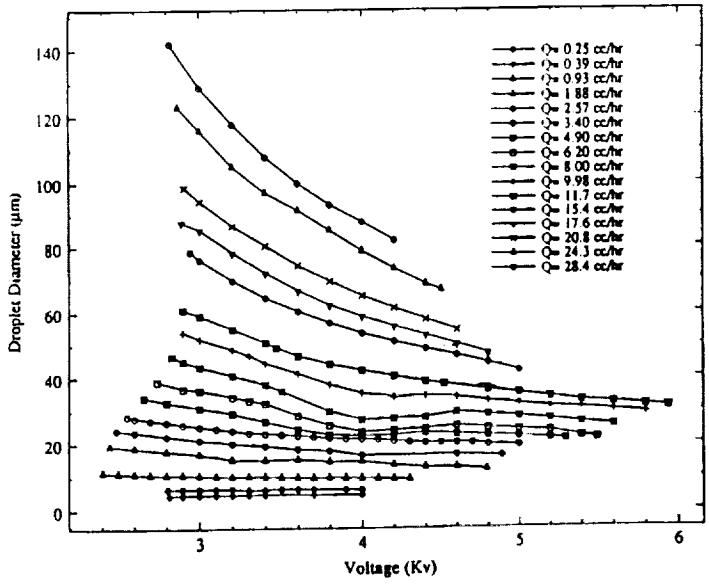

Fig.. 2 Droplet average diameter versus applied voltage for various liquid flow rates.

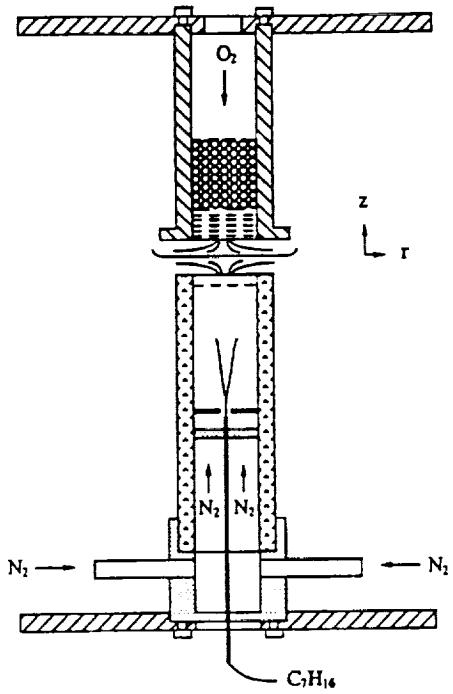

Fig. 3 Counteflow spray diffusion flame burner.

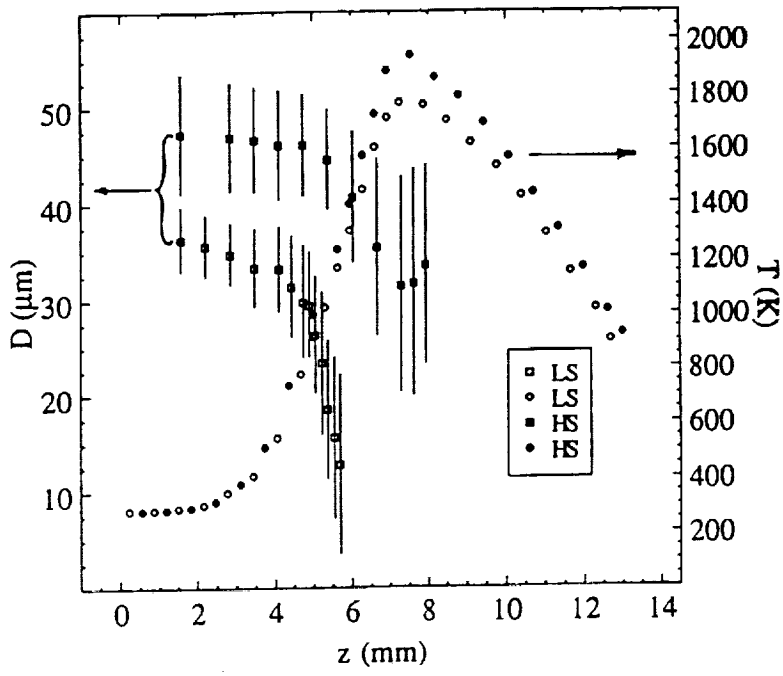

Fig. 4 Average droplet diameter (squares) and gas-phase temperature (circles) measured along the burner axis versus distance from the bottom burner rim.

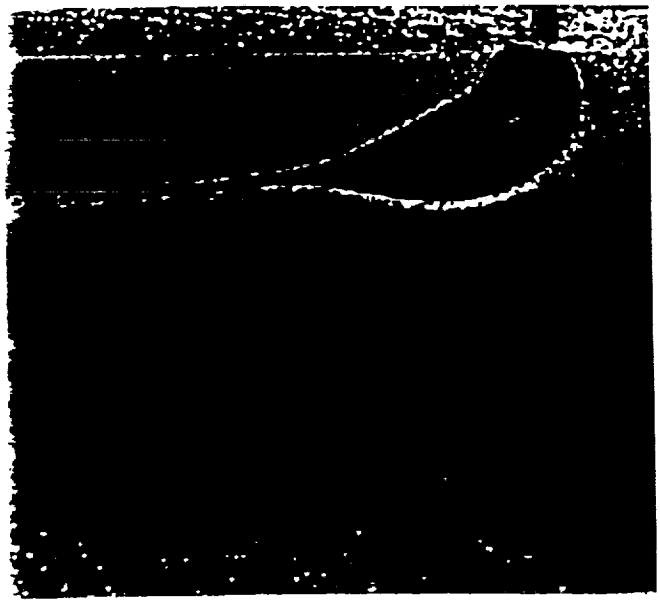

Fig. 5 Microphotograph of a droplet in the act of disintegrating.

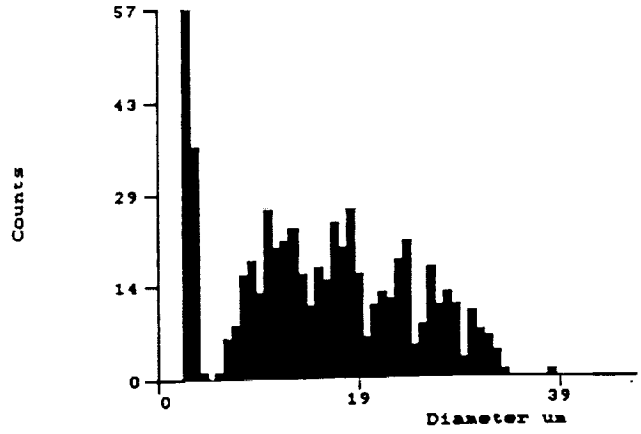

Fig. 6 Droplet size distribution measured at z=5.5 mm in Flame LS.

See Color Plate G-6

CHARACTERIZING DROPLET COMBUSTION OF PURE AND MULTI-COMPONENT LIQUID FUELS IN A MICROGRAVITY ENVIRONMENT

N93-20219

Gregory S. Jackson and C. Thomas Avedisian
Sibley School of Mechanical and Aerospace Engineering
Cornell University
Ithica, New York 14853

Introduction

The importance of understanding the effects of fuel composition, length scales, and other parameters on the combustion of liquid fuels has motivated the examination of simple flames which have easily characterized flow fields and hence, the potential of being modeled accurately. One such flame for liquid fuel combustion is the spherically symmetric droplet flame which can be achieved in an environment with sufficiently low gravity (i.e., low buoyancy). To examine fundamental characteristics of spherically symmetric droplet combustion, a drop tower facility has been employed to provide a microgravity environment to study droplet combustion. This paper gives a brief review of results obtained over the past three years under NASA sponsorship (grant NAG3 -987).

Important aspects which were studied to characterize the burning of liquid droplets included: 1) droplet burning rate constants (K) which assess the rate of heat transfer to the liquid fuel from the exothermic gas-phase reactions, 2) extinction of the droplet flame before complete vaporization which indicates the possibility of incomplete combustion, 3) soot formation inside the spherical droplet flame, and 4) microexplosions and preferential vaporization exhibited by multi-stage combustion for droplets of miscible mixtures. The spherically symmetric configuration of microgravity droplet combustion allows for parameters such as average burning rates, flame stand-off ratios, and location of soot agglomerates in the flame to be defined without the effects of natural convective flows, and effects of droplet size in microgravity combustion are not masked by the length scale dependence of natural convective flows.

A wide range of pure and blended fuels were studied in air at standard room temperature and pressure in a low gravity environment on board the drop tower. Results from some of these fuels are briefly reviewed here: pure n-heptane, pure 1-chloro-octane, heptane/monochloro-octane mixtures, pure methanol, methanol/toluene mixtures, and methanol/dodecanol mixtures. The bulk of experimental results reported here were obtained by studying free unsupported droplets with initial diameters (D_o) ranging from 0.4 to 0.7 mm. A more limited series of experiments were carried out on fiber-suspended droplets, with D_o up to 1.1 mm, to examine the effect of initial diameter on the burning of sooting fuels. Different mixture compositions were burned to assess the affects of additives on soot emissions, extinction, and microexplosions.

Experimental Set-up and Data Extraction

The original drop tower facility as well as the technique for creating free-floating stationary droplets has been described in detail previously [ref. 1, 2]. Many modifications were implemented over the past three years to improve the quality of data obtained from the experiments [refs. 3, 4, 7]. The experimental package contains a combustion chamber with the droplet generator, ignition circuitry, a high-speed movie camera, and a low-lux CCD camera for visualization of the flame boundary. The drop package experiences free fall for about 1.2 s. Some previous experiments showed that the increase in gravity levels in the latter half of free fall due to air drag around the package increased buoyant flows around larger droplets with $D_o > 0.80$ mm [ref. 3]. Thus, in order to observe spherically symmetric combustion for the longer-burning larger droplets, a drag shield was built in which the experimental package can fall freely with minimal air drag for the entire period of free fall.

Two types of burning droplet experiments were performed in the drop tower: free unsupported droplets and fiber-suspended droplets. To effectively levitate unsupported droplets in microgravity, a droplet deployment technique based on the "ink jet" method was employed [refs 1, 7]. For the suspended droplets, a 30 to 50 μm diameter quartz

fiber was used. The fiber diameter was kept very small in order to minimize its influence on the burning process. Unsupported droplet experiments reported here included the following fuels: n-heptane, methanol, methanol/toluene mixtures, and methanol/dodecanol mixtures. Suspended droplet experiments reviewed here include pure heptane, pure monochloro-octane, and monochloro-octane/heptane mixtures. Because suspended n-heptane droplets had burning rates and flame stand-off ratios which agreed well with burning rates and flame stand-off ratios of similarly-sized unsupported droplets, the fiber was assumed to have a negligible impact on the combustion process.

Droplets were ignited about 15 ms after the package was released into free fall by two spark discharges on opposite sides of the droplet. Considerable efforts were spent to develop a multiple spark circuit with the capability of adjusting the spark energy, which was controlled by varying the spark duration, the voltage of the energy-storing capacitors, and/or the current through the electrodes. The electrodes for the spark were retracted away from the flame after ignition. Retraction was initially performed by a solenoid-activated spring mechanism which retracted the entire electrode mount upwardly [ref. 3, 5, 7], but more recent experiments have used a mechanism where only the electrodes are retracted in a radially outward direction [ref. 4].

Droplet diameter measurements were obtained from the high-speed movie records with framing rates ranging from 100 to 250 frames per second. Measurements were taken with a computer-based image analysis system (Image Analyst™, Automatix Inc., Billerica, MA). For suspended droplets, measurements were not taken when the average droplet diameter became less than 8 times the nominal fiber diameter because of concerns about the influence of the fiber on the burning process when the fiber diameter becomes a significant fraction of the droplet diameter. The region for calculating the average droplet radius for the suspended droplets was defined as lying between the locations where the liquid surface changed concavity near the fiber, both at the top and at the bottom of the droplet.

Results and Discussion

Heptane, Monochloro-octane, and Heptane/Monochloro-octane Mixtures

Burning rate constants were found for unsupported and suspended n-heptane droplets with D_o ranging from 0.40 to 1.05 mm and for suspended 1-chloro-octane droplets with D_o from 0.45 to 1.10 mm [ref. 3 - 5]. N-heptane droplets larger than 0.9 mm and 1-chloro-octane droplets larger than 0.8 mm had burning times longer than the duration of free-fall. However, enough of the burning history was recorded for these larger droplets to get a reasonable assessment of K during the period of so-called steady burning after the initial heat-up period. Representative examples of droplet diameter-squared profiles for unsupported n-heptane droplets are shown in fig. 1. Burning rate constants were found with a least-squared linear regression of the droplet diameter-squared data vs. time. Data from the initial period of droplet heat-up and gas-phase vapor accumulation were excluded from the linear regression. The differences in the slopes of the two profiles in fig. 1 reflect a decreased burning rate for the larger n-heptane droplets. For both n-heptane and monochloro-octane droplets with D_o around 0.60 mm, K consistently had values which were more than 20% higher than those for droplets with D_o around 1.00 mm.

Both heptane and monochloro-octane droplets exhibited common trends in the development of the flame and a shell-like structure of soot (i.e., soot shell) between the droplet and the flame. Soot particles form rapidly enough for all but the smaller-sized heptane droplets, such that thermophoretic forces overtake outward inertia created from the Stefan flow and the particles are pushed inward to a region where the themrophoretic forces balance the outwardly directed drag forces. The soot shell begins to take shape as new particles collect in this region. As burning progresses, the particles begin to agglomerate and the large soot agglomerates are eventually pushed away from the droplet and into the flame zone because the outward drag force increases more rapidly with particle size than does the thermophoretic force [ref. 3]. The soot agglomerates generally escape the flame without complete oxidation implying a loss in heat generation due to unoxidized carbon. As vaporization is completed, the contracting flame passes through and disrupts the remaining soot.

Fig. 2 shows two representative photographic sequences of n-heptane droplets burning at low gravity: an unsupported droplet with D_o = 0.69 mm and a suspended droplet with D_o = 0.75 mm. The two sequences have approximately the same t/D_o^2 values to provide some basis for comparison and to show the similarities between the unsupported droplet flames and the suspended droplet flames. The bright particles in fig. 2 are radiating soot particles emitted from the flame without undergoing complete oxidation. The fiber-supported droplet sequence shows some soot agglomerates collecting on the fiber, perhaps due to thermophoresis. However, because burning rates and dimensionless soot shell diameters for fiber-supported droplets agreed well with those of unsupported droplets of similar initial size, the effect on burning of the soot/fiber interactions was assumed to be negligible.

The smaller heptane droplets did not show any soot shell formation until near the end of burning, perhaps due to their higher vaporization rates and the lower residence times for fuel particles inside the flame. On the other hand, the larger heptane droplets (D_o > 0.6 mm) formed soot shells early in the combustion process and emitted soot agglomerates as combustion proceeded until the end of burning. The smaller monochloro-octane droplets exhibited soot shell development, but their soot structures were much less dense and their emissions greatly reduced in comparison to the larger monochloro-octane droplets.

The flame luminosity, soot emissions, and burning rates of 25%, 50%, and 75% v/v heptane in monochloro-octane suspended droplets fell between those of the two pure components [ref. 3]. The photographic records suggest that more than 25% v/v heptane must be added to monochloro-octane before soot emissions are noticeably reduced as the 25% heptane mixture droplets appeared to soot almost as heavily as pure monochloro-octane droplets of similar size. No multi-stage combustion process was observed for these mixtures.

Photographic records of the pure heptane and monochloro-octane droplets suggest that the amount of soot collected in the shell and unoxidized by the flame may be a more sensitive function of the droplet diameter than a D^2 dependence. Longer residence time for fuel molecules inside the droplet flame should promote fuel pyrolysis and soot production. An approximate estimate for the residence time of fuel molecules inside the flame is obtained by integrating with respect to radial position the inverse of the average velocity of fuel molecules inside the flame. This residence time can be shown to scale with D^2 [ref. 3]. Therefore, larger droplets have more time for fuel pyrolysis and soot formation. A large amount of soot formation early in the combustion process of large droplets may encourage further soot formation by surface reactions on newly-formed soot particles. If the amount of soot formed is more sensitive to droplet diameter than D^2, proportionately more carbon atoms from the vaporized fuel goes into forming soot for larger droplets than for smaller droplets. This lowers the proportionate amount of heat released for droplet vaporization and the corresponding burning rate constant.

Methanol and Methanol/Toluene Mixtures

Experimental results of pure methanol droplets showed that methanol droplets produce virtually non-luminous flames in microgravity at atmospheric pressure [ref. 6]. Pure toluene droplets, however, have been shown to produce highly sooting flames with the formation of dense soot shells between the droplet and the flame [ref. 1, 5]. Furthermore, pure methanol droplets exhibit flame extinction, attributed to water vapor absorption into the liquid phase, and pure toluene droplets have been shown to emit large quantities of soot due to the break-up of the soot shell near the end of burning. These differences in the behavior of methanol and toluene motivated the study of mixture droplets of these two fuels [ref. 7] in order to ascertain whether some of the less favorable characteristics of the spherically symmetric combustion of the pure components could be eliminated. Pure methanol droplets were burned in the microgravity environment in order to provide a basis for comparison with the mixtures which included 5%, 25%, and 50% v/v toluene in methanol.

Pure methanol droplets with D_o from 0.40 to 0.45 mm burned with a faint non-luminous flame and exhibited extinction at droplet diameters ranging from 160 to 190 μm. 5% v/v toluene in methanol droplets, with D_o ranging from 0.5 to 0.6 mm, burned without any observable difference from the pure methanol droplets. The flame did not appear luminous or exhibit soot formation. Average K values of the 5% toluene droplets before extinction matched those for pure methanol droplets, and extinction of the 5% toluene droplets consistently occurred at droplet diameters similar to those of pure methanol droplets. In fact, all toluene/methanol droplets had similar droplet diameter-squared profiles as shown by the sample in fig. 3 in spite of tremendous differences in flame luminosity and soot production, demonstrated partly by the photographic sample of the 50% toluene mixture droplet in fig. 4.

Marked increases in the flame luminosity indicating oxidation of soot precursors resulted from the burning of 25% v/v toluene droplets, with D_o between 0.45 and 0.60 mm. The visibility of the flame increased as combustion proceeded as demonstrated by the two sequences shown in fig. 5. This increase with time may be explained by the fact that the fractional vaporization of toluene increased as combustion proceeded. Furthermore, the intensity of the flame luminosity appeared to be sensitive to droplet size as shown in comparing the two sequences in fig. 5. Nonetheless, the flames for all 25% toluene droplets studied (D_o between 0.45 and 0.60 mm) did not produce soot agglomerates, which suggests that this mixture might be useful in promoting flame luminosity for methanol-based fuels without soot emissions. However, flame extinction was still observed for this mixture as shown in the characteristic diameter squared profile of fig. 3. Extinction diameters and burning rate constants before extinction were again similar to those for pure methanol droplets (~ 160 - 180 μm).

The 50% v/v toluene mixtures burned with a dramatic increase in soot production to the extent that a dense soot shell eventually formed around the droplet and large agglomerates of soot were emitted through the flame near the end of burning, as in the combustion of pure toluene droplets. However, unlike the combustion of pure toluene droplets, the mixture droplets (ranging in D_o from 0.45 to 0.55 mm) burned with an initial stage of low luminosity, which suggests an initial period where the fractional vaporization of toluene is low. As methanol is preferentially removed from the droplet surface in the early period of combustion, the fractional vaporization of toluene increases to eventually cause the rapid production of soot particles in the gas phase, demonstrated in the photographs of fig. 4. The soot particles rapidly agglomerate and form a soot shell around the droplet much like the heptane and monochloro-octane droplets mentioned above. The collapse of the flame near the end of burning results in the disruption of the soot shell. The flame extinguishes before the droplet is completely vaporized. The size of the remaining droplets after the collapse of the flame is clearly smaller (< 140 μm) than the extinction diameter of the other two methanol/toluene mixtures studied. The differences in the behaviors of the 50% toluene droplets can in part be explained by vapor/liquid equilibrium data for methanol and toluene which shows that the 50% toluene mixture lies on the toluene rich side of a negative azeotrope for methanol/toluene mixtures [ref. 7].

Methanol/Dodecanol Mixtures

Adding dodecanol to methanol resulted in different droplet combustion behavior than with adding toluene to methanol. 25% v/v and 50% v/v dodecanol in methanol mixture droplets were burned in the low-gravity environment. The following burning characteristics of the methanol/dodecanol mixture droplets, with D_o ranging from 0.50 to 0.60 mm, were observed [ref. 6]: 1) droplet burning appeared to be a multi-stage process for both mixture compositions studied, 2) microexplosions were observed for some of the 25% dodecanol droplets, and 3) extinction did not occur for the mixtures.

Multi-stage combustion in mixture droplets is characterized by a period midway through combustion when the droplet diameter remains relatively constant as its temperature rises and the liquid density correspondingly decreases due to the fractional vaporization of the less volatile component. Such a period is clearly evident in the D^2 profiles for both the 50% v/v and a 25% v/v dodecanol in methanol mixture droplets in fig. 6. The multi-stage combustion for the methanol/dodecanol droplets is caused by diffusion-controlled vaporization where the more volatile methanol gradually is depleted at the droplet surface and cannot be replenished fast enough at the surface due to slow liquid-phase diffusion. The droplet volume reduction before the intermittent period of heating (e.g., ~25% for the 50% methanol mixture) leaves some methanol in the droplet interior, and thus in the final stage of combustion both dodecanol and methanol are being vaporized.

Microexplosions did not occur for the 50% dodecanol droplets burning in microgravity, while microexplosions were observed for over two thirds of the 25% dodecanol droplets. Microexplosions were characterized by the rapid formation and expansion of a bubble within the droplet, which eventually bursts as shown in fig. 7. The initiation of microexplosion is caused by the droplet temperature reaching the superheat limit as discussed in ref. 6.

Methanol/dodecanol mixtures cannot attain temperatures higher than the boiling point of dodecanol during burning. Therefore, any methanol/dodecanol mixture composition with a superheat limit above the dodecanol boiling point will not undergo microexplosion. Calculation of methanol/dodecanol mixture superheat limits at one atmosphere showed that the 50% dodecanol mixture had a superheat limit that was too high for microexplosion while the 25% dodecanol mixture superheat limit was slightly lower than the dodecanol boiling point [ref. 7]. This sheds light on the experimental results which showed microexplosion for only two thirds of the 25% dodecanol mixture droplets. Because the 25% dodecanol mixture has a superheat limit near the boiling point of dodecanol, it is not surprising that some 25% dodecanol droplets did not exhibit microexplosion.

The addition of dodecanol to methanol was found to suppress extinction exhibited as all the 50% dodecanol and non-exploding 25% dodecanol mixture droplets appeared to burn to completion. Water absorption within the droplet may be insignificant during combustion of these mixture droplets because of the higher droplet surface temperatures and the lower solubility of water in dodecanol.

Conclusions

The microgravity environment has proven a very useful tool in examining different aspects of droplet combustion. The spherically symmetric droplet flames simplified the interpretation of all of these phenomena because the interactions between the liquid and the gas-phase were more clearly defined. These aspects included: 1) an influence of droplet size on soot formation in heptane and monochloro-octane droplets, 2) the possibility that

increased soot formation and emissions of larger droplets encourage a decrease in the burning rate constant with initial droplet size for sooting fuels, 3) the usefulness of mixing methanol and toluene to achieve a luminous droplet flame without soot emissions, 4) microexplosions of methanol/dodecanol mixture droplets, and 5) the potential of mixing a heavier alcohol (such as dodecanol) with methanol to suppress flame extinction exhibited by pure methanol droplet. Future work will seek to further quantify the influence of soot on the burning process and to examine a wide range of fuel mixtures.

References

1. Avedisian, C.T., Yang, J.C., and Wang, C.H., "On low gravity droplet combustion", *Proc. R. Soc. Lond.* **A420**, 1988, pp. 183-200.
2. Yang, J.C., An experimental method for studying combustion of an unsupported fuel droplet at reduced gravity, Ph.D. thesis, Cornell University, Ithaca, New York, 1990.
3. Jackson, G.S., Avedisian, C.T., and Yang, J.C., "Observations of Soot during Droplet Combustion at Low Gravity: Heptane and Heptane/Monochloro-alkane Mixtures", *Int. J. Heat Mass Trans.* **35** (8), 1992, pp. 2017-2033.
4. Jackson, G.S. and Avedisian, C.T., "Experiments on the Effect of Initial Diameter in Spherically Symmetric Droplet Combustion of Sooting Fuels", Paper no. 93-0130, AIAA 31st Aerospace Sciences Meeting, Reno, Nevada, 1993.
5. Jackson, G.S. and Avedisian, C.T., "Possible Effect of Initial Diameter in Spherically Symmetric Combustion of Sooting Fuels", Paper no. 110, Eastern States Section Meeting of the Combustion Institute, Ithaca, NY, October, 1991.
6. Yang, J.C., Jackson, G.S. Avedisian, C.T., Combustion of unsupported methanol/dodecanol mixture droplets at low gravity, *Twenty-Third Symp. (Int.) on Comb.*, The Combustion Institute, Pittsburgh, 1990, pp. 1619-1625.
7. Jackson, G.S., Avedisian, C.T., and Yang, J.C., "Soot Formation During Combustion of Unsupported Methanol/Toluene Mixture Droplets in Microgravity", *Proc. R. Soc. Lond.* **A435**, 1991, pp. 359-369.

Figures

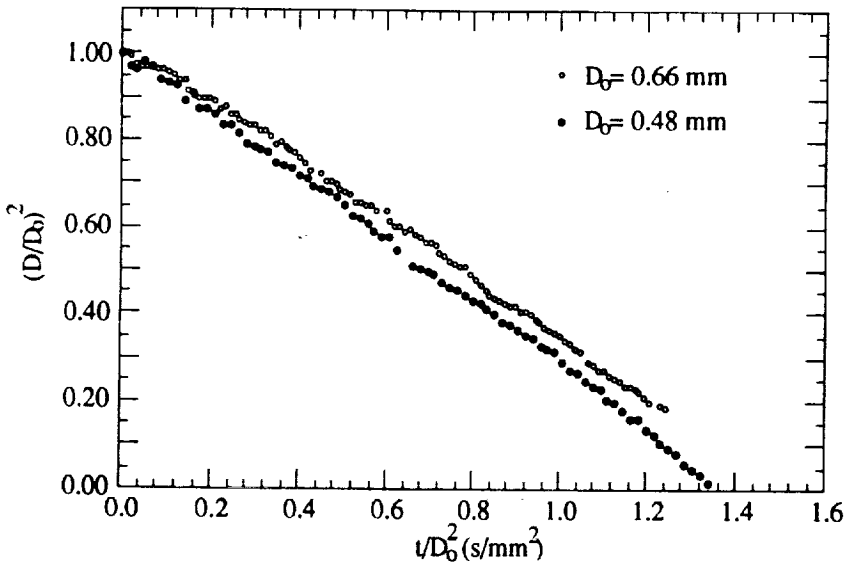

Figure 1. -- Two examples of dimensionless diameter-squared profiles for unsupported heptane droplets burning in microgravity [ref. 4].

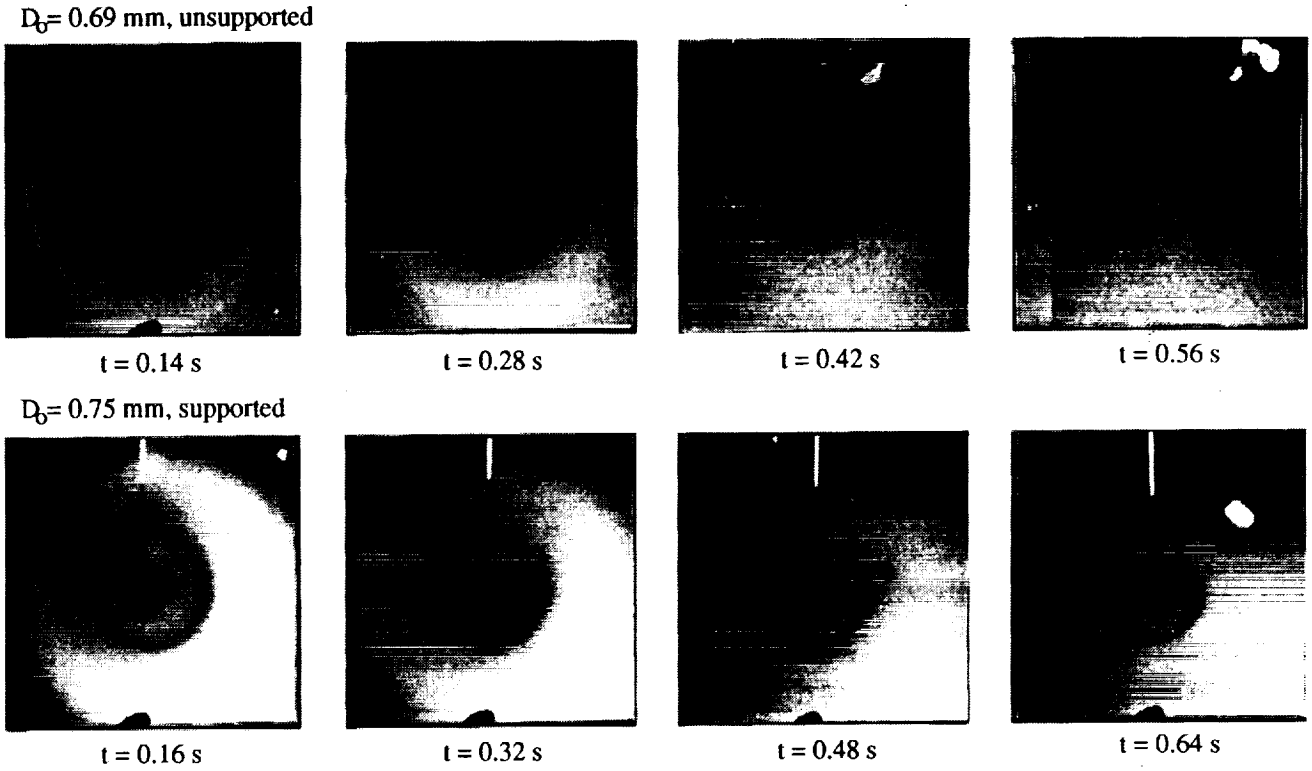

Figure 2. -- Comparison of unsupported and suspended heptane droplets burning in microgravity [ref. 4].

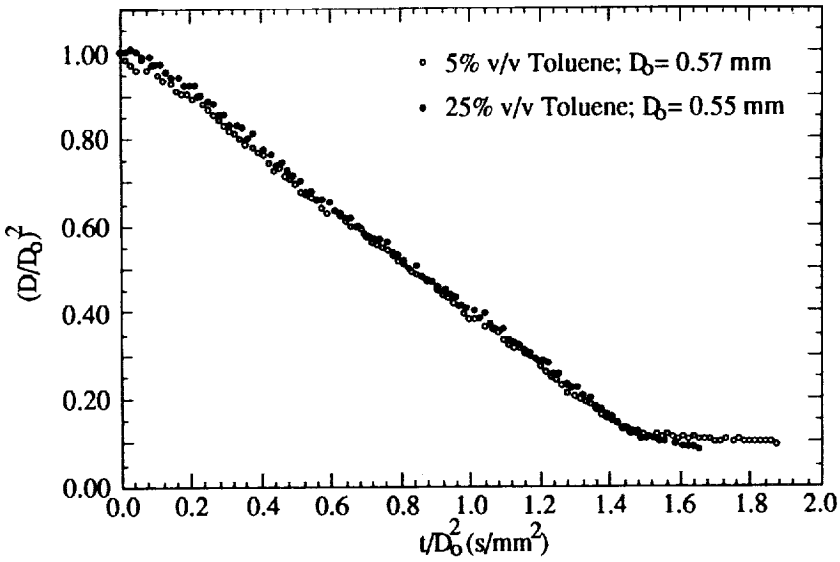

Figure 3. -- Dimensionless diameter-squared profiles for two methanol/toluene mixture droplets burning in microgravity [ref. 7].

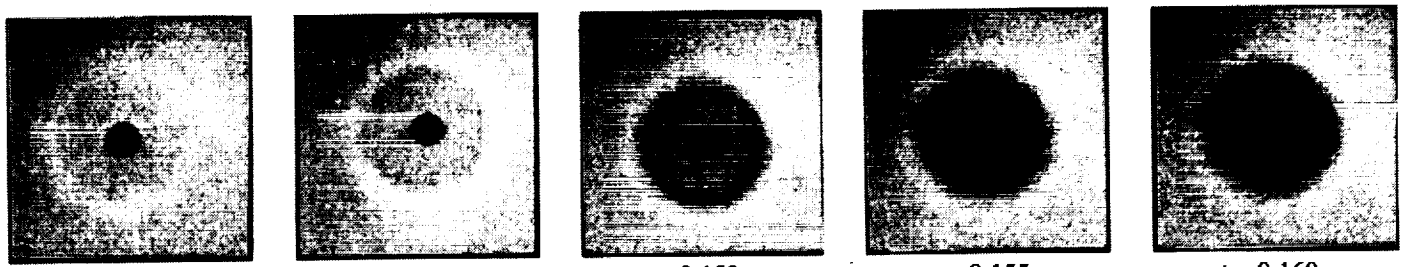

Figure 4. --50% v/v toluene in methanol droplet burning at low gravity, exhibiting rapid formation of soot [ref. 7].

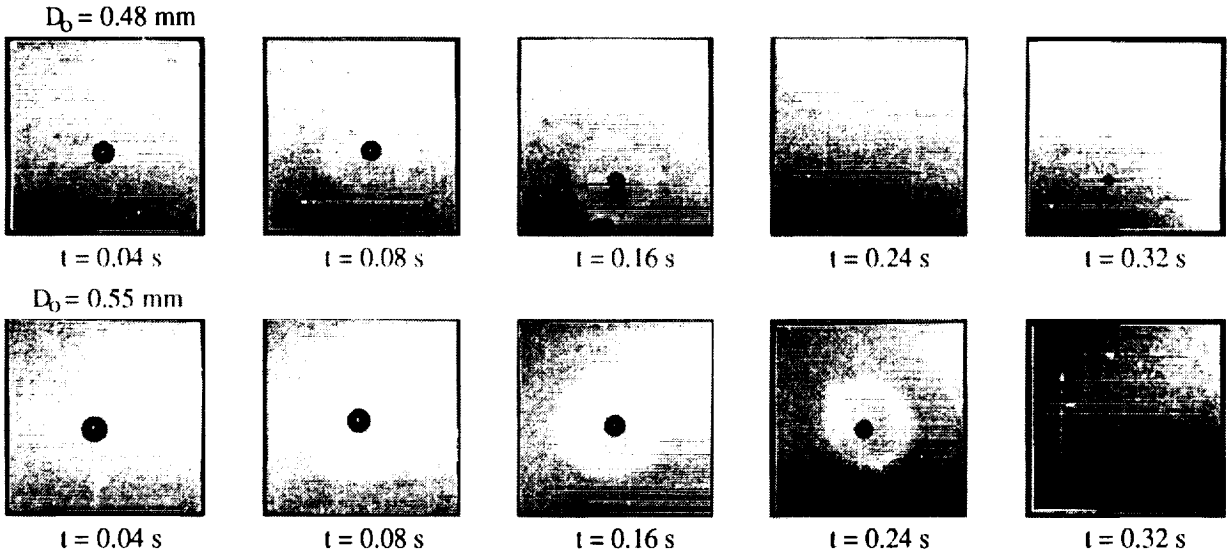

Figure 5. -- Comparison of flame luminosity of two 25% v/v toluene in methanol droplets with different initial diameters burning in microgravity [ref. 7].

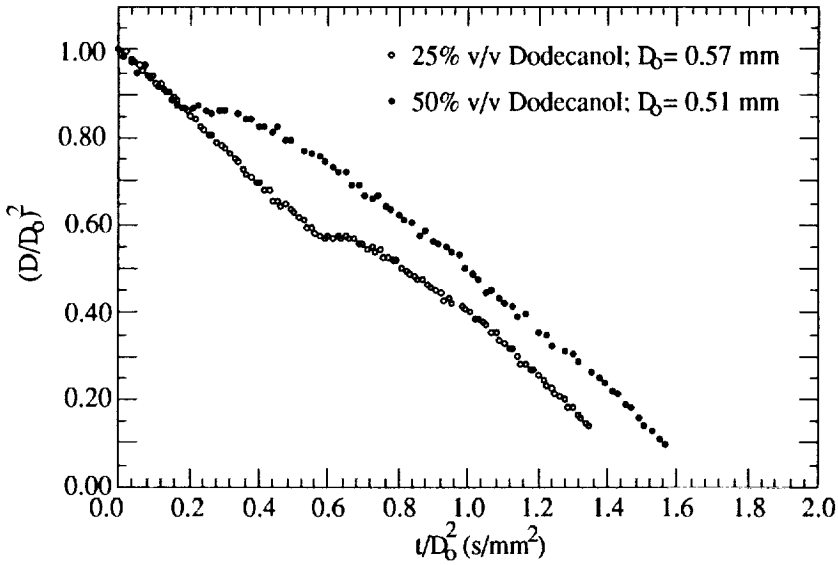

Figure 6. -- Dimensionless diameter-squared profiles for two methanol/dodecanol droplets burning in microgravity illustrating multi-staged combustion.

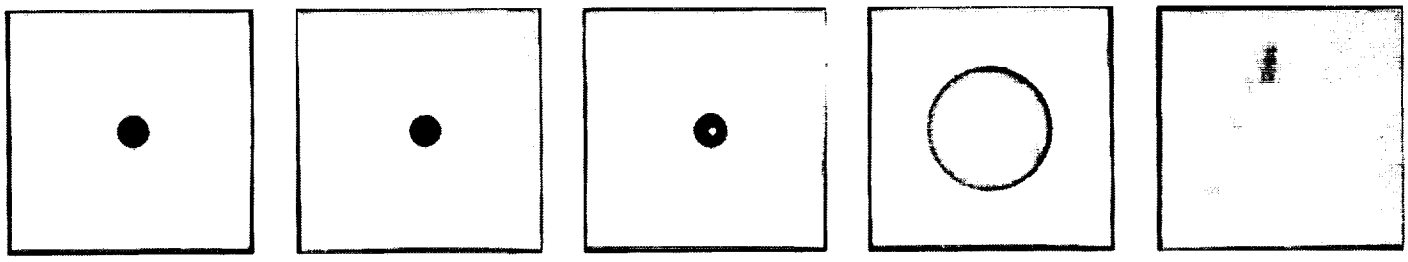

Figure 7. -- 75% v/v methanol in dodecanol droplet burning in microgravity which illustrates microexplosion [ref. 6].

SESSION H - FINAL PLENARY SESSION

(Chair, Bradley Carpenter)

SESSION SUMMARIES

SUMMARY OF SESSION C - Diffusion Flames and Diagnostics

(Robert Santoro, session chair)

The session on Diffusion Flames and Diagnostics contained a balanced treatment of these topical areas in microgravity research. Four papers were presented on diffusion flames involving both laminar and turbulent flow conditions. These papers were completed by three diagnostic contributions which reviewed present capabilities as well as previewing future developments.

From the presentations in this session some general observations can be drawn regarding both topical areas. First, turning to the diffusion flame studies in microgravity conditions, current work is emphasizing the measurement and prediction of flame shape for both laminar and turbulent flame conditions. The presence of soot particles in these flames has been used as a key diagnostic tool because the luminous characteristics of soot particles provide for convenient visualization of the flame boundary. Consequently, studies are also focusing on soot formation effects themselves as a phenomenon of interest. Furthermore, the present results for these flames have revealed several interesting effects on soot formation under microgravity conditions, including what appears to be enhanced formation rates. With respect to the modeling of these flames, current models emphasize the prediction of the species concentration, temperature and velocity fields from which the flame boundaries are obtained and compared with experiments. Because of the lack of diagnostic techniques suitable to the microgravity experimental facilities (i.e., drop towers, KC-135 flights and Space Shuttle experiments) prediction will continue to be relied upon for determination of these quantities.

With regard to the area of diagnostics for microgravity studies, the video camera has truly become the visualization detector of choice. The advent of intensified cameras is extending the application of this technique to low light levels and holds the promise of providing spectral measurements as well. The implementation of thermophoretic probe sampling of soot particles represents a significant advance. The application of intrusive probes for the measurement of other combustion products would be a major diagnostic enhancement. Thus, the thermophoretic probe results may spur similar intrusive probe development for other measurement needs. It is clear that rapid and significant advances have been made in the area of combustion diagnostics for microgravity experiments since the First International Microgravity Combustion Workshop was held.

Turning to the specific presentations made during the session, several interesting and significant results were presented. Bahadori et al. reviewed their extensive work in the area of laminar and turbulent diffusion flame studies. Of particular note were the turbulent flames results, which were reported to have significantly different blowoff, flame length and vortex development behavior as compared to similar flames in normal gravity environments. These results will offer new challenges to models predicting mixing, near-limit phenomena (e.g. extinction) and flame stability properties in turbulent flames.

Faeth et al. reported on studies conducted on laminar diffusion flames, which are oriented towards better understanding the soot and thermal radiation emissions from luminous flames. The results presented for low pressure diffusion flames were quite novel. Low pressure conditions were used to simulate microgravity conditions and revealed new insight in smoke-point behavior and soot formation processes. A major advantage of this low pressure environment is the opportunity for extensive measurements of flame properties over periods of time longer than than typically available in current microgravity facilities. These experiments hold the potential for providing a unique environment in which to study soot formation and the development of state relationships aimed at predicting soot formation in turbulent combustion systems.

Atreya et al. reported on their modeling efforts with respect to soot formation in counterflow diffusion flames. These modeling results are being compared to recent normal gravity flame measurements and will be extended to zero gravity studies to be initiated soon in the NASA-Lewis 2.2 sec microgravity drop tower. Ku et al. similarly reported on their efforts to model turbulent flames in a microgravity environment in which

soot formation is explicitly modeled. Both these studies are incorporating normal gravity results for the key submodels of soot formation, turbulence and radiation. In this respect, they will challenge current understanding, while presenting new opportunities to reveal modeling successes and deficiencies.

The last three presentations of the session focused on diagnostics for microgravity studies. Weiland reported on the current capabilities with respect to imaging and visualization of flames. Both qualitative and quantitative aspects were discussed. The application of intensified solid-state cameras to recent experiments was discussed and the potential of these techniques for future drop tower and space-based studies was clearly demonstrated. Extension of solid-state camera capabilities into the infrared region was also described. Finally, developments in the area of compact solid-state lasers were reviewed. Griffin and Greenberg reviewed applications of rainbow schlieren deflectometry and thermophoretic sampling of soot particles in separate microgravity studies. These techniques were demonstrated to have suitable performance in microgravity experimental facilities such as the NASA-Lewis microgravity drop towers. Both of these talks from the NASA Lewis Research Center were clear evidence of the advances made in the past four years with respect to microgravity diagnostics. Finally, Winter described his work on droplet diagnostics and reviewed plans to extend that work to a microgravity environment, using recently developed compact-laser technology. This work clearly points to the promising future for diagnostics development for microgravity studies.

The session on Diffusion Flames and Diagnostics provided a suitable overview and summary of microgravity research in these areas. From this session chairman's viewpoint, it also identified some research needs. In-situ measurements of species, temperature or density under microgravity conditions would provide critically needed test data for model predictions of these quantities. Current experiments rely heavily on models to provide these properties and comparative results do not presently exist against which to validate models. Studies of finite rate chemistry effects have not yet been pursued. In fact, studies that differentiate between soot and flame chemistry effects are absent. Presently, soot is a key diagnostic tool for the study of flame structure. Direct measurements of combustion species such as OH or CO would yield further insights into flame structure under microgravity conditions. All of these needs appear to be in the mix of future studies and, with proper development of diagnostics capabilities, we can look forward to stimulating presentations on these topics in future microgravity combustion workshops.

SUMMARY OF SESSION D - Premixed Flames
(Mitchell Smooke, session chair)

The Wednesday afternoon session on premixed flames consisted of eight presentations. Most of the talks were experimental in focus, though two were computational and theoretical in orientation, and one was entirely computational. The presentations ranged from studies of premixed laminar and turbulent flames in microgravity conditions, to combustion of particles and dust-cloud suspensions, to the combustion synthesis of ceramic composites. Each of the eight talks is discussed in some detail below.

The presentation by Paul Ronney (Princeton University) considered combustion limits in premixed flames in microgravity. He examined the effects of radiation on these systems as well as the structure and stability of these flames at low Lewis numbers. His work also considered flame propagation in cylindrical tubes and the simulation of combustion via autocatalytic chemical reactions.

John Buckmaster's (University of Illinois) presentation focused on the analytical and numerical modeling of configurations undergoing experimental study in NASA's microgravity combustion program. The major areas of study were flame balls, particle cloud flames and self extinguishing flames.

Research of K. Kailasanath (NRL) and G. Patnaik's (Berkeley Research Associates) investigates computationally concerns the propagation and extinction of gas-phase flames in both microgravity and Earth environments. They computed time-dependent multidimensional flames that propagated downward. They analyzed a chemical kinetics instability issue for rich hydrogen-air flames and they studied thermodiffusive and buoyancy interactions.

The work by Eng, Zhu, and Law (Princeton University) combined experimental and theoretical analyses of cylindrical and spherical premixed and nonpremixed flames in microgravity. The premixed work focused on stabilization issues and the measurement of the laminar flame speed. The nonpremixed work examined extinction and soot layer properties in the inner flame region.

Researchers at LBL (Kostiuk, Zhou, and Cheng) used moderate-to-low turbulence Reynolds number flames (wrinkled) to characterize and quantify turbulent flame structure under microgravity. Qualitative and quantitative flow visualization techniques were coupled with video recording and computer-controlled image analysis.

The research group at McGill University (Lee, Peraldi, and Knystautas) is examining microgravity combustion of dust suspensions. They have carried out a number of studies aboard the KC-135 and the ESA Caravelle. Preliminary experiments have demonstrated the feasibility of obtaining a quiescent dust cloud for fundamental flame propagation studies in microgravity.

A combined theoretical and numerical study of particle cloud premixed flames was undertaken by Seshadri at UCSD. The work provided a description of the structure of planar laminar flames propagating a medium containing a uniform cloud of fuel particles premixed with air.

The final presentation of the afternoon was by Moore, Feng and Hunter (Colorado Center for Advanced Ceramics) and Wirth (Coors Ceramics Company). An experimental program in self-propagating high temperature synthesis (SHS) was described in which several model composite systems were investigated. The work has the potential of impacting catalyst support systems, filters, and ultra-light structural materials.

Due to the length and the number of talks, the session ended close to 6 P.M., so there was not time for a general wrap-up discussion in which outstanding problems, issues and concerns of the researchers could be voiced. Overall, the talks were well received and we look forward to the next round of results.

SUMMARY OF SESSION F - Ignition, Smolder, and Flame Spread of Condensed Phase Fuels
(Raymond Friedman, session chair)

The session consisted of seven presentations. The investigators were from 10 organizations. Each presentation included some discussion or at least mention of a mathematical model of the combustion phenomenon of interest, as well as references to experimental results. The papers dealt with ignition, flame spread, and in some cases, extinction for a wide variety of condensed-phase combustibles: (1) thin paper; (2) thermally thick polymethyl methacrylate; (3) flexible polyurethane foam; (4) flammable liquids (methanol, butanol, decane); and (5) metals (iron, steel, titanium, copper, aluminum, nickel, Monel, tungsten). Other variables were gravitational field, total pressure, partial pressure of oxygen, incident thermal radiation, approach flow velocity, and sample thickness. In each study, the goal is to establish the physico-chemical mechanism by which the ignition and propagation occur, both at normal gravity and at microgravity. In no case was it possible to draw final conclusions, but it was clear that progress is occurring in each of these ongoing investigations.

From an experimental point of view, certain things emerged: (1) it is indeed possible to perform good microgravity combustion experiments with condensed-phased materials; there are clearly observable differences from normal-gravity combustion, (2) there would be a great advantage in having higher-resolution non-intrusive instrumentation, and (3) much more experimental data will be needed before firm conclusions on mechanisms can be established. As for the theoretical side, the most advanced models presented were those of Kashiwagi and Baum (ignition and spread); Tien et al. (steady spread, limits), and Sirignano et al. (unsteady spread with circulation in both liquid and gas). All these models will require further development (three-dimensionality, better chemical kinetic representation, inclusion of gaseous radiation, effect of diluents).

Ultimately, we look forward to the convergence of the experimental and theoretical work.

SUMMARY OF SESSION G - Droplet and Spray Combustion
(Forman Williams, session chair)

This proved to be a lively session involving a considerable number of new research results, especially concerning droplet combustion. Different studies of droplet burning focused on different fuels, including heptane, decane, methanol, heptane-hexadecane mixtures and (in work reported orally) methanol-dodecanol and methanol-toluene mixtures as well. The oxidizing atmospheres were mainly normal air, air diluted with nitrogen, or air enriched with oxygen. Very broad pressure ranges, from 0.1 atm to 100 atm, were considered in different investigations. In addition to these single-droplet studies, there were two reports of preliminary results on burning of droplet arrays and one outlining investigations of counterflow spray combustion.

An area of emphasis in droplet combustion concerned the burning of single-component and two-component fuels at elevated pressures, extending beyond the critical pressures of the fuels, confirming the increase in the burning-rate constant with increasing pressure, up to the critical pressure. The burning-rate constant achieves a maximum at or above the critical pressure, with the maximum occurring at higher pressures for lower peak temperatures, as found in burning in diluted atmospheres or, in extreme cases, in vaporization without burning. This behavior is explicable on the basis of the reduced partial pressure of the fuel in the gas at the droplet surface under conditions of reduced partial pressure of the fuel in the gas at the droplet surface under conditions of reduced peak temperatures and correspondingly reduced burning rates.

The question of whether three-stage combustion of two-component fuels extends to supercritical pressures could not be addressed in ground-based experiments employing fiber-supported droplets, because the droplets fall off the fiber as the critical point is approached, due to the reduced surface tensions. Microgravity investigations have now demonstrated that three-stage behavior does indeed extend to supercritical conditions. Preliminary explanations of the new results were offered in terms of buildup of surface layers of different composition through fuel diffusion effects.

Other results, indicated as having been obtained since the previous workshop, included the observation of the slow regime of heptane combustion, encountered for near-spherical burning with weak ignitions, and the demonstration of a decreasing burning-rate constant for methanol with increasing time, as a consequence of absorption, within the liquid fuel, of water produced in the flame. A number of new observations of sooting phenomena. Droplet disruption events during combustion also were reported, further emphasizing relationships between sooting and disruption.

Studies directed towards flame extinction helped to clarify extinction conditions in droplet burning for methanol and for alkanes. In particular, significant uncertainties in important alkane fuel chemistry were identified, which can result in differences of two orders of magnitude in predicted heptane droplet extinction diameters. Experiments are being designed to measure the extinction diameters under microgravity conditions, to help reduce the uncertainties in the predictions.

The two studies of droplet arrays involve two or three fiber-supported droplets, side by side, burning in chambers in drop towers. One study is directed towards normal pressures and the other towards two-component fuels at elevated pressures. Both are directed towards obtaining information that can be used in describing influences of droplet interactions in spray combustion, and both are just beginning. So scientific conclusions have not been drawn, although useful observations have been made on ways to make droplet arrays burn symmetrically.

The investigation of counterflow sprays employed electrostatically-formed sprays and demonstrated combustion-zone structures in the counterflow configuration and how those structures can depend on initial droplet-size distributions. The role of microgravity in this investigation was indicated as involving possible reaction-zone displacement through buoyancy effects and group-combustion phenomena that may occur at higher droplet number densities.

Most of the droplet-burning investigations have been performed employing drop-tower facilities. Drop towers are considered to be well-suited to many droplet-combustion studies, because the burning times often are compatible with such facilities, and the low g-levels required are achievable therein. For conditions under which longer burning times occur, the Hokkaido 10-second tower is a very attractive facility, especially since its gentler deceleration admits use of more advanced instrumentation, which often is more sensitive to rapid deceleration. The g-levels in aircraft typically are high enough to produce some degradation in droplet-burning results. One investigation is directed towards experiments in the Space Shuttle for conditions involving burning times too long for drop towers. In another, an ESA project, there are plans to employ a sounding rocket. It will be interesting to see what facilities result in the most useful droplet-combustion data.

In what directions might future new investigations best proceed? It was suggested that new emphasis might be placed on burning in atmospheres having high or low oxygen concentrations, on burning in atmospheres having high or low oxygen concentrations, on burning in atmospheres having inerts other than nitrogens, and on burning more exotic fuels, such as monopropellants or liquid metals. These seemed to be topics for which unknowns are relatively great.

A final question concerned types of instrumentation for use in microgravity studies of droplet and spray combustion. Most previous work has involved mainly motion-picture photography. Recent use has been made of ultraviolet filters to isolate OH radiation emission, and a project directed towards development of laser instrumentation has been initiated. It seemed to be felt to be highly desirable to explore further many new instrumentation approaches for such microgravity studies, but without discontinuing the photographic methods that to date have provided virtually all of the useful experimental information obtained under microgravity conditions for droplet combustion.

OPEN DISCUSSION

Question (Jack Salzman, NASA Lewis Research Center): Were liquid phase dynamics (e.g., internal droplet flows) discussed? Could this be an important area of research?

Answer: (Forman Williams, U. of California, San Diego) Yes, there was discussion of liquid-phase dynamics, for example in connection with Professor Dryer's presentation. I neglected to mention that in my summary. It certainly could be an important area of research because the roles of phenomena such as Marangoni flow, for example, in droplet and spray combustion are poorly understood.

Question (John Moore, Colorado School of Mines)

The combustion science research community now has an ideal opportunity to embrace a new and highly logical research area of the synthetics of advanced materials in favorable combustion technology.

(1) Need: more research on the potential of coupling combustion synthesis and microgravity to produce new and unique advanced materials. The will complement and aid the Federal government's new research directive in Advanced Materials and Processing Program (AMPP)

(2) In particular: need to conduct research on:

(a) Synergistic effects of the coupling of combustion synthesis with microgravity and liquid and/or gaseous (fluid) phase transport (i.e., deliberately generating liquids and/or gases at the combustion point to aid in the synthesis kinetics and provide new and/or unique microstructure and morphologies with improved properties (e.g., in-situ synthesis of composites; whiskers; fine and ultrafine powders; foamed (expanded) ceramics; dense near net-shape ceramic and metal matrix composites.

(b) Modeling of the above advanced combustion synthesis processes to high synthesis parameters (e.g., particle size, green density, stoichiometry, physico-chemical properties of reactants and products, ignition and combustion temperatures, etc, which provide control of the combustion synthesis and predict product microstructure and properties.

(c) other areas (e.g., flame synthesis of powders, including composite powders), whiskers and fibers and Fullerenes. etc.

Answer (Brad Carpenter, NASA Headquarters): So noted, and we will certainly take that into consideration when preparing the scope of the next NRA.

COLOR PLATES

Fig. 1 Measurement of internal circulation from within droplets using fluorescence quenching.

ORIGINAL PAGE
COLOR PHOTOGRAPH

Winter
Color Plate C-7a

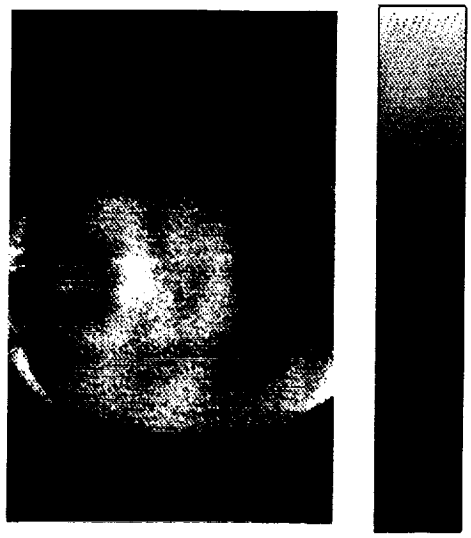

Fig. 2 Surface fluorescence quenching from a droplet supported on a fiber.

Winter
Color Plate C-7b

ORIGINAL PAGE
COLOR PHOTOGRAPH

Comparison of OH concentration in upward-, zero-gravity and downward- propagating flames with heat loss to walls.

Kailasanath
Color Plate D-3

Fig. 2a. Low strain rate, sooty counterflow diffusion flame on the oxidizer side of the stagnation plane

Fig. 2b. Same as Fig. 2a. The $TiCl_4$ streak shows the location of the stagnation plane

Fig. 3a. Low strain rate, sooty counterflow diffusion flame on the fuel side of the stagnation plane

Fig. 3b. Same as Fig. 3a. The $TiCl_4$ streak shows the location of the stagnation plane

Atreya
Color Plate C3

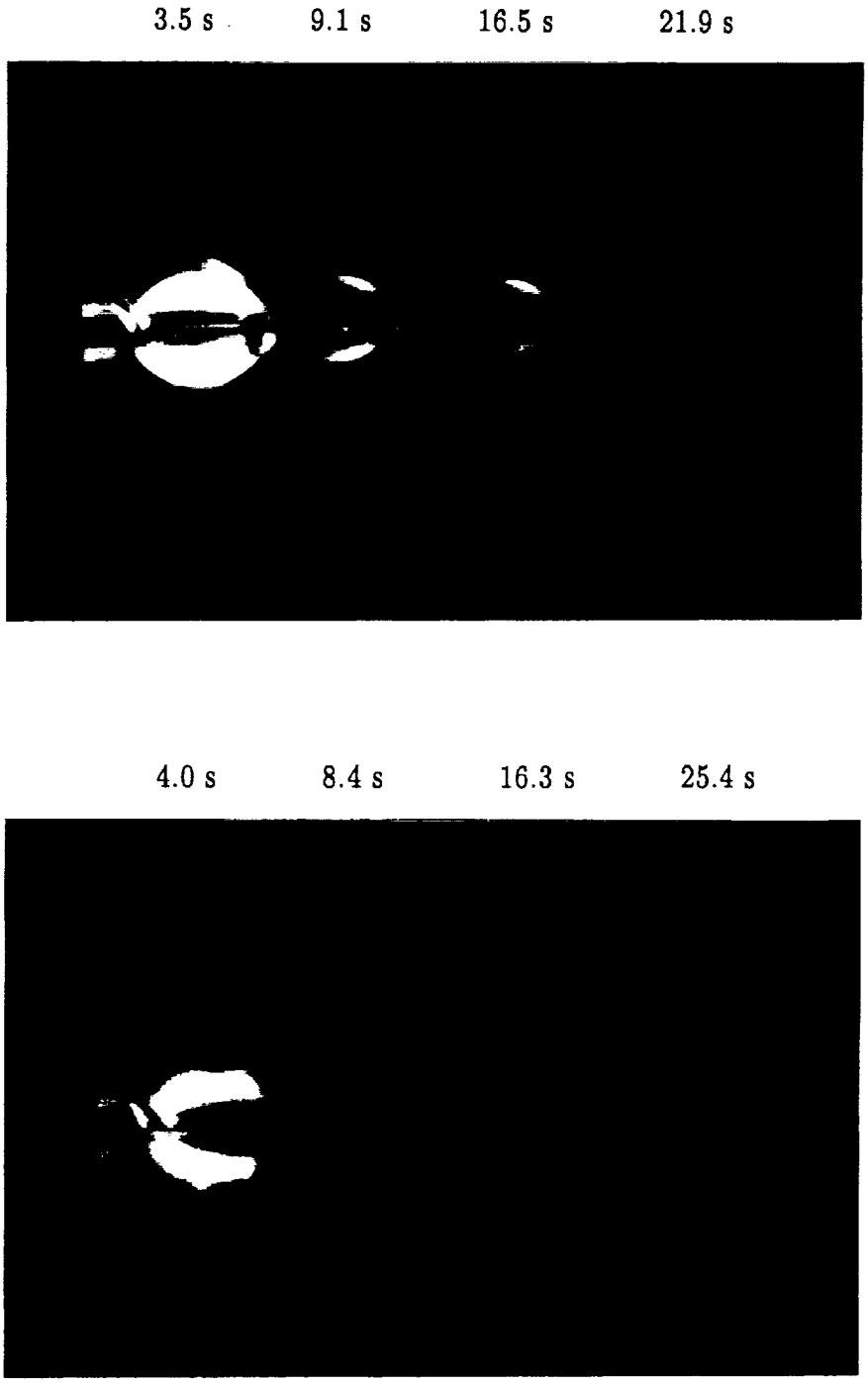

Fig. 1. Four frames from 16 mm film of flame spread over ashless filter paper in the SSCE at 50% O_2 at 1.5 atm (top) and 1.0 atm (bottom). Times are time from the first appearance of a flame–like image on the film.

Altenkirch
Color Plate F-2

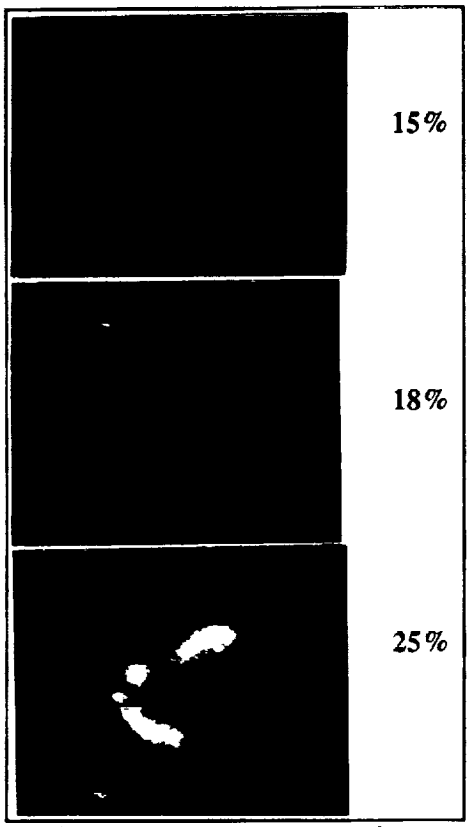

Fig. 6 Flame Shapes at 5cm/sec Relative Concurrent Flow

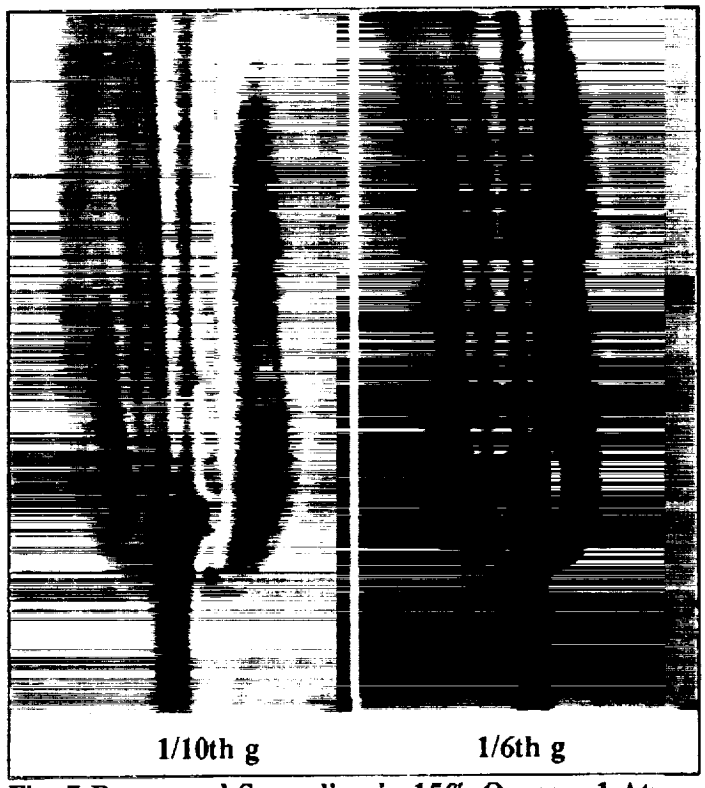

Fig. 7 Downward Spreading in 15% Oxygen, 1 Atm

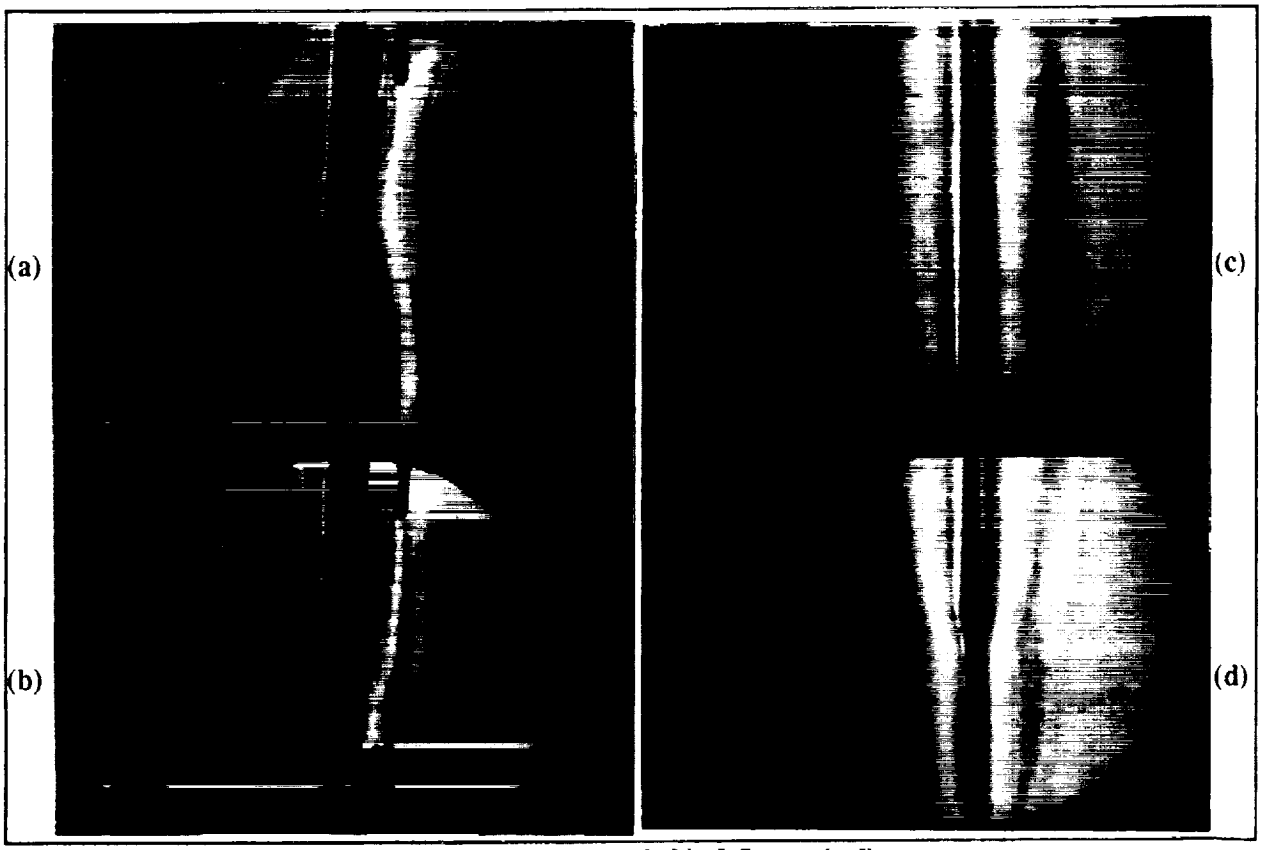

Fig. 8 Upward Spreading in 15% Oxygen, 1 atm (a,b), 0.5 atm (c,d)

T'ien
Color Plate F-3

FIGURE 1: RSD Visualization of a butanol-air flame at 23 C. Flame spreads from left to right. The pool depth is 1 cm.

FIGURE 2: PIV of a butanol-air flame at 23 C. Flame spread is from right to left. Time lapse is 0.33 sec. Pool depth is 1 cm; note that the field of vie[illegible]'s picture is different than that of Figure 1.

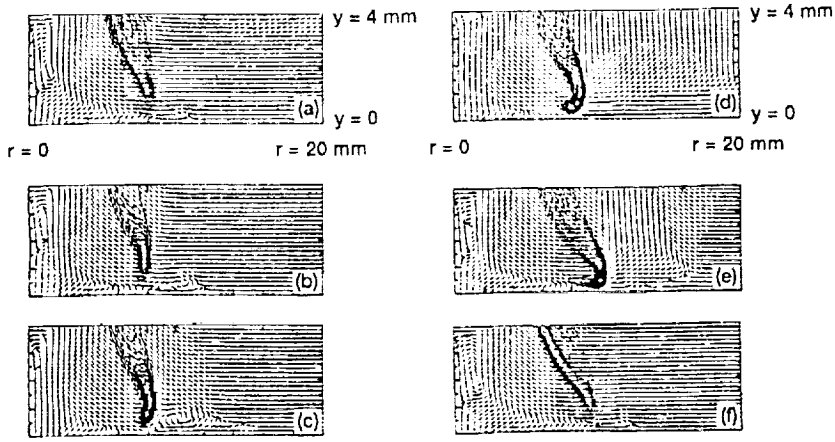

Figure 3.—Flow pattern and flame structure for one flame pulsation at normal gravity. In (d)-(f), the recirculation cell structure in front of the flame leading edge is destroyed during the premixed burning portion of the flame. Hot gas expansion opposes the flow of fresh oxygen to the reaction zone, and the flame moves backwards (as if it were being extinguished). The gas expansion rate decreases after the flame propagates through the premixed region, and, subsequently, the buoyant forces recover to provide fresh oxygen to the reaction zone.

Ross
Color Plate F--5

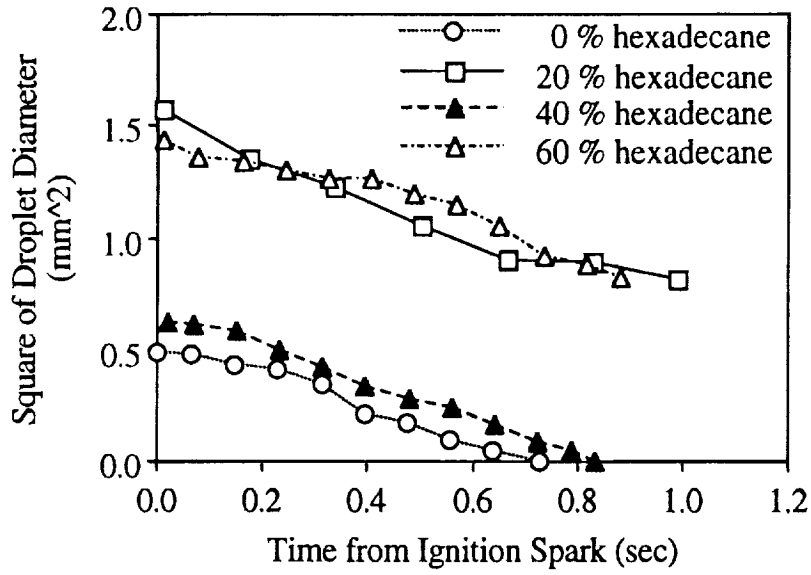

Figure 1.--Plots of squares of measured droplet diameters vs. time.

0.794 sec 0.860 sec 0.990 sec

Figure 2.--Sequence of images showing flame contraction and growth for a droplet composed initially of 20% n-hexadecane and 80% n-heptane. Times are after the ignition spark. Visible flame diameters (measured perpendicular to the fiber) for this droplet are plotted in Fig. 3.

ORIGINAL PAGE
COLOR PHOTOGRAPH

Shaw
Color Plate G2A

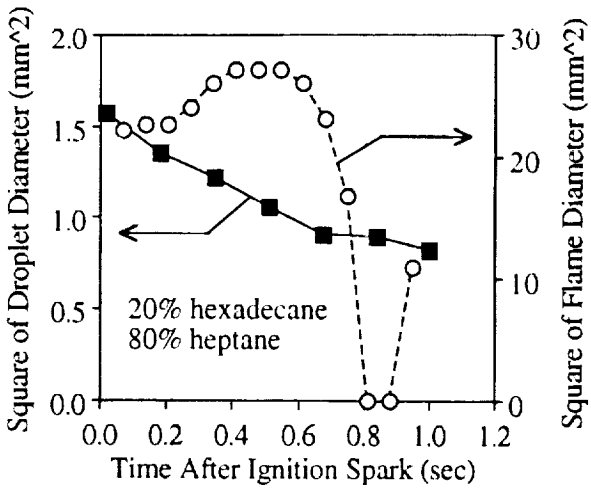

Figure 3.--Plots of squares of droplet and flame diameters for a droplet composed initially of 20% n-hexadecane and 80% n-heptane.

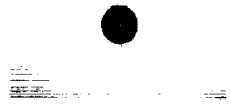

Figure 4.--Image of a droplet (initially 60% n-hexadecane and 40% n-heptane) showing the support fiber and the soot "shell". The droplet diameter is about 1.07 mm.

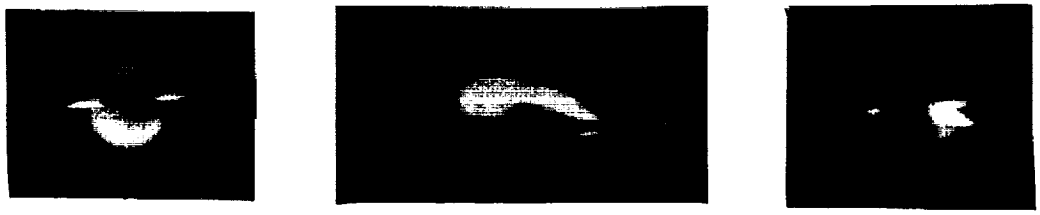

0.324 sec 0.333 sec 0.342 sec

Figure 5.--Sequence of images showing the flame behavior just prior to, during and after what appears to be disruption of a droplet initially composed only of n-heptane. Times are after the ignition spark. For a scale reference, the visible flame diameter at 0.324 sec is about 4.7 mm (measured perpendicular to the fiber).

ORIGINAL PAGE
COLOR PHOTOGRAPH

Shaw
Color Plate G2b

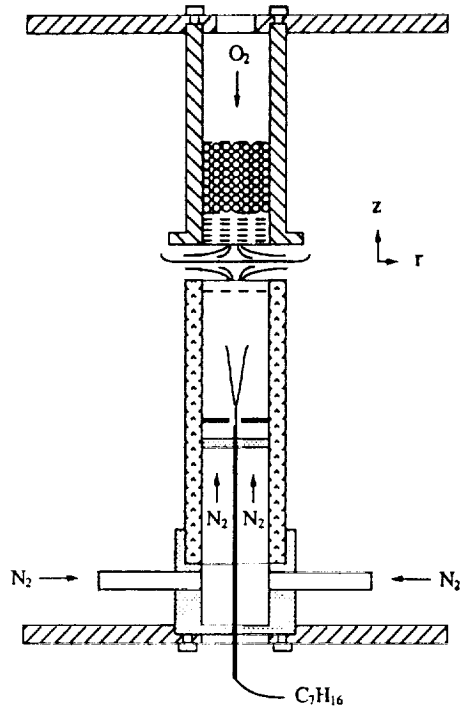

Fig. 3 Counteflow spray diffusion flame burner.

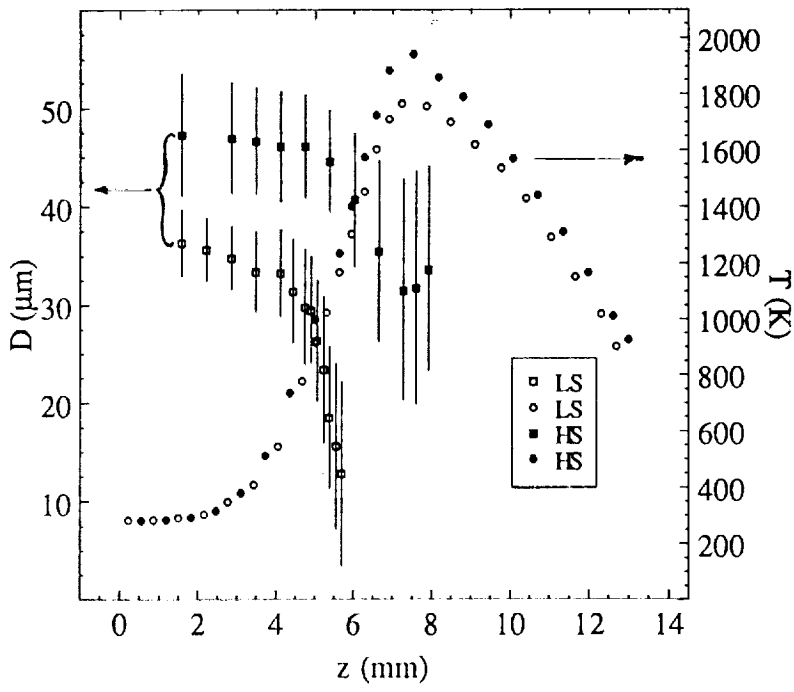

Fig. 4 Average droplet diameter (squares) and gas-phase temperature (circles) measured along the burner axis versus distance from the bottom burner rim.

Fig. 5 Microphotograph of a droplet in the act of disintegrating.

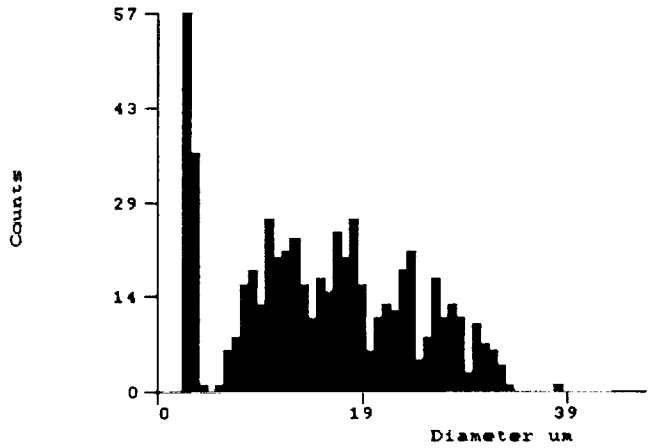

Fig. 6 Droplet size distribution measured at z=5.5 mm in Flame LS.

Gomez
Color Plate G-6

LIST OF ATTENDEES

SECOND INTERNATIONAL MICROGRAVITY COMBUSTION WORKSHOP

September 15-17, 1992

ATTENDEE LIST

Suresh Aggarwal
Univ. of Illinois at Chicago
Mechanical Engineering
Box 4348
Chicago, IL 60680
312-996-2235

Sanjay Agrawal
Michigan State University
Department of Mechanical Engineering
East Lansing, MI 48824
517-353-9950

Ajay Agrawal
Clemson University
Mechanical Engineering Department
318 Riggs Hall
Clemson, SC 29631
203-656-5643

Robert Altenkirch
Mississippi State University
P.O. Drawer DE
Mississippi State, MS 39762
601-325-2270

George Apostolakis
University of California, Los Angeles
Mech. Aerospace & Nuclear Engr. Dept.
38-137 Engineering IV
Los Angeles, CA 90024-1597
213-825-1300

Arvind Atreya
Michigan State University
Department of Mechanical Engineering
A-104 RCE
East Lansing, MI 48824
517-353-6356

Thomas Avedisian
Cornell University
Department of Mechanical & Aero Engr.
Upson Hall Room 112
Ithaca, NY 14853-7501
607-255-5105

Richard Axelbaum
Washington University
Dept. of Mechanical Engineering
St. Louis, MO 63130
314-935-7560

Yousef Bahadori
Science Applications International Corp.
M.S. 500-217
21000 Brookpark Rd.
Cleveland, OH 44135
216-433-8574

Kirk Barrow
Jet Propulsion Laboratory
M.S. 301-375
4800 Oak Grove Dr.
Pasadena, CA 91109
818-354-6345

Howard Baum
NIST
Building 224, Room B268
Gaithersburg, MD 20899
301-975-6668

Barney Bellagh
ADF, Inc.
3003 Aerospace Parkway
Brook Park, OH 44142
216-977-0375

Subrata Bhattacharjee
San Diego State University
Dept. of Mechanical Engineering
San Diego, CA 92182
619-594-6080

Nora Bozzolo
Analex
3001 Aerospace Parkway
Brook Park, OH 44142
216-977-0086

Melvyn Branch
University of Colorado, Boulder
Mechanical Engineering
Boulder, CO 80309-0427
303-492-6318

Kenneth Brezinsky
Princeton University
E. Quad D329
Princeton, NJ 08544
609-258-5225

John Buckmaster
University of Illinois
Aero & Astro Engr.
104 S. Mathews Ave
Urbana, IL 61801-2007
217-333-1803

Dan Bulzan
NASA Lewis Research Center
21000 Brookpark Rd.
Cleveland, OH 44135
216-433-5848

Brad Carpenter
NASA Headquarters
Code SNB
Washington, DC 20546
202-358-0818

Ivan Catton
University of California, Los Angeles
Mech. Aerospace & Nuclear Engr.
48-121 Engineering IV
Los Angeles, CA 90024-1597
310-825-5320

Dee Chapman
Boeing
P.O. Box 240002
Huntsville, AL 35824

Christian Chauveau
CNRS - CRCCHT
1C, Av. Recherche Scientifique
45071 ORLEANS Cedex 2
FRANCE,
3338515485

Gung Chen
Yale University
Dept. of Mechanical Engineering
P.O. Box 2159, Yale Station
New Haven, CT 06520
203-432-4390

Robert Cheng
University of California
1 Cyclotron Rd.
B29C
Berkeley, CA 94720
415-486-5438

Daniel Dietrich
Sverdrup Technology, Inc.
M.S. 500-217
21000 Brookpark Rd.
Cleveland, OH 44135
216-433-8759

James Driscoll
University of Michigan
312 Aerospace Engineering Bldg.
Ann Arbor, MI 48109

Frederick Dryer
Princeton University
C-316 Engineering Quadrangle
Princeton, NJ 08544
609-987-2916

Cory Dunsky
Sandia National Labs
Combustion Research Facility
P.O. Box 969, Division 8362
Livermore, CA 94551-0969
510-294-1005

Ray Edelman
Rockwell International Corporation
23146 Cumorah Crest Drive
Woodland Hills, CA 91364
805-371-7196

S. Elghobashi
University of California
Dept. of Mechanical Engineering
Irvine, CA 92717
714-856-6131

James Eng
Princeton University
Dept. of Mech. & Aero. Engr.
Princeton, NJ 08544
609-258-5649

Ofodike Ezekoye
NIST
B-258, Building 224
Building & Fire Research Lab.
Gaithersburg, MD 20899
301-975-2593

Gerard Faeth
University of Michigan
218 Aerospace Engineering Building
Ann Arbor, MI 48109-2140
313-764-7202

Bakhtier Farouk
Drexel University
Dept. of Mechanical Engineering
Philadelphia, PA 19104
215-895-2287

Patrick Farrell
University of Wisconsin, Madison
Department of Mechanical Engineering
1500 Johnson Drive
Madison, WI 53706
608-263-1686

Francis Fendell
TRW
R1/1062
One Space Park
Redondo Beach, CA 90025
310-812-0327

Paul Ferkul
NASA Lewis Research Center
M.S. 500-217
21000 Brookpark Rd.
Cleveland, OH 44135
216-433-8107

A. Carlos Fernandez-Pello
University of California, Berkeley
Department of Mechanical Engineering
Berkeley, CA 94720
415-642-6554

Patrick Finnegan
Analex
3001 Aerospace Parkway
Brook Park, OH 44142
216-977-0188

Michael Frenklach
Penn State University
202 Academic Projects Bldg.
University Park, PA 16802
816-865-4392

Robert Friedman
NASA Lewis Research Center
M.S. 500-217
21000 Brookpark Rd.
Cleveland, OH 44135
216-433-5697

Raymond Friedman
Factory Mutual Research
1151 Boston-Providence Turnpike
Norwood, MA 02062
617-762-4300

Osamu Fujita
Hokkaido University
Dept. Mechanical Engineering
Sapporo, Hokkaido, 060 JAPAN

Tony Galambos
Analex
3001 Aerospace Parkway
Brook Park, OH 44142
216-977-0144

George Gogos
Rutgers University
Dept. of Mech. & Aero. Engr.
P.O. Box 909
Piscataway, NJ 08855
908-932-3797

Iskender Gokalp
C.N.R.S. -LCSR
1 C, av de la Recherche Scientifique
45071 Orleans Cedex 2
France

Suleyman Gokoglu
NASA Lewis Research Center
M.S. 106-1
21000 Brookpark Rd.
Cleveland, OH 44135
216-433-5499

Jeffrey S. Goldmeer
Case Western Reserve University
Department of Mech. & Aero. Engr.
Cleveland, OH 44106
216-791-8555

Alessandro Gomez
Yale University
Dept. of Mechanical Engineering
P.O. Box 2159
New Haven, CT 06520
203-432-4384

Jay Gore
University of Maryland
School of Mechanical Engineering
2177F Engineering Building
College Park, MD 27907
317-494-1452

Samuel Goroshin
438 90th Street Apt. #3B
Brooklyn, NY 11209
718-921-1504

Helen Grant
NASA Headquarters
Code SNC
300 E Street SW
Washington, DC 20546
202-358-0825

Paul Greenberg
NASA Lewis Research Center
M.S. 500-217
21000 Brookpark Rd.
Cleveland, OH 44135
216-433-3621

DeVon Griffin
Sverdrup Technology, Inc.
M.S. 500-217
21000 Brookpark Rd.
Cleveland, OH 44135
216-433-8109

Mark Guenther
Michigan State University
1637 Lake Dr. Apt. 80
Haslett, MI 48840

George Haddad
NASA Lewis Research Center
21000 Brookpark Rd.
Cleveland, OH 44135
216-433-2714

John Haggard
NASA Lewis Research Center
M.S. 500-217
21000 Brookpark Rd.
Cleveland, OH 44135
216-433-2832

Bert Hansen
NASA Headquarters
Code SN
Washington, DC 20546
202-358-0818

William Hartz
Analex
3001 Aerospace Parkway
Brook Park, OH 44142
216-433-0084

Mohammad Hassani
The University of Michigan
College of Engineering
Department of Mech. Engr. & Appl. Mech.
Ann Arbor, MI 48109-2121
313-767-3588

Uday Hegde
Sverdrup Technology, Inc.
2001 Aerospace Parkway
Brook Park, OH 44142
216-433-8744

Warren Hodges
NASA Headquarters
Code SN
Washington, DC 20546
202-453-1741

Jack Howard
MIT
Room 66-454
Cambridge, MA 02139
617-253-4574

Thomas Hunter
Penn State University
Mechanical Engineering Department
310 Reber Bldg.
University Park, PA 16802
814-863-2945

Soon Muk Hwang
NASA Lewis Research Center
M.S. 5-11
21000 Brookpark Rd.
Cleveland, OH 44135
216-433-6504

Farrokh Issacci
University of California, Los Angeles
MANE
Los Angeles, CA 90024-1597
310-206-4848

Greg Jackson
Cornell University
Upson Hall Box 34
Ithaca, NY 14853
607-255-9109

Dick Jacobs
Analex
3001 Aerospace Parkway
Brook Park, OH 44142

Dwight Janoff
Lockheed ESC
2400 NASA 1 MS B22
Houston, TX 77058
713-333-6072

Hang Jia
Rutgers University
Dept. of Mechanical & Aerospace Engr.
P.O. Box 909
Piscataway, NJ 08855
908-932-3674

Stan Jones
University of California, Los Angeles
MANE
38-137 Engineering IV
Los Angeles, CA 90024-1597
310-825-1300

K. Kailasanath
Naval Research Laboratory
Code 4410
Lab for Computational Physics
Washington, DC 20375-5000
202-767-2402

Takashi Kashiwagi
National Institute of Standards and Tech
Center for Fire Research
B258/224
Gaithersburg, MD 20899
301-975-6699

Larry Kostiuk
Lawrence Berkeley Laboratory
MS-B29C 1 Cyclotron Road
Berkeley, CA 94720
510-486-6683

John Koudelka
NASA Lewis Research Center
M.S. 500-217
21000 Brookpark Rd.
Cleveland, OH 44135
215-433-2852

Jerry Ku
Wayne State University
Mechanical Engineering Department
Detroit, MI 48202
313-577-3814

Ming-Chi Lai
Wayne State University
Mechanical Engineering Department
2129 Engineering Building
Detroit, MI 48202
313-577-3893

Chung K. Law
Princeton University
Department of Mech. & Aero.
Engineering Quadrangle
Princeton, NJ 08544
609-452-5271

Paul Ledoux
McDonnell Douglas
16055 Space Center Blvd.
Houston, TX 77062
713-335-4133

John Lee
McGill University
Department of Mechanical Engineering
817 Sherbrooke St. W.
Montreal Quebec H3A 2K6 CANADA
514-398-6301

Jack Lekan
NASA Lewis Research Center
M.S. 500-217
21000 Brookpark Rd.
Cleveland, OH 44135
216-433-3459

Gregory Linteris
NIST
Bldg. 224, Room A345
Gaithersburg, MD 20899
301-975-2283

David Lozinski
University of Ill. Urbana-Champagne
Dept. of Aero & Astro Engr.
Urbana, IL 61810
217-244-4372

Bernard Matkowsky
Northwestern University
The Technological Institute
Dept. of Engr. Sci. & Appl. Math
Evanston, IL 60208
708-491-5396

Carl Meade
NASA Johnson Space Center
Astronaut's Office
Houston, TX 77058

C. M. Megaridis
Univ. of Illinois at Chicago
Mech. Engr.
M/C 251 Box 4348
Chicago, IL 60680
312-996-3436

A.M. Mellor
Vanderbilt University
Box 1592, Station B
Nashville, TN 37235-1592
615-343-6214

Clayton Meyers
NASA Lewis Research Center
M.S. 86-15
21000 Brookpark Rd.
Cleveland, OH 44135
216-433-3882

K. Clark Midkiff
University of Alabama
Department of Mechanical Engr.
Box 870276
Tuscaloosa, AL 35487-0276
205-348-1645

Masato Mikami
University of Tokyo
7-3-1 Hongo, Bunkyo-ku
Tokyo 113, JAPAN

Fletcher Miller
NASA Lewis Research Center
M.S. 500-217
21000 Brookpark Rd.
Cleveland, OH 44135
216-433-8845

Moti Mittal
Ohio Supercomputer Center
1224 Kinnear Rd.
Columbus, OH 43212
614-292-2552

John Moore
Colorado School of Mines
Dept. of Metallurgical and Mat. Engr.
Golden, CO 80401
303-273-3770

Dan Morilak
NASA Lewis Research Center
M.S. 500-322
21000 Brookpark Rd.
Cleveland, OH 44135

Edward Mularz
NASA Lewis Research Center
M/S 5-11
21000 Brookpark Rd.
Cleveland, OH 44135
216-433-5850

Vedha Nayagam
Analex
3001 Aerospace Parkway
Brook Park, OH 44142
216-977-0139

Sandra Olson
NASA Lewis Research Center
M.S. 500-217
21000 Brookpark Rd.
Cleveland, OH 44135
216-433-2859

Howard Palmer
Penn State University
224 Academic Proj. Bldg.
University Park, PA 16802

Mary Palumbo
NASA Lewis Research Center
M.S. 86-12
21000 Brookpark Rd.
Cleveland, OH 44135
216-433-2043

Gopal Patnaik
Berkley Research Associates
P.O. Box 852
Springfield, VA 22150
202-767-3531

Mark Paul
University of California, Los Angeles
MANE
38-137 Engineering IV
Los Angeles, CA 90024-1597
310-825-1300

Todd Paulos
University of California, Los Angeles
MANE
38-137 Engineering IV
Los Angeles, CA 90024-1597
310-825-1300

Kevin Paxton
University of California
MANE
38-137 Engineering IV
Los Angeles, CA 90024-1597
310-825-1300

Howard Pearlman
NASA Lewis Research Center
21000 Brookpark Rd.
Cleveland, OH 44135

Robert Pitz
Vanderbilt University
Mechanical Engineering
Box 54, Station B
Nashville, TN 37205
615-322-0209

Joseph Powers
University of Notre Dame
Dept. of Aero. & Mech. Engr.
Notre Dame, IN 46556
219-239-5978

Joseph Prahl
Case Western Reserve University
Dept. Mech. & Aero. Engr.
Cleveland, OH 44106
216-368-2941

Alden Presler
Analex
3005 Aerospace Parkway
Brook Park, OH 44142
216-977-0194

Ishwar Puri
University of Illinois at Chicago
Dept. of Mech. Engr.
M/C 251, Box 4348
Chicago, IL 60680
312-413-7560

Marty Rabinowitz
NASA Lewis Research Center
M.S. 5-11
21000 Brookpark Rd.
Cleveland, OH 44135
216-433-5847

Surya Raghu
State Univ. of New York at Stony Brook
Department of Mechanical Engineering
Stony Brook, NY 11794-2300
516-632-8343

Anjay Ray
Michigan State University
Department of Mechanical Engineering
Combustion/Heat Transfer Lab
East Lansing, MI 48824
517-353-9950

D.R. Reddy
NASA Lewis Research Center
M.S. 5-11
21000 Brookpark Rd.
Cleveland, OH 44135
216-433-8133

Robert Rhome
NASA Headquarters
Code SN
Washington, DC 20546
202-453-1425

Paul Ronney
Princeton University
The Engineering Quadrangle
Princeton, NJ 08544
609-452-5278

Howard Ross
NASA Lewis Research Center
M.S. 500-217
21000 Brookpark Rd.
Cleveland, OH 44135

Kurt Sacksteder
NASA Lewis Research Center
M.S. 500-217
21000 Brookpark Rd.
Cleveland, OH 44135
216-433-2857

Jack Salzman
NASA Lewis Research Center
M.S. 500-205
21000 Brookpark Rd.
Cleveland, OH 44135
216-433-2868

Robert Santoro
The Pennsylvania State University
Department of Mechanical Engineering
240 Research Building E
University Park, PA 16802-2320
814-863-1285

Jun'ichi Sato
IHI Research Institute
3-1-15 Toyosu, Koto-ku, Tokyo 135
JAPAN,
813-534-3360

David Schiller
University of California, Irvine
945 Engineering Building
Irvine, CA 92717
714-856-7160

James Seaba
University of Missouri - Columbia
1020 EBE, MAE Department
Columbia, MO 65211
314-882-3655

K. Seshadri
University of California at San Diego
Dept. AMES
Mail Code B-010
La Jolla, CA 92093-0310
619-534-4876

Ben Shaw
University of California at Davis
MAME Department
Davis, CA 95616
916-752-4130

Nancy Shaw
NASA Lewis Research Center
M.S. 500-205
21000 Brookpark Rd.
Cleveland, OH 44135
216-433-3285

Martin Sichel
University of Michigan
Dept. of Aerospace Engr.
Ann Arbor, MI 48109-2140
313-764-3388

Joel Silver
Southwest Sciences, Inc.
1570 Pacheco St., E-11
Santa Fe, NM 87501
505-984-1322

Y.R. Sivathanu
Purdue University
School of Mechanical Engr.
125 Chafee Hall, TSPC Sch. of Mech. Engr.
W. Layfayette, IN 47907
317-494-9364

Mitchell Smooke
Yale University
New Haven, CT
203-432-4344

Mark Stack
Bradley University
1539 California St.
Elk Grove, IL 60007
708-529-7877

Theodore Steinberg
Lockheed - ESC
P.O. Drawer MM
Las Cruces, NM 88004
505-524-5680

Russ Stienbach
Analex
3001 Aerospace Parkway
Brook Park, OH 44142

Dennis Stocker
NASA Lewis Research Center
M.S. 500-217
21000 Brookpark Rd.
Cleveland, OH 44135
216-433-2166

James Tien
Case Western Reserve University
Dept. of Mechanical & Aerospace Engr.
Cleveland, OH 44106-7222
216-368-4581

Robert Tacina
NASA Lewis Research Center
21000 Brookpark Rd.
Cleveland, OH 44135
216-433-3588

Fumiaki Takahashi
University of Dayton Research Institute
KL465
300 College Park
Dayton, OH 45469-0140
513-252-5577

Tesfahunet Tecle
NASA Lewis Research Center
21000 Brookpark Rd.
Cleveland, OH 44135
216-433-6620

Larry Torre
Boeing
P.O. Box 240002, MS JC-26
Huntsville, AL 35824
205-461-3516

Paul Trimarchi
NASA Lewis Research Center
M.S. 86-12
21000 Brookpark Rd.
Cleveland, OH 44135
216-433-3824

David Urban
Sverdrup Technology, Inc.
M.S. 500-217
21000 Brookpark Rd.
Cleveland, OH 44135
216-433-2835

Randy Vander Wal
Sverdrup Technology, Inc.
2001 Aerospace Parkway
Brook Park, OH 44142
216-234-2111

Denise Varga
NASA Lewis Research Center
M.S. 11-2
21000 Brookpark Rd.
Cleveland, OH 44135
216-433-5190

Richard Verbus
Analex
3001 Aerospace Parkway
Brook Park, OH 44142
216-977-0192

Vladimir Volpert
Northwestern University
Dept. of Engineering Sci. & Appl. Math.
Evanston, IL 60208
708-491-5396

Joyce Wanhainen
NASA Lewis Research Center
M.S. 86-12
21000 Brookpark Rd.
Cleveland. OH 44135
216-433-3820

Curtis Watts
Grumman Space Station Int. Div.
620 Discovery Drive, 3rd Floor
Huntsville, AL 35806
205-971-6107

Joseph Wehrmeyer
University of Missouri-Columbia
Mech. and Aerospace Engr. Dept.
1020 Engr. Building East
Columbia. MO 65211
314-882-0878

Karen Weiland
NASA Lewis Research Center
M.S. 500-217
21000 Brookpark Rd.
Cleveland. OH 44135
216-433-3623

Carl Wickstrom
University of Arkansas
Dept. of Mech. Engr.
Fayetteville. AK 72701
501-575-4503

Forman Williams
University of California, San Diego
9500 Gilman Drive
B-010
La Jolla. CA 92093
619-534-5492

Michael Winter
United Technologies Research
M/S 90
Silver Lane
E. Hartford. CT 06108
203-727-7805

Sylvia Yang
NASA Lewis Research Center
M.S. 86-5
21000 Brookpark Rd.
Cleveland. OH 44135
216-433-3889

Michael Zachariah
NIST
Gaithersburg, MD 20899

Liming Zhou
7710 Lucerne Dr. #R-30
Middleburg Hts., OH 44130
216-433-0820

REPORT DOCUMENTATION PAGE

Form Approved
OMB No. 0704-0188

1. AGENCY USE ONLY (*Leave blank*)	2. REPORT DATE	3. REPORT TYPE AND DATES COVERED
	February 1993	Conference Publication

4. TITLE AND SUBTITLE

Second International Microgravity Combustion Workshop

5. FUNDING NUMBERS

WU-674-22-05

6. AUTHOR(S)

7. PERFORMING ORGANIZATION NAME(S) AND ADDRESS(ES)

National Aeronautics and Space Administration
Lewis Research Center
Cleveland, Ohio 44135-3191

8. PERFORMING ORGANIZATION REPORT NUMBER

E-7309

9. SPONSORING/MONITORING AGENCY NAMES(S) AND ADDRESS(ES)

National Aeronautics and Space Administration
Washington, D.C. 20546-0001

10. SPONSORING/MONITORING AGENCY REPORT NUMBER

NASA CP-10113

11. SUPPLEMENTARY NOTES

Responsible person, Howard D. Ross, (216) 433-2562.

12a. DISTRIBUTION/AVAILABILITY STATEMENT

Unclassified - Unlimited
Subject Category 29

12b. DISTRIBUTION CODE

13. ABSTRACT (*Maximum 200 words*)

This CP contains 40 papers presented at the Second International Microgravity Combustion Workshop held in Cleveland, Ohio from September 15 to 17, 1992. The purpose of the workshop was twofold: to exchange information about the progress and promise of combustion science in microgravity and to provide a forum to discuss which areas in microgravity combustion science need to be expanded profitably and which should be included in upcoming NASA Research Announcements (NRA).

14. SUBJECT TERMS

Microgravity and fire; Combustion; Flammability

15. NUMBER OF PAGES
389

16. PRICE CODE
A17

17. SECURITY CLASSIFICATION OF REPORT	18. SECURITY CLASSIFICATION OF THIS PAGE	19. SECURITY CLASSIFICATION OF ABSTRACT	20. LIMITATION OF ABSTRACT
Unclassified	Unclassified	Unclassified	

END DATE APRIL 5, 1993